

Distribution Agreement

In presenting this thesis or dissertation as a partial fulfillment of the requirements for an advanced degree from Emory University, I hereby grant to Emory University and its agents the non-exclusive license to archive, make accessible, and display my thesis or dissertation in whole or in part in all forms of media, now or hereafter known, including display on the world wide web. I understand that I may select some access restrictions as part of the online submission of this thesis or dissertation. I retain all ownership rights to the copyright of the thesis or dissertation. I also retain the right to use in future works (such as articles or books) all or part of this thesis or dissertation.

Signature:

Autumn R. Flynn

Date

Structure, Synthesis, and Reactivity:
Intentional Design Approaches to Agonists for Liver Receptor Homolog-1
and
Photochemical Arene Dearomatization

By
Autumn R. Flynn
Doctor of Philosophy
Chemistry

Nathan T. Jui, Ph.D.
Advisor

Dennis C. Liotta, Ph.D.
Committee Member

Eric A. Ortlund, Ph.D.
Committee Member

Lanny L. Liebeskind, Ph.D.
Committee Member

Accepted:

Dean of the Graduate School
Lisa A. Tedesco, Ph.D.

Date

Structure, Synthesis, and Reactivity:
Intentional Design Approaches to Agonists for Liver Receptor Homolog-1
and
Photochemical Arene Dearomatization

By

Autumn R. Flynn
B.A., College of Saint Benedict, 2015

Advisor: Nathan T. Jui, Ph.D.

An abstract of
A dissertation submitted to the Faculty of the
James T. Laney School of Graduate Studies of Emory University
in partial fulfillment of the requirements for the degree of
Doctor of Philosophy
in Chemistry
2020

Abstract

Structure, Synthesis, and Reactivity:

Intentional Design Approaches to Agonists for Liver Receptor Homolog-1
and
Photochemical Methods for Arene Dearomatization

By: Autumn R. Flynn

The nuclear receptor Liver Receptor Homolog-1 (LRH-1) is a high-value therapeutic target for inflammatory bowel diseases due to its ability to combat tissue damage specifically in the gastrointestinal tract. Developing activators (agonists) for LRH-1 would be highly beneficial to people with these autoimmune disorders, like ulcerative colitis, because the agonists would stimulate endogenous anti-inflammatory activity in the gut without global immunosuppression.

Unfortunately, LRH-1 is historically difficult to target with small molecules because of its spacious and largely hydrophobic ligand binding domain that prefers to bind lipids, which cannot be used as pharmaceuticals because of their poor metabolic profiles and low potency.

Here, crystallographic studies have driven the design of synthetic targets, each of which interrogates a specific question relating to LRH-1 activation by small molecules. By combining these intentional synthetic efforts with pointed biological feedback, we have successfully developed the only small molecule agonists that activate LRH-1 with nanomolar potencies. Additionally, we have developed a synthetic strategy to install phospholipid-mimicking groups that act synergistically with the core of our agonists to result in the most activating and potent LRH-1 ligands to date. These activators indeed bind to LRH-1 exactly as designed and are strikingly effective at restoring colitis-induced intestinal inflammation in a mouse model of colitis.

Structure, Synthesis, and Reactivity:
Intentional Design Approaches to Agonists for Liver Receptor Homolog-1
and
Photochemical Arene Dearomatization

By
Autumn R. Flynn
B.A., College of Saint Benedict, 2015

Advisor: Nathan T. Jui, Ph.D.

A dissertation submitted to the Faculty of the
James T. Laney School of Graduate Studies of Emory University
in partial fulfillment of the requirements for the degree of
Doctor of Philosophy
in Chemistry
2020

Acknowledgements

Chemists are in a uniquely powerful position to use their knowledge of how to make changes on the atomic level that will impact the world. The field of chemistry as a whole often finds itself rationalizing much of its work by illustrating how it will impact our quality of life, and as a research group, we have strived to do the same. Though my respective place in the field (and the Jui group) has been highly intersectional, I have also found myself driven by what I can do at the bench that will somehow, someday, make an impact on people. To this end, I haven't actually found myself focusing on a single project—but instead learning as much and as broadly as I can while given the freedom and resources to do so. I think this dissertation reflects that.

For the luxury of this playground, permission for autonomy, unwavering support, and constructive frustration: thank you, Nate. I entered graduate school with limited expectations—yet none of them were “working for an assistant professor.” I am lucky to have had the incomparable experience of working with you in your pre-tenure years. Thank you for choosing me to be a part of your story, I am honored and excited to be the first (of what will doubtlessly become a legacy of chemists) to earn their Ph.D. under your guidance.

I'm forever indebted to the members of my committee that have dedicated their time and brains to my development as a scientist: Dennis Liotta, Lanny Liebeskind, and Eric Ortlund. Dr. Liotta—you were the first person (outside of Nate and Eric) I experienced encouragement from for my work on the LRH-1 project, the genuine interest you show to the projects and the students you oversee—even outside of your own group—is so treasured. Dr. Liebeskind—you defended one of my crazy sulfur-fluorine proposals in my third-year exam when I didn't believe in it enough on my own. That was a turning point for me, and I haven't let anybody tell me to not try an idea

I've had since then. Eric—I have been so inspired by your ideas and your authentic enthusiasm for research. You have a talent for invigorating a group of people that I've never experienced before: every time I leave an LRH-1 meeting it makes me excited to get right back into the lab. I've learned a lot by seeing the way you run your group and advocate for the projects and people in your lab—I hope to take a lot of what I learned from you with me to my own career.

To David, Ally, and Adam:

This entire experience would have been unbearable if we weren't going through it together. Reflecting too long on what we built together makes me all teary, the Core Four is one of the coolest groups of people I've ever known. I wholeheartedly think part of the reason we all made it through (and all got our “hands” with nearly zero benchwork mentorship) was because we used our collective competitive dispositions to push each other to *be better*, had the courage to ask each other our stupid questions (and were accepting enough to listen to all the stupid questions), dared each other to run the rogue reactions, and *just do it*. I love you guys.

Especially David. It goes without saying that I take back all the times I told my friends and family I'd never marry a chemist. In you I've found my perfect complement and it turns out that actually satiates my competitive side—I'm so grateful that you taught me that about myself. In fact, you've taught me so much about everything: not only chemistry (you're so smart) but also about all your hobbies (3D printing, woodworking, mountain biking, engineering, the list goes on!). I'm excited to learn together for life and I'm constantly looking forward to our next project!

Penelope—I wish you could read. Aside from David you're the most important companion I have and it would have been difficult to stay afloat without you by my side.

Maya & McCauley—you two are phenomenal friends and I love how endlessly interested you are by the things I'm doing in the lab even if you have no reason to be. You've both been

incredibly supportive through the whole planning-a-wedding-and-also-defending-a-PhD-and-moving-across-the-country thing, thank you for all the effort you've put in to make it all possible.

To some of my lifelong lifelines—Shenandoah and Jackson—thinking about you two never fails to pop the “chemistry world” bubble when I'm overwhelmed. You remind me what matters most, and that it's ultimately not chemistry. Watching the two of you find your place in the world and lead your own lives makes me so proud to be your big sister.

Mom and Dad—thanks for not complaining too much when I keep moving further and further away from home, and for keeping me in touch (but not too in touch) with everything around me. Your support means the world. Know you can always call whenever you want even if you don't have any news.

Dear me (for when you finally can get yourself to open this again 10 years down the road): look how *cool* this chemistry was! I hope you're still proud of this stepping-stone, the grit and determination it took to build it, and where it allowed you to climb to.

TABLE OF CONTENTS

PART 1: RATIONAL DESIGN OF LRH-1 AGONISTS.....

USING LRH-1 TO LOCALLY COMBAT INFLAMMATION..... 1

CHAPTER 1: IDENTIFYING A TARGETING STRATEGY FOR LRH-1... 4

1.1 TWO MODES OF LRH-1 ACTIVATION 5

1.2 CRYSTAL STRUCTURES OF RJW100 BOUND TO LRH-1 8

1.3 IDENTIFYING A SYNTHETIC LIGAND DESIGN STRATEGY FOR LRH-1 16

1.4 SUPPORTING INFORMATION 17

CHAPTER 2: PHOSPHOLIPID-MIMICKING CHIMERAS AS LRH-1

AGONISTS..... 33

2.1 OPTIMIZING A SYNTHETIC ROUTE TO RJW100-DLPC HYBRID PRECURSORS 34

2.3 DESIGN AND EVALUATION OF AN RJW100-DLPC CHIMERA 37

2.3 OPTIMIZATION OF CHIMERAS *VIA* SIMPLIFICATION..... 39

2.4 CONCLUSIONS 44

2.5 SUPPORTING INFORMATION. 44

CHAPTER 3: MECHANISM OF ACTIVATION AND THERAPEUTIC

EFFECTS OF LRH-1 AGONIST 10CA..... 86

3.1 PHOSPHOLIPID SIGNALING AXES..... 87

3.2 THE APPARENT IMPORTANCE OF LINKER-LENGTH ON ACTIVATION 88

3.3 CRYSTAL STRUCTURES OF PL MIMETICS BOUND TO LRH-1 90

3.4 SURFACE RESIDUE CONTACTS DRIVE BINDING AND ACTIVATION BY PL MIMETICS 91

3.5 CHIMERAS AFFECT COREGULATOR ASSOCIATION SIGNATURES AND STABILIZE AFS 93

3.6 EFFICACY OF 10CA IN MURINE MODELS OF COLITIS.....	96
3.6 CONCLUSIONS.....	99
3.7 SUPPORTING INFORMATION.....	99
CHAPTER 4: LRH-1-RJW100 CRYSTAL STRUCTURES ENABLE A COMPREHENSIVE STRUCTURE-ACTIVITY RELATIONSHIP	111
4.1 SYNTHESIZING A LIBRARY.....	112
4.2 THE FIRST LOW NANOMOLAR LRH-1 AGONIST.....	115
4.3 CONTACTS THAT DRIVE LRH-1 ACTIVATION BY 6N.....	117
4.4 6N STABILIZES AFS, STRENGTHENS ALLOSTERIC SIGNALING, AND PROMOTES COACTIVATOR RECRUITMENT.....	122
4.5 EVALUATION OF 6N IN MURINE INTESTINAL ORGANOIDS.....	126
4.6 CONCLUSIONS.....	128
4.7 SUPPORTING INFORMATION.....	130
CHAPTER 5: OPTIMIZATION OF LEAD AGONISTS	195
5.1 STRATEGY.....	196
5.2 CARBOXYLATE REPLACEMENT.....	196
5.3 6N-10CA HYBRID.....	199
5.4 SUPPORTING INFORMATION.....	202
CHAPTER 6: DESIGNING NEW CHEMICAL TOOLS TO STUDY THE HUMAN NR5A RECEPTORS LRH-1 AND SF-1	216
6.1 NR5A NUCLEAR RECEPTORS.....	217
6.1 DEVELOPMENT OF A FLUORESCENCE POLARIZATION ASSAY TO DETECT BINDING.....	218
6.3 EVALUATION OF THE FLUORESCENT PROBE 6N-FAM.....	220
6.4 UTILIZATION OF 6N-FAM TO DETECT PHOSPHOLIPID BINDING TO NR5A RECEPTORS.....	222

6.5 SYNTHETIC AGONIST BINDING AFFINITY CORRELATION WITH STABILITY AND ACTIVITY	224
6.6 FP ASSAY VALIDATION BY COMPARING TO EMSA AND SPR	225
6.7 CONCLUSIONS	227
6.8 SUPPORTING INFORMATION	228
LRH-1: SUMMARY AND FUTURE DIRECTIONS	245
PART 2: ARENE DEAROMATIZATION	25247
A CALL FOR IMPROVED DEAROMATIVE TECHNOLOGIES	248
PRINCIPLES OF PHOTOCHEMISTRY	250
CHAPTER 7: DEAROMATIZATION VIA RADICAL HYDROARYLATION	254
7.1 OUR AROMATIC FUNCTIONALIZATION SPACE	254
7.2 DEAROMATIVE HYDROARYLATION DESIGN STRATEGY	256
7.3 KEY DIFFERENCES AND ASSETS TO PHOTOCHEMICAL DEAROMATIVE HYDROARYLATION	259
7.4 THE SCOPE	260
7.5 SELECTIVITY RATIONALE	263
7.6 COMPARATIVE SYNTHESIS OF A PHARMACEUTICAL CANDIDATE	266
7.7 CONCLUSIONS	267
7.8 SUPPORTING INFORMATION	267
CHAPTER 8: PHOTOCHEMICAL DEAROMATIZATION OF BENZENOIDS	326
8.1 PHOTOCHEMICAL ACTIVATION OF MONOCYCLIC AROMATICS	327
8.2 PROOF-OF-CONCEPT AND PRELIMINARY SCOPE	328
8.3 PROPOSED MECHANISM	329

8.4 PROBING MECHANISM WITH EXPERIMENTATION	331
8.5 SUPPORTING INFORMATION	335
PHOTOCHEMICAL DEAROMATIZATION: SUMMARY AND FUTURE DIRECTIONS	338

List of Figures

Chapter 1: Identifying an LRH-1 Targeting Strategy		
1.1	LRH-1 Mechanism of Activation	6
1.2	GSK8470 Crystal Structure	7
1.3	<i>Exo</i> -R JW100 Crystal Structure	8
1.4	<i>Exo</i> -R JW100 vs. DLPC HDX-MS	10
1.5	X-Ray structures of <i>exo</i> -R JW100 vs. GSK8470	11
1.6	LRH-1 LBD Mutations and their effect on receptor melting	13
1.7	LRH-1 LBD Mutations and their effect on receptor activity	14
1.8	<i>Endo</i> -R JW100 Crystal Structure	15

Chapter 2: Phospholipid-Mimicking Chimeras as LRH-1 Agonists		
2.1	Design of Hybrid PL Mimics	35
2.2	Synthetic approach to hybrid compounds	36
S2.1	Luciferase data for compounds 12	84
S2.2	Luciferase data for compounds 13	85

Chapter 3: Mechanism of Activation and Therapeutic Effects of LRH-1 Agonist 10CA		
3.1	Activation dependence on linker length	89
3.2	Crystal Structure of 10CA bound in the LBD of LRH-1	91
3.3	LRH-1 LBD mutations effect activity and binding	92
3.4	9CA and 10CA stabilize LRH-1 relative to 4CA and 5CA	94
3.5	9CA and 10CA effect coregulator recruitment more strongly than 4CA and 5CA	96
3.6	Therapeutic effects of 10CA in disease model	98

Chapter 4: LRH-1–R JW100 Crystal Structure Enables a Comprehensive SAR		
4.1	Structure based design of LRH-1 agonists	113
4.2	Synthesis of LRH-1 targeted compounds	114
4.3	Optimization of R ¹ modification improves potency by two orders of magnitude	116
4.4	A hydrogen-bond donating nitrogen linker in the R ¹ groups improves potency and selectivity	118
4.5	Crystal structures of LRH-1 bound to novel agonists	120
4.6	Compound 6N promotes allosteric communication to AFS and coactivator recruitment	125

4.7	Compound 6N induces intestinal epithelial steroidogenesis in humanized LRH-1 mouse enteroids	127
S4.1	Dose-response curves from luciferase reporter assays in HeLa cells	191
S4.2	HDX data for RJW100, 5N, and 6N	192
S4.3	Ensemble refinement and B-factor analysis	193
<hr/>		
Chapter 5: Optimization of Lead Agonists		
<hr/>		
5.1	Polar groups to be investigated as replacements for carboxylates and synthetic routes to each compound	197
5.2	Synthesis of 6N-10CA hybrid and <i>in vitro</i> activity	200
5.3	Crystal structure of 6N-10CA hybrid	201
<hr/>		
Chapter 6: Designing New Chemical Tools to Study the Human NR5A Receptors LRH-1 and SF-1		
<hr/>		
6.1	Structure-guided design of NR5A probe	219
6.2	Validation of fluorescence polarization	221
6.3	FP assay detects lipid binding	223
6.4	Binding affinity correlates with in-cell activity and receptor stability for LRH-1, but not SF-1	224
6.5	FP measurements for synthetic ligands	226
S6.1	SF-1 binding to R ¹ compounds	242
S6.2	LRH-1 binding to R ¹ compounds	243
S6.3	Representative thermal shift curves	244
<hr/>		
Chapter 7: Dearomatization via Radical Hydroarylation		
<hr/>		
7.1	The principles of photoredox catalysis	251
7.2	Photocatalytic quenching pathways and common sacrificial oxidants and reductants	252
7.3	Structures of organic photoredox catalyst classes	253
7.4	Dearomative radical Hydroarylation strategy	257
7.5	Design of dearomative spirocyclization and support for each component	258
7.6	Modulation of lactam product ratios by reductant concentration	264
7.7	Computational structure of anion orbitals as a rationale for observed regioselectivity	265
7.8	Photocatalytic dearomatization provides an efficient route to anti-obesity candidate 36	267
S7.1	Stern-Volmer plots	274

Chapter 8: Photochemical Dearomatization of Benzenoids

8.1	Mechanistic blueprint for photochemical dearomatization	330
8.2	Luminescence quenching experiment suggests endergonic SET as operative mechanism	332
8.3	Varying concentration and pK_a 's of acids does not change quenching efficiency	333
8.4	Deuteration experiment suggests consecutive reduction-protonation sequence	334
8.5	Current photochemical arene dearomatization conditions	335

List of Schemes

Chapter 2: Phospholipid-Mimicking Chimeras as LRH-1 Agonists		
2.1	Synthesis and biological evaluation of DLPC/RJW100 hybrid 11 from 5e	38
2.2	Synthesis and evaluation of simplified phosphorylcholine hybrids 12	40
2.3	Synthesis and evaluation of simplified carboxylic acid hybrids 13	42

Chapter 6: Designing New Chemical Tools to Study the Human NR5A Receptors LRH-1 and SF-1		
6.1	Chemical synthesis of 6N-FAM (6)	220

Chapter 8: Photochemical Dearomatization of Benzenoids		
8.1	Preliminary results for arene dearomatization	329

List of Tables

<hr/>		
Chapter 2: Phospholipid-Mimicking Chimeras as LRH-1 Agonists		
<hr/>		
2.1	Summarized activity data for hybrid PL mimics	43
S2.1	Luciferase data for compounds 12	84
S2.2	Luciferase data for compounds 13	85
<hr/>		
Chapter 3: Mechanism of Activation and Therapeutic Effects of LRH-1 Agonist 10CA		
<hr/>		
S3.1	List of primers for qPCR	113
<hr/>		
Chapter 5: Optimization of Lead Agonists		
<hr/>		
S5.1	Summary of <i>in vitro</i> data for new compounds	199
<hr/>		
Chapter 6: Designing New Chemical Tools to Study the Human NR5A Receptors LRH-1 and SF-1		
<hr/>		
S6.1	Summary K _i table	241
<hr/>		
Chapter 7: Dearomatization via Radical Hydroarylation		
<hr/>		
7.1	Photocatalytic radical Hydroarylation of aromatics: scope of spirocyclic products	262
S7.1	Optimization of arene dearomatization via Hydroarylation reaction	272
S7.2	Fluorescence quenching data	275
S7.3	Preliminary results for electrochemical spirocyclization	276
<hr/>		
Chapter 8: Photochemical Dearomatization of Benzenoids		
<hr/>		
S8.1	Optimization of reduction reaction	336
S8.2	Fluorescence quenching data	337

List of Abbreviations

3DPA2FBN	2,4,6-Tris(diphenylamino)-3,5-difluorobenzonitrile
3DPAFIPN	2,4,6-Tris(diphenylamino)-5-fluoroisophthalonitrile
4CzIPN	1,2,3,5-Tetrakis(carbazol-9-yl)-4,6-dicyanobenzene
5CzBN	pentabenzyl 6-cyanobenzene-1,2,3,4,5-pentacarboxylate
6HP	Hexahydropentalene
AAV8	Adeno-associated virus serotype 8
AcOH	Acetic acid
AF-B	Activation function B
AF-H	Activation function helix
AFS	Activation function surface
AIBN	Azobisisobutyronitrile
APCI	Atmospheric pressure chemical ionization
Bn	Benzyl
Boc	<i>Tert</i> -butoxy carbonyl
CA	Carboxylic acid
Cbz	Carboxybenzyl
CDI	Carbonyldiimidazole
CHAPS	3-[(3-Cholamidopropyl)dimethylammonio]-1-propanesulfonate
CI	Confidence interval
CMV	Cytomegalovirus
CYP11A1	Cytochrome P450 Family 11 Subfamily A Member 1

CYP11B1	Cytochrome P450 Family 11 Subfamily B Member 1
DAX1	Dosage sensitive sex reversal adrenal hypoplasia congenita critical region on the X chromosome, gene 1 (also known as NR0B1)
DCIA	7-Diethylamino-3-[4-(iodoacetamido)phenyl]-4-methylcoumarin
DCM	Dichloromethane
DFT	Density functional theory
DIPEA	Diisopropylethylamine
DLPC	Dilauroylphosphatidylcholine
DLPE	Dilauroylphosphatidylethanolamine
DMA	Dimethylacetamide
DMAD	Dimethylacetylenedicarboxylate
DMF	Dimethylformamide
DMS	Dimethylsulfide
DMSO	Dimethylsulfoxide
DNA	Deoxyribonucleic acid
DPP	Deep-polar part of the LRH-1 pocket
dr	Diastereomeric ratio
DSF	Differential scanning fluorimetry
DSS	Dextran sodium sulfate
DTT	Dithiothreitol
EC₅₀	Half maximal effective concentration
EDCI	1-Ethyl-3-(3-dimethylaminopropyl)carbodiimide

EDTA	Ethylenediaminetetraacetic acid
EMSA	Electrophoretic mobility shift assay
EnT	Energy transfer
ESI-TOF	Electrospray ionization time-of-flight mass spectrometry
EtOAc	Ethyl acetate
FA	Formic acid
FAM	Fluoresceinamine
FDA	Food and drug administration
FP	Fluorescence polarization
FRET	Förster Resonance Energy Transfer
GCMS	Gas chromatography mass spectrometry
GI	Gastrointestinal tract
HBTU	(2-(1H-benzotriazol-1-yl)-1,1,3,3-tetramethyluronium hexafluorophosphate
HDH	Hydrodehalogenation
HDX-MS	Hydrogen deuterium exchange mass spectrometry
Hex	Hexanes
HMPA	Hexamethylphosphoramide
HOMO	Highest occupied molecular orbital
HPLC	High performance liquid chromatography
IBD	Inflammatory bowel disease
IC₅₀	Half maximal inhibitory concentration
IL-10	Interleukin 10

IL1B	Interleukin 1 beta
IPTG	Isopropyl β -d-1-thiogalactopyranoside
LBD	Ligand binding domain
LCMS	Liquid chromatography mass spectrometry
LCOR	Ligand dependent corepressor
LDA	Lithiumdiisopropylamide
LED	Light emitting diode array
LRH-1	Liver receptor homolog 1
LUMO	Lowest occupied molecular orbital
MARCoNI	Microarray assay for realtime coregulator-nuclear receptor interaction
MCD	Methionine-choline deficient
MDS	Molecular dynamics simulation
MeCN	Acetonitrile
MEMα	Mimimum essential media alpha
MeOH	Methanol
MOM	Methoxymethyl
mRNA	Messenger RNA
MsCl	Methanesulfonyl chloride
N-POX(Ph₂)₂	3,7-di([1,1'-biphenyl]-4-yl)-10-(naphthalen-1-yl)-10 <i>H</i> -phenoxazine
NBD	nitrobenzofurazan
NCOA1	Nuclear receptor coactivator 1

NCOA3	Nuclear receptor coactivator 3
NCOR1	Nuclear receptor corepressor 1
NMO	n-methyl morpholine oxide
NMR	Nuclear magnetic resonance
NR	Nuclear receptor
OD	Optical density
PBS	Phosphate buffered saline
PC	Phosphatidylcholine
PCC	Pyridinium chlorochromate
PCET	Proton-coupled electron transfer
PCR	Polymerase chain reaction
PDB	Protein data bank
PEG	Polyethyleneglycol
Ph	phenyl
PhC	Phosphorylcholine
PIP	Phosphatidylinositol
PL	phospholipid
PTFE	Polytetrafluoroethylene
PTLC	Preparative thin layer chromatography
qRT-PCR	Quantitative reverse transcription polymerase chain reaction (qPCR)
RE	Relative efficacy
RNA	Ribonucleic acid

RPM	Rotations per minute
rt	Room temperature
SAR	Structure-activity relationship
SCE	Standard calomel electrode
SEM	Standard error of the mean
SET	Single electron transfer
SF-1	Steroidogenic factor 1
SHP	Small heterodimer partner
SPR	Surface plasmon resonance
TBAF	Tetrabutylammonium fluoride
TBDMS-OTf	<i>Tert</i> -butyldimethylsilyl trifluoromethanesulfonate
TBDPS-Cl	<i>Tert</i> -butyldiphenylchloro silane
^tBuBrettPhos	2-(Di- <i>tert</i> -butylphosphino)-2',4',6'- triisopropyl-3,6-dimethoxy-1,1'-biphenyl
^tBuXPhos	2-Di- <i>tert</i> -butylphosphino-2',4',6'-triisopropylbiphenyl
TCEP	Tris(2-carboxyethyl)phosphine
TEA	Triethylamine
TEMPO	(2,2,6,6,-tetramethylpiperidin-1)oxyl
TEV	Tobacco etch virus
TFA	Trifluoroacetic acid
THF	tetrahydrofuran
Tif2	Transcriptional intermediary factor 2
TLC	Thin layer chromatography

TMS	trimethylsilyl
TNFα	Tumor necrosis factor alpha
TPAP	Tetrapropylammonium perrhuthenate
TREF-1	Transcriptional regulating factor 1
UPLC	Ultra performance liquid chromatography
V	volts
W	Watts
WT	Wild type

Part 1: Rational Design of LRH-1 Agonists

Using LRH-1 to locally combat inflammation

Nuclear receptors (NRs) are a class of mammalian proteins that typically sense hormones and are responsible for the expression of specific genes that can have drastic effects on human physiology. Because their mechanism of action includes binding to DNA and regulating the downstream transcription of adjacent genes, they are also commonly termed transcription factors.

The human NR superfamily is comprised of 48 ligand-regulated transcription factors that control diverse biological processes, including metabolism, inflammation, immune response, development, and steroidogenesis. Though the powerful control of gene expression that NRs demonstrate make them attractive pharmacological targets, only 17 NRs have been successfully targeted in the clinic.¹ Despite this seemingly small percentage, the therapeutics that *have* been developed by targeting NRs account for 13% of all FDA approved drugs.²

Of the remaining, untargeted NRs, many are known to respond to lipids and lipid metabolites, but their exact endogenous ligands are unknown.³ These NRs (without known native ligands) are termed “orphan” nuclear receptors and represent a very attractive—but extremely challenging—class of therapeutic targets. When endogenous ligands are unknown, the contacts important for binding and precise mode of activation is difficult to elucidate.

One of these orphan nuclear receptors is a lipid-sensing NR with exceptionally promising therapeutic potential: liver receptor homolog-1 (LRH-1; NR5A2). LRH-1 is highly expressed in

¹ Rask-Andersen, M.; Almén, M. S.; Schiöth, H. B. Trends in the Exploitation of Novel Drug Targets. *Nat. Rev. Drug Discov.* **2011**, *10* (8), 579–590

² Overington, J. P.; Overington, J. P.; Al-Lazikani, B.; Al-Lazikani, B.; Hopkins, A. L.; Hopkins, A. L. How Many Drug Targets Are There? *Nat. Rev. Drug Discov.* **2006**, *5* (12), 993–996

³ (a) Zhi, X.; Zhou, X. E.; Melcher, K.; Xu, H. E. Structures and Regulation of Non-X Orphan Nuclear Receptors: A Retinoid Hypothesis. *J. Steroid Biochem. Mol. Biol.* **2016**, *157*, 27–40 (b) Kelly, M. E.; Mohan, H. M.; Baird, A. W.; Ryan, E. J.; Winter, D. C. Orphan Nuclear Receptors in Colorectal Cancer. *Pathol. Oncol. Res.* **2018**, *24* (4), 815–819

the intestine, where there is strong evidence that the receptor is a therapeutic target for inflammatory bowel diseases (IBD), such as ulcerative colitis and Crohn's disease.⁴

IBD is estimated to currently affect over 1.6 million Americans, and the resulting financial burden on the United States public is approximately \$32 billion.⁵ While the exact cause of IBD is unknown, these diseases result from the immune system errantly targeting the gastrointestinal (GI) tract, which results in chronic inflammation and formation of ulcers. Current therapeutic strategies fall into two categories: targeting the signaling axis of tumor necrosis factor alpha (TNF α), a protein that causes inflammation, or alleviating inflammation through the use of anti-inflammatories. The current most commonly employed drugs for IBD contain (or are prodrugs of) aminosalicylate, a nonsteroidal anti-inflammatory. Though the precise mechanism of action is unknown, aminosalicylate-containing drugs are generally well-tolerated. However, they often fail to sustain disease remission.⁶ Flare-ups can be effectively treated with corticosteroids like prednisone and prednisolone, but the debilitating long-term use of steroidal anti-inflammatories (e.g. osteoporosis that leads to bone fragmentation, easy bruising, increased risk of infections, and elevated blood-sugar levels) preclude corticosteroids as a generalized strategy to treat IBD.⁶ More recently, anti-TNF α monoclonal antibodies (often broadly termed 'biologics') have been used to

⁴ (a) Fayard, E.; Auwerx, J.; Schoonjans, K. LRH-1: An Orphan Nuclear Receptor Involved in Development, Metabolism and Steroidogenesis. *Trends Cell Biol.* **2004**, *14* (5), 250–260 (b) Venteclef, N.; Jakobsson, T.; Steffensen, K. R.; Treuter, E. Metabolic Nuclear Receptor Signaling and the Inflammatory Acute Phase Response. *Trends Endocrinol. Metab.* **2011**, *22* (8), 333–343 (c) Coste, A.; Dubuquoy, L.; Barnouin, R.; Annicotte, J. S.; Magnier, B.; Notti, M.; Corazza, N.; Antal, M. C.; Metzger, D.; Desreumaux, P.; Brunner, T.; Auwerx, J.; Schoonjans, K. LRH-1-Mediated Glucocorticoid Synthesis in Enterocytes Protects against Inflammatory Bowel Disease. *Proc. Natl. Acad. Sci. U. S. A.* **2007**, *104* (32), 13098–13103

⁵ (a) Gibson, T. B.; Ng, E.; Ozminowski, R. J.; Wang, S.; Burton, W. N.; Goetzel, R. Z.; Maclean, R. The Direct and Indirect Cost Burden of Crohn's Disease and Ulcerative Colitis. *J. Occup. Environ. Med.* **2008**, *50* (11), 1261–1272 (b) Kappelman, M. D.; Rifas-Shiman, S. L.; Porter, C. Q.; Ollendorf, D. A.; Sandler, R. S.; Galanko, J. A.; Finkelstein, J. A. Direct Health Care Costs of Crohn's Disease and Ulcerative Colitis in US Children and Adults. *Gastroenterology* **2008**, *135* (6), 1907–1913 (c) Longobardi, T.; Jacobs, P.; Bernstein, C. N. Work Losses Related to Inflammatory Bowel Disease in the United States: Results from the National Health Interview Survey. *Am. J. Gastroenterol.* **2003**, *98* (5), 1064–1072

⁶ Kozuch, P. L.; Hanauer, S. B. Treatment of Inflammatory Bowel Disease: A Review of Medical Therapy. *World J. Gastroenterol.* **2008**, *14* (3), 354–377

globally suppress TNF α .^{6,7} TNF α is an inflammatory cytokine (signaling protein) which, in the case of IBD, is errantly secreted by the immune system in the colon and destroys colon tissue. Global suppression of TNF α (and therefore the body's natural immune response) to combat IBD, however, leaves the body vulnerable to opportunistic mycobacterial, fungal, viral, and parasitic pathogens.⁸ There is a clear need for new therapeutics that effectively target inflammation in the gut without the detrimental consequences of global immunosuppression.

The NR LRH-1 is located in intestinal crypts, where intestinal stem cells reside.⁹ Here, LRH-1 contributes to epithelial renewal by decreasing TNF α expression and critically regulating the synthesis of immunoregulatory glucocorticoids.¹⁰ In fact, deletion of LRH-1 in mouse intestinal epithelium predisposes them to develop inflammatory diseases specifically due to the absence of local glucocorticoid production.^{10,11} We hypothesized that the reverse of this process—increasing the activity of LRH-1 in the intestine—would result in a synergistic localized increase in glucocorticoid production coupled to decreased TNF α expression, effectively developing a viable strategy to combat inflammation in the intestine without global immunosuppression.

⁷ (a) Sands, B. E.; Kaplan, G. G. The Role of TNF α in Ulcerative Colitis. *J. Clin. Pharmacol.* **2007**, *47* (8), 930–941
(b) Monaco, C.; Nanchahal, J.; Taylor, P.; Feldmann, M. Anti-TNF Therapy: Past, Present and Future. *Int. Immunol.* **2015**, *27* (1), 55–62

⁸ Ali, T.; Bronze; Kaitha; Mahmood; Ftaiis; Stone. Clinical Use of Anti-TNF Therapy and Increased Risk of Infections. *Drug. Healthc. Patient Saf.* **2013**, *79*

⁹ Botrugno, O. A.; Fayard, E.; Annicotte, J. S.; Haby, C.; Brennan, T.; Wendling, O.; Tanaka, T.; Kodama, T.; Thomas, W.; Auwerx, J.; Schoonjans, K. Synergy between LRH-1 and β -Catenin Induces G1 Cyclin-Mediated Cell Proliferation. *Mol. Cell* **2004**, *15* (4), 499–509

¹⁰ Mueller, M.; Cima, I.; Noti, M.; Fuhrer, A.; Jakob, S.; Dubuquoy, L.; Schoonjans, K.; Brunner, T. The Nuclear Receptor LRH-1 Critically Regulates Extra-Adrenal Glucocorticoid Synthesis in the Intestine. *J. Exp. Med.* **2006**, *203* (9), 2057–2062

¹¹ Coste, A.; Dubuquoy, L.; Barnouin, R.; Annicotte, J. S.; Magnier, B.; Notti, M.; Corazza, N.; Antal, M. C.; Metzger, D.; Desreumaux, P.; Brunner, T.; Auwerx, J.; Schoonjans, K. LRH-1-Mediated Glucocorticoid Synthesis in Enterocytes Protects against Inflammatory Bowel Disease. *Proc. Natl. Acad. Sci. U. S. A.* **2007**, *104* (32), 13098–13103

Chapter 1: Identifying a targeting strategy for LRH-1

Adapted and Reprinted in part with permission from J. Biol. Chem. 2016, *291*(49), 25281–25291

Copyright 2016 The American Society for Biochemistry and Molecular Biology, Inc.

<https://www.jbc.org/content/291/49/25281>

1.1 Two Modes of LRH-1 Activation

The link between dietary and microbial-derived lipids and the immune system has been suggested for a long time, but only recently we have begun to elucidate the precise role they play. Phosphatidylcholines (PCs), specifically, are known to bind to NRs and therefore serve as powerful signaling molecules.¹² For transcription factors in general, upon binding of a ligand, NRs enter the nucleus of a cell and associate with DNA at a specific recognition site as dictated by their DNA binding domain. The ligand binding event to the NR triggers an allosteric conformational change to a distal portion of the receptor called the “activation function surface” (AFS). This conformational change allows coregulators to bind to the AFS, and, depending on the identity of the ligand present in the ligand binding pocket (LBD) the AFS can bind to a profile of coregulators specific to the bound ligand. This allows antagonists to recruit corepressors to the AFS, and agonists to recruit coactivators (Fig. 1.1).

LRH-1 is known to bind the dietary PC dilauroylphosphatidylcholine (DLPC; 12:0/12:0), which in turn activates the receptor through an allosteric conformational change which allows coactivators to bind to its AFS.¹³ Because of this, DLPC has been used as an effective preliminary

¹² (a) Musille, P. M.; Pathak, M.; Lauer, J. L.; Hudson, W. H.; Griffin, P. R.; Ortlund, E. A. Antidiabetic Phospholipid – Nuclear Receptor Complex Reveals the Mechanism for Phospholipid Driven Gene Regulation. *Nat Struct Mol Biol.* **2012**, *19* (5), 532 (b) Miranda, D. A.; Krause, W. C.; Cazenave-Gassiot, A.; Suzawa, M.; Escusa, H.; Foo, J. C.; Shihadih, D. S.; Stahl, A.; Fitch, M.; Nyangau, E.; Hellerstein, M.; Wenk, M. R.; Silver, D. L.; Ingraham, H. A. LRH-1 Regulates Hepatic Lipid Homeostasis and Maintains Arachidonoyl Phospholipid Pools Critical for Phospholipid Diversity. *JCI Insight* **2018**, *3* (5), 1–15 (c) Musille, P. M.; Kohn, J. A.; Ortlund, E. A. Phospholipid – Driven Gene Regulation. *FEBS Lett.* **2013**, *587*, 1238–1246 (d) Blind, R. D.; Sablin, E. P.; Kuchenbecker, K. M.; Chiu, H. J.; Deacon, A. M.; Das, D.; Fletterick, R. J.; Ingraham, H. A. The Signaling Phospholipid PIP3 Creates a New Interaction Surface on the Nuclear Receptor SF-1. *Proc. Natl. Acad. Sci. U. S. A.* **2014**, *111* (42), 15054–15059 (e) Ma, K.; Saha, P. K.; Chan, L.; Moore, D. D. Farnesoid X Receptor Is Essential for Normal Glucose Homeostasis. *J Clin Invest* **2006**, *116* (4), 1102–1109 (f) Walker, A. K.; Jacobs, R. L.; Watts, J. L.; Rottiers, V.; Jiang, K.; Finnegan, D. M.; Shioda, T.; Hansen, M.; Yang, F.; Niebergall, L. J.; Vance, D. E.; Tzoneva, M.; Hart, A. C.; Näär, A. M. A Conserved SREBP-1/Phosphatidylcholine Feedback Circuit Regulates Lipogenesis in Metazoans. *Cell* **2011**, *147* (4), 840–852 (g) Crowder, M. K.; Seacrist, C. D.; Blind, R. D. Phospholipid Regulation of the Nuclear Receptor Superfamily. *Adv. Biol. Regul.* **2017**, *63*, 6–14

¹³ (a) Musille, P. M.; Pathak, M.; Lauer, J. L.; Hudson, W. H.; Griffin, P. R.; Ortlund, E. A. Antidiabetic Phospholipid – Nuclear Receptor Complex Reveals the Mechanism for Phospholipid Driven Gene Regulation. *Nat Struct Mol Biol.* **2012**, *19* (5), 532 (b) Musille, P. M.; Kossmann, B. R.; Kohn, J. A.; Ivanov, I.; Ortlund, E. A. Unexpected Allosteric

probe for the physiological consequences of LRH-1 activation. Unfortunately, DLPC has low specificity for LRH-1 and readily binds to a number of receptors with hydrophobic binding pockets.^{12g} Additionally, it displays relatively low affinity to LRH-1, and only mild levels of activation.^{13a} Furthermore, PCs are prone to biological remodeling and have poor pharmacokinetic properties, limiting their use as therapeutic candidates.¹⁴

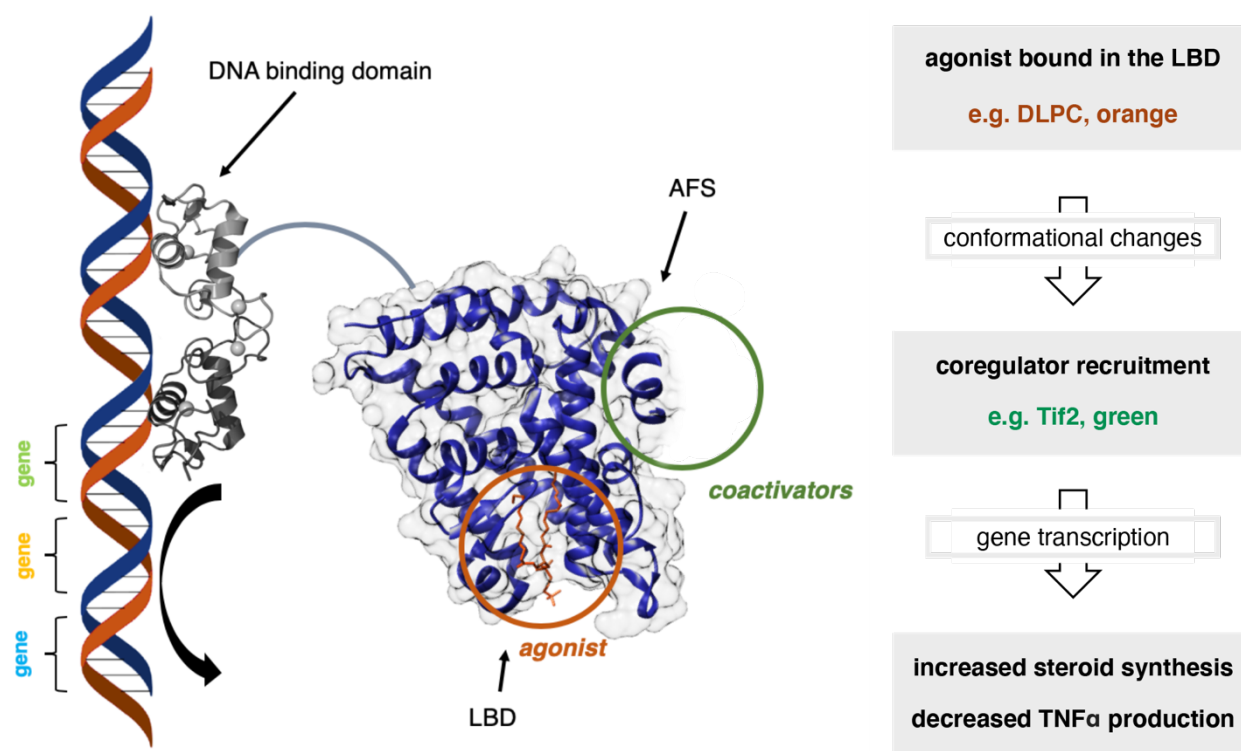


Figure 1.1 LRH-1 Mechanism of Activation

Small molecules can act as modulators for NRs, however LRH-1 has been historically challenging to target with small molecules, as its endogenous ligand is not known. The large, extremely lipophilic binding pocket of LRH-1 has made ligand identification and design especially difficult. To combat the difficult design aspects of designing ligands for this receptor, a number of

Network Contributes to LRH-1 Co-Regulator Selectivity. *J. Biol. Chem.* **2016**, *291* (3), 1411–1426

¹⁴ (a) MacDonald, J. I.; Sprecher, H. Phospholipid Fatty Acid Remodeling in Mammalian Cells. *Biochim. Biophys. Acta* **1991**, *1084* (2), 105–121 (b) Exton, J. H. Phosphatidylcholine Breakdown and Signal Transduction. *Biochim. Biophys. Acta* **1994**, *1212*, 26–42

groups have launched widespread, high-throughput screens in an attempt to find a class of molecules that could act as groundwork to build agonists for this important NR. In 2006, a group at Southampton University in collaboration with GlaxoSmithKline identified the first small-molecule activator of LRH-1: termed GSK8470 (Fig. 1.2).¹⁵ Soon after, a crystal structure of GSK8470 bound in the LBD of LRH-1 was elucidated (Fig. 1.2).¹⁶

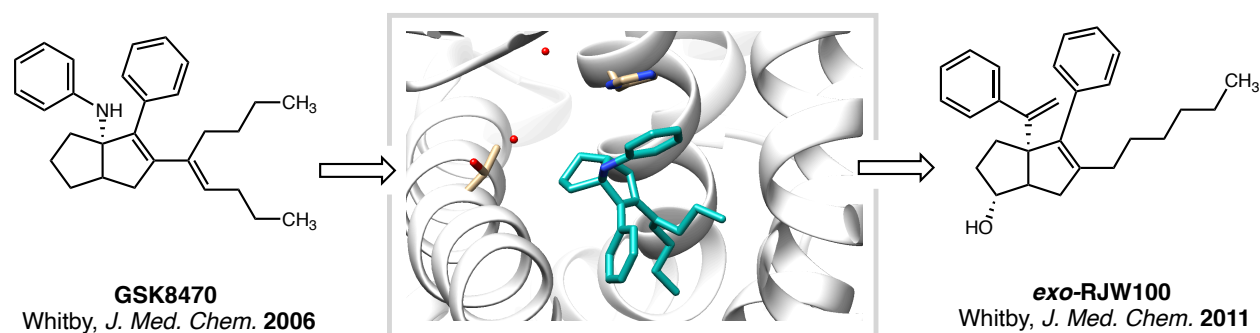


Figure 1.2: GSK8470 crystal structure. The determination of the crystal structure of GSK8470 bound in the LBD of LRH-1 launched a structure-activity relationship study, which resulted in RJW100. Shown: T352 and H390, two residues hypothesized to be critical to LRH-1 activation depending on ligand class.

Based on the crystal structure of GSK8470, an extensive structure-activity relationship (SAR) was launched to improve on GSK8470.¹⁶ Namely, the authors hoped to improve acid stability, as GSK8470 is so sensitive to acid that that storage in glassware that has not been base washed will degrade the compound. Their efforts were ultimately successful and produced RJW100 (Fig. 1.2) in 2011. Unfortunately, the attempt to establish a clear structure-activity relationship between modifications made to the bicyclic scaffold and observed activity could not be achieved, and the authors were unable to further improve upon RJW100 with the information at hand. For years,

¹⁵ Whitby, R.J.; Dixon, S.; Maloney, P.R.; Delerive, P.; Goodwin, B. J.; Parks, D.J.; Willson, T.M. Identification of Small Molecule Agonists of the Orphan Nuclear Receptors Liver Receptor. *J. Med. Chem.* **2006**, *49*, 6652–6655

¹⁶ Whitby, R. J.; Stec, J.; Blind, R. D.; Dixon, S.; Leesnitzer, L. M.; Orband-Miller, L. a.; Williams, S. P.; Willson, T. M.; Xu, R.; Zuercher, W. J.; Cai, F.; Ingraham, H. a. Small Molecule Agonists of the Orphan Nuclear Receptors Steroidogenic Factor-1 (SF-1, NR5A1) and Liver Receptor Homologue-1 (LRH-1, NR5A2). *J. Med. Chem.* **2011**, *54* (7), 2266–2281

RJW100 was the leading LRH-1 agonist, but its low potency and the lack of information on how exactly it activated the receptor limited the studies that were able to hinge on this small molecule.

1.2 Crystal Structures of RJW100 bound to LRH-1

Our efforts to develop an effective synthetic ligand started with an investigation of *how* RJW100 activates LRH-1. We made a successful attempt to co-crystallize *exo* RJW100 (the slightly more active diastereomer) bound to LRH-1, and determined the X-ray crystal structure of LRH-1 LBD bound to the *exo* diastereomer of RJW100 to 1.85 Å (Fig. 1.3).¹⁷

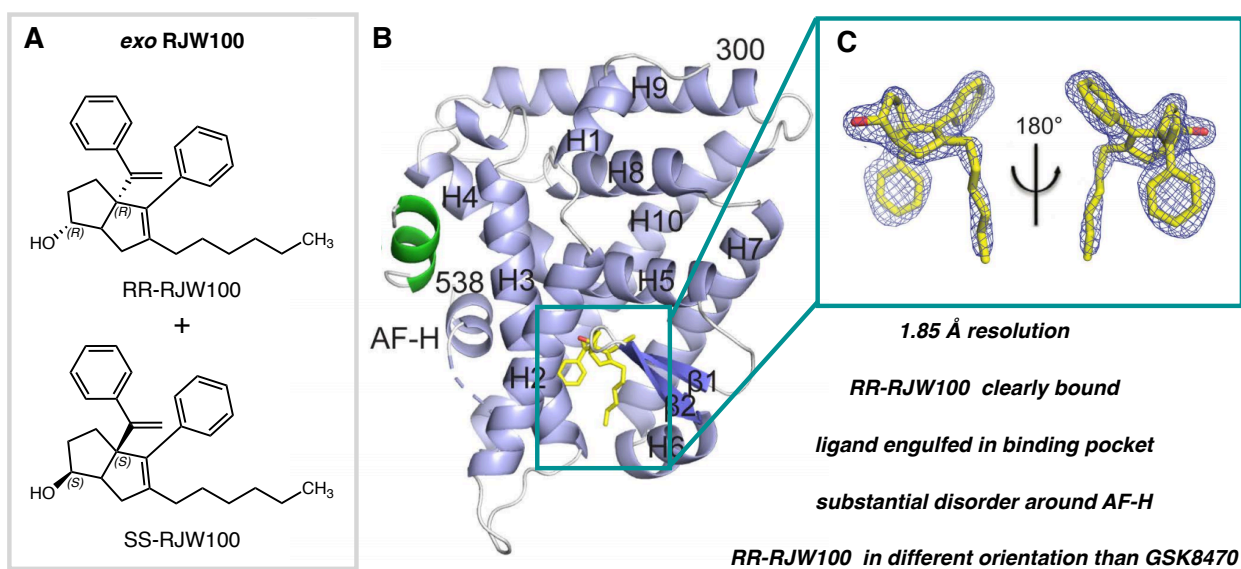


Figure 1.3. *exo* RJW100 Crystal Structure. (A) enantiomers of *exo*-RJW100. (B) overall structure, with α -helices shown in light blue and β -sheets in slate. The Tif2 peptide (green) is bound at the AFS. The ligand (yellow) is bound at a single site in the binding pocket. Dashed line, region of disorder in the protein backbone that could not be modeled. Omit map ($F_o - F_c$, contoured at 2.5σ) showing that a single enantiomer of RJW100 is bound in the structure.

¹⁷ Mays, S. G.; Okafor, C. D.; Whitby, R. J.; Goswami, D.; Stec, J.; Flynn, A. R.; Dugan, M. C.; Jui, N. T.; Griffin, P. R.; Ortlund, E. A. Crystal Structures of the Nuclear Receptor, Liver Receptor Homolog 1, Bound to Synthetic Agonists. *J. Biol. Chem.* **2016**, *291* (49), 25281–25291

Although the RJW100 used for the crystallization was a racemic mixture of the two *exo* stereoisomers, the electron density in the structure unambiguously indicates that a single enantiomer is bound, where the 1- and 3a- positions are both R (RR-RJW100). The ligand is bound at a single site deep in the hydrophobic binding pocket and is fully engulfed within it, effectively contracting the LBD nearly 40% versus DLPC (by volume).

This binding mode is markedly different than DLPC, where the alkyl chain tails sit within the hydrophobic binding pocket and the phosphorylcholine headgroup extends, stabilizing the mouth of the LBD in an open conformation to make key hydrophilic contacts to K520, Y516 and the backbone of G421, and protruding into the solvent (Fig. 1.1).^{12a} The overall crystal structure of RJW100 depicts the helices that comprise the AFS (Helices H3, H4, and the activation function helix 'AF-H') in their active conformation and the Tif2 coactivator peptide bound at this AFS, as expected with agonists (Fig. 1.3, green). However, there are a few indications that the active state may not be fully stabilized (relative to DLPC). There is substantial disorder in the loop connecting Helix 10 to the AF-H, and three residues within this loop cannot be modeled (dotted line in Fig. 1.3). This is unlike the crystal structures of LRH-1 bound to DLPC or GSK8470. The disorder in the vicinity of the AFS in our structure suggests this region is mobile when RJW100 is bound. To test this explicitly, we utilized solution-based hydrogen-deuterium exchange mass spectrometry (HDX-MS) to compare dynamics of purified LRH-1 LBD bound to enantiomerically pure RR-RJW100 or to DLPC. As shown in Figure 1.4, RR-RJW100 indeed destabilizes the bottom of H10 and the pre-AF-H loop relative to DLPC, although the AF-H itself is highly stabilized. Interestingly, this localized destabilization occurs even though RJW100 increases overall thermostability of LRH-1 compared to compared to DLPC (Fig. 1.4). This finding may indicate

room for improvement in agonist design: compounds that provide a stable surface for coactivator recruitment would likely be more potent activators.

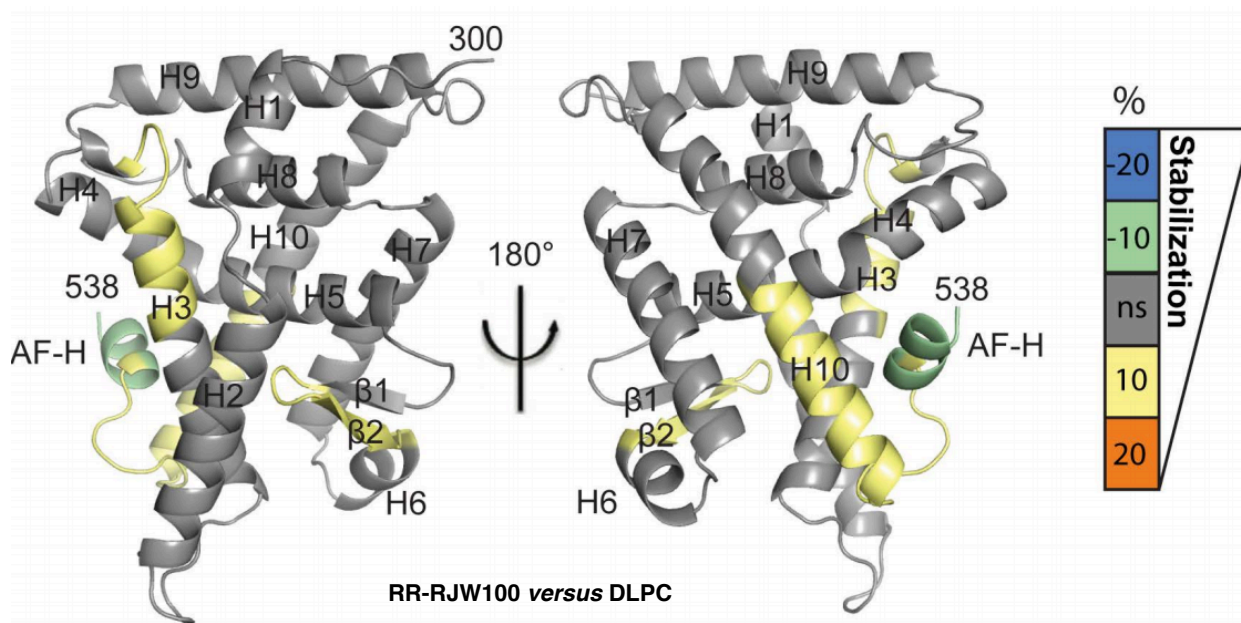


Figure 1.4. *exo*-RJW100 vs. DLPC HDX-MS. HDX was used to probe differential effects on protein dynamics by the two ligands. The scale refers to the difference in percent deuterium incorporation for RR-RJW100-bound LRH-1 minus DLPC-bound LRH-1. The scale reflects the difference in average percent deuterium incorporation for RR-RJW100-bound versus DLPC-bound LRH-1 LBD. For example, negative numbers reflect slower deuterium incorporation (less motion) for RR-RJW100 versus DLPC. Results are mapped onto PDB 4DOS.

Perhaps the most striking observation from our structure comes from comparison with GSK8470-bound LRH-1 (PDB 3PLZ).¹⁶ Overall protein conformation is highly similar, but overall there is a substantial difference in the positioning of these agonists within the binding pocket. Although GSK8470 (Fig. 1.5A) and RR-RJW100 (Fig. 1.5B) bind in the same vicinity, they are rotated nearly 180° from each other, causing the tails to be pointed in opposite directions (Fig. 1.5C). Such a propensity to rotate within the pocket may have contributed to the difficulties in

predicting modifications that would improve agonist activity by modification of the GSK8470 scaffold.

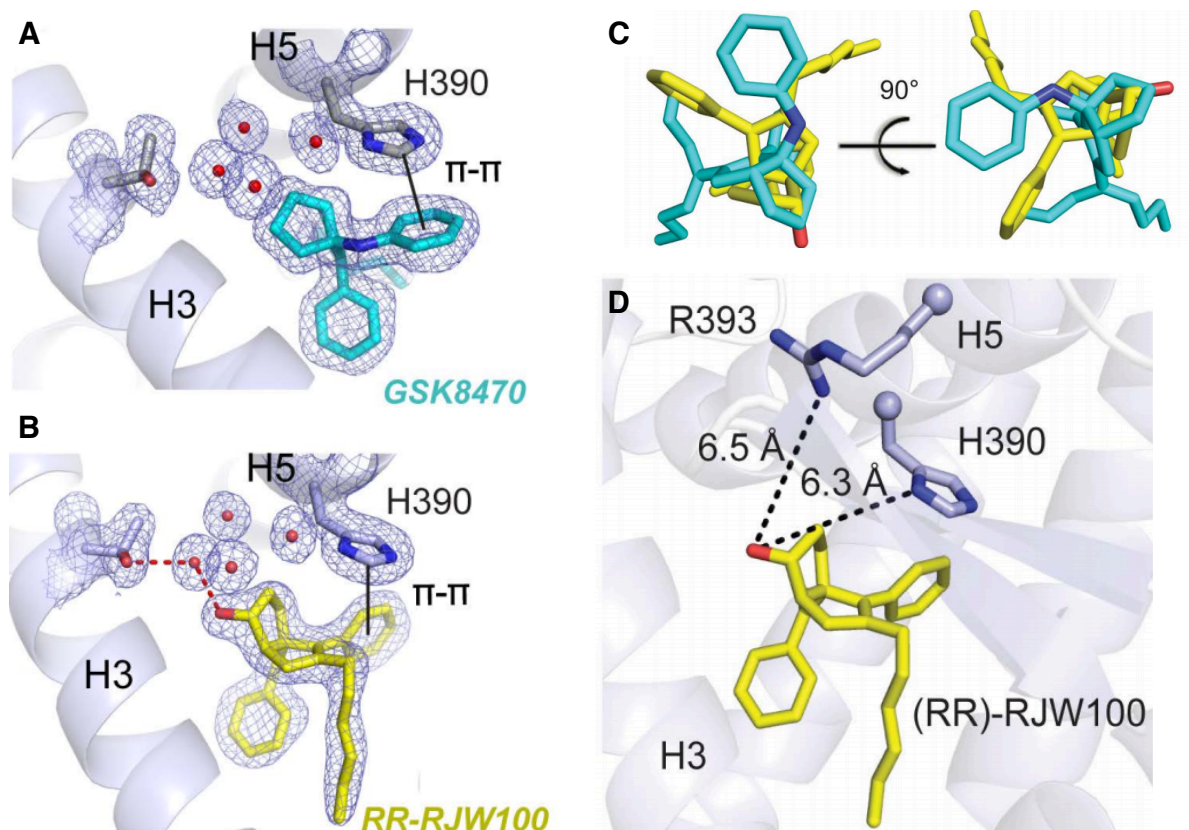


Figure 1.5. X-Ray structures of *exo*-RJW100 vs. GSK8470. (A) GSK8470 bound in the LBD of LRH-1, makes a face to face π -stacking contact with H390. (B) RR-RJW100 bound in the LBD of LRH-1, makes both an edge-to-face π -stacking contact with H390 and a water-mediated contact to T352. (C) superposition of RR-RJW100 (yellow) and GSK8470 (teal) coordinates. (D) Other possible water-mediated interactions that could affect ligand-receptor stabilization or

Notably, the conformation of RR-RJW100 in the pocket shows the hydroxyl group participating in an indirect polar contact with residues T352 via a water molecule (Fig. 1.5B) Although this T352 interaction is indirect, we observed that the water molecule involved is part of a network of waters found in every LRH-1 crystal structure in the same location (e.g. PDBs 4DOS,

1YUC, 3PLZ and 4DOR),^{12a,16,18} and may play a role in receptor function or stability through contact to nearby polar residues (Fig. 1.5A,B,D).

To test the hypothesis that this water molecule was influencing ligand positioning, we analyzed the stability of the bond through molecular dynamics simulations (MDS). Throughout each 200 ns simulation, the water molecule network remained in the same position. Residue T352 maintained a hydrogen bond with the water molecule for 100% of each simulation, regardless of the bound ligand. Additionally, RR-RJW100 maintained its hydrogen bonding with a water molecule for 53.7% of the simulation. Also seen in the crystal structure of LRH-1 bound to RR-RJW100 is a potential interaction with a phenyl ring with H390 (Fig. 1.5B) Over the course of a 200ns MDS, it was determined that the indicated phenyl ring in RR-RJW100 was edge-to-face π - π stacking with H390 59.6% of the MDS time.¹⁷

The importance of the T352 and H390 interactions for binding and activation of LRH-1 by the agonists was investigated using mutagenesis. Binding and stabilization of LRH-1 were detected using differential scanning fluorimetry (DSF), and activation of LRH-1 was detected using a luciferase reporter assay.

We first introduced a T352V mutant, which was designed to remove the water-mediated hydrogen bond with bound ligands. As seen in Figure 1.6 (left), this had little effect on the overall thermostability of DLPC-bound LRH-1, but completely abolished the stabilizing effect of RR-RJW100. To further probe this effect, we used an RJW100 analog lacking the hydroxyl group (named 18a by Whitby, Fig. 1.6). This analogue did not induce the positive T_m shift in wild-type (WT) LRH-1, lending further evidence to the importance of the water-mediated contact by the

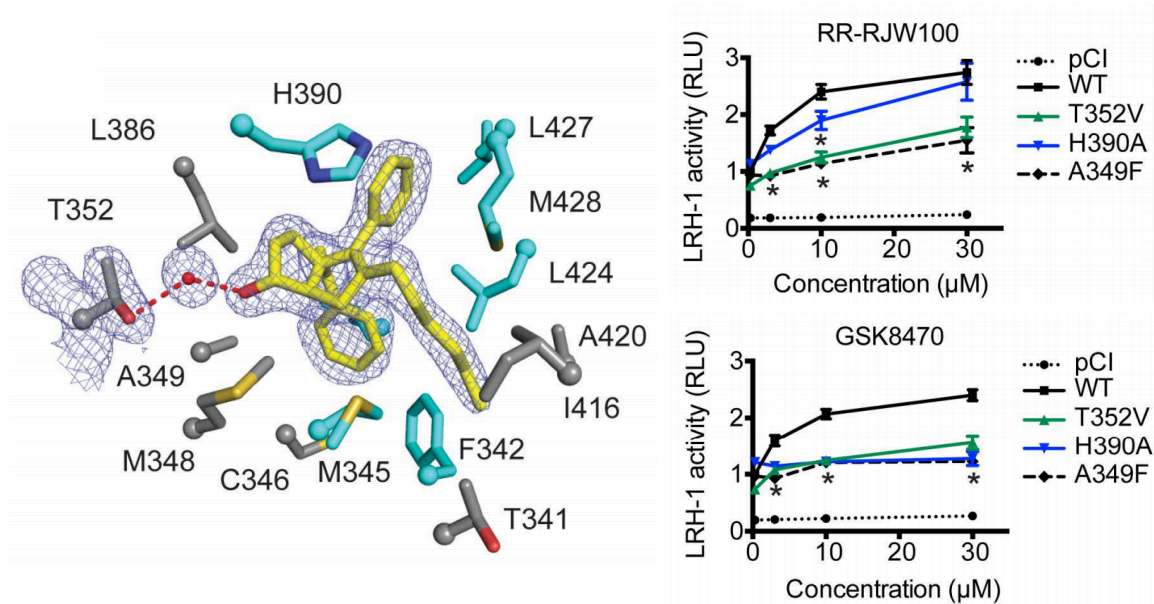
¹⁸ Ortlund, E. A.; Lee, Y.; Solomon, I. H.; Hager, J. M.; Safi, R.; Choi, Y.; Guan, Z.; Tripathy, A.; Raetz, C. R. H.; McDonnell, D. P.; Moore, D. D.; Redinbo, M. R. Modulation of Human Nuclear Receptor LRH-1 Activity by Phospholipids and SHP. *Nat. Struct. Mol. Biol.* **2005**, *12* (4), 357–363

RJW100 ligands. The melting profile of LRH-1 was not affected by GSK8470 (which does not contact T352) in WT or T352V protein, supporting the notion that the hydroxyl group is important for LRH-1 stabilization by small molecule agonists (Fig. 1.6).



Figure 1.6. LRH-1 LBD mutations and their effect on receptor melting. Left: Introduction of the T352V mutation to LRH-1 ablates the stabilizing effects of RR-RJW00 and endo-RJW100. Purified LRH-1 LBD, initially bound to DLPC for homogeneity, was incubated with either DMSO (control) or synthetic agonist dissolved in DMSO. Right: The structure of 18a, a Whitby compound lacking the hydroxyl group of RJW100, does not stabilize wild-type LRH-1 in DSF assays.

These results were also echoed in luciferase reporter assays summarized in Figure 1.7: compound 18a (lacking the hydroxyl group and therefore unable to make the water-mediated T352 interaction)¹⁶ was an extremely poor LRH-1 activator. RR-RJW100 and GSK8470 were equally effective toward WT LRH-1: both increased activity by approximately 2.5-fold compared to DMSO at their highest doses, and both had EC₅₀s of around 4 μM in this initial assay. A T352V mutation greatly reduced the ability of RR-RJW100 to activate LRH-1 compared to WT protein, while not affecting baseline activity. Coupled with MDS data, we have hypothesized that the water network stabilized by T352 plays an important role in ligand mediated activation of LRH-1.



The role of H390 for activation for either ligand as evidenced by a H390A mutation is well-defined. GSK8470 was completely unable to activate H390A-LRH-1. In the H390A-LRH-1 mutant, RR-RJW100 mediated activation was not disrupted. This differential reliance on H390 for activation is consistent with MDS, where GSK8470 has a more stable and consistent interaction with H390 than RR-RJW100 over a 200 ns simulation. This also provides evidence that RR-RJW100 must utilize a different mechanism of action than GSK8470 for LRH-1 activation—and we conclude, based on this data, it is the water-mediated T352 interaction.

To add to the growing body of evidence that the T352 interaction is critical for activation and ligand orientation, we investigated *endo* RJW100 (Fig. 1.8A). Using racemic *endo* RJW100, we solved the crystal structure of *endo* RJW100 bound to the LBD of LRH-1 at 1.93 Å (Fig. 1.8B). This crystal structure (like *exo* RJW100) also unambiguously shows one enantiomer bound (SR-RJW100, Fig. 1.8C).

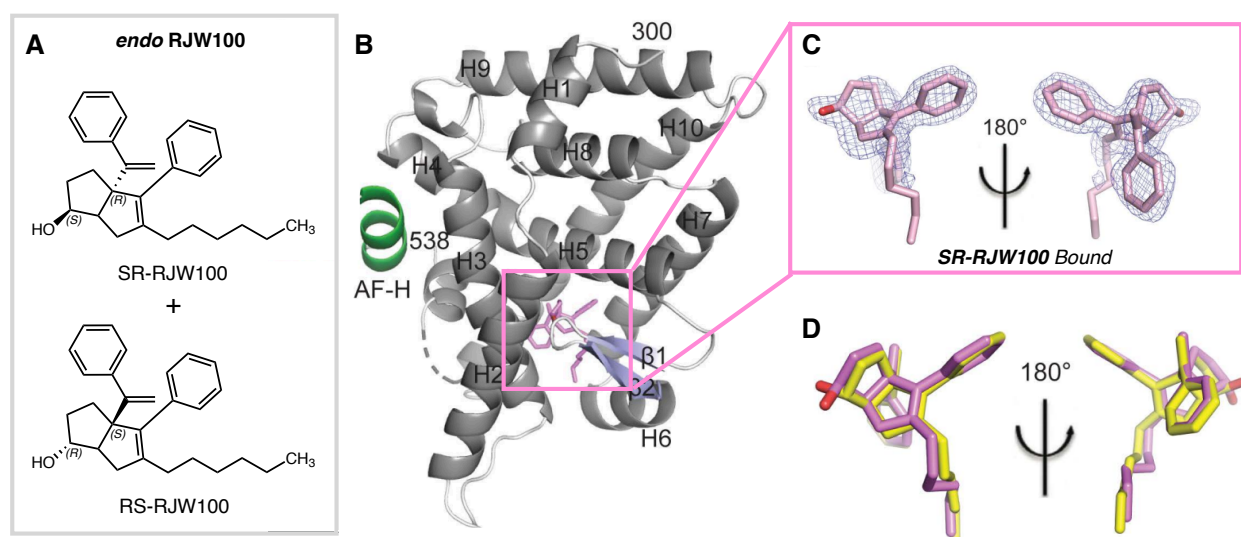


Figure 1.8. *endo*-RJW100 crystal structure. (A) enantiomers of *endo*-RJW100. (B) Overall structure. The Tif2 peptide (green) is bound at the AFS. The ligand (pink) is bound at a single site in the binding pocket. Dashed line, region of disorder in the protein backbone that could not be modeled. (C) Omit map ($F_o - F_c$, contoured at 2.5σ) showing that a single enantiomer of RJW100 is bound in the structure. (D) Superposition of SR-RJW100 (pink) with RR-RJW100 (yellow) showing a very similar position in the binding pocket.

The overall protein conformation is highly similar to that of the RR-RJW100 structure, and there is also disorder at the same portion of the protein backbone within the pre-AFH loop (dotted line, Fig. 1.8B). Superposition of the ligand coordinates from the RR-RJW100 and SR-RJW100 structures reveals nearly identical positioning, with the exception of the hydroxyl group because

of the opposite stereochemistry at this position (seen in Fig. 1.8D). The atomic motion for SR-RJW100 is higher than for RR-RJW100, suggested that the ligand has a reduced ability to engage in stabilizing intermolecular interactions in the pocket (as evidenced by ligand B-factors, and a higher EC₅₀ value, see supporting information), which may stem from a disruption in the water-mediated T352 interaction based on hydroxyl stereochemistry. The T352V mutation also ameliorates the ability of SR-RJW100 to activate the receptor (Fig. 1.6).

1.3 Identifying a Synthetic Ligand Design Strategy for LRH-1

In a previous study, *exo*-RJW100 was the most effective in a large series of GSK8470 derivatives but still only modestly increased LRH-1 activation.¹⁶ We find these two agonists are statistically indistinguishable in luciferase reporter assays measuring LRH-1 activity. Given the similarities in structures and efficacies for these ligands, we expected them to utilize similar mechanisms of action; however, this is not the case. Our crystal structure reveals a dramatically different binding mode for RR-RJW100 compared to GSK8470. While this was surprising, it is not unreasonable, considering that LRH-1 has a very large hydrophobic binding pocket and that these agonists are also quite hydrophobic, filling only 37% of the available space (excluding waters). It is possible that many of the GSK8470 analogs investigated in the previous SAR study adopt a variety of conformations. Importantly, however, the repositioning of RR-RJW100 in our structure appears to be driven by particular interactions, since SR-RJW100 assumes a very similar pose. A major factor driving the repositioning of the RJW100 enantiomers (versus GSK8470) was the through-water hydrogen bonding interaction made by the hydroxyl group with T352. Although this contact is indirect, it is a major driving force for activation of LRH-1 as evidenced by a T352V mutation in luciferase reporter assays.

Based on this new information, we hypothesized two major areas of expansion on the RJW100 scaffold which are the basis of Part 1 of this dissertation.

- 1) (Chapter 2, 3, 5, 6): The water mediated T352 contact will position ligands in a consistent orientation, allowing elaboration of the RJW100 scaffold to incorporate polar moieties that contact canonical phospholipid residues at the mouth of the pocket.
- 2) (Chapter 4, 5): Replacing the RJW100 hydroxyl group with a larger polar moiety may allow direct contact with T352, leading to a stronger interaction. Furthermore, consistent positioning of the core structure will allow for a proper SAR around the RJW100 core to be conducted.

1.4 Supporting Information

Materials and reagents

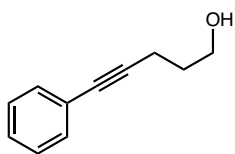
All reactions were carried out in oven-dried glassware, equipped with a stir bar and under a nitrogen atmosphere with dry solvents under anhydrous conditions, unless otherwise noted. Solvents used in anhydrous reactions were purified by passing over activated alumina and storing under argon. Yields refer to chromatographically and spectroscopically (^1H NMR) homogenous materials, unless otherwise stated. Reagents were purchased at the highest commercial quality and used without further purification, unless otherwise stated. n-Butyllithium (n-BuLi) was used as a 1.6 M or a 2.5 M solution in hexanes (Aldrich), was stored at 4°C and titrated prior to use. Organic solutions were concentrated under reduced pressure on a rotary evaporator using a water bath. Chromatographic purification of products was accomplished using forced-flow chromatography on 230-400 mesh silica gel. Preparative thin-layer chromatography (PTLC) separations were carried out on 1000 μm SiliCycle silica gel F-254 plates. Thin-layer chromatography (TLC) was

performed on 250 μ m SiliCycle silica gel F-254 plates. Visualization of the developed chromatogram was performed by fluorescence quenching or by staining using KMnO₄, p-anisaldehyde, or ninhydrin stains. ¹H and ¹³C NMR spectra were obtained from the Emory University NMR facility and recorded on a Bruker Avance III HD 600 equipped with cryo-probe (600 MHz), INOVA 600 (600 MHz), INOVA 500 (500 MHz), INOVA 400 (400 MHz), VNMR 400 (400 MHz), or Mercury 300 (300 MHz), and are internally referenced to residual protio solvent signals. Data for ¹H NMR are reported as follows: chemical shift (ppm), multiplicity (s = singlet, d = doublet, t = triplet, q = quartet, m = multiplet, dd = doublet of doublets, dt = doublet of triplets, ddd = doublet of doublet of doublets, dtd = doublet of triplet of doublets, b = broad, etc.), coupling constant (Hz), integration, and assignment, when applicable. Data for decoupled ¹³C NMR are reported in terms of chemical shift and multiplicity when applicable. Gas Chromatography Mass Spectrometry (GC-MS) was performed on an Agilent 5977A mass spectrometer with an Agilent 7890A gas chromatography inlet. Liquid Chromatography Mass Spectrometry (LC-MS) was performed on an Agilent 6120 mass spectrometer with an Agilent 1220 Infinity liquid chromatography inlet.

RR-RJW100 was separated from SS-RJW100 by chiral preparative chromatography (Diacel OD-H column, (31)). Endo-RJW100 is a diastereoisomer of RJW100, previously referred to as “24-endo” (23). In this paper, we use “SR-RJW100” to refer to the enantiomers of endo-RJW100 (Fig. 1.3A, 1.8A). pCI empty vector was purchased from Promega. The SHP-luc and Renilla reporters, as well as pCI LRH-1, have been previously described (20). The vector for His-tagged tobacco etch virus (TEV) was a gift from John Tesmer (University of Texas at Austin). The pMSC7 (LIC_HIS) vector was provided by John Sondek (University of North Carolina at Chapel Hill). The Tif2 NR Box 3 peptide was purchased from RS Synthesis (Louisville, KY). DNA

oligonucleotide primers were synthesized by IDT (Coralville, IA). Protein expression and purification—LRH-1 LBD (residues 299-541) in the pMSC7 vector was expressed and purified as previously described.¹⁹ Briefly, protein was expressed in BL21(DE3) pLysS *E. coli* by induction with IPTG (1 mM) for 4 hr at 30°C. Protein was purified by nickel affinity chromatography. Protein used for DSF experiments was incubated with DLPC (five-fold molar excess) for four hours at room temperature, and then repurified by size-exclusion into an assay buffer of 20 mM Tris-HCl, pH 7.5, 150 mM NaCl, and 5% glycerol. Protein used for crystallization was incubated with TEV protease to cleave the His tag. The cleaved protein was then separated from the His tag and TEV by a second round of nickel affinity chromatography. To make protein-ligand complexes, protein was incubated with ligands overnight (10-fold molar excess) and repurified by size-exclusion, using a final buffer of 100 mM ammonium acetate, pH 7.4, 150 mM sodium chloride, 1 mM DTT, 1 mM EDTA, and 2 mM CHAPS.

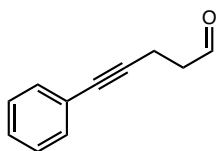
Chemical Syntheses



5-phenylpent-4-yn-1-ol: A round bottom flask equipped with magnetic stir bar was charged with bis(triphenylphosphine)palladium dichloride (347.7 mg, 0.5 mmol, 0.01 equiv) and copper iodide (323.2 mg, 1.7 mmol, 0.03 equiv). The flask was placed under nitrogen and triethylamine (52 mL) was added via syringe. The solution was treated with iodobenzene (10.7 g, 52 mmol, 1.0 equiv),

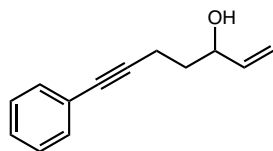
¹⁹ Goodwin, B.; Jones, S. A.; Price, R. R.; Watson, M. A.; McKee, D. D.; Moore, L. B.; Galardi, C.; Wilson, J. G.; Lewis, M. C.; Roth, M. E.; Maloney, P. R.; Willson, T. M.; Kliewer, S. A. A Regulatory Cascade of the Nuclear Receptors FXR, SHP-1, and LRH-1 Represses Bile Acid Biosynthesis. *Mol. Cell* **2000**, *6* (3), 517–526

then sparged with nitrogen for 30 minutes. 4-pentyn-1-ol (5.4 g, 64 mmol, 1.2 equiv) was then added via syringe. The sparging needle was removed from the solution and replaced with a vent needle under positive nitrogen pressure. The solution was vigorously stirred at 60°C for 2 hours, at which point the reaction was complete by TLC. The reaction was cooled and precipitated with ether. The entire reaction was filtered over a plug of celite (eluted with ether). The filtrate was concentrated in vacuo to afford a rust-colored oil, which was purified on silica (30% EtOAc/Hex eluent) to afford the title compound as a clear, colorless oil. (8.4 g, >99% yield). Spectral data were consistent with reported values.²⁰

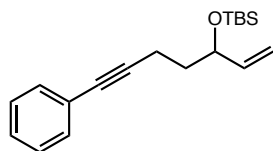


5-phenylpent-4-ynal: Under nitrogen, a solution of oxalyl chloride (4.5 mL, 52 mmol, 1.1 equiv) in DCM (400 mL) was cooled to -78 °C. A solution of dimethylsulfoxide (4.4 mL, 62 mmol, 1.3 equiv) in DCM (30 mL) was added dropwise. After effervescence ceased (ca. 30 minutes), 5-phenylpent-4-yn-1-ol (7.6 g, 48 mmol, 1.0 equiv) was added dropwise in DCM. The reaction mixture was stirred at -78 °C for 1.5 h before the addition of triethylamine (17 mL, 123 mmol, 2.5 equiv). The solution was allowed to warm to room temperature before the addition of saturated ammonium chloride (excess). The reaction mixture was then poured onto water and extracted with EtOAc, dried with MgSO₄, concentrated, and purified by silica gel chromatography (10-20% EtOAc/Hex 6.8 g, 91 %). Spectral data were consistent with reported values.¹⁶

²⁰ Fujii, K.; Morimoto, T.; Tsutsumi, K.; Kakiuchi, K. Rh(I)-Catalyzed CO Gas-Free Cyclohydrocarbonylation of Alkynes with Formaldehyde to α,β -Butenolides. *Chem. Commun.* **2005**, No. 26, 3295–3297

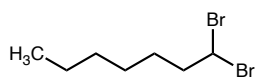


7-phenylhept-1-en-6-yn-3-ol: Under nitrogen, a solution of 5-phenylpent-4-ynal (5.8 g, 37 mmol, 1.0 equiv) in anhydrous THF was cooled to $-78\text{ }^{\circ}\text{C}$. The solution was treated with vinylmagnesium bromide (58 mL of a 1.0M solution in THF, 58 mmol, 1.5 equiv.). The reaction was stirred and allowed to warm to room temperature over 16 h, then saturated ammonium chloride was added. The reaction mixture was poured onto water and extracted with EtOAc, dried with MgSO_4 , and concentrated before purification on silica (5-10% EtOAc/Hex eluent) to give the title compound (5.5 g, 81%). Spectral data are consistent with reported values.¹⁶



tert-butyldimethyl((7-phenylhept-1-en-6-yn-3-yl)oxy)silane: A 3-neck flask was charged with imidazole (2.7g, 39 mmol, 4.0 equiv) and DMAP (2.5 g, 20 mmol, 2 equiv), a magnetic stirrer, and placed under nitrogen. Dry THF was added to make a 0.1 M solution, and the flask was cooled to $0\text{ }^{\circ}\text{C}$ in an ice bath. TBDMS-OTf was added dropwise and allowed to stir for 10 minutes at $0\text{ }^{\circ}\text{C}$. 7-phenylhept-1-en-6-yn-3-ol was added dropwise as a solution in THF *via* syringe and the reaction was allowed to warm to room temperature and stir for 16 h. Upon reaction completion, the reaction was quenched with water and extracted with ether 3 x. The combined organic layers were washed with brine, dried with Na_2SO_4 , and concentrated. The crude residue was purified on silica in 5% Et_2O /Hex eluent to give the title compound as a colorless oil (2.2 g, 72% yield). Spectral data are consistent with literature values.¹⁶

$^1\text{H NMR}$ (300 MHz, CDCl_3) δ 7.48 – 7.37 (m, 2H), 7.37 – 7.27 (m, 3H), 5.85 (ddd, $J = 17.1, 10.4, 6.1$ Hz, 1H), 5.23 (ddd, $J = 17.2, 1.8, 1.3$ Hz, 1H), 5.09 (ddd, $J = 10.3, 1.8, 1.2$ Hz, 1H), 4.32 (d, $J = 7.0$ Hz, 1H), 2.66 – 2.37 (m, 2H), 1.97 – 1.70 (m, 2H), 1.38 – 1.20 (m, 1H), 0.94 (s, 9H), 0.13 (s, 3H), 0.08 (s, 3H).



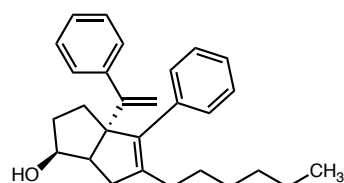
1,1-dibromoheptane: Under nitrogen, triphenylphosphite (11.4 mL, 40 mmol 1.1 equiv) was dissolved in DCM and cooled to -78°C . Bromine (2.0 mL, 40 mmol 1.1 equiv) was added dropwise and stirred briefly. Heptanal (4.2 g, 37 mmol 1.0 equiv.) was then added dropwise in DCM and the reaction was allowed to come to room temperature over 3 hours. The reaction mixture was then filtered through silica and concentrated in vacuo. The crude oil was purified by silica gel chromatography in 100% hexanes to afford a clear, colorless oil (6.3 g, 66% yield). Spectral data is consistent with reported values.²¹

$^1\text{H NMR}$ (600 MHz, CDCl_3) δ 5.67 (t, $J = 6.2$ Hz, 1H), 2.38–2.33 (m, 2H), 1.51 (dd, $J = 5.9, 3.3$ Hz, 2H), 1.35–1.23 (m, 6H), 0.86 (t, $J = 6.9$ Hz, 3H).

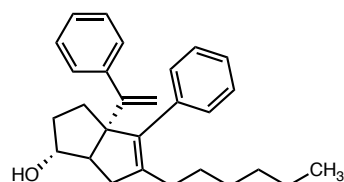
RJW100: Hexahydropentalene formation was accomplished through slight modification of Whitby's procedure. Prior to cyclization, all non-volatile reagents were dried by azeotropic removal of water using benzene. A dry round bottom flask containing bis(cyclopentadienyl)zirconium(IV) dichloride (1.2 equiv) under nitrogen, was dissolved in

²¹ Hoffman, R. W.; Bovicelli, P. Conversion of Aldehydes into 1,1-Dibromoalkanes. *Synthesis (Stuttg)*. **1990**, *8*, 657–659

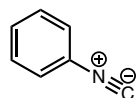
anhydrous, degassed tetrahydrofuran (THF, 50 mL/mmol enyne) and cooled to -78 °C. The resulting solution was treated with n-BuLi (2.4 equiv.) and the light yellow solution was stirred for 30 minutes. A solution of tertbutyldimethyl((7-phenylhept-1-en-6-yn-3-yl)oxy)silane (1.0 equiv) in anhydrous, degassed THF (5 mL/mmol) was added. The resulting light yellow mixture was stirred at -78 °C for 30 minutes, the cooling bath removed, and the reaction mixture was allowed to warm to ambient temperature with stirring (2.5 hours total). The reaction mixture was then cooled to -78 °C and the required 1,1-dibromoheptane (1.1 equiv) was added as a solution in anhydrous THF (5 mL/mmol) followed by freshly prepared lithium diisopropylamide (LDA, 1.0 M, 1.1 equiv.). After 15 minutes, a freshly prepared solution of lithium phenylacetylide (3.6 equiv.) in anhydrous THF was added dropwise and the resulting rust-colored solution was stirred at -78 °C for 1.5 hours. The reaction was quenched with methanol and saturated aqueous sodium bicarbonate and allowed to warm to room temperature, affording a light yellow slurry. The slurry was poured onto water and extracted with ethyl acetate four times. The combined organic layers were washed with brine, dried with MgSO₄, and concentrated *in vacuo*. The resulting yellow oil was passed through a short plug of silica (20% EtOAc/Hex eluent) and concentrated. The crude product was dissolved in THF and treated with solid tetrabutylammonium fluoride hydrate (ca. 2.0 equiv.) and the resulting solution stirred at room temperature for 16 h. The reaction mixture was concentrated and the diastereomers were purified and separated by careful silica gel chromatography (5-20% EtOAc/Hex eluent) to afford RJW100 *exo* and RJW100 *endo* in a 1.6:1 ratio, respectfully, as determined by characteristic ¹H NMR signals. The spectral data reported are consistent with literature values. (402.0 mg combined *exo* and *endo*, 58 %).

**Endo:**

¹H NMR: (400 MHz, CDCl₃) δ 7.38 – 7.12 (m, 10H), 5.05 (d, J = 1.4 Hz, 1H), 4.92 (d, J = 1.4 Hz, 1H), 4.16 (ddd, J = 9.0, 8.6, 5.4 Hz, 1H), 2.60 (dd, J = 17.3, 2.0 Hz, 1H), 2.46 (td, J = 8.7, 2.2 Hz, 1H), 2.13 – 1.95 (m, 3H), 1.84 (ddt, J = 10.1, 5.5, 4.6 Hz, 1H), 1.72 – 1.64 (m, 2H), 1.60 – 1.31 (m, 3H), 1.33 – 1.13 (m, 7H), 0.83 (t, J = 7.0 Hz, 3H).

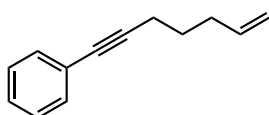
**Exo:**

¹H NMR: (400 MHz, CDCl₃) δ 7.37 – 7.14 (m, 10H), 5.05 (d, J = 1.4 Hz, 1H), 4.97 (d, J = 1.4 Hz, 1H), 3.99 – 3.85 (m, 1H), 2.35 (dd, J = 16.6, 9.4 Hz, 1H), 2.27 (d, J = 9.4 Hz, 1H), 2.09 – 1.96 (m, 4H), 1.74 – 1.61 (m, 3H), 1.44 – 1.11 (m, 9H), 0.84 (t, J = 7.0 Hz, 3H).



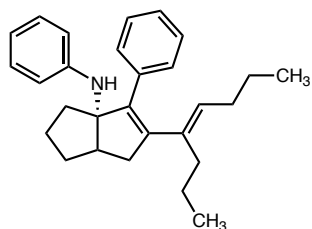
Isocyanobenzene: Aniline (2.0 mL, 22 mmol, 1.0 equiv) was added to a round bottom flask charged with magnetic stir bar was diluted with, 50% NaOH in water (w/v) (17 g in 17 mL) and the solution was stirred vigorously. Tetrabutylammoniumbromide (86 mg, 0.3 mmol, ~ 1 mol%) was added to the solution. Chloroform (2.7 mL, 33 mmol, 1.5 equiv) was added to the solution. The flask was fitted with a reflux condenser with water cooling and heated to reflux overnight.

Upon starting material (aniline) consumption (as determined by GCMS), the reaction was cooled to room temperature, diluted with water, and extracted with dichloromethane 3 x. The organic layers were washed with brine, dried with MgSO₄, and concentrated. The crude mixture was purified on silica in 20–40% DCM/Hex to afford the title compound. CAUTION: isonitriles have an *extremely distressing odor*. Concentrate *in vacuo* with a rotary evaporator inside a fume hood.



hept-6-en-1-yn-1-ylbenzene: To a 3-neck flask equipped with magnetic stir bar under nitrogen was added phenylacetylene (1.5 mL, 14 mmol, 1.6 equiv). Dry THF was then added to the flask to make a 0.1 M solution. The reaction was cooled to -78 °C before the dropwise addition of n-BuLi (as a 2.0 M solution in hexanes, 6.8 mL, 14 mmol, 1.6 equiv). The reaction was allowed to stir at -78 °C for 30 minutes before the addition of hexamethylphosphoramide (HMPA, 2.4 mL, 14 mmol, 1.6 equiv). 5-bromo-1-pentene (1.0 mL, 8.5 mmol, 1.0 equiv) was then added *via* syringe to the solution. The reaction was stirred and allowed to warm to room temperature over 16 h before being quenched with saturated ammonium chloride. The solution was partitioned between EtOAc and water. The organic layer was washed with brine (3 x), dried over Na₂SO₄, and concentrated. The crude residue was purified on silica in 100% Hex to afford the title compound as a colorless liquid (1.0 g, 64%). Spectral data were consistent with reported values.¹⁵

¹H NMR (300 MHz, CDCl₃) δ 7.45 – 7.38 (m, 2H), 7.32 – 7.23 (m, 3H), 5.85 (ddt, J = 16.9, 10.2, 6.7 Hz, 1H), 5.09 (dq, J = 17.1, 1.7 Hz, 1H), 5.02 (ddt, J = 10.2, 2.2, 1.2 Hz, 1H), 2.44 (t, J = 7.1 Hz, 2H), 2.24 (dt, J = 7.9, 6.6, 1.4 Hz, 2H), 1.72 (p, J = 7.2 Hz, 2H).



GSK8470: A dry 3-neck round bottom flask equipped with magnetic stir bar and reflux condenser was placed under nitrogen. To the flask bis(cyclopentadienyl)zirconium(IV) dichloride (azeotroped with benzene 3 x, 270 mg, 0.9 mmol, 1.0 equiv) was added as a solution in dry THF (~ 1 M) and cooled to -78 °C. The resulting solution was treated with n-BuLi (2.0 equiv) and the solution was stirred for 1 h. Hept-6-en-1-yn-1-ylbenzene (1148 mg, 0.9 mmol, 1.0 equiv) as a 1 M solution in THF was added dropwise *via* syringe. The resulting solution was stirred at -78 °C for 1 h, the cooling bath was removed, and the reaction mixture was allowed to warm to ambient temperature with stirring for an additional 2 h. The reaction mixture was then cooled to -40 °C, and phenylisocyanide (excess, ca 5 equiv) was added, followed by 4-octyne (131 mg, 1.2 mmol, 1.3 equiv). The resulting claret-red solution was heated to reflux and allowed to react for 2 h before being cooled to room temperature and quenched with methanol, followed by water. The slurry was partitioned between water and ether, and extracted 3 x with ether. The combined organic layers were washed with brine, dried with MgSO₄ and concentrated. A preparative TLC plate was basified with hexanes and 1% TEA and allowed to dry completely before the crude residue was loaded and purified on the preparative TLC plate in 10% EtOAc/Hex (1% TEA additive) to afford 22 mg (7% yield) of the title compound as a colorless oil. Spectral data were consistent with reported values. *Caution:* This compound is extremely acid labile: base-wash glassware before storing.

¹H NMR (600 MHz, CDCl₃) δ 7.18 – 7.08 (m, 5H), 6.97 – 6.94 (m, 2H), 6.66 (tt, *J* = 7.3, 1.0 Hz, 1H), 6.62 – 6.55 (m, 2H), 5.29 – 5.25 (m, 1H), 3.97 (s, 1H), 3.00 (dd, *J* = 17.3, 9.7 Hz, 1H), 2.80 (td, *J* = 8.9, 3.0 Hz, 1H), 2.33 (dd, *J* = 17.3, 3.5 Hz, 1H), 2.00 – 1.87 (m, 5H), 1.78 – 1.48 (m, 4H), 1.36 – 1.13 (m, 5H), 0.79 – 0.67 (m, 6H).

Crystallization

Protein-ligand complexes were incubated with a peptide derived from human Tif2 NR Box 3 (⁺H₃N-KENALLRYLLDKDDT⁻CO₂) at four-fold molar excess for two hours at room temperature and then concentrated to 6.5 mg/ml. A crystallant of 0.05 M sodium acetate, pH 4.6, 5-11% PEG 4000 and 0-10% glycerol was used. Crystals were grown by hanging drop vapor diffusion in drops containing 1 μl protein and 1 μl crystallant, at a temperature of 18-20°C.

Structure Determination

Crystals were flash frozen in liquid nitrogen, using a cryopreservative consisting of crystallant plus 30% glycerol. Data were collected remotely from the South East Regional Collaborative Access Team at the Advanced Photon Source, 22ID beamline (Argonne National Laboratories, Chicago, IL). Data were processed and scaled using HKL2000²² and phased by molecular replacement using Phaser-MR (Phenix²³). For the RR-RJW100 structure, PDB 3PLZ¹⁶ was used as the search model, with the ligand and a portion of the bottom of the receptor omitted. For the SR-RJW100 structure,

²² Otwinowski, Z.; Minor, W. Processing of X-Ray Diffraction Data Collected in Oscillation Mode. *Methods Enzymol.* **1997**, *276*, 307–326

²³ Adams, P. D.; Afonine, P. V.; Bunkóczi, G.; Chen, V. B.; Davis, I. W.; Echols, N.; Headd, J. J.; Hung, L. W.; Kapral, G. J.; Grosse-Kunstleve, R. W.; McCoy, A. J.; Moriarty, N. W.; Oeffner, R.; Read, R. J.; Richardson, D. C.; Richardson, J. S.; Terwilliger, T. C.; Zwart, P. H. PHENIX: A Comprehensive Python-Based System for Macromolecular Structure Solution. *Acta Crystallogr. Sect. D Biol. Crystallogr.* **2010**, *66* (2), 213–221

the search model was the RR-RJW100 structure with the ligand omitted. Model building and refinement were conducted with Coot²⁴ and phenix.refine²³, respectively. Figures were constructed using Pymol (Schrödinger, LLC)²⁵

Structure Analysis

Dimensions of the binding pocket in the presence of various ligands were calculated using CastP software.²⁶ Ligplot+ was used to identify residues interacting with the ligands.²⁷

Mutagenesis

Mutations were introduced to pMSC7 and pCI LRH-1 constructs using the Quikchange site-directed mutagenesis kit (Stratagene). Constructs were sequence-verified prior to use.

Cell Culture

HeLa cells were purchased from Atlantic Type Culture Collection and grown in phenol red-free MEM α media (CellGro) supplemented with 10% charcoal-stripped fetal bovine serum (Atlanta Biologicals). Cells were maintained using standard culture conditions.

²⁴ Emsley, P.; Cowtan, K. Coot: Model-Building Tools for Molecular Graphics. *Acta Crystallogr. Sect. D Biol. Crystallogr.* **2004**, *60* (12 I), 2126–2132

²⁵ DeLano, W. L. (2010) The PyMOL Molecular Graphics System, Version 1.3r1, Schrödinger, LLC, New York

²⁶ Binkowski, T. A., Naghibzadeh, S., and Liang, J. CASTp: computed atlas of surface topography of proteins. *Nucleic Acids Res*, **2003**, *31*, 3352–3355

²⁷ Laskowski, R. A., and Swindells, M. B. LigPlot+, multiple ligand protein interaction diagrams for drug discovery. *J. Chem. Inf. Model*, **2011**, *51*, 2778–2786

Reporter Gene Assays

HeLa cells were seeded at a density of 10,000 cells per well in white-walled, clear-bottomed 96-well culture plates. The next day, cells were transfected with LRH-1 and reporters, using Fugene HD (Roche) at a ratio of 5:2 Fugene:DNA. The transfected plasmids included full-length LRH-1 in a pCI vector (5 ng/ well), and a SHP-luc reporter, encoding the LRH-1 response element and surrounding sequence from the SHP promoter cloned upstream of firefly luciferase in the pGL3 basic vector (50 ng/ well). Cells were also cotransfected with a constitutive Renilla luciferase reporter (utilizing the CMV promoter), which was used for normalization of firefly signal (1 ng/ well). Control cells received pCI empty vector at 5 ng/ well in place of LRH-1-pCI. Following an overnight transfection, cells were treated with agonists for 24 hours at the concentrations indicated in the figure legends. Agonists were dissolved in DMSO and then diluted into media, with a final concentration of 0.3% DMSO in all wells. Luciferase signal was quantified using the DualGlo kit (Promega). Experiments were conducted at least three times in triplicate.

Hydrogen-Deuterium exchange mass spectrometry

Purified LRH-1 LBD protein (His tag removed) was incubated with of a five-fold molar excess DLPC or synthetic agonist overnight at 4°C. Protein-ligand complexes were then repurified by size exclusion to remove displaced phospholipids and unbound ligands. An additional bolus of agonist or DLPC (5-fold molar excess) was added to the complexes prior to analysis by HDX. The assay buffer consisted of 20 mM Tris HCl, pH 7.4, 150 mM NaCl, and 5% glycerol. Solution-phase amide HDX was carried out with a fully automated system as described previously.²⁸

²⁸ Goswami, D., Devarakonda, S., Chalmers, M. J., Pascal, B. D., Spiegelman, B. M., and Griffin, P. R. Time window expansion for HDX analysis of an intrinsically disordered protein. *J. Am. Soc. Mass Spectrom.* **2013**, *24*, 1584–1592

Briefly, 5 μ l of protein was diluted to 25 μ l with D₂O-containing HDX buffer and incubated at 25 qC for 10 s, 30 s, 60 s, 900 s or 3,600 s. Following on exchange, back exchange was minimized and the protein was denatured by dilution to 50 μ L in a low pH and low temperature buffer containing 0.1% (v/v) trifluoroacetic acid in 5 M urea (held at 1 qC). Samples were then passed across an immobilized pepsin column (prepared in house) at 50 μ l min⁻¹ (0.1% v/v TFA, 15 qC); the resulting peptides were trapped on a C8 trap cartridge (Hypersil Gold, Thermo Fisher). Peptides were then gradient-eluted (4% (w/v) CH₃CN to 40% (w/v) CH₃CN, 0.3% (w/v) formic acid over 5 min, 2 qC) across a 1 mm \times 50 mm C18 HPLC column (Hypersil Gold, Thermo Fisher) and electrosprayed directly into an Orbitrap mass spectrometer (Q Exactive, Thermo Fisher). Data were processed with in-house software²⁹ and visualized with PyMOL (Schrödinger, LLC,²⁵). To measure the difference in exchange rates, we calculated the average percent deuterium uptake for hLRH-1 LBD – RR-RJW100 complexes following 10, 30, 60, 900 and 3,600 s of on exchange. From this value, we subtracted the average percent deuterium uptake measured for the DLPC-hLRH-1 LBD complex. Negative perturbation values indicate exchange rates are slower for these regions within the RR-RJW100-LRH-1 complex relative to DLPC-bound LRH-1.

Differential Scanning Fluorimetry (DSF)

Purified LRH-1 LBD-His protein (0.2 mg/ml) was incubated overnight with 50 μ M of each compound at 4°C. The final DMSO concentration in the reactions was 1%. SYPRO orange dye (Invitrogen) was then added at a 1:1000 dilution. Reactions were heated at a rate of 0.5°C per

²⁹ Pascal, B. D., Willis, S., Lauer, J. L., Landgraf, R. R., West, G. M., Marciano, D., Novick, S., Goswami, D., Chalmers, M. J., and Griffin, P. R. HDX workbench: software for the analysis of H/D exchange MS data. *J. Am. Soc. Mass Spectrom*, **2012**, *23*, 1512–1521

minute, using a StepOne Plus Real Time PCR System (ThermoFisher). Fluorescence was recorded at every degree using the ROX filter (602 nm). Data were analyzed by first subtracting baseline fluorescence (ligands + SYPRO with no protein) and then fitting the curves using the Boltzmann equation (GraphPad Prism, v6) to determine the T_m .

Model Construction for Molecular Dynamics Simulations

Three crystal structures of LRH-1 LBD in complex with Tif2 were used to construct models for the simulations. These were (1) PDB 3PLZ, chains B and D (GSK8470 ligand), (2) PDB 5L11 (RR-RJW100 ligand), and (3) PDB 5SYZ (SR-RJW100 ligand). For consistency, the structures were modified at the N- and C-termini so that all contained residues 300-540 of LRH-1 and residues 742-751 of the Tif2 peptide. Missing residues within this protein sequence were added, as well as missing protein sidechains (3PLZ). The T352V mutation was introduced by mutating the sequence of WT LRH-1 in each of these structures. Finally, in a separate simulation, RR-RJW100 ligand was artificially reoriented in WT LRH-1 to be aligned with GSK8470, allowing a face-to-face π - π -stacking interaction of LRH-1 residue H390 with the aniline ring of RR-RJW100. Seven complexes in total were used in molecular dynamics simulations.

Molecular Dynamics Simulations

The complexes were solvated in an octahedral box of TIP3P water with a 10 Å buffer around the protein complex. Na^+ and Cl^- ions were added to neutralize the protein and achieve physiological conditions. All systems were set up using xleap in AmberTools³⁰ with the parm99-bsc0

³⁰ Case, D., and Kollman, P. (2012) AmberTools, Version 12, University of California, San Francisco

forcefield.³¹ Parameters for all ligands (GSK8470, RR-RJW100, and SR-RJW100) were obtained using Antechamber³² in AmberTools. All minimizations and simulations were performed with Amber14.³³ Systems were minimized with 5000 steps of steepest decent followed by 5000 steps of conjugate gradient minimization with 500 kcal/mol·Å² restraints on all atoms. Restraints were removed from all atoms excluding the atoms in both the ligand and the Tif2 peptide, and the previous minimization was repeated. The systems were heated from 0 to 300 K using a 100-ps run with constant volume periodic boundaries and 5 kcal/mol·Å² restraints on all protein and ligand atoms. Twelve ns of MD equilibration was performed with 10 kcal/mol·Å² restraints on protein and ligand atoms using the NPT ensemble. Restraints were reduced to 1 kcal/mol·Å² for an additional 10 ns of MD equilibration. Then restraints were removed and 200 ns production simulations were performed for each system in the NPT ensemble. A 2-fs timestep was used and all bonds between heavy atoms and hydrogens were fixed with the SHAKE algorithm.³⁴ A cut-off distance of 10 Å was used to evaluate long-range electrostatics with Particle Mesh Ewald (PME) and for van der Waals forces. 10,000 evenly spaced frames were taken from each simulation for analysis. Analysis was performed with the CPPTRAJ module³⁵ of AmberTools.

³¹ Pérez, A., Marchán, I., Svozil, D., Sponer, J., Cheatham, T. E., 3rd., Laughton, C. A., and Orozco, M. Refinement of the AMBER force field for nucleic acids: improving the description of α/γ conformers. *Biophys. J.* **2007**, *92*, 3817–3829

³² Wang, J., Wang, W., Kollman, P. A., and Case, D. A. Automatic atom type and bond type perception in molecular mechanical calculations. *J. Mol. Graph. Model.* **2006**, *25*, 247–260

³³ Case, D., Babin, V., Berryman, J., Betz, R., Cai, Q., Cerutti, D., Cheatham Iii, T., Darden, T., Duke, R., and Gohlke, H. (2014) Amber Tools, Version 14, University of California, San Francisco

³⁴ Ryckaert, J.-P., Ciccotti, G., and Berendsen, H. J. Numerical integration of the cartesian equations of motion of a system with constraints: molecular dynamics of n-alkanes. *J. Comput. Phys.* **1997**, *23*, 327–341

³⁵ Roe, D. R., and Cheatham, T. E., 3rd. PTRAJ and CPPTRAJ: software for processing and analysis of molecular dynamics trajectory data. *J. Chem. Theory Comput.* **2013**, *9*, 3084–3095

Chapter 2: Phospholipid-mimicking chimeras as LRH-1 agonists

Adapted and Reprinted in part with permission from ACS Med. Chem. Lett. 2018, 9, 1051–1056
Copyright 2018 American Chemical Society
<https://pubs.acs.org/doi/10.1021/acsmchemlett.8b00361>

2.1 Optimizing a synthetic route to RJW100-DLPC hybrid precursors

In the crystal structure of DLPC (**1**) bound in the LBD of LRH-1, it is clear that the alkyl tails are buried deep in the LBD, while the phosphatidylcholine makes important contacts at the mouth of the LBD of LRH-1.¹³ Specifically, DLPC activates LRH-1 through an allosteric network by contacting G421, Y516, and K520.^{12a} Unlike DLPC, however, hexahydropentalenes operate through differing modes of activation. We were able to show that the most well-known ligand of this class, RJW100 (**2**), activates LRH-1 through a separate allosteric network by indirectly contacting (namely) T352 deep in the binding pocket of LRH-1 through a conserved network of water molecules (Chapter 1).¹⁷ Superposition of the cocrystal structures of both *exo*-RJW100 and DLPC in the LBD reveals direct intersection of the hexyl tail of *exo*-RJW100 and the Sn1-lauroyl tail of DLPC (Fig. 2.1). We questioned whether the binding features of both ligand classes (i.e., phospholipid interactions with surface residues and the hydroxyl interaction with deep pocket residues) could be achieved by a single scaffold, thus achieving greater engagement with the ligand binding pocket. We designed a series of hybrid phospholipid mimics with three distinct regions: the hexahydropentalene (6HP) core of RJW100 to interact with T352, modular alkyl linkers to maintain hydrophobic interactions, and terminal polar groups to engage the PC headgroup binding near the mouth of the pocket.³⁶

³⁶ Flynn, A. R.; Mays, S. G.; Ortlund, E. A.; Jui, N. T. Development of Hybrid Phospholipid Mimics as Effective Agonists for Liver Receptor Homologue-1. *ACS Med. Chem. Lett.* **2018**, *9* (10), 1051–1056

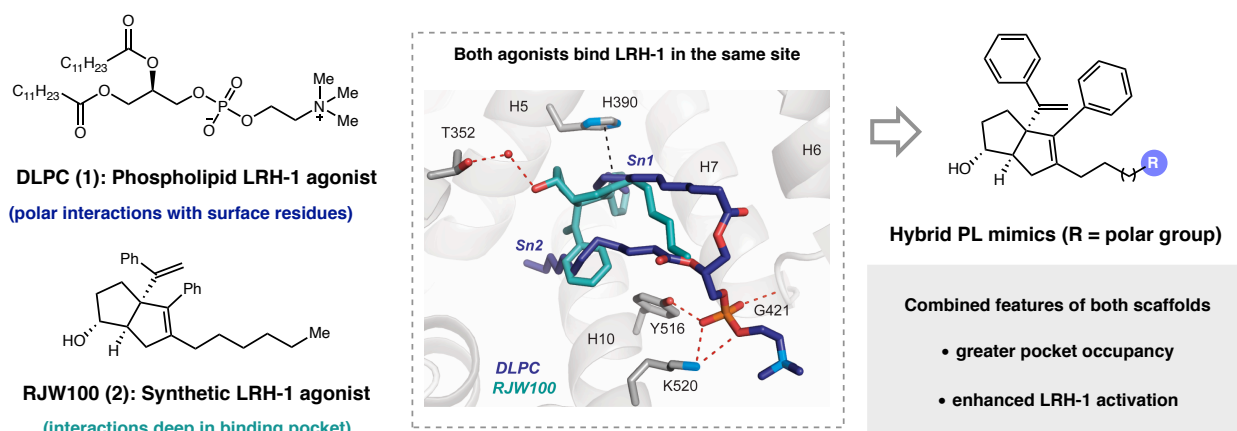


Figure 2.1. Design of hybrid PL mimics. Two different agonist classes are combined into a single scaffold. In addition to the shown hydrophilic and π -stacking interactions, each ligand makes extensive hydrophobic interactions (omitted for clarity).

To generate the targeted phospholipid (PL) mimics, we employed Whitby's carbene-interrupted Pauson–Khand reaction, where zirconocene-mediated reaction of silyl ether-containing 1,1-dibromoalkanes (**3a–3h**), enyne (**4**), and phenylacetylene would deliver the 6HP-containing primary alcohols **5a–5h**.³⁷ We developed this specific approach because it would allow for systematic variation of the alkyl linker length, and the primary alcohols could be easily manipulated into a range of polar head groups. This retrosynthetic disconnection is ideal, in part, because it utilizes readily accessible precursors of similar complexity in the convergent 6HP-forming step. Whitby (and we) showed that, although *exo* and *endo* diastereomers of RJW100 are roughly equipotent, the *exo* diastereomer is a more effective agonist for LRH-1.^{16,17} Moreover, we have found that *endo* RJW100 is a poor LRH-1 activator in cellular assays. As such, we sought reaction conditions to selectively produce the *exo* isomer.

³⁷ Stec, J.; Thomas, E.; Dixon, S.; Whitby, R. J. Tandem Insertion of Halocarbenoids and Lithium Acetylides into Zirconacycles: A Novel Rearrangement to Zirconium Alkenylidenates by β -Addition to an Alkynyl Zirconocene. *Chem. - A Eur. J.* **2011**, *17* (17), 4896–4904

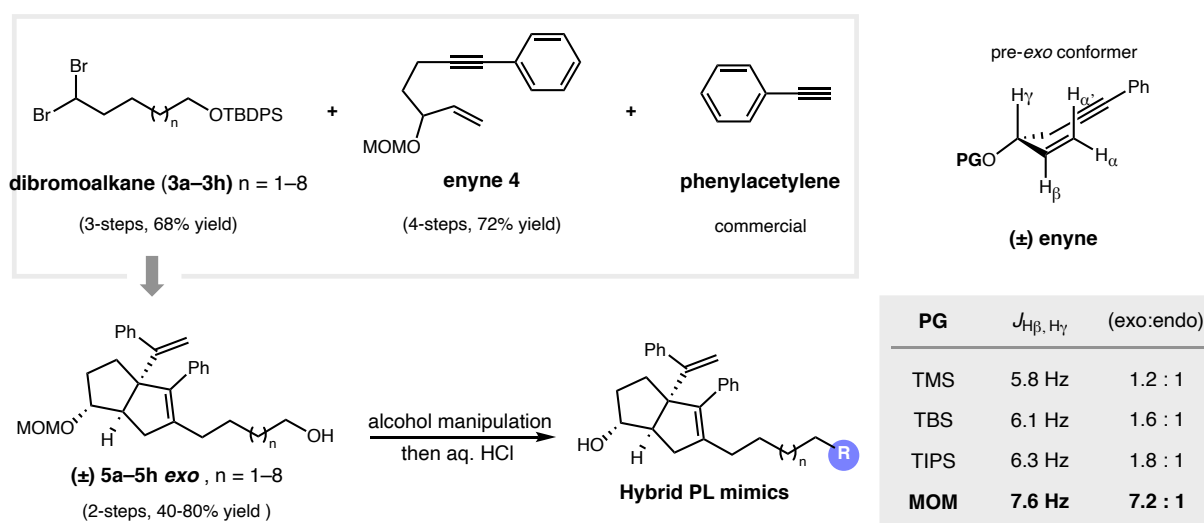


Figure 2.2. Synthetic approach to hybrid compounds.

Similar to other Pauson–Khand reactions, Whitby’s system operates through an early transition state, where diastereoselectivity is dictated by the conformational preference of the corresponding enyne starting materials. We prepared a small collection of enynes with different alcohol protecting groups and found that the *exo*-selectivity increased with relative population of the pre-*exo* conformer (as indicated by $J_{H\gamma}$),³⁸ where a methoxymethyl (MOM) ether gave the desired *exo*-6HP diastereomer in 7.2:1 d.r. In addition to providing diastereocontrol, MOM protection to give **4** was strategically enabling due to its orthogonal reactivity to silyl protecting groups. This allowed for chemoselective manipulation of the primary alcohol. Using *exo*-selective cyclization conditions, we utilized a series of intermediates to afford the requisite hybrid precursors as diastereomeric mixtures (~7:1 d.r. favoring the desired *exo* isomers).

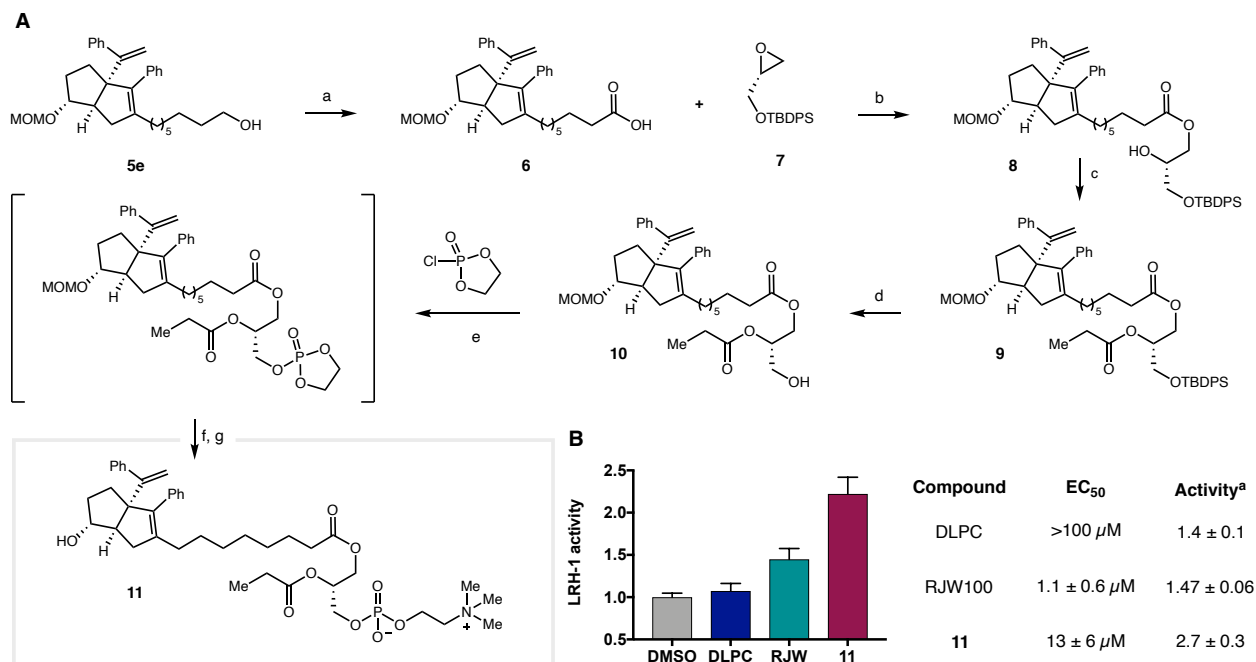
³⁸ Adrio, J.; Rivero, M. R.; Carretero, J. C. Endo-Selective Intramolecular Pauson ± Khand Reactions Of Gamma-Oxygenated Alpha,Beta-Unsaturated Phenylsulfones. *Synthesis*. **2001**, 7(11),2435–2448

2.3 Design and evaluation of an RJW100-DLPC chimera

To directly examine the effect of combining PC binding elements with those of the 6HP scaffold, we designed a hybrid compound where the RJW100 core was appended to a glycerophosphorylcholine headgroup. Analysis of the crystallographic data described above indicated that this could be achieved via extension of the RJW100 alkyl chain (along the trajectory of the Sn1 lipid tail) along with truncation of the Sn2 tail (to avoid disruption of 6HP binding). Accordingly, our synthetic efforts, as shown in Scheme 2.1, began with alcohol precursor **5e** to provide the required seven methylene units between the 6HP core and acylglycerol. Ley–Griffith oxidation of **5e** efficiently yielded terminal carboxylic acid **6**, which participated in a regioselective cobalt-mediated opening of epoxide **7** to give ester **8**.³⁹ Sequential acylation and deprotection with tetrabutylammonium fluoride (TBAF) afforded primary alcohol **10**. Terminal phosphorylcholine construction commenced with reaction of **10** with 2-chloro-1,3,2-dioxaphospholane 2-oxide in toluene. After filtration and concentration of the reaction mixture, the crude cyclic phospholane was opened with trimethylamine.

³⁹ Jacobsen, E. N.; Kakiuchi, F.; Konsler, R. G.; Larrow, J. F.; Tokunaga, M. Enantioselective Catalytic Ring Opening of Epoxides with Carboxylic Acids. *Tetrahedron Lett.* **1997**, *38* (5), 773–776

Scheme 2.1. Synthesis and Biological Evaluation of DLPC/RJW100 Hybrid **11** from **5e**^a



^a (A) *Reagents and conditions*: (a) TPAP, NMO, H₂O, MeCN, 23 °C; 1 h, 85% yield; (b) i. Co(salen), Et₂O, 23 °C; 1 h; ii. DIPEA, neat, 60 °C, 16 h, 24% yield; (c) propionyl chloride, DMAP, THF, 23 °C; 30 min, 77% yield; (d) TBAF, THF, 23 °C; 16 h, 76% yield; (e) 2-chloro-1,3,2-dioxaphospholane 2-oxide, TEA, toluene, 23 °C; 4 h; (f) trimethylamine, MeCN, 90 °C, 16 h; (g) conc. aq. HCl, MeCN, 23 °C; 10 min, purified by preparative HPLC (4% isolated yield over three steps e–g). (B) Ligand-driven LRH-1 activity using a Luciferase reporter assay. Maximum activation value for each ligand (fold vs vehicle) at a single point (30 μM).

Finally, acidic cleavage of the MOM-ether and isolation by preparative HPLC gave the hexahydropentalene-phospholipid hybrid **11**. We evaluated the efficacy of **11** using a luciferase reporter assay, which measures LRH-1 activity in intact (HeLa) cells. This functional assay utilizes a reporter plasmid in which the gene for luciferase is cloned downstream of a LRH-1 response element. In this way, luciferase is generated in response to LRH-1 transactivation. Maximum LRH-1 activation values for DLPC, RJW100, and **11** at 30 μM ligand concentration are given in Scheme 2.1B, and dose-dependent increases in luminescence was observed in all cases. EC₅₀ and maximum activation were calculated from the resulting dose–response curves. We found that **11**

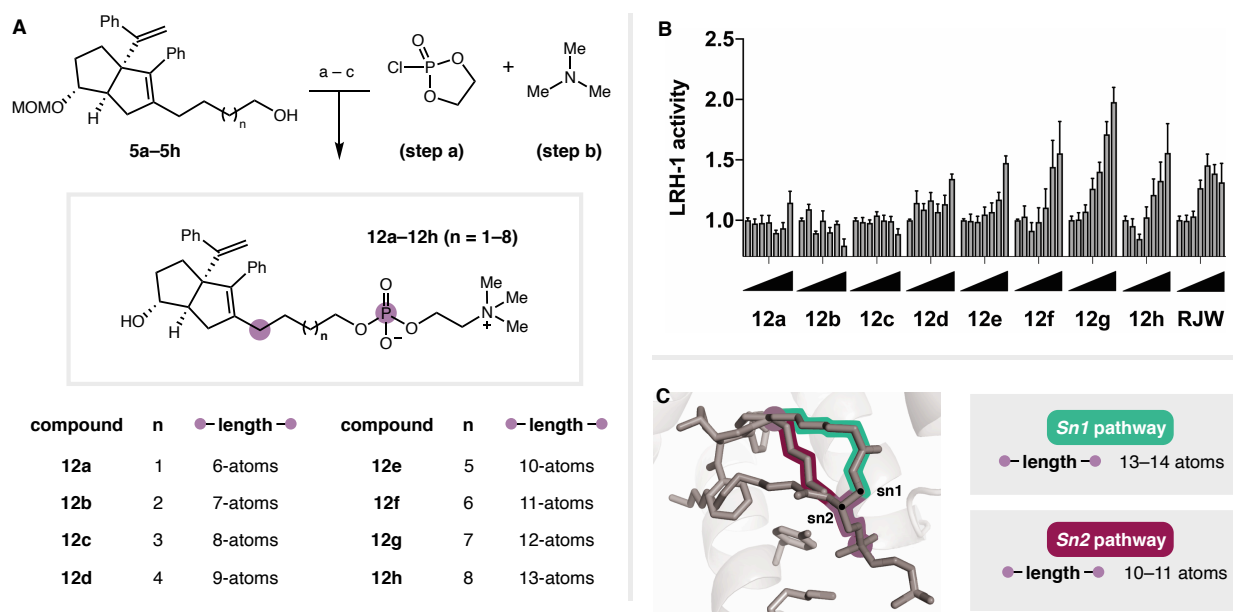
was considerably more potent than the parent phospholipid DLPC (EC_{50} of $13 \pm 6 \mu\text{M}$ vs $>100 \mu\text{M}$ for DLPC). The low potency of DLPC in this assay is consistent with previous reports.⁴⁰ RJW100 is more potent than **11**, with an EC_{50} of $1.1 \pm 0.6 \mu\text{M}$; however, **11** induced higher levels of LRH-1 activation than either DLPC or RJW100 in these experiments (Scheme 2.1B). Encouraged by this result, we were motivated to refine the structure of the LRH-1 hybrid agonists. To do this, we aimed to remove the hydrolytic and enzymatic liabilities inherent to the glyceryl esters while retaining the 6HP core and phosphorylcholine elements.

2.3 Optimization of chimeras *via* simplification

Also key to this study was the systematic evaluation of distance between these binding elements. In the overlaid ligand poses of **1** and **2**, the linear measured distance between the first methylene unit in the hexyl tail off the 6HP core and the DLPC phosphate is 10.0 \AA . However, the ligand binding pocket is fluxional; we have observed a change in the shape of the LRH-1 LBD to accommodate either DLPC or RJW100.¹⁷ We anticipated that hybrid ligand would be anchored at either end (by 6HP and polar group), though hydrophobic interactions within the pocket could enforce a nonlinear trajectory of the hybrid tail, underscoring the importance of systematic evaluation of linker length. As such, we targeted a series of hybrid compounds **12a–12h** comprising the 6HP core, phosphorylcholine polar group, and alkyl linker with systematically varied lengths. Importantly, this series would enable evaluation of the central hybrid design strategy, and the compounds would be considerably more synthetically accessible. The synthesis of **12a–12h** is summarized in Scheme 2.2A.

⁴⁰ Lee, J. M.; Lee, Y. K.; Mamrosh, J. L.; Busby, S. A.; Patrick, R.; Pathak, M. C.; Ortlund, E. A.; Moore, D. D. Antidiabetic Actions of a Phosphatidylcholine Ligand for Nuclear Receptor LRH-1. *Nature* **2011**, *474* (7352), 506–510

Scheme 2.2. Synthesis and Evaluation of Simplified Phosphorylcholine Hybrids **12**^a



^a (A) *Reagents and conditions*: (a) 2-chloro-1,3,2-dioxaphospholane 2-oxide, TEA, toluene, 23 °C; 4 h; (b) trimethylamine, MeCN, 90 °C, 16 h; (c) conc. aq. HCl, MeCN, 23 °C; 10 min. 12–49% over three steps and after purification by preparative HPLC. (B) Luciferase reporter assay demonstrating ligand efficacy, each bar represents activity at a different concentration of designated compound, from right to left: 0.003, 0.03, 0.3, 1.0, 3.0, 10, and 30 μ M. Represented as a measure of fold increase in activity over vehicle. (C) Overlay of DLPC and RJW100 in LRH-1 LBD. Number of atoms in linker is counted between the 6HP core and key PC binding element.

Beginning with primary alcohols **5a–5h**, transformation to their corresponding cyclic phospholanes followed by ring opening with trimethylamine afforded the crude MOM-protected phosphorylcholines. Direct cleavage of the MOM group with aqueous hydrochloric acid and purification by HPLC gave rise to the exo-compounds **12** with linkers between 6- and 13-atoms long. Evaluation of this series revealed that the improvement to LRH-1 activity that was observed with the hybrid **11** could be retained, in spite of significant structural simplification. Scheme 2.2B shows LRH-1 activity in the presence of these ligands, where each vertical bar represents activity

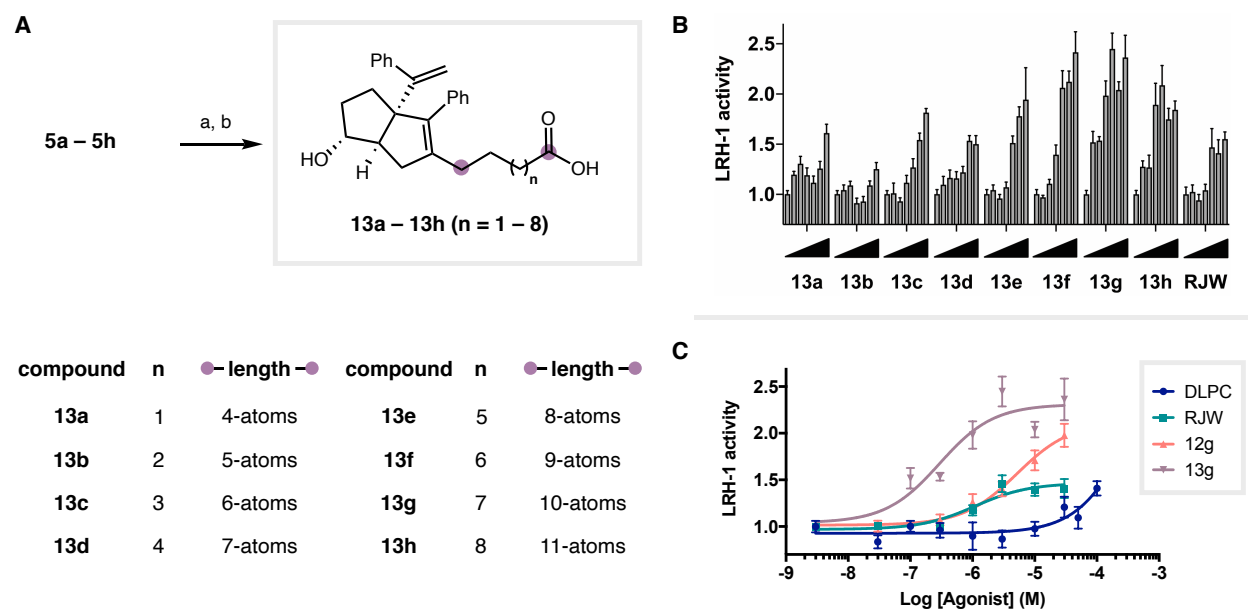
at a given dose of each compound (concentration increases from 0–30 μM , represented by triangles). Agonism was clearly related to linker length; compounds with shorter linkers (**12a–12c**, $n = 1–3$) did not induce luciferase expression at greater levels than vehicle alone, while **12d** and **12e** ($n = 4,5$) had only moderate activity at the highest dose. Compounds with longer linkers (**12f–12h**, $n = 6–8$) induced robust, dose-dependent LRH-1 activation, presumably through enhanced pocket engagement. Notably, the optimal alkyl linker length is 12-atoms, as demonstrated by the activity of compound **12g**, where the maximum LRH-1 activity was significantly higher than RJW100. Maximum LRH-1 activity, driven by **12g**, was 2.1-fold over DMSO, and potency was largely retained ($\text{EC}_{50} = 5 \pm 2 \mu\text{M}$). Visual examination of the plot in Scheme 2.2B reveals that ligand-driven LRH-1 activity is diminished on either side of the optimal linker length. As illustrated in Scheme 2.2C, the findings presented here are consistent with proposed hydrophobic and hydrophilic interactions outlined in the design scheme. Though tracing the specific conformation of the alkyl chain (i.e., emulating the phospholipid Sn1 or Sn2 pathway) will require structural studies, correlation between length and activation are most consistent with the Sn2 pathway.

Having established that our ligand hybrid design strategy could be used to improve agonist efficacy and that structural simplification is well tolerated, we sought to further optimize our hybrid scaffold. While our most effective phosphorylcholine hybrid (**12g**) demonstrated that the ester units are unnecessary, removing the choline moiety and synthesizing the directly analogous phosphates would likely hinder further development. Ultimately, phosphates can be poorly cell permeant, and cellular stability can be low due to the action of phosphatases.⁴¹ Accordingly, we considered a number of phosphate isosteres. Of these, carboxylic acids were attractive because

⁴¹ Rye, C. S.; Baell, J. B. Phosphate Isosteres in Medicinal Chemistry. *Curr. Med. Chem.* **2005**, *12* (26), 3127–3141

they are chemically stable and readily accessible from our collection of primary alcohols **5**. If successful, phosphate substitution in this manner could illuminate avenues for further scaffold optimization as carboxylic acid isosteres have been extensively studied.⁴²

Scheme 2.3. Synthesis and Evaluation of Simplified Carboxylic Acid Hybrids **13**^a



^a (A) *Reagents and conditions*: (a) TPAP, NMO, H₂O, MeCN, 23 °C; 1 h; (b) conc. aq. HCl, MeCN, 23 °C, 10 min. 40–85% yield over two steps. (B) Luciferase reporter assay demonstrating ligand efficacy, each bar represents activity at a different concentration of designated compound, from right to left: 0.003, 0.03, 0.3, 1.0, 3.0, 10, and 30 μM. Represented as a measure of fold increase in activity over vehicle. (C) Overlaid dose–response curves of indicated ligands.

In addition to improved binding properties, other polar groups would offer the ability to improve the aqueous solubility of this agonist scaffold. As summarized in Scheme 2.3A, Ley–Griffith oxidation of each parent alcohol **5a–5h** followed by MOM deprotection gave the

⁴² Ballatore, C.; Huryn, D. M.; Smith, A. B. Carboxylic Acid (Bio)Isosteres in Drug Design. *ChemMedChem* **2013**, *8* (3), 385–395

desired carboxylic acid hybrids as diastereomeric mixtures that were separated by HPLC to afford the pure *exo*-isomers.

Again we observed highly pronounced length-dependent LRH-1 activation by luciferase expression. While the hybrid compounds with shorter linkers (**13a–13d**, $n = 1–4$) did not appear to be better LRH-1 agonists than RJW100, the compounds with longer linkers were significantly more effective (activity of each compound by dose is visually depicted in Scheme 2.3B). The most efficacious agonist **13g (10CA)** effectively drives LRH-1 transcriptional activity (maximum activity = 2.3 ± 0.2 fold over vehicle) with significantly improved potency ($EC_{50} = 0.4 \pm 0.4 \mu\text{M}$), and length deviation on either side (i.e., shorter or longer linkers) resulted in loss of activity. Dose-response curves for the key compounds in this study are given in Scheme 2.3C. Although activities of the phosphorylcholine compounds **12** and DLPC do not appear to reach saturation (potentially due to low solubility and membrane incorporation), the synthetic hybrid **13g (10CA)** displayed a sigmoidal activation curve in this concentration range (Table 2.1).

Table 2.1. Summarized Activity Data for Hybrid PL Mimics

compound	EC_{50} (μM)	max. LRH-1 activation ^a
RJW100 (1)	1.1 ± 0.6	1.47 ± 0.06
11	13 ± 6	2.7 ± 0.3
12g	5 ± 2	2.1 ± 0.1
10CA (13g)	0.4 ± 0.4	2.3 ± 0.2

^a Maximum LRH-1 activation was calculated at the top of the resulting dose–response curves, as a fold increase in LRH-1 activity over baseline (vehicle).

2.4 Conclusions

Guided by structural insights from our laboratories (Chapter 1), we have incorporated key binding elements from two discrete ligand classes into a single hybrid scaffold. This ideal was first validated through synthesis of a 6HP phospholipid hybrid (**11**), which displayed significantly higher LRH-1 activation than either of the parent structures (RJW100 and DLPC). Simplification of this scaffold and systematic evaluation of various alkyl linkers revealed a clear correlation between linker length and LRH-1 activation, in support of our hypothesis that agonism could be improved through a dual binding mode. Substitution of the terminal phosphate groups with carboxylic acids afforded **10CA (13g)**, the most highly efficacious and potent LRH-1 agonist that has been reported to date.

2.5 Supporting Information.

General Synthetic Information

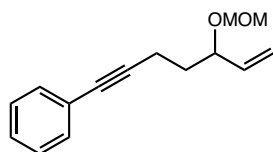
All reactions were carried out in oven-dried glassware, equipped with a stir bar and under a nitrogen atmosphere with dry solvents under anhydrous conditions, unless otherwise noted. Solvents used in anhydrous reactions were purified by passing over activated alumina and storing under argon. Yields refer to chromatographically and spectroscopically (¹H NMR) homogenous materials, unless otherwise stated. Reagents were purchased at the highest commercial quality and used without further purification, unless otherwise stated. n-Butyllithium (n-BuLi) was used as a 1.6 M or a 2.5 M solution in hexanes (Aldrich), was stored at 4°C and titrated prior to use. Organic solutions were concentrated under reduced pressure on a rotary evaporator using a water bath. Chromatographic purification of products was accomplished using forced-flow chromatography

on 230-400 mesh silica gel. Preparative thin-layer chromatography (PTLC) separations were carried out on 1000 μ m SiliCycle silica gel F-254 plates. Thin-layer chromatography (TLC) was performed on 250 μ m SiliCycle silica gel F-254 plates. Visualization of the developed chromatogram was performed by fluorescence quenching or by staining using KMnO_4 , p-anisaldehyde, or ninhydrin stains. ^1H and ^{13}C NMR spectra were obtained from the Emory University NMR facility and recorded on a Bruker Avance III HD 600 equipped with cryo-probe (600 MHz), INOVA 600 (600 MHz), INOVA 500 (500 MHz), INOVA 400 (400 MHz), VNMR 400 (400 MHz), or Mercury 300 (300 MHz), and are internally referenced to residual protio solvent signals. Data for ^1H NMR are reported as follows: chemical shift (ppm), multiplicity (s = singlet, d = doublet, t = triplet, q = quartet, m = multiplet, dd = doublet of doublets, dt = doublet of triplets, ddd = doublet of doublet of doublets, dtd = doublet of triplet of doublets, b = broad, etc.), coupling constant (Hz), integration, and assignment, when applicable. Data for decoupled ^{13}C NMR are reported in terms of chemical shift and multiplicity when applicable. IR spectra were recorded on a Thermo Fisher DiamondATR and reported in terms of frequency of absorption (cm^{-1}). High Resolution mass spectra were obtained from the Emory University Mass Spectral facility. Gas Chromatography Mass Spectrometry (GC-MS) was performed on an Agilent 5977A mass spectrometer with an Agilent 7890A gas chromatography inlet. Liquid Chromatography Mass Spectrometry (LC-MS) was performed on an Agilent 6120 mass spectrometer with an Agilent 1220 Infinity liquid chromatography inlet. Preparative High Pressure Liquid chromatography (Prep-HPLC) was performed on an Agilent 1200 Infinity Series chromatograph using an Agilent Prep-C18 30 x 250 mm 10 μ m column, or an Agilent Prep-C18 21.2 x 100 mm, 5 μ m column.

Evaluation of Compound Purity

Purity of all tested compounds was determined by HPLC analysis, using the methods given below (as indicated for each compound). Method A: A linear gradient using water and 0.1 % formic acid (FA) (Solvent A) and MeCN and 0.1% FA (Solvent B); t = 0 min, 50% B, t = 4 min, 99% B (held for 1 min), then 50% B for 1 min, was employed on an Agilent Poroshell 120 EC-C18 2.7 micron, 3.0 mm x 50 mm column (flow rate 1 mL/min) or an Agilent Zorbax SB-C18 1.8 micron, 2.1 mm x 50 mm column (flow S2 rate 0.8 mL/min). The UV detection was set to 254 nm. The LC column was maintained at ambient temperature. Method B: An isocratic method using 65% MeCN, 45% water, and 0.1 % FA was employed on an Agilent Poroshell 120 EC-C18 2.7 micron, 3.0 mm x 50 mm column (flow rate 1 mL/min) or an Agilent Zorbax SB-C18 1.8 micron, 2.1 mm x 50 mm column (flow rate 0.8 mL/min). The UV detection was set to 254 nm. The LC column was maintained at ambient temperature.

Chemical Syntheses

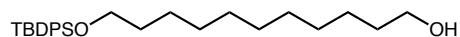


(5-(methoxymethoxy)hept-6-en-1-yn-1-yl)benzene: Under nitrogen, 7-phenylhept-1-en-6-yn-3-ol (1.97 g, 11 mmol, 1.0 equiv) was dissolved in DCM (50 mL), followed by the addition of N,N-diisopropylethylamine (2.3 mL, 13 mmol, 1.2 equiv) and chloromethyl methyl ether (1.2 mL, 16 mmol, 1.5 equiv). The reaction was stirred at 30 °C for 4 h, then cooled to ambient temperature

and poured onto water, extracted with DCM, and washed with 1M HCl. The combined organic layers were dried with MgSO₄, filtered, and concentrated before purification on silica (5% EtOAc/Hex eluent) to afford the title compound (2.4 g, 98%).

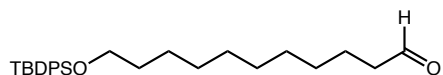
¹H NMR (600 MHz, CDCl₃) δ 7.42 – 7.35 (m, 2H), 7.32 – 7.22 (m, 3H), 5.70 (ddd, J = 17.6, 10.4, 7.6 Hz, 1H), 5.27 (dt, J = 17.1, 1.4 Hz, 1H), 5.22 (dt, J = 10.4, 1.3 Hz, 1H), 4.73 (d, J = 6.8 Hz, 1H), 4.57 (d, J = 6.7 Hz, 1H), 4.22 (td, J = 7.8, 5.3 Hz, 1H), 3.40 (d, J = 1.5 Hz, 3H), 2.60 – 2.45 (m, 2H), 1.95 – 1.84 (m, 1H), 1.84 – 1.76 (m, 1H).

¹³C NMR (151 MHz, CDCl₃) δ 137.7, 131.5, 128.2, 127.6, 123.9, 117.7, 93.8, 89.4, 81.0, 75.8, 55.5, 34.4, 15.6.



Representative Dibromoalkane Synthesis: Compound 3g 11-((tert-butyldiphenylsilyl)oxy)undecan-1-ol (S1a): A solution of 1,11-undecanediol (6.9 g, 37 mmol, 2.0 equiv) in THF (100 mL) was treated with imidazole (1.2 g, 18 mmol, 1.0 equiv) and tert-butyldiphenylsilylchloride (TBDPS-Cl, 4.9 g, 18 mmol, 1.0 equiv). The reaction was stirred for 16 h. The entire reaction was passed through celite to remove ammonium salts, then the filtrate was concentrated. The crude oil was purified on silica (5-20% EtOAc/Hex eluent) to give the desired compound S1a as a clear, colorless oil (5.7 g, 74%).

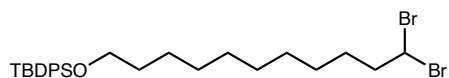
¹H NMR (600 MHz, CDCl₃) δ 7.68 – 7.61 (m, 4H), 7.45 – 7.32 (m, 6H), 3.68 – 3.54 (t, 4H), 1.64 – 1.44 (m, 4H), 1.37 – 1.21 (m, 14H), 1.03 (s, 9H). ¹³C NMR (126 MHz, CDCl₃) δ 135.6, 134.2, 129.5, 127.5, 64.0, 63.1, 32.8, 32.6, 29.6, 29.5, 29.43, 29.37, 26.9, 25.8, 25.7, 19.2.



11-((tertbutyldiphenylsilyloxy)undecanal (S1b): A solution of S1a (2.2 g, 5.2 mmol, 1.0 equiv) was dissolved in DCM (100 mL). Trichloroisocyanuric acid (1.35 g, 5.8 mmol, 1.1 equiv) and (2,2,6,6-tetramethylpiperidin-1-yl)oxyl (TEMPO, 76.7 mg, 0.5 mmol, 0.01 equiv.) were added. The reaction mixture was allowed to stir at room temperature until the reaction was complete by TLC (fewer than 5 minutes). The reaction was quenched with saturated aqueous NaHCO₃ and stirred for 5 minutes. The reaction mixture was poured onto water and extracted with DCM three times. The combined organic layers were washed with 1M aqueous HCl, brine, dried with MgSO₄, and concentrated. The crude oil was purified on silica (5-10% EtOAc/Hex eluent) to afford the title compound S1b as a clear, colorless oil (2.0 g, 93%)

¹H NMR (600 MHz, CDCl₃) δ 9.74 (t, J = 1.9 Hz, 1H), 7.65 (m, 4H), 7.42 – 7.33 (m, 6H), 3.63 (td, J = 6.5, 3.4 Hz, 2H), 2.40 (m, 2H), 1.60 (m, 2H), 1.53 (m, 2H), 1.35 – 1.20 (m, 12H), 1.06 – 1.00 (s, 9H).

¹³C NMR (151 MHz, CDCl₃) δ 202.9, 135.5, 134.1, 129.4, 127.5, 63.9, 43.9, 32.5, 29.34, 29.26, 29.1, 26.8, 25.8, 25.7, 19.2.



tert-butyl((11,11-dibromoundecyl)oxy)diphenylsilane (3g): Under nitrogen, a solution of triphenylphosphite (4.0 mL, 15 mmol, 1.1 equiv) in DCM (100 mL) was cooled to -78 °C. Bromine (0.8 mL, 16 mmol, 1.1 equiv) and triethylamine (2.2 mL, 16 mmol, 1.1 equiv) were sequentially added dropwise at -78 °C. The reaction was stirred for 5 minutes, then S1b (5.8 g, 14 mmol, 1.0

equiv) was added as a solution in DCM (10 mL) via syringe at -78 °C. The reaction was stirred for 5 h and allowed to warm to ambient temperature. The whole reaction was then poured over a pad of silica. The filtrate was concentrated and purified on a short plug of silica in 100% Hex to afford the title compound as a clear, colorless oil (7.7 g, 99%).

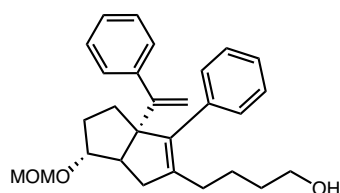
¹H NMR (600 MHz, CDCl₃) δ 7.68 – 7.62 (m, 4H), 7.44 – 7.33 (m, 6H), 5.68 (t, J = 6.2 Hz, 1H), 3.63 (t, J = 6.6 Hz, 2H), 2.41 – 2.31 (m, 2H), 1.57 – 1.46 (m, 4H), 1.35 – 1.20 (m, 12H), 1.03 (s, 9H).

¹³C NMR (75 MHz, CDCl₃) δ 135.6, 134.1, 129.5, 127.6, 64.0, 46.4, 45.4, 32.5, 29.4, 29.3, 28.2, 28.1, 26.9, 25.7, 19.2.

Cyclization Procedure: Compounds 5a–h

Hexahydropentalene formation was accomplished through slight modification of Whitby's procedure.¹⁶ Prior to cyclization, all reagents were dried by azeotropic removal of water using benzene. A dry round bottom flask containing bis(cyclopentadienyl)zirconium(IV) dichloride (1.2 equiv) under nitrogen, was dissolved in anhydrous, degassed tetrahydrofuran (THF, 50 mL/mmol enyne) and cooled to -78 °C. The resulting solution was treated with n-BuLi (2.4 equiv.) and the light yellow solution was stirred for 30 minutes. A solution of **4** (5- (methoxymethoxy)hept-6-en-1-yn-1-yl)benzene (1.0 equiv) in anhydrous, degassed THF (5 mL/mmol) was added. The resulting salmon-colored mixture was stirred at -78 °C for 30 minutes, the cooling bath removed, and the reaction mixture was allowed to warm to ambient temperature with stirring (2.5 hours total). The reaction mixture was then cooled to -78 °C and the required 1,1-dibromoalkane (**3a–3h**, 1.1 equiv) was added as a solution in anhydrous THF (5 mL/mmol) followed by freshly prepared lithium diisopropylamide (LDA, 1.0 M, 1.1 equiv.). After 15 minutes, a freshly prepared solution of

lithium phenylacetylide (3.6 equiv.) in anhydrous THF was added dropwise and the resulting rust-colored solution was stirred at $-78\text{ }^{\circ}\text{C}$ for 1.5 hours. The reaction was quenched with methanol and saturated aqueous sodium bicarbonate and allowed to warm to room temperature, affording a light yellow slurry. The slurry was poured onto water and extracted with ethyl acetate four times. The combined organic layers were washed with brine, dried with MgSO_4 , and concentrated in vacuo. The resulting yellow oil was passed through a short plug of silica (20% EtOAc/Hex eluent) and concentrated. The crude product was dissolved in THF (50–100 mL) and treated with solid tetrabutylammonium fluoride hydrate (ca. 2.0 equiv.) and the resulting solution stirred at room temperature for 16 h. The reaction mixture was concentrated and purified by silica gel chromatography (20% EtOAc/Hex eluent) to afford the title compound **5a–5h** as a 7:1 mixture of diastereomers, favoring the desired exo-isomer (drawn).



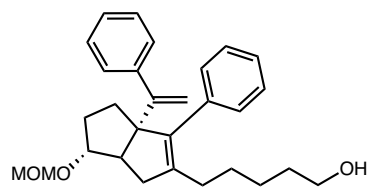
4-(6-exo-(methoxymethoxy)-3-phenyl-3a-(1-phenylvinyl)-1,3a,4,5,6,6a-hexahydroindolen-2-yl)butan-1-ol (5a): According to the general procedure, tert-butyl((5,5-dibromopentyl) oxy) diphenylsilane (798.6 mg, 1.7 mmol) was reacted with **4** (342.2 mg, 1.5 mmol,) to give the title compound (7:1 dr) as a yellow oil (349.4 mg, 56% over 2 steps).

For the exo diastereomer (drawn): $^1\text{H NMR}$ (400 MHz, CDCl_3) δ 7.35 – 7.11 (m, 10H), 5.03 (d, $J = 1.5\text{ Hz}$, 1H), 4.99 (d, $J = 1.5\text{ Hz}$, 1H), 4.60 – 4.52 (m, 2H), 3.81 – 3.71 (m, 1H), 3.54 (t, $J = 6.2\text{ Hz}$, 2H), 3.29 (s, 3H), 2.47 – 2.35 (m, 1H), 2.31 – 2.26 (m, 1H), 2.09 – 1.99 (m, 4H), 1.78 – 1.54 (m, 4H), 1.52 – 1.35 (m, 3H).

^{13}C NMR (126 MHz, CDCl_3) δ 154.4, 144.0, 140.8, 139.7, 137.3, 129.6, 127.8, 127.70, 127.65, 126.6, 114.9, 94.7, 86.7, 69.1, 62.6, 55.2, 52.8, 40.4, 32.7, 32.4, 31.5, 29.4, 24.0.

LRMS (ESI, APCI) m/z : calc'd for $\text{C}_{27}\text{H}_{31}\text{O}_2$ $[\text{M}-\text{OCH}_3]^+$ 387.2, found 386.9.

For the *endo* diastereomer (characteristic signals): ^1H NMR (400 MHz, CDCl_3) δ 5.06 (d, $J = 1.3$ Hz, 1H), 4.84 (d, $J = 1.4$ Hz, 1H), 4.00 (td, $J = 9.8, 6.1$ Hz, 1H), 2.64 (dd, $J = 17.1, 2.4$ Hz, 1H), 2.53 (td, $J = 9.0, 2.2$ Hz, 1H).

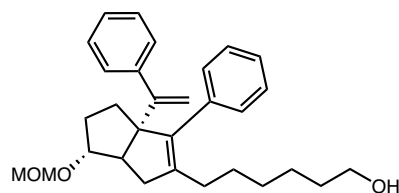


5-(6-*exo*-(methoxymethoxy)-3-phenyl-3a-(1-phenylvinyl)-1,3a,4,5,6,6a-hexahydropentalen-2-yl)pentan-1-ol (5b): According to the general procedure, *tert*-butyl((6,6-dibromohexyl)oxy)diphenylsilane (529.1 mg, 0.95 mmol) was reacted with **4** (203.4 mg, 0.88 mmol) to give the title compound (7:1 dr) as a yellow oil (301.0 mg, 70% over 2 steps).

For the *exo* diastereomer (drawn): ^1H NMR (600 MHz, CDCl_3) δ 7.41 – 7.10 (m, 10H), 5.01 (d, $J = 1.4$ Hz, 1H), 4.97 (d, $J = 1.4$ Hz, 1H), 4.60 – 4.51 (m, 2H), 3.76 (s, 1H), 3.55 (t, $J = 6.5$ Hz, 2H), 3.27 (s, 3H), 2.39 (d, $J = 8.6$ Hz, 1H), 2.29 (dd, $J = 18.2, 9.6$ Hz, 1H), 2.10 – 1.88 (m, 4H), 1.75 – 1.50 (m, 2H), 1.50 – 1.42 (m, 2H), 1.41 – 1.22 (m, 5H).

LRMS (ESI, APCI) m/z : calc'd for $\text{C}_{28}\text{H}_{33}\text{O}_2$ $[\text{M}-\text{OCH}_3]^+$ 401.2, found 401.2.

For the *endo* diastereomer (characteristic signals): ^1H NMR (600 MHz, CDCl_3) δ 5.07 (d, $J = 1.3$ Hz, 1H), 4.84 (d, $J = 1.4$ Hz, 1H), 4.00 (td, $J = 10.3, 5.8$ Hz, 1H), 2.63 (dd, $J = 17.3, 2.3$ Hz, 1H), 2.52 (td, $J = 9.2, 2.1$ Hz, 1H).



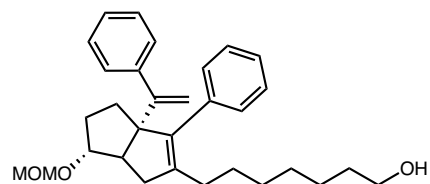
6-(6-*exo*-(methoxymethoxy)-3-phenyl-3a-(1-phenylvinyl)-1,3a,4,5,6,6a-hexahydropentalen-2-yl)hexan-1-ol (5c): According to the general procedure, *tert*-butyl((7,7-dibromoheptyl)oxy)diphenylsilane (908.2 mg, 1.8 mmol) was reacted with **4** (355.9 mg, 1.5 mmol) to give the title compound (7:1 dr) as a yellow oil (431.8 mg, 63% over 2 steps).

For the *exo* diastereomer (drawn): $^1\text{H NMR}$ (600 MHz, CDCl_3) δ 7.36 – 7.11 (m, 10H), 5.03 (s, 1H), 4.98 (s, 1H), 4.61 – 4.51 (m, 2H), 3.77 (s, 1H), 3.57 (t, $J = 6.7$ Hz, 2H), 3.29 (s, 3H), 2.40 (d, $J = 9.1, 1.8$ Hz, 1H), 2.30 (dd, $J = 16.9, 9.3$ Hz, 1H), 2.10 – 1.96 (m, 4H), 1.79 – 1.53 (m, 2H), 1.54 – 1.45 (m, 2H), 1.43 – 1.23 (m, 7H).

$^{13}\text{C NMR}$ (126 MHz, CDCl_3) δ 154.5, 144.1, 141.1, 139.4, 137.4, 134.8, 129.6, 127.8, 127.63, 126.59, 114.9, 94.7, 86.7, 69.1, 62.8, 55.1, 52.8, 40.5, 32.6, 32.41, 31.42, 29.6, 29.4, 27.8, 25.5.

LRMS (ESI, APCI) m/z : calc'd for $\text{C}_{29}\text{H}_{35}\text{O}_2$ $[\text{M}-\text{OCH}_3]^+$ 415.3, found 415.3.

For the *endo* diastereomer (characteristic signals): $^1\text{H NMR}$ (600 MHz, CDCl_3) δ 5.08 (d, $J = 1.4$ Hz, 1H), 4.85 (d, $J = 1.4$ Hz, 1H), 4.01 (td, $J = 9.8, 5.6$ Hz, 1H), 2.65 (dd, $J = 17.3, 2.2$ Hz, 1H), 2.54 (td, $J = 9.1, 2.3$ Hz, 1H).



7-(6-*exo*-(methoxymethoxy)-3-phenyl-3a-(1-phenylvinyl)-1,3a,4,5,6,6a-hexahydropentalen-2-yl)heptan-1-ol (5d): According to the general procedure, *tert*-butyl((8,8-

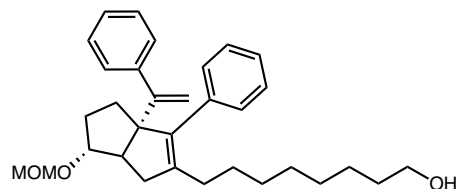
dibromooctyl)oxy)diphenylsilane (732.9 mg, 1.4 mmol) was reacted with **4** (287.5 mg, 1.2 mmol) to give the title compound (7:1 dr) as a yellow oil (303.2 mg, 55% over 2 steps).

For the *exo* diastereomer: $^1\text{H NMR}$ (600 MHz, CDCl_3) δ 7.46 – 7.02 (m, 10H), 5.05 (s, 1H), 5.00 (s, 1H), 4.62 – 4.56 (m, 2H), 3.79 (s, 1H), 3.66 – 3.60 (m, 2H), 3.30 (s, 3H), 2.41 (d, $J = 9.4$ Hz, 1H), 2.32 (dd, $J = 17.0, 9.2$ Hz, 1H), 2.08 – 1.92 (m, 4H), 1.78 – 1.67 (m, 2H), 1.59 – 1.49 (m, 2H), 1.44 – 1.19 (m, 9H).

$^{13}\text{C NMR}$ (126 MHz, CDCl_3) δ 154.5, 144.1, 141.2, 139.3, 137.5, 129.6, 127.8, 127.63, 126.57, 114.9, 94.7, 86.7, 69.1, 63.0, 55.1, 52.8, 40.5, 32.7, 32.4, 31.4, 29.64, 29.58, 29.2, 27.7, 25.6.

LRMS (ESI, APCI) m/z : calc'd for $\text{C}_{30}\text{H}_{37}\text{O}_2$ $[\text{M}-\text{OCH}_3]^+$ 429.3, found 428.8.

For the *endo* diastereomer (characteristic signals): $^1\text{H NMR}$ (600 MHz, CDCl_3) δ 5.08 (d, $J = 1.3$ Hz, 1H), 4.85 (d, $J = 1.2$ Hz, 1H), 4.00 (td, $J = 9.6, 5.6$ Hz, 1H), 2.65 (dd, $J = 17.4, 2.1$ Hz, 1H), 2.53 (td, $J = 8.9, 2.2$ Hz, 1H).



8-(6-*exo*-(methoxymethoxy)-3-phenyl-3a-(1-phenylvinyl)-1,3a,4,5,6,6a-hexahydropentalen-2-yl)octan-1-ol (5e): According to the general procedure, *tert*-butyl((9,9-dibromononyl)oxy)diphenylsilane (709.8 mg, 1.3 mmol) was reacted with **4** (274.4 mg, 1.2 mmol) to afford the title compound (7:1 dr) as a yellow oil (441.5 mg, 78% over 2 steps).

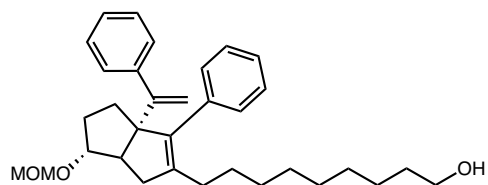
For the *exo* diastereomer: $^1\text{H NMR}$ (500 MHz, CDCl_3) δ 7.41 – 7.18 (m, 10H), 5.05 (d, $J = 1.5$ Hz, 1H), 5.01 (d, $J = 1.5$ Hz, 1H), 4.63 – 4.53 (m, 2H), 3.79 (s, 1H), 3.62 (t, $J = 6.7$ Hz, 2H), 3.31

(s, 3H), 2.42 (d, $J = 9.4$, 1.8 Hz, 1H), 2.32 (dd, $J = 16.9$, 9.1 Hz, 1H), 2.11 – 1.97 (m, 4H), 1.83 – 1.54 (m, 4H), 1.59 – 1.50 (m, 2H), 1.38 – 1.17 (m, 9H).

^{13}C NMR (126 MHz, CDCl_3) δ 154.5, 144.1, 141.3, 139.3, 137.5, 129.6, 127.8, 127.6, 126.59, 126.55, 114.8, 94.7, 86.7, 69.1, 63.0, 55.1, 52.8, 40.5, 32.8, 32.4, 31.4, 29.7, 29.6, 29.33, 29.27, 27.8, 25.7.

LRMS (ESI, APCI) m/z : calc'd for $\text{C}_{31}\text{H}_{39}\text{O}_2$ $[\text{M}-\text{OCH}_3]^+$ 443.3, found 442.9.

For the *endo* diastereomer (characteristic signals): ^1H NMR (500 MHz, CDCl_3) δ 5.08 (d, $J = 1.3$ Hz, 1H), 4.85 (d, $J = 1.3$ Hz, 1H), 4.01 (td, $J = 9.6$, 5.8 Hz, 1H), 2.65 (dd, $J = 17.4$, 2.1 Hz, 1H), 2.53 (td, $J = 8.9$, 2.2 Hz, 1H).



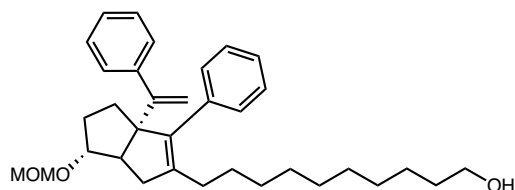
9-(6-*exo*-(methoxymethoxy)-3-phenyl-3a-(1-phenylvinyl)-1,3a,4,5,6,6a-hexahydropentalen-2-yl)nonan-1-ol (5f): According to the general procedure, *tert*-butyl((10,10-dibromodecyl)oxy)diphenylsilane (577.2 mg, 1.0 mmol) was reacted with **4** (206.7 mg, 0.9 mmol) to give the title compound (7:1 dr) as a yellow oil (249.6 mg, 57% over 2 steps).

For the *exo* diastereomer: ^1H NMR (500 MHz, CDCl_3) δ 7.39 – 7.15 (m, 10H), 5.06 (d, $J = 1.4$ Hz, 1H), 5.01 (d, $J = 1.5$ Hz, 1H), 4.62 – 4.56 (m, 2H), 3.80 (s, 1H), 3.62 (t, $J = 6.7$ Hz, 2H), 3.32 (s, 3H), 2.43 (d, $J = 9.1$, 1.7 Hz, 1H), 2.33 (dd, $J = 16.9$, 9.2 Hz, 1H), 2.11 – 1.99 (m, 4H), 1.79 – 1.60 (m, 4H), 1.60 – 1.51 (m, 2H), 1.43 – 1.17 (m, 11H).

^{13}C NMR (126 MHz, CDCl_3) δ 154.5, 144.1, 141.3, 139.2, 137.5, 129.6, 127.8, 127.6, 126.62, 126.56, 114.9, 94.7, 86.7, 69.1, 63.0, 55.2, 52.7, 40.5, 32.8, 32.4, 31.4, 29.7, 29.6, 29.5, 29.4, 29.3, 27.8, 25.7.

LRMS (ESI, APCI) m/z : calc'd for $C_{32}H_{41}O_2$ $[M-CH_3O]^+$ 457.3, found 457.8.

For the *endo* diastereomer (characteristic signals): **1H NMR** (500 MHz, $CDCl_3$) δ 5.09 (d, $J = 1.4$ Hz, 1H), 4.86 (d, $J = 1.4$ Hz, 1H), 4.01 (td, $J = 9.6, 5.8$ Hz, 1H), 2.66 (dd, $J = 17.3, 2.4$ Hz, 1H), 2.54 (td, $J = 9.0, 2.3$ Hz, 1H).



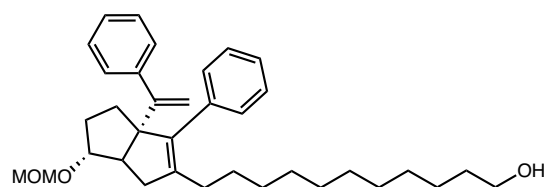
10-(6-*exo*-(methoxymethoxy)-3-phenyl-3a-(1-phenylvinyl)-1,3a,4,5,6,6a-hexahydropentalen-2-yl)decan-1-ol (5g): According to the general procedure, *tert*-butyl((11,11-dibromoundecyl)oxy)diphenylsilane (1.24 g, 2.2 mmol) was reacted with **4** (463.9 mmol, 2.0 mmol) to give the title compound (7:1 dr) as a yellow oil (584.1 mg, 58% over 2 steps).

For the *exo* diastereomer: **1H NMR** (500 MHz, $CDCl_3$) δ 7.41 – 7.17 (m, 10H), 5.07 (d, $J = 1.4$ Hz, 1H), 5.02 (d, $J = 1.5$ Hz, 1H), 4.64 – 4.56 (m, 2H), 3.81 (p, $J = 2.1$ Hz, 1H), 3.62 (d, $J = 6.6$ Hz, 2H), 3.32 (s, 3H), 2.44 (dq, $J = 9.2, 1.7$ Hz, 1H), 2.35 (dd, $J = 16.9, 9.2$ Hz, 1H), 2.11 – 2.00 (m, 4H), 1.81 – 1.63 (m, 4H), 1.57 (m, 2H), 1.40 – 1.19 (m, 13H).

^{13}C NMR (126 MHz, $CDCl_3$) δ 154.5, 144.1, 141.3, 139.2, 137.5, 129.6, 127.8, 127.6, 126.62, 126.56, 114.9, 94.7, 86.7, 69.1, 63.0, 55.2, 52.7, 40.5, 32.8, 32.4, 31.4, 29.7, 29.6, 29.5, 29.4, 29.3, 27.8, 25.7.

LRMS (ESI, APCI) m/z : calc'd for $C_{33}H_{43}O_2$ $[M-CH_3O]^+$ 471.3, found 470.9.

For the *endo* diastereomer (characteristic signals): **1H NMR** (500 MHz, $CDCl_3$) δ 5.10 (d, $J = 1.3$ Hz, 1H), 4.87 (d, $J = 1.4$ Hz, 1H), 4.03 (td, $J = 9.7, 5.6$ Hz, 1H), 2.68 (dd, $J = 17.3, 2.3$ Hz, 1H), 2.56 (td, $J = 9.0, 2.3$ Hz, 1H).



11-(6-*exo*-(methoxymethoxy)-3-phenyl-3a-(1-phenylvinyl)-1,3a,4,5,6,6a-hexahydropentalen-2-yl)undecan-1-ol (5h): According to the general procedure, *tert*-butyl((12,12-dibromododecyl)oxy)diphenylsilane (703.6 mg, 1.2 mmol) was reacted with **4** (250.2 mg, 1.1 mmol) to give the title compound (7:1 dr) as a yellow oil (325.7 mg, 58% over 2 steps).

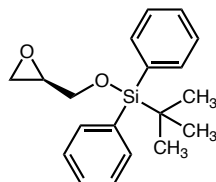
For the *exo* diastereomer: $^1\text{H NMR}$ (500 MHz, CDCl_3) δ 7.42 – 7.16 (m, 10H), 5.08 (d, $J = 1.5$ Hz, 1H), 5.03 (d, $J = 1.5$ Hz, 1H), 4.65 – 4.56 (m, 3H), 3.82 (s, 1H), 3.64 (t, $J = 6.7$ Hz, 2H), 3.33 (s, 3H), 2.45 (d, $J = 9.2, 1.7$ Hz, 1H), 2.36 (dd, $J = 16.9, 9.2$ Hz, 1H), 2.13 – 2.00 (m, 4H), 1.89 – 1.61 (m, 4H), 1.62 – 1.51 (m, 2H), 1.41 – 1.19 (m, 15H).

$^{13}\text{C NMR}$ (126 MHz, CDCl_3) δ 154.5, 144.1, 141.4, 139.2, 137.5, 129.6, 127.8, 127.7, 126.64, 126.58, 114.9, 94.7, 86.8, 69.1, 62.9, 55.2, 52.7, 40.6, 32.8, 32.5, 31.5, 29.7, 29.7, 29.61, 29.58, 29.54, 29.46, 29.4, 27.9, 25.8.

LRMS (ESI, APCI) m/z : calc'd for $\text{C}_{34}\text{H}_{45}\text{O}_2$ $[\text{M}-\text{CH}_3\text{O}]^+$ 485.3, found 484.9.

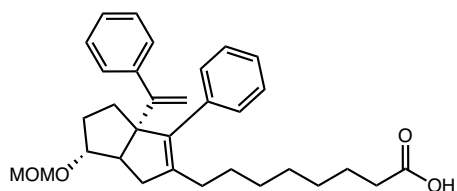
For the *endo* diastereomer (characteristic signals): $^1\text{H NMR}$ (500 MHz, CDCl_3) δ 5.11 (d, $J = 1.4$ Hz, 1H), 4.88 (d, $J = 1.4$ Hz, 1H), 4.03 (td, $J = 9.8, 5.8$ Hz, 1H), 2.68 (dd, $J = 17.3, 2.3$ Hz, 1H), 2.57 (td, $J = 9.0, 2.3$ Hz, 1H).

Synthesis of PL Mimic 11



(*R*)-tert-butyl(oxiran-2-ylmethoxy)diphenylsilane (7): A solution of (*S*)-oxiran-2-ylmethanol (1.1 g, 15 mmol, 1.0 equiv) in THF (50 mL) was treated with TBDPS-Cl (4.9 g, 18 mmol, 1.2 equiv) and imidazole (1.2 g, 18 mmol, 1.2 equiv.) The resulting suspension was stirred for 16 h. The entire reaction was filtered through celite, the filtrate was concentrated, and the crude oil was purified on silica (5% EtOAc/Hex eluent) to afford the title compound as a clear, colorless oil (3.5g, 74%).

¹H NMR (500 MHz, CDCl₃) δ 7.82 – 7.63 (m, 4H), 7.54 – 7.33 (m, 6H), 3.91 (dd, *J* = 11.8, 3.2 Hz, 1H), 3.75 (dd, *J* = 11.9, 4.7 Hz, 1H), 3.17 (ddt, *J* = 4.9, 4.2, 2.9 Hz, 1H), 2.77 (dd, *J* = 5.2, 4.1 Hz, 1H), 2.65 (dd, *J* = 5.2, 2.7 Hz, 1H), 1.11 (s, 9H). Spectroscopic data are consistent with reported values.⁴³



8-(6-*exo*-(methoxymethoxy)-3-phenyl-3a-(1-phenylvinyl)-1,3a,4,5,6,6a-hexahydropentalen-2-yl)octanoic acid (6): A solution of **5e** (449.0 mg, 1.2 mmol) in acetonitrile (20 mL) was treated with tetrapropylammonium perruthenate (TPAP, 4.4 mg, 0.01 mmol, 0.1 equiv), N-

⁴³ Díaz, Y.; Bravo, F.; Castillón, S. J. Org. Chem. 1999, 64, 6508.

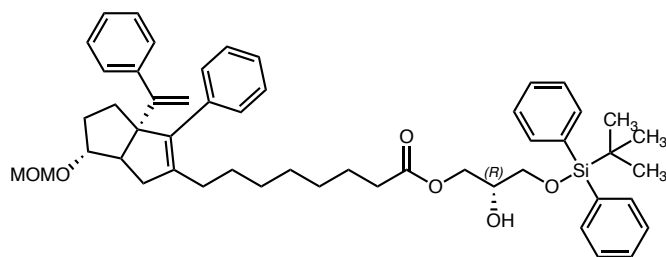
Methylmorpholine-N-Oxide (NMO, 700.2 mg, 6 mmol, 5.0 equiv.), and water (100 μ L, 6 mmol, 5 equiv.). The reaction mixture was allowed to stir until complete by TLC and LCMS, 1-16 h. Upon reaction completion, the reaction mixture was directly concentrated and purified on silica (20-50% EtOAc (containing 0.1% AcOH)/Hex to afford the title compound **6** (7:1 dr) as a clear, colorless oil (489.9 mg, 85%).

For the *exo* diastereomer: $^1\text{H NMR}$ (500 MHz, CDCl_3) δ 7.40 – 7.19 (m, 10H), 5.07 (d, $J = 1.5$ Hz, 1H), 5.02 (d, $J = 1.5$ Hz, 1H), 4.64 – 4.59 (m, 2H), 3.81 (s, 1H), 3.33 (s, 3H), 2.44 (d, $J = 9.5$ Hz, 1H), 2.38 – 2.29 (m, 3H), 2.12 – 1.99 (m, 5H), 1.81 – 1.56 (m, 5H), 1.40 – 1.19 (m, 7H).

For the *endo* diastereomer (characteristic signals): (500 MHz, CDCl_3) δ 5.08 (d, $J = 1.4$ Hz, 1H), 4.85 (d, $J = 1.3$ Hz, 1H), 4.01 (td, $J = 9.1, 5.6$ Hz, 1H), 2.64 (d, $J = 17.5$ Hz, 1H), 2.54 (t, $J = 9.1$ Hz, 1H).

$^{13}\text{C NMR}$ (126 MHz, CDCl_3) δ 179.7, 154.5, 144.1, 141.2, 139.4, 137.4, 129.6, 127.8, 127.7, 127.6, 126.62, 126.60, 114.9, 94.7, 86.8, 69.1, 55.1, 52.8, 40.5, 34.0, 32.4, 31.5, 29.6, 29.4, 28.9, 29.0, 27.7, 24.7.

LRMS (ESI, APCI) m/z : calc'd for $\text{C}_{32}\text{H}_{39}\text{O}_4$ [$\text{M}-\text{H}$] $^-$ 487.3, found 487.2. Calc'd for $\text{C}_{31}\text{H}_{37}\text{O}_3$ [$\text{M}-\text{CH}_3\text{O}$] $^+$ 457.3, found 456.8.



***R*-3-((*tert*-butyldiphenylsilyl)oxy)-2-hydroxypropyl 8-(6-(*exo*)-(methoxymethoxy)-3-phenyl-3a-(1-phenylvinyl)-1,3a,4,5,6,6a-hexahydropentalen-2-yl)octanoate (**8**):** A solution of **6** (111.9 mg, 0.23 mmol) in diethyl ether (1 mL) was treated with co[*salen*] ((*S,S*)-(+)-*N,N'*bix(3,5-di-*tert*-

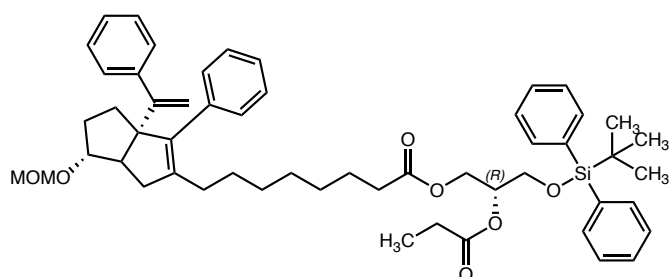
butylsalicylidene)-1,2-cyclohexanediamono cobalt (II) (3.6 mg, 0.006 mmol, 0.03 equiv) and the reaction was allowed to stir for 1 h open to air. After 1 h, the diethylether was evaporated. **7** (76.1 mg, 0.24 mmol, 1.0 equiv) and diisopropylethylamine (40 μ L, 0.23 mmol, 1.0 equiv) were added and the reaction was stirred neat at ambient temperature for 16 h. The crude reaction mixture was directly purified on silica (5-10% EtOAc/Hex eluent) to give the title compound (**7**:1 dr) as a clear, colorless oil (44.0 mg, 24%).

For the *exo* diastereomer: **¹H NMR** (600 MHz, CDCl₃) δ 7.70 – 7.62 (m, 4H), 7.47 – 7.18 (m, 16H), 5.05 (d, J = 1.4 Hz, 1H), 5.00 (d, J = 1.4 Hz, 1H), 4.63 – 4.56 (m, 2H), 4.18 (dd, J = 11.5, 4.7 Hz, 1H), 4.15 (dd, J = 11.2, 6.3 Hz, 1H), 3.94 (p, J = 5.5 Hz, 1H), 3.80 – 3.77 (m, 1H), 3.71 (dd, J = 10.4, 4.8 Hz, 1H), 3.66 (dd, J = 10.4, 5.6 Hz, 1H), 3.31 (s, 3H), 2.54 (d, J = 5.5 Hz, 1H), 2.41 (d, J = 9.0 Hz, 1H), 2.32 (dd, J = 16.9, 9.3 Hz, 1H), 2.27 (t, J = 7.5 Hz, 2H), 2.09 – 1.97 (m, 4H), 1.78 – 1.68 (m, 1H), 1.69 – 1.60 (m, 1H), 1.60 – 1.47 (m, 2H), 1.36 – 1.15 (m, 9H), 1.06 (s, 9H).

¹³C NMR (126 MHz, CDCl₃) δ 173.8, 154.5, 144.1, 141.2, 139.3, 137.4, 135.73, 135.69, 135.5, 132.9, 129.9, 129.6, 127.8, 127.7, 127.64, 127.61, 126.60, 126.57, 114.9, 94.7, 86.7, 70.1, 69.1, 65.0, 64.5, 63.6, 55.1, 52.8, 40.5, 34.1, 32.4, 31.4, 29.7, 29.5, 29.0, 27.8, 26.9, 26.8, 24.8.

LRMS (ESI, APCI) m/z : calc'd for C₅₀H₆₁O₅Si [M-OCH₃]⁺ 769.4, found 769.6.

For the *endo* diastereomer (characteristic signals): **¹H NMR** (600 MHz, CDCl₃) δ 5.08 (d, J = 1.3 Hz, 1H), 4.85 (d, J = 1.3 Hz, 1H), 4.00 (td, J = 9.5, 5.9 Hz, 1H), 2.65 (d, J = 17.3 Hz, 1H).



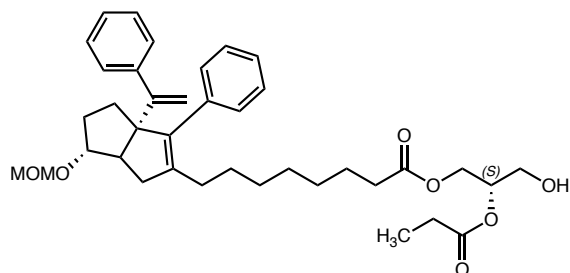
(R)-3-((tert-butyl-diphenylsilyloxy)-2-(propionyloxy)propyl 8-(6-(exo)-(methoxymethoxy)-3-phenyl-3a-(1-phenylvinyl)-1,3a,4,5,6,6a-hexahydropentalen-2-yl)octanoate (9): A solution of **8** (44 mg, 0.05 mmol, 1.0 equiv) in DCM (4 mL) was treated with propionyl chloride (18 μ L, 0.2 mmol, 4.0 equiv) and DMAP (29.4 mg, 0.24 mol, 4.8 equiv). The reaction was allowed to stir for 4 h. The resulting reaction mixture was directly concentrated and purified on silica (5-10% EtOAc/Hex eluent) to give the title compound (7:1 dr) as a clear, colorless oil (35.0 mg, 77%).

For the *exo* diastereomer: $^1\text{H NMR}$ (500 MHz, CDCl_3) δ 7.69 – 7.60 (m, 4H), 7.50 – 7.16 (m, 16H), 5.23 – 5.14 (m, 1H), 5.06 (s, 1H), 5.02 (s, 1H), 4.62 – 4.58 (m, 2H), 4.41 (dt, $J = 11.9, 3.4$ Hz, 1H), 4.23 (ddd, $J = 11.8, 6.3, 2.5$ Hz, 1H), 3.83 – 3.79 (m, 1H), 3.81 – 3.74 (m, 2H), 3.33 (s, 3H), 2.43 (d, $J = 8.8$ Hz, 1H), 2.38 – 2.20 (m, 5H), 2.11 – 1.97 (m, 4H), 1.80 – 1.71 (m, 1H), 1.71 – 1.60 (m, 1H), 1.60 – 1.51 (m, 2H), 1.42 – 1.13 (m, 9H), 1.12 (t, $J = 7.6$ Hz, 3H), 1.05 (s, 9H).

$^{13}\text{C NMR}$ (126 MHz, CDCl_3) δ 173.6, 173.3, 154.5, 144.1, 141.2, 139.3, 137.4, 135.6, 135.5, 133.1, 133.0, 129.8, 129.6, 127.8, 127.74, 127.72, 127.65, 127.62, 126.61, 126.59, 114.9, 94.8, 86.7, 71.6, 69.1, 62.4, 62.3, 55.1, 52.8, 40.5, 34.1, 32.4, 31.5, 29.7, 29.5, 29.04, 29.03, 27.8, 27.6, 26.7, 24.8, 19.2, 9.0.

LRMS (ESI) m/z : calc'd for $\text{C}_{53}\text{H}_{65}\text{O}_6\text{Si}$ $[\text{M}-\text{OCH}_3]^+$ 825.45504, found 825.45507.

For the *endo* diastereomer (characteristic signals): $^1\text{H NMR}$ (500 MHz, CDCl_3) δ 5.09 (d, $J = 1.3$ Hz, 1H), 4.87 (d, $J = 1.4$ Hz, 1H), 4.03 (t, $J = 9.9, 5.9$ Hz, 1H), 2.66 (d, $J = 17.3$ Hz, 1H), 2.55 (t, $J = 8.9$ Hz, 1H).

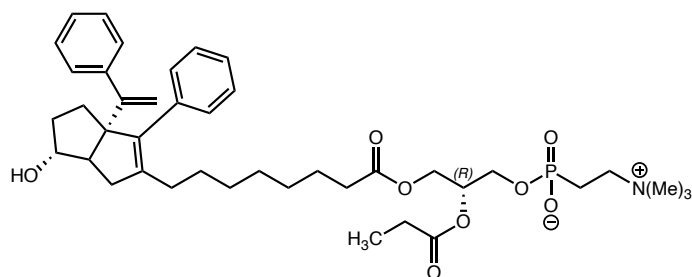


(S)- 3- hydroxy- 2- (propionyloxy)propyl 8- (6- (exo)- (methoxymethoxy)- 3- phenyl -3a- (1- phenylvinyl) -1,3a,4,5,6,6a-hexahydropentalen-2-yl)octanoate (10): A solution of **9** (35.0 mg, 0.041 mmol, 1.0 equiv) in THF was treated with TBAF (13.2 mg, 0.047 mmol, 1.1 equiv) and stirred for 16 h. The resulting mixture was directly concentrated and purified on silica (20-50% EtOAc/Hex eluent) to give the desired compound (7:1 dr) as a clear, colorless oil (19.3 mg, 76%).
For the *exo* diastereomer: $^1\text{H NMR}$ (500 MHz, CDCl_3) δ 7.39 – 7.17 (m, 10H), 5.10 – 5.07 (m, 1H), 5.05 (d, $J = 1.4$ Hz, 1H), 5.00 (d, $J = 1.4$ Hz, 1H), 4.62 – 4.57 (m, 2H), 4.19 (ddd, $J = 11.5, 4.3, 1.7$ Hz, 2H), 4.13 (ddd, $J = 11.4, 5.8, 2.1$ Hz, 2H), 4.12 – 4.04 (m, 1H), 3.81 – 3.76 (m, 1H), 3.73 (s, 1H), 3.31 (s, 3H), 2.45 – 2.27 (m, 6H), 2.09 – 1.98 (m, 4H), 1.79 – 1.53 (m, 4H), 1.36 – 1.19 (m, 8H), 1.15 (t, $J = 7.2$ Hz, 3H).

$^{13}\text{C NMR}$ (126 MHz, CDCl_3) δ 174.5, 173.8, 154.5, 144.1, 141.2, 139.3, 137.4, 129.6, 127.8, 127.64, 127.61, 126.60, 126.57, 114.9, 94.7, 86.7, 69.1, 68.3, 65.1, 65.0, 55.1, 52.8, 40.5, 34.0, 32.4, 31.4, 29.7, 29.5, 29.0, 27.7, 27.4, 24.8.

LRMS (ESI, APCI) m/z : calc'd for $\text{C}_{37}\text{H}_{47}\text{O}_6$ $[\text{M}-\text{OCH}_3]^+$ 587.3, found 586.8.

For the *endo* diastereomer (characteristic signals): $^1\text{H NMR}$ (500 MHz, CDCl_3) δ 5.08 (d, $J = 1.2$ Hz, 1H), 4.85 (d, $J = 1.4$ Hz, 1H), 4.01 (td, $J = 9.2, 5.7$ Hz, 1H), 2.65 (dd, $J = 17.3, 2.4$ Hz, 1H).



(2*R*)-3-((8-(6-(*exo*)-hydroxy-3-phenyl-3a-(1-phenylvinyl)-1,3a,4,5,6,6a-hexahydropentalen-2-yl)octanoyl)oxy)-2-(propionyloxy)propyl (2-(trimethylammonio)ethyl) phosphate (11): A solution of **10** (31.8 mg, 0.05 mmol, 1.0 equiv) in toluene was treated with 2-chloro-1,3,2-dioxaphospholane 2-oxide (10 μ L, 0.11 mmol, 2.2 equiv) was added, followed by DMAP (13.1 mg, 0.11 mmol, 2.2 equiv.) The resulting reaction mixture was stirred for 4 h, until reaction was complete by LCMS. The resulting mixture was filtered over a cotton plug to remove excess ammonium salts and concentrated. The crude reaction mixture dissolved in acetonitrile, transferred into a pressure tube, and cooled to -78 $^{\circ}$ C. Trimethylamine (neat, 2-5mL) was condensed into the pressure tube at -78 $^{\circ}$ C. The tube was capped, allowed to warm to room temperature, and heated to 90 $^{\circ}$ C for 16 h. After the reaction was complete, the pressure tube was allowed to cool to ambient temperature before being further cooled to -78 $^{\circ}$ C and uncapped. The solution was allowed to re-warm to room temperature before being concentrated *inside a fume hood* and used without further purification. The crude reaction mixture was dissolved in acetonitrile, and 2 drops of concentrated HCl was added. The mixture was allowed to stir until the reaction was complete (ca. 5 min, monitored by LCMS), and then concentrated. Purification *via* preparative HPLC on an Agilent 1200 Infinity Series chromatograph using an Agilent Prep-C18 30 x 250 mm 10 μ m column, with a linear gradient using water and 0.1% formic acid (FA) (Solvent A) and MeCN and 0.1% FA (Solvent B); $t=0$ min, 30% B, $t = 10$ min, 99% B, with a flow rate 40 mL/min, afforded the title compounds **11** as its *exo* diastereomer, as a mixture of regioisomers. Purity established as a mixture

of regioisomers using Method A: >99% (91.3% sn-1 connectivity (desired, shown), 8.6 % sn-2 connectivity). $t_R = 0.72$ min (Sn1), 0.78 min (Sn2).

$^1\text{H NMR}$ (600 MHz, CDCl_3) δ 7.37 – 7.15 (m, 10H), 5.04 (s, 1H), 4.98 (s, 1H), 4.51 (s, 1H), 4.44 – 4.28 (m, 4H), 4.28 – 4.17 (m, 2H), 4.18 – 4.06 (m, 1H), 3.92 (s, 1H), 3.80 – 3.69 (m, 2H), 3.30 (s, 9H), 2.38 – 2.22 (m, 6H), 2.12 – 1.93 (m, 4H), 1.60 – 1.48 (m, 4H), 1.38 – 1.13 (m, 9H), 1.10 (t, $J = 7.5$ Hz, 3H).

LRMS (ESI, APCI) m/z : calc'd for $\text{C}_{41} [\text{M}]^+$ 739.4, found 739.6.

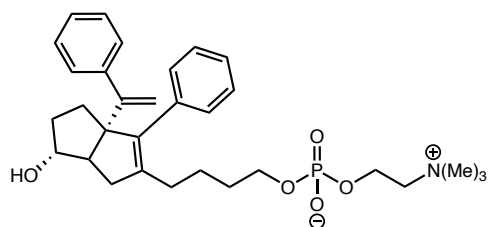
HRMS (ESI) m/z : calc'd for $\text{C}_{41}\text{H}_{59}\text{O}_9\text{NP} [\text{M}+\text{H}]^+$ 740.3939, found 740.3922. Calc'd for $\text{C}_{41}\text{H}_{48}\text{O}_9\text{NPNa} [\text{M}+\text{Na}]^+$ 762.3757, found 762.3741.

Phosphorylcholine Synthesis: Compounds 12a–h.

General Procedure:

A solution of the required alcohol (**5a–5h**, 1.0 equiv) in toluene was treated with 2-chloro-1,3,2-dioxaphospholane 2-oxide (2.0 equiv), followed by triethylamine (2.0 equiv). The reaction mixture was stirred for 1-4 h, until reaction was complete by LCMS. The resulting mixture was filtered through a cotton plug to remove ammonium salts and concentrated. The crude reaction mixture was dissolved in acetonitrile, transferred into a pressure tube, and cooled to -78 °C. Trimethylamine (neat, 2-5mL) was condensed into the pressure tube at -78 °C. The tube was capped, allowed to warm to room temperature, and then heated to 90 °C for 16 h. After the reaction was complete, the pressure tube was allowed to cool to ambient temperature before being further cooled to -78 °C and uncapped. The solution was allowed to re-warm to room temperature before being concentrated *inside a fume hood* and used without further purification. The crude reaction mixture was dissolved in acetonitrile, and 2-5 drops of concentrated HCl was added. The mixture

was allowed to stir until the reaction was complete (5-30 min, monitored by LCMS), and concentrated. Purification *via* preparative HPLC on an Agilent 1200 Infinity Series chromatograph using an Agilent Prep-C18 30 x 250 mm 10 μ m column, with a linear gradient using water and 0.1% formic acid (FA) (Solvent A) and MeCN and 0.1% FA (Solvent B); t=0 min, 30% B, t = 10 min, 99% B, flow rate 40 mL/min, afforded the desired compounds (**12a–12h**) as their *exo* diastereomer as clear, colorless oils.

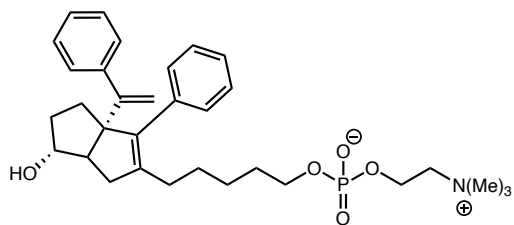


4-(6-*exo*-hydroxy-3-phenyl-3a-(1-phenylvinyl)-1,3a,4,5,6,6a-hexahydropentalen-2-yl)butyl (2-(trimethylammonio)ethyl) phosphate (12a): **5a** was reacted and purified according to the general procedure to give the title compound. Purity established as the *exo* diastereomer by Method A: >99%, *exo* t_R = 0.33 min.

^1H NMR (500 MHz, CDCl_3) δ 7.28 – 7.13 (m, 10H), 5.02 (s, 1H), 4.99 (s, 1H), 4.19 (s, 2H), 3.81 (s, 1H), 3.76 (s, 2H), 3.64 (s, 2H), 3.21 (s, 9H), 2.26 – 2.05 (m, 3H), 2.01 – 1.87 (m, 1H), 1.68 – 1.36 (m, 9H).

^{31}P NMR (121 MHz, CDCl_3) δ -0.76.

LRMS (ESI, APCI) m/z : calc'd for $\text{C}_{31}\text{H}_{43}\text{O}_5\text{NP}$ $[\text{M}+\text{H}]^+$: 540.3, found 540.3.

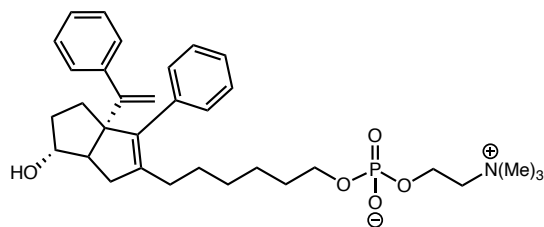


5-(6-*exo*-hydroxy-3-phenyl-3a-(1-phenylvinyl)-1,3a,4,5,6,6a-hexahydropentalen-2-yl)pentyl (2-(trimethylammonio)ethyl) phosphate (12b): **5b** was reacted and purified according to the general procedure to give the title compound. Purity established as the *exo* diastereomer by Method A: 95.8%, $t_R = 0.28$ min.

$^1\text{H NMR}$ (600 MHz, CDCl_3) δ 7.31 – 7.24 (m, 4H), 7.25 – 7.14 (m, 6H), 4.99 (s, 2H), 4.19 (s, 2H), 3.86 (s, 1H), 3.75 (s, 2H), 3.63 (s, 2H), 3.20 (s, 9H), 2.25 – 2.18 (m, 1H), 2.16 – 2.04 (m, 2H), 1.95 – 1.87 (m, 1H), 1.70 – 1.60 (m, 1H), 1.60 – 1.52 (m, 4H), 1.53 – 1.43 (m, 1H), 1.42 – 1.30 (m, 3H), 1.31 – 1.18 (m, 2H).

$^{31}\text{P NMR}$ (121 MHz, CDCl_3) δ -0.82.

LRMS (ESI, APCI) m/z : calc'd for $\text{C}_{32}\text{H}_{45}\text{O}_5\text{NP}$ $[\text{M}+\text{H}]^+$: 554.3, found 554.2.

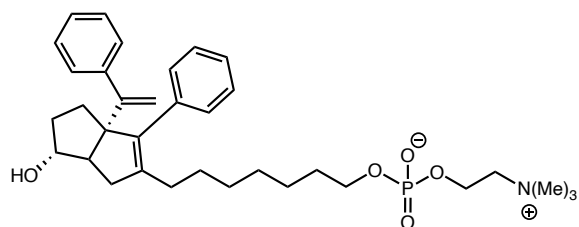


6-(6-*exo*-hydroxy-3-phenyl-3a-(1-phenylvinyl)-1,3a,4,5,6,6a-hexahydropentalen-2-yl)hexyl (2-(trimethylammonio)ethyl) phosphate (12c): **5c** was reacted and purified according to the general procedure to give the title compound. Purity established as the *exo* diastereomer by Method A: >99%, *exo* $t_R = 0.47$ min.

$^1\text{H NMR}$ (500 MHz, CDCl_3) δ 7.41 – 7.26 (m, 4H), 7.28 – 7.12 (m, 6H), 5.03 (s, 1H), 5.01 (s, 1H), 4.24 (s, 2H), 3.88 (s, 1H), 3.80 – 3.67 (m, 4H), 3.28 (s, 9H), 2.28 – 2.05 (m, 3H), 2.01 – 1.80 (m, 1H), 1.72 – 1.49 (m, 3H), 1.40 – 0.82 (m, 10H).

$^{31}\text{P NMR}$ (121 MHz, CDCl_3) δ -0.59.

LRMS (ESI, APCI) m/z : calc'd for $\text{C}_{33}\text{H}_{47}\text{O}_5\text{NP}$ $[\text{M}+\text{H}]^+$ 568.3, found 568.2



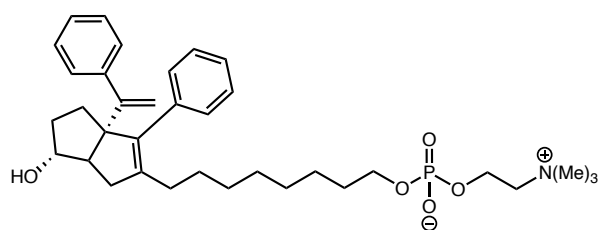
7-(6-*exo*-hydroxy-3-phenyl-3a-(1-phenylvinyl)-1,3a,4,5,6,6a-hexahydropentalen-2-yl)heptyl (2-(trimethylammonio)ethyl) phosphate (12d): **5d** was reacted and purified according to the general procedure to give the title compound. Purity established as the *exo* diastereomer by Method B: 95.9%, $t_R = 0.48$ min.

$^1\text{H NMR}$ (500 MHz, CDCl_3) δ 7.37 – 7.11 (m, 10H), 5.02 (s, 1H), 4.99 (s, 1H), 4.21 (s, 2H), 3.87 (s, 1H), 3.77 (s, 2H), 3.67 (s, 1H), 3.25 (s, 9H), 2.29 – 2.16 (m, 1H), 2.15 – 2.02 (m, 2H), 2.00 – 1.90 (m, 1H), 1.72 – 1.57 (m, 3H), 1.57 – 1.48 (m, 3H), 1.37 – 1.14 (m, 9H).

$^{13}\text{C NMR}$ (300 MHz, CDCl_3) δ 154.6, 144.1, 140.9, 139.6, 137.4, 129.6, 127.8, 127.7, 126.64, 114.7, 81.5, 69.1, 66.1, 65.7, 59.2, 55.7, 54.3, 40.0, 34.2, 32.0, 30.8, 29.5, 29.3, 29.2, 27.6, 25.6.

$^{31}\text{P NMR}$ (300 MHz, CDCl_3) δ -0.51.

HRMS (ESI) m/z : calc'd for $\text{C}_{34}\text{H}_{49}\text{O}_5\text{NP}$ $[\text{M}+\text{H}]^+$: 582.3343, found 582.3338.



8-(6-*exo*-hydroxy-3-phenyl-3a-(1-phenylvinyl)-1,3a,4,5,6,6a-hexahydropentalen-2-yl)octyl (2-(trimethylammonio)ethyl) phosphate (12e): **5e** was reacted and purified according to the general procedure to give the title compound. Purity established as the *exo* diastereomer by Method A: >99%, $t_R = 0.68$ min.

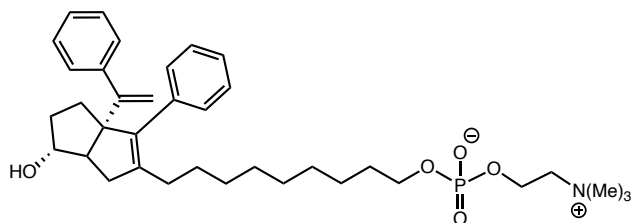
¹H NMR (600 MHz, CDCl₃) δ 7.33 –7.15 (m, 10H), 5.00 (s, 1H), 4.96 (s, 1H), 4.22 (s, 2H), 3.89 (s, 1H), 3.81 – 3.75 (m, 2H), 3.74 – 3.66 (m, 2H), 3.27 (s, 9H), 2.28 – 2.17 (m, 2H), 2.10 – 2.04 (m, 1H), 1.96 – 1.87 (m, 1H), 1.71 – 1.58 (m, 3H), 1.57 – 1.48 (m, 2H), 1.36 – 1.13 (m, 12H).

¹³C NMR (151 MHz, CDCl₃) δ 154.6, 144.1, 141.0, 139.5, 137.4, 129.6, 127.8, 127.6, 126.61, 126.55, 114.8, 81.7, 69.2, 66.3, 59.1, 55.6, 54.4, 53.4, 40.1, 37.1, 34.3, 32.0, 30.8, 29.4, 29.2, 28.9, 28.8, 27.5, 25.6, 22.6.

³¹P NMR (300 MHz, CDCl₃) δ -0.43.

LRMS (ESI, APCI) *m/z*: calc'd for C₃₅H₅₁O₅NP [M+H]⁺ 596.3, found 596.3.

HRMS (ESI) *m/z*: calc'd for C₃₅H₅₁O₅NP [M+H]⁺ : 596.3499, found 596.3494.



9-(6-*exo*-hydroxy-3-phenyl-3a-(1-phenylvinyl)-1,3a,4,5,6,6a-hexahydropentalen-2-yl)nonyl (2-(trimethylammonio)ethyl) phosphate (12f): **5f** was reacted and purified according to the general procedure to give the title compound. Purity established as the *exo* diastereomer using Method A: 94.8%, *exo* t_R = 0.89 min.

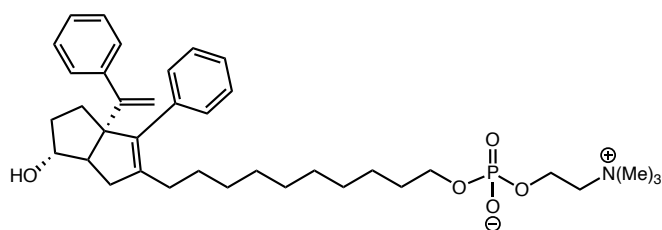
¹H NMR (600 MHz, CDCl₃) δ 7.32 – 7.14 (m, 10H), 5.01 (d, *J* = 7.6 Hz, 1H), 4.95 (d, *J* = 7.9 Hz, 1H), 4.20 (s, 2H), 3.87 (s, 1H), 3.75 (s, 3H), 3.67 (s, 3H), 3.25 (s, 9H), 2.27 – 2.18 (m, 2H), 2.06 – 1.98 (m, 2H), 1.94 (p, *J* = 7.0 Hz, 1H), 1.70 – 1.58 (m, 4H), 1.58 – 1.48 (m, 3H), 1.36 – 1.10 (m, 12H).

^{13}C NMR (126 MHz, CDCl_3) δ 154.7, 144.2, 141.1, 139.4, 137.4, 129.7, 127.8, 127.7, 127.6, 126.63, 126.57, 114.9, 81.7, 69.3, 66.2, 65.9, 59.3, 55.7, 54.4, 40.2, 34.2, 32.1, 30.9, 29.5, 29.3, 29.2, 27.7, 27.6, 25.8.

^{31}P NMR (121 MHz, CDCl_3) δ -0.73.

LRMS (ESI, APCI) m/z : calc'd for $\text{C}_{36}\text{H}_{53}\text{O}_5\text{NP}$ $[\text{M}+\text{H}]^+$ 610.4, found 609.8.

HRMS (ESI) m/z : calc'd for $\text{C}_{36}\text{H}_{53}\text{O}_5\text{NP}$ $[\text{M}+\text{H}]^+$: 610.3656, found 610.3655.



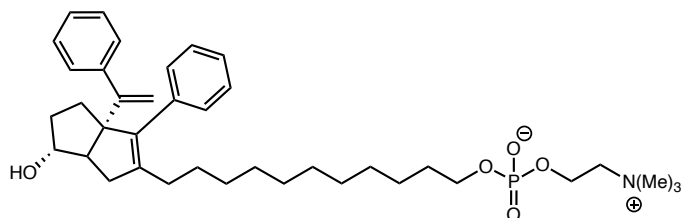
10-(6-*exo*-hydroxy-3-phenyl-3a-(1-phenylvinyl)-1,3a,4,5,6,6a-hexahydropentalen-2-yl)decyl (2-(trimethylammonio)ethyl) phosphate (12g): **5g** was reacted and purified according to the general procedure to give the title compound. Purity established as the *exo* diastereomer by Method A: 95.8%, $t_{\text{R}} = 0.74$ min.

^1H NMR (600 MHz, CDCl_3) δ 7.34 – 7.14 (m, 10H), 5.03 (d, $J = 4.9$ Hz, 1H), 4.95 (d, $J = 5.0$ Hz, 1H), 4.24 (s, 2H), 3.90 (s, 1H), 3.79 (q, $J = 6.4$ Hz, 2H), 3.74 (s, 2H), 3.28 (s, 9H), 2.34 – 2.23 (m, 2H), 2.10 – 1.92 (m, 3H), 1.64 (q, $J = 10.2, 6.5$ Hz, 2H), 1.56 (t, $J = 7.3$ Hz, 2H), 1.37 – 1.10 (m, 16H).

^{13}C NMR (126 MHz, CDCl_3) δ 154.7, 144.2, 141.1, 139.4, 137.4, 129.7, 127.73, 127.70, 127.6, 126.63, 126.56, 81.7, 69.3, 66.2, 65.9, 59.3, 55.6, 54.3, 40.2, 34.1, 32.2, 30.91, 30.86, 29.6, 29.3, 29.22, 29.17, 27.6, 25.8.

^{31}P NMR (121 MHz, CDCl_3) δ -0.75.

LRMS (ESI, APCI) m/z : calc'd for $\text{C}_{37}\text{H}_{55}\text{O}_5\text{NP}$ $[\text{M}+\text{H}]^+$: 624.4, found 624.3.



11-(6-*exo*-hydroxy-3-phenyl-3a-(1-phenylvinyl)-1,3a,4,5,6,6a-hexahydropentalen-2-yl)undecyl (2-(trimethylammonio)ethyl) phosphate (12h): **5h** was reacted and purified according to the general procedure to give the title compound. Purity established as the *exo* diastereomer by Method A: 95.4%, $t_R = 0.74$ min.

^1H NMR (600 MHz, CDCl_3) δ 7.35 – 7.15 (m, 12H), 5.03 (s, 1H), 4.96 (s, 1H), 4.26 (s, 2H), 3.91 (s, 1H), 3.85 – 3.77 (m, 2H), 3.75 (s, 2H), 3.29 (s, 9H), 2.32 (dd, $J = 16.7, 9.4$ Hz, 1H), 2.26 (d, $J = 9.6$ Hz, 1H), 2.10 – 1.94 (m, 4H), 1.71 – 1.61 (m, 3H), 1.61 – 1.53 (m, 2H), 1.38 – 1.14 (m, 16H).

^{13}C NMR (126 MHz, CDCl_3) δ 154.7, 144.2, 141.1, 139.3, 137.4, 129.7, 114.9, 81.7, 69.3, 66.2, 65.9, 59.3, 55.7, 54.4, 40.3, 34.0, 32.2, 31.6, 30.91, 30.86, 29.6, 29.5, 29.43, 29.40, 29.36, 29.3, 29.2, 27.7, 25.8, 22.7.

^{31}P NMR (121 MHz, CDCl_3) δ -0.90.

LRMS (ESI, APCI) m/z : calc'd for $\text{C}_{38}\text{H}_{57}\text{O}_5\text{NP}$ $[\text{M}+\text{H}]^+$ 638.4, found 637.8

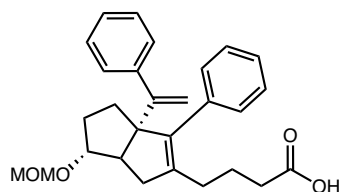
HRMS (ESI) m/z : calc'd for $\text{C}_{38}\text{H}_{57}\text{O}_5\text{NP}$ $[\text{M}+\text{H}]^+$: 638.3969, found 638.3974.

Carboxylate Synthesis: Compounds 13a–h.

General Ley-Griffith Oxidation General Procedure:

A solution of the required alcohol (**5a–5h**, 1.0 equiv) in acetonitrile was treated with tetrapropylammonium perruthenate (TPAP, 0.1 equiv), N-Methylmorpholine-N-Oxide (NMO, 5

equiv), and water (5 equiv). The reaction mixture was allowed to stir until complete by TLC and LCMS (1-16 h). The reaction mixture was directly concentrated and purified on silica (20-50% EtOAc (containing 0.1% AcOH)/Hex eluent).



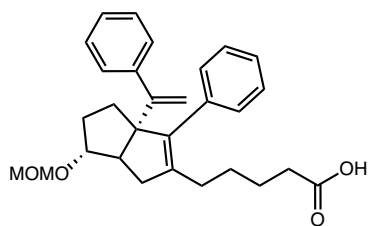
4-(6-*exo*-(methoxymethoxy)-3-phenyl-3a-(1-phenylvinyl)-1,3a,4,5,6,6a-hexahydropentalen-2-yl)butanoic acid (S2a): **5a** (262.8 mg, 0.63 mmol) was reacted and purified according to the general procedure to give the title compound as a clear, colorless oil (161.2 mg, 59%).

For the *exo* diastereomer: $^1\text{H NMR}$ (500 MHz, CDCl_3) δ 7.47 – 7.05 (m, 10H), 5.07 (s, 1H), 5.01 (s, 1H), 4.66 – 4.52 (m, 2H), 3.80 (s, 1H), 3.31 (s, 3H), 2.45 (d, $J = 8.9$ Hz, 1H), 2.37 – 2.20 (m, 2H), 2.13 – 1.98 (m, 4H), 1.81 – 1.57 (m, 3H), 1.36 – 1.18 (m, 3H).

For the *endo* diastereomer (characteristic signals): $^1\text{H NMR}$ (500 MHz, CDCl_3) δ 5.08 (s, 1H), 4.88 (s, 1H), 4.06 – 3.98 (m, 1H), 2.67 (d, $J = 17.8$ Hz, 1H).

$^{13}\text{C NMR}$ (126 MHz, CDCl_3) δ 179.0, 154.3, 143.9, 140.6, 139.7, 137.1, 129.5, 127.80, 127.75, 127.7, 126.8, 115.0, 94.7, 86.6, 69.1, 55.2, 52.8, 40.3, 33.6, 32.4, 31.5, 29.1, 22.9.

LRMS (ESI, APCI) m/z : calc'd for $\text{C}_{27}\text{H}_{29}\text{O}_3$ $[\text{M}-\text{OCH}_3]^+$ 401.2, found 400.8.



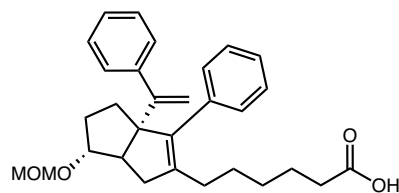
5-(6-*exo*-(methoxymethoxy)-3-phenyl-3a-(1-phenylvinyl)-1,3a,4,5,6,6a-hexahydropentalen-2-yl)pentanoic acid (S2b): **5b** (50.6 mg, 0.12 mmol) was reacted and purified according to the general procedure to give the title compound as a clear, colorless oil. (41.2 mg, 79 %).

For the *exo* diastereomer: $^1\text{H NMR}$ (500 MHz, CDCl_3) δ 7.37 – 7.14 (m, 10H), 5.06 (d, $J = 1.4$ Hz, 1H), 5.02 (d, $J = 1.4$ Hz, 1H), 4.63 – 4.57 (m, 2H), 3.80 (s, 1H), 3.32 (s, 3H), 2.43 (d, $J = 9.2$ Hz, 1H), 2.35 – 2.26 (m, 3H), 2.10 – 2.00 (m, 4H), 1.79 – 1.53 (m, 4H), 1.46 – 1.20 (m, 3H).

For the *endo* diastereomer (characteristic signals): $^1\text{H NMR}$ (500 MHz, CDCl_3) δ 5.07 (d, $J = 1.3$ Hz, 1H), 4.85 (d, $J = 1.3$ Hz, 1H), 3.99 (dt, $J = 9.6, 5.8$ Hz, 1H), 2.63 (dd, $J = 17.2, 1.8$ Hz, 1H), 2.54 (dd, $J = 9.5, 2.2$ Hz, 1H).

$^{13}\text{C NMR}$ (151 MHz, CDCl_3) δ 179.5, 154.3, 144.0, 140.4, 139.9, 137.2, 129.5, 127.8, 127.7, 127.6, 126.7, 126.6, 114.9, 86.6, 69.1, 55.1, 52.7, 40.3, 32.4, 31.4, 29.9, 29.3, 27.2, 24.6.

LRMS (ESI, APCI) m/z : calc'd for $\text{C}_{29}\text{H}_{33}\text{O}_4$ $[\text{M}-\text{H}]^-$ 445.2, found 445.1. Calc'd for $\text{C}_{28}\text{H}_{31}\text{O}_3$ $[\text{M}-\text{OCH}_3]^+$ 415.2, found 415.2.



6-(6-*exo*-(methoxymethoxy)-3-phenyl-3a-(1-phenylvinyl)-1,3a,4,5,6,6a-hexahydropentalen-2-yl)hexanoic acid (S2c): **5c** (45.8 mg, 0.10 mmol) was reacted and purified according to the general procedure to give the title compound as a clear, colorless oil (35.5 mg, 75 %).

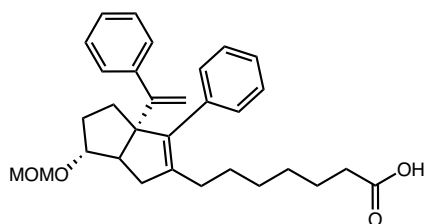
For the *exo* diastereomer: $^1\text{H NMR}$ (500 MHz, CDCl_3) δ 7.36 – 7.11 (m, 10H), 5.05 (d, $J = 1.4$ Hz, 1H), 5.02 (d, $J = 1.5$ Hz, 1H), 3.80 (s, 1H), 3.33 (s, 3H), 2.41 (d, $J = 8.7$ Hz, 1H), 2.38 – 2.29

(m, 2H), 2.24 (dd, $J = 17.0, 8.9$ Hz, 1H), 2.12 – 1.98 (m, 4H), 1.79 – 1.49 (m, 7H), 1.47 – 1.18 (m, 4H).

For the *endo* diastereomer: $^1\text{H NMR}$ (600 MHz, CDCl_3) δ 5.06 (d, $J = 1.3$ Hz, 1H), 4.84 (d, $J = 1.3$ Hz, 1H), 4.00 (td, $J = 9.8, 5.8$ Hz, 1H), 2.63 (dd, $J = 17.4, 2.2$ Hz, 1H), 2.53 (td, $J = 9.0, 2.2$ Hz, 1H).

$^{13}\text{C NMR}$ (151 MHz, CDCl_3) δ 179.5, 144.1, 140.7, 139.5, 137.2, 129.6, 127.72, 127.69, 127.66, 126.66, 126.65, 115.0, 82.0, 69.3, 60.4, 53.4, 40.1, 34.0, 32.0, 31.6, 29.4, 29.0, 27.4, 27.0, 22.6, 21.1.

LRMS (ESI, APCI) m/z : calc'd for $\text{C}_{30}\text{H}_{35}\text{O}_4$ $[\text{M}-\text{H}]^-$ 459.3, found 459.3. Calc'd for $\text{C}_{29}\text{H}_{33}\text{O}_3$ $[\text{M}-\text{OCH}_3]^+$ 429.2, found 429.3.



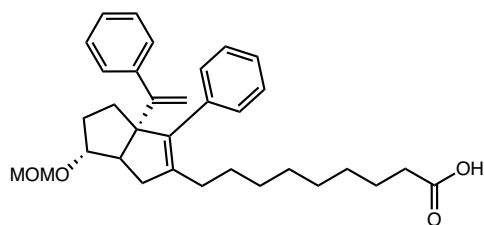
7-(6-*exo*-(methoxymethoxy)-3-phenyl-3a-(1-phenylvinyl)-1,3a,4,5,6,6a-hexahydropentalen-2-yl)heptanoic acid (S2d): **5d** (303.1 mg, 0.66 mmol) was reacted and purified according to the general procedure to give the title compound as a clear, colorless oil (126.3 mg, 40%).

$^1\text{H NMR}$ (500 MHz, CDCl_3) δ 7.60 – 7.02 (m, 10H), 5.05 (d, $J = 1.5$ Hz, 1H), 5.00 (d, $J = 1.5$ Hz, 1H), 4.66 – 4.52 (m, 2H), 3.79 (s, 1H), 3.31 (s, 3H), 2.42 (d, $J = 9.3, 1.7$ Hz, 1H), 2.40 – 2.27 (m, 3H), 2.10 – 1.97 (m, 4H), 1.79 – 1.50 (m, 4H), 1.52 – 1.18 (m, 7H).

For the *endo* diastereomer (characteristic signals): $^1\text{H NMR}$ (500 MHz, CDCl_3) δ 5.08 (d, $J = 1.4$ Hz, 1H), 4.85 (d, $J = 1.4$ Hz, 1H), 4.01 (td, $J = 9.1, 5.8$ Hz, 1H), 2.64 (d, $J = 17.5$ Hz, 1H), 2.54 (t, $J = 9.1$ Hz, 1H).

$^{13}\text{C NMR}$ (126 MHz, CDCl_3) δ 179.5, 154.5, 144.1, 141.1, 139.4, 137.4, 134.6, 129.6, 127.8, 127.7, 126.6, 114.9, 94.7, 86.7, 69.1, 55.1, 52.8, 40.5, 33.9, 32.4, 31.4, 29.6, 29.2, 28.8, 27.6, 24.5.

LRMS (ESI, APCI) m/z : calc'd for $\text{C}_{31}\text{H}_{37}\text{O}_4$ $[\text{M}-\text{H}]^-$ 473.3, found 473.4.



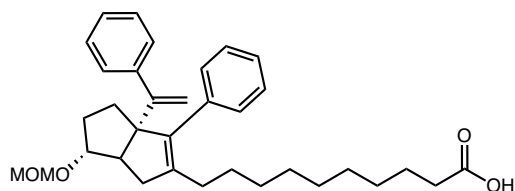
9-(6-*exo*-(methoxymethoxy)-3-phenyl-3a-(1-phenylvinyl)-1,3a,4,5,6,6a-hexahydropentalen-2-yl)nonanoic acid (S2f): **5f** (559.0 mg, 1.1 mmol) was reacted and purified according to the general procedure to give the title compound as a clear, colorless oil (489.9 mg, >85 %).

For the *exo* diastereomer: $^1\text{H NMR}$ (500 MHz, CDCl_3) δ 7.39 – 7.18 (m, 10H), 5.05 (d, $J = 1.4$ Hz, 1H), 5.00 (d, $J = 1.5$ Hz, 1H), 4.65 – 4.57 (m, 2H), 3.80 (d, $J = 2.1$ Hz, 1H), 3.32 (d, $J = 0.7$ Hz, 3H), 2.42 (d, 1H), 2.37 – 2.29 (m, 3H), 2.10 – 1.98 (m, 4H), 1.69 – 1.58 (m, 5H), 1.44 – 1.08 (m, 11H).

For the *endo* diastereomer (characteristic signals): $^1\text{H NMR}$ (500 MHz, CDCl_3) δ 5.09 (d, $J = 1.3$ Hz, 1H), 4.85 (d, $J = 1.4$ Hz, 1H), 4.02 (td, $J = 9.8, 5.4$ Hz, 1H), 2.65 (dd, $J = 17.7, 2.1$ Hz, 1H), 2.54 (td, $J = 9.4, 2.1$ Hz, 1H).

^{13}C NMR (126 MHz, CDCl_3) δ 179.2, 154.5, 144.1, 141.3, 139.3, 137.4, 129.6, 127.8, 127.6, 126.61, 126.57, 114.9, 94.6, 86.8, 69.1, 55.1, 52.8, 40.5, 33.9, 32.4, 31.4, 29.7, 29.5, 29.2, 29.1, 29.0, 27.7, 24.7.

LRMS (ESI, APCI) m/z : calc'd for $\text{C}_{33}\text{H}_{41}\text{O}_4$ $[\text{M}-\text{H}]^-$ 501.3, found 501.4. Calc'd for $\text{C}_{32}\text{H}_{39}\text{O}_3$ $[\text{M}-\text{CH}_3\text{O}]^+$ 471.3, found 470.8.



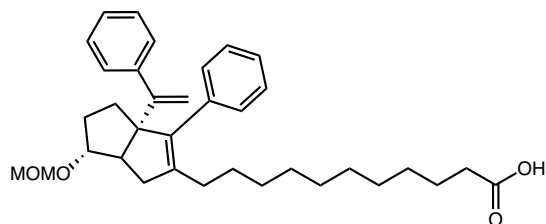
10-(6-*exo*-(methoxymethoxy)-3-phenyl-3a-(1-phenylvinyl)-1,3a,4,5,6,6a-hexahydropentalen-2-yl)decanoic acid (S2g): **5g** (584.5 1.2 mmol) was reacted and purified according to the general procedure to give the title compound as a clear, colorless oil (498.2 mg, 88%).

For the *exo* diastereomer: ^1H NMR (500 MHz, CDCl_3) δ 7.38 – 7.18 (m, 10H), 5.05 (d, J = 1.4 Hz, 1H), 5.01 (d, J = 1.5 Hz, 1H), 4.61 – 4.59 (m, 2H), 3.80 (s, 1H), 3.32 (s, 3H), 2.42 (d, J = 9.2, 1.7 Hz, 1H), 2.38 – 2.29 (m, 3H), 2.11 – 1.97 (m, 4H), 1.70 – 1.59 (m, 5H), 1.37 – 1.18 (m, 13H).

For the *endo* diastereomer (characteristic signals): ^1H NMR (500 MHz, CDCl_3) δ 5.09 (d, J = 1.3 Hz, 1H), 4.86 (d, J = 1.3 Hz, 1H), 4.02 (td, J = 9.7, 5.5 Hz, 1H), 2.65 (dd, J = 17.7, 2.2 Hz, 1H), 2.54 (td, J = 9.3, 2.2 Hz, 1H).

^{13}C NMR (126 MHz, CDCl_3) δ 179.4, 154.5, 144.1, 141.3, 139.2, 137.5, 129.6, 127.8, 127.6, 126.61, 126.56, 114.9, 94.7, 86.7, 69.1, 55.1, 52.7, 40.5, 34.0, 32.4, 31.4, 29.7, 29.6, 29.30, 29.26, 29.2, 29.0, 27.8, 24.7.

LRMS (ESI, APCI) m/z : calc'd for $\text{C}_{34}\text{H}_{43}\text{O}_4$ $[\text{M}-\text{H}]^-$ 515.3, found 515.1. Calc'd for $\text{C}_{33}\text{H}_{41}\text{O}_3$ $[\text{M}-\text{CH}_3\text{O}]^+$ 485.3, found 484.9.



11-(6-*exo*-(methoxymethoxy)-3-phenyl-3a-(1-phenylvinyl)-1,3a,4,5,6,6a-hexahydropentalen-2-yl)undecanoic acid (S2h): **5h** (325.7 mg, 0.63 mmol) was reacted and purified according to the general procedure to give the title compound as a clear, colorless oil (334.0 mg, > 99 %).

For the *exo* diastereomer: $^1\text{H NMR}$ (500 MHz, CDCl_3) δ 7.39 – 7.18 (m, 10H), 5.05 (d, $J = 1.2$ Hz, 1H), 5.00 (d, $J = 1.2$ Hz, 1H), 4.64 – 4.58 (m, 2H), 3.80 (s, 1H), 3.32 (s, 3H), 2.42 (d, $J = 8.8$ Hz, 1H), 2.38 – 2.30 (m, 3H), 2.11 – 1.98 (m, 4H), 1.72 – 1.59 (m, 5H), 1.44 – 1.17 (m, 16H).

For the *endo* diastereomer (characteristic signals): $^1\text{H NMR}$ (500 MHz, CDCl_3) δ 5.09 (d, $J = 1.2$ Hz, 1H), 4.86 (d, $J = 1.2$ Hz, 1H), 4.02 (td, $J = 9.4, 5.7$ Hz, 1H), 2.66 (dd, $J = 17.6, 2.2$ Hz, 1H), 2.54 (td, $J = 9.9, 2.1$ Hz, 1H).

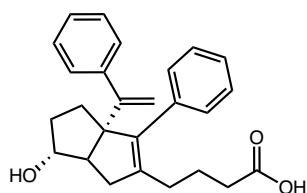
$^{13}\text{C NMR}$ (126 MHz, CDCl_3) δ 179.2, 154.5, 144.1, 141.4, 139.2, 137.5, 129.6, 127.8, 127.63, 126.60, 126.55, 114.9, 94.7, 86.7, 69.1, 55.1, 52.7, 40.5, 33.9, 32.4, 31.4, 29.7, 29.6, 29.38, 29.36, 29.3, 29.2, 29.0, 27.8, 24.7.

LRMS (ESI, APCI) m/z : calc'd for $\text{C}_{35}\text{H}_{46}\text{O}_4$ $[\text{M}-\text{H}]^-$ 529.3, found 529.5. Calc'd for $\text{C}_{34}\text{H}_{43}\text{O}_3$ $[\text{M}-\text{CH}_3\text{O}]^+$ 499.3, found 498.9.

General Deprotection Procedure:

A solution of **S2a-S2h** (1.0 equiv) in acetonitrile was treated with 2-5 drops of concentrated aqueous HCl and stirred until complete by TLC and LCMS (5-30 min). The resulting solution was

directly purified *via* preparatory HPLC on an Agilent 1200 Infinity Series chromatograph using an Agilent Prep-C18 30 x 250 mm 10 μ m column, with a linear gradient using water and 0.1% formic acid (FA) (Solvent A) and MeCN and 0.1% FA (Solvent B); $t=0$ min, 50% B, $t = 10$ min, 99% B, flow rate 40 mL/min, to afford the desired compounds as their *exo* diastereomer as clear, colorless oils (**13a–13h**).



4-(6-*exo*-hydroxy-3-phenyl-3a-(1-phenylvinyl)-1,3a,4,5,6,6a-hexahydropentalen-2-

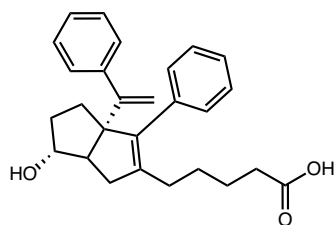
yl)butanoic acid (13a): **S2a** (169.2 mg, 0.39 mmol) was reacted and purified according to the general procedure to give the title compound as a clear, colorless oil (47.8 mg, 31%). Purity was established as the *exo* diastereomer by Method A: >99%, *exo* $t_R = 1.63$ min.

$^1\text{H NMR}$ (500 MHz, CDCl_3) δ 7.38 – 7.16 (m, 10H), 5.08 (d, $J = 1.4$ Hz, 1H), 5.00 (d, $J = 1.4$ Hz, 1H), 3.97 (s, 1H), 2.42 – 2.36 (m, 1H), 2.37 – 2.31 (m, 2H), 2.30 – 2.23 (m, 2H), 2.14 – 2.06 (m, 4H), 1.75 – 1.65 (m, 5H).

$^{13}\text{C NMR}$ (126 MHz, CDCl_3) δ 178.7, 154.4, 144.0, 140.4, 139.6, 137.0, 129.6, 127.8, 127.7, 126.81, 126.75, 115.2, 82.0, 69.4, 55.7, 40.1, 34.0, 33.8, 32.0, 29.1, 22.9.

LRMS (ESI, APCI) m/z : calc'd for $\text{C}_{26}\text{H}_{27}\text{O}_3$ $[\text{M}-\text{H}]^-$ 387.2, found 387.1.

HRMS calcd for $\text{C}_{26}\text{H}_{27}\text{O}_3$ $[\text{M}-\text{H}]^-$: 387.1966, found 387.1969.



5-(6-hydroxy-3-phenyl-3a-(1-phenylvinyl)-1,3a,4,5,6,6a-hexahydropentalen-2-yl)pentanoic acid (13b):

S2b (40.6 mg, 0.09 mmol) was reacted according to the general procedure and purified on silica (20-50% EtOAc (0.1% AcOH)/Hex eluent) to give the title compound as a mixture of diastereomers as a clear, colorless oil (36.1 mg, >99%). Purity was established as a mixture of diastereomers by Method B: 96.8% (83.9% *exo* 12.9% *endo*), *exo* t_R = 1.07 min, *endo* t_R = 1.28 min.

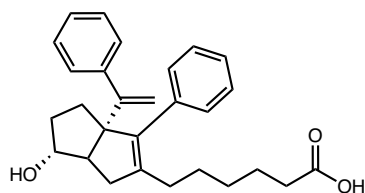
For the *exo* diastereomer: $^1\text{H NMR}$ (600 MHz, CDCl_3) δ 7.56 – 6.96 (m, 10H), 5.05 (d, J = 1.4 Hz, 1H), 4.97 (d, J = 1.4 Hz, 1H), 3.93 (s, 1H), 2.38 – 2.23 (m, 4H), 2.13 – 1.97 (m, 5H), 1.74 – 1.62 (m, 3H), 1.53 (p, J = 7.4 Hz, 2H), 1.44 – 1.32 (m, 2H).

For the *endo* diastereomer (characteristic signals): $^1\text{H NMR}$ (600 MHz, CDCl_3) δ 5.07 (d, J = 1.6 Hz, 1H), 4.94 (d, J = 1.4 Hz, 1H), 4.20 (td, J = 9.0, 5.7 Hz, 1H), 2.64 (dd, J = 17.3, 2.0 Hz, 1H), 2.50 (td, J = 8.6, 1.9 Hz, 1H).

$^{13}\text{C NMR}$ (126 MHz, CDCl_3) δ 177.8, 154.5, 144.1, 140.3, 139.8, 137.2, 129.7, 127.8, 127.7, 126.8, 126.7, 115.1, 82.0, 69.4, 55.8, 40.1, 34.0, 33.5, 32.1, 29.3, 27.2, 24.6.

LRMS (ESI, APCI) m/z : calc'd for $\text{C}_{27}\text{H}_{30}\text{O}_3$ $[\text{M}-\text{H}]^-$ 401.2, found 401.5. Calc'd for $\text{C}_{27}\text{H}_{29}\text{O}_2$ $[\text{M}-\text{OH}]^+$ 385.2, found 385.2

HRMS calc'd for $\text{C}_{27}\text{H}_{31}\text{O}_3$ $[\text{M}+\text{H}]^+$: 403.2268, found 403.2266.



6-(6-*exo*-hydroxy-3-phenyl-3a-(1-phenylvinyl)-1,3a,4,5,6,6a-hexahydropentalen-2-

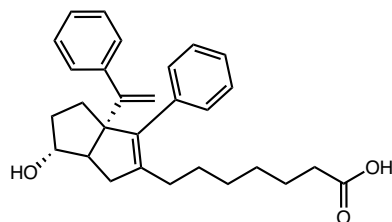
yl)hexanoic acid (13c): S2c (169.6 mg, 0.37 mmol) was reacted and purified according to the general procedure to give the title compound as a clear, colorless oil (94.3 mg, 61%). Purity was established as the *exo* diastereomer by Method A: >99%, *exo* t_R = 2.26 min.

$^1\text{H NMR}$ (600 MHz, CDCl_3) δ 7.49 – 7.05 (m, 10H), 5.05 (d, J = 1.5 Hz, 1H), 4.97 (d, J = 1.4 Hz, 1H), 3.93 (s, 1H), 2.36 – 2.21 (m, 4H), 2.10 – 1.97 (m, 5H), 1.73 – 1.61 (m, 3H), 1.59 – 1.51 (m, 2H), 1.34 (p, J = 7.6 Hz, 2H), 1.28 – 1.20 (m, 2H).

$^{13}\text{C NMR}$ (126 MHz, CDCl_3) δ 179.4, 154.5, 144.1, 140.7, 139.5, 137.3, 129.6, 127.8, 127.70, 127.68, 126.7, 115.0, 82.1, 69.3, 55.7, 40.2, 34.0, 33.8, 32.0, 29.5, 29.0, 27.4, 24.5.

LRMS (ESI, APCI) m/z : calc'd for $\text{C}_{28}\text{H}_{31}\text{O}_3$ $[\text{M}-\text{H}]^-$ 415.2, found 414.9. Calc'd for $\text{C}_{28}\text{H}_{31}\text{O}_2$ $[\text{M}-\text{OH}]^+$ 399.2, found 399.2

HRMS calc'd for $\text{C}_{28}\text{H}_{32}\text{O}_3\text{Na}$ $[\text{M}+\text{Na}]^+$: 439.2235, found 439.2237.



7-(6-*exo*-hydroxy-3-phenyl-3a-(1-phenylvinyl)-1,3a,4,5,6,6a-hexahydropentalen-2-

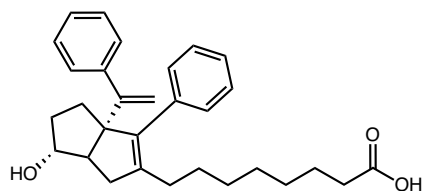
yl)heptanoic acid (13d): S2d (126.3 mg, 0.27 mmol) was reacted and purified according to the general procedure to give the title compound as a clear, colorless oil (95.3 mg, 83%). Purity was established as the *exo* diastereomer by Method A: >99%, *exo* t_R = 2.53 min.

^1H NMR (600 MHz, CDCl_3) δ 7.37 – 7.14 (m, 9H), 5.05 (d, $J = 1.5$ Hz, 1H), 4.97 (d, $J = 1.4$ Hz, 1H), 3.93 (s, 1H), 2.38 – 2.25 (m, 4H), 2.11 – 1.97 (m, 4H), 1.76 – 1.47 (m, 4H), 1.33 (p, $J = 7.6$ Hz, 2H), 1.29 – 1.14 (m, 6H).

^{13}C NMR (126 MHz, CDCl_3) δ 179.9, 154.5, 144.1, 140.9, 139.3, 137.3, 129.7, 127.74, 127.70, 127.66, 126.7, 115.0, 82.1, 69.3, 55.6, 40.2, 34.0, 33.9, 32.0, 29.6, 29.2, 28.8, 27.6, 24.6.

LRMS (ESI, APCI) m/z : calc'd for $\text{C}_{29}\text{H}_{33}\text{O}_3$ $[\text{M}-\text{H}]^-$ 429.3, found 429.3. Calc'd for $\text{C}_{29}\text{H}_{33}\text{O}_2$ $[\text{M}-\text{OH}]^+$ 413.2, found 413.28

HRMS calc'd for $\text{C}_{29}\text{H}_{33}\text{O}_3$ $[\text{M}-\text{H}]^-$: 429.2435, found 429.2378.



8-(6-*exo*-hydroxy-3-phenyl-3a-(1-phenylvinyl)-1,3a,4,5,6,6a-hexahdropentalen-2-

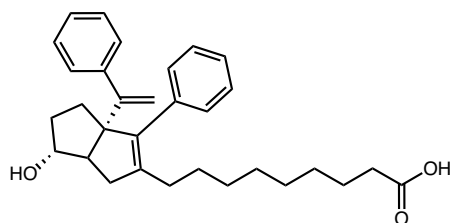
yl)octanoic acid (13e): **S2e** (147.2 mg, 0.30 mmol) was reacted and purified according to the general procedure to give the title compound as a clear, colorless oil (95.9 mg, 72%). Purity was established as the *exo* diastereomer by Method A: >97.3%, $t_R = 2.84$ min.

^1H NMR (600 MHz, CDCl_3) δ 7.81 – 7.13 (m, 10H), 5.05 (s, 1H), 4.97 (s, 1H), 3.93 (s, 1H), 2.37 – 2.22 (m, 5H), 2.09 – 1.94 (m, 5H), 1.79 – 1.58 (m, 6H), 1.38 – 1.16 (m, 5H).

^{13}C NMR (126 MHz, CDCl_3) δ 180.0, 154.5, 144.1, 141.0, 139.2, 137.3, 129.7, 127.74, 127.68, 127.6, 126.7, 115.0, 82.1, 69.3, 55.6, 40.2, 34.0, 33.8, 32.0, 29.4, 28.94, 28.88, 27.7, 24.6, 21.0.

LRMS (ESI, APCI) m/z : calc'd for $\text{C}_{30}\text{H}_{35}\text{O}_3$ $[\text{M}-\text{H}]^-$ 443.3, found 443.2. Calc'd for $\text{C}_{30}\text{H}_{35}\text{O}_2$ $[\text{M}-\text{OH}]^+$ 427.3, found 427.4

HRMS calc'd for $\text{C}_{30}\text{H}_{35}\text{O}_3$ $[\text{M}-\text{H}]^-$: 443.2592, found 443.2593



9-(6-*exo*-hydroxy-3-phenyl-3a-(1-phenylvinyl)-1,3a,4,5,6,6a-hexahydropentalen-2-

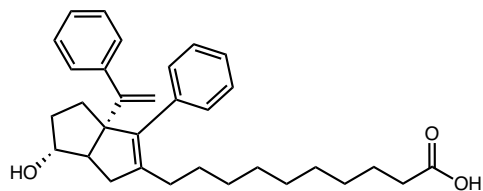
yl)nonanoic acid (13f): S2f (39.4 mg, 0.83 mmol) was reacted and purified according to the general procedure to give the title compound as a clear, colorless oil (34.3 mg, 90%). Purity was established as the *exo* diastereomer by Method A: >99%, $t_R = 3.22$ min.

$^1\text{H NMR}$ (500 MHz, CDCl_3) δ 7.41 – 7.15 (m, 10H), 5.07 (d, $J = 1.4$ Hz, 1H), 4.99 (d, $J = 1.4$ Hz, 1H), 3.95 (s, 1H), 2.39 – 2.27 (m, 5H), 2.12 – 1.97 (m, 5H), 1.76 – 1.56 (m, 6H), 1.40 – 1.15 (m, 7H).

$^{13}\text{C NMR}$ (126 MHz, CDCl_3) δ 179.5, 154.6, 144.1, 141.1, 139.2, 137.4, 129.7, 127.74, 127.71, 127.6, 126.7, 126.6, 115.0, 82.1, 69.3, 55.7, 40.2, 34.0, 32.1, 29.6, 29.5, 29.2, 29.1, 29.0, 24.7.

LRMS (ESI, APCI) m/z : calc'd for $\text{C}_{31}\text{H}_{37}\text{O}_3$ $[\text{M}-\text{H}]^-$ 457.3, found 457.3. Calc'd for $\text{C}_{31}\text{H}_{37}\text{O}_2$ $[\text{M}-\text{OH}]^+$ 441.3, found 440.8

HRMS (ESI) m/z : calc'd for for $\text{C}_{31}\text{H}_{37}\text{O}_3$ $[\text{M}-\text{H}]^-$ 457.2748, found 457.2749.



10-(6-*exo*-hydroxy-3-phenyl-3a-(1-phenylvinyl)-1,3a,4,5,6,6a-hexahydropentalen-2-

yl)decanoic acid (6HP-CA 13g): S2g (498.2 mg, 0.96 mmol) was reacted and purified according

to the general procedure to give the title compound as a clear, colorless oil (434.9 mg, 95%). Purity was established as the *exo* diastereomer using Method A: 98.5%, $t_R = 3.64$ min.

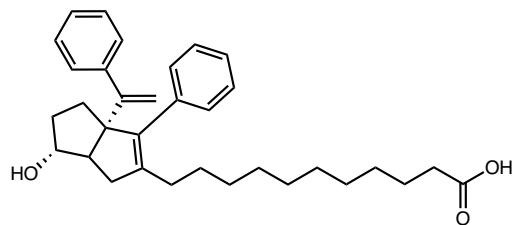
$^1\text{H NMR}$ (500 MHz, CDCl_3) δ 7.39 – 7.15 (m, 10H), 5.07 (d, $J = 1.6$ Hz, 1H), 4.99 (d, $J = 1.6$ Hz, 1H), 3.95 (s, 1H), 2.41 – 2.24 (m, 5H), 2.15 – 1.94 (m, 5H), 1.75 – 1.50 (m, 6H), 1.42 – 1.09 (m, 9H).

$^{13}\text{C NMR}$ (126 MHz, CDCl_3) δ 179.4, 154.6, 144.2, 141.2, 139.1, 137.4, 129.7, 127.74, 127.71, 127.6, 126.7, 126.6, 115.0, 82.1, 69.3, 55.7, 40.3, 34.0, 33.9, 32.1, 29.7, 29.6, 29.30, 29.28, 29.2, 29.0, 27.8, 24.7.

LRMS (ESI, APCI) m/z : calc'd for $\text{C}_{32}\text{H}_{39}\text{O}_3$ $[\text{M}-\text{H}]^-$ 471.3, found 471.3. Calc'd for $\text{C}_{32}\text{H}_{39}\text{O}_2$ $[\text{M}-\text{OH}]^+$ 455.3, found 454.8

HRMS (ESI) m/z : calc'd for $\text{C}_{32}\text{H}_{39}\text{O}_3$ $[\text{M}-\text{H}]^-$ 471.2882, found 471.2905.

FT-IR (neat): 3360(b), 1708 (s) cm^{-1} .



11-(6-*exo*-hydroxy-3-phenyl-3a-(1-phenylvinyl)-1,3a,4,5,6,6a-hexahydropentalen-2-

yl)undecanoic acid (13h): **S2h** (38.9 mg, 0.07 mmol) was reacted and purified according to the general procedure to give the title compound as a clear, colorless oil (30.8 mg, 87%). Purity was established as the *exo* diastereomer by Method A: 98.0%, *exo* $t_R = 3.71$ min.

¹H NMR (500 MHz, CDCl₃) δ 7.41 – 7.12 (m, 10H), 5.07 (d, *J* = 1.4 Hz, 1H), 4.99 (d, *J* = 1.5 Hz, 1H), 3.99 – 3.92 (s, 1H), 2.38 – 2.26 (m, 5H), 2.11 – 1.98 (m, 5H), 1.75 – 1.58 (m, 6H), 1.36 – 1.17 (m, 11H).

¹³C NMR (126 MHz, CDCl₃) δ 179.4, 154.6, 144.2, 141.2, 139.1, 137.4, 129.7, 127.74, 127.71, 127.6, 126.7, 126.6, 115.0, 82.1, 69.3, 55.7, 40.2, 34.0, 33.9, 32.1, 29.7, 29.6, 29.4, 29.3, 29.2, 29.0, 27.8, 24.7.

LRMS (ESI, APCI) *m/z*: calc'd for C₃₃H₄₁O₃ [M-H]⁻ 485.3, found 485.3. Calc'd for C₃₃H₄₁O₂ [M-OH]⁺ 469.3, found 468.9

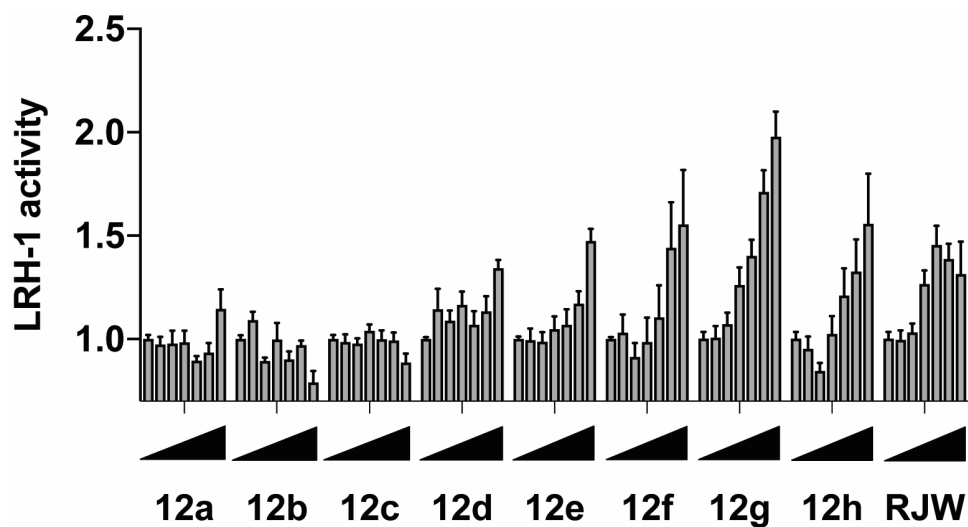
HRMS (ESI) *m/z* : calc'd for C₃₃H₄₁O₃ [M-H]⁻ 485.3061, found 485.3065.

Detailed Biological Procedures

We performed cellular assays with HeLa cells which were reverse-transfected with three vectors: (1) full-length, human LRH-1 in a pCI vector, (2) a firefly reporter (pGL3 Basic) with a portion of the SHP promoter cloned upstream of the firefly luciferase gene, and (3) a constitutively active vector expressing Renilla luciferase under control of the cytomegalovirus (CMV) promoter. The following day, cells were treated with each compound or vehicle control for 24 hours (in the case of all synthetic compounds, vehicle was DMSO). In most cases, six points in the concentration range of 0.03—30 μM were used, with a final DMSO concentration of 0.3% in all wells. Luciferase expression was measured using the DualGlo Kit (Promega). Firefly luciferase signal was normalized to Renilla luciferase signal in each well. EC₅₀ values were calculated using three-parameter curve-fitting (GraphPad Prism, v.7). Assays were conducted in triplicate with at least two independent biological replicates.

DLPC was purchased from Avanti Polar Lipids (Alabaster, AL) and dissolved in ethanol for delivery to cells (with a final concentration of 0.3% ethanol in each well). A concentration range of 0-100 μM was used. Fold change in LRH-1 activation for DLPC-treated cells was calculated relative to response in cells treated with 0.3% ethanol vehicle alone.

Additional Activity Data: Compounds 12

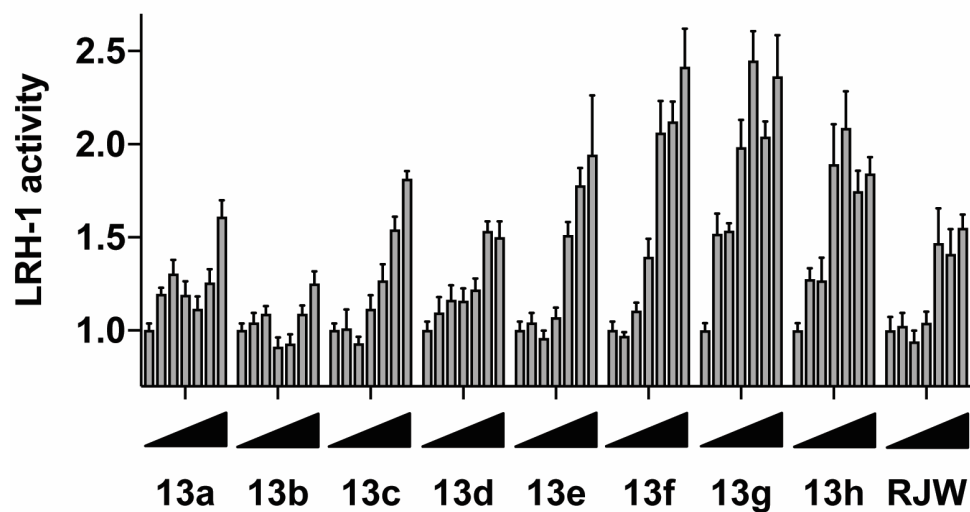


Supporting Figure S2.1. Luciferase Data for Compounds 12

Supporting Table S2.1. Luciferase Data for Compounds 12

Compound	EC₅₀ (μM)	Maximum LRH-1 Activity (curve fit)	Maximum LRH-1 Activity (SEM)
12a	N/A	inactive	--
12b	N/A	inactive	--
12c	N/A	inactive	--
12d	N/A	inactive	--
12e	>30	4	7
12f	2 +/- 3	2.3	0.2
12g	5 +/- 2	2.1	0.1
12h	5.1 +/- 0.5	1.4	0.06

Additional Activity Data: Compounds 13



Supporting Figure S2.2. Luciferase Data for Compounds 13

Supporting Table S2.2. Luciferase Data for Compounds 13

Compound	EC ₅₀ (μM)	Maximum LRH-1 Activity (curve fit)	Maximum LRH-1 Activity (SEM)
13a	N/A	inactive	--
13b	N/A	inactive	--
13c	9 +/- 3	2	0.1
13d	4 +/- 3	1.6	0.1
13e	4 +/- 2	2.1	0.1
13f	1.8 +/- 0.7	2.5	0.1
13g (6HP-CA)	0.4 +/- 0.4	2.3	0.2
13h	0.3 +/- 0.3	1.9	0.1

Chapter 3:
Mechanism of Activation and Therapeutic Effects
of LRH-1 Agonist 10CA

3.1 Phospholipid Signaling Axes

The successful rational design of LRH-1 chimera agonist **10CA** is not only exciting as a potential therapeutic lead, but also represents a broader opportunity to study LRH-1. Understanding phosphatidylcholine–NR signaling axes is vital to understanding NR biology and may illuminate other novel general strategies for NR-targeted drug design. Here, we aimed to deeply understand how **10CA** binding leads to LRH-1 activation, evaluate its potential as a therapeutic candidate, and broadly elucidate **10CA** signaling pathways and understand this chimera’s role in NR biology.

There are several models that shown a relationship between phosphatidylcholine (PC) levels and LRH-1 activity. Depletion of endogenous PCs in mice by administration of a methionine and choline-deficient (MCD) diet induces an “antagonist” pattern of gene expression similar to that seen in LRH-1 knockout mice.⁴⁴ In related work, depletion of dietary methionine of *C. Elegans* reduces endogenous PC levels via perturbation of the one-carbon cycle.⁴⁵ This inhibits the worm LRH-1 ortholog, and causes fat accumulation that is rescued by PC agonists. In human hepatocytes, LRH-1 senses PCs generated via methyl metabolism to control beta-oxidation of fatty acids and mitochondrial biogenesis.⁴⁶ Finally, exogenous administration of DLPC has demonstrated therapeutic potential via activation of LRH-1. DLPC induces potent anti-diabetic

⁴⁴ Wagner, M.; Choi, S.; Panzitt, K.; Mamrosh, J. L.; Man Lee, J.; Zaufel, A.; Xiao, R.; Wooton-Kee, R.; Ståhlman, M.; Newgard, C. B.; Borén, J.; Moore, D. D. LRH-1 Is a Critical Determinant of Methyl-Pool Metabolism - Prepublication. *Hepatology* **2015**, *63* (1), n/a-n/a

⁴⁵ (a) Walker, A. K. 1-Carbon Cycle Metabolites Methylate Their Way to Fatty Liver. *Trends Endocrinol. Metab.* **2017**, *28* (1), 63–72 (b) Klapper, M.; Findeis, D.; Koefeler, H.; Döring, F. Methyl Group Donors Abrogate Adaptive Responses to Dietary Restriction in *C. Elegans*. *Genes Nutr.* **2016**, *11* (1), 1–12

⁴⁶ (a) Stein, S.; Lemos, V.; Xu, P.; Demagny, H.; Wang, X.; Ryu, D.; Jimenez, V.; Bosch, F.; Lüscher, T. F.; Oosterveer, M. H.; Schoonjans, K. Impaired SUMOylation of Nuclear Receptor LRH-1 Promotes Nonalcoholic Fatty Liver Disease. *J. Clin. Invest.* **2017**, *127* (2), 583–592 (b) Choi, S.; Dong, B.; Lin, C. C. J.; Heo, M. J.; Kim, K. H.; Sun, Z.; Wagner, M.; Putluri, N.; Suh, J. M.; Wang, M. C.; Moore, D. D. Methyl-Sensing Nuclear Receptor Liver Receptor Homolog-1 Regulates Mitochondrial Function in Mouse Hepatocytes. *Hepatology* **2019**, *0* (0), 1–15

effects in mouse models of obesity-induced insulin resistance that occur via LRH-1-dependent repression of de novo lipogenesis in the liver.^{12a}

The sensitivity of LRH-1 to endogenous PC levels suggests a specific regulatory circuit connecting PC availability to LRH-1-controlled gene expression. However, because of their insolubility, rapid metabolism, and unselective binding, PCs are poor probes to study LRH-1 specific biology. Our RJW100–DLPC chimera **10CA**, however, is an effective synthetic ligand that acts as an agonist, activating LRH-1 robustly.

3.2 The Apparent Importance of Linker-Length on Activation

The addition of polar groups—here, phosphorylcholines (PhCs) or carboxylic acids (CAs) to the RJW100 scaffold dramatically increases LRH-1 transcriptional activity in luciferase reporter assays, depending on the length of the alkyl linker connecting the bicyclic core to the modified group. Compounds with short alkyl linkers (4-5 carbons) for both classes do not significantly activate the receptor at doses up to 30 μM (Fig. 3.1A). Conversely, compounds containing linkers of 9–10 carbons are the strongest activators for both classes (Fig. 3.1A), and the optimal linker length corresponds to distances of 18–20 Å from the bicyclic core to the terminal polar group (for PhCs) and 15–17 Å for the CAs (Chapter 2 and Fig. 3.1). We questioned whether the terminal polar group must contain an anionic component to make the appropriate contacts with the residues at the mouth of the LBD of LRH-1 to increase activity. We synthesized a panel of compounds with a terminal hydroxyl group, which will not be deprotonated at physiological pH, and found that they do not activate the receptor over the level of RJW100 regardless of linker length (Fig. 3.1A). This data suggests that PL-mimicking groups may indeed form productive interactions with LRH-1 which results in greatly increased LRH-1-dependent transcriptional output. We also investigated

whether the binding constants of the alcohol, carboxylic acid, and phosphorylcholine series to LRH-1 were affected by linker length (Fig. 3.1C, D, E). In the case of the PhCs and CAs (Fig. 3.1C, D), binding affinity increased with increasing linker length (presumably positioning the pharmacophore closer to the mouth of the pocket).

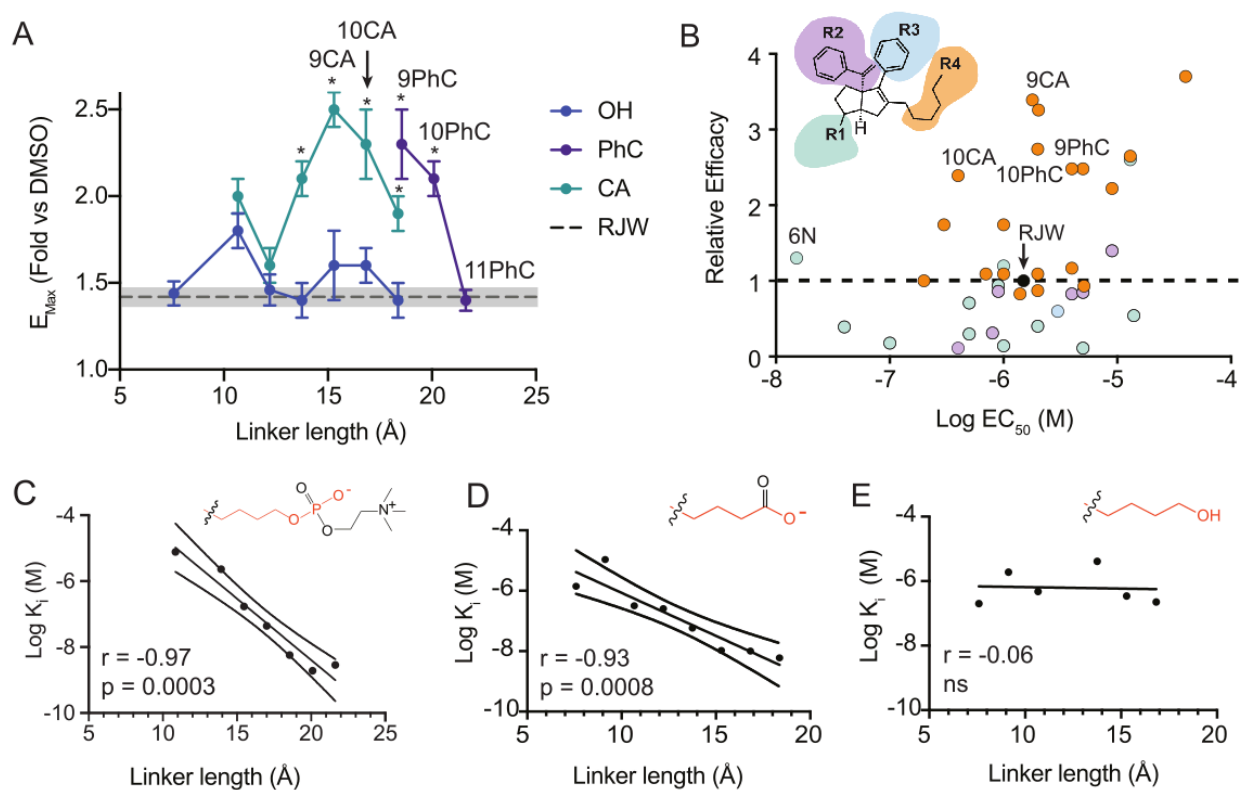


Figure 3.1. Activation dependence on linker length (A) Maximum Activation versus linker length. RJW100 maximum activation is used as a reference (black line). (B) Relative efficacy (as calculated in the Supporting Information) of synthesized agonists. Orange dots represent compounds the R^4 series (Chapter 2 and 3). Teal, blue, and purple dots will be discussed in Chapter 4. RJW100 is the black dot. (C) Binding efficacy of phosphorylcholine-terminated compounds versus linker length shows that binding is correlated to linker length and enhanced with longer linkers. (D) Binding efficacy of carboxylate-terminated compounds versus linker length. (E) Binding efficacy of alcohol-terminated compounds versus linker length.

However, this was not the case with the alcohol series, where binding affinity was not correlated to linker length. This observation is consistent with the hypothesis that CAs and PhCs make specific interactions with the mouth of the pocket that the alcohol-terminated compounds are unable to make. Figure 3.1B compares all synthesized hexahydropentalenes and highlights that, while many modifications can affect the potency of LRH-1 ligands, PhCs and CAs have the unique ability to affect receptor activation: almost the entirety of compounds more activating than RJW100 are represented by R⁴ modifications (orange dots).

3.3 Crystal Structures of PL Mimetics Bound to LRH-1

To unambiguously determine whether our binding pose hypothesis was correct, and PL-mimicking contacts were being made by the PhC and CA series of compounds, we determined X-ray crystal structures of the LRH-1 LBD bound to **10CA** and **9PhC** at resolutions of 2.3 Å and 2.6 Å, respectively (**10CA**: Fig. 3.3A). In both cases, the electron density surrounding the ligands indicates the position of the 6HP core. The agonists' cores adopt nearly identical positions in the deep binding pocket as RJW100, anchored by the proposed through-water contact to T352, and phenyl ring π - π edge-to-face interaction with H390, exactly as hypothesized in Chapter 1.

In the cocrystal structure of **10CA** bound to the LBD of LRH-1 (Fig. 3.2A), the extended alkyl linker and terminal polar groups are also well-defined by strong electron density (Fig. 3.2B). Remarkably, the **10CA** alkyl chain extends towards the mouth of the pocket, with the head groups within 2 Å of the DLPC phosphate head group (seen by superposition with PDB 4DOS, Fig. 3.2D), as designed. It can be seen that the carboxylate makes very similar contacts near the mouth of the pocket as DLPC, including hydrogen bonds with Y516 and G421, and a 3.45 Å interaction with the K520 sidechain (Fig. 3.3C). **10CA** also makes an additional contact to L424, strengthening the

association with the mouth of the pocket (Fig. 3.2C). Molecular dynamics simulations (MDS) with the **10CA** structure predict that the interacts with Y516 and K520 persist for 50.2% and 37.6% of the 1 μ s simulation, respectively, which is similar to DLPC (Fig. 3.2E).

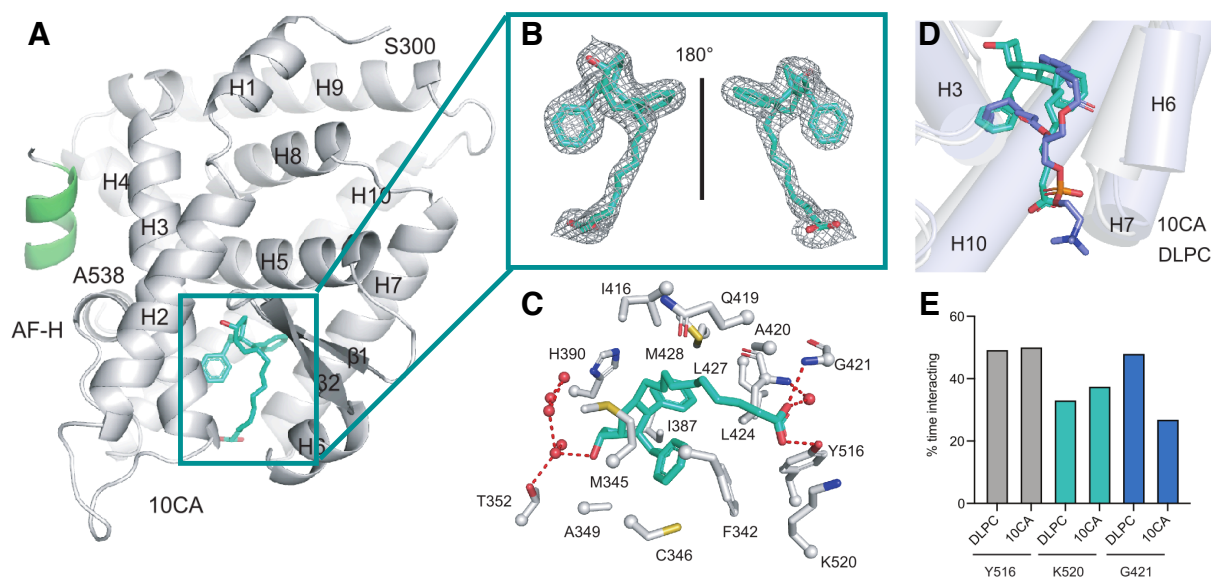


Figure 3.2. Crystal Structure of 10CA bound in the LBD of LRH-1(A) Overall structure shows the Tif2 peptide (green) bound at the AFS and the ligand (teal) bound in the LBD. The ligand is bound at a single site in the binding pocket. (B) Omit map ($2F_o - F_c$, contoured at 1σ) showing that a single enantiomer of RJW100 is bound. (C) Close-up views of the binding pocket from the structure of LRH-1 bound to 10CA, depicting side chains of amino acid residues that interact with the ligand. (D) Superposition of DLPC and RJW100, showing their similar binding poses. (E) MDS analysis reveals that **10CA** makes contacts to Y516, K520, and G421 for amounts of time similar to DLPC.

3.4 Surface Residue Contacts Drive Binding and Activation by PL Mimetics

To interrogate the function of these PL-like interactions made by long-tailed PhCs and CAs, we mutated key LRH-1 residues and measured the impact on binding affinity and transcriptional activity. Introduction of a Y516A or K520A mutation nearly ablates DLPC binding, reducing affinity by more than an order of magnitude and greatly compromising its ability to

displace a fluorescent probe—the design of which is described in detail in Chapter 6 (Fig. 3.3A). Likewise, for **9CA** and **10CA**, both the K520A and Y516A mutations significantly decrease binding affinity. For **9PhC** and **10PhC**, these mutations are also detrimental for binding. This data supports the hypothesis that the PL-mimicking contacts by these ligands are critical for effective binding.

Surprisingly, in luciferase activity assays the K520A mutation affects LRH-1 activation by the phosphorylcholines and carboxylates differently. For **9PhC** and **10PhC** (Fig. 3.3C) the Y516A mutation prevents activation, but the K520A mutation has no impact on LRH-1 activation. For **9CA** and **10CA**, however, both mutations prevent ligand-driven activity (Fig. 3.3B).

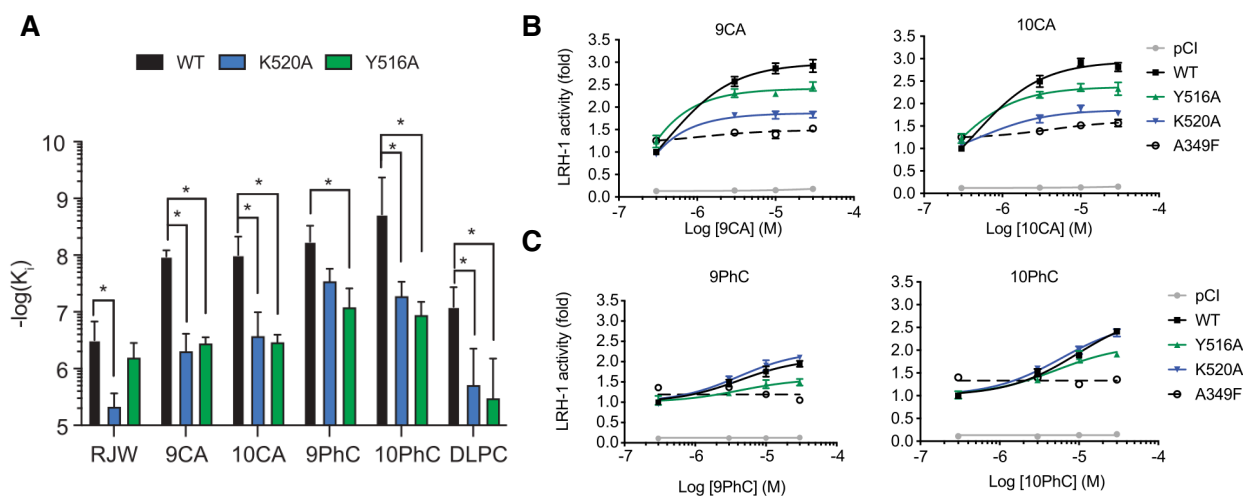


Figure 3.3. LRH-1 LBD mutations effect activity and binding. (A) Binding affinity of both CAs and PhCs are decreased when mutations that disrupt binding at the mouth of the pocket are introduced. (B) Transcriptional activity of LRH-1 by CAs is decreased when mutations that disrupt binding at the mouth of the pocket are introduced. (C) Transcriptional activity of LRH-1 by PhCs is only moderately decreased or not affected when mutations that disrupt binding at the mouth of the pocket are introduced. C, D: A349F introduces a bulky mutation that prohibits ligand binding, this mutation is used as a negative control.^{69a}

The difference in PhC *versus* CA activities may be because of the increased number of polar contacts, size, and different geometry of the pharmacophore in the PhCs, which may allow them to rely more heavily on a different residue for activation when one is mutated, whereas the CA compounds may have less flexibility in this regard due to their smaller, planar geometry.

The LRH-1-**10CA** structure and subsequent binding and activation data provides the first evidence of a synthetic molecule that makes polar contacts both in the deep part of the pocket (water-mediated T352 interaction, H390) and near the mouth (Y516, K520, G421).

3.5 Chimeras Affect Coregulator Association Signatures and Stabilize AFS

To uncover how the effective agonists (namely, **9CA** and **10CA**) specifically impact the mechanism of activation of LRH-1, we investigated how activating *versus* non-activating CAs effect LRH-1 conformation in solution using hydrogen-deuterium exchange mass spectrometry (HDX-MS). We used four CAs for HDX-MS: two that bind LRH-1 but are relatively inactive (**4CA**, **5CA**) and two highly activating agonists (**9CA**, **10CA**). We found that relative to the inactive compounds, **9CA** and **10CA** impart overall stability to Helix 3 and the pre-AFH loops in the LRH-1 activation function surface (AFS) as seen by the relative deuterium uptake over time in these different parts of the AFS (Fig. 3.4A).

Figure 3.4B and C illustrate the exact sites of differential deuterium uptake for LRH-1 relative to **4CA** and **5CA**. Compounds **9CA** and **10CA** stabilize the AFS relative to **4CA** and **5CA**. This is especially exciting because we had previously identified stabilization of the AFS as a desirable quality of strongly activating ligands (Chapter 1).

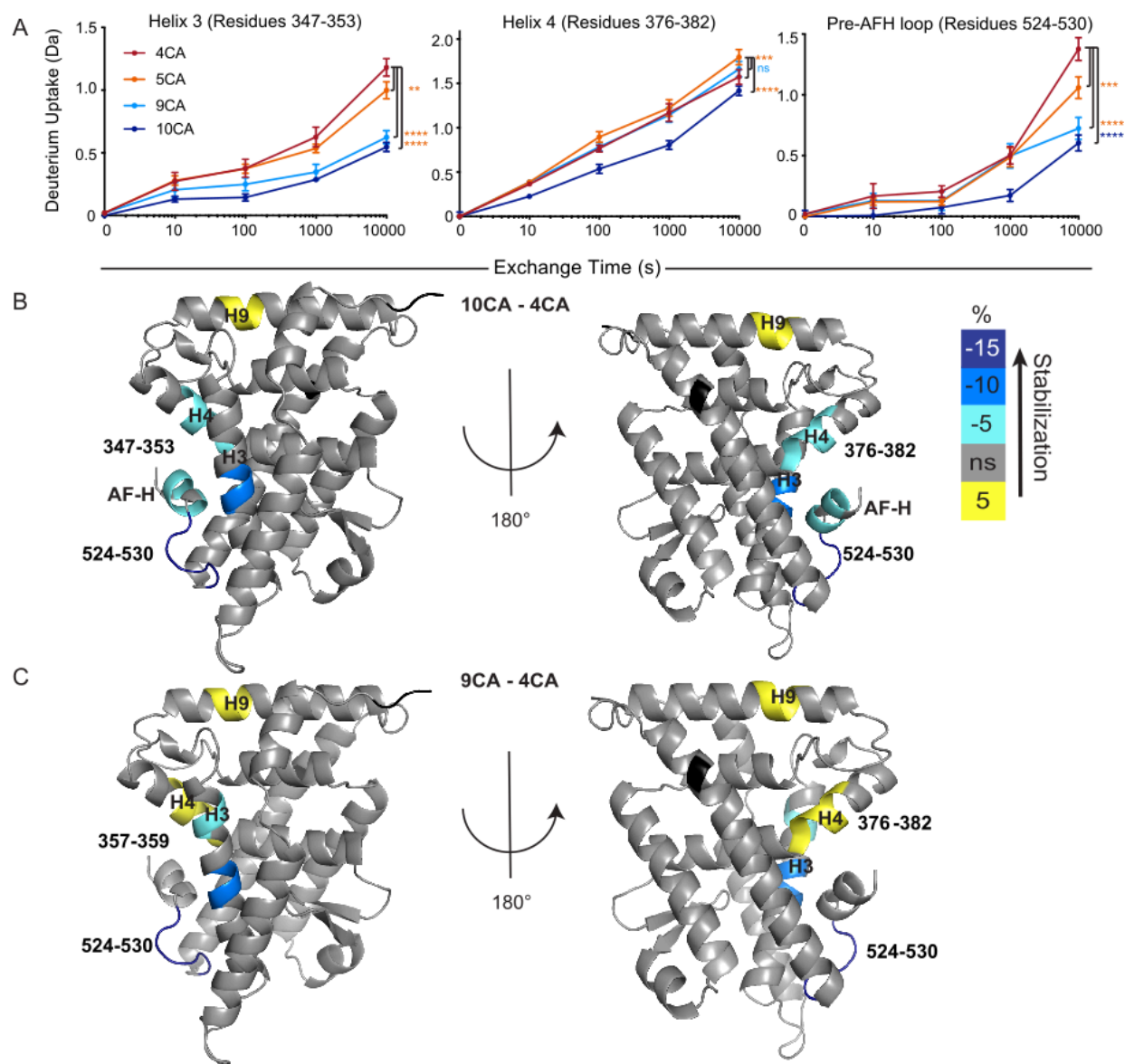


Figure 3.4. 9CA and 10CAs stabilize LRH-1 relative to 4CA and 5CA. HDX was used to probe differential effects on protein dynamics by four ligands, 4CA, 5CA, 9CA, and 10CA. (A) Deuterium uptake over time in helix 3, 4, and the pre-AFH loop as a function of ligand binding. (B) The scale reflects the difference in percent deuterium incorporation for 10CA bound LRH-1 minus 4CA-bound LRH-1. For example, negative numbers reflect slower deuterium incorporation (less motion) for RR-RJW100 versus DLPC. (C) The scale reflects the difference in percent deuterium incorporation for 9CA bound LRH-1 minus 4CA-bound LRH-1.

The stabilization of the AFS observed with HDX-MS suggests that **9CA** and **10CA** likely modulate coregulator binding at this site. To evaluate specific patterns of coregulator associations promoted by these agonists, we conducted coregulator profiling using the Microarray Assay for Real-time Coregulator-Nuclear Receptor Interactions (MARCoNI), a microarray that quantifies association of 154 peptides containing NR interaction motifs from 64 coregulators.⁴⁷ We conducted an experiment using purified LRH-1 LBD incubated with ligands at saturating concentrations. Patterns of coregulator preferences in this context provide a readout of ligand-induced conformational changes at the AFS. We first investigated how **4CA**, **5CA**, **9CA** and **10CA**s affect coregulator binding to the LRH-1 AFS *versus* unligated LRH-1 (apo).

The AFS of unligated LRH-1 exhibits a strong preference for binding known LRH-1 *corepressors* (i.e. nuclear receptor corepressor 1 (NCOR1), nuclear receptor subfamily 0 group B member 1 (NR0B1/DAX1), and nuclear receptor subfamily 0 group B member 2 (NR0B2/SHP), and NF κ B inhibitor beta (I κ B β), which is classified as “antagonist” behavior.

Compounds **9CA** and **10CA** profoundly alter coregulator associations *versus* the unligated protein. Both agonists disrupt many of the strongest coregulator interactions with unligated LRH-1 (i.e. I κ B β , NCOR1, and transcriptional cofactor of *c-fos* (TREF1)). **9CA** and **10CA** also increase association of a specific complement of coregulators (e.g. ligand dependent nuclear receptor corepressor (LCOR), nuclear receptor coactivator A1 (NCOA1) and nuclear receptor coactivator A3 (NCOA3). In contrast, **4CA** and **5CA** have weaker effects on coregulator associations in general. These results suggest that **9CA** and **10CA** promote conformational changes to the LBD

⁴⁷ Desmet, S. J.; Dejager, L.; Clarisse, D.; Thommis, J.; Melchers, D.; Bastiaensen, N.; Ruijtenbeek, R.; Beck, I. M.; Libert, C.; Houtman, R.; Meijer, O. C.; De Bosscher, K. Cofactor Profiling of the Glucocorticoid Receptor from a Cellular Environment. In *Steroid Receptors: Methods and Protocols*; Castoria, G., Auricchio, F., Eds.; Springer New York: New York, NY, 2014; pp 83–94

that affect coregulator recognition of the AFS, consistent with observations from HDX-MS. This study also delineates which specific coregulators are recruited to LRH-1 *in vitro* and *in vivo* to cause specific patterns of “agonistic” transactivation. Here, **9CA** and **10CA** seem to synergistically both downregulate corepressors *and* upregulate coactivators of LRH-1, demonstrating their power to potentially act as strong therapeutic leads.

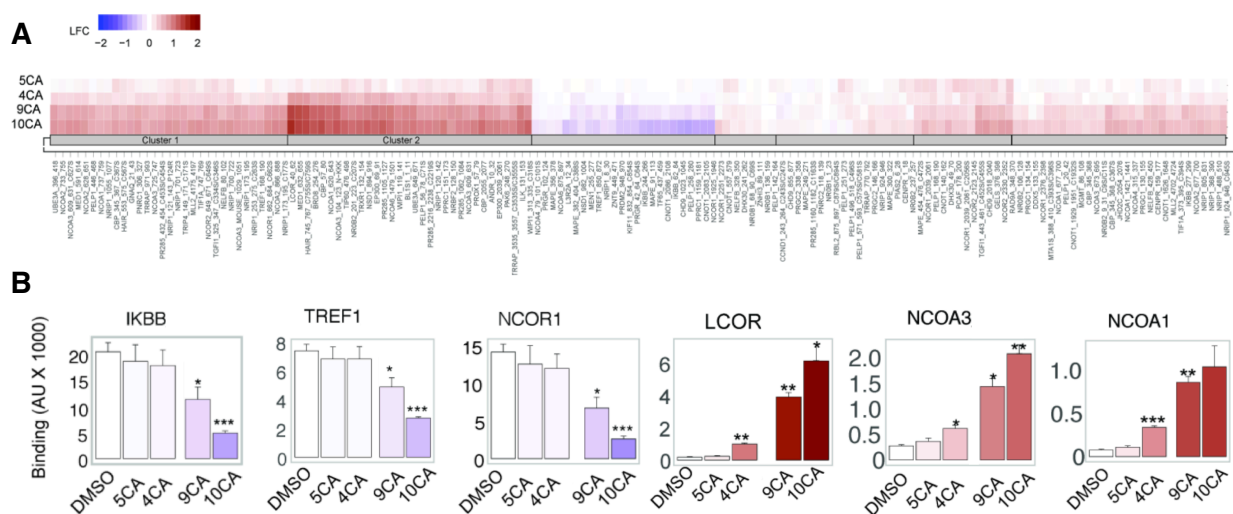


Figure 3.5. 9CA and 10CA effect coregulator recruitment more strongly than 4CA and 5CA. (A) overall clustered difference in coregulator recruitment to LRH-1 induced by **4CA**, **5CA**, **9CA**, and **10CA**. (B) Notable coregulator up- and down-recruitment induced by activating CAs. A,B: Log fold change (LFC) of peptides corresponding to the binding interface of coregulators is indicated. * = $p < 0.05$; ** $p < 0.01$. Student’s t-test, FDR.

3.6 Efficacy of 10CA in Murine Models of Colitis

LRH-1 has the potential to have a ligand-regulated therapeutic effect in inflammatory bowel diseases (IBD), which are characterized by chronic inflammation in the GI tract.⁴⁸ LRH-1 locally suppresses inflammation in the GI tract through regulation of corticosterone production

⁴⁸ Hanauer, S.B. Inflammatory Bowel Disease, Epidemiology, Pathogenesis, and Therapeutic Opportunities. *Inflamm. Bowel Dis.* **2006**, *12*(1), S3–S9.

and regulates maintenance of the epithelial cell barrier to promote intestinal cell survival.^{10,49} With a highly activating ligand for LRH-1 (**10CA**) in hand, we sought to determine whether the patterns of activity we discovered indeed could mitigate the effects of IBD.

We began with an organoid model from intestinal crypts of humanized LRH-1 mice (enteroids), which we and others have used to characterize anti-inflammatory effects of compounds.⁵⁰ Overnight treatment of enteroids with **10CA** induced transcription of the LRH-1 targets *Cyp11A1* and *Cyp11B1*, two steroidogenic genes which regulate corticosterone production (Fig. 3.6A). Additionally, **10CA** treatment increased transcript levels of the anti-inflammatory cytokine *Il-10* (which is important for protecting against colitis-induced inflammation) and, importantly, reduced levels of pro-inflammatory cytokines *Il-1B* and *TNF α* , which are overactive in colitis models (Fig. 3.6B,C).⁵¹ These results demonstrate robust activation of LRH-1 in a cellular model of IBD, and we were encouraged to pursue *in vivo* studies with **10CA**.

For this study, we utilized a dextran sulfate sodium (DSS)-induced murine model of IBD, with humanized LRH-1 mice which express only human LRH-1 in enterocytes.⁵² After 5 days of DSS treatment, mice had lost a significant amount of weight—a primary disease marker for IBD (Fig. 3.6D). Mice then received **10CA** or vehicle for 7 days. Treated mice quickly and significantly regained weight to their pre-DSS levels, and also demonstrated significantly improved symptom

⁴⁹ Fernandez-Marcos, P. J.; Auwerx, J.; Schoonjans, K. Emerging Actions of the Nuclear Receptor LRH-1 in the Gut. *Biochim. Biophys. Acta - Mol. Basis Dis.* **2011**, *1812* (8), 947–955

⁵⁰ Basak, O.; Beumer, J.; Wiebrands, K.; Seno, H.; van Oudenaarden, A.; Clevers, H. Induced Quiescence of *Lgr5+* Stem Cells in Intestinal Organoids Enables Differentiation of Hormone-Producing Enteroendocrine Cells. *Cell Stem Cell* **2017**, *20* (2), 177-190

⁵¹ Shouval, D. S.; Biswas, A.; Kang, Y. H.; Griffith, A. E.; Konnikova, L.; Mascanfroni, I. D.; Redhu, N. S.; Frei, S. M.; Doty, A. L.; Goldsmith, J. D.; Bhan, A. K.; Loizides, A.; Weiss, B.; Yerushalmi, B.; Yanagi, T.; Lui, X.; Francisco, J.; Muise, A. M.; Klein, C.; Horwitz, B. H.; Glover, C.; Bousvaros, A.; Snapper, S. B.; Children, B.; Hashomer, T.; Aviv, T.; Hospital, W.; Hospital, W.; Children, B.; Hospital, M. G.; Unit, G. Interleukin 1 Beta Mediates Intestinal Inflammation in Mice and Patients with IL10 Receptor Deficiency. *Gastroenterology*, **2017**, *151* (6), 1100–1104

⁵² Chassaing, B.; Aitken, J. D.; Malleshappa, M.; Vijay-Kumar, M. Dextran Sulfate Sodium (DSS)-Induced Colitis in Mice. *Curr. Protoc. Immunol.* **2014**, No. SUPPL.104, 1–14

scores (Fig. 3.6E) and intestinal histology (untreated: Fig. 3.6F, treated: Fig 3.6G). Conversely, vehicle-treated mice did not experience the same level of weight gain or improvement to symptom scores or intestinal histology. This is the first LRH-1 small molecule agonist to show *in vivo* efficacy in IBD, and these results excitingly affirm the promise of LRH-1 as a therapeutic target.

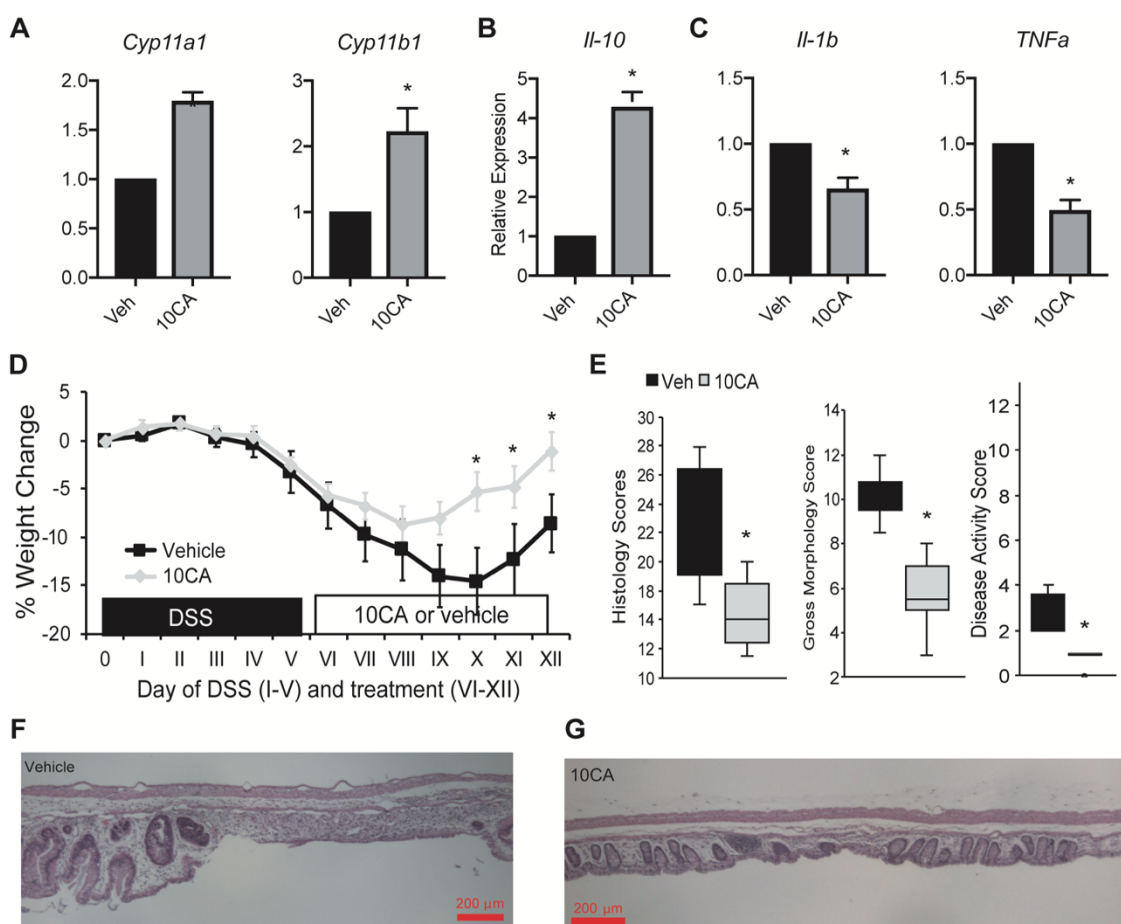


Figure 3.6. Therapeutic effects of 10CA in disease model. (A) Compound 10CA induces mRNA expression of steroidogenic enzymes Cyp11a1 and Cyp11b1. (B) Compound 10CA induces mRNA expression of anti-inflammatory cytokine IL-10. (C) Compound 10CA reduces mRNA expression of inflammatory cytokines IL-1 β (left) and TNF α (right). Error bars represent the standard deviation from six biological replicates for mouse enteroids. (D) Average % weight change in mice treated with DSS for 5 days, then 10CA or vehicle for 7 days. (E) Histology, gross morphology, and disease activity scores for mice treated with vehicle or 10CA. (F) colon tissue from mice treated with vehicle. (G) colon tissue from mice treated with 10CA.

3.6 Conclusions

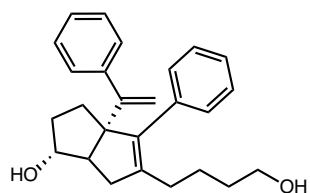
The discovery that phosphatidylcholines act as nuclear receptor ligands has illuminated the potential for novel signaling axes connecting phospholipid metabolism with gene expression. A leap forward in this area of research was realized when we synthesized 10CA, a highly efficacious LRH-1 agonist that acts as a hybrid between synthetic agonist RJW100 and dietary phospholipid DLPC. We were able to study the mechanism of activation of 10CA through crystallography, MDS, and HDX-MS where we made the discoveries that **10CA** binds in the LBD of LRH-1 and makes the proposed contacts as designed. HDX-MS revealed that **10CA** stabilizes the AFS of LRH-1. We investigated the coregulator association profile of **10CA** and identified coregulators that are potentially responsible for the downstream transcriptional activity we have seen in intestinal organoid models. An exciting study where we induced colitis in mice with DSS and then treated them with our agonist **10CA** reveals **10CA** as a viable therapeutic lead for IBD.

3.7 Supporting Information

Chemical Syntheses

General Procedure for Diol MOM Deprotection

To a solution of (**S1a-h**, Chapter 2) in MeCN was added concentrated HCl in excess (5-20 equiv.). The solution was stirred for 5 minutes or until the reaction was completed by TLC/LCMS. The resulting solution as concentrated *in vacuo* and subjected to preparatory HPLC to isolate the desired product as the major *exo* diastereomer.

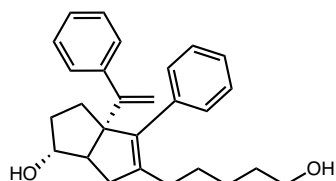


Exo-5-(4-hydroxybutyl)-4-phenyl-3a-(1-phenylvinyl)-1,2,3,3a,6,6a-hexahydropentalen-1-ol

(1): S1a (18.3 mg, 0.04 mmol) was reacted and purified according to the general procedure to give the title compound as a clear, colorless oil (13.0 mg, 79% yield).

¹H NMR (600 MHz, CDCl₃) δ 7.33 – 7.24 (m, 6H), 7.23 (s, 2H), 7.20 – 7.16 (m, 2H), 5.05 (d, *J* = 1.4 Hz, 1H), 4.97 (d, *J* = 1.5 Hz, 1H), 3.93 (s, 1H), 3.55 (t, *J* = 6.2 Hz, 2H), 2.36 (dd, *J* = 16.9, 9.3 Hz, 1H), 2.29 (d, *J* = 6.9 Hz, 1H), 2.10 – 2.02 (m, 4H), 1.74 – 1.61 (m, 3H), 1.50 – 1.37 (m, 4H).

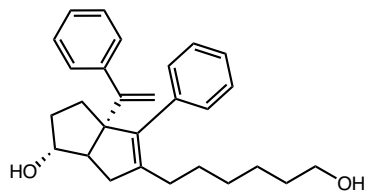
¹³C NMR (500 MHz, CDCl₃) δ 154.6, 144.1, 140.8, 139.4, 137.3, 129.6, 127.7, 127.7, 127.6, 126.6, 116.6, 114.8, 81.8, 69.3, 62.4, 55.7, 40.1, 33.9, 32.7, 32.0, 29.4, 24.0, 22.5, 10.6. **HRMS** calcd for C₂₆H₃₁O₂ [M+H]⁺: 375.23186, found 375.23145



Exo-5-(5-hydroxypentyl)-4-phenyl-3a-(1-phenylvinyl)-1,2,3,3a,6,6a-hexahydropentalen-1-ol

(2): S1b (21.2 mg, 0.05 mmol) was reacted and purified according to the general procedure to give the title compound as a clear, colorless oil (19.0 mg, >99% yield). **¹H NMR** (500 MHz, CDCl₃) δ 7.43 – 7.28 (m, 7H), 7.28 – 7.19 (m, 3H), 5.09 (d, *J* = 1.4 Hz, 1H), 5.01 (d, *J* = 1.4 Hz, 1H), 3.97 (s, 1H), 3.61 (t, *J* = 6.6 Hz, 2H), 2.38 (dd, *J* = 16.8, 9.4 Hz, 1H), 2.31 (d, *J* = 9.3, 1.5 Hz, 1H), 2.16 – 2.03 (m, 4H), 1.77 – 1.65 (m, 3H), 1.56 – 1.48 (m, 3H), 1.43 – 1.25 (m, 3H). **¹³C NMR** (500 MHz, CDCl₃) δ 154.5, 144.1, 140.8, 139.3, 137.3, 131.5, 129.6, 128.2, 127.7, 127.6, 126.7, 126.6,

115.0, 82.0, 69.3, 62.9, 61.9, 55.8, 40.3, 34.0, 32.5, 32.1, 31.3, 29.7, 27.6, 25.8, 16.0. **HRMS** calcd for $C_{27}H_{33}O_2$ $[M+H]^+$: 389.24751, found 398.24762

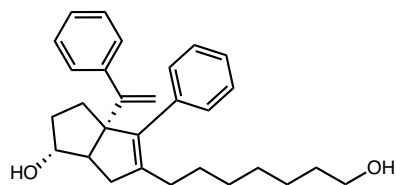


Exo-5-(6-hydroxyhexyl)-4-phenyl-3a-(1-phenylvinyl)-1,2,3,3a,6,6a-hexahydropentalen-1-ol

(3): S1c (9.5 mg, 0.02 mmol) was reacted and purified according to the general procedure to give the title compound as a clear, colorless oil (6.8 mg, 79% yield).

1H NMR (600 MHz, $CDCl_3$) δ 7.36 – 7.25 (m, 6H), 7.24 – 7.15 (m, 4H), 5.05 (s, 1H), 4.97 (s, 1H), 3.93 (s, 1H), 3.58 (t, $J = 6.6$ Hz, 2H), 2.35 (dd, $J = 16.9, 9.4$ Hz, 1H), 2.28 (d, $J = 9.4$ Hz, 1H), 2.11 – 1.97 (m, 4H), 1.75 – 1.62 (m, 3H), 1.53 – 1.46 (m, 2H), 1.38 – 1.15 (m, 6H).

^{13}C NMR (600 MHz, $CDCl_3$) δ 154.5, 144.1, 140.9, 139.2, 137.3, 129.7, 127.7, 127.6, 126.7, 126.6, 115.0, 110.0, 82.0, 69.3, 63.0, 55.8, 40.3, 34.0, 32.6, 32.1, 29.6, 29.4, 27.7, 25.5, **HRMS** calcd for $C_{28}H_{35}O_2$ $[M+H]^+$: 403.26316, found 403.26338



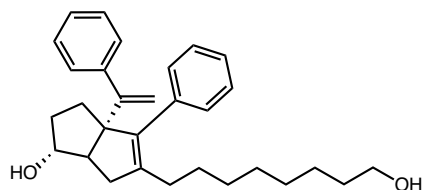
Exo-5-(7-hydroxyheptyl)-4-phenyl-3a-(1-phenylvinyl)-1,2,3,3a,6,6a-hexahydropentalen-1-ol

(4): S1d (11.6 mg, 0.03 mmol) was reacted and purified according to the general procedure to give the title compound as a clear, colorless oil (8.5 mg, 81% yield).

1H NMR (600 MHz, $CDCl_3$) δ 7.35 – 7.25 (m, 5H), 7.24 – 7.15 (m, 5H), 5.05 (d, $J = 1.4$ Hz, 1H), 4.97 (d, $J = 1.4$ Hz, 1H), 3.93 (s, 1H), 3.60 (t, $J = 6.7$ Hz, 2H), 2.35 (dd, $J = 16.9, 9.3$ Hz, 1H), 2.28 (d, $J = 9.4$ Hz, 1H), 2.09 – 1.98 (m, 5H), 1.73 – 1.61 (m, 3H), 1.36 – 1.19 (m, 10H).

^{13}C NMR (600 MHz, CDCl_3) δ 154.5, 144.1, 141.0, 139.2, 137.3, 129.7, 127.7, 127.6, 126.64, 126.59, 115.0, 82.0, 69.3, 63.0, 58.5, 55.8, 50.9, 40.2, 34.0, 32.7, 32.1, 29.63, 29.58, 29.2, 27.7, 25.6, 18.4.

HRMS calcd for $\text{C}_{29}\text{H}_{36}\text{O}_2\text{Cl}$ $[\text{M}+\text{Cl}]^-$: 451.24093, found 451.24179

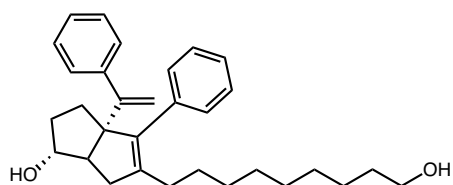


Exo-5-(8-hydroxyoctyl)-4-phenyl-3a-(1-phenylvinyl)-1,2,3,3a,6,6a-hexahydropentalen-1-ol

(5): S1e (4.6 mg, 0.01 mmol) was reacted and purified according to the general procedure to give the title compound as a clear, colorless oil (2.3 mg, 55% yield)

^1H NMR (600 MHz, CDCl_3) δ 7.35 – 7.25 (m, 6H), 7.24 – 7.16 (m, 4H), 5.05 (d, $J = 1.4$ Hz, 1H), 4.97 (d, $J = 1.4$ Hz, 1H), 3.93 (s, 1H), 3.61 (t, $J = 6.7$ Hz, 2H), 2.35 (dd, $J = 16.9, 9.3$ Hz, 1H), 2.28 (d, $J = 9.2$ Hz, 1H), 2.10 – 2.01 (m, 2H), 2.00 – 1.97 (m, 2H), 1.74 – 1.61 (m, 3H), 1.35 – 1.16 (m, 13H).

HRMS calcd for $\text{C}_{30}\text{H}_{38}\text{O}_2\text{Cl}$ $[\text{M}+\text{Cl}]^-$: 465.25658, found 465.25703



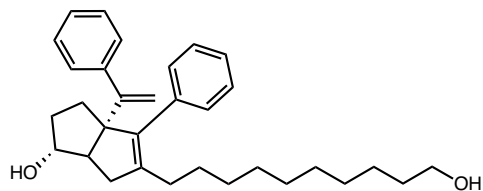
Exo-5-(9-hydroxynonyl)-4-phenyl-3a-(1-phenylvinyl)-1,2,3,3a,6,6a-hexahydropentalen-1-ol

(6): S1f (9.4 mg, 0.02 mmol) was reacted and purified according to the general procedure to give the title compound as a clear, colorless oil (8.2 mg, 96% yield.)

¹H NMR (600 MHz, CDCl₃) δ 7.39 – 7.26 (m, 5H), 7.24 – 7.14 (m, 5H), 5.05 (d, *J* = 1.4 Hz, 1H), 4.97 (d, *J* = 1.4 Hz, 1H), 3.93 (s, 1H), 3.62 (t, *J* = 9.4 Hz, 2H), 2.34 (dd, *J* = 16.7, 9.4 Hz, 1H), 2.27 (d, *J* = 9.3 Hz, 1H), 2.12 – 2.03 (m, 2H), 2.01 – 1.96 (m, 1H), 1.74 – 1.58 (m, 3H), 1.34 – 1.17 (m, 18H).

¹³C NMR (600 MHz, CDCl₃) δ 154.6, 144.2, 141.1, 139.1, 137.4, 129.7, 127.71, 127.70, 127.59, 126.64, 126.57, 115.0, 82.1, 69.3, 63.1, 55.8, 40.2, 34.0, 32.8, 32.1, 29.7, 29.6, 29.5, 29.4, 29.3, 27.8, 25.7.

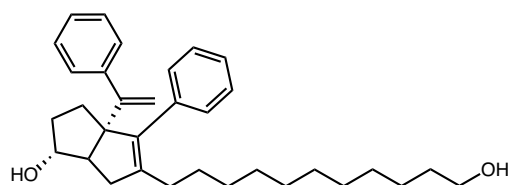
HRMS calcd for C₃₁H₄₀O₂Cl [M+Cl]⁻ : 479.27223, 479.27260



Exo-5-(10-hydroxydecyl)-4-phenyl-3a-(1-phenylvinyl)-1,2,3,3a,6,6a-hexahydropentalen-1-ol (7): S1g (81.4 mg, 0.16 mmol) was reacted and purified according to the general procedure to give the title compound as a clear, colorless oil (62.0 mg, 83% yield).

¹H NMR (600 MHz, CDCl₃) δ 7.35 – 7.25 (m, 5H), 7.24 – 7.16 (m, 5H), 5.05 (d, *J* = 1.4 Hz, 1H), 4.97 (d, *J* = 1.4 Hz, 1H), 3.93 (s, 1H), 3.61 (t, *J* = 6.7 Hz, 2H), 2.34 (dd, *J* = 16.9, 9.4 Hz, 1H), 2.27 (d, *J* = 9.2 Hz, 1H), 2.11 – 2.00 (m, 3H), 1.73 – 1.62 (m, 3H), 1.54 (dq, *J* = 8.2, 6.7 Hz, 2H), 1.34 – 1.17 (m, 17H).

LRMS [APCI] calcd for C₃₂H₄₁O₂ [M-H]⁻ : 457.3, found 457.2



Exo-5-(11-hydroxyundecyl)-4-phenyl-3a-(1-phenylvinyl)-1,2,3,3a,6,6a-hexahydropentalen-1-ol (8): **S1h** (7.7 mg, 0.015 mmol) was reacted and purified according to the general procedure to give the title compound as a clear, colorless oil (5.4 mg, 78% yield).

¹H NMR (600 MHz, CDCl₃) δ 7.34 – 7.25 (m, 4H), 7.24 – 7.16 (m, 5H), 5.05 (d, *J* = 1.4 Hz, 1H), 4.96 (d, *J* = 1.3 Hz, 1H), 3.93 (s, 1H), 3.61 (t, *J* = 6.7 Hz, 2H), 2.33 (dd, *J* = 17.2, 9.8 Hz, 1H), 2.26 (d, *J* = 9.3 Hz, 1H), 2.09 – 1.99 (m, 1H), 2.02 – 1.99 (m, 5H), 1.72 – 1.61 (m, 3H), 1.57 – 1.51 (m, 2H), 1.40 – 1.11 (m, 10H).

LRMS [APCI] calcd for C₃₃H₄₃O₂ [M-H]⁻ : 471.3, found 471.0

Ligand binding assay.

All assays were conducted in black, polystyrene, non-binding surface 384-well plates (Corning Inc., Corning, NY) with 30 μL volumes in assay buffer (150 mM NaCl, 20 mM Tris-HCl pH 7.4, 5% glycerol). Binding affinity of the fluorescein amidite (FAM)-labeled probe (6N-FAM, Chapter 6) for WT and mutant LRH-1 was determined as described⁵³ and used to determine probe and protein concentrations used in competition experiments. Competition assays were conducted with 10 nM 6N-FAM (10, 0.6, and 1.1 times the K_d of wildtype, K520A, and Y516A LRH-1, respectively, for 6N-FAM). For protein concentration, 5, 10, and 15 nM wildtype, K520A, or Y516A LRH-1 were used, representing 50-80% of the B_{max} from the 6N-FAM binding curves for

⁵³ D'Agostino, E. H.; Flynn, A. R.; Cornelison, J. L.; Mays, S. G.; Patel, A.; Jui, N. T.; Ortlund, E. A. Development of a Versatile and Sensitive Direct Ligand Binding Assay for Human NR5A Nuclear Receptors. *ACS Med. Chem. Lett.* **2019**

each protein variant. Assay conditions were validated using unlabeled compound 6N. Competition experiments used unlabeled agonists at a concentration range of 200 pM-200 μ M. Plates were incubated overnight at 4°C and centrifuged at 2,000 x g for 2 minutes before polarization measurement. Polarization was monitored on a Neo plate reader (Biotek, Winooski, VT) at an excitation/emission wavelength of 485/528 nm. The experiment was conducted twice in quadruplicate, and GraphPad Prism version 7 was used to analyze compiled data. Data were baseline subtracted, then normalized to the 6N competition curve (representing complete competition) and fit using a one-site, fit K_i curve. Mutants were normalized to their respective 6N curves. To compare K_i values for wildtype versus K520A and Y516A mutants, two-way Anova with Dunnett's test for multiple comparisons was used (GraphPad Prism v7).

Differential scanning fluorimetry.

Purified protein, pre-exchanged with DLPC (0.2 mg/mL), was combined with agonists overnight at 4 °C. SYPRO orange dye was added to the complexes the next day, at a final dilution of 1:1000. Complexes were heated at a rate of 0.5 °C/ minute on a StepOne Plus thermocycler, using the ROX filter for fluorescence detection. T_m was calculated using the Boltzman equation (GraphPad Prism, V7). Assays were conducted in triplicate, with three biological replicates.

Mutagenesis

Mutations were introduced using the Quikchange Lightning site-directed mutagenesis kit as directed by the manufacturer (Agilent). Constructs were sequenced prior to use in binding or activity assays.

Cell Culture

Hela cells were purchased from Atlantic Type Culture Collection and cultured in MEM α medium supplemented with 10% charcoal-stripped fetal bovine serum. Cells were maintained under standard culture conditions.

Reporter gene assays

Hela cells were seeded into 96-well culture plates at 7500 cells/ well and transfected with reporter plasmids and either pCI empty vector or full-length LRH-1-pCI. Reporter plasmids consisted of (1) the pGLC3 basic vector containing a portion of the SHP promoter containing the LRH-1 response element cloned upstream of firefly luciferase and (2) a constitutively active vector encoding *Renilla* luciferase used for normalization. Transfections utilized the FugeneHD transfection reagent at a ratio of 5 μ l Fugene: 2 μ g DNA. Cells were treated with agonists 24 hours after transfection at concentrations indicated in the figure legends. 24 hours after treatment, luminescence was quantified using the DualGlo kit from Promega on a BioTek Neo plate reader.

LRH-1 LBD purification.

LRH-1 LBD (residues 299-541) in the pMSC7 vector was transformed in *E. coli* strain BL21(pLysS) for expression. Cultures were grown at 37 °C in liquid broth to an OD₆₀₀ of 0.6 prior to induction of protein expression with 1 mM isopropyl-1-thio-D-galactopyranoside (IPTG). Cultures were grown for 4 hours at 30 °C following induction. Protein was purified by nickel affinity chromatography with Buffer A of 20 mM Tris HCl (pH 7.4), 150 mM NaCl, 5% glycerol, and 25 mM imidazole and Buffer B of 150 mM Tris HCl (pH 7.4), 150 mM NaCl, 5% glycerol,

and 500 mM imidazole (HisTrap FF; GE Healthcare, Little Chalfont, UK). Protein was incubated with DLPC (4-fold molar excess) overnight at 4 °C, repurified by size exclusion into assay buffer (150 mM NaCl, 20 mM Tris-HCl (pH 7.4), and 5% glycerol, concentrated to approximately 3 mg/mL, and stored at -80°C until use. The same purification strategy was utilized for protein containing the point mutations described in the text.

Generation of apo LRH-1

To extract lipids from the LRH-1 LBD, 1 mL of purified protein (3 mg) was treated with 3.75 mL of chloroform-methanol solution (1:2 v/v) and vortexed briefly. An additional 2.5 mL chloroform:water solution (1:1 v/v) was added and the mixture was vortexed again. The stripped and unfolded protein was pelleted by centrifugation at 1000 rpm for 10 minutes. The resulting protein pellet was dissolved into 0.5 mL of buffer containing 50 mM Tris (pH 8.0), 6 M guanidine hydrochloride and 2 mM DTT. Protein was refolded by fast dilution at 4 °C into 25 mL of buffer containing 20 mM Tris (pH 8.5), 1.7 M urea, 4% glycerol and 2 mM DTT. The final urea concentration was adjusted to 2 M, and protein was concentrated to ~ 1.5 mL, followed by overnight dialysis against PBS containing 2 mM DTT at 4 °C. Refolded protein was purified by size exclusion chromatography to remove aggregates and remaining unfolded protein, and ligand binding ability was verified by fluorescence polarization.

Crystallography

6X-His-LRH-1 LBD was expressed and purified by nickel affinity chromatography as described above. The His tag was cleaved overnight at 4 °C using TEV protease with dialysis against buffer containing 150 mM NaCl, 5% glycerol, and 20 mM Tris HCl (pH 7.4). Cleaved protein was

isolated using nickel affinity chromatography. To generate protein-ligand complexes, purified protein was incubated overnight at 4 °C with 4-5-fold molar excess of ligand. Complexes were purified by size exclusion chromatography into crystallization buffer (150 mM NaCl, 100 mM ammonium acetate (pH 7.4), 1 mM DTT, 1 mM EDTA, 2 mM 3-[(3-cholamidopropyl)dimethylammonio]-1propanesulfonic acid (CHAPS)), and then incubated with 4-fold molar excess of Tif2 peptide for two hours at room temperature (Tif2 peptide sequence was H₃N-KENALLRYLLDKDDT-CO₂⁻, or a shorter version for the 10CA-LRH-1 structure, H₃N-KENALLRYLLDK-CO₂⁻). Crystallization conditions for each complex were as follows:

LRH-1-10CA-Tif2: The LRH-1-10CA-Tif2 complex was concentrated to 5 mg/mL and screened using the Classics screen (Qiagen) and a Phoenix Liquid Handler (Art Robbins Instruments) in 96-well sitting drop plates. Crystals were generated at room temperature in 0.4 M N/K tartrate.

LRH-1-9CA-Tif2: Crystals were generated by microseeding, using LRH-1-RJW100-Tif2 crystals as seed stocks. Crystals used as seeds were grown as previously described. The complex was crystallized by sitting drop vapor diffusion with drops of 1 µl purified LRH-1-9CA-Tif2 (6 mg/ml), 1 µl seed stock, and 2 µl crystallant (0.2 M ammonium formate (pH 6.6), 20% PEG 3350).

LRH-1-11CA-Tif2: Crystals were generated by hanging drop vapor diffusion, using a crystallant of 0.05 M sodium acetate (pH 4.6), 5-11% PEG 4000, and 0-10% glycerol. LRH-1-9PC-Tif2 and

LRH-1-11PC-Tif2: Crystals were generated by soaking the ligands into LRH-1-RJW100-Tif2 crystals. Drops of purified complexes were added to cover slides next to drops containing LRH-1-RJW100 crystals and combined with crystallant at a ratio of 1:1. Drops were equilibrated for 2 days at 18 °C. LRH-1-RJW100 crystals were then individually transferred into the equilibrated drops for ligand exchange.

Structure Determination

Crystals were flash-frozen in liquid nitrogen using a cryoprotectant of 30% glycerol in crystallant. Data were collected remotely from Argonne National Laboratory (South East Regional Collaborative Access Team, Lemont, IL) using the 22ID beamline. Data were processed and scaled using HKL2000²² and phased by molecular replacement using Phaser-MR (Phenix²³) with PDB 5L11 as the search model. Coot²⁴ and Phenix.refine²³ were used for model building and refinement, respectively. Figures were constructed using Pymol.²⁵ Ligplot+²⁷ was used to identify residues interacting with the ligands.

Hydrogen-deuterium exchange mass spectrometry (HDX-MS)

Following affinity purification and removal of the His-tag as described above, LRH-1 LBD protein was repurified by size exclusion chromatography into an assay buffer of phosphate-buffered saline, pH 7.5, plus 5% glycerol. Protein aliquots (2 mg/ml) were incubated with carboxylic acid derivatives **4CA**, **5CA**, **9CA**, or **10CA** at 5-fold molar excess, overnight at 4 °C. Samples were diluted 1:7 (v/v) into 10 mM phosphate buffer in 99.9 % D₂O to initialize exchange reactions. The reactions were quenched after 0, 10, 100, 1000 and 10000 seconds by adding equal volume of precooled quenching buffer (100 mM phosphate, 0.5 M tris(2-carboxyethyl) phosphine, 0.8% formic acid, and 2% acetonitrile, pH 2.5). Reactions for each sample at each time point were performed in triplicate. Quenched samples were passed through an Enzymate BEH pepsin column (Waters Corp, Milford, MA). Fragmented peptides were separated by an C18 UPLC column and analyzed by a Q-ToF Premier mass spectrometer. ProteinLynx Global SERVER™ (PLGS) was used to identify peptides by database searching of LRH-1 LBD sequence. The HDX-MS data were

further processed using DynamX (v3.0) and the differential HDX between ligand-bound states was calculated by comparing the relative fractional uptake for each residue at given time.

In vitro NR-coregulator recruitment by MARCoNI

Assay mixes of 50 nM His-SUMO-hLRH-1-LBD (bound to copurifying PL from *E. coli* or preloaded with compound during purification), 25 nM ALEXA488-conjugated penta-His antibody (Qiagen # 35310), 50 μ M DTT, 10 μ M freshly added compound (or 2% DMSO) were made in 20mM Tris(pH 7.4), 250mM NaCl and 0.5 mM TCEP and stored on ice. LRH-1 in the assay mixes for was functionally analyzed by applying Micro array Assay for Real-time Coregulator Nuclear Receptor Interaction (MARCoNI), using PamChip #88101 with 154 unique coregulator sequences. In short, each condition was tested using three technical replicates (arrays), and LRH-1 binding to each coregulator motif was quantified using BioNavigator software (PamGene). The modulation index (MI, defined as the compound-induced log-fold change of LRH-1 binding to each coregulator) and statistical significance (Student's t-test) were calculated and visualized using R software (R Core Team, 2017). Compound and interaction (dis-)similarity was calculated by Hierarchical Clustering on Euclidean Distance and Ward's agglomeration.

Animals

For the experiments involving enteroids and in vivo IBD, the work was done in collaboration with Dr. David Moore. The study protocol was approved by the Animal Care and Use Committee of the Baylor College of Medicine and was in accordance with the Guide for the Care and Use of Laboratory Animals [DHHS publication no. (NIH) 85-23, revised 1985, Office of Science and Health Reports, DRR/NIH, Bethesda, MD 20205].

Chapter 4:
**LRH-1-RJW100 Crystal Structures Enable a
Comprehensive Structure-Activity Relationship**

Adapted and Reprinted in part with permission from J. Med. Chem. 2019, 62, 11022–11034
Copyright 2019 American Chemical Society
<https://pubs.acs.org/doi/10.1021/acs.jmedchem.9b00753>

4.1 Synthesizing a Library

Our structural studies have revealed that highly similar LRH-1 synthetic agonists can bind unpredictably within the hydrophobic binding pocket, which has presented a challenge for improving agonist design in a rational manner (Fig 4.1A, and Chapter 1).¹⁷ In addition to our efforts to contact the mouth of the pocket (Chapter 2, 3),³⁶ we reasoned that strengthening contacts within the deep polar part of the LBD (e.g. T352, H390—this space hereafter abbreviated DPP) may anchor synthetic compounds in a consistent orientation and improve potency. To evaluate this hypothesis, we synthesized RJW100 analogs with polar groups in place of the RJW100 hydroxyl (R^1), aiming to displace bridging waters and to generate direct interactions with Thr352 or other nearby polar residues (Fig. 4.1B). In parallel, we synthesized compounds designed to interact with other sites in the DPP by (1) modifying the external styrene (R^2) to promote interactions with helix 3 or to fill a hydrophobic pocket in the vicinity or (2) incorporating hydrogen bond donors at the meta position of the internal styrene (R^3) to promote hydrogen bonding with His390 (also via water displacement) (Fig. 4.1B).⁵⁴

⁵⁴ Mays, S. G.; Flynn, A. R.; Cornelison, J. L.; Okafor, C. D.; Wang, H.; Wang, G.; Huang, X.; Donaldson, H. N.; Millings, E. J.; Polavarapu, R.; Moore, D. D.; Calvert, J. W.; Jui, N. T.; Ortlund, E. A. Development of the First Low Nanomolar Liver Receptor Homolog-1 Agonist through Structure-Guided Design. *J. Med. Chem.* **2019**, *62* (24), 11022–11034

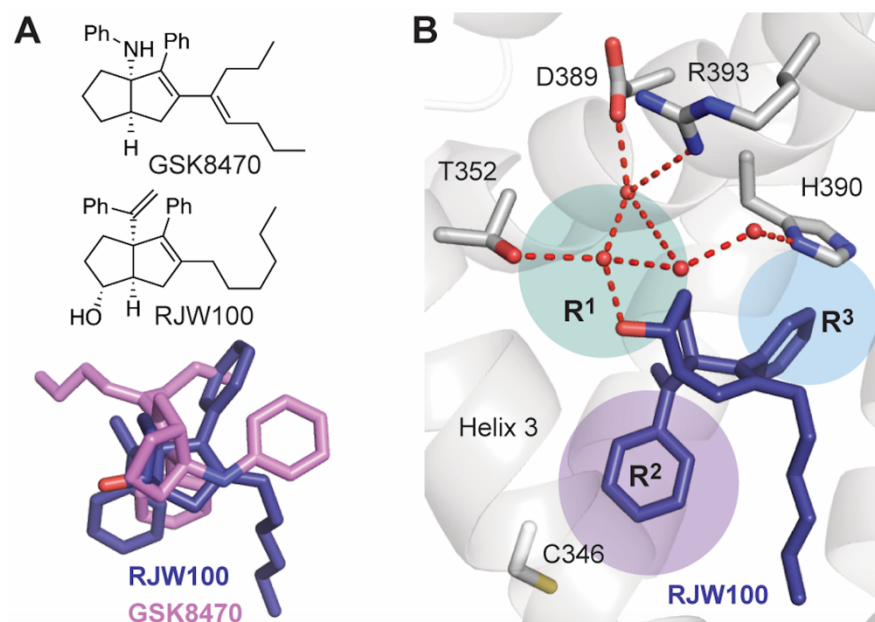


Figure 4.1. Structure-based design of LRH-1 agonists. (A) Top, chemical structures of the agonists GSK8470 and RJW100. Bottom, the superposition of GSK8470 and RJW100 (from PDB 3PLZ and 5L11, respectively)^{12,13} show the very different binding modes for these similar agonists. (B) RJW100 interacts with LRH-1 residue Thr352 via water. The four water molecules shown coordinate a group of polar residues deep in the binding pocket. The colored circles indicate the areas targeted by modifications to the RJW100 scaffold in this work.

To prepare this compound library, we utilized Whitby's zirconocene-mediated Pauson–Khand-type cyclization,³⁷ or the diastereoselective variant that we have developed.³⁶ This highly modular approach unites three readily available precursors (an enyne, an alkyne, and 1,1-dibromoheptane) to generate all-carbon bridgehead [3.3.0]-bicyclic systems with varying functionalities at positions R¹, R², and R³ (Fig. 4.2A). R¹ was most conveniently varied through modification of the RJW100 alcohol to yield derivatives **1–8**, which were synthesized separately as both the endo (N) or exo (X) diastereomers (Fig. 4.2B). Oxygen-linked analogs **3** and **5** were formed directly from the diastereomerically appropriate parent alcohol. Nitrogen-linked analogs **1, 2, 4, 6, and 8** were prepared through alcohol activation (mesylate **S4**) and substitution (azide **S2**, nitrile **S3**) (Fig. 4.2B and Supporting Information). Alteration of R² was accomplished by

introducing phenylacetylene derivatives as the alkyne in the cyclization step (Fig. 4.2A), generating **9–15** (Fig. 4.2B). R^3 variants **16–23** were prepared using functionalized enyne starting materials. The detailed chemical syntheses of all intermediates and tested compounds are provided in the supplementary information.

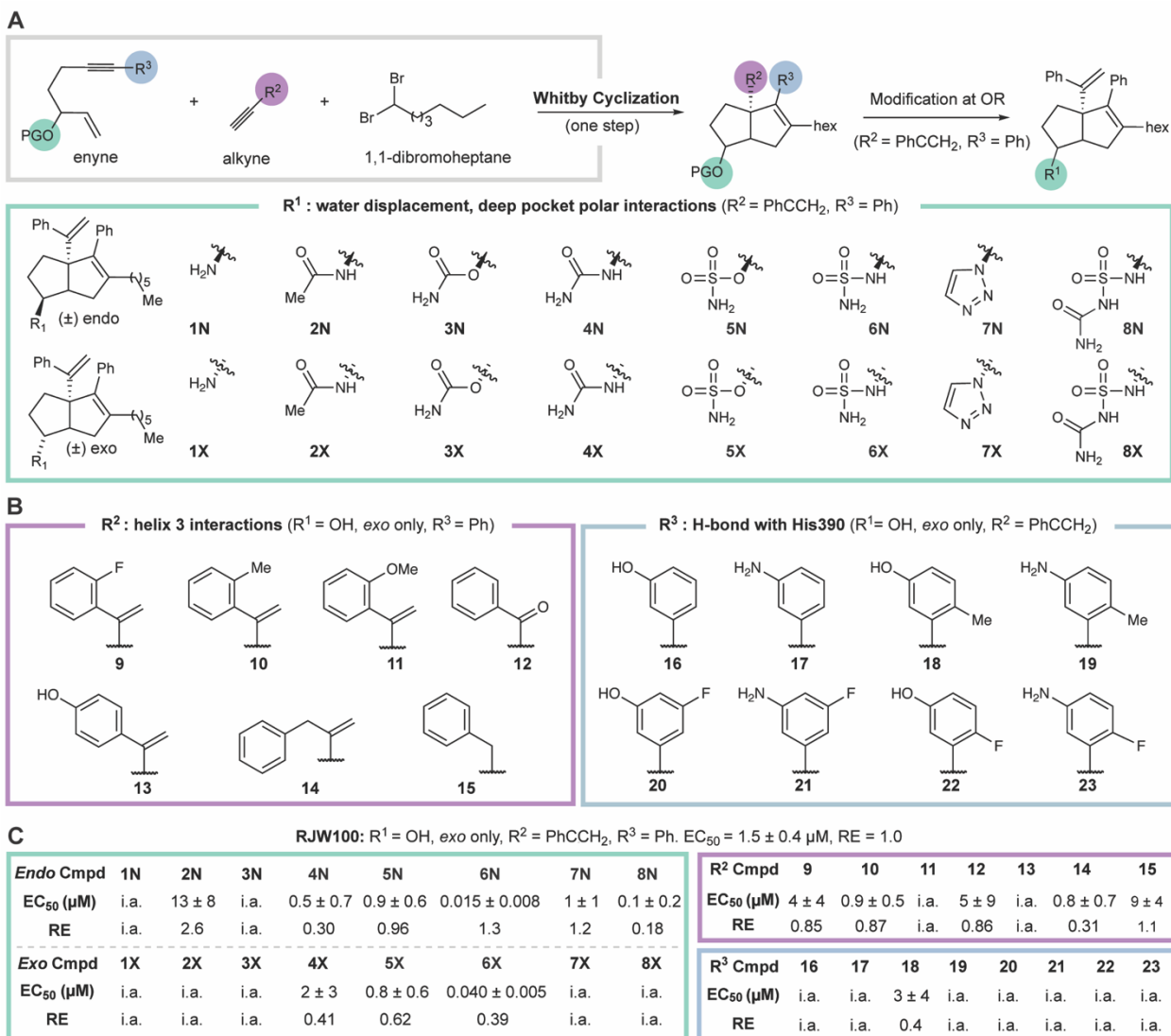


Figure 4.2. Synthesis of LRH-1-targeted compounds. (A) Overview of the synthetic strategy used to generate agonists based on modification of the [3.3.0]-bicyclic hexahydropentalene scaffold. (B) Modifications to the scaffold evaluated in this study, grouped by the site of modification by colored boxes. (C) Summary of EC_{50} and efficacy relative to RJW100 relative efficacy (RE). RE was calculated as described in the methods section. RJW100 RE = 1.0 and $\text{EC}_{50} = 1.5 \pm 0.4 \mu\text{M}$. The abbreviation “i.a.” refers to inactive compounds for which EC_{50} values could not be calculated.

4.2 The First Low Nanomolar LRH-1 Agonist

We evaluated the new compounds using differential scanning fluorimetry (DSF) because entropic gain from displacement of buried water molecules or favorable energetics from bond formation would result in global stabilization of the LRH-1-agonist complex. DSF assays were paired with cellular luciferase reporter assays to determine effects on LRH-1 transcriptional activity. Luciferase data are summarized in Figure 4.2C and dose-response curves are shown in Figure S4.1. As previously observed, RJW100 stabilizes the LRH-1 ligand binding domain (LBD) by around 3 °C relative to a PL ligand in DSF assays (Fig. 4.3A). While the R²- and R³-modified compounds (**9–23**) destabilize the receptor relative to RJW100 (Fig. 4.3A) and tend to be poor activators (Fig. 4.2C and S4.1), certain R¹ modifications are highly stabilizing, with T_m values 3–8 °C higher than RJW100 (Fig. 4.3A and Supporting Information).

There is a striking correlation between potency in luciferase reporter assays and LRH-1 stabilization by DSF for the R¹-modified compounds, where lower EC₅₀s are associated with higher T_m values (Pearson correlation coefficient = -0.71; p = 0.0009, Fig. 4.3B). This correlation provides a direct link between cellular activity and receptor stabilization. There is no correlation between T_m and EC₅₀ for the R²- and R³-modified compounds (data not shown), suggesting that improved potency is due to specific polar interactions mediated by the R¹ group. The R¹ modifications are diverse, ranging from small to large polar groups, including hydrogen bond donors and acceptors and *endo* and *exo* diastereomers (Fig. 4.2B). Both the size and stereochemistry of the R¹ group are important for activity. Mid-sized polar groups, mainly tetrahedral in geometry, tend to increase potency relative to RJW100 (Fig. 4.2C). The close relationship between the R¹ size, agonist potency, and LRH-1 stabilization is evident looking at DSF results, where a strong peak in stabilization occurs for compounds **5–6** and **8N** (Fig. 4.3A).

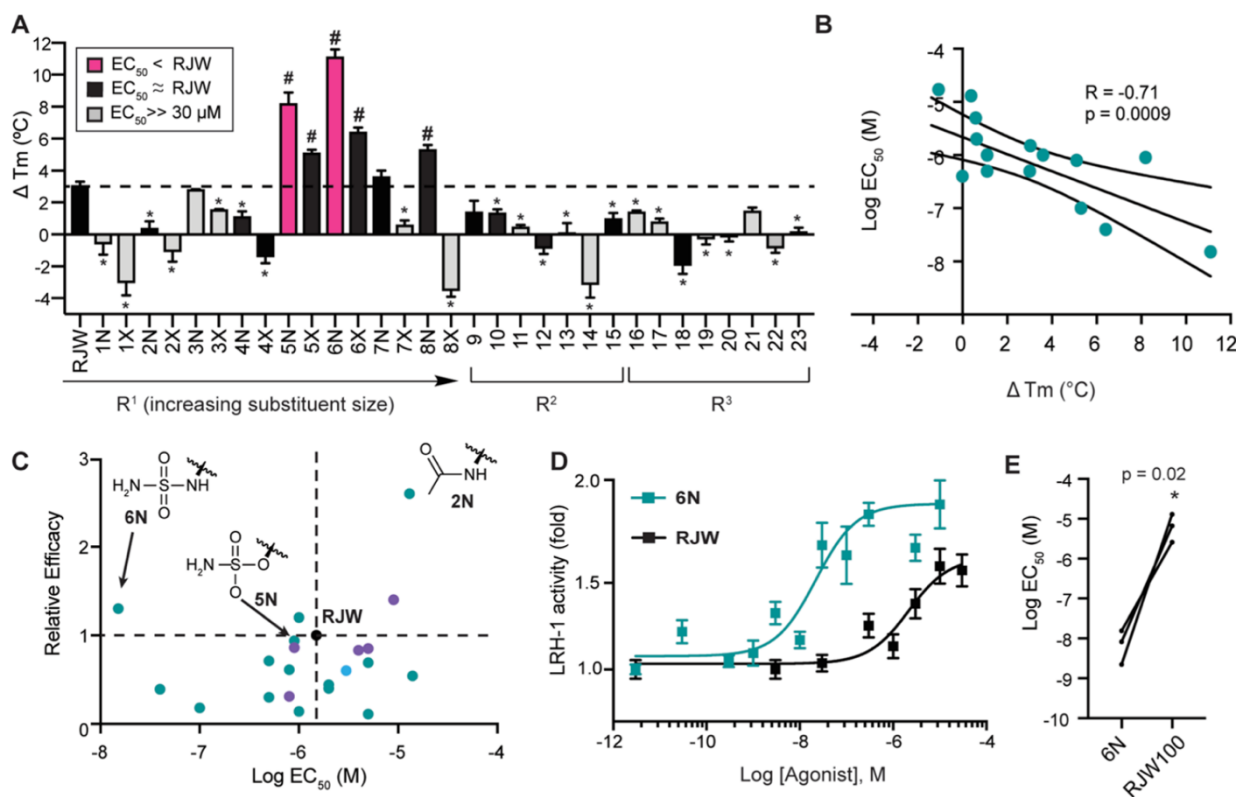


Figure 4.3. Optimization of R¹ modification improves potency by two orders of magnitude.

(A) DSF assays demonstrate that the site of modification, R¹ substituent size, and stereochemistry affect global LRH-1 stabilization. Colored bars represent EC₅₀s relative to RJW100 as indicated in the legend. Each bar represents three experiments conducted in triplicate. *, $p < 0.05$ for T_m decrease vs RJW100. #, $p < 0.05$ T_m increase vs RJW100. Significance was assessed by one-way ANOVA followed by Dunnett's multiple comparisons test. The dotted line indicates the T_m change induced by RJW100 relative to the PL agonist, DLPC. (B) Scatter plot showing the correlation between T_m shift in DSF assay (x-axis) and EC₅₀ from luciferase reporter assays (y-axis) for the R¹-modified compounds. Data were analyzed by linear regression (curved lines are the 95% confidence interval). (C) Scatter plot comparing potency (EC₅₀) and efficacy relative to RJW100 (RE) for all compounds for which EC₅₀ values could be calculated. Dots are color-coded by the site of modification (as indicated in Figure 4.2). The black dot is RJW100. The EC₅₀ values and efficacies of compounds 2N, 5N, and 6N are indicated. RE was calculated as described in the methods section. (D) Dose response curves comparing 6N and RJW100 in luciferase reporter assays. Each point represents the mean \pm SEM for three experiments conducted in triplicate. (E) Significance of difference in potency for 6N vs RJW100 was determined by a two-tailed, paired Student's t-test from parallel experiments.

Another strong trend among the data is that unlike RJW100, *endo* diastereomers of the bulkier groups are better activators (and more stabilizing) than the corresponding *exo* diastereomers (as seen for the triazoles **7**, sulfamides **6**, and acetamides **2**, Fig. 4.2 and 4.3). While the compounds display a wide range of potencies and efficacies, the *endo* sulfamide (**6N**) stands out as being the most potent (Fig. 4.3C). With an EC₅₀ of 15 nM, **6N** is two orders of magnitude more potent than RJW100 (Fig. 4.3D,E). This is the first discovery of a low-nanomolar LRH-1 modulator, representing a leap forward in developing agonists for this challenging target.

4.3 Contacts that Drive LRH-1 Activation by **6N**

The improved potency of **6N** is particularly striking considering that a very similar, highly stabilizing compound (**5N**) is not much more potent or effective for transcriptional activation than RJW100 (Fig. 4.3C). We speculated the dramatic increase in potency for **6N** relative to **5N** is driven by replacement of oxygen with nitrogen in the R¹ linker, as this is the only difference between the two compounds. Remarkably, a nitrogen-containing linker improves potency relative to an oxygen linker for several pairs of compounds that differ only at this site (Fig. 4.4A). The NH linker also contributes to selectivity for LRH-1 over its closest homolog, steroidogenic factor-1 (SF-1). Compound **6N** is a weaker activator of SF-1 than LRH-1, and **2N** (the *endo* acetamide) displays no activity against SF-1 while strongly activating LRH-1 (Fig. 4.4B). In contrast, **5N** and RJW100 equally activate both receptors (Fig. 4.4B).

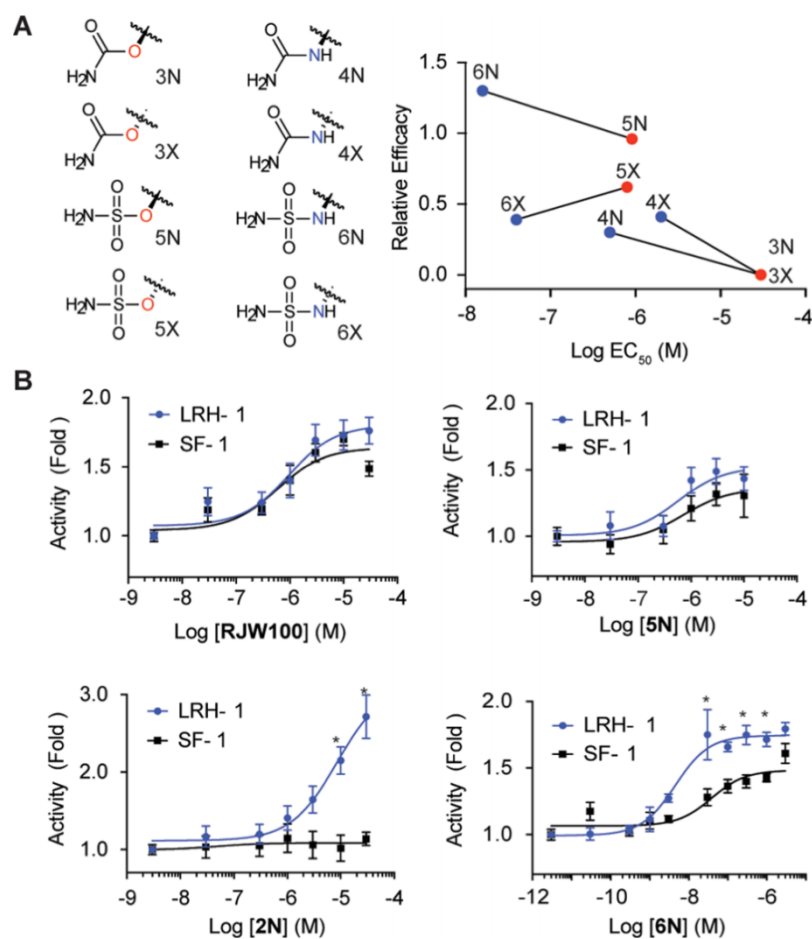


Figure 4.4. A hydrogen-bond donating nitrogen linker in the R¹ group improves potency and selectivity. (A) Comparison of potencies and efficacies for four sets of compounds that are identical except for the presence of a R¹ linker containing an oxygen (red dots) or nitrogen (blue dots). (B) Dose response curves comparing activation of LRH-1 and SF-1 by select compounds. Significance of differences in activities of each compound for LRH-1 vs SF-1 was determined by two-way ANOVA followed by Sidak's multiple comparisons test. *, p < 0.05.

To investigate the role of the R¹ linker in agonist activity and to gain insights into mechanisms underlying the potency of **6N**, we determined the X-ray crystal structure of **6N** bound to the LRH-1 LBD at a resolution of 2.23 Å (Fig. 4.5A, Table S4.1). For comparison and to delineate the function of the NH containing linker, we also determined structures of LRH-1 bound to **2N** (with an NH-linker, 2.2 Å) and **5N** (with an oxygen linker, 2.0 Å). The complexes were

crystallized with a fragment of the coactivator protein, transcriptional intermediary factor 2 (Tif2), which is bound at the AF-2 activation function surface (AFS) at the interface between helices 3, 4, and the activation function helix (AF-H, Fig. 4.5A). Overall protein conformation does not differ greatly and is similar to the LRH-1-RJW100 structure (root mean-square deviations are within 0.2 Å). The ligands are well defined by electron density, with the exception of the alkyl “tails” (Fig. 4.5B). The disorder in the tail is also seen in the *endo* RJW100 structure and may be a general feature of *endo* agonists with this scaffold. One of the main goals for these studies was to develop ligands that bind with consistent positions of the bicyclic cores. These structures demonstrate that this strategy was successful. Superposition of RJW100, **2N**, **5N**, and **6N** from the crystal structures shows nearly identical conformation of the agonists’ cores and phenyl groups, with slight variation in the positions of the R¹ polar groups (Fig. 4.5C). All three polar moieties protrude into the DPP, filling space typically occupied by one or more water molecules and making several polar contacts (Fig. 4.5D). For both **5N** and **6N**, there is strong tetrahedral density indicating the position of the R¹ groups; however, analysis of structure B factors and ensemble refinement suggest that the R¹ groups are somewhat mobile and capable of making transient interactions in the pocket that differ from the modeled states (Fig. S4.3). Studies with LRH-1 mutants helped to elucidate mechanistic differences between these agonists. While the binding modes of the three agonists are similar, mutagenesis studies show that they activate LRH-1 through different mechanisms (Fig. 4.5E).

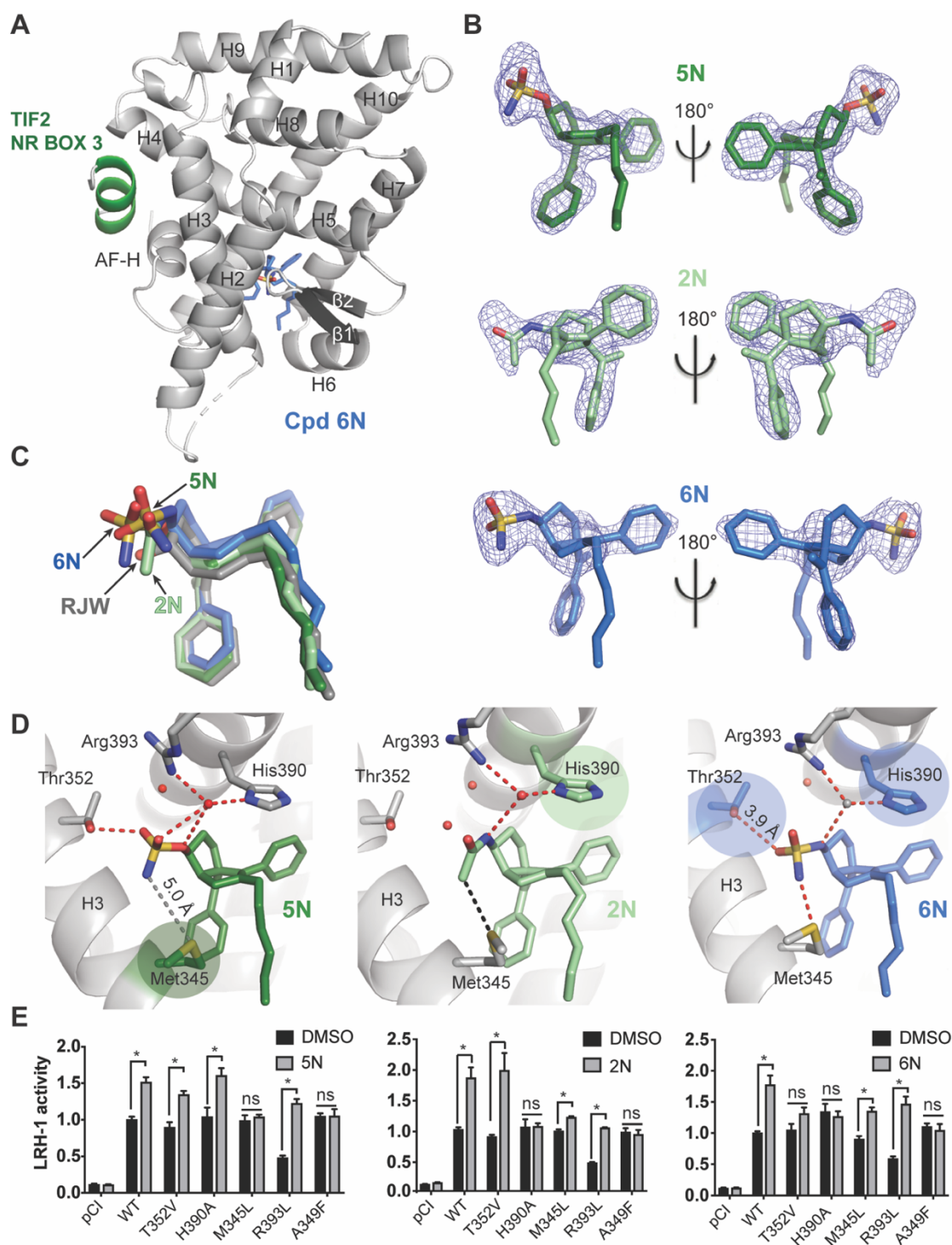


Figure 4.5. Crystal structures of LRH-1 bound to novel agonists. (A) Overall structure of the LRH-1 LBD (gray) bound to 6N (blue sticks). Tif2 is shown in green. The dotted line indicates a disordered region that could not be modeled. (B). Omit maps for 2N, 5N, and 6N. Maps are $F_o - F_c$, contoured at 2.5σ . (C) Superposition of ligands from the crystal structures showing a consistent

position of the cores of the modified agonists compared to RJW100. (D) Close view of the LRH-1 binding pocket with **5N**, **2N**, or **6N** bound showing a subset of interactions made by the R¹ groups. Colored circles highlight interactions that are important for LRH-1 activation by each agonist. Red spheres are water molecules (the gray sphere in the LRH-1-**6N** structure is a water molecule typically present in the LRH-1 pocket that could not be modeled because of poor crystallographic order). Red dotted lines indicate hydrogen bonds and black dotted lines indicate hydrophobic contacts. The interaction indicated by the gray dotted line in the LRH-1-**5N** structure is outside of hydrogen bonding distance in the structure but important for activity in mutagenesis studies. (E) Luciferase reporter assays showing how the interactions made by the agonists affect LRH-1 activity. The A349F mutation occludes the DPP and was used as a negative control. Each bar represents the mean \pm SEM for three independent experiments conducted in triplicate. Cells were treated with 10 μ M **2N**, 10 μ M **5N**, or 0.3 μ M **6N** for 24 h (concentrations chosen based on agonist EC₅₀ toward wild-type LRH-1). *, $p < 0.05$ by two-way ANOVA followed by Dunnett's multiple comparisons test. PDB codes for the structures compared in this figure are as follows: LRH-1-RJW100, 5L11; LRH-1-**5N**, 6OQX; LRH-1-**6N**, 6OQY; LRH-1-**2N**, 6OR1.

The first major difference is with the T352 interaction. Both **5N** and **6N** directly interact with T352, but the differential impact of a T352V mutation shows that this interaction only contributes to agonist-mediated LRH-1 activity in the case of **6N** (Fig. 4.5E). Compound **2N** is not well-positioned to interact with the water coordinating T352 because of the planar geometry of the R¹ acetamide group, and the T352V mutation has no effect on LRH-1 activity (Fig. 4.5E). The agonists also demonstrate a differential reliance on the interaction with M345: **5N** is unable to activate a M345L LRH-1 mutant, but **6N** and **2N** activate it significantly above basal levels (Fig. 4.5E). We were particularly interested in how interactions made by the NH linker contribute to agonist activity. All three agonists are positioned to make water-mediated hydrogen bonds with LRH-1 residue H390 via the R¹ linkers (Fig. 4.5D). In the case of **6N**, we were unable to model the bridging water molecule seen in the other two structures (and in other published LRH-1 LBD structures) because of weak electron density. The weak density for the water molecule is likely a consequence of poor crystallographic order because very few waters could be modeled in this structure (24 total, unusual for a 2.2 Å structure). However, luciferase reporter assays with LRH-

1 mutants indicate that **6N** interacts with H390 and that the interaction is critical for transcriptional activity (Fig. 4.5E). Compound **2N** is also unable to activate the LRH-1 H390A mutant, supporting the idea that a productive water-mediated interaction with H390 is made by the NH-linker (Fig. 4.5E). Compound **5N**, with an oxygen linker, interacts with H390 with both the linker and sulfonyl oxygens (Fig. 4.5D). However, **5N** does not utilize the H390 interaction for activation because mutating H390 to alanine has no effect on its ability to activate LRH-1 (Fig. 4.5E). Therefore, while **5N** and **6N** make very similar contacts, the presence of a hydrogen bond donor in the R¹ linker is uniquely able to drive activation of LRH-1 via H390. This provides a potential mechanism through which a nitrogen linker increases agonist potency.

4.4 6N Stabilizes AFS, Strengthens Allosteric Signaling, and Promotes Coactivator Recruitment

To investigate how **6N** alters LRH-1 dynamics to drive receptor activation, we determined its effects on LRH-1 conformation in solution using hydrogen–deuterium exchange (HDX) mass spectrometry. The most significant changes occur at sites involved in ligand-driven recruitment of coregulators: (1) the AFS and (2) a region of the receptor involved in allosteric signaling to the AFS, located near helix 6 and the beta sheets¹³¹² (this site is called activation function B and abbreviated “AF-B”). Relative to RJW100, **6N** impacts the conformation of AF-B by destabilizing the N-terminal portion of helix 7 and stabilizing the loop between helices 6 and 7 (Fig. 4.6A). Rigidification of the loop between these helices may induce pressure to unwind helix 7, which could explain this pattern of motion. In addition to these changes near AF-B, **6N** strongly stabilizes a portion of helix 4 near the AFS (Fig. 4.6A). Compound **5N** stabilizes the same region of helix 4 relative to RJW100 and **6N**, but it also destabilizes the AF-H, a critical part of the AFS that tunes

coregulator associations through subtle changes to its conformation¹³ (Fig. 4.6B). Because **6N** alters LRH-1 conformation at AF-B and the AFS, we hypothesized that it increases communication between these two sites. To quantify the predicted strength of agonist-driven communication between AF-B and the AFS, we conducted 1 μ s molecular dynamics simulations (MDS) using the crystal structures as starting models. Correlated motions of residues within a protein facilitate allosteric coupling between distant sites. Communication paths can traverse thousands of possible routes through the receptor, and the chains of residues with the strongest patterns of correlated motion the optimal path and a subset of suboptimal paths are thought to convey the most information. We therefore constructed dynamical networks of LRH-1-agonist complexes, using calculated covariance to weight the strength of communication between pairs of residues.

The resulting covariance matrices were used to identify the strongest suboptimal paths facilitating communication between AF-B and the Tif2 coactivator (bound at the AFS). The number of strong paths markedly increases when **2N**, **5N**, or **6N** are bound compared to RJW100, with **6N** exhibiting the strongest communication between these sites (Fig. 4.6C). There are also significant differences in the directionality of the paths promoted by each agonist. Although all paths traverse helix 5, indicating that correlated motion is induced in this region, compounds **2N**, **5N**, and **6N** also induce strong communication along helix 3. Compound **6N** also induces highly interconnected communication within the AFS and the Tif2 coactivator, including significant involvement of the AF-H. This important helix in the AFS is notably excluded from the paths when the other agonists are bound (Fig. 4.6C). The stabilization of the AFS by **6N** is associated with enhanced coactivator recruitment. In a fluorescence polarization-based coregulator binding assay, RJW100, **5N**, and **6N** dose-dependently recruit fluorescein-labeled Tif2 peptide to LRH-1 and exhibit similar EC₅₀s (50% of maximum Tif2 binding occurs with ~600–700 nM agonist, Fig.

4.6D). Each curve reaches a well-defined plateau that indicates maximum response with saturating concentrations of the agonist; however, curve maxima are lower for RJW100 and **5N** than **6N** by 50–60%, which is characteristic of partial agonists. Although the endogenous ligand has not been identified for comparison, **6N** behaves more like a full agonist than **5N** or RJW100 in this assay. Therefore, we have elucidated a novel mechanism of action utilized by **6N**, whereby specific interactions by the sulfamide and R¹ linker promote allosteric signaling to the AFS, stabilizing the site of coactivator interaction and increasing Tif2 association.

Figure 6

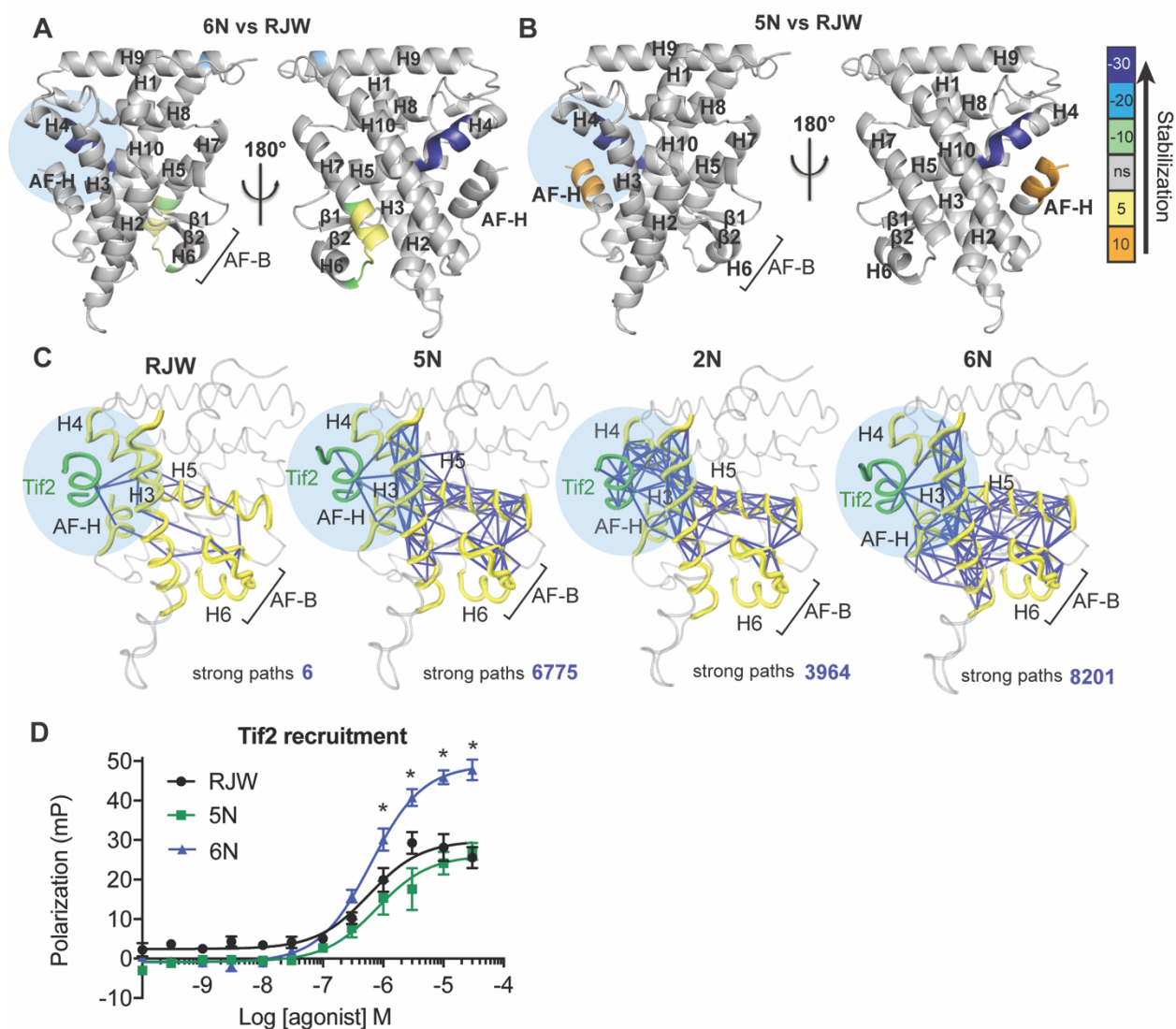


Figure 4.6. Compound 6N promotes allosteric communication to the AFS and coactivator recruitment. (A,B) Differential HDX comparing 5N to RJW100 (A) or 6N to RJW100 (B). Color bar indicates the percent difference in deuterium uptake when 5N or 6N is bound compared to RJW100. A positive number indicates more deuterium exchange, indicating relative destabilization. A negative number indicates relative stabilization. (C) Molecular dynamics simulations (MDS) results showing the strongest suboptimal paths (blue lines) between AF-B and the Tif2 coactivator (green) when the indicated agonists are bound. The AFS is highlighted in light blue in panels (A–C) and the position of AF-B is indicated with brackets. The PDB codes for the starting models used in MD are as follows: LRH-1-RJW100, 5L11; LRH-1-5N, 6OQX; LRH-1-6N, 6OQY; LRH-1-2N, 6OR1. (D) Compound 6N promotes recruitment of the Tif2 coactivator to purified LRH-1 LBD in a fluorescence polarization based binding assay. Each point represents the mean \pm SEM for three independent experiments conducted in triplicate. *, $p < 0.05$ by two-way ANOVA followed by Sidak's multiple comparisons test.

4.5 Evaluation of **6N** in Murine Intestinal Organoids

The discovery of the first highly potent LRH-1 agonist provides the opportunity to elucidate ligand regulated transcriptional pathways controlled by this receptor bound to **6N**. The recent development of methods to culture organoids of intestinal crypts (enteroids, Fig. 4.7A) has provided an excellent research tool for drug discovery for IBD.⁵⁰ When stimulated with inflammatory cytokines, enteroids mimic features of gut epithelia in IBD.⁵⁰ To investigate anti-inflammatory properties of **6N**, we measured the effects of the new agonist on gene expression in humanized LRH-1 mouse enteroids in the context of TNF α -induced inflammation. Expression of human LRH-1 in the enteroids was verified by qRT-PCR (Fig. 4.7B). The treatment with 1 μ M **6N** in hLRH-1-expressing enteroids (but not knockout enteroids) significantly increased mRNA expression of the steroidogenic enzymes Cyp11a1 and Cyp11b1, which are LRH-1 transcriptional targets (Fig. 4.7C). Like with **10CA**, there was a concomitant increase in expression of the anti-inflammatory cytokine IL-10 and decreases in expression of the inflammatory cytokines IL-1 β and TNF α (Fig. 4.7D,E).

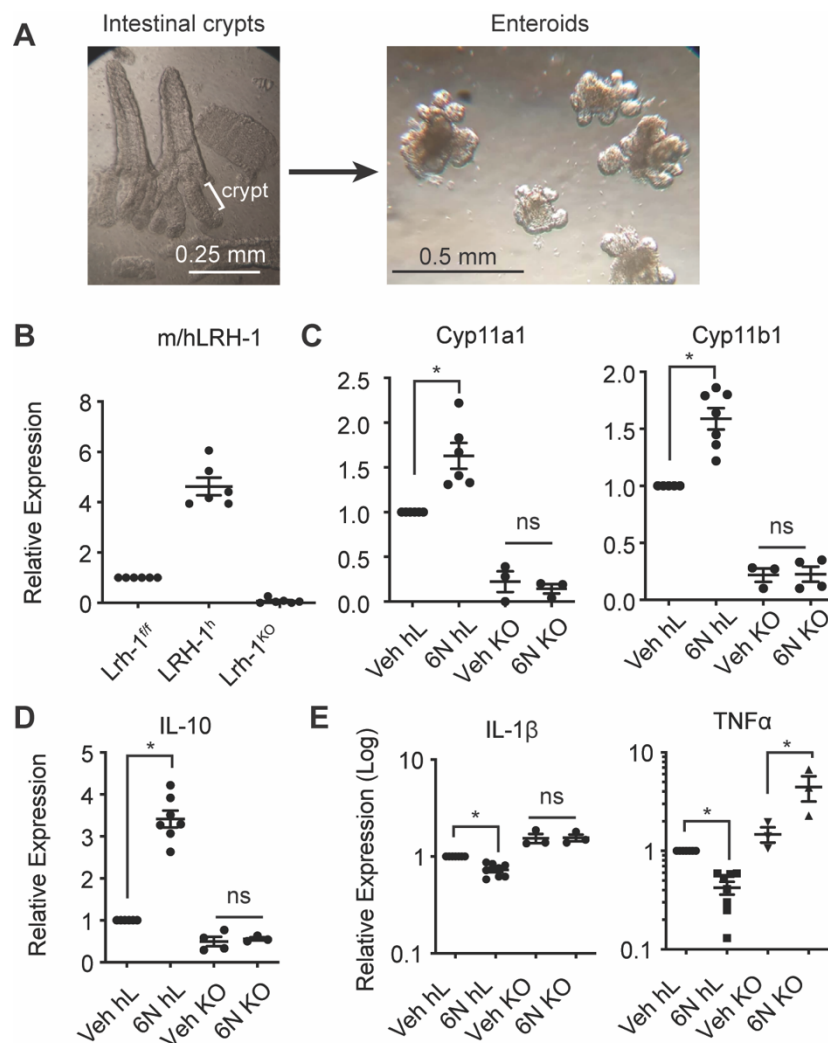


Figure 4.7. Compound 6N induces intestinal epithelial steroidogenesis in humanized LRH-1 mouse enteroids. (A) Enteroids were generated through isolation and culture of intestinal crypts from mice expressing human LRH-1. (B) Mouse or human (m/h) LRH-1 mRNA expression in the intestinal enteroids of Lrh-1^{fl/fl}, Lrh-1^{KO}, and LRH-1^h mouse lines. (C) Compound 6N induces mRNA expression of steroidogenic enzyme Cyp11a1 and Cyp11b1. (D) Compound 6N induces anti-inflammatory cytokine *IL-10*. (E) Compound 6N reduces inflammatory cytokine *IL-1 β* (left) and TNF α (right). Error bars represent the standard deviation from six biological replicates for mouse enteroids expressing human LRH-1 (hL) and three biological replicates from Lrh-1 knockout (KO) mouse enteroids. *, $p < 0.01$ (one-way ANOVA followed by Tukey's multiple comparisons test).

These data suggest a role for **6N** in reducing inflammation in the gut via upregulation of steroidogenesis. These findings are in stark contrast with previous enteroid studies with RJW100, which was inactive at doses up to 20 μM ,¹⁰ (dosage information not reported but obtained by personal communication). While the involvement of LRH-1 in IBD is clear from gain- and loss-of function studies, this is the first demonstration of an agonist that can stimulate LRH-1-driven epithelial steroidogenesis. This discovery demonstrates the tremendous potential for LRH-1 as a drug target for this disease.

4.6 Conclusions

By exploiting a novel polar interaction in the LRH-1 DPP, we have overcome the challenge of developing tightly-binding ligands for LRH-1 and have made substantial progress in agonist development. Systematic variation of three sites on the RJW100 scaffold has revealed a robust structure–activity relationship. The modifications to the styrene sites that we examined (R^2 and R^3) do not significantly improve performance and often ablate activity; however, modifications at R^1 increase potency in transactivation assays (Fig. 4.2C and S4.1). The increased potency is associated with global receptor stabilization by DSF promoted by tetrahedral, polar R^1 substituents with endo stereochemistry (Fig. 4.3). In addition, the composition of the R^1 group, particularly the linker, is critical for activity. This is exemplified through the comparison of **5N** and **6N**, which differ only at the R^1 linker. Compound **6N** utilizes interactions with both Thr352 and His390 to activate LRH-1, the latter of which is likely mediated by the linker nitrogen (Fig. 4.5D). This novel binding mode leads to a distinct mechanism of action for **6N** compared to similar, less potent compounds, inducing conformational changes at AF-B, stabilizing the AFS, and increasing coactivator association (Fig. 4.6). Results from MDS support the idea that **6N** promotes very strong

allostery to the AFS, evidenced in the strong communication between the AF-B and the AFS predicted to occur when **6N** is bound compared to less potent agonists (Fig. 4.6). With three separate crystal structures, we demonstrated that polar modifications at the RJW100 R¹ group do not cause major repositioning of the scaffold (Fig. 4.5), supporting our hypothesis that this polar group acts as an important anchor point. This finding was not only key to the success of the current study, but it will also greatly benefit future work. The ability to anchor the scaffold consistently provides an opportunity to tune for additional desired effects, such as solubility or selectivity. Moreover, the trajectory of the alkyl “tails” of these molecules is amenable for introduction of modifications that could engage residues near the mouth of the pocket in a PL-like manner.^{12d,13} Initial studies in this vein have been fruitful, leading to the discovery of highly active compounds.³⁶ Finally, the establishment of a predictable binding mode may open avenues for antagonist design; for example, by modifying the scaffold to promote displacement of the AF-H and recruitment of corepressors. This approach has been successful for other nuclear receptors⁵⁵ and could generate LRH-1 antagonists useful as therapeutics for certain cancers in which LRH-1 is aberrantly active.⁵⁶

⁵⁵ (a) Raaijmakers, H. C. A.; Versteegh, J. E.; Ulddehaag, J. C. M. The X-Ray Structure of RU486 Bound to the Progesterone Receptor in a Destabilized Agonistic Conformation. *J. Biol. Chem.* **2009**, *284* (29), 19572–19579 (b) Shiau, A. K.; Barstad, D.; Loria, P. M.; Cheng, L.; Kushner, P. J.; Agard, D. A.; Greene, G. L. The Structural Basis of Estrogen Receptor/Coactivator Recognition and the Antagonism of This Interaction by Tamoxifen. *Cell* **1998**, *95* (7), 927–937

⁵⁶ (a) Thiruchelvam, P. T. R.; Lai, C. F.; Hua, H.; Thomas, R. S.; Hurtado, A.; Hudson, W.; Bayly, A. R.; Kyle, F. J.; Periyasamy, M.; Photiou, A.; Spivey, A. C.; Ortlund, E. A.; Whitby, R. J.; Carroll, J. S.; Coombes, R. C.; Buluwela, L.; Ali, S. The Liver Receptor Homolog-1 Regulates Estrogen Receptor Expression in Breast Cancer Cells. *Breast Cancer Res. Treat.* **2011**, *127* (2), 385–396 (b) Safi, R.; Kovacic, A.; Gaillard, S.; Murata, Y.; Simpson, E. R.; McDonnell, D. P.; Clyne, C. D. Coactivation of Liver Receptor Homologue-1 by Peroxisome Proliferator-Activated Receptor γ Coactivator-1 α on Aromatase Promoter II and Its Inhibition by Activated Retinoid X Receptor Suggest a Novel Target for Breast-Specific Antiestrogen Therapy. *Cancer Res.* **2005**, *65* (24), 11762–11770 (c) Nadolny, C.; Dong, X. Liver Receptor Homolog-1 (LRH-1): A Potential Therapeutic Target for Cancer. *Cancer Biol. Ther.* **2015**, *16* (7), 997–1004 (d) Lin, Q.; Aihara, A.; Chung, W.; Li, Y.; Huang, Z.; Chen, X.; Weng, S.; Carlson, R. I.; Wands, J. R.; Dong, X. LRH1 as a Driving Factor in Pancreatic Cancer Growth. *Cancer Lett.* **2014**, *345* (1), 85–90 (e) Busby, S.; Nuhant, P.; Cameron, M.; Mercer, B. A.; Hodder, P.; Roush, W. R.; Griffin, P. R. *Discovery of Inverse Agonists for the Liver Receptor Homologue-1 (LRH1; NR5A2)*; National Center for Biotechnology Information (US), 2010 (f) Bayrer, J. R.; Mukkamala, S.; Sablin, E. P.; Webb, P.; Fletterick, R. J. Silencing LRH-1 in Colon Cancer Cell Lines Impairs Proliferation and Alters Gene Expression Programs. *Proc. Natl. Acad. Sci. U. S. A.* **2015**, *112* (8), 2467–2472

⁵⁶ (g) Lai, C.-F.; Flach, K. D.; Alexi, X.; Fox, S. P.; Ottaviani, S.; Thiruchelvam, P. T. R.; Kyle, F. J.; Thomas, R. S.; Launchbury, R.; Hua, H.; Callaghan, H. B.; Carroll, J. S.; Charles Coombes, R.; Zwart, W.; Buluwela, L.; Ali, S. Co-

A systematic, structure-guided approach has resulted in the discovery of the first low nanomolar LRH-1 agonist and elucidated a novel mechanism of action. This agonist has great potential as a tool to uncover novel aspects of LRH-1 biology and as a potential therapeutic for IBD and obesity associated metabolic diseases. The discovery of elements that stabilize the orientation of the hexahydropentalene scaffold, greatly improve potency, and drive activation of LRH-1 is invaluable for understanding ligand regulation of this receptor and for future modulator design. It should be noted, however, that **6N** does not increase LRH-1 maximum activation or transcription of LRH-1 regulated genes as highly as **10CA**. The combination of these two highly desirable traits (the ability of **6N** to improve potency, and the ability of **10CA** to improve activation) will be addressed in detail in Chapter 5.

4.7 Supporting Information

General Synthetic Information

All reactions were carried out in oven-dried glassware, equipped with a stir bar and under a nitrogen atmosphere with dry solvents under anhydrous conditions, unless otherwise noted. Solvents used in anhydrous reactions were purified by passing over activated alumina and storing under argon. Yields refer to chromatographically and spectroscopically (¹H NMR) homogenous materials, unless otherwise stated. Reagents were purchased at the highest commercial quality and used without further purification, unless otherwise stated. n-Butyllithium (n-BuLi) was used as a 1.6 M or a 2.5 M solution in hexanes (Aldrich), was stored at 4°C and titrated prior to use. Organic solutions were concentrated under reduced pressure on a rotary evaporator using a water bath.

Chromatographic purification of products was accomplished using forced-flow chromatography on 230-400 mesh silica gel. Preparative thin-layer chromatography (PTLC) separations were carried out on 1000 μ m SiliCycle silica gel F-254 plates. Thin-layer chromatography (TLC) was performed on 250 μ m SiliCycle silica gel F-254 plates. Visualization of the developed chromatogram was performed by fluorescence quenching or by staining using KMnO₄, p-anisaldehyde, or ninhydrin stains. ¹H and ¹³C NMR spectra were obtained from the Emory University NMR facility and recorded on a Bruker Avance III HD 600 equipped with cryo-probe (600 MHz), INOVA 600 (600 MHz), INOVA 500 (500 MHz), INOVA 400 (400 MHz), VNMR 400 (400 MHz), or Mercury 300 (300 MHz), and are internally referenced to residual protio solvent signals. Data for ¹H NMR are reported as follows: chemical shift (ppm), multiplicity (s = singlet, d = doublet, t = triplet, q = quartet, m = multiplet, dd = doublet of doublets, dt = doublet of triplets, ddd = doublet of doublet of doublets, dtd = doublet of triplet of doublets, b = broad, etc.), coupling constant (Hz), integration, and assignment, when applicable. Data for decoupled ¹³C NMR are reported in terms of chemical shift and multiplicity when applicable. IR spectra were recorded on a Thermo Fisher DiamondATR and reported in terms of frequency of absorption (cm⁻¹). High Resolution mass spectra were obtained from the Emory University Mass Spectral facility. Gas Chromatography Mass Spectrometry (GC-MS) was performed on an Agilent 5977A mass spectrometer with an Agilent 7890A gas chromatography inlet. Liquid Chromatography Mass Spectrometry (LC-MS) was performed on an Agilent 6120 mass spectrometer with an Agilent 1220 Infinity liquid chromatography inlet. Preparative High Pressure Liquid chromatography (Prep-HPLC) was performed on an Agilent 1200 Infinity Series chromatograph using an Agilent Prep-C18 30 x 250 mm 10 μ m column, or an Agilent Prep-C18 21.2 x 100 mm, 5 μ m column. HPLC analyses were performed using the following conditions.

Evaluation of Compound Purity.

Purity of all tested compounds was determined by HPLC analysis, using the methods given below (as indicated for each compound).

Method A: A linear gradient using water and 0.1 % formic acid (FA) (Solvent A) and MeCN and 0.1% FA (Solvent B); t = 0 min, 30% B, t = 4 min, 99% B (held for 1 min), then 50% B for 1 min, was employed on an Agilent Poroshell 120 EC-C18 2.7 micron, 3.0 mm x 50 mm column (flow rate 1 mL/min) or an Agilent Zorbax SB-C18 1.8 micron, 2.1 mm x 50 mm column (flow rate 0.8 mL/min). The UV detection was set to 254 nm. The LC column was maintained at ambient temperature.

Method B: A linear gradient using water and 0.1 % formic acid (FA) (Solvent A) and MeCN and 0.1% FA (Solvent B); t = 0 min, 70% B, t = 4 min, 99% B (held for 1 min), then 50% B for 1 min, was employed on an Agilent Poroshell 120 EC-C18 2.7 micron, 3.0 mm x 50 mm column (flow rate 1 mL/min) or an Agilent Zorbax SB-C18 1.8 micron, 2.1 mm x 50 mm column (flow rate 0.8 mL/min). The UV detection was set to 254 nm. The LC column was maintained at ambient temperature.

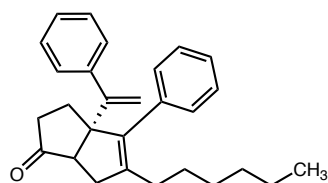
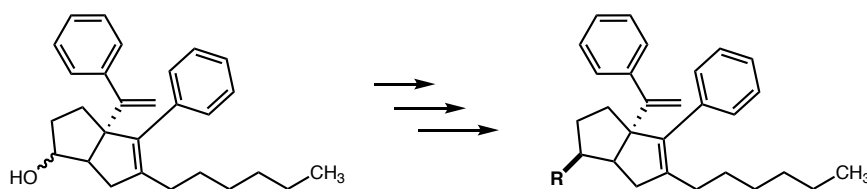
Method C: An isocratic method using 75% MeCN, 35% water, and 0.1 % FA was employed on an Agilent Poroshell 120 EC-C18 2.7 micron, 3.0 mm x 50 mm column (flow rate 1 mL/min) or an Agilent Zorbax SB-C18 1.8 micron, 2.1 mm x 50 mm column (flow rate 0.8 mL/min). The UV detection was set to 254 nm. The LC column was maintained at ambient temperature.

Method D: An isocratic method using 85% MeCN, 15% water, and 0.1% FA was employed on an Agilent Poroshell 120 EC-C18 2.7 micron, 3.0 mm x 50 mm column (flow rate 1 mL/min) or an

Agilent Zorbax SB-C C18 1.8 micron, 2.1 mm x 50 mm column (flow rate 0.8 mL/min). The UV detection was set to 254 nm. The LC column was maintained at ambient temperature.

Detailed Syntheses of Tested Compounds 1 – 23

Hydroxyl modifications 1 – 8

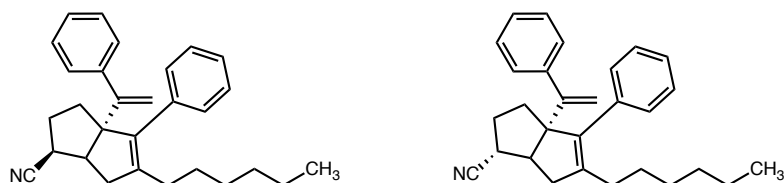


5-hexyl-4-phenyl-3a-(1-phenylvinyl)-3,3a,6,6a-tetrahydropentalen-1(2H)-one (S1): A solution of RJW100 (mixture of diastereomers (124.5 mg, 0.3 mmol 1.0 equiv) in acetonitrile was treated with N-methylmorpholine oxide (380.7 mg, 3.2 mmol, 10 equiv) and allowed to stir to homogeneity before the addition of tetrapropylammonium perruthenate (12.6 mg, 0.04 mmol, 0.1 equiv). The solution was stirred at room temperature until completion as determined by TLC (ca. 10 min). The solution was concentrated and subjected directly to silica gel chromatography in 10% EtOAc/Hex eluent to afford the title compound as a clear, colorless oil (118.8 mg, 95% yield).

¹H NMR (400 MHz, CDCl₃) δ 7.38 – 7.25 (m, 6H), 7.24 – 7.19 (m, 4H), 5.20 (d, *J* = 1.4 Hz, 1H), 5.09 (d, *J* = 1.4 Hz, 1H), 2.44 (d, *J* = 7.5 Hz, 1H), 2.34 – 2.23 (m, 2H), 2.15 – 1.95 (m, 5H), 1.89 (ddt, *J* = 16.5, 7.8, 1.1 Hz, 1H), 1.29 – 1.09 (m, 8H), 0.82 (t, *J* = 7.0 Hz, 3H).

¹³C NMR (101 MHz, CDCl₃) δ 222.8, 153.2, 144.9, 142.5, 137.3, 136.6, 129.0, 128.2, 128.1, 127.6, 127.03, 126.96, 115.3, 110.0, 65.4, 55.5, 38.8, 37.5, 31.5, 30.0, 29.4, 28.3, 27.6, 22.5, 14.1.

LRMS (ESI, APCI) *m/z*: calc'd for C₂₈H₃₅O [M+H]⁺ 385.2, found 385.3



(endo or exo)-5-hexyl-4-phenyl-3a-(1-phenylvinyl)-1,2,3,3a,6,6a-hexahydro-pentalene-1-carbonitrile (S2N, S2X): A solution of sodium cyanide (10.0 equiv) in DMF was treated with **S4X** (99 mg, 0.2 mmol, 1.0 equiv) or **S4N** (50 mg, 0.1 mmol, 1.0 equiv) as a solution in DMF. The mixture was allowed to stir at 100 °C for about 16 h. The reaction was cooled to ambient temperature, diluted with water, and extracted with EtOAc three times. The combined organic layers were washed with water and brine, dried with Na₂SO₄, filtered, and concentrated. The crude oil was purified by silica gel chromatography in 5% EtOAc/Hex eluent to afford the title compound. (**S2N endo**: 21.9 mg, 26% yield; **S2X exo**: 19.9 mg, 47% yield) (Note: An appreciable amount of E₂ elimination product is typically also observed, despite optimization of reaction conditions.) (Note: inversion of stereochemistry). (Caution: inorganic cyanides must be handled carefully due to toxicity).

S2N endo ¹H NMR (600 MHz, CDCl₃) δ 7.34 – 7.23 (m, 8H), 7.22 – 7.19 (m, 2H), 5.08 (s, 1H), 4.98 (s, 1H), 2.91 – 2.84 (m, 1H), 2.60 (t, *J* = 9.0 Hz, 1H), 2.53 (d, *J* = 17.5 Hz, 1H), 2.30 (dd, *J* =

17.6, 8.6 Hz, 1H), 2.15 – 1.97 (m, 3H), 1.83 – 1.75 (m, 2H), 1.74 – 1.66 (m, 1H), 1.39 (p, $J = 7.6$ Hz, 2H), 1.31 – 1.17 (m, 6H), 0.84 (d, $J = 7.0$ Hz, 3H).

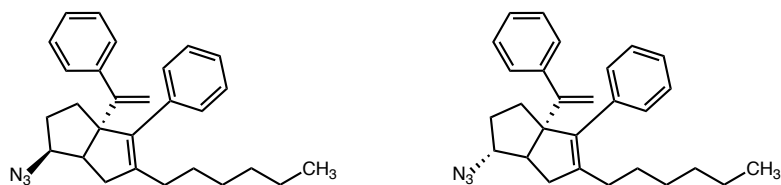
S2N endo ^{13}C NMR (126 MHz, CDCl_3) δ 153.4, 143.23, 143.22, 137.9, 136.6, 129.6, 127.9, 127.8, 127.7, 127.1, 126.9, 121.1, 115.8, 69.8, 46.5, 39.1, 34.9, 34.7, 31.6, 30.6, 29.8, 29.5, 27.7, 22.6, 14.1.

S2N endo LRMS (ESI, APCI) m/z : calc'd for $\text{C}_{29}\text{H}_{35}\text{N}$ $[\text{M}+\text{H}]^+$ 396.6 found 396.4

S2X exo ^1H NMR (600 MHz, CDCl_3) δ 7.38 – 7.20 (m, 10H), 5.09 (s, 1H), 5.08 (s, 1H), 2.71 (dd, $J = 7.9, 4.9$ Hz, 1H), 2.53 (q, $J = 11.0, 5.9$ Hz, 1H), 2.29 (dd, $J = 17.9, 8.4$ Hz, 1H), 2.12 – 1.98 (m, 4H), 1.92 – 1.86 (m, 2H), 1.72 (dt, $J = 13.1, 5.2$ Hz, 1H), 1.36 – 1.15 (m, 8H), 0.84 (t, $J = 7.0$ Hz, 3H).

S2X exo ^{13}C NMR (75 MHz, CDCl_3) δ 153.1, 142.9, 141.5, 138.6, 136.6, 129.4, 128.0, 127.9, 127.8, 126.99, 126.95, 123.1, 115.4, 69.6, 51.8, 41.7, 37.5, 33.8, 31.6, 30.5, 29.7, 29.4, 27.8, 22.6, 14.1.

S2X exo LRMS (ESI, APCI) m/z : calc'd for $\text{C}_{29}\text{H}_{36}\text{N}$ $[\text{M}+\text{H}]^+$ 398.3, found 398.3



(endo or exo)-5-hexyl-4-phenyl-3a-(1-phenylvinyl)-1,2,3,3a,6,6a-hexahydropentalen-1-amine (S3N, S3X): A solution of **S4X** (139.8 mg, 0.3 mmol, 1.0 equiv) or **S4N** (57 mg, 0.12 mmol, 1.0 equiv) in DMF was treated with sodium azide (10.0 equiv) and the reaction was stirred 16 h at 80 °C behind a blast shield. The solution was allowed to cool to room temperature and poured over water and extracted with EtOAc three times. The combined organic layers were

washed with water and brine, dried over MgSO_4 , and concentrated. The reaction mixture was purified on silica in 0-10% EtOAc/Hex eluent. (**S3N** *endo*: 117.6 mg, 95% yield; **S3X** *exo*: 45.6 mg, 90% yield) (Note: inversion of stereochemistry). (Warning: caution must be exercised when handling organic and inorganic azides for their toxicity and instability. Aqueous layers were basified and disposed of appropriately).

S3N *endo* ^1H NMR (600 MHz, CDCl_3) δ 7.36 – 7.26 (m, 8H), 7.23 – 7.18 (m, 2H), 5.10 (d, J = 1.3 Hz, 1H), 4.94 (d, J = 1.3 Hz, 1H), 3.87 (ddd, J = 10.5, 8.8, 5.9 Hz, 1H), 2.62 – 2.51 (m, 2H), 2.16 – 2.01 (m, 4H), 1.97 – 1.88 (m, 1H), 1.79 (ddd, J = 12.4, 5.9, 1.8 Hz, 1H), 1.71 (td, J = 12.4, 5.2 Hz, 1H), 1.67 – 1.59 (m, 1H), 1.40 (p, J = 7.5 Hz, 2H), 1.31 – 1.19 (m, 5H), 0.87 (t, J = 7.2 Hz, 3H).

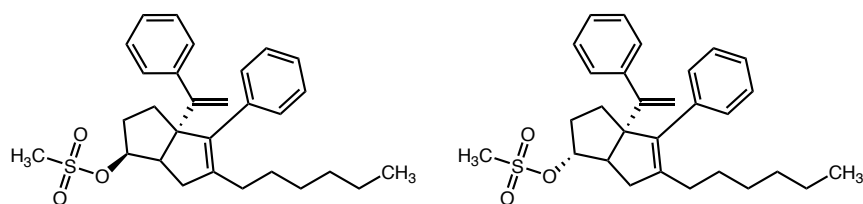
S3N *endo* ^{13}C NMR (126 MHz, CDCl_3) δ 154.2, 143.8, 143.4, 138.5, 136.8, 129.8, 127.8, 127.7, 126.9, 126.7, 115.5, 69.1, 64.9, 47.9, 35.7, 32.5, 31.7, 30.2, 29.8, 29.5, 27.8, 22.6, 14.1.

S3N *endo* LRMS (ESI) m/z : calc'd for $\text{C}_{28}\text{H}_{34}\text{N}_3$ 412.3 $[\text{M}+\text{H}]^+$, found 411.8

S3X *exo* ^1H NMR (500 MHz, CDCl_3) δ 7.36 – 7.24 (m, 8H), 7.21 (dt, J = 7.5, 1.4 Hz, 2H), 5.09 (s, 1H), 5.00 (s, 1H), 3.64 (s, 1H), 2.44 – 2.35 (m, 2H), 2.14 – 1.93 (m, 5H), 1.83 – 1.67 (m, 3H), 1.40 – 1.30 (m, 2H), 1.32 – 1.17 (m, 5H), 0.86 (d, J = 7.1 Hz, 3H).

S3X *exo* ^{13}C NMR (126 MHz, CDCl_3) δ 153.8, 143.8, 141.3, 139.1, 137.0, 129.6, 127.78, 127.77, 127.72, 126.80, 126.75, 115.3, 71.3, 69.3, 52.1, 41.1, 32.6, 31.6, 31.2, 29.7, 29.4, 27.8, 22.6, 14.1.

S3X *exo* LRMS (ESI) m/z : calc'd for $\text{C}_{28}\text{H}_{34}\text{N}_3$ $[\text{M}+\text{H}]^+$ 412.3, found 412.3



(endo or exo) 5-hexyl-4-phenyl-3a-(1-phenylvinyl)-1,2,3,3a,6,6a-hexahydropentalen-1-yl methanesulfonate (S4N, S4X): A solution of RJW100 *endo* (54.4 mg, 0.14 mmol, 1.0 equiv) or RJW100 *exo* (122.5 mg, 0.3 mmol, 1.0 equiv) in dichloromethane was treated with methanesulfonyl chloride (5.0 equiv), then triethylamine (5.0 equiv). The reaction mixture was allowed to stir 1 h before concentrating and purifying on silica in 30% EtOAc/Hex eluent. (**S4N** *endo*: 62.1 mg, 95% yield; **S4X** *exo*: 139 mg, >99% yield)

S4N endo ^1H NMR (500 MHz, CDCl_3) δ 7.36 – 7.26 (m, 8H), 7.24 – 7.17 (m, 2H), 5.13 (d, $J = 1.1$ Hz, 1H), 5.04 – 4.92 (m, 1H), 4.95 (d, $J = 1.2$ Hz, 1H), 3.00 (s, 3H), 2.70 (t, $J = 9.0$, 1.8 Hz, 1H), 2.60 (d, $J = 17.4$ Hz, 1H), 2.17 (dd, $J = 17.5$, 9.1 Hz, 1H), 2.08 (tt, $J = 13.5$, 6.8, 4.9 Hz, 4H), 1.92 – 1.76 (m, 3H), 1.72 (td, $J = 12.5$, 5.8 Hz, 1H), 1.40 (p, 2H), 1.33 – 1.18 (m, 4H), 0.88 (t, $J = 7.2$ Hz, 3H).

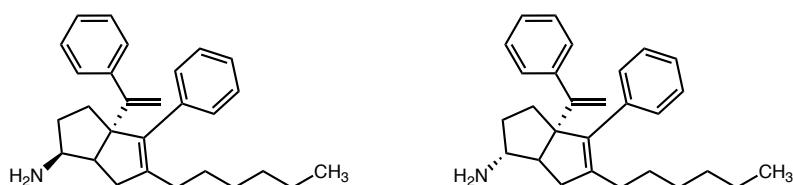
S4N endo ^{13}C NMR (126 MHz, CDCl_3) δ 153.7, 143.4, 143.2, 138.5, 136.5, 129.8, 127.9, 127.7, 127.6, 127.0, 126.8, 115.7, 82.9, 68.2, 47.4, 38.2, 34.9, 31.7, 31.1, 31.0, 29.8, 29.4, 27.8, 22.6, 14.1.

S4N endo LRMS (ESI, APCI) m/z : calc'd for $\text{C}_{29}\text{H}_{33}$ $[\text{M}-\text{CH}_3\text{O}_3\text{S}]^+$ 369.2, found $[\text{M}-\text{CH}_3\text{O}_3\text{S}]^+$ 368.9.

S4X exo ^1H NMR (500 MHz, CDCl_3) δ 7.37 – 7.25 (m, 8H), 7.27 – 7.19 (m, 2H), 5.11 (d, $J = 1.3$ Hz, 1H), 5.01 (d, $J = 1.3$ Hz, 1H), 4.83 (d, $J = 4.0$ Hz, 1H), 2.95 (s, 3H), 2.63 (d, $J = 9.2$ Hz, 1H), 2.41 (dd, $J = 17.4$, 9.5 Hz, 1H), 2.14 (dd, $J = 17.5$, 2.0 Hz, 1H), 2.11 – 1.98 (m, 4H), 1.90 – 1.75 (m, 2H), 1.40 – 1.31 (m, 2H), 1.32 – 1.17 (m, 6H), 0.87 (t, $J = 7.1$ Hz, 3H).

S4X *exo* ^{13}C NMR (151 MHz, CDCl_3) δ 153.5, 143.6, 141.3, 138.8, 136.8, 132.8, 129.6, 127.83, 127.76, 127.6, 126.90, 126.86, 115.6, 92.1, 69.2, 53.0, 40.0, 38.7, 32.4, 32.1, 31.6, 29.6, 29.4, 27.8, 22.6, 14.1.

S4X *exo* LRMS (ESI, APCI) m/z : calc'd for $\text{C}_{29}\text{H}_{33}$ $[\text{M}-\text{CH}_3\text{O}_3\text{S}]^+$ 369.2, found $[\text{M}-\text{CH}_3\text{O}_3\text{S}]^+$ 368.9



(endo or exo)-5-hexyl-4-phenyl-3a-(1-phenylvinyl)-1,2,3,3a,6,6a-hexahydropentalen-1-amine (1N, 1X): A solution of **S3N** *endo* (54 mg, 0.13 mmol, 1.0 equiv) or **S3X** *exo* (46 mg, 0.1 mmol, 1.0 equiv) in anhydrous Et_2O was cooled to $0\text{ }^\circ\text{C}$ and treated dropwise with LiAlH_4 (4.0M in Et_2O , 10.0 equiv). The reaction was stirred at ambient temperature for ca. 1 h, until the reaction was complete by TLC. The reaction was cooled to $0\text{ }^\circ\text{C}$, diluted with anhydrous Et_2O , and slowly treated with water (1mL/g LiAlH_4). Excess 4 M NaOH was added slowly and the solution was extracted with EtOAc three times. The combined organic layers were washed with Rochelle's salt and brine, dried over MgSO_4 , and concentrated. The crude oil was purified by silica gel chromatography in 50% EtOAc/Hex eluent (1% triethylamine) to afford the title compounds as colorless oils. (**1N** *endo*: 47.9 mg, 95% yield; **1X** *exo*: 40.0 mg, 92% yield). Purity was established by Method C: *endo* $t_r = 0.302$ min, 98.6%, *exo* $t_r = 0.290$ min, 77.5%.

1N *endo* ^1H NMR (600 MHz, CDCl_3) δ 7.37 – 7.19 (m, 10H), 5.08 (d, $J = 1.4$ Hz, 1H), 4.94 (d, $J = 1.5$ Hz, 1H), 3.30 (ddd, $J = 11.0, 8.8, 5.7$ Hz, 1H), 2.48 (d, $J = 17.4$ Hz, 1H), 2.42 (t, $J = 9.0$

Hz, 1H), 2.12 – 2.00 (m, 2H), 1.83 – 1.78 (m, 1H), 1.73 – 1.68 (m, 2H), 1.46 – 1.37 (m, 2H), 1.35 – 1.20 (m, 8H), 0.88 (t, $J = 7.1$ Hz, 3H).

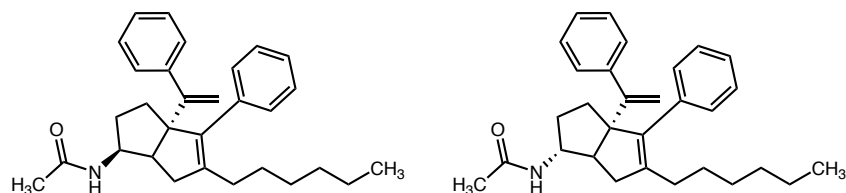
1N *endo* ^{13}C NMR (151 MHz, CDCl_3) δ 155.1, 144.2, 142.9, 139.4, 137.2, 129.8, 127.72, 127.66, 127.56, 126.6, 126.5, 115.0, 69.5, 55.3, 49.1, 34.6, 34.1, 33.3, 31.7, 29.9, 29.5, 28.0, 22.6, 14.1.

1N *endo* LRMS (ESI, APCI) m/z : calc'd for $\text{C}_{28}\text{H}_{36}\text{N}$ $[\text{M}+\text{H}]^+$ 386.28, found 385.9

1X *exo* ^1H NMR (600 MHz, CDCl_3) δ 7.33 – 7.28 (m, 4H), 7.28 – 7.21 (m, 6H), 5.04 (d, $J = 1.5$ Hz, 1H), 5.03 (d, $J = 1.4$ Hz, 1H), 3.01 (dt, $J = 5.4, 3.9$ Hz, 1H), 2.32 – 2.26 (m, 1H), 2.08 – 2.02 (m, 4H), 1.79 – 1.72 (m, 1H), 1.65 – 1.60 (m, 1H), 1.42 – 1.17 (m, 10H), 0.85 (t, $J = 7.2$ Hz, 3H).

1X *exo* ^{13}C NMR (126 MHz, CDCl_3) δ 153.8, 143.4, 141.3, 139.0, 137.1, 129.5, 128.1, 127.8, 127.6, 126.71, 126.67, 114.9, 69.2, 61.2, 40.5, 32.1, 31.6, 30.3, 29.7, 29.4, 27.8, 22.6, 14.1.

1X *exo* LRMS (ESI, APCI) m/z : calc'd for $\text{C}_{28}\text{H}_{36}\text{N}$ $[\text{M}+\text{H}]^+$ 386.28, found 385.9



N-((*endo* or *exo*)-5-hexyl-4-phenyl-3a-(1-phenylvinyl)-1,2,3,3a,6,6a-hexahydropentalen-1-yl)acetamide (2N, 2X): A solution of **1N** (23 mg, 0.06 mmol, 1.0 equiv) or **1X** (8.4 mg, 0.02 mmol, 1.0 equiv) in DCM was cooled to 0 °C and treated with acetyl chloride (1.5 equiv) and triethylamine (3.0 equiv), then stirred for 1 h. The solution was diluted with water and extracted with DCM three times. The combined organic layers were washed with water and brine, dried with Na_2SO_4 , filtered, and concentrated. The crude oil was purified on silica gel in 35% EtOAc/Hex eluent to afford the title compound as a colorless oil (**2N *endo***: 21.1 mg, 83% yield; **2X *exo***: 6.6

mg, 71% yield.). Purity was established by Method D: *endo* $t_R = 1.00$ min, 96.3 %. *Exo* $t_R = 1.04$ min, 96.4 min.

2N *endo* ^1H NMR (500 MHz, CDCl_3) δ 7.35 – 7.27 (m, 5H), 7.25 – 7.22 (m, 5H), 5.35 (d, $J = 8.1$ Hz, 1H), 5.06 (d, $J = 1.5$ Hz, 1H), 5.02 (d, $J = 1.5$ Hz, 1H), 4.25 (dtd, $J = 10.5, 8.6, 6.2$ Hz, 1H), 2.66 (ddd, $J = 16.9, 8.4, 1.6$ Hz, 1H), 2.14 – 2.00 (m, 4H), 1.99 (s, 3H), 1.87 (dtd, $J = 11.7, 6.0, 2.3$ Hz, 1H), 1.76 (td, $J = 12.2, 11.7, 5.8$ Hz, 1H), 1.66 (ddd, $J = 12.7, 5.9, 2.3$ Hz, 1H), 1.43 – 1.26 (m, 1H), 1.30 – 1.18 (m, 8H), 0.87 (t, $J = 7.0$ Hz, 3H).

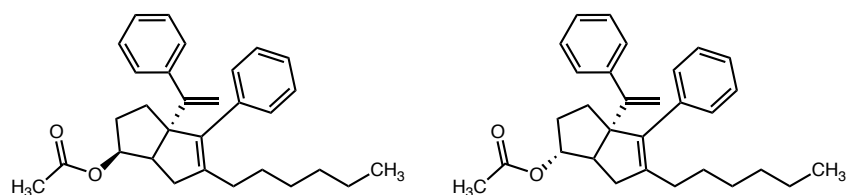
2N *endo* ^{13}C NMR (126 MHz, CDCl_3) δ 169.3, 154.6, 143.6, 141.7, 138.9, 137.2, 129.6, 127.9, 127.8, 127.7, 126.9, 126.6, 114.8, 69.0, 59.5, 54.4, 40.9, 33.0, 32.1, 31.6, 29.8, 29.4, 27.8, 26.0, 23.6, 22.6, 14.1.

2N *endo* LRMS (ESI, APCI) m/z : calc'd for $\text{C}_{30}\text{H}_{39}\text{NO}$ $[\text{M}+\text{H}]^+$ 430.3, found 430.3

2X *exo* ^1H NMR (500 MHz, CDCl_3) δ 7.35 – 7.25 (m, 8H), 7.27 – 7.19 (m, 2H), 5.35 (d, $J = 7.4$ Hz, 1H), 5.07 (s, 2H), 3.96 (dd, $J = 8.2, 4.0$ Hz, 1H), 2.34 (dd, $J = 17.2, 8.6$ Hz, 1H), 2.25 (d, $J = 7.1$ Hz, 1H), 2.22 – 2.16 (m, 1H), 2.08 – 2.02 (m, 2H), 1.93 (s, 3H), 1.90 – 1.82 (m, 2H), 1.75 – 1.66 (m, 1H), 1.40 – 1.14 (m, 9H), 0.86 (t, $J = 7.1$ Hz, 3H).

2X *exo* ^{13}C NMR (126 MHz, CDCl_3) δ 169.5, 154.3, 143.5, 143.0, 141.3, 139.3, 136.0, 129.5, 128.0, 127.8, 127.7, 126.7, 115.0, 69.0, 53.1, 47.4, 35.2, 32.1, 31.7, 29.9, 29.6, 28.1, 23.3, 22.6, 14.1.

2X *exo* LRMS (ESI, APCI) m/z : calc'd for $\text{C}_{30}\text{H}_{39}\text{NO}$ $[\text{M}+\text{H}]^+$ 430.3, found 430.3



(endo or exo)-5-hexyl-4-phenyl-3a-(1-phenylvinyl)-1,2,3,3a,6,6a-hexahydropentalen-1-yl carbamate (3N, 3X): A solution of RJW100 *endo* (25 mg, 0.07 mmol, 1.0 equiv) or RJW100 *exo* (22 mg, 0.06 mmol, 1.0 equiv) in acetonitrile was cooled to $-15\text{ }^{\circ}\text{C}$ and treated with chlorosulfonyl isocyanate (2.0 equiv) before stirring for 2 h. Concentrated hydrochloric acid (0.5 mL) was added slowly and the reaction was stirred 4 h. The solution was quenched with NaHCO_3 , diluted with water, and extracted with EtOAc three times. The combined organic layers were rinsed with brine, dried with Na_2SO_4 , filtered, and concentrated. The crude oil was purified by silica gel chromatography in 5-30% EtOAc/Hex eluent to afford the title compounds as yellow oils (**3N** *endo*: 20.4mg, 73% yield. **3X** *exo*: 16.6 mg, 68% yield). Purity was established by Method D: *endo* $t_{\text{R}} = 1.20\text{ min}$, 93.3%. *exo* $t_{\text{R}} = 1.26\text{ min}$, >99%.

3N endo $^1\text{H NMR}$ (400 MHz, CDCl_3) δ 7.34 – 7.23 (m, 5H), 7.24 – 7.18 (m, 5H), 5.04 (d, $J = 1.4\text{ Hz}$, 1H), 4.93 (d, $J = 1.4\text{ Hz}$, 1H), 4.91 – 4.87 (m, 1H), 4.54 (s, 2H), 2.66 (td, $J = 8.9, 1.8\text{ Hz}$, 1H), 2.32 (dd, $J = 17.7, 1.9\text{ Hz}$, 1H), 2.10 – 1.95 (m, 3H), 1.93 – 1.83 (m, 1H), 1.73 – 1.59 (m, 2H), 1.36 (p, $J = 7.3\text{ Hz}$, 2H), 1.29 – 1.16 (m, 7H), 0.84 (t, $J = 7.0\text{ Hz}$, 3H).

3N endo $^{13}\text{C NMR}$ (101 MHz, CDCl_3) δ 156.4, 154.3, 143.7, 143.3, 138.5, 136.9, 129.7, 127.8, 127.7, 127.6, 126.7, 126.6, 115.2, 68.54 47.0, 34.5, 31.7, 31.1, 30.1, 29.8, 29.4, 27.8, 22.6, 14.1.

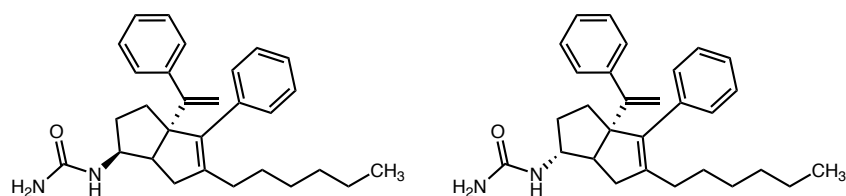
3N endo LRMS (ESI, APCI) m/z : calc'd for $\text{C}_{29}\text{H}_{39}\text{NO}_3$ $[\text{M}+\text{H}_2\text{O}]^-$ 449.3, 449.1

3X exo $^1\text{H NMR}$ (500 MHz, CDCl_3) δ 7.41 – 7.19 (m, 10H), 5.08 (d, $J = 1.6\text{ Hz}$, 1H), 5.02 (d, $J = 1.6\text{ Hz}$, 1H), 4.77 (dt, $J = 4.2, 1.4\text{ Hz}$, 1H), 4.56 (s, 2H), 2.42 (d, $J = 8.1\text{ Hz}$, 1H), 2.36 (dd, $J =$

16.3, 8.9 Hz, 1H), 2.19 (d, $J = 17.0$ Hz, 1H), 2.14 – 1.88 (m, 4H), 1.85 – 1.63 (m, 3H), 1.41 – 1.29 (m, 2H), 1.31 – 1.16 (m, 5H), 0.88 (t, $J = 7.0$ Hz, 3H).

3X *exo* ^{13}C NMR (126 MHz, CDCl_3) δ 156.6, 154.5, 143.9, 141.9, 138.5, 137.3, 129.6, 127.8, 127.7, 126.8, 126.7, 115.0, 85.6, 69.4, 53.0, 40.3, 32.4, 31.7, 31.5, 29.7, 29.4, 27.8, 22.6, 14.1.

3X *exo* LRMS (ESI, APCI) m/z : calc'd for $\text{C}_{29}\text{H}_{39}\text{NO}_3$ $[\text{M}+\text{H}_2\text{O}]^-$ 449.3, found 449.3



1-((endo or exo)-5-hexyl-4-phenyl-3a-(1-phenylvinyl)-1,2,3,3a,6,6a-hexahydropentalen-1-yl)urea (4N, 4X): A solution of **1N** (15 mg, 0.04 mmol, 1.0 equiv) or **1X** (11 mg, 0.03 mmol, 1.0 equiv) in water was treated with sodium cyanate (10.0 equiv) and 1M aqueous hydrochloric acid (2.0 equiv). The reaction was heated to 90°C and stirred for approximately 72 hours before being cooled to room temperature, diluted with 3M aqueous NaOH and extracted with Et_2O three times. The combined organic layers were washed with water and brine, dried with Na_2SO_4 , filtered, and concentrated. The crude oil was purified on silica in 100% EtOAc eluent to afford the title compound as a white solid. (**4N** *endo*: 6.9 mg, 41% yield; **4X** *exo*: 4.5 mg, 37% yield). Purity was established by Method B: *endo* $t_{\text{R}} = 2.19$ min, 96.5%. *exo* $t_{\text{R}} = 4.05$ min, >99%.

4N *endo* ^1H NMR (600 MHz, CDCl_3) δ 7.34 – 7.19 (m, 10H), 5.06 (d, $J = 1.4$ Hz, 1H), 4.99 (d, $J = 1.4$ Hz, 1H), 4.48 (d, $J = 7.7$ Hz, 1H), 4.32 (s, 2H), 3.97 (s, 1H), 2.60 (t, $J = 8.7$ Hz, 1H), 2.22 (d, $J = 17.3$ Hz, 1H), 2.09 – 2.03 (m, 2H), 1.93 – 1.85 (m, 1H), 1.73 (td, $J = 12.5, 5.7$ Hz, 1H),

1.67 (ddd, $J = 12.9, 6.1, 1.9$ Hz, 1H), 1.39 – 1.31 (m, 2H), 1.29 – 1.17 (m, 8H), 0.86 (t, $J = 7.1$ Hz, 3H).

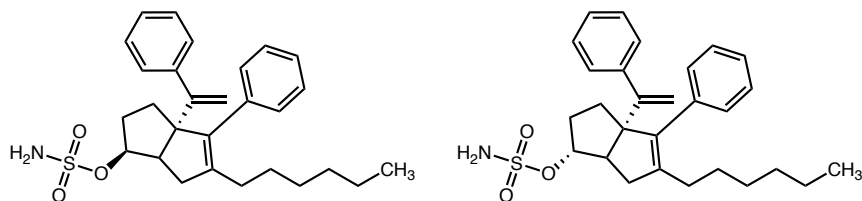
4N *endo* ^{13}C NMR (126 MHz, CDCl_3) δ 157.9, 154.4, 143.6, 143.2, 139.0, 136.8, 129.5, 127.9, 127.72, 127.68, 126.8, 126.7, 115.1, 69.2, 47.6, 35.1, 32.1, 31.9, 31.6, 29.9, 29.5, 28.0, 22.6, 14.1.

4N *endo* LRMS (ESI, APCI) m/z : calc'd for $\text{C}_{29}\text{H}_{37}\text{N}_2\text{O}$ $[\text{M}+\text{H}]^+$ 429.7, found 428.9

4X *exo* ^1H NMR (600 MHz, CDCl_3) δ 7.34 – 7.19 (m, 10H), 5.06 (d, $J = 1.3$ Hz, 1H), 5.03 (d, $J = 1.4$ Hz, 1H), 4.42 (d, $J = 7.4$ Hz, 1H), 4.25 (s, 2H), 3.70 (s, 1H), 2.36 (dd, $J = 17.2, 8.9$ Hz, 1H), 2.22 – 2.17 (m, 2H), 2.05 (q, $J = 7.0$ Hz, 2H), 1.94 – 1.80 (m, 2H), 1.72 – 1.66 (m, 1H), 1.59 – 1.52 (m, 1H), 1.33 (q, $J = 7.4$ Hz, 2H), 1.28 – 1.17 (m, 6H), 0.85 (t, $J = 7.2$ Hz, 3H).

4X *exo* ^{13}C NMR (126 MHz, CDCl_3) δ 157.7, 154.5, 143.6, 141.5, 139.0, 137.2, 129.6, 127.83, 127.77, 127.7, 126.8, 126.7, 114.9, 69.0, 60.9, 54.4, 41.1, 32.8, 32.4, 31.6, 29.8, 29.7, 29.4, 27.8, 22.6, 14.1.

4X *exo* LRMS (ESI, APCI) m/z : calc'd for $\text{C}_{29}\text{H}_{37}\text{N}_2\text{O}$ $[\text{M}+\text{H}]^+$ 429.7, found 428.9



(*endo* or *exo*)-5-hexyl-4-phenyl-3a-(1-phenylvinyl)-1,2,3,3a,6,6a-hexahydropentalen-1-yl

sulfamate (5N, 5X): A 1M solution of sulfamoyl chloride (2.5 equiv) in DMA was cooled to 0°C .

A solution of the appropriate RJW100 alcohol isomer (*endo* (224.3 mg, 0.6 mmol 1.0 equiv) or *exo* (26 mg, 0.07 mmol, 1.0 equiv)) in DMA was added slowly, followed by triethylamine (excess, ca. 5 equiv); the resulting solution was stirred for one hour. The solution was then diluted with

water and extracted with EtOAc three times. The combined organic layers were washed with water and brine, dried with MgSO₄, filtered, and concentrated. The crude oil was purified by silica gel chromatography in 20% EtOAc/Hex eluent (with 0.5% triethylamine), to afford the title compound as a clear oil (**5N endo**: 182 mg, 67% yield. **5X exo**: 16.5 mg, 52% yield). Purity was established by Method D: *endo* t_R = 1.15 min, 95.3%. *exo* t_R = 0.97 min, 95.1%.

5N endo ¹H NMR (500 MHz, CDCl₃) δ 7.35 – 7.24 (m, 8H), 7.23 – 7.15 (m, 2H), 5.11 (s, 1H), 4.92 (s, 1H), 4.87 (td, *J* = 9.1, 5.2 Hz, 1H), 4.64 (s, 2H), 2.71 (d, *J* = 9.0 Hz, 1H), 2.60 (d, *J* = 17.5 Hz, 1H), 2.17 (dd, *J* = 17.7, 9.3 Hz, 1H), 2.10 – 2.01 (m, 3H), 1.92 – 1.83 (m, 1H), 1.83 – 1.76 (m, 1H), 1.68 (td, *J* = 12.6, 5.6 Hz, 1H), 1.45 – 1.35 (m, 2H), 1.32 – 1.16 (m, 6H), 0.86 (t, *J* = 7.1 Hz, 3H).

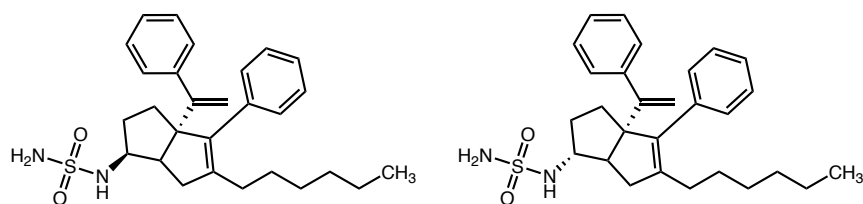
5N endo ¹³C NMR (126 MHz, CDCl₃) δ 153.8, 143.5, 143.2, 138.5, 136.5, 129.8, 127.9, 127.7, 127.6, 127.0, 126.8, 115.7, 84.1, 68.2, 47.1, 34.9, 31.6, 31.2, 30.5, 29.8, 29.4, 27.7, 22.6, 14.1.

5N endo LRMS (ESI, APCI) *m/z*: calc'd for C₂₈H₃₆NO₃S [M-H]⁻ 465.3, found 465.4

5X exo ¹H NMR (500 MHz, CDCl₃) δ 7.36 – 7.28 (m, 7H), 7.29 – 7.16 (m, 3H), 5.10 (d, *J* = 1.3 Hz, 1H), 5.00 (d, *J* = 1.3 Hz, 1H), 4.75 (d, *J* = 4.4 Hz, 1H), 4.62 (s, 2H), 2.68 (d, *J* = 9.1 Hz, 1H), 2.40 (dd, *J* = 18.1, 9.4 Hz, 1H), 2.19 – 2.01 (m, 6H), 1.88 – 1.73 (m, 2H), 1.38 – 1.16 (m, 7H), 0.87 (t, *J* = 7.1 Hz, 3H).

5X exo ¹³C NMR (126 MHz, CDCl₃) δ 153.6, 143.7, 141.4, 138.8, 136.8, 129.6, 127.8, 127.8, 127.7, 126.89, 126.86, 115.6, 93.7, 69.3, 52.8, 40.1, 32.1, 32.0, 31.6, 29.7, 29.4, 27.8, 22.6, 14.1.

5X exo LRMS (ESI, APCI) *m/z*: calc'd for C₂₈H₃₆NO₃S [M-H]⁻ 465.3, found 465.2



(endo or exo)-5-hexyl-4-phenyl-3a-(1-phenylvinyl)-1,2,3,3a,6,6a-hexahydropentalen-1-yl sulfamide (6N, 6X): A solution of **1N** (30 mg, 0.08 mmol, 1.1 equiv) or **1X** (12 mg, 0.03 mmol, 1.1 equiv) in DCM was treated with triethylamine (2.0 equiv.) and solution of 2-oxo-1,3-oxazolidine-3-sulfonyl chloride (0.5 M in DCM, 1.0 equiv). The reaction was stirred at room temperature for 3 h then concentrated. The residue was treated with ammonia (0.5 M in dioxane, 1.5 equiv) and triethylamine (3.0 equiv). The solution was heated in a sealed tube at 85°C for 16 h behind a blast shield. After cooling to ambient temperature, the reaction was diluted with 3:3:94 MeOH:Et₃N:EtOAc and passed through a pad of silica. The eluent was concentrated, and the crude oil was purified on silica in 20-30% EtOAc/Hex eluent to afford the title compound as a colorless oil. (**6N endo**: 21.6 mg, 60% yield; **6X exo**: 5.4 mg, 36% yield) Purity was established by Method C: *endo* t_R = 2.0 min, 96.6%. *exo* t_R = 1.89 min, 79.6%.

6N endo ¹H NMR (600 MHz, CDCl₃) δ 7.33 – 7.23 (m, 8H), 7.20 – 7.17 (m, 2H), 5.09 (d, *J* = 1.3 Hz, 1H), 4.96 (d, *J* = 1.3 Hz, 1H), 4.44 (s, 2H), 4.36 (d, *J* = 8.0 Hz, 1H), 3.84 – 3.77 (m, 1H), 2.62 (td, *J* = 8.9, 2.0 Hz, 1H), 2.38 (dd, *J* = 17.5, 2.0 Hz, 1H), 2.20 – 2.13 (m, 1H), 2.08 – 2.04 (m, 2H), 2.00 – 1.95 (m, 1H), 1.74 – 1.70 (m, 2H), 1.50 – 1.43 (m, 1H), 1.42 – 1.16 (m, 8H), 0.86 (t, *J* = 7.1 Hz, 3H).

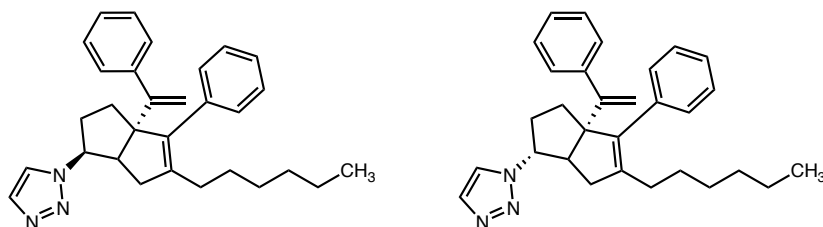
6N endo ¹³C NMR (126 MHz, CDCl₃) δ 154.1, 143.6, 142.8, 139.3, 136.6, 129.6, 127.8, 127.7, 126.9, 126.8, 115.5, 68.8, 57.2, 47.4, 35.4, 32.3, 32.0, 31.6, 29.8, 29.5, 27.9, 22.6, 14.1.

6N endo LRMS (ESI, APCI) *m/z*: calc'd for C₂₈H₃₇N₂O₂S [M+H]⁺ 465.7, found 464.8

6X *exo* ^1H NMR (600 MHz, CDCl_3) δ 7.34 – 7.24 (m, 8H), 7.23 – 7.18 (m, 2H), 5.08 (d, $J = 1.2$ Hz, 1H), 5.01 (d, $J = 1.2$ Hz, 1H), 4.38 (s, 2H), 4.21 (d, $J = 7.2$ Hz, 1H), 3.58 – 3.52 (m, 1H), 2.40 (dd, $J = 16.9, 8.9$ Hz, 1H), 2.36 – 2.31 (m, 1H), 2.18 (d, $J = 16.9$ Hz, 1H), 2.05 (td, $J = 7.5, 2.6$ Hz, 2H), 1.99 – 1.85 (m, 2H), 1.76 – 1.69 (m, 2H), 1.38 – 1.30 (m, 1H), 1.30 – 1.15 (m, 7H), 0.86 (t, $J = 7.2$ Hz, 3H).

6X *exo* ^{13}C NMR (126 MHz, CDCl_3) δ 154.1, 143.5, 141.2, 139.3, 136.9, 129.6, 127.9, 127.7, 126.9, 126.8, 115.2, 68.8, 63.8, 54.0, 40.8, 32.8, 32.3, 31.6, 29.71, 29.69, 29.4, 27.8, 22.6, 14.1.

6X *exo* LRMS (ESI, APCI) m/z : calc'd for $\text{C}_{29}\text{H}_{37}\text{N}_2\text{O}$ $[\text{M}+\text{H}]^+$ 465.7, found 464.8



(endo or exo) 5-hexyl-4-phenyl-3a-(1-phenylvinyl)-1,2,3,3a,6,6a-hexahydropentalen-1-yl)-1H-1,2,3-triazole (7N, 7X): A solution of ascorbic acid (1.0 equiv), and potassium carbonate (6.0 equiv) in water was treated with copper sulfate pentahydrate (1.0 equiv) and stirred briefly. Trimethylsilyl acetylene (6.0 equiv.) was added in MeOH before addition of **SN *endo*** (29 mg, 0.07 mmol, 1.0 equiv) or **S3X *exo*** (29 mg, 0.07 mmol, 1.0 equiv) in MeOH. The reaction mixture was stirred 16 h, diluted with water, and extracted with EtOAc three times. The combined organics were washed with brine and dried over MgSO_4 before concentration. The crude oil was purified by silica gel chromatography in 30% EtOAc/Hex eluent to afford the title compounds (**7N *endo***: 19.0 mg, 62% yield, **7X *exo***: 14.7 mg, 48% yield). Purity was established by: *endo* (Method B) $t_{\text{R}} = 2.88$ min, 97.5%. *exo* (Method D) $t_{\text{R}} = 1.46$ min, 78.0%.

7N endo ^1H NMR (600 MHz, CDCl_3) δ 7.70 (s, 1H), 7.49 (s, 1H), 7.36 – 7.25 (m, 8H), 7.24 – 7.21 (m, 2H), 5.14 (s, 1H), 5.00 (s, 1H), 4.96 (ddd, $J = 11.5, 9.5, 6.7$ Hz, 1H), 2.94 (td, $J = 9.2, 1.9$ Hz, 1H), 2.29 – 2.20 (m, 2H), 2.03 – 1.84 (m, 5H), 1.27 – 1.09 (m, 9H), 0.81 (t, $J = 7.0$ Hz, 3H).

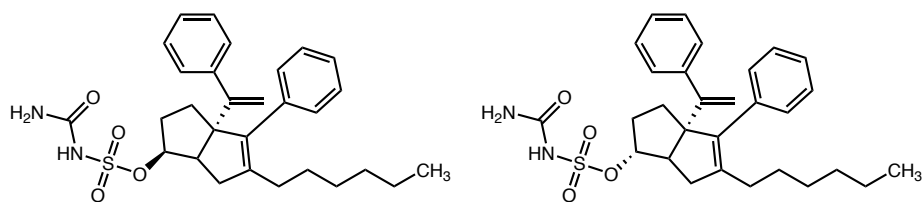
7N endo ^{13}C NMR (126 MHz, CDCl_3) δ 153.8, 143.5, 138.4, 133.3, 129.7, 127.9, 127.8, 127.7, 127.0, 126.9, 122.9, 115.9, 69.1, 63.4, 48.6, 35.7, 32.6, 31.5, 29.7, 29.4, 29.3, 27.7, 22.6, 14.1.

7N endo LRMS (ESI, APCI) m/z : calc'd for $\text{C}_{30}\text{H}_{38}\text{N}_3$ $[\text{M}+\text{H}]^+$ 440.3, found 440.4

7X exo ^1H NMR (600 MHz, CDCl_3) δ 7.66 (s, 1H), 7.43 (s, 1H), 7.37 – 7.20 (m, 10H), 5.13 (dd, $J = 0.9$ Hz, 1H), 5.09 (d, $J = 0.9$ Hz, 1H), 4.79 – 4.72 (m, 1H), 2.79 (dd, $J = 8.6, 3.8$ Hz, 1H), 2.41 (dd, $J = 17.2, 8.6$ Hz, 1H), 2.28 (d, $J = 17.5$ Hz, 1H), 2.18 – 1.98 (m, 4H), 1.85 – 1.77 (m, 1H), 1.40 – 1.33 (m, 2H), 1.29 – 1.16 (m, 7H), 0.85 (t, $J = 7.1$ Hz, 3H).

7X exo ^{13}C NMR (101 MHz, CDCl_3) δ 153.4, 143.2, 141.3, 139.2, 136.7, 129.6, 128.0, 127.0, 127.8, 127.1, 126.9, 121.7, 115.7, 110.0, 70.0, 69.3, 53.1, 41.2, 33.0, 32.9, 31.6, 29.8, 29.4, 27.8, 22.6, 14.1.

7X exo LRMS (ESI, APCI) m/z : calc'd for $\text{C}_{30}\text{H}_{38}\text{N}_3$ $[\text{M}+\text{H}]^+$ 440.3, found 440.3



(endo or exo) 5-hexyl-4-phenyl-3a-(1-phenylvinyl)-1,2,3,3a,6,6a-hexahydropentalen-1-yl carbamoylsulfamate (8N, 8X): To a solution of sodium hydride (60% suspension in mineral oil, 2.0 equiv) at 0 °C was added either **5X** (49.7 mg, 0.11 mmol, 1.0 equiv) or **5N** (33.6 mg, 0.07 mmol, 1.0 equiv) in THF at 0 °C for 1 h and allowed to warm to room temperature. A solution of carbonyldiimidazole (1.5 equiv) in THF was added to the reaction mixture at room temperature.

The resulting solution was stirred for 1 h before slow addition of excess ammonia in methanol (7N). The solution was allowed to stir for an additional 3 h. The crude reaction mixture was dissolved in EtOAc, washed with brine, and dried in MgSO₄. The organic layer was concentrated, and the crude mixture was purified via preparatory HPLC (8N endo: 6.1 mg, 16% yield, 8X exo: 2.5 mg, 5% yield). Purity was established by Method D: endo tR = 1.74 min, 96.2%. exo tR = 1.74 min, >99%.

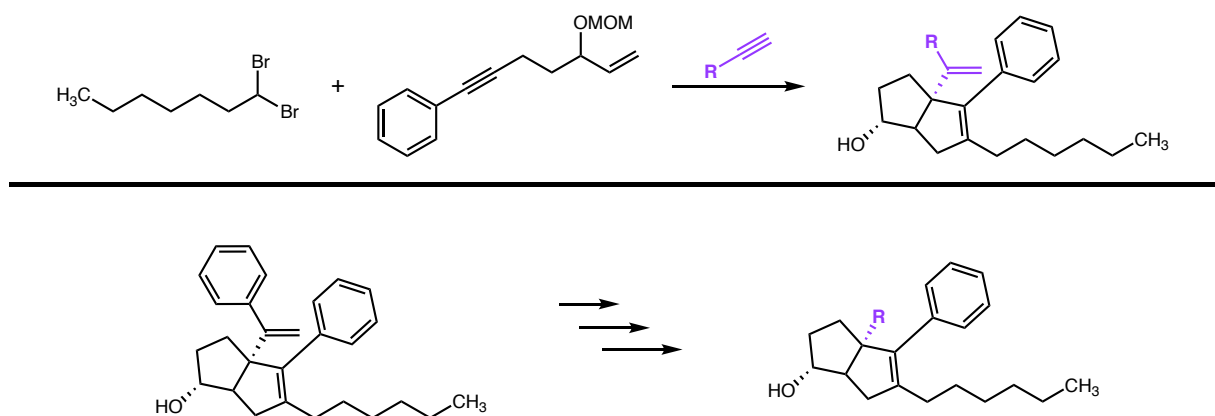
8N endo ¹H NMR (400 MHz, CDCl₃) δ 7.35 (s, 1H), 7.33 – 7.20 (m, 8H), 7.19 – 7.13 (m, 2H), 5.08 (d, J = 1.2 Hz, 1H), 5.02 (td, J = 9.1, 6.0 Hz, 1H), 4.91 (d, J = 1.4 Hz, 1H), 3.74 (s, 2H), 2.67 (td, J = 9.0, 2.3 Hz, 1H), 2.58 (dd, J = 17.5, 2.1 Hz, 1H), 2.17 – 1.99 (m, 3H), 1.91 – 1.62 (m, 3H), 1.40 – 1.27 (m, 2H), 1.27 – 1.15 (m, 7H), 0.83 (t, J = 7.0 Hz, 3H).

8N endo LRMS (ESI, APCI) m/z: calc'd for C₂₈H₃₃ [M-CH₃N₂O₄S]⁺ 369.6, found 369.2. calc'd for C₂₉H₃₅N₂O₄S [M-H]⁻ 507.7, found 507.2.

8X exo ¹H NMR (400 MHz, CDCl₃) δ 7.32 – 7.11 (m, 11H), 4.99 (s, 1H), 4.93 (s, 1H), 4.69 (s, 1H), 3.60 – 3.48 (m, 2H), 2.60 (d, J = 9.1 Hz, 1H), 2.25 (dd, J = 17.4, 9.2 Hz, 1H), 2.11 – 1.90 (m, 3H), 1.75 – 1.54 (m, 2H), 1.32 – 1.07 (m, 10H), 0.81 (t, J = 7.1 Hz, 3H).

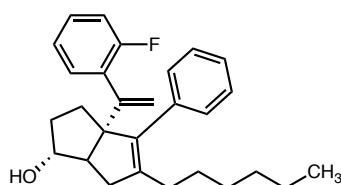
8X exo LRMS (ESI, APCI) m/z: calc'd for C₂₈H₃₃ [M-CH₃N₂O₄S]⁺ 369.6, found 369.2. calc'd for C₂₉H₃₅N₂O₄S [M-H]⁻ 507.7, found 507.2.

R2: Styrene Modifications 9 – 15



Hexahydropentalene formation was accomplished through slight modification of Whitby's procedure. Prior to cyclization, all non-volatile reagents were dried by azeotropic removal of water using benzene. A dry round bottom flask containing bis(cyclopentadienyl)zirconium(IV) dichloride (1.2 equiv) under nitrogen, was dissolved in anhydrous, degassed tetrahydrofuran (THF, 50 mL/mmol enyne) and cooled to $-78\text{ }^{\circ}\text{C}$. The resulting solution was treated with *n*-BuLi (2.4 equiv.) and the light yellow solution was stirred for 30 minutes. A solution of (5-(methoxymethoxy)hept-6-en-1-yn-1-yl)benzene (1.0 equiv) (prepared according to a literature procedure)⁵⁷ in anhydrous, degassed THF (5 mL/mmol) was added. The resulting salmon-colored mixture was stirred at $-78\text{ }^{\circ}\text{C}$ for 30 minutes, the cooling bath removed, and the reaction mixture was allowed to warm to ambient temperature with stirring (2.5 hours total). The reaction mixture was then cooled to $-78\text{ }^{\circ}\text{C}$ and the required 1,1-dibromoheptane (1.1 equiv) was added as a solution in anhydrous THF (5 mL/mmol) followed by freshly prepared lithium diisopropylamide (LDA, 1.0 M, 1.1 equiv.). After 15 minutes, a freshly prepared solution of lithium phenylacetylide (3.6 equiv.) in anhydrous THF was added dropwise and the resulting rust-colored solution was stirred

at -78 °C for 1.5 hours. The reaction was quenched with methanol and saturated aqueous sodium bicarbonate and allowed to warm to room temperature, affording a light yellow slurry. The slurry was poured onto water and extracted with ethyl acetate four times. The combined organic layers were washed with brine, dried with MgSO₄, and concentrated in vacuo. The resulting yellow oil was passed through a short plug of silica (20% EtOAc/Hex eluent) and concentrated. The crude product was dissolved in acetonitrile and treated with concentrated aqueous hydrochloric acid (ca 5 equiv) and the resulting solution stirred at room temperature until completion of the reaction was detected (typically fewer than 10 minutes). The reaction mixture was concentrated and purified by silica gel chromatography (20% EtOAc/Hex eluent) to afford the title compounds **9** – **15** as a 7:1 mixture of diastereomers, favoring the desired *exo*-isomer.



(*exo*)-3a-(1-(2-fluorophenyl)vinyl)-5-hexyl-4-phenyl-1,2,3,3a,6,6a-hexahydropentalen-1-ol

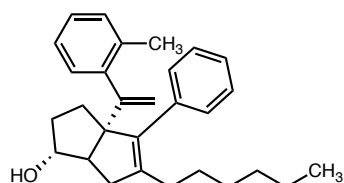
(9): According to the general procedure, (5-(methoxymethoxy)hept-6-en-1-yn-1-yl)benzene (179.7 mg, 0.8 mmol) was reacted with 1-ethynyl-2-fluorobenzene (320 μ L, 2.8 mmol). The crude oil was purified in 5-20% EtOAc/Hex eluent to give the title compound (35.5 mg, 11% yield over two steps). Purity was established as the *exo* diastereomer by Method D: $t_R = 1.44$ min, 98.3%.

¹H NMR (500 MHz, CDCl₃) δ 7.38 – 7.17 (m, 7H), 7.03 (dtt, $J = 13.0, 7.5, 1.1$ Hz, 2H), 5.27 (s, 1H), 5.11 (s, 1H), 3.92 (d, $J = 4.3$ Hz, 1H), 2.31 (d, $J = 14.3$ Hz, 2H), 2.15 – 1.95 (m, 4H), 1.76 – 1.57 (m, 4H), 1.40 – 1.15 (m, 7H), 0.86 (t, $J = 7.1$, 3H).

^{13}C NMR (126 MHz, CDCl_3) δ 160.6, 158.6, 147.9, 141.8, 138.3, 137.4, 130.4, 129.7, 128.4, 128.3, 127.7, 126.6, 123.2, 116.7, 115.4, 115.2, 82.0, 69.4, 56.8, 39.7, 34.7, 31.7, 31.2, 29.8, 29.4, 27.9, 22.6, 14.1.

^{19}F NMR (282 MHz, CDCl_3) δ -113.74.

LRMS (ESI, APCI) m/z : calc'd for $\text{C}_{28}\text{H}_{36}\text{FO}$ $[\text{M}+\text{H}]^+$ 405.3, found 405.9



(*exo*)-5-hexyl-4-phenyl-3a-(1-(*o*-tolyl)vinyl)-1,2,3,3a,6,6a-hexahydropentalen-1-ol (10):

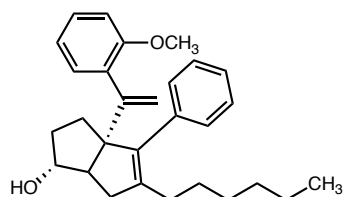
According to the general procedure, (5-(methoxymethoxy)hept-6-en-1-yn-1-yl)benzene (144.4 mg, 0.6 mmol) was reacted with 1-ethynyl-2-methylbenzene (280 μL , 2.2 mmol). The crude oil was purified in 10% EtOAc/Hex eluent to give the title compound (62.9 mg, 25% over two steps).

Purity was established as the *exo* diastereomer by Method B: $t_{\text{R}} = 3.66$ min, 98.3%.

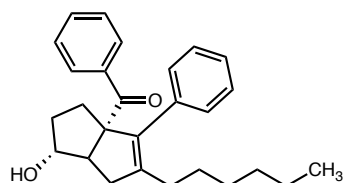
^1H NMR (600 MHz, CDCl_3) δ 7.36 – 7.30 (m, 2H), 7.30 – 7.26 (m, 1H), 7.24 (d, $J = 7.5$ Hz, 2H), 7.18 (d, $J = 7.5$ Hz, 1H), 7.14 (t, $J = 7.4$ Hz, 1H), 7.04 (t, $J = 7.4$ Hz, 1H), 5.08 (s, 1H), 4.95 (s, 1H), 3.91 (s, 1H), 2.26 (s, 3H), 2.25 – 2.12 (m, 2H), 2.06 – 1.88 (m, 4H), 1.76 – 1.66 (m, 2H), 1.61 (dd, $J = 11.9, 6.3$ Hz, 1H), 1.42 – 1.28 (m, 3H), 1.28 – 1.22 (m, 1H), 1.22 – 1.15 (m, 4H), 0.85 (t, $J = 7.2$ Hz, 3H).

^{13}C NMR (126 MHz, CDCl_3) δ 152.3, 142.9, 141.7, 138.5, 137.7, 135.6, 130.1, 130.0, 127.6, 126.6, 126.5, 124.8, 115.5, 82.1, 74.7, 70.0, 55.7, 39.8, 34.6, 31.8, 31.7, 29.7, 29.3, 27.9, 22.6, 20.7, 14.1.

LRMS (ESI, APCI) m/z : calc'd for $\text{C}_{29}\text{H}_{39}\text{O}$ $[\text{M}+\text{H}]^+$ 401.3, found 401.0



(*exo*)-5-hexyl-3a-(1-(2-methoxyphenyl)vinyl)-4-phenyl-1,2,3,3a,6,6a-hexahydropentalen-1-ol (11): According to the general procedure, (5-(methoxymethoxy)hept-6-en-1-yn-1-yl)benzene (146.5 mg, 0.6 mmol) was reacted with 1-ethynyl-2-methoxybenzene (300 μ L, 2.3 mmol). The crude oil was purified in 10-20% EtOAc/Hex eluent to give the title compound (12.2 mg, 5% yield over two steps). Purity was established as the *exo* diastereomer by Method B: $t_R = 2.95$ min, 97.6% $^1\text{H NMR}$ (600 MHz, CDCl_3) δ 7.36 – 7.18 (m, 6H), 6.95 (d, $J = 7.1$ Hz, 1H), 6.88 – 6.81 (m, 2H), 5.18 (d, $J = 1.8$ Hz, 1H), 5.01 (d, $J = 1.8$ Hz, 1H), 3.86 (s, 1H), 3.75 (s, 3H), 2.50 (dd, $J = 16.6, 9.1$ Hz, 1H), 2.45 (d, $J = 8.6$ Hz, 1H), 2.08 (d, $J = 16.6$ Hz, 1H), 2.01 (t, $J = 7.7$ Hz, 2H), 1.81 – 1.72 (m, 2H), 1.65 – 1.58 (m, 2H), 1.58 – 1.53 (m, 1H), 1.36 – 1.29 (m, 2H), 1.27 – 1.20 (m, 2H), 1.21 – 1.14 (m, 2H), 0.84 (t, $J = 7.2$ Hz, 3H). $^{13}\text{C NMR}$ (151 MHz, CDCl_3) δ 172.5, 169.6, 156.4, 151.5, 140.5, 137.7, 132.6, 130.1, 129.8, 128.0, 127.5, 126.4, 120.4, 115.6, 110.8, 81.7, 69.3, 57.6, 55.6, 51.3, 39.6, 34.6, 31.6, 31.1, 29.6, 29.2, 28.0, 22.6, 14.1. **LRMS** (ESI, APCI) m/z : calc'd for $\text{C}_{29}\text{H}_{39}\text{O}_2$ $[\text{M}+\text{H}]^+$ 417.3, found 417.9



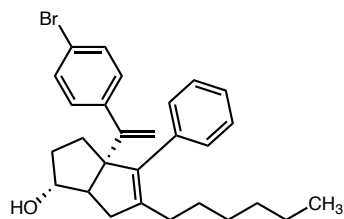
(*exo*)-5-hexyl-1-hydroxy-4-phenyl-2,3,6,6a-tetrahydropentalen-3a(1*H*)-yl)(phenyl)methanone (12):

A solution of RJW100 (11.2 mg, 0.03 mmol) in DCM was cooled to -78°C and treated with ozone until the solution was blue. At this point, the stream of ozone was stopped and the reaction was stirred until the blue color dissipated. DMS was added (11 μL , 0.15 mmol, 5.0 equiv) and briefly stirred. The reaction solution was concentrated, and the crude reaction mixture was purified on silica in 0-20% EtOAc/Hex to afford a clear, colorless oil (9.4 mg, 81% yield). Purity was established by Method D: $t_{\text{R}} = 1.43$ min, 96.5%.

^1H NMR (600 MHz, CDCl_3) δ 7.86 (d, $J = 7.7$ Hz, 2H), 7.46 (t, $J = 7.4$ Hz, 1H), 7.35 (dd, $J = 8.7$, 6.7 Hz, 2H), 7.18 (d, $J = 6.6$ Hz, 3H), 6.87 (dd, $J = 7.2$, 2.3 Hz, 2H), 4.06 (s, 1H), 3.02 (dd, $J = 17.5$, 10.2 Hz, 1H), 2.90 (d, $J = 11.2$ Hz, 1H), 2.76 – 2.64 (m, 1H), 2.33 (dd, $J = 17.7$, 3.5 Hz, 1H), 2.09 (t, $J = 7.8$ Hz, 2H), 2.00 (d, $J = 12.2$ Hz, 1H), 1.85 – 1.66 (m, 2H), 1.49 – 1.36 (m, 2H), 1.29 – 1.15 (m, 6H), 0.85 (dd, $J = 14.0$, 7.2 Hz, 3H).

^{13}C NMR (101 MHz, CDCl_3) δ 203.4, 142.0, 140.0, 138.6, 136.2, 131.8, 129.0, 128.6, 128.1, 128.1, 127.0, 80.8, 76.3, 54.6, 40.5, 32.7, 31.6, 30.5, 29.4, 29.3, 27.8, 22.6, 21.6, 14.1.

LRMS (ESI, APCI) m/z : calc'd for $\text{C}_{27}\text{H}_{35}\text{O}_2$ $[\text{M}+\text{H}]^+$ 389.6, found 389.2



(*exo*)-3a-(1-(4-bromophenyl)vinyl)-5-hexyl-4-phenyl-1,2,3,3a,6,6a-hexahydropentalen-1-ol

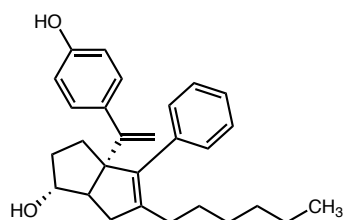
(S9): According to the general procedure, (5- (methoxymethoxy)hept-6-en-1-yn-1-yl)benzene

(273.6 mg, 1.2 mmol) was reacted with 1-bromo-4-ethynylbenzene (776.3 mg, 4.3 mmol). The crude oil was purified in 10% EtOAc/Hex eluent to give the title compound (105.0 mg, 19% yield over two steps).

¹H NMR (500 MHz, CDCl₃) δ 7.38 (d, *J* = 8.1 Hz, 2H), 7.34 – 7.27 (m, 3H), 7.23 (d, *J* = 8.1 Hz, 2H), 7.16 (d, *J* = 8.6 Hz, 2H), 5.06 (s, 1H), 5.01 (s, 1H), 3.96 (s, 1H), 2.38 (dd, *J* = 17.2, 9.4 Hz, 1H), 2.26 (d, *J* = 9.4 Hz, 1H), 2.13 – 1.98 (m, 4H), 1.72 – 1.65 (m, 3H), 1.33 (d, *J* = 7.5 Hz, 3H), 1.29 – 1.18 (m, 5H), 0.87 (t, *J* = 7.1 Hz, 3H).

¹³C NMR (126 MHz, CDCl₃) δ 153.6, 143.1, 141.5, 138.9, 137.2, 130.8, 129.6, 129.4, 127.7, 126.7, 120.8, 115.5, 82.0, 69.2, 55.7, 40.3, 34.0, 32.1, 31.6, 29.7, 29.4, 27.8, 22.6, 14.1.

LRMS (ESI, APCI) *m/z*: calc'd for C₂₈H₃₆BrO [M+H]⁺ 465.2, found 465.7



(*exo*)-5-hexyl-3a-(1-(4-hydroxyphenyl)vinyl)-4-phenyl-1,2,3,3a,6,6a-hexahydropentalen-1-ol

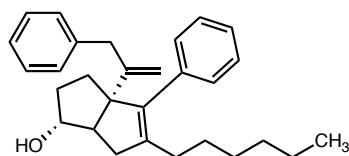
(13): A solution of potassium hydroxide (13.5 mg, 0.24 mmol, 3.0 equiv.), tris(dibenzylideneacetone)dipalladium(0) (1.8 mg, 0.002 mmol, ca 0.03 equiv), and ^tBuXPhos (2.8 mg, 0.007 mmol, ca 0.1 equiv) in 1,4-dioxane (ca 2 mL) in a reaction tube under nitrogen was treated with water and (*exo*)-3a-(1-(4-bromophenyl)vinyl)-5-hexyl-4-phenyl-1,2,3,3a,6,6a-hexahydropentalen-1-ol (**S9**) (30.7 mg, 0.07 mmol, 1.0 equiv) as a solution in dioxane (ca 1 mL). Water (ca 0.5 mL) was added, and the reaction mixture was heated to 80 °C for 16 hours. After reaction completion, the reaction was allowed to cool to ambient temperature before poured onto water and extracted with ethyl acetate three times. The combined organic layers were washed with

water then brine, dried with MgSO_4 , concentrated, and purified on silica in 20-50% EtOAc/Hex eluent to afford the title compound. (6.2 mg, 26% yield). Note: for larger scale reactions palladium loading can be brought down to 0.01 equiv, and ligand to 0.04 equiv. Purity was established as the *exo* diastereomer by Method B: $t_R = 1.33$ min, 95.6%.

$^1\text{H NMR}$ (500 MHz, CDCl_3) δ 7.38 – 7.27 (m, 4H), 7.24 – 7.14 (m, 3H), 6.78 – 6.70 (m, 2H), 5.03 (d, $J = 1.4$ Hz, 1H), 4.96 (d, $J = 1.5$ Hz, 1H), 4.74 (s, 1H), 3.95 (s, 1H), 2.38 (dd, $J = 16.9, 9.4$ Hz, 1H), 2.28 (d, $J = 9.3$ Hz, 1H), 2.12 – 1.93 (m, 4H), 1.78 – 1.62 (m, 3H), 1.33 (dd, $J = 14.0, 6.7$ Hz, 3H), 1.31 – 1.17 (m, 5H), 0.86 (t, $J = 7.1$ Hz, 3H).

$^{13}\text{C NMR}$ (126 MHz, CDCl_3) δ 154.6, 154.0, 141.1, 139.1, 137.4, 136.6, 129.7, 129.0, 127.6, 126.6, 114.5, 82.2, 69.5, 55.7, 40.3, 34.0, 32.0, 31.7, 29.7, 29.4, 27.8, 22.6, 14.1.

LRMS (ESI, APCI) m/z : calc'd for $\text{C}_{28}\text{H}_{37}\text{O}_2$ $[\text{M}+\text{H}]^+$ 403.3, found 403.9



(*exo*)-5-hexyl-4-phenyl-3a-(3-phenylprop-1-en-2-yl)-1,2,3,3a,6,6a-hexahydropentalen-1-ol

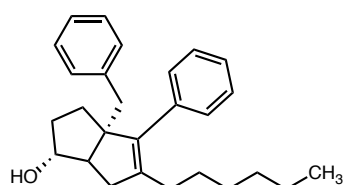
(14): According to the general procedure, (5-(methoxymethoxy)hept-6-en-1-yn-1-yl)benzene (57.0 mg, 0.25 mmol) was reacted with 3-phenyl-1-propyne (110 μL , 0.9 mmol) and purified in 5-20% EtOAc/Hex eluent to afford the title compound (38.7 mg, 39% yield over two steps). Purity was established as the *exo* diastereomer by Method B: $t_R = 3.89$ min, >99%.

$^1\text{H NMR}$ (500 MHz, CDCl_3) δ 7.34 – 7.27 (m, 4H), 7.25 – 7.17 (m, 4H), 7.11 – 7.07 (m, 2H), 4.93 (d, $J = 1.1$ Hz, 1H), 4.50 (d, $J = 1.4$ Hz, 1H), 3.99 (s, 1H), 3.50 (d, $J = 16.4$ Hz, 1H), 3.39 (d, $J = 16.4$ Hz, 1H), 2.89 (dd, $J = 17.2, 9.3$ Hz, 1H), 2.39 (d, 1H), 2.25 (dd, $J = 17.3, 2.0$ Hz, 1H), 2.17 –

2.03 (m, 3H), 1.80 – 1.70 (m, 1H), 1.56 – 1.51 (m, 1H), 1.42 – 1.35 (m, 2H), 1.28 – 1.12 (m, 7H), 0.84 (t, $J = 7.1$ Hz, 3H).

^{13}C NMR (126 MHz, CDCl_3) δ 153.2, 140.9, 140.1, 139.1, 137.3, 129.7, 129.3, 128.3, 127.7, 126.5, 126.0, 95.5, 82.5, 70.2, 55.6, 40.7, 39.4, 34.2, 31.6, 30.2, 29.5, 29.2, 28.1, 22.6, 14.1.

LRMS (ESI, APCI) m/z : calc'd for $\text{C}_{29}\text{H}_{39}\text{O}$ $[\text{M}+\text{H}]^+$ 401.3, found 401.0



(*exo*)-3a-benzyl-5-hexyl-4-phenyl-1,2,3,3a,6,6a-hexahydropentalen-1-ol (15):

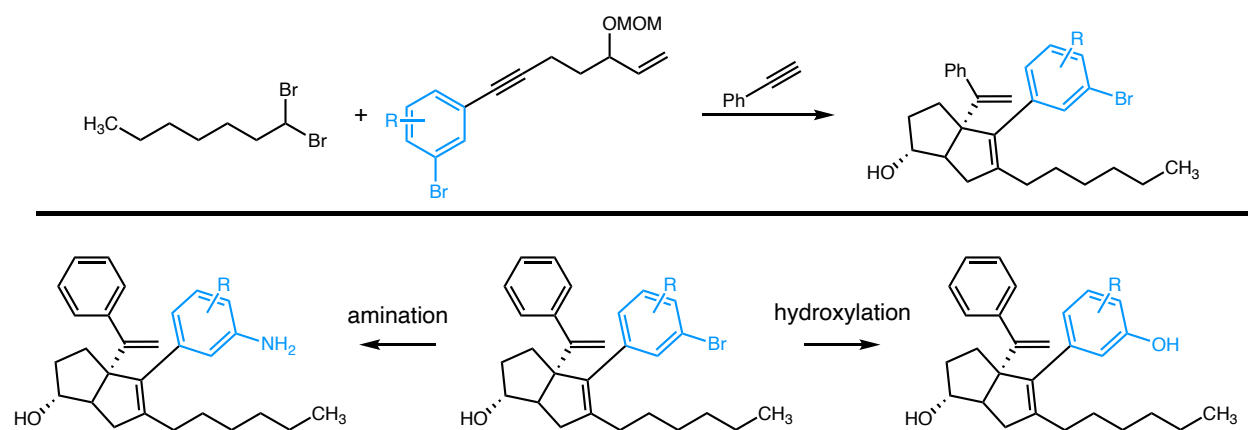
A solution of (12) (9.0 mg, 0.02 mmol, 1.0 equiv) in ethylene glycol was treated with hydrazine hydrate (0.5 mL, 0.16 mmol, 8 equiv) and heated to 100 °C for 1 hour. Potassium hydroxide (19 mg, 0.3 mmol, 15 equiv) was added and the reaction mixture was stirred at 150 °C for 48 h, at which point the reaction was allowed to come to ambient temperature, poured onto water and extracted with EtOAc three times. The combined organic layers were dried with MgSO_4 , filtered, and concentrated. The crude reaction mixture was purified on silica in 10-20% EtOAc/Hex eluent (2.6 mg, 30% yield). Purity was established as the *exo* diastereomer by Method D: $t_{\text{R}} = 1.35$ min, 95.3%.

^1H NMR (600 MHz, CDCl_3) δ 7.37 – 7.33 (m, 3H), 7.30 – 7.27 (m, 1H), 7.24 – 7.22 (m, 1H), 7.21 – 7.17 (m, 3H), 7.16 – 7.11 (m, 2H), 3.83 (s, 1H), 2.93 (d, $J = 13.6$ Hz, 1H), 2.73 (d, $J = 13.6$ Hz, 1H), 2.38 (dd, $J = 15.6, 8.4$ Hz, 1H), 2.34 (d, $J = 10.6$ Hz, 1H), 2.05 – 1.99 (m, 1H), 1.89 – 1.83 (m, 2H), 1.74 – 1.67 (m, 3H), 1.49 – 1.44 (m, 1H), 1.29 – 1.18 (m, 5H), 1.12 (dt, $J = 6.0, 4.2$ Hz, 3H), 0.82 (td, $J = 7.2, 0.6$ Hz, 3H).

^{13}C NMR (101 MHz, CDCl_3) δ 140.9, 139.8, 139.4, 138.0, 130.5, 129.9, 127.9, 126.5, 126.0, 81.8, 64.3, 52.6, 44.0, 38.9, 33.8, 32.1, 31.6, 29.2, 29.0, 27.8, 22.6, 14.1.

LRMS (ESI, APCI) m/z : calc'd for $\text{C}_{26}\text{H}_{35}$ $[\text{M}-\text{H}_2\text{O}]^+$ 358.3, found 358.3

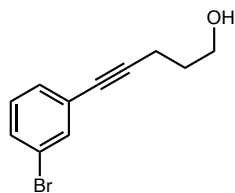
R3: Internal Styrene Modifications 16 – 23



General Sonogashira coupling procedure (S5a – S8a):

A roundbottom flask equipped with magnetic stir bar was charged with bis(triphenylphosphine) palladium dichloride (0.01 equiv) and copper iodide (0.03 equiv). The flask was placed under nitrogen and triethylamine (1M with respect to aryl halide) was added via syringe. The solution was treated with iodobenzene (1.0 equiv), then sparged with nitrogen for 30 minutes. 4-pentyn-1-ol (1.2 equiv) was then added via syringe. The sparging needle was removed from the solution and replaced with a vent needle under positive nitrogen pressure. The solution was vigorously stirred at 60°C for 2 hours, at which point the reaction was complete by TLC. The reaction was cooled and precipitated with ether. The entire reaction was filtered over a plug of celite (eluted with ether).

The filtrate was concentrated in vacuo to afford a rust-colored oil, which was purified on silica (10–30% EtOAc/Hex eluent) to afford the title compounds.

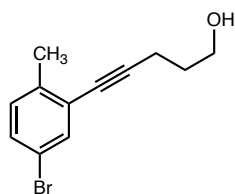


5-(3-bromophenyl)pent-4-yn-1-ol (S5a): According to the general procedure, 1-bromo-3-iodobenzene (3.6 g, 12.5 mmol) was reacted with 4-pentyn-1-ol (1.3 g, 15 mmol) to give the title compound as a yellow oil. (3.1 g, 92% yield).

¹H NMR (500 MHz, CDCl₃) δ 7.54 (t, *J* = 1.8 Hz, 1H), 7.40 (ddd, *J* = 8.1, 2.0, 1.0 Hz, 1H), 7.31 (dt, *J* = 7.7, 1.3 Hz, 1H), 7.15 (t, *J* = 7.9 Hz, 1H), 3.81 (t, *J* = 6.2 Hz, 2H), 2.54 (t, *J* = 7.0 Hz, 2H), 1.86 (tt, *J* = 6.9, 6.1 Hz, 2H), 1.59 (s, 1H).

¹³C NMR (126 MHz, CDCl₃) δ 134.3, 130.8, 130.1, 129.6, 125.7, 122.0, 90.9, 79.7, 61.7, 31.2, 15.9.

LRMS (EI) *m/z*: calc'd for C₁₁H₁₁BrO [M]⁺ 238.0, found 238.0.

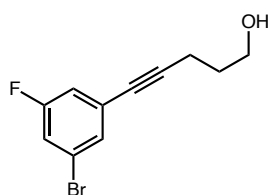


5-(5-bromo-2-methylphenyl)pent-4-yn-1-ol (S6a): According to the general procedure, 4-methyl-2-iodo-1-methylbenzene (2.5 mL, 17 mmol) was reacted with 4-pentyn-1-ol (2.2 mL, 22 mmol) to give the title compound as a yellow oil (3.6 g, 81% yield).

¹H NMR (600 MHz, CDCl₃) δ 7.48 (d, *J* = 2.2 Hz, 1H), 7.28 (dd, *J* = 8.2, 2.2 Hz, 1H), 7.03 (d, *J* = 8.2 Hz, 1H), 3.83 (t, *J* = 6.1 Hz, 2H), 2.58 (t, *J* = 6.9 Hz, 2H), 2.34 (s, 3H), 1.87 (p, *J* = 6.8 Hz, 2H), 1.55 (s, 1H).

¹³C NMR (126 MHz, CDCl₃) δ 138.8, 134.3, 130.8, 130.6, 125.6, 118.6, 94.7, 78.7, 61.7, 31.4, 20.3, 16.1.

LRMS (EI) *m/z*: calc'd for C₁₂H₁₃BrO [M]⁺ 252.0, found 252.0



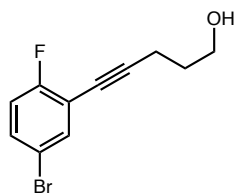
5-(3-bromo-5-fluorophenyl)pent-4-yn-1-ol (S7a): According to the general procedure, 1-bromo-3-fluoro-5-iodobenzene (4.6 g, 15 mmol) was reacted with 4-pentyn-1-ol (1.5 g, 18 mmol) to give the title compound as a yellow oil (3.5 g 90% yield).

¹H NMR (500 MHz, CDCl₃) δ 7.32 (t, *J* = 1.6 Hz, 1H), 7.16 (dt, *J* = 8.2, 2.1 Hz, 1H), 7.02 (ddd, *J* = 9.0, 2.4, 1.3 Hz, 1H), 3.79 (t, *J* = 6.2 Hz, 2H), 2.53 (t, *J* = 7.0 Hz, 2H), 1.85 (p, *J* = 6.6 Hz, 2H), 1.69 (s, 1H).

¹⁹F NMR (282 MHz, CDCl₃) δ -111.19 (t, *J* = 8.7 Hz).

¹³C NMR (126 MHz, CDCl₃) δ 162.1 (d, *J* = 250.6 Hz), 130.4 (d, *J* = 3.3 Hz), 127.0 (d, *J* = 10.3 Hz), 122.2 (d, *J* = 10.7 Hz), 118.7 (d, *J* = 24.6 Hz), 117.3 (d, *J* = 22.6 Hz), 92.2, 78.7 (d, *J* = 3.5 Hz), 61.5, 31.1, 15.9.

LRMS (EI) *m/z*: calc'd for C₁₁H₉BrFO [M]⁺ 256.0, found 256.1



5-(5-bromo-2-fluorophenyl)pent-4-yn-1-ol (S8a): According to the general procedure, 4-bromo-1-fluoro-2-iodobenzene (2.6 mL, 20 mmol) was reacted with 4-pentyn-1-ol (2.2 mL, 22 mmol) to give the title compound as a yellow oil (3.9 g, 76% yield).

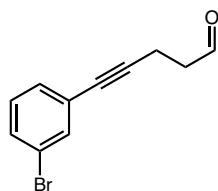
¹H NMR (500 MHz, CDCl₃) δ 7.51 (dd, *J* = 6.3, 2.5 Hz, 1H), 7.35 (ddd, *J* = 8.8, 4.6, 2.6 Hz, 1H), 6.93 (t, *J* = 8.8 Hz, 1H), 3.83 (t, *J* = 6.1 Hz, 2H), 2.59 (t, *J* = 6.9 Hz, 2H), 1.88 (tt, *J* = 6.7, 6.1 Hz, 2H), 1.39 (s, 1H).

¹³C NMR (126 MHz, CDCl₃) δ 161.9 (d, *J* = 251.0 Hz), 135.9 (d, *J* = 1.9 Hz), 132.1 (d, *J* = 7.8 Hz), 117.0 (d, *J* = 22.8 Hz), 116.0 (d, *J* = 3.8 Hz), 114.3 (d, *J* = 17.3 Hz), 96.5 (d, *J* = 3.4 Hz), 73.2, 61.6, 31.1, 16.1.

¹⁹F NMR (282 MHz, CDCl₃) δ -113.28 (ddd, *J* = 9.0, 6.3, 4.6 Hz).

LRMS (EI) *m/z*: calc'd for C₁₁H₁₀BrFO [M]⁺ 256.0, found 256.0

General Swern Oxidation Procedure (S5b – S8b): Under nitrogen, a solution of oxalyl chloride (1.1 equiv) in DCM (0.1 M with respect to alcohol) was cooled to -78 °C. A solution of dimethylsulfoxide (1.3 equiv) in DCM was added dropwise. After effervescence ceased (ca. 30 minutes), the required alcohol (1.0 equiv) was added dropwise in DCM. The reaction mixture was stirred at -78 °C for 1.5 h before the addition of triethylamine (2.5 equiv). The solution was allowed to warm to room temperature before the addition of saturated ammonium chloride (excess). The reaction mixture was then poured onto water and extracted with EtOAc, dried with MgSO₄, concentrated, and purified by silica gel chromatography.



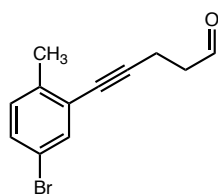
5-(3-bromophenyl)pent-4-ynal (S5b):

According to the general procedure, 5-(3-bromophenyl)pent-4-yn-1-ol (**S5a**) (4.2 g, 18 mmol) was reacted to give the title compound. The crude oil was purified on silica gel with 10-50% EtOAc/Hex eluent (3.4g, 81%).

$^1\text{H NMR}$ (600 MHz, CDCl_3) δ 9.85 (t, $J = 1.1$ Hz, 1H), 7.53 (t, $J = 1.8$ Hz, 1H), 7.41 (ddd, $J = 8.0, 2.1, 1.0$ Hz, 1H), 7.30 (dt, $J = 7.7, 1.4$ Hz, 1H), 7.15 (t, $J = 7.9$ Hz, 1H), 2.80 – 2.71 (m, 4H).

$^{13}\text{C NMR}$ (126 MHz, CDCl_3) δ 200.1, 134.4, 131.1, 130.1, 129.7, 125.3, 122.0, 89.3, 80.0, 42.5, 12.6.

LRMS (ESI) m/z : calc'd for $\text{C}_{11}\text{H}_9\text{BrO}$ $[\text{M}]^+$ 236.0, found 236.0

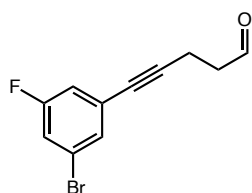


5-(5-bromo-2-methylphenyl)pent-4-ynal (S6b): According to the general procedure, 5-(5-bromo-2-methylphenyl)pent-4-yn-1-ol (**S6a**) (3.6 g, 14 mmol) was reacted to give the title compound. The crude oil was purified on silica gel with 10% EtOAc/Hex (0.6 g, 17%).

^1H NMR (500 MHz, CDCl_3) δ 9.86 (s, 1H), 7.48 (d, $J = 2.2$ Hz, 1H), 7.29 (dd, $J = 8.2, 2.2$ Hz, 1H), 7.04 (d, $J = 8.2$ Hz, 1H), 2.78 (s, 4H), 2.33 (s, 3H).

^{13}C NMR (151 MHz, CDCl_3) δ 200.2, 172.5, 139.0, 134.3, 130.8, 125.1, 118.6, 93.0, 79.1, 42.7, 20.2, 12.8.

LRMS (EI) m/z : calc'd for $\text{C}_{12}\text{H}_{11}\text{BrO}$ $[\text{M}]^+$ 250.0, found 250.0



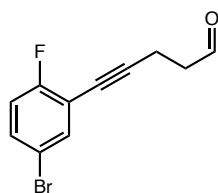
5-(3-bromo-5-fluorophenyl)pent-4-ynal (S7b): According to the general procedure, 5-(3-bromo-5-fluorophenyl)pent-4-yn-1-ol (S7a) (1.4 g, 5.5 mmol) was reacted to give the title compound. The crude oil was purified on silica gel with 10-20% EtOAc/Hex, (700 mg, 50%).

^1H NMR (500 MHz, CDCl_3) δ 9.81 (t, $J = 1.0$ Hz, 1H), 7.30 – 7.27 (m, 1H), 7.15 (ddd, $J = 8.1, 2.4, 1.8$ Hz, 1H), 6.99 (ddd, $J = 9.1, 2.4, 1.3$ Hz, 1H), 2.79 – 2.71 (m, 2H), 2.73 – 2.66 (m, 2H).

^{13}C NMR (126 MHz, CDCl_3) δ 199.8, 162.1 (d, $J = 250.7$ Hz), 130.5 (d, $J = 3.3$ Hz), 126.6 (d, $J = 10.4$ Hz), 122.2 (d, $J = 10.5$ Hz), 118.9 (d, $J = 24.5$ Hz), 117.3 (d, $J = 22.7$ Hz), 90.6, 78.9 (d, $J = 3.5$ Hz), 42.3, 12.5.

^{19}F NMR (282 MHz, CDCl_3) δ -111.00 (t, $J = 8.6$ Hz).

LRMS (EI) m/z : calc'd for $\text{C}_{11}\text{H}_9\text{BrFO}$ $[\text{M}]^+$ 254.0, found 254.0



5-(5-bromo-2-fluorophenyl)pent-4-ynal (S8b): According to the general procedure, 5-(5-bromo-2-fluorophenyl)pent-4-yn-1-ol (**S8a**) (3.9 g, 15 mmol) was reacted to give the title compound. The crude oil was purified on silica gel with 10-20% EtOAc/Hex (2.4 g, 62%).

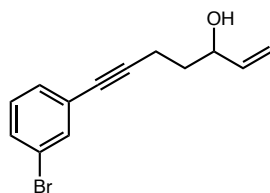
¹H NMR (500 MHz, CDCl₃) δ 9.84 (s, 1H), 7.49 (dd, *J* = 6.3, 2.5 Hz, 1H), 7.35 (ddd, *J* = 8.8, 4.6, 2.6 Hz, 1H), 6.93 (t, *J* = 8.8 Hz, 1H), 2.82 – 2.73 (m, 4H).

¹³C NMR (126 MHz, CDCl₃) δ 199.9, 161.9 (d, *J* = 251.5 Hz), 135.9 (d, *J* = 1.8 Hz), 132.4 (d, *J* = 7.7 Hz), 117.0 (d, *J* = 22.5 Hz), 116.0 (d, *J* = 3.4 Hz), 113.9 (d, *J* = 20.5 Hz), 94.8 (d, *J* = 3.4 Hz), 73.5, 42.3, 12.8.

¹⁹F NMR (282 MHz, CDCl₃) δ -113.04 (ddd, *J* = 8.9, 6.3, 4.5 Hz).

LRMS (EI) *m/z*: calc'd for C₁₁H₈BrFO [M]⁺ 254.0, found 254.0

General Grignard Addition Procedure (S5c – S8c): Under nitrogen, a solution of aldehyde **S2b** – **S5b** (1.0 equiv) in anhydrous THF (0.5 M) was cooled to -78 °C. The solution was treated with vinylmagnesium bromide (1.0M solution in THF, 1.5 equiv). The reaction was stirred and allowed to warm to room temperature over 16 h, then saturated ammonium chloride was added. The reaction mixture was poured onto water and extracted with EtOAc, dried with MgSO₄, and concentrated before purification on silica to give the title compounds.



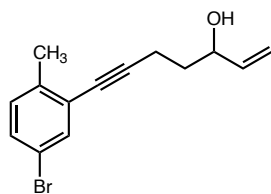
7-(3-bromophenyl)hept-1-en-6-yn-3-ol (S5c): According to the general procedure, 5-(3-bromophenyl)pent-4-ynal (**S5b**) (3.4 g, 14 mmol) was reacted with vinylmagnesium bromide (21

mL of a 1.0M solution in THF, 21 mmol). The crude oil was purified on silica gel with 5-10% EtOAc/Hex eluent, (2.0 g, 53% yield).

¹H NMR (600 MHz, CDCl₃) δ 7.53 (t, *J* = 1.8 Hz, 1H), 7.40 (ddd, *J* = 8.1, 2.1, 1.1 Hz, 1H), 7.30 (dt, *J* = 7.8, 1.3 Hz, 1H), 7.14 (t, *J* = 7.9 Hz, 1H), 5.90 (ddd, *J* = 17.2, 10.4, 6.1 Hz, 1H), 5.29 (dt, *J* = 17.3, 1.4 Hz, 1H), 5.16 (dt, *J* = 10.5, 1.3 Hz, 1H), 4.31 (qt, *J* = 6.0, 1.3 Hz, 1H), 2.72 – 2.33 (m, 2H), 1.96 – 1.69 (m, 2H).

¹³C NMR (126 MHz, CDCl₃) δ 140.4, 134.3, 130.8, 130.1, 129.6, 125.8, 122.0, 115.3, 91.0, 79.7, 71.9, 35.4, 15.6.

LRMS (ESI) *m/z*: calc'd for C₁₃H₁₄BrO [M+H]⁺ 265.0, found 265.0

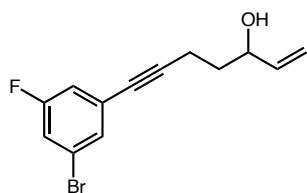


7-(5-bromo-2-methylphenyl)hept-1-en-6-yn-3-ol (S6c): According to the general procedure, 5-(5-bromo-2-methylphenyl)pent-4-ynal (**S6b**) (0.6 g, 2.4 mmol) was reacted with vinyl magnesium bromide (3.6 mL of a 1.0 M solution in THF, 3.6 mmol). The crude oil was purified on silica gel in 20% EtOAc/Hex eluent, (0.2 g, 32% yield).

¹H NMR (600 MHz, CDCl₃) δ 7.49 (d, *J* = 2.2 Hz, 1H), 7.28 (dd, *J* = 8.2, 2.2 Hz, 1H), 7.04 (d, *J* = 8.2 Hz, 1H), 5.95 – 5.87 (m, 1H), 5.30 (dt, *J* = 17.3, 1.4 Hz, 1H), 5.17 (dt, *J* = 10.6, 1.4 Hz, 1H), 4.34 (q, *J* = 6.4 Hz, 1H), 2.57 (qt, *J* = 17.1, 7.1 Hz, 2H), 2.35 (s, 3H), 1.84 (q, *J* = 6.9 Hz, 2H), 1.67 (s, 1H).

¹³C NMR (126 MHz, CDCl₃) δ 140.4, 138.8, 134.3, 130.8, 130.6, 125.6, 118.6, 115.3, 94.8, 78.8, 72.0, 35.6, 20.3, 15.8.

LRMS (ESI) *m/z*: calc'd for C₁₄H₁₆BrO [M+H]⁺ 279.0, found 279.0.



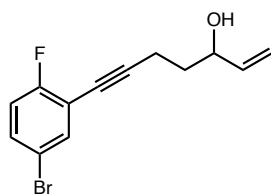
7-(3-bromo-5-fluorophenyl)hept-1-en-6-yn-3-ol (S7c): According to the general procedure, 5-(3-bromo-5-fluorophenyl)pent-4-yn-1-ol (**S7b**) (700 mg, 2.7 mmol) was reacted with vinylmagnesium bromide (5 mL of a 1.0M solution in THF, 5 mmol, 1.9 equiv). The crude oil was purified on silica gel in 20% EtOAc/Hex, (497 mg, 64% yield).

¹H NMR (500 MHz, CDCl₃) δ 7.33 (s, 1H), 7.17 (ddd, *J* = 8.2, 2.4, 1.8 Hz, 1H), 7.02 (ddd, *J* = 9.1, 2.5, 1.3 Hz, 1H), 5.90 (ddd, *J* = 17.1, 10.4, 6.1 Hz, 1H), 5.30 (dt, *J* = 17.2, 1.4 Hz, 1H), 5.18 (dt, *J* = 10.4, 1.3 Hz, 1H), 4.30 (d, *J* = 10.3 Hz, 1H), 2.60 – 2.45 (m, 3H), 1.85 – 1.78 (m, 3H), 1.66 (d, *J* = 4.3 Hz, 1H).

¹³C NMR (126 MHz, CDCl₃) δ 140.3, 130.4 (d, *J* = 3.2 Hz), 122.2 (d, *J* = 10.7 Hz), 118.8 (d, *J* = 24.6 Hz), 117.3 (d, *J* = 22.6 Hz), 115.3, 92.3, 78.7, 71.9, 35.3, 15.6.

¹⁹F NMR (282 MHz, CDCl₃) δ -111.22 (t, *J* = 8.6 Hz).

LRMS (ESI) *m/z*: calc'd for C₁₃H₁₂BrFO [M]⁺ 282.0, found 282.1



7-(5-bromo-2-fluorophenyl)hept-1-en-6-yn-3-ol (S8c): According to the general procedure, 5-(5-bromo-2-fluorophenyl)pent-4-ynal (**S8b**) (2.4 g, 9.3 mmol) was reacted with vinylmagnesium bromide (14 mL of a 1.0M solution in THF, 14 mmol). The crude oil was purified on silica gel in 20% EtOAc/Hex eluent, (1.7 g, 64% yield).

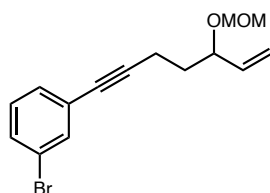
¹H NMR (600 MHz, CDCl₃) δ 7.51 (dd, *J* = 6.4, 2.4 Hz, 1H), 7.36 – 7.33 (m, 1H), 6.93 (t, *J* = 8.9, Hz, 1H), 5.90 (m, 1H), 5.31 (dq, *J* = 17.2, 1.2 Hz, 1H), 5.17 (dq, *J* = 10.4, 1.2 Hz, 1H), 4.34 (q, *J* = 6.5 Hz, 1H), 2.58 (qt, *J* = 17.2, 7.1 Hz, 3H), 1.87 – 1.80 (m, 2H), 1.67 (s, 1H).

¹³C NMR (126 MHz, CDCl₃) δ 161.9 (d, *J* = 250.6 Hz), 140.3, 135.9 (d, *J* = 1.9 Hz), 132.1 (d, *J* = 7.8 Hz), 117.0 (d, *J* = 23.0 Hz), 116.0 (d, *J* = 3.6 Hz), 115.3, 114.4 (d, *J* = 17.3 Hz), 96.6 (d, *J* = 3.4 Hz), 73.2, 71.9, 35.3, 15.8.

¹⁹F NMR (282 MHz, CDCl₃) δ -113.24 (ddd, *J* = 9.0, 6.3, 4.5 Hz).

LRMS (ESI) *m/z*: calc'd for C₁₃H₁₃BrFO [M+H]⁺ 283.0, found 283.0

General procedure for methoxymethyl (MOM) ether alcohol protection (S5d–S8d): The required enyne (**S5c** – **S8c**) (1.0 equiv.) was dissolved in DCM (0.5 M), followed by diisopropylethyl amine (1.25 equiv.) Chloromethyl methyl ether (1.5 equiv.) was added and the reaction mixture was stirred at 30 °C until completion was detected by TLC (typically 1-4 hours). The reaction mixture was cooled to room temperature, poured onto water, and extracted with DCM. The combined organic layers were washed with dilute HCl (1 M) and brine, dried with MgSO₄, filtered, and concentrated before purification on silica to give the title compounds.

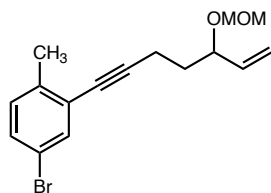


1-bromo-3-(5-(methoxymethoxy)hept-6-en-1-yn-1-yl)benzene (S5d): According to the general procedure, 7-(3-bromophenyl)hept-1-en-6-yn-3-ol (**S5c**) (2.0 g, 7.5 mmol) was reacted with chloromethyl methyl ether. The crude oil was purified in 5% EtOAc/Hex eluent (2.1 g, 92% yield).

¹H NMR (600 MHz, CDCl₃) δ 7.53 (t, *J* = 1.8 Hz, 1H), 7.40 (m, 1H), 7.32 – 7.29 (m, 1H), 7.14 (t, *J* = 7.9 Hz, 1H), 5.70 (ddd, *J* = 17.8, 10.3, 7.6 Hz, 1H), 5.31 – 5.21 (m, 2H), 4.73 (d, *J* = 6.8 Hz, 1H), 4.57 (d, *J* = 6.7 Hz, 1H), 4.19 (td, *J* = 7.8, 5.2 Hz, 1H), 3.40 (s, 3H), 2.63 – 2.42 (m, 2H), 1.93 – 1.86 (m, 1H), 1.84 – 1.76 (m, 1H).

¹³C NMR (126 MHz, CDCl₃) δ 137.6, 134.3, 130.8, 130.1, 129.6, 125.9, 122.0, 117.9, 93.8, 91.0, 79.6, 75.8, 55.5, 34.2, 15.6.

LRMS (ESI) *m/z*: calc'd for C₁₅H₁₆BrO₂ [M-H]⁺ 307.0, found 307.0, calc'd for C₁₄H₁₄BrO [M-OCH₃]⁺ 277.0, found 277.1, calc'd for C₁₃H₁₂BrO [M-C₂H₅O]⁺ 263.0, found 263.0.

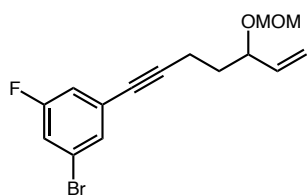


4-bromo-2-(5-(methoxymethoxy)hept-6-en-1-yn-1-yl)-1-methylbenzene (S6d): According to the general procedure, 7-(5-bromo-2-methylphenyl)hept-1-en-6-yn-3-ol (**S6c**) (0.2 g, 0.7 mmol) was reacted with chloromethyl methyl ether. The crude oil was purified in 2-10% EtOAc/Hex eluent (0.18 g, 78% yield).

¹H NMR (600 MHz, CDCl₃) δ 7.48 (d, *J* = 2.2 Hz, 1H), 7.28 (dd, *J* = 8.2, 2.2 Hz, 1H), 7.04 (d, *J* = 8.2 Hz, 1H), 5.71 (m, 1H), 5.31 – 5.20 (m, 2H), 4.74 (d, *J* = 6.7 Hz, 1H), 4.57 (d, *J* = 6.7 Hz, 1H), 4.22 (td, *J* = 7.7, 5.3 Hz, 1H), 3.40 (s, 3H), 2.63 – 2.50 (m, 2H), 2.35 (s, 3H), 1.91 (dtd, *J* = 13.8, 7.6, 6.2 Hz, 1H), 1.81 (dtd, *J* = 13.2, 7.6, 5.4 Hz, 1H).

¹³C NMR (126 MHz, CDCl₃) δ 138.8, 137.6, 134.3, 130.8, 130.6, 125.7, 118.6, 117.9, 94.9, 93.8, 78.6, 75.8, 55.5, 34.5, 20.2, 15.8.

LRMS (ESI) *m/z*: calc'd for C₁₆H₁₉BrO₂ [M-H]⁺ 321.0, found 321.0, calc'd for C₁₅H₁₆BrO [M-OCH₃]⁺ 291.0, found 291.0, calc'd for C₁₄H₁₄BrO [M-C₂H₅O]⁺ 277.0, found 277.0.

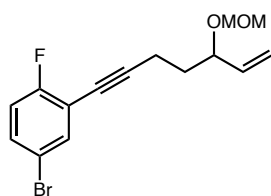


1-bromo-3-fluoro-5-(5-(methoxymethoxy)hept-6-en-1-yn-1-yl)benzene (S7d): According to the general procedure, 7-(3-bromo-5-fluorophenyl)hept-1-en-6-yn-3-ol (**S7c**) (497.1 mg, 1.8 mmol) was reacted with chloromethyl methyl ether. The crude oil was purified in 2-10% EtOAc/Hex (270 mg, 47% yield).

¹H NMR (500 MHz, CDCl₃) δ 7.32 (s, 1H), 7.16 (ddd, *J* = 8.2, 2.4, 1.7 Hz, 1H), 7.02 (ddd, *J* = 9.1, 2.4, 1.3 Hz, 1H), 5.70 (ddd, *J* = 17.2, 10.3, 7.5 Hz, 1H), 5.28 (ddd, *J* = 17.3, 1.6, 1.0 Hz, 1H), 5.24 (ddd, *J* = 10.3, 1.6, 0.8 Hz, 1H), 4.73 (d, *J* = 6.7 Hz, 1H), 4.56 (d, *J* = 6.7 Hz, 1H), 3.40 (s, 3H), 2.58 – 2.42 (m, 2H), 1.88 (dtd, *J* = 13.9, 7.8, 6.1 Hz, 1H), 1.80 (dtd, *J* = 13.6, 7.7, 5.3 Hz, 1H).

¹³C NMR (126 MHz, CDCl₃) δ 162.1 (d, *J* = 250.6 Hz), 137.5, 130.4 (d, *J* = 3.3 Hz), 127.1 (d, *J* = 10.2 Hz), 122.2 (d, *J* = 10.6 Hz), 118.7 (d, *J* = 24.6 Hz), 117.8, 117.3 (d, *J* = 22.6 Hz), 93.8, 92.3, 78.6 (d, *J* = 3.4 Hz), 75.7, 55.5, 34.1, 15.5.

¹⁹F NMR (282 MHz, CDCl₃) δ -111.22 (t, *J* = 8.6 Hz).



4-bromo-1-fluoro-2-(5-(methoxymethoxy)hept-6-en-1-yn-1-yl)benzene (S8d): According to the general procedure, 7-(5-bromo-2-fluorophenyl)hept-1-en-6-yn-3-ol (**S8c**) (1.7 g, 6 mmol) was

reacted with chloromethyl methyl ether. The crude oil was purified in 2-10% EtOAc/Hex eluent (1.6 g, 80% yield).

¹H NMR (600 MHz, CDCl₃) δ 7.50 (dd, *J* = 6.3, 2.5 Hz, 1H), 7.34 (m, 1H), 6.93 (t, *J* = 8.8 Hz, 1H), 5.70 (m, 1H), 5.31 – 5.21 (m, 2H), 4.73 (d, *J* = 6.7 Hz, 1H), 4.57 (d, *J* = 6.7 Hz, 1H), 4.20 (td, *J* = 7.8, 5.3 Hz, 1H), 3.40 (s, 3H), 2.63 – 2.50 (m, 2H), 1.94 – 1.87 (m, 1H), 1.85 – 1.78 (m, 1H).

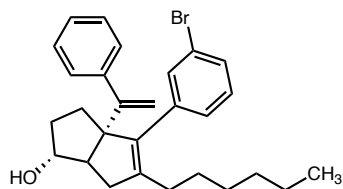
¹³C NMR (126 MHz, CDCl₃) δ 161.9 (d, *J* = 251.0 Hz), 137.6, 135.9 (d, *J* = 1.8 Hz), 132.1 (d, *J* = 7.8 Hz), 117.9, 117.0 (d, *J* = 22.6 Hz), 116.0 (d, *J* = 3.6 Hz), 114.5 (d, *J* = 17.4 Hz), 96.6 (d, *J* = 3.4 Hz), 93.9, 75.7, 73.1, 55.5, 34.1, 15.8.

¹⁹F NMR (282 MHz, CDCl₃) δ -113.23 (ddd, *J* = 9.3, 6.4, 4.6 Hz).

LRMS (ESI) *m/z*: calc'd for C₁₅H₁₅BrFO₂ [M-H]⁺ 325.0, found 325.0, calc'd for C₁₄H₁₃BrFO [M-OCH₃]⁺ 295.0, found 295.1, calc'd for C₁₃H₁₁BrFO [M-C₂H₅O]⁺ 281.0, found 281.0.

Hexahydropentalene formation was accomplished through slight modification of Whitby's procedure.¹ Prior to cyclization, all non-volatile reagents were dried by azeotropic removal of water using benzene. A dry round bottom flask containing bis(cyclopentadienyl)zirconium(IV) dichloride (1.2 equiv) under nitrogen, was dissolved in anhydrous, degassed tetrahydrofuran (THF, 50 mL/mmol enyne) and cooled to -78 °C. The resulting solution was treated with n-BuLi (2.4 equiv.) and the light yellow solution was stirred for 30 minutes. A solution of **S5d** – **S8d** (1.0 equiv) in anhydrous, degassed THF (5 mL/mmol) was added. The resulting salmon-colored mixture was stirred at -78 °C for 30 minutes, the cooling bath removed, and the reaction mixture was allowed to warm to ambient temperature with stirring (2.5 hours total). The reaction mixture was then cooled to -78 °C and the required 1,1-dibromoheptane (1.1 equiv) was added as a solution

in anhydrous THF (5 mL/mmol) followed by freshly prepared lithium diisopropylamide (LDA, 1.0 M, 1.1 equiv.). After 15 minutes, a freshly prepared solution of lithium phenylacetylide (3.6 equiv.) in anhydrous THF was added dropwise and the resulting rust-colored solution was stirred at -78 °C for 1.5 hours. The reaction was quenched with methanol and saturated aqueous sodium bicarbonate and allowed to warm to room temperature, affording a light yellow slurry. The slurry was poured onto water and extracted with ethyl acetate four times. The combined organic layers were washed with brine, dried with MgSO₄, and concentrated *in vacuo*. The resulting yellow oil was passed through a short plug of silica (20% EtOAc/Hex eluent) and concentrated. The crude product was dissolved in acetonitrile and treated with concentrated aqueous hydrochloric acid (ca 5 equiv) and the resulting solution stirred at room temperature until completion of the reaction was detected (typically fewer than 10 minutes). The reaction mixture was concentrated and purified by silica gel chromatography (5-20% EtOAc/Hex eluent) to afford the title compounds **S5e** – **S8e** as a 7:1 mixture of diastereomers, favoring the desired *exo*-isomer.



(*exo*)-4-(3-bromophenyl)-5-hexyl-3a-(1-phenylvinyl)-1,2,3,3a,6,6a-hexahydropentalen-1-ol

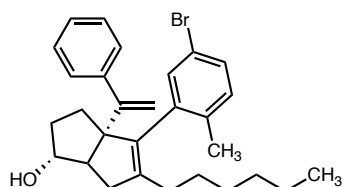
(S5e): According to the general procedure, 1-bromo-3-(5-(methoxymethoxy)hept-6-en-1-yn-1-yl)benzene (**S5d**) (234 mg, 0.76 mmol) was reacted with 1,1-dibromoheptane (215 mg, 0.84 mmol) and phenylacetylide to afford the title compound (21.2 mg, 6% yield) over two steps.

¹H NMR (500 MHz, CDCl₃) δ 7.43 – 7.37 (m, 1H), 7.36 – 7.29 (m, 3H), 7.29 – 7.26 (m, 2H), 7.24 – 7.08 (m, 3H), 5.10 (d, *J* = 1.3 Hz, 1H), 5.00 (d, *J* = 1.2 Hz, 1H), 3.95 (s, 1H), 2.38 (dd, *J* = 17.0,

9.4 Hz, 1H), 2.30 (d, $J = 9.5$ Hz, 1H), 2.14 – 1.97 (m, 5H), 1.74 – 1.65 (m, 3H), 1.39 – 1.15 (m, 7H), 0.87 (t, $J = 7.2$ Hz, 3H).

^{13}C NMR (126 MHz, CDCl_3) δ 154.3, 144.0, 142.4, 139.6, 137.7, 132.5, 129.7, 129.2, 128.4, 127.8, 127.6, 126.8, 121.8, 115.3, 81.9, 69.3, 55.8, 40.3, 34.0, 32.1, 31.6, 29.7, 29.3, 27.7, 22.6, 14.1.

LRMS (ESI, APCI) m/z : calc'd for $\text{C}_{28}\text{H}_{36}\text{BrO}$ $[\text{M}+\text{H}]^+$ 465.2, found 465.7



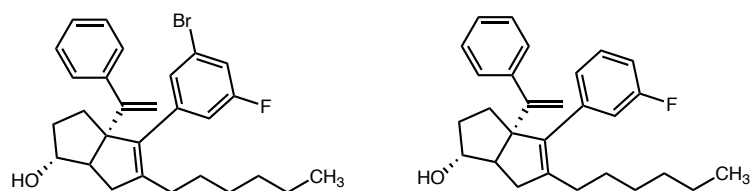
(exo)-4-(5-bromo-2-methylphenyl)-5-hexyl-3a-(1-phenylvinyl)-1,2,3,3a,6,6a-

hexahydropentalen-1-ol (S6e): According to the general procedure, 4-bromo-2-(5-(methoxymethoxy)hept-6-en-1-yn-1-yl)-1-methylbenzene (**S6d**) (317.5 mg, 1 mmol) was reacted with 1,1-dibromoheptane (282.8 mg, 1.1 mmol) and phenylacetylide to afford the title compound (20.4 mg, 4% yield over two steps).

^1H NMR (500 MHz, CDCl_3) δ 7.39 – 7.34 (m, 2H), 7.32 – 7.27 (m, 3H), 7.26 – 7.22 (m, 2H), 7.11 (d, $J = 8.2$ Hz, 1H), 5.22 (d, $J = 1.1$ Hz, 1H), 4.85 (d, $J = 1.1$ Hz, 1H), 3.98 (dd, $J = 3.8, 1.8$ Hz, 1H), 2.63 (dd, $J = 17.4, 10.0$ Hz, 1H), 2.34 (ddt, $J = 10.0, 3.0, 1.7$ Hz, 1H), 2.15 (s, 3H), 2.09 – 1.99 (m, 3H), 1.87 (t, $J = 7.9$ Hz, 2H), 1.84 – 1.69 (m, 2H), 1.37 (td, $J = 7.9, 5.1$ Hz, 2H), 1.30 – 1.11 (m, 6H), 0.86 (t, $J = 7.2$ Hz, 3H).

^{13}C NMR (126 MHz, CDCl_3) δ 154.5, 141.4, 138.1, 136.4, 136.2, 133.2, 131.3, 129.7, 128.1, 127.8, 127.2, 126.8, 116.4, 81.3, 55.5, 40.3, 33.8, 33.0, 31.6, 30.1, 29.5, 27.1, 22.6, 19.5, 14.1.

LRMS (ESI, APCI) m/z : calc'd for $\text{C}_{29}\text{H}_{38}\text{BrO}$ $[\text{M}+\text{H}]^+$ 479.2, found 479.7



(*exo*)-4-(3-bromo-5-fluorophenyl)-5-hexyl-3a-(1-phenylvinyl)-1,2,3,3a,6,6a-

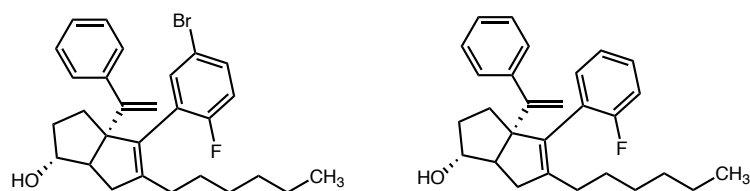
hexahydropentalen-1-ol (S7e): According to the general procedure, 1-bromo-3-fluoro-5-(5-(methoxymethoxy)hept-6-en-1-yn-1-yl)benzene (S7d) (345.6 mg, 1 mmol) was reacted with 1,1-dibromoheptane (300.5 mg, 1.2 mmol) and phenylacetylide to afford both the desired compound and lithium-halogen exchange byproduct in an appreciable amount (72.4 mg combined, over two steps) This mixture was carried on without further purification. Spectral data are representative of both hydrodehalogenation (33%) and desired (67%) products.

¹H NMR (500 MHz, CDCl₃) δ 7.36 – 7.23 (m, 4H), 7.20 – 7.12 (m, 1H), 7.01 – 6.87 (m, 3H), 5.12 (d, *J* = 1.3 Hz, 0.5H), 5.10 (d, *J* = 1.4 Hz, 0.3H), 5.04 (d, *J* = 1.3 Hz, 0.6H), 5.02 (d, *J* = 1.4 Hz, 0.3H), 3.94 (s, 1H), 2.43 – 2.34 (m, 1H), 2.31 (dt, *J* = 9.4, 1.9 Hz, 1H), 2.15 – 2.07 (m, 1H), 2.06 – 1.99 (m, 2H), 1.72 – 1.60 (m, 3H), 1.36 (d, *J* = 7.8 Hz, 4H), 1.31 – 1.17 (m, 5H), 0.91 – 0.82 (m, 3H).

¹³C NMR (126 MHz, CDCl₃) δ 154.4, 154.2, 143.7, 143.4, 129.1, 129.0, 128.5, 127.9, 127.8, 127.7, 127.6, 126.9, 126.8, 125.5, 117.4, 117.2, 116.5, 116.3, 115.52, 115.47, 115.4, 115.2, 113.6, 113.4, 81.9, 81.8, 69.3, 55.8, 40.3, 34.0, 32.1, 31.62, 31.59, 29.68, 29.65, 29.4, 29.3, 27.74, 27.67, 22.6, 14.1.

¹⁹F NMR (282 MHz, CDCl₃) δ -111.56, -113.95.

LRMS (ESI, APCI) *m/z*: calc'd for C₂₈H₃₅BrFO [M+H]⁺ 483.2, found 483.1, calc'd for C₂₈H₃₆FO [M+H]⁺ 405.3, found 405.2



(exo)-4-(5-amino-2-fluorophenyl)-5-hexyl-3a-(1-phenylvinyl)-1,2,3,3a,6,6a-

hexahydropentalen-1-ol (S8e): According to the general procedure, 4-bromo-1-fluoro-2-(5-(methoxymethoxy)hept-6-en-1-yn-1-yl)benzene (**S8d**) (417.6 mg, 1.8 mmol) was reacted with 1,1-dibromoheptane (371.6 mg, 1.4 mmol) and phenylacetylide, affording both the desired compound and lithium-halogen exchange byproduct in an appreciable amount (63.3 mg, combined, over two steps). This mixture was carried on without further purification. Spectral data are representative of both hydrodehalogenation (67%) and desired (33%) products.

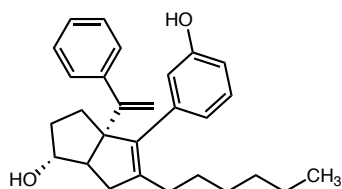
¹H NMR (500 MHz, CDCl₃) δ 7.41 – 7.24 (m, 6H), 7.21 (td, *J* = 7.6, 1.7 Hz, 0.67H), 7.10 – 7.02 (m, 1H), 6.96 (t, *J* = 8.8 Hz, 0.33H), 5.12 (d, *J* = 1.3 Hz, 0.33H), 5.07 (d, *J* = 1.3 Hz, 0.67H), 4.90 (d, *J* = 1.3 Hz, 0.33H), 4.87 (d, *J* = 1.3 Hz, 0.67H), 4.11 – 3.90 (m, 1H), 2.54 (dd, *J* = 16.1, 8.7 Hz, 1H), 2.32 (d, *J* = 9.7 Hz, 1H), 2.12 – 2.02 (m, 2H), 1.94 (t, *J* = 7.7 Hz, 2H), 1.88 – 1.63 (m, 2H), 1.36 (q, *J* = 7.0, 6.4 Hz, 2H), 1.29 – 1.14 (m, 7H), 0.86 (q, *J* = 7.0 Hz, 3H).

¹³C NMR (126 MHz, CDCl₃) δ 161.6, 160.8, 159.7, 158.8, 154.6, 154.4, 144.57, 144.55, 144.3, 143.3, 134.2, 134.1, 132.6, 131.8, 131.7, 131.5, 131.4, 128.5, 128.5, 127.9, 127.9, 127.5, 127.4, 126.8, 126.7, 124.5, 124.4, 123.08, 123.05, 117.1, 116.9, 115.74, 115.71, 115.5, 115.4, 115.3, 115.1, 82.0, 81.8, 69.69, 69.66, 55.4, 55.3, 40.6, 33.58, 33.56, 33.2, 31.61, 31.59, 30.00, 29.95, 29.3, 27.2, 27.2, 22.6, 14.1.

¹⁹F NMR (282 MHz, CDCl₃) δ -113.58, -115.34.

LRMS (ESI, APCI) *m/z*: calc'd for C₂₈H₃₅BrFO [M+H]⁺ 483.2, found 483.1, calc'd for C₂₈H₃₆FO [M+H]⁺ 405.3, found 405.2.

General Procedure for Hydroxyl Coupling (16, 18, 20, 22): Potassium hydroxide (3.0 equiv.), tris(dibenzylideneacetone)dipalladium(0) (0.01 equiv.), and ^tBuXPhos (0.04 equiv.) were placed in a reaction tube, which was evacuated and backfilled with nitrogen three times. The solids were then suspended in degassed 1,4-dioxane under nitrogen. The required brominated [3.3.0] bicycle (**S5e** – **S8e**) was added in 1,4-dioxane. Water (~10 equiv.) was added. The reaction mixture was heated to 80 °C and stirred for 16 hours. After stirring, the mixture was poured over water and extracted with EtOAc three times. The combined organic layers were washed with water and brine, dried with MgSO₄, concentrated, and purified on silica in 20% EtOAc/Hex eluent.



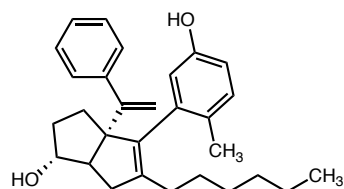
(*exo*)-5-hexyl-4-(3-hydroxyphenyl)-3a-(1-phenylvinyl)-1,2,3,3a,6,6a-hexahydropentalen-1-ol

(16): (*exo*)-6-(3-bromophenyl)-5-hexyl-3-(methoxymethoxy)-6a-(1-phenylvinyl)-1,2,3,3a,4,6a-hexahydropentalen-1-ol (**S5e**) (9.1 mg, 0.02 mmol) was reacted and purified according to the general procedure to give the title compound (3.4 mg, 43% yield). Purity was established as the *exo* diastereomer by Method A: *t*R = 1.02 min, 89.2%.

¹H NMR (500 MHz, CDCl₃) δ 7.30 (d, *J* = 41.7 Hz, 5H), 7.17 (t, *J* = 7.8 Hz, 1H), 6.75 (t, *J* = 9.3 Hz, 2H), 6.69 (s, 1H), 5.07 (s, 1H), 5.02 (s, 1H), 4.88 (s, 1H), 3.94 (s, 1H), 2.35 (dd, *J* = 17.3, 8.0 Hz, 1H), 2.27 (d, *J* = 9.4 Hz, 1H), 2.05 (dt, *J* = 21.8, 6.9 Hz, 4H), 1.77 – 1.48 (m, 5H), 1.35 – 1.16 (m, 8H), 0.86 (t, *J* = 7.0 Hz, 3H).

¹³C NMR (126 MHz, CDCl₃) δ 154.9, 154.6, 144.1, 141.4, 139.1, 138.6, 128.8, 127.72, 126.68, 122.4, 116.4, 115.1, 113.6, 82.1, 69.3, 55.8, 40.2, 34.0, 32.1, 31.7, 29.7, 29.4, 27.9, 27.8, 22.6, 14.1.

LRMS (ESI, APCI) *m/z*: calc'd for C₂₈H₃₇O₂ [M+H]⁺ 403.3, found 403.8

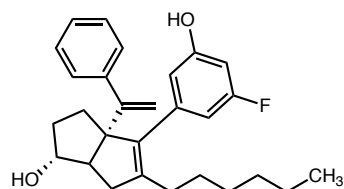


(*exo*)-5-hexyl-4-(5-hydroxy-2-methylphenyl)-3a-(1-phenylvinyl)-1,2,3,3a,6,6a-

hexahydropentalen-1-ol (18): (*exo*)-4-(5-bromo-2-methylphenyl)-5-hexyl-3a-(1-phenylvinyl)-1,2,3,3a,6,6a-hexahydropentalen-1-ol (**S6e**) (10.2 mg, 0.02 mmol) was reacted and purified according to the general procedure to give the title compound (2.4 mg, 27% yield). Purity was established as the *exo* diastereomer by Method B: *t_R* = 1.25 min, 97.6%.

¹H NMR (500 MHz, CDCl₃) δ 7.46 – 7.39 (m, 2H), 7.31 – 7.27 (m, 3H), 7.09 (d, *J* = 8.3 Hz, 1H), 6.67 (dd, *J* = 8.3, 2.8 Hz, 1H), 6.56 (d, *J* = 2.8 Hz, 1H), 5.20 (d, *J* = 1.1 Hz, 1H), 4.88 (d, *J* = 1.2 Hz, 1H), 4.52 (s, 1H), 3.99 (s, 1H), 3.49 (s, 3H), 2.64 (dd, *J* = 17.3, 10.2 Hz, 1H), 2.33 (d, *J* = 9.5 Hz, 1H), 2.10 – 1.99 (m, 3H), 1.94 – 1.77 (m, 3H), 1.71 (ddd, *J* = 19.1, 13.3, 6.6 Hz, 2H), 1.42 – 1.12 (m, 7H), 0.85 (t, *J* = 7.1 Hz, 3H).

LRMS (ESI, APCI) *m/z*: calc'd for C₂₉H₃₇O₂ [M+H]⁺ 417.3, found 416.9.



(*exo*)-4-(3-fluoro-5-hydroxyphenyl)-5-hexyl-3a-(1-phenylvinyl)-1,2,3,3a,6,6a-

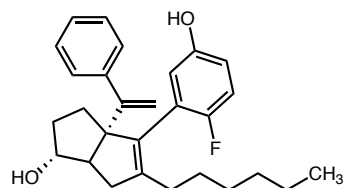
hexahydropentalen-1-ol (20): (*exo*)-4-(3-bromo-5-fluorophenyl)-5-hexyl-3a-(1-phenylvinyl)-1,2,3,3a,6,6a-hexahydropentalen-1-ol (**S7e**) (27.9 mg, 0.06 mmol) was reacted and purified according to the general procedure to give the title compound (5.9 mg, 24%). Purity was established as the *exo* diastereomer by Method B: $t_R = 1.14$ min, 97.3%.

$^1\text{H NMR}$ (500 MHz, CDCl_3) δ 7.35 – 7.28 (m, 2H), 7.26 (d, $J = 6.2$ Hz, 3H), 6.55 – 6.45 (m, 3H), 5.09 (s, 1H), 5.04 (s, 1H), 4.94 (s, 1H), 3.93 (s, 1H), 2.35 (dd, $J = 17.0, 9.3$ Hz, 1H), 2.28 (d, $J = 9.5$ Hz, 1H), 2.15 – 1.99 (m, 4H), 1.73 – 1.64 (m, 3H), 1.38 – 1.18 (m, 6H), 0.90 – 0.83 (m, 3H).

$^{13}\text{C NMR}$ (126 MHz, CDCl_3) δ 162.0, 156.2, 154.4, 143.9, 142.3, 137.8, 127.8, 127.7, 126.8, 115.3, 112.4, 109.2, 109.0, 101.7, 101.5, 82.0, 69.3, 55.8, 40.2, 34.0, 32.0, 31.6, 29.7, 29.4, 27.7, 22.6, 14.1.

$^{19}\text{F NMR}$ (282 MHz, cdcl_3) δ -112.75.

LRMS (ESI, APCI) m/z : calc'd for $\text{C}_{28}\text{H}_{36}\text{FO}_2$ $[\text{M}+\text{H}]^+$ 421.3, found 421.9

**(*exo*)-4-(2-fluoro-5-hydroxyphenyl)-5-hexyl-3a-(1-phenylvinyl)-1,2,3,3a,6,6a-**

hexahydropentalen-1-ol (22): (*exo*)-4-(5-amino-2-fluorophenyl)-5-hexyl-3a-(1-phenylvinyl)-1,2,3,3a,6,6a-hexahydropentalen-1-ol (**S8e**) (29.8 mg, 0.06 mmol) was reacted and purified

according to the general procedure to give the title compound (3.4 mg, 13% yield). Purity was established as the *exo* diastereomer by Method B: $t_R = 1.03$ min, 96.9%.

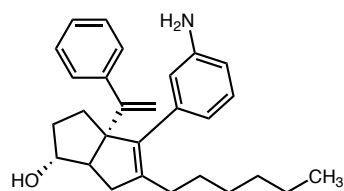
^1H NMR (500 MHz, CDCl_3) δ 7.39 – 7.35 (m, 2H), 7.31 – 7.27 (m, 3H), 6.93 (t, $J = 8.8$ Hz, 1H), 6.70 (dt, $J = 8.6, 3.5$ Hz, 1H), 6.65 (dd, $J = 5.6, 3.2$ Hz, 1H), 5.10 (d, $J = 1.2$ Hz, 1H), 4.93 (d, $J = 1.3$ Hz, 1H), 4.61 (s, 1H), 3.97 (s, 1H), 2.52 (dd, $J = 17.3, 9.7$ Hz, 1H), 2.30 (d, $J = 9.7$ Hz, 1H), 2.12 – 2.03 (m, 2H), 1.95 (t, $J = 7.8$ Hz, 2H), 1.87 – 1.78 (m, 1H), 1.73 (dd, $J = 12.3, 6.3$ Hz, 1H), 1.68 (dd, $J = 13.1, 5.9$ Hz, 1H), 1.45 – 1.27 (m, 2H), 1.29 – 1.16 (m, 6H), 0.86 (t, $J = 7.1$ Hz, 3H).
 ^{13}C NMR (126 MHz, CDCl_3) δ 156.1, 154.5, 154.2, 150.6, 144.4, 143.6, 127.9, 127.4, 126.8, 117.7, 117.6, 115.9, 115.7, 115.5, 114.9, 114.9, 81.9, 69.6, 55.4, 40.6, 33.6, 33.1, 31.6, 30.0, 29.4, 27.2, 22.6, 14.1.

^{19}F NMR (282 MHz, CDCl_3) δ -124.47.

LRMS (ESI, APCI) m/z : calc'd for $\text{C}_{28}\text{H}_{36}\text{FO}_2$ $[\text{M}+\text{H}]^+$ 421.2, found 421.9

General Procedure for Amination (17, 19, 21, 23)

A solution of $^t\text{BuBrettPhos}$ (0.04 equiv), sodium *tert* butoxide (3.0 equiv) in 1,4-dioxane was treated with **S5e** – **S8e** as a solution in 1,4-dioxane and ammonia (0.5M in dioxane, ca. 10 equiv) (tube A). In a separate reaction tube (B), a solution of $^t\text{BuBrettPhos}$ precatalyst (0.04 equiv.) in 1,4-dioxane was prepared. The solution in tube B was transferred to tube A. The reaction mixture in tube A was heated in a closed reaction tube at 80 °C for 16 hours behind a blast shield (for larger reaction quantities, a pressure tube behind a blast shield is recommended). The mixture was cooled to room temperature, diluted with water and extracted with EtOAc three times. The combined organics were washed with water and brine, dried over MgSO_4 , and concentrated. The crude oil was purified by silica gel chromatography in EtOAc/Hex eluent.

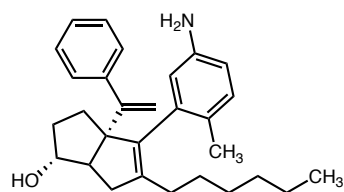


(*exo*)-4-(3-aminophenyl)-5-hexyl-3a-(1-phenylvinyl)-1,2,3,3a,6,6a-hexahydropentalen-1-ol

(17): (*exo*)-6-(3-bromophenyl)-5-hexyl-3-(methoxymethoxy)-6a-(1-phenylvinyl)-1,2,3,3a,4,6a-hexahydropentalen-1-ol (**S5e**) (8.3 mg, 0.02 mmol) was reacted according to the general procedure. The crude oil was purified by silica gel chromatography in 20% EtOAc/Hex eluent (2.6 mg, 36% yield). Purity was established as the *exo* diastereomer by Method B: $t_R = 0.89$ min, 90.1%. $^1\text{H NMR}$ (500 MHz, CDCl_3) δ 7.49 – 7.20 (m, 5H), 7.09 (dd, $J = 9.6, 5.6$ Hz, 1H), 6.61 (d, $J = 7.4$ Hz, 2H), 6.55 (s, 1H), 5.06 (d, $J = 3.9$ Hz, 1H), 5.02 (d, $J = 4.2$ Hz, 1H), 3.93 (s, 1H), 3.52 (s, 2H), 2.32 (dt, $J = 13.6, 6.7$ Hz, 1H), 2.25 (d, $J = 8.8$ Hz, 1H), 2.04 (ddd, $J = 21.8, 11.9, 4.7$ Hz, 5H), 1.77 – 1.62 (m, 3H), 1.38 – 1.06 (m, 8H), 0.86 (t, $J = 7.1$ Hz, 3H).

$^{13}\text{C NMR}$ (126 MHz, CDCl_3) δ 154.7, 145.6, 144.2, 141.0, 139.0, 138.5, 128.5, 127.8, 127.7, 126.6, 120.5, 116.4, 114.9, 113.6, 110.0, 82.1, 55.9, 40.2, 34.1, 32.0, 31.7, 29.8, 29.4, 27.8, 22.6, 14.1.

LRMS (ESI, APCI) m/z : calc'd for $\text{C}_{28}\text{H}_{38}\text{NO}$ $[\text{M}+\text{H}]^+$ 402.3, found 401.9



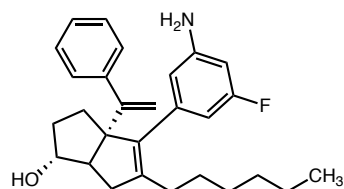
(*exo*)-4-(5-amino-2-methylphenyl)-5-hexyl-3a-(1-phenylvinyl)-1,2,3,3a,6,6a-

hexahydropentalen-1-ol (19): (*exo*)-4-(5-bromo-2-methylphenyl)-5-hexyl-3a-(1-phenylvinyl)-1,2,3,3a,6,6a-hexahydropentalen-1-ol (**S6e**) (10.2 mg, 0.02 mmol) was reacted according to the general procedure. The crude oil was purified by silica gel chromatography in 20-30% EtOAc/Hex

eluent (1.2 mg, 14% yield). Purity was established as the *exo* diastereomer by Method B: $t_R = 0.53$ min, 97.5%.

$^1\text{H NMR}$ (500 MHz, CDCl_3) δ 7.44 – 7.38 (m, 2H), 7.33 – 7.27 (m, 2H), 7.02 (d, $J = 8.0$ Hz, 1H), 6.85 (dd, $J = 8.9, 5.0$ Hz, 1H), 6.54 (dd, $J = 8.0, 2.5$ Hz, 1H), 6.47 (d, $J = 2.5$ Hz, 1H), 5.18 (d, $J = 1.1$ Hz, 1H), 4.89 (d, $J = 1.2$ Hz, 1H), 3.98 (s, 1H), 3.79 (s, 2H), 3.53 (s, 3H), 2.61 (dd, $J = 17.2, 10.0$ Hz, 1H), 2.30 (d, $J = 9.7$ Hz, 1H), 2.06 – 1.99 (m, 2H), 1.97 – 1.79 (m, 2H), 1.77 – 1.68 (m, 2H), 1.38 – 1.07 (m, 11H), 0.86 (t, $J = 7.1$ Hz, 3H).

LRMS (ESI, APCI) m/z : calc'd for $\text{C}_{29}\text{H}_{38}\text{NO}$ $[\text{M}+\text{H}]$ 416.3, found 415.9.



(*exo*)-4-(3-amino-5-fluorophenyl)-5-hexyl-3a-(1-phenylvinyl)-1,2,3,3a,6,6a-

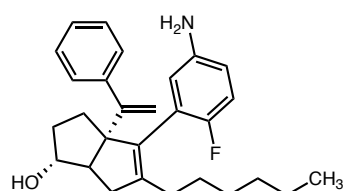
hexahydropentalen-1-ol (21): (*exo*)-4-(3-bromo-5-fluorophenyl)-5-hexyl-3a-(1-phenylvinyl)-1,2,3,3a,6,6a-hexahydropentalen-1-ol (**S7e**) (44.5 mg, 0.09 mmol) was reacted according to the general procedure. The crude oil was purified by silica gel chromatography in 20-30% EtOAc/Hex eluent (3.2 mg, 8% yield). Purity was established as the *exo* diastereomer by method B: $t_R = 1.16$ min, 95.9%.

$^1\text{H NMR}$ (500 MHz, CDCl_3) δ 7.36 – 7.30 (m, 2H), 7.31 – 7.20 (m, 3H), 6.41 – 6.21 (m, 3H), 5.08 (d, $J = 1.6$ Hz, 1H), 5.05 (d, $J = 1.6$ Hz, 1H), 3.92 (s, 1H), 3.79 (d, $J = 1.7$ Hz, 1H), 3.70 (s, 2H), 3.53 (d, $J = 1.6$ Hz, 1H), 2.32 (dd, $J = 16.7, 9.3$ Hz, 1H), 2.25 (d, $J = 9.4$ Hz, 1H), 2.13 – 1.97 (m, 4H), 1.79 – 1.63 (m, 3H), 1.42 – 1.12 (m, 6H), 0.87 (t, $J = 7.1, 6.5$ Hz, 3H).

^{13}C NMR (126 MHz, CDCl_3) δ 164.2, 162.3, 154.5, 147.2, 147.1, 144.0, 141.8, 140.2, 140.1, 138.2, 127.7, 126.7, 119.7, 115.1, 112.1, 106.9, 106.7, 100.7, 100.5, 82.0, 69.2, 55.9, 40.2, 34.1, 32.0, 31.7, 31.1, 29.7, 29.4, 28.2, 27.7, 25.4, 23.9, 23.5, 22.6, 14.1.

^{19}F NMR (282 MHz, CDCl_3) δ -114.23.

LRMS (ESI, APCI) m/z : calc'd for $\text{C}_{28}\text{H}_{37}\text{FNO}$ $[\text{M}+\text{H}]^+$ 420.3, found 420.8



(*exo*)-4-(5-amino-2-fluorophenyl)-5-hexyl-3a-(1-phenylvinyl)-1,2,3,3a,6,6a-

hexahydropentalen-1-ol (23): (*exo*)-4-(5-amino-2-fluorophenyl)-5-hexyl-3a-(1-phenylvinyl)-1,2,3,3a,6,6a-hexahydropentalen-1-ol (**S8e**) (33.5 mg, 0.07 mmol) was reacted according to the general procedure. The crude oil was purified by silica gel chromatography in 30-50% EtOAc/Hex eluent (5.2 mg, 18 yield%). Purity was established as the *exo* diastereomer by Method B: t_{R} = 0.81 min, 98.5%.

^1H NMR (500 MHz, CDCl_3) δ 7.38 (dd, J = 6.7, 2.9 Hz, 2H), 7.32 – 7.25 (m, 2H), 6.99 – 6.79 (m, 2H), 6.56 (dt, J = 8.6, 3.5 Hz, 1H), 6.50 (dd, J = 6.0, 2.9 Hz, 1H), 5.09 (d, J = 1.3 Hz, 1H), 4.93 (d, J = 1.3 Hz, 1H), 3.96 (d, J = 3.6 Hz, 1H), 3.79 (s, 1H), 3.53 (s, 1H), 3.46 (s, 2H), 2.56 – 2.44 (m, 1H), 2.28 (d, J = 9.7 Hz, 1H), 2.10 – 2.02 (m, 2H), 1.96 (t, J = 7.8 Hz, 2H), 1.88 – 1.78 (m, 1H), 1.75 (dd, J = 12.0, 6.4 Hz, 1H), 1.67 (dd, J = 12.9, 5.8 Hz, 1H), 1.35 (q, J = 6.9 Hz, 1H), 1.32 – 1.15 (m, 6H), 0.86 (t, J = 7.0 Hz, 3H).

¹³C NMR (126 MHz, CDCl₃) δ 154.7, 144.6, 135.5, 129.6, 127.9, 127.6, 127.5, 126.7, 120.1, 119.7, 117.7, 115.6, 115.3, 114.9, 82.0, 69.6, 55.4, 40.5, 33.6, 33.0, 31.7, 31.1, 30.0, 29.4, 28.2, 27.3, 26.8, 25.4, 23.9, 23.5, 22.6, 14.1.

¹⁹F NMR (282 MHz, CDCl₃) δ -126.95

LRMS (ESI, APCI) *m/z*: calc'd for C₂₈H₃₇FNO [M+H]⁺ 420.3, found 419.9

Biology: Materials and Reagents

pCI empty vector was purchased from Promega. The SHP-luc and Renilla reporters, as well as pCI LRH-1, have been previously described.¹⁸ The vector for Histagged tobacco etch virus (TEV) was a gift from John Tesmer (University of Texas at Austin). The pMSC7 (LIC-HIS) vector was provided by John Sondek (University of North Carolina at Chapel Hill). The Tif2 NR Box 3 peptide was purchased from RS Synthesis. DNA oligonucleotide primers were synthesized by Integrated DNA Technologies.

Protein Purification

Purification of human LRH-1 LBD (residues 300–537) in a pMCSG7 expression vector was performed as described. Briefly, protein was expressed in BL21 PLYS E. coli, using 1 mM IPTG for 4 h (30 °C) to induce expression. The protein was purified by nickel affinity chromatography. For DSF assays, the protein eluted from the nickel column was exchanged with DLPC (5- fold molar excess overnight at 4 °C), followed by repurification by size exclusion to remove displaced lipids. The assay buffer was 20 mM Tris-HCl, pH 7.5, 150 mM sodium chloride, and 5% glycerol. Cleaved LRH-1 was then incubated with ligands overnight at 4 °C prior to repurification by size exclusion, using the same assay buffer as used for DSF. The protein used for

crystallography was prepared as for coregulator recruitment, except that it was sized into a buffer of 100 mM ammonium acetate (pH 7.5), 150 mM sodium chloride, 1 mM DTT, 1 mM EDTA, and 2 mM CHAPS.

Differential Scanning Fluorimetry

DSF assays were conducted on a StepOne Plus thermocycler as previously described.^{13,15} Briefly, aliquots of purified LRH-1 LBD protein (0.2 mg/mL) were incubated with saturating concentrations of the ligand overnight at 4 °C. Protein–ligand complexes were heated in the presence of the SYPRO orange dye at a rate of 0.5°/min. Complexes were excited at 488 nm, and fluorescence emissions at each degree Celsius were measured using the ROX filter (~600 nm). T_m values were calculated using the Boltzmann equation in GraphPad Prism, v7.

Crystallography

Compounds **5N**, **6N**, or **2N** were incubated with purified LRH-1 LBD (His tag removed) at 5-fold molar excess overnight at 4 °C. The complexes were re-purified by size exclusion chromatography into the crystallization buffer (see above). Protein was concentrated to 5–6 mg/mL and combined with a peptide from human Tif2 NR Box 3 (H₃N-KENALLRYLLDKDDT-CO₂) at fourfold molar excess. Crystals were generated by hanging drop vapor diffusion at 18 °C, using a crystallant of 0.05 M sodium acetate (pH 4.6), 5–11% PEG 4000, and 0–10% glycerol. Crystals of **2N** with LRH-1 were generated by microseeding, using RJW100-LRH-1 crystals as the seed stocks (crystals used for seeding were grown as described).¹⁷

Structure Determination

Crystals were flash-frozen in liquid nitrogen, using a cryoprotectant of the crystallant plus 30% glycerol. Diffraction data were collected remotely from Argonne National Laboratory, Southeast Regional Collaborative Access Team, Beamline 22ID. Data were processed and scaled using HKL2000.²² Structures were phased by molecular replacement using Phenix,²³ with PDB 5L11 used as the search model. The structure was refined using phenix.refine²³ and Coot,²⁴ with some additional refinement done using the PDB Redo web server.⁵⁸

Tissue Culture

HeLa cells were purchased from Atlantic-Type Culture Collection and cultured in phenol red-free MEM α media supplemented with 10% charcoal–dextran-stripped fetal bovine serum. Cells were maintained under standard culture conditions.

Reporter Gene Assays

HeLa cells were reverse-transfected with three vectors: (1) full-length, human LRH-1 in a pCI vector, (2) a firefly reporter (pGL3 Basic) with a portion of the SHP promoter cloned upstream of the firefly luciferase gene, and (3) a constitutively active vector expressing Renilla luciferase under control of the CMV promoter. To study SF-1 activity, cells were transfected with the same constructs, except that full-length SF-1 (in a pcDNA3.1 vector) was overexpressed instead of LRH-1, with empty pcDNA3.1 used as the negative control. Transfections utilized the Fugene HD transfection reagent at a ratio of 5 μ L per 2 μ g DNA. To perform reverse transfections, cells were

⁵⁸ Joosten, R. P.; Long, F.; Murshudov, G. N.; Perrakis, A. The Pdb_Redo Server for Macromolecular Structure Model Optimization. *IUCrJ* **2014**, *1*, 213–220.

trypsinized, combined with the transfection mixture, and plated at densities of 7500 cells per well in white-walled 96-well plates. The following day, cells were treated with each compound (or DMSO control) for 24 h. In most cases, six points in the concentration range of 0.03–30 μ M were used (exceptions noted in figures), with a final DMSO concentration of 0.3% in all wells. Luciferase expression was measured using the Dual-Glo Kit (Promega). The firefly luciferase signal was normalized to the Renilla luciferase signal in each well. EC₅₀ values were calculated using three parameter curve-fitting (GraphPad Prism, v.7). Assays were conducted in triplicate with at least two independent biological replicates. Significance of differences in the luminescence signal for LRH-1 versus SF-1 promoted by particular agonists was determined using two-way ANOVA followed by Sidak's multiple comparisons test.

Calculation of RE

This value was calculated from curve-fitting to data from luciferase reporter assays. To compare the maximum activities of the new compounds to RJW100, we used the formula $(\text{Max}_{\text{cpd}} - \text{Min}_{\text{cpd}})/(\text{Max}_{\text{RJW100}} - \text{Min}_{\text{RJW100}})$, where “Max” and “Min” denote the dose response curve maximum and minimum, respectively. A RE of 0 indicates a completely inactive compound, a value of 1 indicates equal activity to RJW100, and values above 1 indicate greater activity.

Mutagenesis

Mutations were introduced to LRH-1 in the pCI vector using the Quikchange Lightning site-directed mutagenesis kit (Ambion). Constructs were sequenced prior to use in reporter gene assays as described above.

Model Construction for MDS

Four LRH-1 LBD complexes were prepared for MDS. (1) LRH-1-Tif2-RJW100 (PDB 5L11), (2) LRH-1-Tif2-5N. 3LRH-1-Tif2-2N, LRH-1-Tif2-6N. For consistency, all structures contained LRH-1 residues 300–540. Missing residues (i.e. that could not be modeled in the structures) were added to the models used in the simulations.

Table S4.1 List of Primers for qPCR

gene	forward (5'→3')	reverse (5'→3')
m/hLRH-1 ⁴²	GTGTCTCAAT TTAAAATGGT GAATTACTCC TATGATGAAG ATCTGGAAGAGCT	AAT AAGTTTGGGC CAATGTACAA GAGAGACAGG GC
Cyp11a1	GCTGGAAGGTGTAGCTCAGG	CACTGGTGTGGAACATCTGG
Cyp11b1	primers purchased from QuantiTect, Qiagen (NM_001033229, catalog # QT01198575)	
IL-10	GCCTTATCGGAAATGATCCAGT	GCTCCACTGCCTTGCTCTTATT
IL-1 β	primers purchased from QuantiTect, Qiagen (NM_008361, catalog # QT01048355)	
TNF α	CCAGAAAAGACACCATGAGCAC	GGGCCATAGAAGTATGATGAGAGG
Rplp0(36B4)	GAAACTGCTGCCTCACATCCG	GCTGGCACAGTGACCTCACAC

⁴²This set of primers are designed to amplify both mouse and human (m/h) LRH-1 cDNA.

Molecular Dynamics Simulations

The complexes were solvated in an octahedral box of TIP3P water with a 10-Å buffer around the protein complex. Na⁺ and Cl⁻ ions were added to neutralize the protein and achieve physiological buffer conditions. All systems were set up using the xleap tool in AmberTools17 with the ff14SB forcefield.⁵⁹ Parameters for the agonist ligands 6N, 2N, and 5N were obtained using Antechamber also in AmberTools17.³² All minimizations and simulations were performed with Amber16.^{59a} Systems were minimized with 5000 steps of steepest descent followed by 5000

⁵⁹ (a) Case, D.; Cerutti, D.; Cheatham, T., III; Darden, T.; Duke, R.; Giese, T.; Gohlke, H.; Goetz, A.; Greene, D.; Homeyer, N.; Izadi, S.; Kovalenko, A.; Lee, T.; LeGrand, S.; Li, P.; Lin, C.; Liu, J.; Luchko, T.; Luo, R.; Mermelstein, D.; Merz, K. M.; Monard, G.; Nguyen, H.; Omelyan, I.; Onufriev, A.; Pan, F.; Qi, R.; Roe, D. R.; Roitberg, A.; Sagui, C.; Simmerling, C.; Botello-Smith, W.; Swails, J.; Walker, R.; Wang, J.; Wolf, R.; Wu, X.; Xiao, L.; York, D.; Kollman, P. Amber 2017; University of California: San Francisco, 2017 (b) Maier, J. A.; Martinez, C.; Kasavajhala, K.; Wickstrom, L.; Hauser, K. E.; Simmerling, C. Ff14sb: Improving the Accuracy of Protein Side Chain and Backbone Parameters from Ff99sb. *J. Chem. Theory Comput.* 2015, 11, 3696–3713.

steps of conjugate gradient minimization with 500 kcal/mol·Å² restraints on all solute atoms. Restraints were removed excluding the atoms in both the ligand and the Tif2 peptide, and previous minimization was repeated. This minimization was repeated with restraints lowered to 100 kcal/mol·Å². Finally, all restraints were removed for a last minimization step. The systems were heated from 0 to 300 K using a 100 ps run with constant volume periodic boundaries and 5 kcal/mol·Å² restraints on all protein and ligand atoms. MD equilibration was performed for 12 ns with 10 kcal/mol·Å² restraints on the Tif2 peptide and ligand atoms using the NPT ensemble. Restraints were reduced to 1 kcal/mol·Å² for an additional 10 ns of MD equilibration. Then, restraints were removed and 1000 ns production simulations were performed for each system in the NPT ensemble. A 2 fs time step was used with all bonds between heavy atoms and hydrogens fixed with the SHAKE algorithm.³⁴ A cutoff distance of 10 Å was used to evaluate long-range electrostatics with particle mesh Ewald and for van der Waals forces. Fifty thousand evenly spaced frames were taken from each simulation for analysis, using the CPPTRAJ module³⁵ of AmberTools. The NetworkView plugin⁶⁰ in VMD54 and the Carma program⁶¹ were used to produce dynamic networks for each system. In brief, networks are constructed by defining all protein C- α atoms as nodes, using Cartesian covariance to measure communication within the network. Pairs of nodes that reside within a 4.5 Å cutoff for 75% of the simulation are connected via an edge. Edge weights are inversely proportional to the covariance between the nodes. Networks were constructed using 500 ns of the MDS trajectories, to enable direct comparison with our previous LRH-1-RJW MDS.⁶² Suboptimal paths between the AF-B and Tif2 peptide were

⁶⁰ Sethi, A.; Eargle, J.; Black, A. A.; Luthey-Schulten, Z. Dynamical Networks in Trna:Protein Complexes. *Proc. Natl. Acad. Sci. U.S.A.* 2009, 106, 6620–6625

⁶¹ Glykos, N. M. Software News and Updates Carma: A Molecular Dynamics Analysis Program. *J. Comput. Chem.* 2006, 27, 1765–1768.

⁶² Mays, S. G.; Okafor, C. D.; Tuntland, M. L.; Whitby, R. J.; Dharmarajan, V.; Stec, J.; Griffin, P. R.; Ortlund, E. A. Structure and Dynamics of the Liver Receptor Homolog 1-PGC1 α Complex. *Mol. Pharmacol.* 2017, 92 (1), 1–11

identified using the Floyd–Warshall algorithm.⁶³ Suboptimal path analyses were performed using Carma and the subopt program in NetworkView. Cross-correlation matrices for C- α atoms in each system were computed with Carma.

Coregulator Recruitment Assays

Synthetic agonists were titrated in the presence of purified LRH-1 LBD protein (2 μ M) and a fluorescein (FAM)-labeled peptide corresponding to the Tif2 NR box 3 (FAM-H₃N-PVSPKKKENALLRYLLDKDDT-CO₂⁻) (50 nM). Protein and probe concentrations were determined from preliminary experiments titrating LRH-1 protein with no ligand added in the presence of FAM-Tif2 (2 μ M was slightly above the Tif2 K_d in these experiments). Tif2 binding was detected by fluorescence polarization, using a BioTek Neo plate reader. Assays were conducted three times in triplicate, using two separate protein preparations. Significance of differences in Tif2 association at each dose was determined using two-way ANOVA followed by Tukey's multiple comparisons test.

HDX Mass Spectrometry

Following cleavage of the His tag from purified LRH-1 LBD with TEV protease as described above, the protein was further purified by size exclusion chromatography into a buffer of phosphate buffered saline (PBS) (pH 7.5) plus 5% glycerol. Protein purity exceeded 98% by Coomassie staining. Protein–ligand complexes were prepared by adding each ligand at 5-fold molar excess to 2 mg/mL protein and incubating overnight at 4 °C. Complexes were centrifuged

⁶³ Floyd, R. W. Algorithm 97: Shortest Path. *Commun. ACM* **1962**, 5, 345.

to remove any aggregates prior to analysis by HDX-MS. HDX-MS was conducted using Waters' UPLC HDX system coupled with a Q-ToF Premier mass spectrometer (Waters Corp, Milford, MA). Protein–ligand complexes were diluted 1:7 (v/v) into labeling buffer (protein buffer containing D₂O instead of water) via an autosampler. Labeling took place at 20 °C for time periods of 100, 1000, and 10,000 s prior to quenching with an equal volume of precooled quenching buffer (100 mM phosphate, 0.5 M (tris(2- carboxyethyl)phosphine, 0.8% FA, and 2% acetonitrile, pH 2.5, 1 °C). After quenching, samples were applied to a Waters enzymate pepsin column (2.1 × 30 mm). Peptides from the pepsin column were separated in-line on a Waters Acuity UPLC BEH C18 column (1.7 μM, 1.0 × 100 mm) at a flow of 40 μL/min for 12 min (8–40% linear gradient, mobile phase: 0.1% FA in acetonitrile) at 1 °C. The mass spectrometer was operated with the electrospray ionization source in the positive ion mode, and the data were acquired in elevated-energy mass spectrometry mode. For internal calibration, a reference lockmass of Glu-Fibrinopeptide (Sigma-Aldrich, St Louis, MO) was acquired along with each sample data collection. Peptides were identified by comparison to the human LRH-1 protein sequence using the ProteinLynx Global SERVER (version 3.02). HDX data were processed in DynamX (version 3.0). Mass assignment for each peptide at 0 s of exchange was checked manually, and any assignment with mass deviation >0.2 Da was removed. HDX protection was quantified by comparison of hydrogen exchange profiles at different time points. Peptide coverage was 99.2% for this experiment (Fig. S4.2).

Humanized LRH-1 Mouse Intestinal Enteroid Culture

The study protocol was approved by the Animal Care and Use Committee of the Baylor College of Medicine and was in accordance with the Guide for the Care and Use of Laboratory Animals [DHHS publication no. (NIH) 85-23, revised 1985, Office of Science and Health Reports,

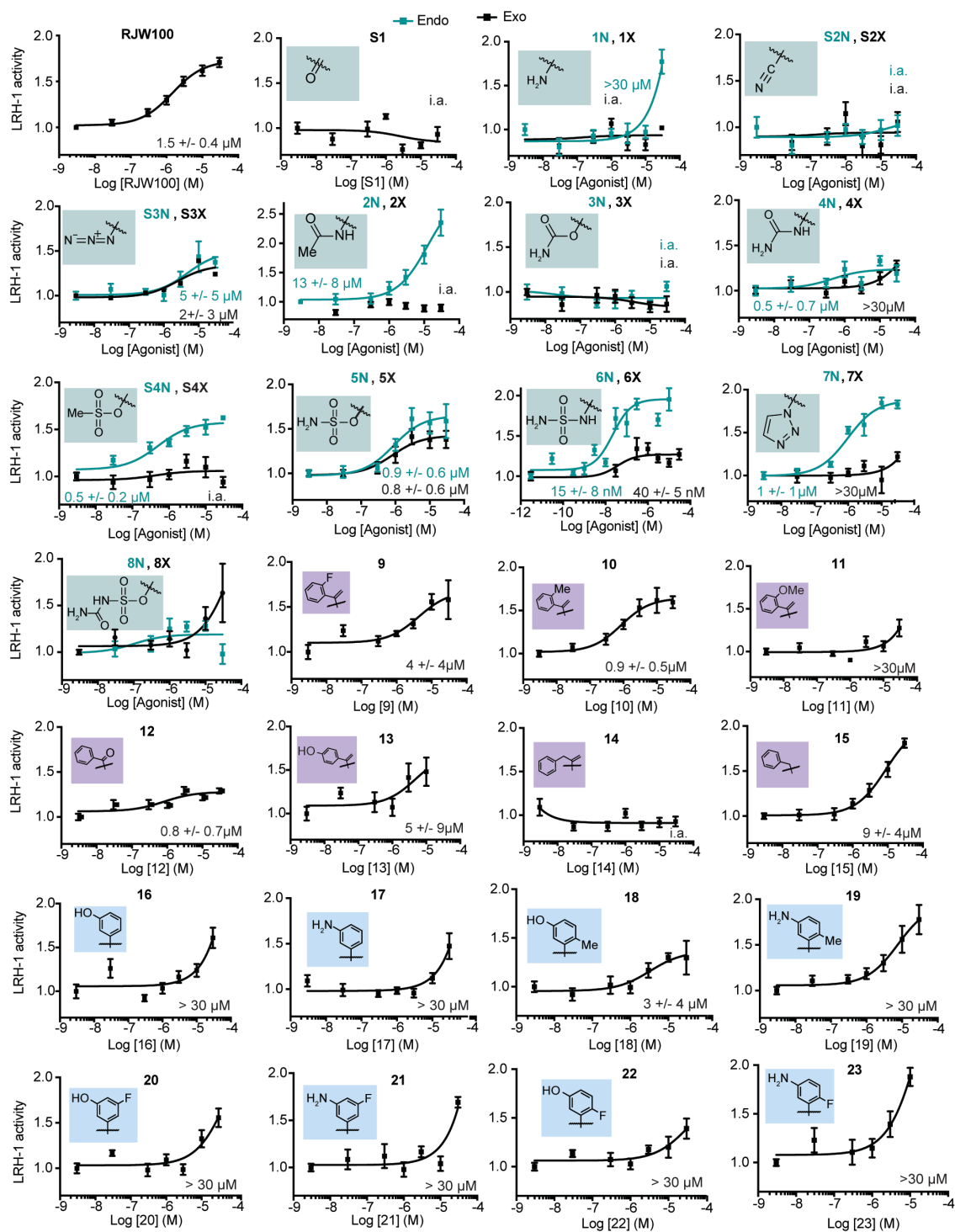
DRR/NIH, Bethesda, MD 20205]. The humanized LRH-1 allele (LRH-1h) is obtained on a mouse line with a human LRH-1 transgene using the Rosa26-loxP-STOPloxP strategy to allow villin-cre-mediated expression of human LRH-1 (LRH-1^{ΔΔ}) in enterocytes with knockout of the endogenous mLRH-1 (Lrh-1^{f/f}). Intestinal crypt culture (enteroids) were derived from Lrh1^{f/f}, Lrh-1 K O (Lrh1^{f/f}; Villin-Cre⁺), and LRH-1 h (Lrh1^{f/f}; hLRH1^{ΔΔ}; Villin-Cre⁺) male mice (6–8 weeks old). Briefly, the small intestine was isolated and flushed with ice-cold PBS, opened longitudinally, then cut into 1–2 mm pieces. Intestinal fragments were incubated in an EDTA (4 mM) containing solution at 4 °C for 60 min on a tube rocker. The intestinal fragment suspension was fractionated by vertical shaking manually and crypt-containing fractions passed through a 70 μm cell strainer for plating in Matrigel. Crypt-Matrigel suspension was allowed to polymerize at 37 °C for 15 min. Intestinal organoids were grown in base culture media (Advanced DMEM/F12 media, HEPES, GlutaMax, penicillin, and streptomycin) supplemented with growth factors (EGF, Noggin, Rspodin, R&D Systems), B27 (Life Technologies), N2 (Life Table 1 gene forward (5'→3') reverse (5'→3'))

m/hLRH-1a GTGTCTCAAT TAAAAATGGT GAATTACTCC TATGATGAAG
ATCTGGAAGAGCT AAT AAGTTTGGGC CAATGTACAA GAGAGACAGG GC Cyp11a1
GCTGGAAGGTGTAGCTCAGG CACTGGTGTGGAACATCTGG Cyp11b1 primers
purchased from QuantiTect, Qiagen (NM_001033229, catalog # QT01198575) IL-10
GCCTTATCGGAAATGATCCAGT GCTCCACTGCCTTGCTCTTATT IL-1β primers
purchased from QuantiTect, Qiagen (NM_008361, catalog # QT01048355) TNFα
CCAGAAAAGACACCATGAGCAC GGGCCATAGAAGTATGATGAGAGG Rplp0(36B4)
GAAACTGCTGCCTCACATCCG GCTGGCACAGTGACCTCACAC a This set of primers are
designed to amplify both mouse and human (m/h) LRH-1 cDNA and N-acetyl cysteine (NAC,
Sigma). Intestinal enteroids were passaged every 3 days. Established LRH-1h enteroids were

treated with mouse TNF- α overnight to provoke inflammatory changes, then treated with vehicle (DMSO) or compound 6N (1 μ M) overnight. Following the treatment, enteroid tissues were harvested for real-time PCR.

RNA Isolation and PCR

Intestinal enteroids were washed in ice cold PBS and suspended in Trizol solution (Sigma). RNA was isolated with RNeasy spin columns (Qiagen). DNase-treated total RNA was used to generate cDNA using Superscript II (Quanta). Sybr green-based qPCR (Kapa Biosystems) was performed on a Roche LightCycler 480 II with primers as shown below. The $\Delta\Delta$ Ct method was used for calculating gene expression fold changes using Rplp0 (ribosomal protein, large, P0, known as 36B4) as the reference. Primer sequences are shown in Table S4.1.

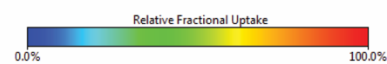


Supporting Figure S4.1. Dose response curves from luciferase reporter assays in HeLa cells. Each point represents the mean \pm SEM for three experiments conducted in triplicate.

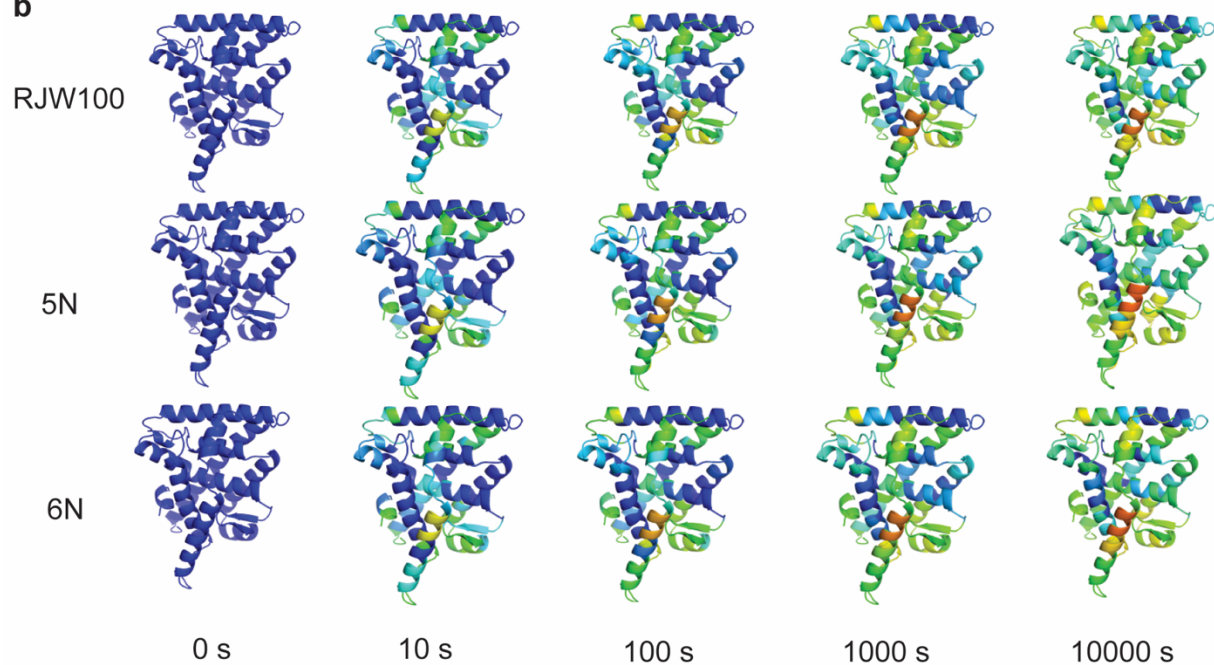
a



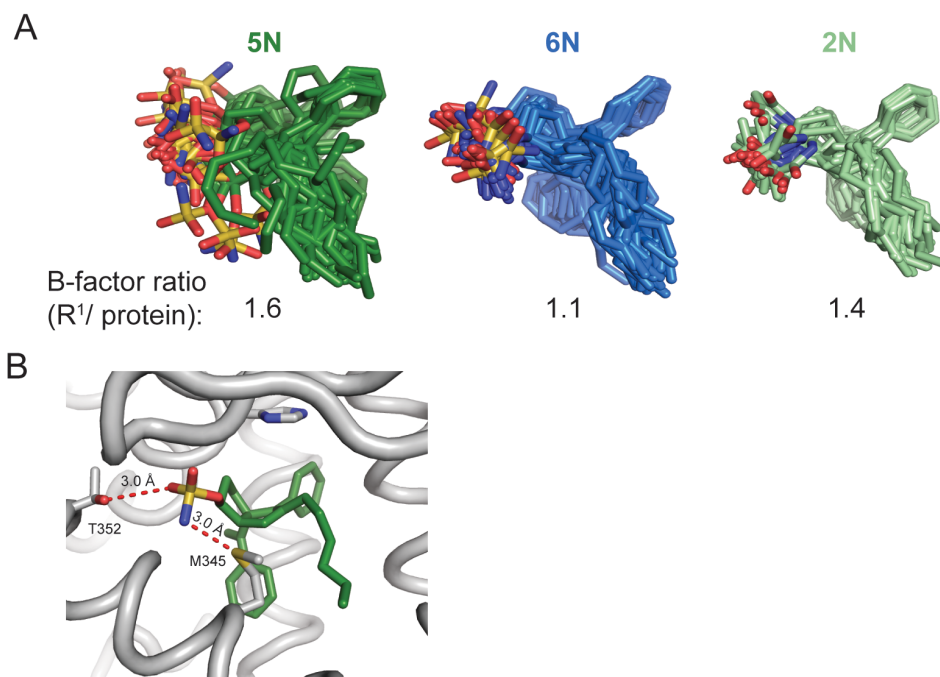
Total: 133 Peptides, 99.2% Coverage, 6.68 Redundancy



b



Supporting Figure S4.2. HDX data for RJW100, 5N, and 6N. A. Map of peptide coverage. B. Fractional uptake of deuterium over time.



Supporting Figure S4.3. Ensemble refinement and B factor analysis. A. Superposition of each ligand following Ensemble Refinement in Phenix. The program generates an ensemble of models to fit the crystallographic data. Numbers below the panel indicate the average B-factors of the atoms in each ligand's R1 group normalized to the average B-factor of protein atoms in each structure. B. Close view of the **5N** ligand in one of the models generated from ensemble refinement, which provides an example of a predicted contact with residue M345.

Supporting Table S4.1: X-ray data collection and refinement statistics.

Data collection	LRH-1 - 5N -Tif2	LRH-1 - 6N - Tif2	LRH-1 - 2N -Tif2
Space group	P4 ₃ 2 ₁ 2	P4 ₃ 2 ₁ 2	P4 ₃ 2 ₁ 2
Cell dimensions			
<i>a, b, c</i> (Å)	46.5, 46.5, 221.0	46.7, 46.7, 218.0	46.7, 46.7, 222.7
α, β, γ (°)	90, 90, 90	90, 90, 90	90, 90, 90
Resolution (Å)	50 – 2.00 (2.07-2.00)	50 – 2.23 (2.31-2.23)	50 – 2.20 (2.28-2.20)
<i>R</i> _{pim}	0.06 (0.52)	0.07 (0.46)	0.04 (0.31)
<i>I</i> / σI	21.3 (1.72)	8.9 (3.2)	18.5 (1.6)
CC _{1/2} in highest shell	0.596	0.976	0.697
Completeness (%)	99.9 (100.0)	97.3 (86.5)	96.6 (87.9)

Redundancy	11.2 (6.8)	16.6 (12.5)	21.1 (13.0)
------------	------------	-------------	-------------

Refinement

Resolution (Å)	2.00	2.23	2.20
No. reflections	17346	12206	13217
$R_{\text{work}} / R_{\text{free}}$ (%)	20.6/ 24.5	23.2/ 26.9	20.0/ 23.9
No. atoms			
Protein	4038	4098	4077
Water	71	24	28
Ligand	68	69	69
B-factors			
Protein	44.8	60.5	59.3
Ligand	53.6	66.1	66.6
Water	44.0	52.7	50.7
R.m.s. deviations			
Bond lengths (Å)	0.002	0.002	0.002
Bond angles (°)	0.504	0.474	0.422
Ramachandran favored (%)	97.6	98.0	97.1
Ramachandran outliers (%)	0.4	0.0	0.0
PDB accession code	6OQX	6OQY	6OR1

Values in parenthesis indicate highest resolution shell.

Chapter 5: Optimization of Lead Agonists

5.1 Strategy

We have described the development of both an efficacious activator of LRH-1 (**10CA**)³⁶ and a highly potent activator of LRH-1 (**6N**).⁵⁴ Though **6N** has undergone significant SAR to realize the most potent and efficacious pharmacophore in the DPP, we questioned whether the carboxylate could also be replaced by another polar group and aimed to find a carboxylate replacement that would improve potency or efficacy. Also important was to combine **10CA** and **6N** into one scaffold to explore whether we could retain the desirable traits of each.

5.2 Carboxylate Replacement

To improve upon the activity of the CA compounds, we aimed to investigate carboxylate bioisosteres.⁴² We targeted polar compounds that may be deprotonated at physiological pH, or that contained bulky polar groups that could make contacts similar to the CAs (Fig. 5.1). Specifically, we chose to synthesize an amide **1** (which may be able to form hydrogen bonds but does not contain a charged portion), a piperazine **2** (which contains a positively charged group at physiological pH), a serine **3** (which is significantly more polar than a carboxylate but contains a similar pharmacophore), a hydroxamic acid **4** (whose nitrogen can be deprotonated easily), and a tetrazole **5**, which is a classical carboxylate isostere and is significantly more polar than a carboxylate.

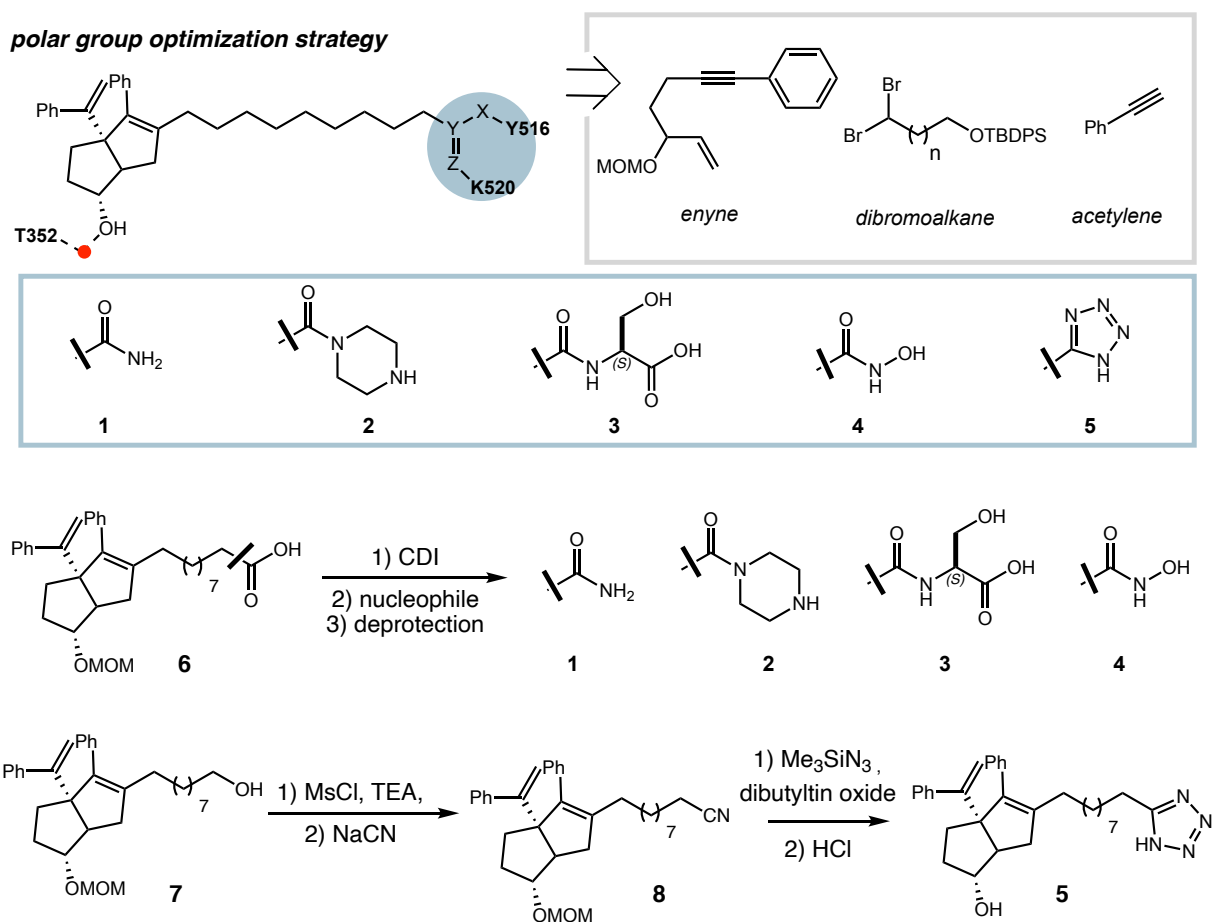


Figure 5.1: Polar groups to be investigated as replacements for the carboxylate and synthetic routes to each compound.

The synthesis for these compounds was relatively straightforward: deprotected **10CA** (intermediate **7**) could be used as to construct compounds **1**, **2**, **3**, and **4**. Activation of **7** by carbonyldiimidazole to make the corresponding activated ester proceeded smoothly, then ammonia addition followed by acidic deprotection created **1**. Piperazine addition to the activated ester followed by deprotection formed **2**. Serine addition to the activated ester followed by deprotection gave rise to **3**, which has multiple polar groups (amide, carboxylate, and alcohol) in the same vicinity. Addition of hydroxylamine hydrochloride then acid to the activated ester gave hydroxamic acid **4**. For compound **5**, a shorter alkyl linker was needed (9 carbons) to give the

correct number of atoms (10) between the core and pharmacophore elements. Cyclization with a 10-carbon dibromoalkane followed by TBAF deprotection gave 9-carbon alcohol **7**, which was treated with mesyl chloride and sodium azide to give nitrile intermediate **8**. Treatment of **8** with dibutyltin oxide and TMS azide gives a tetrazole, which can be deprotected to give **5**. Detailed syntheses can be found in the supporting information.

These compounds were evaluated *in vitro* by luciferase reporter assays to determine their potencies (EC_{50}) and relative efficacies (RE), DSF assays to determine if binding alters the melting profile of the receptor (ΔT_m), and a binding assay to determine their binding constants (K_i). The results of these assays are summarized in Table 6.1. In blue is **10CA**, which is a highly efficacious and reasonably potent compound. We were hoping to develop a compound that displayed improved potency, efficacy, thermal stability, and binding relative to **10CA**. To help visualize how these compounds compare, under-performing numbers are shown in gray, and out-performing numbers are shown in bolded black. Two compounds stand out here—**3** (serine) and **5** (tetrazole). These compounds have comparable EC_{50} s to **10CA** but are not more potent. They both have higher efficacies, impart thermal stability by almost 10 degrees, and demonstrate improved binding efficiencies. Because both **3** and **5** are still less potent than **10CA**, we have not identified a single replacement that we consider significantly better than **10CA**. To determine whether these replacements should be incorporated into future iterations of lead compounds, we are currently investigating their effects on disease models using enteroids and RNA-seq. However, the preliminary data that we have on these compounds are important for the development of new therapeutics based on the hexahydropentalene scaffold as they demonstrate that replacement of the carboxylate (if necessary) is a tolerated strategy to improve or modulate properties of future leads.

compound	EC ₅₀	RE	ΔT _m (°C)	K _i
10CA	0.4 μM	2.39	-0.7	10.0 nM
1	3.9 μM	3.28	4.6	161 nM
2	26.0 μM	13.83	3.3	40.7 nM
3	4.3 μM	3.98	7.6	3.0 nM
4	2.3 μM	6.1	4.4	268 nM
5	2.6 μM	3.57	7.2	4.7 nM

Table 5.1. Summary of *in vitro* data for new compounds.

5.3 6N-10CA Hybrid

We hypothesized that by combining the pharmacophores of **6N** and **10CA**, we could retain the high activity imparted by contacting residues at the mouth of the pocket by **10CA** while imparting the potency gained by the direct T352 contact made by the sulfamide of **6N**. To synthesize this compound (Fig. 5.2) we started with diol **9** as a mixture of *endo* and *exo* stereoisomers. Ley-Griffith oxidation followed by esterification gave the keto-ester **10** in 72% yield over 2 steps. Reductive amination proceeds with good diastereocontrol, giving *endo* amine **11** in >20:1 *endo* : *exo* selectivity and 81% yield. Sulfamide installation to form intermediate **12** followed by global acidic deprotection gave hybrid **13**, called **6N-10CA**.

We evaluated **6N-10CA** in luciferase reporter assays as well as a binding assay (Chapter 6). This compound performs extraordinarily well, and indeed it seems as though the potency and activity imparted by both the sulfamide and acid pharmacophores are additive.

Hybrid compound **6N-10CA** has an EC_{50} of 43 nM, presumably imparted by the sulfamide moiety, a maximum efficacy of 2.1, similar to that of the carboxylate pharmacophore, a binding constant of 180 pM, representing the first picomolar binder for LRH-1, and stabilizes the receptor by nearly 40 degrees ($T_m = 79.7$ °C). The combination of **6N** and **10CA** are completely synergistic—all of these metrics either equal or outperform **6N** and **10CA** in nearly every regard.

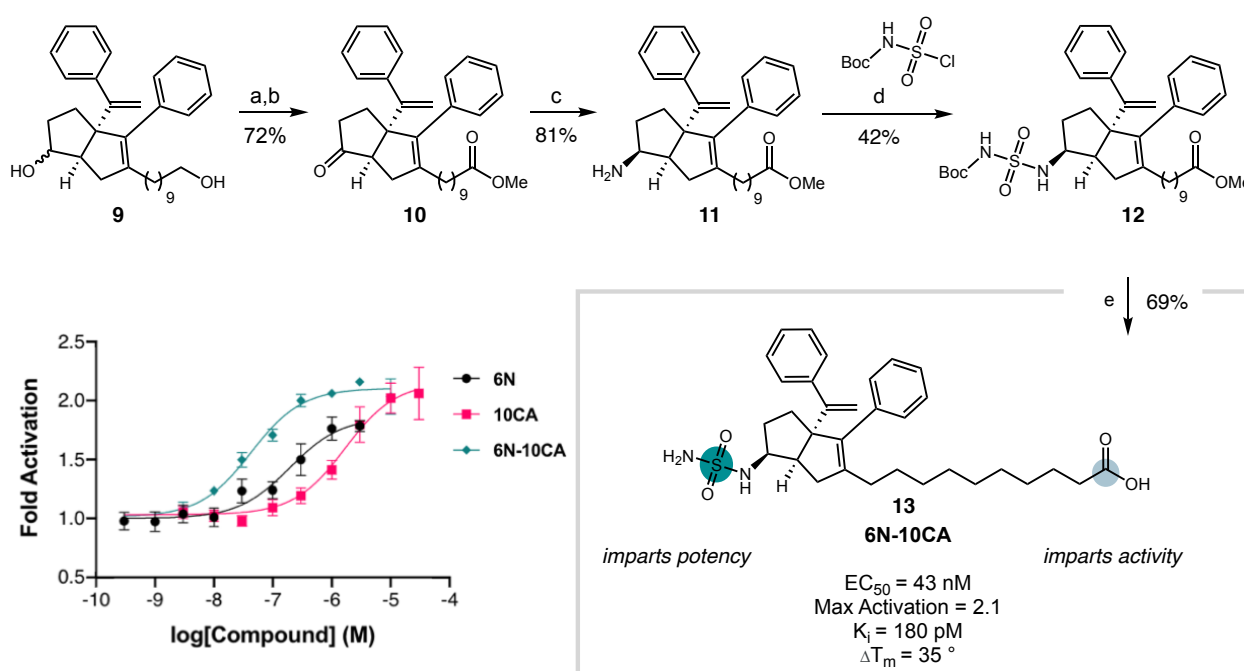


Figure 5.2. Synthesis of **6N-10CA hybrid and *in vitro* activity.** In these assays, **6N-10CA** has an $EC_{50} = 43$ nM, a Max. Activity = 2.1, $K_i = 180$ pM, and $\Delta T_m = 35$ °

Excitingly, we also solved the X-Ray crystal structure of **6N-10CA** bound in the LBD of LRH-1 (Fig. 5.3) at a resolution of 2.8 Å. As seen in Figure 5.3A, the *endo* sulfamide is in position to contact T352 directly, as **6N** does. The alkyl linker tail extends towards the mouth of the receptor and is able to interact with K520 and Y516 at the mouth of the pocket, similar to **10CA**. It is also apparent that the core of the compound overlays with all of our other hexahydropentalene

structures (Fig. 5.3B). The sulfamides of **6N** and **6N-10CA** hybrid overlay, as does the carboxylate pharmacophore of **10CA** and **6N-10CA**.

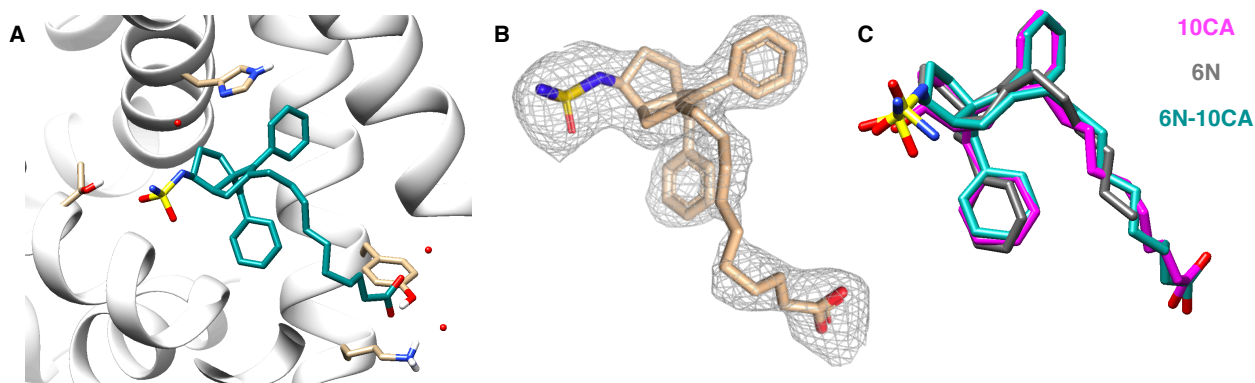


Figure 5.3. Crystal structure of 6N-10CA hybrid. (A) **6N-10CA** hybrid in the ligand binding pocket of LRH-1. (B) Omit map ($F_o - F_c$, contoured at 2.5σ) showing that a single enantiomer of RJW100 is bound (C) The coordinates of **10CA** (pink), **6N** (gray), and **6N-10CA** hybrid (teal) show that all three ligands are oriented similarly in the binding pocket of LRH-1.

This compound, **6N-10CA**, represents the culmination of our current agonist structural studies. We have used the crystal structure of RJW100 bound in the LBD of LRH-1 (Chapter 1) combined with the DLPC-LRH-1 crystal structure to rationally design compounds that would contact multiple sites important for LRH-1 activation. These chimeric molecules represent the current best agonists for LRH-1, and we are currently deeply investigating this hybrid and launching a program to evaluate it in disease models. This agonist will additionally serve as an important chemical probe to elucidate the role of LRH-1 in other tissues.

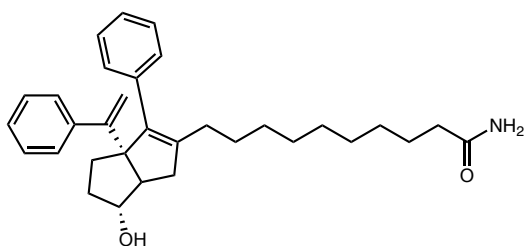
5.4 Supporting information

General Information

All reactions were carried out in oven-dried glassware, equipped with a stir bar and under a nitrogen atmosphere with dry solvents under anhydrous conditions, unless otherwise noted. Solvents used in anhydrous reactions were purified by passing over activated alumina and storing under argon. Yields refer to chromatographically and spectroscopically (^1H NMR) homogenous materials, unless otherwise stated. Reagents were purchased at the highest commercial quality and used without further purification, unless otherwise stated. n-Butyllithium (n-BuLi) was used as a 2.5 M solution in hexanes (Aldrich), was stored at 4 °C and titrated prior to use. Organic solutions were concentrated under reduced pressure on a rotary evaporator using a water bath. Chromatographic purification of products was accomplished using forced-flow chromatography on 230-400 mesh silica gel. Preparative thin-layer chromatography (PTLC) separations were carried out on 1000 μm SiliCycle silica gel F-254 plates. Thin-layer chromatography (TLC) was performed on 250 μm SiliCycle silica gel F-254 plates. Visualization of the developed chromatogram was performed by fluorescence quenching or by staining using KMnO_4 , p-anisaldehyde, or ninhydrin stains. ^1H and ^{13}C NMR spectra were obtained from the Emory University NMR facility and recorded on a INOVA 600 (600 MHz), INOVA 500 (500 MHz), INOVA 400 (400 MHz), VNMR 400 (400 MHz), or Mercury 300 (300 MHz), and are internally referenced to residual protio solvent signals. Data for ^1H NMR are reported as follows: chemical shift (ppm), multiplicity (s = singlet, d = doublet, t = triplet, q = quartet, m = multiplet, dd = doublet of doublets, dt = doublet of triplets, ddd = doublet of doublet of doublets, dtd = doublet of triplet of doublets, b = broad, etc.), coupling constant (Hz), integration, and assignment, when applicable. Data for decoupled ^{13}C NMR are reported in terms of chemical shift and multiplicity when

applicable. Liquid chromatography mass spectrometry (LC-MS) was performed on an Agilent 6120 mass spectrometer with an Agilent 1220 Infinity liquid chromatography inlet. Preparative high pressure liquid chromatography (Prep-HPLC) was performed on an Agilent 1200 Infinity Series chromatograph using an Agilent Prep-C18 30 x 250 mm 10 μ m column.

Chemical Syntheses of Carboxylate Replacements



10-((*exo*)-6-hydroxy-3-phenyl-3a-(1-phenylvinyl)-1,3a,4,5,6,6a-hexahydropentalen-2-

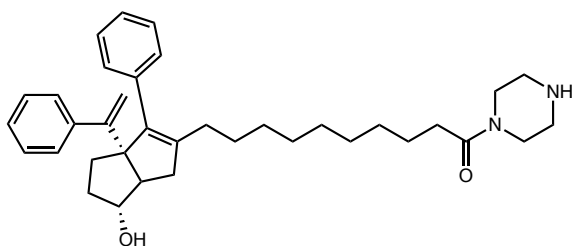
yl)decanamide (1): MOM-protected **10CA (6)** was prepared as described before (Chapter 2) and added to a scintillation vial (52 mg, 0.1 mmol, 1.0 equiv), equipped with a magnetic stir bar and dissolved in THF. Carbonyldiimidazole (35 mg, 0.2 mmol, 2 equiv) was added in small portions (effervesces) and stirred until completion was detected by LCMS (small portions of the activated ester was quenched with methanol to visualize reaction progress). Ammonia (as a 0.5N solution in dioxane, 100 μ L, excess) was added to the reaction mixture, which was stirred at room temperature until completion as detected by TLC and LCMS. The reaction mixture was concentrated and the crude residue was passed through silica (50–100% EtOAc/Hex eluent), concentrated, and dissolved in acetonitrile. A magnetic stirrer was added, and two drops of concentrated HCl was added to the solution. After deprotection was complete (approximately 1 hr

as determined by TLC and LCMS), the reaction mixture was concentrated and purified on silica (50–100% EtOAc/Hex eluent) to give the title compound (10.1 mg, 54% yield).

$^1\text{H NMR}$ (600 MHz, CDCl_3) δ 7.40 – 7.15 (m, 10H), 5.35 (d, $J = 36.9$ Hz, 2H), 5.06 (s, 1H), 4.99 (s, 1H), 3.95 (s, 1H), 2.35 (dd, $J = 16.8, 9.3$ Hz, 1H), 2.29 (d, $J = 8.8$ Hz, 1H), 2.21 (t, $J = 7.6$ Hz, 2H), 2.12 – 1.95 (m, 4H), 1.74 – 1.60 (m, 6H), 1.42 – 1.14 (m, 11H).

$^{13}\text{C NMR}$ (126 MHz, CDCl_3) δ 175.2, 155.0, 143.7, 141.9, 138.9, 137.8, 129.7, 127.8, 127.7, 127.6, 126.7, 126.6, 116.4, 86.0, 70.1, 54.0, 40.2, 35.9, 34.0, 32.1, 29.6, 29.6, 29.3, 29.2, 29.2, 27.3, 25.5.

LRMS (ESI, APCI) m/z : calc'd for $\text{C}_{32}\text{H}_{41}\text{NO}_2$ $[\text{M}+\text{H}]^+$ 472.3, found 471.8

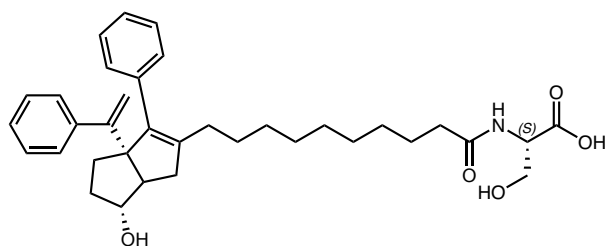


10-((exo)-6-hydroxy-3-phenyl-3a-(1-phenylvinyl)-1,3a,4,5,6,6a-hexahydroindolen-2-yl)-1-(piperazin-1-yl)decan-1-one (2) : MOM-protected 10CA (6) (17 mg, 0.03 mmol, 1.0 equiv) was dissolved in MeCN in a 20 mL scintillation vial equipped with magnetic stir bar. Carbonyldiimidazole (20 mg, 0.1 mmol, 3.7 equiv) was added in small portions (effervesces) and stirred until completion was detected by LCMS (small portions of the activated ester was quenched with methanol to visualize reaction progress). Piperazine (50 mg, 0.6 mmol, 20 equiv) was added to the reaction mixture, which was stirred at room temperature until completion as detected by TLC and LCMS. The reaction mixture was concentrated and the crude residue was passed through silica (65/35/5 DCM/MeOH/ NH_4OH eluent), concentrated, and dissolved in acetonitrile. A

magnetic stirrer was added, and two drops of concentrated HCl was added to the solution. After deprotection was complete (approximately 30 minutes as determined by TLC and LCMS), the reaction mixture was concentrated and purified on silica (5–10% MeOH/DCM + 1% TEA eluent) to give the title compound (5.0 mg, 54% yield).

¹H NMR (399 MHz, CDCl₃) δ 7.47 – 7.05 (m, 10H), 5.04 (s, 1H), 4.97 (s, 1H), 3.97 (s, 1H), 3.93 (s, 1H), 3.84 (s, 1H), 3.63 (s, 1H), 3.30 – 3.12 (m, 4H), 2.46 – 2.23 (m, 5H), 2.16 – 1.90 (m, 6H), 1.79 – 1.52 (m, 5H), 1.34 – 1.12 (m, 11H).

LRMS (ESI, APCI) *m/z*: calc'd for C₃₆H₅₀N₂O₂ [M+H]⁺ 542.4, found 542.8

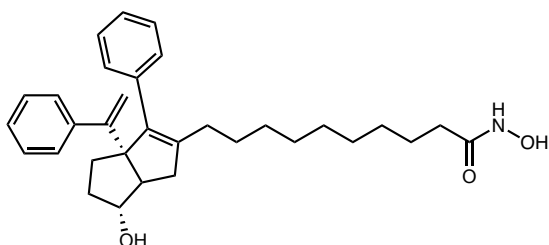


(10-(*exo*)-6-hydroxy-3-phenyl-3a-(1-phenylvinyl)-1,3a,4,5,6,6a-hexahdropentalen-2-yl)decanoyl-L-serine (3): MOM-protected **10CA (6)** (35 mg, 0.07 mmol, 1.0 equiv) was dissolved in THF in a 20 mL scintillation vial equipped with magnetic stir bar. Carbonyldiimidazole (30 mg, 2.5 equiv) was added in small portions (effervesces) and stirred until completion was detected by LCMS (small portions of the activated ester was quenched with methanol to visualize reaction progress). L-Serine methyl ester (16 mg, 0.13 mmol, 2 equiv) was added to the reaction mixture, which was stirred at room temperature until completion as detected by TLC and LCMS. The reaction mixture was extracted into ethyl acetate 3 x. The combined organic layers were dried over MgSO₄, filtered, and concentrated. The resulting residue was dissolved in acetonitrile. A magnetic stirrer was added, and one drop of concentrated HCl was

added to the solution. After deprotection was complete (approximately 1 hr as determined by TLC and LCMS), the reaction mixture was concentrated and dissolved in MeCN/H₂O (3:1 v/v). Lithium hydroxide (excess, ca 10 equiv) was added portionwise and the reaction was stirred at room temperature for 2.5 h. Upon reaction completion (as detected by TLC and LCMS), the reaction mixture was concentrated. The crude residue was and purified on silica in 100% EtOAc + 1% Acetic Acid eluent to give the title compound (10.5 mg, 27% yield over 4 steps).

¹H NMR (500 MHz, CDCl₃) δ 7.42 – 7.07 (m, 10H), 6.76 (s, 1H), 5.05 (s, 1H), 4.99 (s, 1H), 4.57 (s, 1H), 4.10 – 3.77 (m, 5H), 2.39 – 2.18 (m, 4H), 2.14 – 1.94 (m, 6H), 1.77 – 1.55 (m, 5H), 1.38 – 1.09 (m, 11H).

LRMS (ESI, APCI) *m/z*: calc'd for C₃₅H₄₄NO₅ [M-H]⁻ 558.3, found 558.3



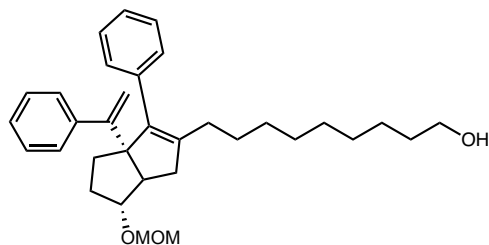
***N*-hydroxy-10-((*exo*)-6-hydroxy-3-phenyl-3a-(1-phenylvinyl)-1,3a,4,5,6,6a-**

hexahydropentalen-2-yl)decanamide (4): MOM-protected **10CA (6)** (49 mg, 0.09 mmol, 1.0 equiv) was dissolved in THF in a 20 mL scintillation vial equipped with magnetic stir bar. Carbonyldiimidazole (42 mg, 3 equiv) was added in small portions (effervesces) and stirred until completion was detected by LCMS (small portions of the activated ester was quenched with methanol to visualize reaction progress). Hydroxylamine hydrochloride (32 mg, 0.4 mmol, 5.0 equiv) was added to the reaction mixture, which was stirred at room temperature until completion as detected by TLC and LCMS. The reaction mixture was concentrated and the crude residue was

passed through silica (50–100% EtOAc/Hex eluent), concentrated, and dissolved in acetonitrile. A magnetic stirrer was added, and one drop of concentrated HCl was added to the solution. After deprotection was complete (approximately 1 hr as determined by TLC and LCMS), the reaction mixture was concentrated and purified by preparatory HPLC (50–99% MeCN/Water) to give the title compound.

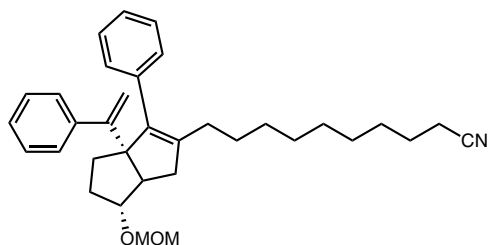
¹H NMR (400 MHz, CDCl₃) δ 7.24 (s, 10H), 5.05 (d, J = 1.4 Hz, 1H), 4.97 (d, J = 1.4 Hz, 1H), 3.93 (s, 1H), 2.39 – 2.23 (m, 2H), 2.15 (t, J = 7.6 Hz, 2H), 2.10 – 1.94 (m, 5H), 1.74 – 1.58 (m, 5H), 1.37 – 1.09 (m, 11H).

LRMS (ESI, APCI) *m/z*: calc'd for C₃₂H₄₂NO₃ [M+H]⁺ 488.3, found 488.6



9-((*exo*)-6-(methoxymethoxy)-3-phenyl-3a-(1-phenylvinyl)-1,3a,4,5,6,6a-

hexahydropentalen-2-yl)nonan-1-ol (7): MOM-protected 9C-OH was prepared as described previously (Chapter 2).

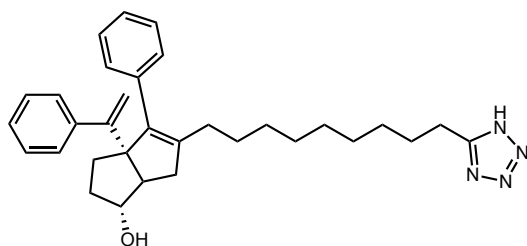


10-((*exo*)-6-(methoxymethoxy)-3-phenyl-3a-(1-phenylvinyl)-1,3a,4,5,6,6a-

hexahydropentalen-2-yl)decanenitrile (8): To a scintillation vial containing

To a scintillation vial equipped with a magnetic stir bar, **7** (168 mg, 0.3 mmol, 1.0 equiv) was added and dissolved in DCM. Methanesulfonyl chloride (50 μ L, 0.6 mmol, 2.0 equiv) and triethylamine (80 μ L, 0.6 mmol, 2.0 equiv) were added portionwise. The reaction was allowed to stir at room temperature for approximately 20 minutes. The crude residue was poured onto water and extracted with EtOAc 3. x. The combined organic layers were dried with MgSO₄, filtered, and concentrated. 51 mg (0.1 mmol, 1.0 equiv) of the mesylate residue was then transferred to a reaction tube in DMF which was equipped with a magnetic stir bar. Sodium cyanide (50 mg, 1 mmol, 10 equiv) was added and the reaction was heated to 110 °C and stirred for 10 minutes. The reaction mixture was allowed to cool to room temperature, diluted with EtOAc, and washed with KOH, water, and brine. The organic layer was dried with MgSO₄, filtered, and concentrated. The crude residue was purified on silica in 10% EtOAc/Hex eluent to afford the title compound (44.8 mg, 82% yield).

¹H NMR (500 MHz, CDCl₃) δ 7.46 – 7.13 (m, 10H), 5.05 (d, J = 1.5 Hz, 1H), 4.99 (d, J = 1.5 Hz, 1H), 4.65 – 4.58 (m, 2H), 3.79 (s, 1H), 3.35 (s, 3H), 2.41 (d, J = 9.3 Hz, 1H), 2.32 (dd, J = 14.6, 9.3 Hz, 2H), 2.11 – 1.95 (m, 6H), 1.86 – 1.59 (m, 5H), 1.43 – 1.10 (m, 11H).



(*exo*)-5-(9-(1H-tetrazol-5-yl)nonyl)-4-phenyl-3a-(1-phenylvinyl)-1,2,3,3a,6,6a-

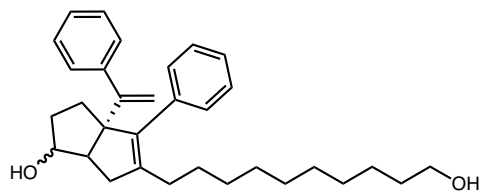
hexahydropentalen-1-ol (5**):** To a scintillation vial equipped with magnetic stir bar was added dibutyltin oxide (5.1 mg, 0.02 mmol, 0.2 equiv). **8** (44.8 mg, 0.09 mmol, 1.0 equiv) in toluene was

added to the scintillation vial, followed by TMS-azide (25 μ L, 0.18 mmol, 2.0 equiv). The reaction mixture was stirred at reflux for 24 hours before being allowed to cool to room temperature and diluted with EtOAc. The organic layer was washed with water and brine, dried with $MgSO_4$, and concentrated. The crude residue was loaded on to a pad of silica and washed with 30% EtOAc/Hex eluent to remove the remaining nitrile starting material. The MOM-protected tetrazole product was eluted off silica in 10% MeOH/DCM. The MOM-protected tetrazole product (16.6 mg, 0.03 mmol, 1 equiv) was then dissolved in MeCN, and 1 drop of concentrated HCl was added. The reaction mixture was stirred for 30 minutes, concentrated, and purified on a pad of silica in 5–10% MeOH/DCM eluent to afford the title compound (2.6 mg, 17% yield).

1H NMR (500 MHz, $CDCl_3$) δ 7.40 – 7.14 (m, 10H), 5.06 (d, J = 1.4 Hz, 1H), 5.00 (d, J = 1.4 Hz, 1H), 3.98 (s, 1H), 2.96 (t, J = 7.4, 6.6 Hz, 2H), 2.41 – 2.23 (m, 2H), 2.21 – 1.95 (m, 4H), 1.86 – 1.52 (m, 6H), 1.44 – 1.10 (m, 11H).

LRMS (ESI, APCI) m/z : calc'd for $C_{32}H_{41}N_4O$ $[M+H]^+$ 497.3, found 497.9

Chemical Syntheses of 6N-10CA Hybrid



5-(10-hydroxydeacyl)-4-phenyl-3a-(1-phenylvinyl)-1,2,3,3a,6,6a-hexahydropentalen-1-ol (1):

Prior to use in the reaction, all reagents were dried by azeotropic removal of water using benzene.

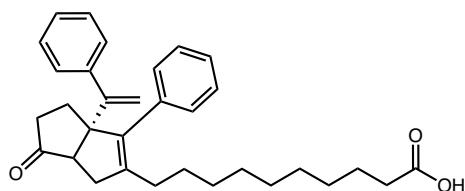
A dry round bottom flask containing bis(cyclopentadienyl)zirconium(IV) dichloride (1.403 g, 4.8

mmol, 1.2 equiv) under nitrogen, was dissolved in anhydrous, degassed tetrahydrofuran (THF, 5 mL/mmol enyne) and cooled to $-78\text{ }^{\circ}\text{C}$. The resulting solution was treated with *n*-BuLi (3.84 mL, 9.6 mmol, 2.4 equiv.) and the light yellow solution was stirred for 50 minutes. A solution of tert-butyltrimethyl((7-phenylhept-1-en-6-yn-3-yl)oxy)silane (1.202 g, 4.0 mmol, 1.0 equiv) in anhydrous, degassed THF (5 mL/mmol) was added. The resulting salmon-colored mixture was stirred at $-78\text{ }^{\circ}\text{C}$ for 45 minutes, the cooling bath removed, and the reaction mixture was allowed to warm to ambient temperature with stirring (2.5 hours total). The reaction mixture was then cooled to $-78\text{ }^{\circ}\text{C}$ for 15 minutes and tert-butyl((10,10-dibromodecyl)oxy)diphenylsilane (2.492 g, 4.4 mmol, 1.1 equiv) was added as a solution in anhydrous THF (5 mL/mmol) followed by freshly prepared lithium diisopropylamide (LDA, 4.4 mL, 4.4 mmol, 1.0 M, 1.1 equiv.). After 30 minutes, a freshly prepared solution of lithium phenylacetylide (14.4 mmol, 3.6 equiv.) in anhydrous THF (2 mL/mmol) was added dropwise and the resulting rust-colored solution was stirred at $-78\text{ }^{\circ}\text{C}$ for 1 hour. The reaction was quenched with methanol and saturated aqueous sodium bicarbonate and allowed to warm to room temperature, affording a light yellow slurry that stirred overnight. The slurry was then poured onto water and extracted with ethyl acetate four times. The combined organic layers were washed with brine, dried with Na_2SO_4 , filtered, and concentrated in vacuo to afford a crude mixture. The resulting crude mixture was dissolved in 200 mL of 1:1 DCM:MeOH in a round bottom flask then 0.5 mL of concentrated HCl added. The resulting solution was stirred at room temperature for 2.5 hours before concentrating in vacuo and subjecting to silica gel chromatography (5-50% EtOAc/Hex eluent) to afford the title compound as a yellow oil and 1.7:1 mixture of diastereomers used in the next step without separation. (1.47 g, 80% over 2 steps).

Exo diastereomer: $^1\text{H NMR}$ (600 MHz, CDCl_3) δ 7.37 – 7.23 (m, 8H), 7.20 (t, $J = 8.0\text{ Hz}$, 2H), 5.07 (d, $J = 1.4\text{ Hz}$, 1H), 4.99 (d, $J = 1.4\text{ Hz}$, 1H), 3.96 – 3.93 (m, 1H), 3.64 (t, $J = 6.6\text{ Hz}$, 2H),

2.36 (dd, $J = 16.9, 9.3$ Hz, 1H), 2.29 (dd, $J = 9.3, 1.8$ Hz, 1H), 2.13 – 1.98 (m, 4H), 1.75 – 1.63 (m, 2H), 1.56 (p, $J = 6.8$ Hz, 3H), 1.43 – 1.17 (m, 14H).

Endo diastereomer: $^1\text{H NMR}$ (600 MHz, CDCl_3) δ 7.37 – 7.23 (m, 8H), 7.20 (t, $J = 7.5$ Hz, 2H), 5.07 (d, $J = 1.4$ Hz, 1H), 4.93 (d, $J = 1.4$ Hz, 1H), 4.18 (td, $J = 8.9, 5.6$, 1H), 3.64 (t, $J = 6.6$ Hz, 2H), 2.62 (dd, $J = 17.5, 2.1$ Hz, 1H), 2.48 (td, $J = 8.7, 2.0$ Hz, 1H), 2.13 – 1.98 (m, 4H), 1.84 (dq, $J = 10.0, 4.9$ Hz, 1H), 1.75 – 1.63 (m, 2H), 1.56 (p, $J = 6.8$ Hz, 2H), 1.43 – 1.17 (m, 14H).



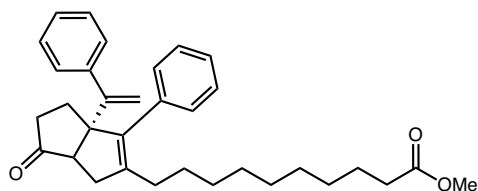
10-(-6-oxo-3-phenyl-3a-(1-phenylvinyl)-1,3a,4,5,6,6a-hexahydropentalen-2-yl)decanoic acid:

To a solution of 5-(10-hydroxydecyl)- 4-phenyl- 3a- (1-phenylvinyl)- 1,2,3,3a,6,6a hexahydropentalen-1-ol (1) in acetonitrile (592 mg, 1.3 mmol, 0.1 M) was added tetrapropylammonium perruthenate (45.3 mg, 0.13 mmol, 0.1 equiv.), N-methylmorpholine N-oxide (2.29 g, 12.9 mmol, 10 equiv.), and water (0.24 mL, 12.9 mmol, 10 equiv.) and stirred at room temperature overnight. The reaction solution was then filtered through a pad of silica with 99:1 EtOAc:AcOH to collect the title compound as a yellow oil (608 mg, >99%).

$^1\text{H NMR}$ (500 MHz, CDCl_3) δ 7.40 – 7.19 (m, 10H), 5.22 (d, $J = 1.5$ Hz, 1H), 5.11 (d, $J = 1.4$ Hz, 1H), 2.46 (d, $J = 7.8$ Hz, 1H), 2.36 – 2.26 (m, 4H), 2.16 – 1.95 (m, 5H), 1.91 (dd, $J = 16.5, 7.8$ Hz, 1H), 1.61 (p, $J = 7.5$ Hz, 2H), 1.46 – 0.97 (m, 12H). Carboxylic acid proton (-COOH) not observed.

$^{13}\text{C NMR}$ (126 MHz, CDCl_3) δ 223.0, 179.9, 153.3, 145.0, 142.6, 137.5, 136.8, 129.1, 128.4, 128.2, 127.7, 127.2, 127.1, 115.4, 65.6, 55.7, 38.9, 37.6, 34.2, 30.1, 29.8, 29.4, 29.3, 29.1, 28.5, 27.7, 24.8.

LRMS (ESI, APCI) m/z : calc'd for $\text{C}_{32}\text{H}_{39}\text{O}_3$ ($\text{M}+\text{H}$) $^+$ 471.3, found 470.8.

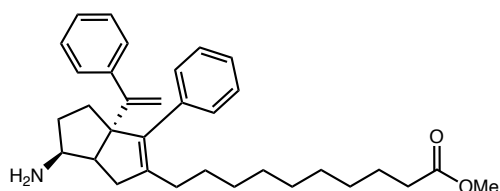


methyl 10-(6-oxo-3-phenyl-3a-(1-phenylvinyl)-1,3a,4,5,6,6a-hexahydropentalen-2-yl)decanoate (2): To a solution of 10-(6-oxo-3-phenyl-3a-(1-phenylvinyl)-1,3a,4,5,6,6a-hexahydropentalen-2-yl)decanoic acid in methanol (945 mg, 2 mmol, 0.1 M) was added 5 drops of concentrated HCl and stirred at room temperature overnight. Reaction solution was then concentrated in vacuo and filtered through a pad of silica to collect the title compound as a yellow oil (930 mg, 96%).

¹H NMR (500 MHz, CDCl₃) δ 7.40 – 7.19 (m, 10H), 5.22 (d, J = 1.3 Hz, 1H), 5.11 (d, J = 1.3 Hz, 1H), 3.66 (s, 3H), 2.46 (d, J = 7.7 Hz, 1H), 2.34 – 2.25 (m, 4H), 2.16 – 1.95 (m, 5H), 1.91 (dd, J = 16.5, 7.8 Hz, 1H), 1.60 (p, J = 7.5 Hz, 2H), 1.33 – 1.10 (m, 12H).

¹³C NMR (126 MHz, CDCl₃) δ 222.7, 174.4, 153.3, 144.9, 142.6, 137.5, 136.7, 129.0, 128.3, 128.2, 127.7, 127.1, 127.1, 115.3, 65.5, 55.6, 51.5, 38.8, 37.6, 34.2, 30.0, 29.7, 29.4, 29.33, 29.27, 29.2, 28.4, 27.7, 25.0.

LRMS (ESI, APCI) m/z: calc'd for C₃₃H₄₁O₃ (M+H)⁺ 485.3, found 484.9.



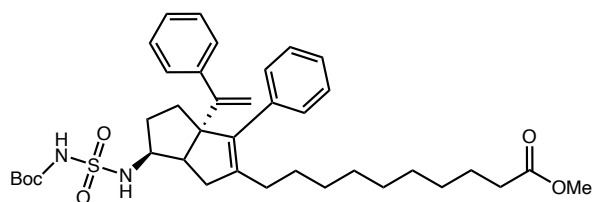
methyl 10-(6-amino-3-phenyl-3a-(1-phenylvinyl)-1,3a,4,5,6,6a-hexahydropentalen-2-yl)decanoate (3): To a screw top test tube charged with a stir bar was added methyl 10-(6-oxo-3-

phenyl-3a-(1-phenylvinyl)-1,3a,4,5,6,6a-hexahydropentalen-2-yl)decanoate (2) (350 mg, 0.72 mmol, 1.0 equiv.) and ethanol (3 mL) and sealed. Ammonia (7 M in methanol, 0.52 mL, 3.61 mmol, 5.0 equiv.) then titanium(IV) isopropoxide (0.33 mL, 1.08 mmol, 1.5 equiv.) were added via syringe and stirred at room temperature for 6 hours. The test tube cap was then removed and sodium borohydride (82 mg, 2.16 mmol, 3 equiv.) added portion-wise. The resulting solution was stirred at room temperature overnight before being quenched with EtOAc, saturated aqueous potassium sodium tartrate, and 2 M aqueous sodium hydroxide. The resulting slurry was then sonicated in the reaction tube for 10 minutes before adding to a separatory funnel. The aqueous layer was then drained and remaining EtOAc washed with 2 x 20 mL of aqueous potassium sodium tartrate and 2 M sodium hydroxide then 20 mL water and 20 mL brine. The remaining organic layer was then dried over Na₂SO₄, filtered, and concentrated *in vacuo* to give the title compound as a yellow oil (283 mg, 81%).

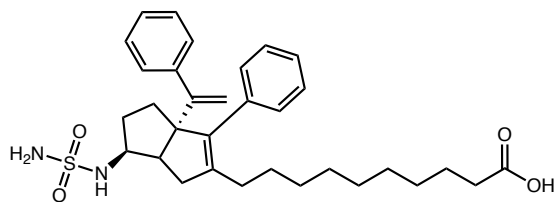
¹H NMR (500 MHz, CDCl₃) δ 7.35 – 7.22 (m, 8H), 7.20 (t, J = 2.0 Hz, 1H), 7.18 (t, J = 1.5 Hz, 1H), 5.07 (d, J = 1.4 Hz, 1H), 4.93 (d, J = 1.5 Hz, 1H), 3.66 (s, 3H), 3.31 (td, J = 8.7, 5.8 Hz, 1H), 2.49 – 2.40 (m, 2H), 2.29 (t, J = 7.6 Hz, 2H), 2.12 – 2.00 (m, 4H), 1.85 – 1.78 (m, 1H), 1.72 – 1.67 (m, 2H), 1.60 (p, J = 7.5 Hz, 2H), 1.42 – 1.15 (m, 12H). Amine protons (-NH₂) not observed.

¹³C NMR (126 MHz, CDCl₃) δ 174.5, 155.1, 144.3, 143.0, 139.5, 137.2, 129.9, 127.9, 127.8, 127.7, 126.8, 126.7, 115.3, 69.6, 55.3, 51.6, 34.4, 34.3, 33.3, 30.0, 29.9, 29.52, 29.50, 29.4, 29.3, 28.1, 25.1.

LRMS (ESI, APCI) m/z: calc'd for C₃₃H₄₄NO₂ (M+H)⁺ 486.3, found 485.8



methyl 10-(6-((N-(tert-butoxycarbonyl) sulfamoyl) amino)- 3-phenyl-3a- (1-phenylvinyl)- 1,3a,4,5,6,6a- hexahydropentalen-2-yl) decanoate (4): To a solution of tert-butyl alcohol (47 mg, 0.64 mmol, 1.1 equiv.) in anhydrous DCM (0.6 mL) in an oven-dried flask under nitrogen at 0 °C was added neat chlorosulfonylisocyanate (0.050 mL, 0.58 mmol, 1.0 equiv.) and stirred for 45 minutes, warming to room temperature in that time. The resulting solution was then added via syringe to a solution of methyl 10-(6-amino-3-phenyl-3a- (1-phenylvinyl)- 1,3a,4,5,6,6a-hexahydropentalen-2-yl) decanoate (3) (283 mg, 0.58 mmol, 1.0 equiv.) and triethylamine (0.12 mL, 0.87 mmol, 1.5 equiv.) in anhydrous DCM (0.6 mL) under nitrogen in an oven-dried flask at 0 °C. The reaction was then stirred and warmed to room temperature over 3 hours before diluting with DCM and washing with 2 x 10 mL 0.5 M aqueous HCl, 10 mL water and 10 mL brine. The organic layer was then dried over Na₂SO₄, filtered, and concentrated in vacuo to give crude material. This material was subjected to silica gel chromatography (10-40% EtOAc/Hex) to collect material taken crude to the next step.



10-(3-phenyl-3a-(1-phenylvinyl)-6-(sulfamoylamino)-1,3a,4,5,6,6a-hexahydropentalen-2-yl)decanoic acid (5): A 20 mL scintillation vial was charged with a stir bar and methyl 10-(6- ((N-

(tert-butoxycarbonyl) sulfamoyl) amino)- 3-phenyl-3a-(1-phenylvinyl)- 1,3a,4,5,6,6a-hexahydropentalen-2-yl) decanoate (4) (160 mg, 0.24 mmol) and cooled to 0 °C. A 3:1 v/v solution of dioxane and concentrated HCl (2 mL) was then added and allowed to warm to room temperature and stirred for 24 hours before heating to 40 °C for 14 hours. The reaction solution was then diluted with EtOAc and washed with 3 x 5 mL 0.5 M aqueous HCl, 5 mL water, and 5 mL brine. The organic layer was then dried over Na₂SO₄, filtered, and concentrated in vacuo to give the title compound as a colorless oil (94 mg, 29% over 2 steps).

¹H NMR (500 MHz, CDCl₃) δ 7.35 – 7.22 (m, 8H), 7.19 (t, J = 2.0 Hz, 1H), 7.17 (t, J = 1.6 Hz, 1H), 5.10 (d, J = 1.3 Hz, 1H), 4.95 (d, J = 1.4 Hz, 1H), 4.84 (d, J = 7.8 Hz, 1H), 4.72 (s, 2H), 3.78 (dtd, J = 11.2, 8.3, 6.0 Hz, 1H), 2.62 (td, J = 8.9, 2.1 Hz, 1H), 2.42 (dd, J = 17.7, 2.1 Hz, 1H), 2.34 (t, J = 7.4 Hz, 2H), 2.16 (dd, J = 17.6, 9.0 Hz, 1H), 2.11 – 2.00 (m, 2H), 1.99 – 1.92 (m, 1H), 1.75 – 1.68 (m, 2H), 1.62 (p, J = 7.4 Hz, 2H), 1.53 – 1.42 (m, 1H), 1.43 – 1.18 (m, 12H).

¹³C NMR (126 MHz, CDCl₃) δ 179.3, 154.3, 143.8, 143.01 139.3, 136.8, 129.8, 128.0, 127.8, 127.0, 126.9, 115.7, 68.9, 57.2, 47.5, 35.6, 34.0, 32.6, 31.8, 29.9, 29.7, 29.2, 29.1, 29.0, 28.9, 27.9, 24.6.

LRMS (ESI, APCI) m/z: calc'd for C₃₂H₄₃N₂O₄S (M+H)⁺ 551.3, found 551.8.

Chapter 6:
Designing New Chemical Tools to Study the
Human NR5A Receptors LRH-1 and SF-1

Adapted and Reprinted in part with permission from ACS Med. Chem. Lett. *In Press*.

Copyright 2019 American Chemical Society

<https://pubs.acs.org/doi/10.1021/acsmchemlett.9b00442>

6.1 NR5A Nuclear Receptors

LRH-1 is part of a subfamily of nuclear receptors: NR5A NRs. The two human NR5A subfamily members are steroidogenic factor-1 (SF-1; NR5A1; Fig. 6.1A) and liver receptor homologue-1 (LRH-1; NR5A2; Fig. 6.1B), and both are lipid-sensing. SF-1 regulates steroidogenesis in the ovaries and adrenal glands, and energy homeostasis in the ventromedial hypothalamus.⁶⁴ Both SF-1 and LRH-1 are also critical for development: SF-1 is necessary for endocrine organ development and differentiation,⁶⁵ and LRH-1 is required for the maintenance of stem cell pluripotency.⁶⁶ Both NR5As also drive cancer progression, with SF-1 involved in adrenocortical carcinoma and LRH-1 in cancers of the breast, colon, pancreas, and prostate.^{56d,56f,67} LRH-1 and SF-1 are highly similar, with 95% sequence similarity in their DNA binding domains and 75% sequence similarity in their ligand binding domains.⁶⁸ The hydrophobicity of the binding pockets creates two challenges in designing ligand-binding assays and screens. First, NR5As favor ligands with low aqueous solubility, hindering ligand binding detection. Second, recombinant proteins copurify with phospholipids, further confounding ligand binding detection. Though direct

⁶⁴ (a) Val, P.; Lefrançois-Martinez, A. M.; Veyssière, G.; Martinez, A. SF-1 a Key Player in the Development and Differentiation of Steroidogenic Tissues. *Nucl. Recept.* **2003**, *1*, 1–23 (b) Majdic, G.; Young, M.; Gomez-Sanchez, E.; Anderson, P.; Szczepaniak, L. S.; Dobbins, R. L.; McGarry, J. D.; Parker, K. L. Knockout Mice Lacking Steroidogenic Factor 1 Are a Novel Genetic Model of Hypothalamic Obesity. *Endocrinology* **2002**, *143* (2), 607–614

⁶⁵ Shinoda, K.; Lei, H.; Yoshii, H.; Nomura, M.; Nagano, M.; Shiba, H.; Sasaki, H.; Osawa, Y.; Ninomiya, Y.; Niwa, O.; Morohashi, K. -I.; Li, E. Developmental Defects of the Ventromedial Hypothalamic Nucleus and Pituitary Gonadotroph in the Ftz-F1 Disrupted Mice. *Dev. Dyn.* **1995**, *204* (1), 22–29

⁶⁶ Gu, P.; Goodwin, B.; Chung, A. C.-K.; Xu, X.; Wheeler, D. A.; Price, R. R.; Galardi, C.; Peng, L.; Latour, A. M.; Koller, B. H.; Gossen, J.; Kliewer, S. A.; Cooney, A. J. Orphan Nuclear Receptor LRH-1 Is Required To Maintain Oct4 Expression at the Epiblast Stage of Embryonic Development. *J. Mol. Cell. Biol.* **2005**, *25* (9), 3492–3505

⁶⁷ (a) Doghman, M.; Karpova, T.; Rodrigues, G. A.; Arhatte, M.; De Moura, J.; Cavalli, L. R.; Virolle, V.; Barbry, P.; Zambetti, G. P.; Figueiredo, B. C.; Heckert, L. L.; Lalli, E. Increased Steroidogenic Factor-1 Dosage Triggers Adrenocortical Cell Proliferation and Cancer. *Mol. Endocrinol.* **2007**, *21* (12), 2968–2987 (b) Xiao, L.; Wang, Y.; Xu, K.; Hu, H.; Xu, Z.; Wu, D.; Wang, Z.; You, W.; Ng, C. F.; Yu, S.; Chan, F. L. Nuclear Receptor LRH-1 Functions to Promote Castration-Resistant Growth of Prostate Cancer via Its Promotion of Intratumoral Androgen Biosynthesis. *Cancer Res.* **2018**, *78* (9), 2205–2218 (c) Chand, A. L.; Herridge, K. A.; Thompson, E. W.; Clyne, C. D. The Orphan Nuclear Receptor LRH-1 Promotes Breast Cancer Motility and Invasion. *Endocr. Relat. Cancer* **2010**, *17* (4), 965–975

⁶⁸ Sablin, E. P.; Krylova, I. N.; Fletterick, R. J.; Ingraham, H. A. Structural Basis for Ligand-Independent Activation of the Orphan Nuclear Receptor LRH-1. *Mol. Cell* **2003**, *11* (6), 1575–1585

binding assays have been reported for the NR5A receptors, they are not amenable to rapid compound screening.^{12d,13b,69} Screens that have been performed have largely relied on indirect methods such as coregulator recruitment and have only identified a handful of small molecule modulators.^{15,69,70} Further, these screens do not necessarily detect binding in the ligand binding pocket, further confounding the rational design of synthetic modulators for the NR5A receptors. The ability to measure direct binding in the ligand-binding pocket would greatly facilitate synthetic ligand screening and development. Thus, we sought to develop a direct binding assay for efficient quantification of binding affinities of a small compound library.

6.1 Development of a Fluorescence Polarization Assay to Detect Binding

Fluorescence polarization (FP) is a direct, equilibrium binding assay commonly used with other NRs. It is solution based, allowing molecules and proteins to retain their native state, uses minimal material, and allows parallel evaluation of several compounds using plate-based fluorescence detectors. We recently developed an NR5A agonist, **6N** (Chapter 4), with low nanomolar potency which facilitated the synthesis of a fluorescent probe for use in FP.⁵⁴ High-affinity compounds are important for FP-based competition binding assays because probe affinity limits detection of the binding constant (K_i) for competing ligands.⁷¹ We hypothesized that this potent agonist would bind the NR5A receptors with high affinity and serve as a scaffold for an FP

⁶⁹ (a) Benod, C.; Carlsson, J.; Uthayaruban, R.; Hwang, P.; Irwin, J. J.; Doak, A. K.; Shoichet, B. K.; Sablin, E. P.; Fletterick, R. J. Structure-Based Discovery of Antagonists of Nuclear Receptor LRH-1. *J. Biol. Chem.* **2013**, *288* (27), 19830–19844 (b) De Jesus Cortez, F.; Suzawa, M.; Irvy, S.; Bruning, J. M.; Sablin, E.; Jacobson, M. P.; Fletterick, R. J.; Ingraham, H. A.; England, P. M. Disulfide-Trapping Identifies a New, Effective Chemical Probe for Activating the Nuclear Receptor Human LRH-1 (NR5A2). *PLoS One* **2016**, *11* (7), 1–14

⁷⁰ (a) Rey, J.; Hu, H.; Kyle, F.; Lai, C. F.; Buluwela, L.; Coombes, R. C.; Ortlund, E. A.; Ali, S.; Snyder, J. P.; Barrett, A. G. M. Discovery of a New Class of Liver Receptor Homolog-1 (LRH-1) Antagonists: Virtual Screening, Synthesis and Biological Evaluation. *ChemMedChem* **2012**, *7* (11), 1909–1914 (b) Corzo, C. A.; Mari, Y.; Chang, M. R.; Khan, T.; Kuruvilla, D.; Nuhant, P.; Kumar, N.; West, G. M.; Duckett, D. R.; Roush, W. R.; Griffin, P. R. Antiproliferation Activity of a Small Molecule Repressor of Liver Receptor Homolog 1. *Mol. Pharmacol.* **2015**, *87* (2), 296–304

⁷¹ Huang, X. Fluorescence Polarization Competition Assay: The Range of Resolvable Inhibitor Potency Is Limited by the Affinity of the Fluorescent Ligand. *J. Biomol. Screen.* **2003**, *8* (1), 34–38

probe. Guided by the crystal structures of LRH-1-6N and LRH-1-10CA, we aimed to extend the 6N hexyl “tail” to 11 carbons and installed a fluoresceinamine (FAM) moiety.

We posited that this linker length was sufficient to position the FAM substituent outside the pocket without interfering with desired deep-pocket contacts anchoring the probe (Fig. 6.1C, D).

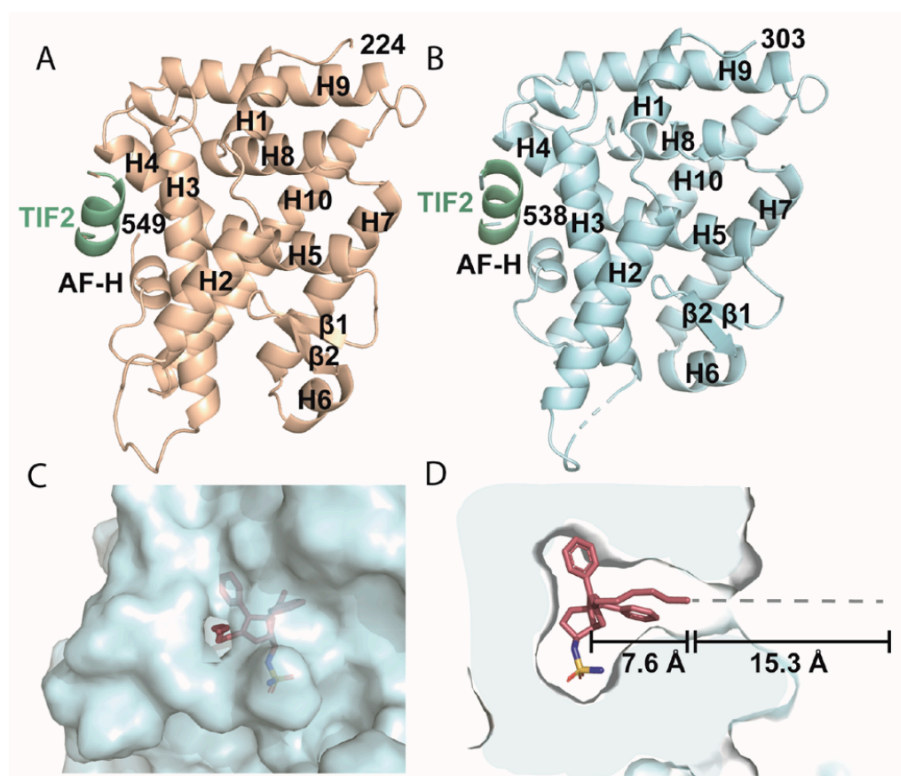
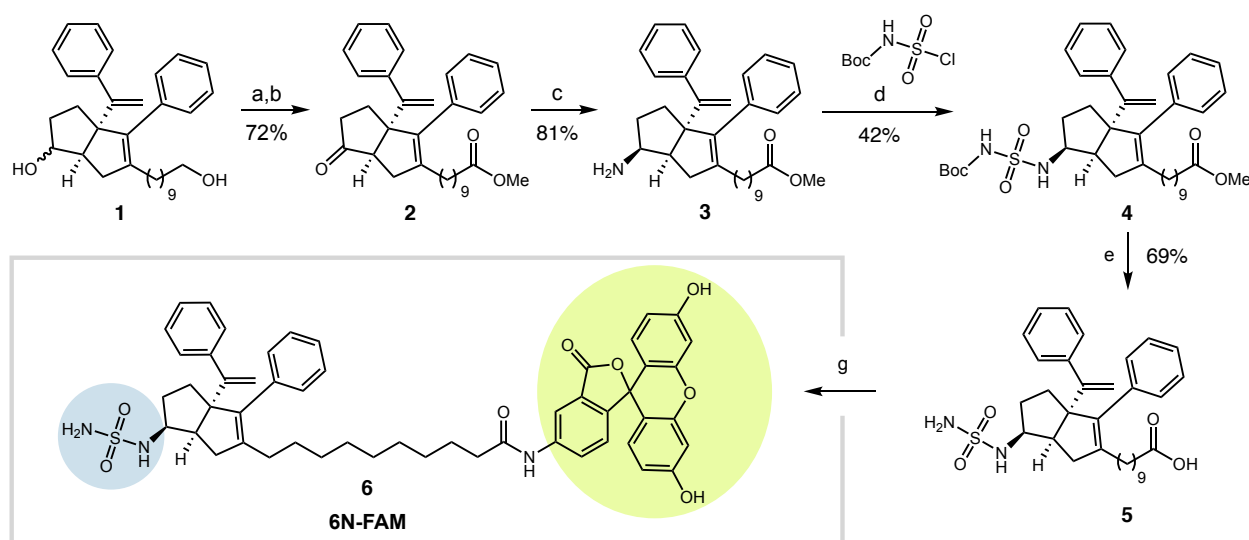


Figure 6.1. Structure-guided design of NR5A probe. Structures of the ligand-binding domains of (A) SF-1 (PDB: 1ZDT) and (B) LRH-1 (PDB: 6OQY). (C) There is a clear exit tunnel from the ligand binding pocket (LRH-1 shown) which can accommodate the 6NFAM linker, and (D) the linker (red) and FAM molecule (dashed line) provide sufficient length to exit the pocket mouth and leave the FAM moiety solvent-exposed for FP detection.

As seen previously (Chapter 2), tail modifications on the hexahdropentalene scaffold are readily incorporated, and NR5A receptors can accommodate a variety of modifications (Chapter 2,3,4). Synthesis of the designed probe involved elaboration of diol **1**, the synthesis of which was

reported previously. Ley-Griffith oxidation afforded the corresponding ketoacid. Esterification gave rise to **2** (in 72% yield over two steps), and diastereoselective reductive amination to **3** provided the endo amine necessary for installation of the sulfamide, which drives potency of the probe. Sulfamide assembly and global deprotection gave **5** which was coupled with fluoresceinamine to furnish the probe **6N-FAM (6)** (Scheme 6.1).

Scheme 6.1: Chemical Synthesis of 6N-FAM (6)^a



^a *Reagents and conditions:* (a) Tetrapropylammonium perruthenate, N-methyl morpholine oxide, H₂O, MeCN, 23 °C, 16 h; (b) MeOH, conc. aq. HCl, 23 °C, 16 h; (c) NH₃ (7N in MeOH), titanium(IV) isopropoxide, 23 °C, 6 h. Sodium borohydride, 16 h; (d) Chlorosulfonyl isocyanate, ^tBuOH, DCM, 0 to 23 °C, 45 min, then TEA, 0 to 23 °C, 3 h; (e) 1,4-dioxane: conc. aq. HCl (3:1 v/v), 40 °C, 14 h; (f) EDCI, fluoresceinamine isomer 1, DMF, 23 °C, 5 h.

6.3 Evaluation of the fluorescent probe 6N-FAM

We first determined the affinities of SF-1 and LRH-1 for **6N-FAM**. Purified SF-1 or LRH-1 ligand-binding domain was titrated against several constant **6N-FAM** concentrations to determine optimal conditions. We chose 10 nM **6N-FAM** as it maximized signal and sensitivity

in competition experiments (below). The K_d of the probe using these conditions was 1.0 nM for LRH-1 (95% confidence interval: [0.8, 1.3]), and 12.3 nM [9.0, 16.7] for SF-1 (Fig. 6.2A, S6.1).

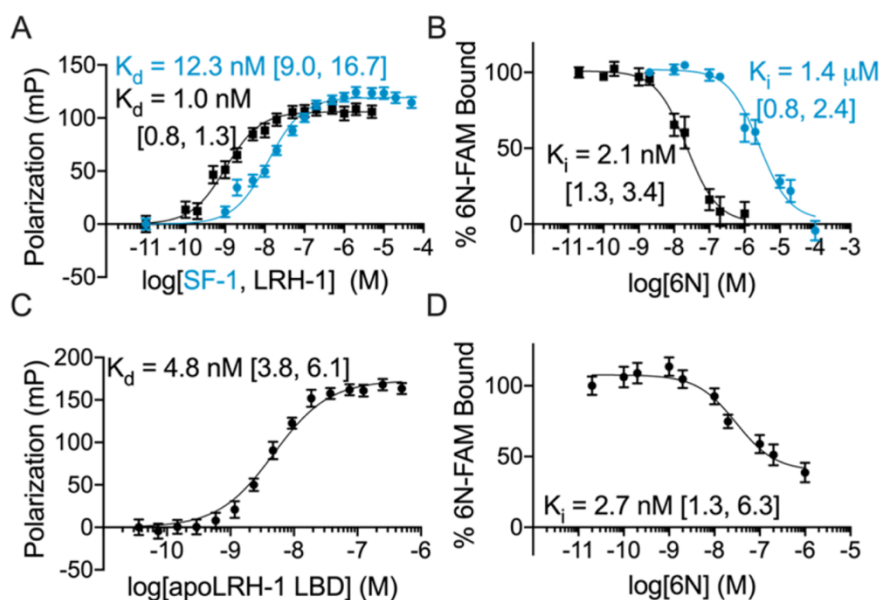


Figure 6.2. Validation of fluorescence polarization. (A) Binding of **6N-FAM** to SF-1 or LRH-1 ($n = 9$). Insets indicate K_d values (95% CI in square brackets). (B) Competitive displacement of the **6N-FAM** probe using unlabeled **6N** ($n = 8$). **6N** completely displaced **6N-FAM** from both SF-1 and LRH-1. Insets indicate the K_i (95% CI in square brackets). (C) **6N-FAM** and (D) Unlabeled **6N** binds apo LRH-1 with comparable affinity to DLPC-exchanged protein (C, $n = 2$; D, $n = 8$). Blue lines, SF-1; black lines, LRH-1; error bars are SEM. Competition experiments used 10 nM **6N-FAM**, 5 nM LRH-1, 25 nM SF-1.

To validate **6N-FAM** in a competition assay, we measured the K_i values of unlabeled **6N** (Fig. 6.2B, S6.1). The unlabeled probe should completely outcompete the labeled probe with a similar inhibition constant (here termed K_i) to the forward binding constant (K_d)⁷¹ Optimized reaction conditions are described in full detail in the Supporting Information. For both LRH-1 and SF-1, unlabeled **6N** dose-dependently decreased millipolarization values and completely outcompeted the probe (Fig. 6.2B, S6.1). For LRH-1, **6N** bound with a K_i of 2.1 nM (95% CI: [1.3, 3.4]), in agreement with the forward binding K_d . Affinities of **6N-FAM** and **6N** were similar when

apo-LRH-1 was used instead of DLPC-exchanged protein (Fig. 6.2C,D, S6.1). Thus, DLPC does not significantly impact affinity measurements, eliminating the need to strip and refold the protein. Surprisingly, the affinity of unlabeled **6N** for SF-1 was much lower than the K_d of the probe, perhaps indicating that the FAM linker makes additional interactions with SF-1 versus LRH-1.

6.4 Utilization of 6N-FAM to Detect Phospholipid Binding to NR5A Receptors

Phospholipid binding assays are challenging to develop, as lipids prefer micellular environments and aggregate in solution. We have previously reported a liposome-based fluorescence resonance energy transfer (FRET)-based assay for LRH-1.^{13b} This assay utilizes donor-quencher vesicles harboring nitrobenzoxadiazole (NBD)-labeled 1,2-dilauroyl-sn-glycero-3-phosphoethanolamine (DLPE) and 7-diethylamino-3-((4'-iodoacetyl)amino)phenyl)-4-methylcoumarin (DCIA)-labeled LRH-1 and requires the nonspecific lipid chaperone β -cyclodextrin to enhance lipid exchange. Though this assay measures binding of a variety of lipids, its lower range of detection is 1 μ M due to the relatively low affinity of DCIA LRH-1 for NBD-DLPE. Thus, we sought to determine whether the FP competition assay, which has a low nanomolar limit of detection, could be used to measure phospholipid binding and evaluate candidate endogenous NR5A ligands. DLPC binds both LRH-1 and SF-1 and is of interest due to its ability to suppress lipogenesis and improve insulin resistance in obese mice. We detected DLPC K_i values of 850 nM [303, 2430] and 81.4 nM [52.7, 126] for SF-1 and LRH-1, respectively (Fig. 6.3A and S6.1).

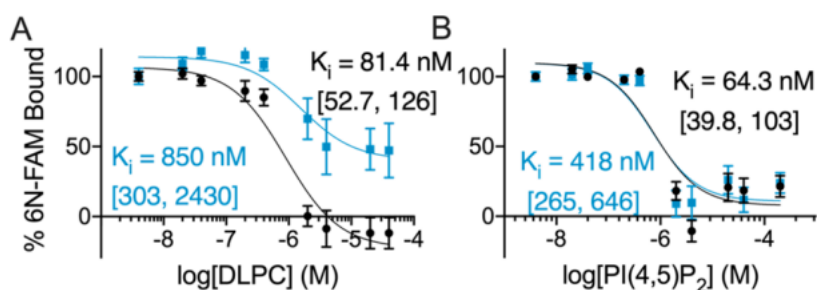


Figure 6.3. FP assay detects lipid binding. Both NR5As bind (A) dilauroylphosphatidylcholine (DLPC) and (B) PI(4,5)P₂ (n = 8). Blue lines, SF-1; black lines, LRH-1; 95% CI is in square brackets; error bars are SEM. Experiments used 10 nM 6N-FAM, 5 nM LRH-1, 25 nM SF-1.

This is 20- fold greater than the 1.9 μ M affinity we measured using the FRET assay with LRH-1. Thus, the FP assay increases our dynamic range 1,000-fold compared to the FRET assay and expands our ability to evaluate potential endogenous ligands for the NR5As. We also measured binding to phosphatidylinositol 4,5- bisphosphate (PI(4,5)P₂), as multiple phosphatidylinositol species have been crystallized with NR5As (Fig. 6.3B and S6.1).^{12d,72} Phosphatidylinositols bind NR5As with high affinity in an electrophoretic mobility shift (EMSA)-based assay.^{12d,72} Affinities for PIP(4,5)P₂ binding of 418 nM [265, 646] and 64.3 nM [39.8, 103] for SF-1 and LRH-1, respectively, were similar to those obtained in the EMSA assay for SF-1 binding to PIP(4,5)P₂ (~250 nM) and LRH-1 binding to PI(3,4,5)P₃ (120 \pm 9 nM). The ligand exchange detected with these PLs indicates that NR5As may follow a canonical model of nuclear receptor activation. Previous reports have proposed that NR5As bind ligand upon folding, are constitutively ligand-bound and active, and do not exist in apo form.^{4a,68} These data indicate that NR5A receptors are dynamic and capable of heterotypic ligand exchange.

⁷² Sablin, E. P.; Blind, R. D.; Uthayaruban, R.; Chiu, H. J.; Deacon, M.; Das, D.; Ingraham, H. A.; Fletterick, R. J. Structure of Liver Receptor Homolog-1 With PIP₃ Hormone Bound in the Ligand Binding Pocket. *J. Struct. Biol.* **2016**, *192* (3), 342–348

6.5 Synthetic Agonist Binding Affinity Correlation with Stability and Activity

We have previously used thermal shift assays (DSF) to detect ligand binding to LRH-1 and assess the effects of ligands on global protein stability. For a subset of these agonists, we have shown that 50% unfolding temperature (T_m) values for LRH-1–ligand complexes strongly correlate with EC_{50} values for LRH-1 activity in cellular luciferase reporter. However, many compounds that bind the NR5As do not induce a strong thermal shift response. We sought to determine whether the FP competition assay could be used to predict compound activity in cells by measuring K_i values for this set of compounds based on the RJW100 scaffold. These compounds, referred to as the R^1 series, include **6N** and contain modifications at the 1-position hydroxyl (Fig. 6.4A).

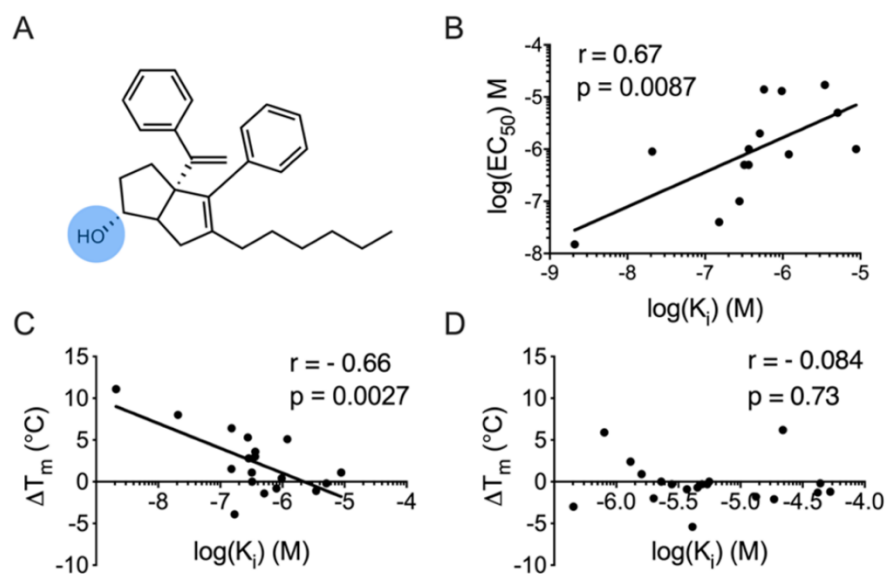


Figure 6.4. Binding affinity correlates with in-cell activity and receptor stability for LRH-1, but not SF-1. (A) Modifications were made to the 1-position hydroxyl (“ R^1 ”) of RJW100, shown in blue, to generate 24 derivatives (reported in). (B) Affinity of R^1 compounds correlates with in-cell potency for LRH-1 in a luciferase reporter assay. Affinity of R^1 compounds also correlated with their effect on receptor stability for LRH-1 (C), but not for SF-1 (D).

We found that LRH-1 K_i values for the R^1 series correlate with EC_{50} values from luciferase reporter assays (Fig. 6.4B, Pearson $r = 0.67$, $p = 0.0087$), indicating that the FP assay can be a screening tool to predict in-cell activity for LRH-1, offering exciting potential for future use in compound development. The LRH-1 K_i values also correlate with T_m values for the R^1 compounds (Fig. 6.4C, Pearson $r = -0.66$, $p = 0.0027$; Fig. S6.1–3). We have not measured in-cell activation of SF-1 by the entire set of R^1 compounds; thus, further investigation is needed to determine whether K_i and EC_{50} correlate for SF-1. However, there is no correlation between the K_i and T_m values for the R^1 series with SF-1 (Fig. 6.4D, Pearson $r = -0.084$, $p = 0.73$; Fig. S6.1–2, 4), perhaps due to distinct effects on SF-1 conformation. The R^1 compounds were designed based on LRH-1 structural studies and generally exhibit poor affinity ($>1 \mu\text{M}$) for SF-1. It remains to be seen whether binding affinities will predict stabilization or in-cell activity of SF-1 for higher affinity compounds.

6.6 FP Assay Validation by Comparing to EMSA and SPR

To further validate our FP competition assay, we compared K_i values to previously reported K_d values (Fig. 6.5 and S6.1). The FP affinity of RJW100 for SF-1 was similar to the value determined by EMSA (EMSA: $1200 \pm 270 \text{ nM}$; FP: $3.3 \mu\text{M}$ [1.9, 5.7]; Fig. 6.5A).^{12d} Our FP values were in agreement with affinities calculated by equilibrium surface plasmon resonance (SPR) for the Cpd3 antagonist for LRH-1 (SPR: $1.5 \pm 0.3 \mu\text{M}$; FP: $2.4 \mu\text{M}$ [0.9, 5.2]; Fig. 6.5B).⁶⁹ Interestingly, the FP assay showed a higher affinity for the PME9 agonist to LRH-1 than SPR (FP, $7.0 \mu\text{M}$ [3.8, 13.0]; SPR, $62.9 \mu\text{M}$; Fig. 6.5C), perhaps due to the time difference between the two assays. SPR was conducted with 60-s contact times, whereas the FP assay requires overnight equilibration to achieve maximum affinity. We next examined the SF-1 isoquinolinone antagonist

SID7969543; no binding data is available for this compound, but its IC_{50} is 30 nM.⁷³ While SID7969543 displaced the 6N-FAM at high concentrations, we were unable to calculate affinity (Fig. 6.5D). Finally, we tested binding of the LRH-1 antagonist SR1848, for which the authors could not detect binding.^{70b} Our FP assay also did not detect binding (Fig. 6.5E), suggesting a novel mechanism of LRH-1 inhibition and also underscoring the difficulty of synthetic modulator development without a direct binding assay to verify compound binding in the ligand-binding pocket.

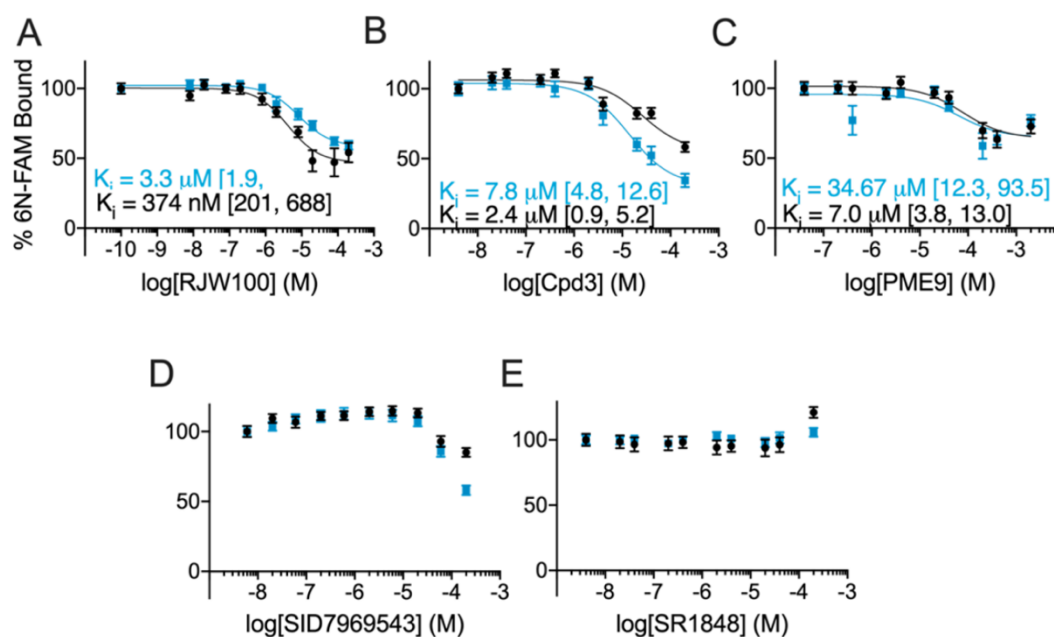


Figure 6.5. FP measurements for synthetic ligands. Both NR5As bind RJW100 (A), Cpd3 (B), and PME9 (C). (D) Binding affinity for SF-1 antagonist SID7969543 cannot be calculated, although probe displacement is detected at high doses. (E) Binding is undetectable for SR1848. Blue lines, SF-1; black lines, LRH-1; error bars are SEM ($n = 8$). Experiments used 10 nM 6N-FAM, 5 nM LRH-1, 25 nM SF-1.

⁷³ Madoux, F.; Li, X.; Chase, P.; Zastrow, G.; Cameron, M. D.; Conkright, J. J.; Griffin, P. R.; Thacher, S.; Hodder, P. Potent, Selective and Cell Penetrant Inhibitors of SF-1 by Functional Ultra-High-Throughput Screening. *Mol. Pharmacol.* **2008**, *73* (6), 1776–1784

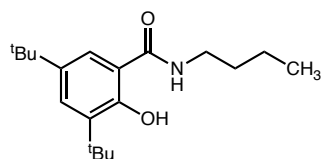
6.7 Conclusions

The NR5A receptors are promising therapeutic targets for metabolic diseases and several cancers, but the hydrophobicity of their binding pockets and preferred ligands has made compound screening and development exceptionally challenging. Without explicit X-ray crystal structure determination, it is difficult to detect direct binding to the LBD of LRH-1, further confounding agonist design. We have developed an FP competition assay to quantify direct ligand binding to NR5A receptors with a 5-log dynamic range. Fluorescence polarization is a simple, inexpensive assay commonly used to quantify ligand binding for NRs (e.g., the PolarScreen FP competition assay is available for seven NRs, Thermo Fisher Scientific, Waltham, MA). It is solution-based, retaining native protein conformation, and equilibrium-based, permitting for measurement of binding regardless of ligand exchange kinetics. We have optimized the assay for 384-well plates, allowing measurement of several compounds in parallel. The assay format ensures that binding will only be detected if a competitor binds in the ligand-binding pocket. This is particularly important for NR5As given that previous screens have largely relied on indirect or virtual screening methods. The flexibility in buffer components provided by FP is critical given the general insolubility of NR5A ligands. We have successfully used 6.7% v/v DMSO and ethanol to increase competitor solubility, allowing competitor ligand concentrations up to 200 μ M. K_i values correlate with in-cell potencies for a series of related NR5A agonists, indicating that this in vitro assay can predict biological activity. In addition to small molecules, the assay detects binding of candidate endogenous phospholipid ligands, which are still under investigation for this subfamily.

6.8 Supporting Information

All reactions were carried out in oven-dried glassware, equipped with a stir bar and under a nitrogen atmosphere with dry solvents under anhydrous conditions, unless otherwise noted. Solvents used in anhydrous reactions were purified by passing over activated alumina and storing under argon. Yields refer to chromatographically and spectroscopically (^1H NMR) homogenous materials, unless otherwise stated. Reagents were purchased at the highest commercial quality and used without further purification, unless otherwise stated. *n*-Butyllithium (*n*-BuLi) was used as a 2.5 M solution in hexanes (Aldrich), was stored at 4 °C and titrated prior to use. Organic solutions were concentrated under reduced pressure on a rotary evaporator using a water bath. Chromatographic purification of products was accomplished using forced-flow chromatography on 230-400 mesh silica gel. Preparative thin-layer chromatography (PTLC) separations were carried out on 1000 μm SiliCycle silica gel F-254 plates. Thin-layer chromatography (TLC) was performed on 250 μm SiliCycle silica gel F-254 plates. Visualization of the developed chromatogram was performed by fluorescence quenching or by staining using KMnO_4 , *p*-anisaldehyde, or ninhydrin stains. ^1H and ^{13}C NMR spectra were obtained from the Emory University NMR facility and recorded on a INOVA 600 (600 MHz), INOVA 500 (500 MHz), INOVA 400 (400 MHz), VNMR 400 (400 MHz), or Mercury 300 (300 MHz), and are internally referenced to residual protio solvent signals. Data for ^1H NMR are reported as follows: chemical shift (ppm), multiplicity (s = singlet, d = doublet, t = triplet, q = quartet, m = multiplet, dd = doublet of doublets, dt = doublet of triplets, ddd = doublet of doublet of doublets, dtd = doublet of triplet of doublets, b = broad, etc.), coupling constant (Hz), integration, and assignment, when applicable. Data for decoupled ^{13}C NMR are reported in terms of chemical shift and multiplicity when applicable. Liquid chromatography mass spectrometry (LC-MS) was performed on an Agilent

6120 mass spectrometer with an Agilent 1220 Infinity liquid chromatography inlet. Preparative high pressure liquid chromatography (Prep-HPLC) was performed on an Agilent 1200 Infinity Series chromatograph using an Agilent Prep-C18 30 x 250 mm 10 μ m column. HPLC analyses were performed using the following conditions. Method A: A linear gradient using water and 0.1 % formic acid (FA) (Solvent A) and MeCN and 0.1% FA (Solvent B); t = 0 min, 75% B, t = 4 min, 99% B (held for 1 min), then 50% B for 1 min, was employed on Agilent Zorbax SB-C18 1.8 micron, 2.1 mm x 50 mm column (flow S2 rate 0.8 mL/min). The UV detection was set to 254 nm. The LC column was maintained at ambient temperature. Method B: A linear gradient using water and 0.1 % formic acid (FA) (Solvent A) and MeCN and 0.1% FA (Solvent B); t = 0 min, 50% B, t = 4 min, 99% B (held for 1 min), then 50% B for 1 min, was employed on Agilent Zorbax SB-C18 1.8 micron, 2.1 mm x 50 mm column (flow S2 rate 0.8 mL/min). The UV detection was set to 254 nm. The LC column was maintained at ambient temperature. Method C: An isocratic method using 60% MeCN, 40% water, and 0.1 % FA was employed on an Agilent Zorbax SB-C18 1.8 micron, 2.1 mm x 50 mm column (flow rate 0.8 mL/min). The UV detection was set to 254 nm. The LC column was maintained at ambient temperature.

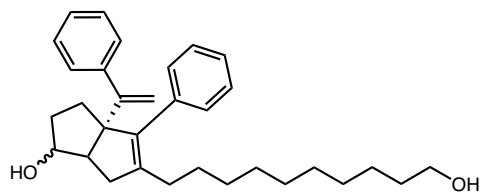


3,5-di-tert-butyl-N-butyl-2-hydroxybenzamide (PME9): To a round bottom flask charged with stir bar was added 3,5-di-tert-butyl-2-hydroxybenzoic acid (311 mg, 1.2 mmol, 1.0 equiv) in THF. 4-nitrophenylchloroformate (284 mg, 1.4 mmol, 1.1 equiv) was added, followed by triethylamine (200 μ L, 1.4, 1.1 equiv). The reaction was stirred at room temperature for 1 h. The volatiles were

concentrated and the crude residue was partitioned between ethyl acetate and water and extracted three times with ethyl acetate. The combined organic layers were washed with NaHCO₃ and brine, dried with MgSO₄, filtered, and concentrated. The crude activated ester was then dissolved in THF and treated with n-butylamine (140 μL, 1.4mmol, 1.1 equiv) and triethylamine (210 μL, 1.5mmol, 1.2 equiv). The reaction was stirred overnight. After reaction completion, the solution was concentrated and subjected to silica gel chromatography in 10% EtOAc/Hex to afford the title compound as a colorless solid (162 mg, 43% yield over 2 steps). Spectral data were consistent with literature values.^{69b}

¹H NMR (600 MHz, CDCl₃) δ 12.73 (s, 1H), 7.44 (d, J = 2.3 Hz, 1H), 7.10 (d, J = 2.3 Hz, 1H), 6.24 (s, 1H), 3.58 – 3.34 (m, 2H), 1.66 – 1.57 (m, 2H), 1.45 – 1.35 (m, 11H), 1.29 (s, 9H), 0.94 (t, J = 7.5 Hz, 3H).

LRMS (ESI, APCI) m/z: calc'd for C₁₉H₃₂NO₂ (M+H)⁺ 306.2, found 305.9. Purity established by HPLC Method A: >99%.



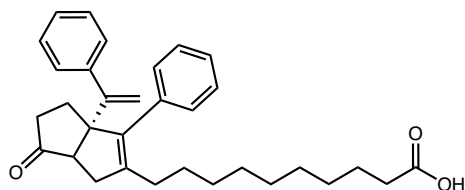
5-(10-hydroxydecyl)-4-phenyl-3a-(1-phenylvinyl)-1,2,3,3a,6,6a-hexahydropentalen-1-ol (1):

Prior to use in the reaction, all reagents were dried by azeotropic removal of water using benzene. A dry round bottom flask containing bis(cyclopentadienyl)zirconium(IV) dichloride (1.403 g, 4.8 mmol, 1.2 equiv) under nitrogen, was dissolved in anhydrous, degassed tetrahydrofuran (THF, 5 mL/mmol enyne) and cooled to -78 °C. The resulting solution was treated with n-BuLi (3.84 mL, 9.6 mmol, 2.4 equiv.) and the light yellow solution was stirred for 50 minutes. A solution of tert-

butyldimethyl((7- phenylhept-1-en-6-yn-3-yl)oxy)silane (1.202 g, 4.0 mmol, 1.0 equiv) in anhydrous, degassed THF (5 mL/mmol) was added. The resulting salmon-colored mixture was stirred at -78 °C for 45 minutes, the cooling bath removed, and the reaction mixture was allowed to warm to ambient temperature with stirring (2.5 hours total). The reaction mixture was then cooled to -78 °C for 15 minutes and tert-butyl((10,10-dibromodecyl)oxy)diphenylsilane (2.492 g, 4.4 mmol, 1.1 equiv) was added as a solution in anhydrous THF (5 mL/mmol) followed by freshly prepared lithium diisopropylamide (LDA, 4.4 mL, 4.4 mmol, 1.0 M, 1.1 equiv.). After 30 minutes, a freshly prepared solution of lithium phenylacetylide (14.4 mmol, 3.6 equiv.) in anhydrous THF (2 mL/mmol) was added dropwise and the resulting rust-colored solution was stirred at -78 °C for 1 hour. The reaction was quenched with methanol and saturated aqueous sodium bicarbonate and allowed to warm to room temperature, affording a light yellow slurry that stirred overnight. The slurry was then poured onto water and extracted with ethyl acetate four times. The combined organic layers were washed with brine, dried with Na₂SO₄, filtered, and concentrated in vacuo to afford a crude mixture. The resulting crude mixture was dissolved in 200 mL of 1:1 DCM:MeOH in a round bottom flask then 0.5 mL of concentrated HCl added. The resulting solution was stirred at room temperature for 2.5 hours before concentrating in vacuo and subjecting to silica gel chromatography (5-50% EtOAc/Hex eluent) to afford the title compound as a yellow oil and 1.7:1 mixture of diastereomers used in the next step without separation. (1.47 g, 80% over 2 steps).

Exo diastereomer: ¹H NMR (600 MHz, CDCl₃) δ 7.37 – 7.23 (m, 8H), 7.20 (t, J = 8.0 Hz, 2H), 5.07 (d, J = 1.4 Hz, 1H), 4.99 (d, J = 1.4 Hz, 1H), 3.96 – 3.93 (m, 1H), 3.64 (t, J = 6.6 Hz, 2H), 2.36 (dd, J = 16.9, 9.3 Hz, 1H), 2.29 (dd, J = 9.3, 1.8 Hz, 1H), 2.13 – 1.98 (m, 4H), 1.75 – 1.63 (m, 2H), 1.56 (p, J = 6.8 Hz, 3H), 1.43 – 1.17 (m, 14H).

Endo diastereomer: $^1\text{H NMR}$ (600 MHz, CDCl_3) δ 7.37 – 7.23 (m, 8H), 7.20 (t, $J = 7.5$ Hz, 2H), 5.07 (d, $J = 1.4$ Hz, 1H), 4.93 (d, $J = 1.4$ Hz, 1H), 4.18 (td, $J = 8.9, 5.6$, 1H), 3.64 (t, $J = 6.6$ Hz, 2H), 2.62 (dd, $J = 17.5, 2.1$ Hz, 1H), 2.48 (td, $J = 8.7, 2.0$ Hz, 1H), 2.13 – 1.98 (m, 4H), 1.84 (dq, $J = 10.0, 4.9$ Hz, 1H), 1.75 – 1.63 (m, 2H), 1.56 (p, $J = 6.8$ Hz, 2H), 1.43 – 1.17 (m, 14H).



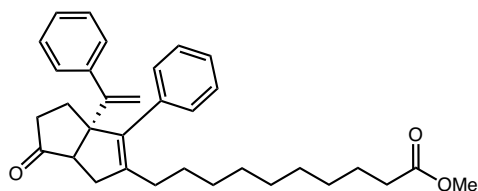
10-(6-oxo-3-phenyl-3a-(1-phenylvinyl)-1,3a,4,5,6,6a-hexahydropentalen-2-yl)decanoic acid:

To a solution of 5-(10-hydroxydecyl)-4-phenyl-3a-(1-phenylvinyl)-1,2,3,3a,6,6a-hexahydropentalen-1-ol in acetonitrile (592 mg, 1.3 mmol, 0.1 M) was added tetrapropylammonium perruthenate (45.3 mg, 0.13 mmol, 0.1 equiv.), N-methylmorpholine N-oxide (2.29 g, 12.9 mmol, 10 equiv.), and water (0.24 mL, 12.9 mmol, 10 equiv.) and stirred at room temperature overnight. The reaction solution was then filtered through a pad of silica with 99:1 EtOAc:AcOH to collect the title compound as a yellow oil (608 mg, >99%).

$^1\text{H NMR}$ (500 MHz, CDCl_3) δ 7.40 – 7.19 (m, 10H), 5.22 (d, $J = 1.5$ Hz, 1H), 5.11 (d, $J = 1.4$ Hz, 1H), 2.46 (d, $J = 7.8$ Hz, 1H), 2.36 – 2.26 (m, 4H), 2.16 – 1.95 (m, 5H), 1.91 (dd, $J = 16.5, 7.8$ Hz, 1H), 1.61 (p, $J = 7.5$ Hz, 2H), 1.46 – 0.97 (m, 12H). Carboxylic acid proton (-COOH) not observed.

$^{13}\text{C NMR}$ (126 MHz, CDCl_3) δ 223.0, 179.9, 153.3, 145.0, 142.6, 137.5, 136.8, 129.1, 128.4, 128.2, 127.7, 127.2, 127.1, 115.4, 65.6, 55.7, 38.9, 37.6, 34.2, 30.1, 29.8, 29.4, 29.3, 29.1, 28.5, 27.7, 24.8.

LRMS (ESI, APCI) m/z : calc'd for $\text{C}_{32}\text{H}_{39}\text{O}_3$ ($\text{M}+\text{H}$) $^+$ 471.3, found 470.8.

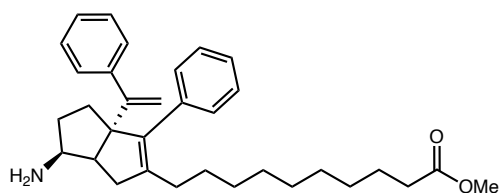


methyl 10-(6-oxo-3-phenyl-3a-(1-phenylvinyl)-1,3a,4,5,6,6a-hexahydropentalen-2-yl)decanoate (2): To a solution of 10-(6-oxo-3-phenyl-3a-(1-phenylvinyl)-1,3a,4,5,6,6a-hexahydropentalen-2-yl)decanoic acid in methanol (945 mg, 2 mmol, 0.1 M) was added 5 drops of concentrated HCl. The reaction mixture was stirred at room temperature overnight. The reaction solution was then concentrated in vacuo and filtered through a pad of silica to collect the title compound as a yellow oil (930 mg, 96%).

¹H NMR (500 MHz, CDCl₃) δ 7.40 – 7.19 (m, 10H), 5.22 (d, J = 1.3 Hz, 1H), 5.11 (d, J = 1.3 Hz, 1H), 3.66 (s, 3H), 2.46 (d, J = 7.7 Hz, 1H), 2.34 – 2.25 (m, 4H), 2.16 – 1.95 (m, 5H), 1.91 (dd, J = 16.5, 7.8 Hz, 1H), 1.60 (p, J = 7.5 Hz, 2H), 1.33 – 1.10 (m, 12H).

¹³C NMR (126 MHz, CDCl₃) δ 222.7, 174.4, 153.3, 144.9, 142.6, 137.5, 136.7, 129.0, 128.3, 128.2, 127.7, 127.1, 127.1, 115.3, 65.5, 55.6, 51.5, 38.8, 37.6, 34.2, 30.0, 29.7, 29.4, 29.33, 29.27, 29.2, 28.4, 27.7, 25.0.

LRMS (ESI, APCI) m/z: calc'd for C₃₃H₄₁O₃ (M+H)⁺ 485.3, found 484.9.



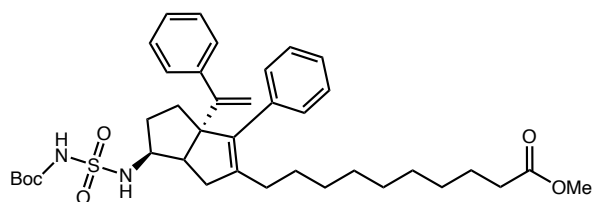
methyl 10-(6-amino-3-phenyl-3a-(1-phenylvinyl)-1,3a,4,5,6,6a-hexahydropentalen-2-yl)decanoate (3): To a screw top test tube charged with a stir bar was added methyl 10-(6-oxo-3-

phenyl-3a-(1-phenylvinyl)-1,3a,4,5,6,6a-hexahydropentalen-2-yl)decanoate (350 mg, 0.72 mmol, 1.0 equiv.) and ethanol (3 mL) and sealed. Ammonia (7 M in methanol, 0.52 mL, 3.61 mmol, 5.0 equiv.) then titanium(IV) isopropoxide (0.33 mL, 1.08 mmol, 1.5 equiv.) were added via syringe and stirred at room temperature for 6 hours. The test tube cap was then removed and sodium borohydride (82 mg, 2.16 mmol, 3 equiv.) added in small portions. The resulting solution was stirred at room temperature overnight before being quenched with EtOAc, saturated aqueous potassium sodium tartrate, and 2 M aqueous sodium hydroxide. The resulting slurry was then sonicated in the reaction tube for 10 minutes before adding to a separatory funnel. The aqueous layer was then drained and remaining EtOAc washed with 2 x 20 mL of aqueous potassium sodium tartrate and 2M sodium hydroxide then 20 mL water and 20 mL brine. The remaining organic layer was then dried over Na₂SO₄, filtered, and concentrated in vacuo to give the title compound as a yellow oil (283 mg, 81%).

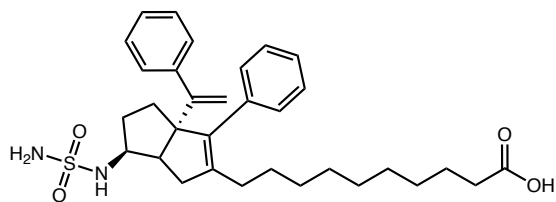
¹H NMR (500 MHz, CDCl₃) δ 7.35 – 7.22 (m, 8H), 7.20 (t, J = 2.0 Hz, 1H), 7.18 (t, J = 1.5 Hz, 1H), 5.07 (d, J = 1.4 Hz, 1H), 4.93 (d, J = 1.5 Hz, 1H), 3.66 (s, 3H), 3.31 (td, J = 8.7, 5.8 Hz, 1H), 2.49 – 2.40 (m, 2H), 2.29 (t, J = 7.6 Hz, 2H), 2.12 – 2.00 (m, 4H), 1.85 – 1.78 (m, 1H), 1.72 – 1.67 (m, 2H), 1.60 (p, J = 7.5 Hz, 2H), 1.42 – 1.15 (m, 12H). Amine protons (-NH₂) not observed.

¹³C NMR (126 MHz, CDCl₃) δ 174.5, 155.1, 144.3, 143.0, 139.5, 137.2, 129.9, 127.9, 127.8, 127.7, 126.8, 126.7, 115.3, 69.6, 55.3, 51.6, 34.4, 34.3, 33.3, 30.0, 29.9, 29.52, 29.50, 29.4, 29.3, 28.1, 25.1.

LRMS (ESI, APCI) m/z: calc'd for C₃₃H₄₄NO₂ (M+H)⁺ 486.3, found 485.8



methyl 10-((N-(tert-butoxycarbonyl) sulfamoyl) amino)-3-phenyl-3a-(1-phenylvinyl)-1,3a,4,5,6,6a-hexahydropentalen-2-yl) decanoate (4): To a solution of tert-butyl alcohol (47 mg, 0.64 mmol, 1.1 equiv.) in anhydrous DCM (0.6 mL) in an oven-dried flask under nitrogen at 0 °C was added neat chlorosulfonylisocyanate (0.050 mL, 0.58 mmol, 1.0 equiv.) and stirred for 45 minutes, warming to room temperature in that time. The resulting solution was then added via syringe to a solution of methyl 10-((6-amino-3-phenyl-3a-(1-phenylvinyl)-1,3a,4,5,6,6a-hexahydropentalen-2-yl) decanoate (283 mg, 0.58 mmol, 1.0 equiv.) and triethylamine (0.12 mL, 0.87 mmol, 1.5 equiv.) in anhydrous DCM (0.6 mL) under nitrogen in an oven-dried flask at 0 °C. The reaction was then stirred and warmed to room temperature over 3 hours before diluting with DCM and washing with 2 x 10 mL 0.5 M aqueous HCl, 10 mL water and 10 mL brine. The organic layer was then dried over Na₂SO₄, filtered, and concentrated in vacuo to give crude material. This material was subjected to silica gel chromatography (10-40% EtOAc/Hex) to collect material taken crude to the next step.



10-(3-phenyl-3a-(1-phenylvinyl)-6-(sulfamoylamino)-1,3a,4,5,6,6a-hexahydropentalen-2-yl)decanoic acid (5): A 20 mL scintillation vial was charged with a stir bar and methyl 10-((N-

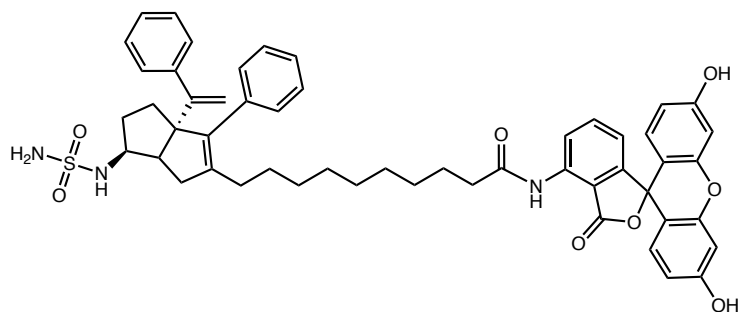
(tert-butoxycarbonyl)sulfamoyl)amino)-3-phenyl-3a-(1-phenylvinyl)-1,3a,4,5,6,6a

hexahydropentalen-2-yl) decanoate (160 mg, 0.24 mmol) and cooled to 0 °C. A 3:1 v/v solution of dioxane and concentrated HCl (2 mL) was then added and allowed to warm to room temperature and stirred for 24 hours before heating to 40 °C for 14 hours. The reaction solution was then diluted with EtOAc and washed with 3 x 5 mL 0.5 M aqueous HCl, 5 ml water, and 5 mL brine. The organic layer was then dried over Na₂SO₄, filtered, and concentrated in vacuo to give the title compound as a colorless oil (94 mg, 29% over 2 steps).

¹H NMR (500 MHz, CDCl₃) δ 7.35 – 7.22 (m, 8H), 7.19 (t, J = 2.0 Hz, 1H), 7.17 (t, J = 1.6 Hz, 1H), 5.10 (d, J = 1.3 Hz, 1H), 4.95 (d, J = 1.4 Hz, 1H), 4.84 (d, J = 7.8 Hz, 1H), 4.72 (s, 2H), 3.78 (dtd, J = 11.2, 8.3, 6.0 Hz, 1H), 2.62 (td, J = 8.9, 2.1 Hz, 1H), 2.42 (dd, J = 17.7, 2.1 Hz, 1H), 2.34 (t, J = 7.4 Hz, 2H), 2.16 (dd, J = 17.6, 9.0 Hz, 1H), 2.11 – 2.00 (m, 2H), 1.99 – 1.92 (m, 1H), 1.75 – 1.68 (m, 2H), 1.62 (p, J = 7.4 Hz, 2H), 1.53 – 1.42 (m, 1H), 1.43 – 1.18 (m, 12H). Carboxylic acid proton (-COOH) not observed.

¹³C NMR (126 MHz, CDCl₃) δ 179.3, 154.3, 143.8, 143.01 139.3, 136.8, 129.8, 128.0, 127.8, 127.0, 126.9, 115.7, 68.9, 57.2, 47.5, 35.6, 34.0, 32.6, 31.8, 29.9, 29.7, 29.2, 29.1, 29.0, 28.9, 27.9, 24.6.

LRMS (ESI, APCI) m/z: calc'd for C₃₂H₄₃N₂O₄S (M+H)⁺ 551.3, found 551.8.



N-(3',6'-dihydroxy-3-oxo-3H-spiro[isobenzofuran-1,9'-xanthen]-5-yl)-10-(3-phenyl-3a-(1-phenylvinyl)-6-(sulfamoylamino)-1,3a,4,5,6,6a-hexahydropentalen-2-yl)decanamide

(6NFAM): A 1 dram vial was charged with a stirbar, 10-(3-phenyl-3a-(1-phenylvinyl)-6-(sulfamoylamino)-1,3a,4,5,6,6a-hexahydropentalen-2-yl)decanoic acid (5) (28.6 mg, 0.05 mmol, 1.0 equiv.), fluoresceinamine isomer 1 (21 mg, 0.06 mmol, 1.2 equiv.), EDCI (11.5 mg, 0.06 mmol, 1.2 equiv.) and DMF (0.65 mL). The resulting solution was stirred at room temperature for 16 hours before diluting with MeCN and subjecting to preparative HPLC to collect the title compound. (9.9 mg, 22%).

¹H NMR (600 MHz, (CD₃)₂CO) δ 9.58 (s, 1H), 8.45 (s, 1H), 7.91 (dd, J = 8.3, 1.9 Hz, 1H), 7.39 – 7.35 (m, 2H), 7.35 – 7.23 (m, 6H), 7.20 (d, J = 7.5 Hz, 2H), 7.17 (d, J = 8.3 Hz, 1H), 6.74 (d, J = 2.3 Hz, 2H), 6.70 (d, J = 8.7 Hz, 2H), 6.62 (dd, J = 8.7, 2.4 Hz, 2H), 5.86 – 5.80 (m, 3H), 5.06 (s, 1H), 4.93 (s, 1H), 3.81 – 3.72 (m, 1H), 2.71 (dd, J = 17.6, 2.2 Hz, 1H), 2.66 (td, J = 9.0, 2.2 Hz, 1H), 2.43 (t, J = 7.4 Hz, 2H), 2.20 (dd, J = 17.5, 9.1 Hz, 1H), 1.95 (m, 1H), 1.75 – 1.66 (m, 4H), 1.62 (qd, J = 11.1, 7.0 Hz, 1H), 1.47 – 1.18 (m, 12H). Phenolic protons (Ar-OH) not observed.

¹³C NMR (151 MHz, (CD₃)₂CO) 172.8, 169.6, 160.6, 156.3, 153.6, 145.1, 144.4, 142.2, 139.9, 138.2, 130.8, 130.39, 130.35, 130.31, 129.0, 128.8, 128.7, 128.6, 127.8, 127.7, 125.3, 115.6, 113.5, 112.0, 103.5, 103.4, 69.9, 58.0, 48.6, 37.9, 36.6, 33.7.

LRMS (ESI, APCI) m/z: calc'd for C₅₂H₅₂N₃O₈S (M-H)⁻ 878.4, found 878.1 (M-H)⁻

Purity established by HPLC Method C: 96%

Other Chemical Sources

SR1848 and Cpd3 were gifted from Patrick Griffin (Scripps University). SID7969543 was purchased from Tocris. DLPC was purchased from Avanti Polar Lipids. PI(4,5)P2 was purchased from Cayman Chemical.

Protein Expression and Purification.

Human LRH-1 LBD (residues 299-541) in the pLIC-His vector was transformed in *E. coli* strain BL21(pLysS) for expression. Cultures (6 L in Liquid Broth, LB) were grown in the presence of ampicillin and chloramphenicol at 37 °C to an OD600 of 0.6. Protein expression was induced with 1 mM isopropyl-1- thio-D-galactopyranoside (IPTG) and grown for 4 hours at 30° C. Cell pellets were resuspended in Buffer A (20 mM Tris-HCl (pH 7.4), 150 mM NaCl, 5% glycerol, 25 mM imidazole), DNase, lysozyme, and phenylmethylsulfonyl fluoride (PMSF). Resuspended cells were sonicated and clarified by centrifugation at 16,000xg for 45 minutes in a Sorvall RC 6+. Protein was purified from the lysate by nickel affinity chromatography (HisTrap FF; GE Healthcare, Little Chalfont, UK): lysate was flowed over the column, washed with Buffer A, and eluted with Buffer B (20 mM Tris-HCl (pH 7.4), 150 mM NaCl, 5% glycerol, 500 mM imidazole). Protein was incubated with DLPC (4-fold molar excess) overnight at 4° C, repurified by size exclusion into assay buffer (150 mM NaCl, 20 mM Tris-HCl (pH 7.4), 5% glycerol) concentrated to approximately 3 mg/mL, and stored at -80 °C until use. SF-1 LBD (residues 218-461) in the pLIC-His vector was transformed in *E. coli* strain BL21(pLysS) for expression. Cultures (6L LB) were grown in the presence of ampicillin and chloramphenicol at 37° C to an OD600 of 0.6. Expression was induced with 0.5 mM IPTG and cultures were grown overnight at 18 °C. Protein

was purified by nickel affinity chromatography as described for LRH-1 (Buffer A: 20 mM Tris-HCl (pH 7.4), 5% glycerol, 500 mM NaCl, 25 mM imidazole, 0.5 mM TCEP; Buffer B: 20 mM Tris-HCl (pH 7.4), 5% glycerol, 500 mM NaCl, 500 mM imidazole, 0.5 mM TCEP), followed by overnight DLPC exchange and size exclusion chromatography into assay buffer. Pure SF-1 protein was concentrated to approximately 3 mg/mL and stored at -80° C until use.

Generation of apo LRH-1.

To extract lipids from the LRH-1 LBD, 4.5 mL of purified protein (15 mg) was treated with 18.75 mL of chloroform-methanol solution (1:2 v/v) and vortexed briefly. An additional 2.5 mL chloroform:water solution (1:1 v/v) was added and the mixture was vortexed again. The stripped and unfolded protein was pelleted by centrifugation at 1000 rpm for 10 minutes. The resulting protein pellet was dissolved into 0.5 mL of buffer containing 50 mM Tris (pH 8.0), 6 M guanidine hydrochloride and 2 mM DTT. Protein was refolded by fast dilution at 4 °C into 50 mL of buffer containing 20 mM Tris (pH 8.5), 1.7 M urea, 4% glycerol and 2 mM DTT. The final urea concentration was adjusted to 2 M, and protein was concentrated to ~ 15 mL, followed by overnight dialysis against assay buffer (see below) containing 2 mM DTT at 4 °C. Refolded protein was purified by size exclusion chromatography to remove aggregates and remaining unfolded protein

Fluorescence Polarization.

All assays were conducted in black, polystyrene, non-binding surface 384- well plates (Corning Inc., Corning, NY) with 30 μ L volumes in assay buffer. Binding affinity for 6N-FAM was determined using 10 nM 6N-FAM and protein concentrations ranging from 1-10⁻⁵ -5 M (SF-

1) or 1-11– 5 -6 M (LRH-1). Plates were incubated overnight at 4 °C and centrifuged at 2,000xg for 2 minutes before polarization measurement. Polarization was monitored on a Neo plate reader (Biotek, Winooski, VT) at an excitation/emission wavelength of 485/528 nm. Nine technical replicates were conducted over three experiments and compiled binding data were baseline-corrected to wells with no protein and fit with a onesite binding curve in GraphPad Prism version 7 (GraphPad, Inc., La Jolla, CA). Competition assays were performed in accordance with development guidelines.³⁶ For LRH-1, 10 nM **6N-FAM** (10 times the affinity of LRH-1 for **6N-FAM**, necessary to obtain adequate signal) and 5 nM LRH-1 (80% of the forward binding B_{max}) were used. For SF-1, 10 nM **6N-FAM** (0.8 times the affinity of SF-1 for **6N-FAM**) and 25 nM SF-1 (60% of the forward binding B_{max}) were used. Competitor ligand concentration ranged from 2^{-11} - 2^{-4} M, and competitor ligand volume was kept constant to maintain constant DMSO in each well (6.7% v/v). Eight technical replicates were performed over two experiments, and GraphPad Prism version 7 was used to analyze compiled data using a one-site, fit K_i curve, with normalization to **6N** competition. For assays with lipids, lipids were solubilized in chloroform and transferred to a clean glass tube. Lipids were dried via evaporation to produce multilamellar sheets. These were resuspended in ethanol and sonicated (twice x 30 seconds) to produce small vesicles for use in FP assays. Differential Scanning Fluorimetry. Purified protein, pre-exchanged with DLPC (0.2 mg/mL), was combined with agonists overnight at 4 °C in assay buffer. SYPRO orange dye was added to the complexes the next day, at a final dilution of 1:1000. Complexes were heated at a rate of 0.5 °C/ minute on a StepOne Plus thermocycler, using the ROX filter for fluorescence detection. The melting temperature (T_m , 50% unfolding) was calculated using the Boltzman equation (GraphPad Prism, V7). Assays were conducted with nine technical replicates over three experiments.

Compound	SF-1 K _i [95% confidence interval]	LRH-1 K _i [95% confidence interval]
6N-FAM (K _d)	12.3 nM [9.0, 16.7]	1.0 nM [0.8, 1.3]; Apo, 4.8 nM [3.8, 6.1]
6N	1.4 μM [0.8, 2.4]	2.1 nM [1.3, 3.4]; Apo, 2.7 nM [1.3, 6.3]
DLPC	850 nM [303, 2430]	81.4 nM [52.7, 126]
PI(4,5)P ₂	9.6 μM [4.3, 21.5]	756 nM [382, 1470]
1N	cnc	cnc
1X	cnc	cnc
S1	4.5 μM [1.8, 10.7]	801 nM [434, 1460]
2N	cnc	973 nM [453, 2060]
2X	18.6 μM [9.3, 36.8]	3.5 μM [1.5, 8.5]
S2N	2.3 μM [0.7, 13.2]	326 nM [181, 580]
S2X	43.9 μM [16.1, 234]	cnc
3N	1.6 μM [0.9, 2.8]	287 nM [174, 468]
3X	1.3 μM [0.8, 1.9]	151 nM [83.0, 263]
S3N	2.8 μM [0.2, 43.1]	cnc
S3X	4.9 μM, 0.8, 31.7]	cnc
4N	5.6 μM [2.4, 19.6]	321 nM [178, 595]
4X	5.4 μM [2.1, 14.5]	508 nM [167, 1670]
5N	21.9 μM [12.4, 39.5]	20.8 nM [11.2, 38.5]
5X	cnc	1.2 μM [0.6, 2.2]
6N	1.4 μM [0.8, 2.4]	2.1 nM [1.3, 3.4]
6X	cnc	152 nM [98.5, 234]
7N	3.7 μM [2.2, 6.9]	366 nM [231, 584]
7X	13.3 μM [8.1, 21.7]	2.2 μM [1.4, 3.4]
8N	2.0 μM [1.4, 2.7]	278 nM [203, 379]
8X	1.2 μM [0.9, 1.7]	170 nM [121, 238]
RJW100	3.3 μM [1.9, 5.7]	316 nM [179, 555]
Cpd3	7.8 μM [4.8, 12.6]	2.4 μM [0.9, 5.2]
PME9	34.6 μM [12.3, 93.5]	7.0 μM [3.8, 13.0]
SID7969543	cnc	cnc
SR1848	cnc	cnc

Table S6.1. Summary K_i Table. K_d and K_i values are presented in the order in which they appear in the manuscript. Experiments were analyzed in Graphpad Prism, v7 using a one-site fit K_i curve (n=8). 95% confidence are reported for each K_i value; cnc (could not calculate) indicates that confidence intervals or K_i values could not be calculated.

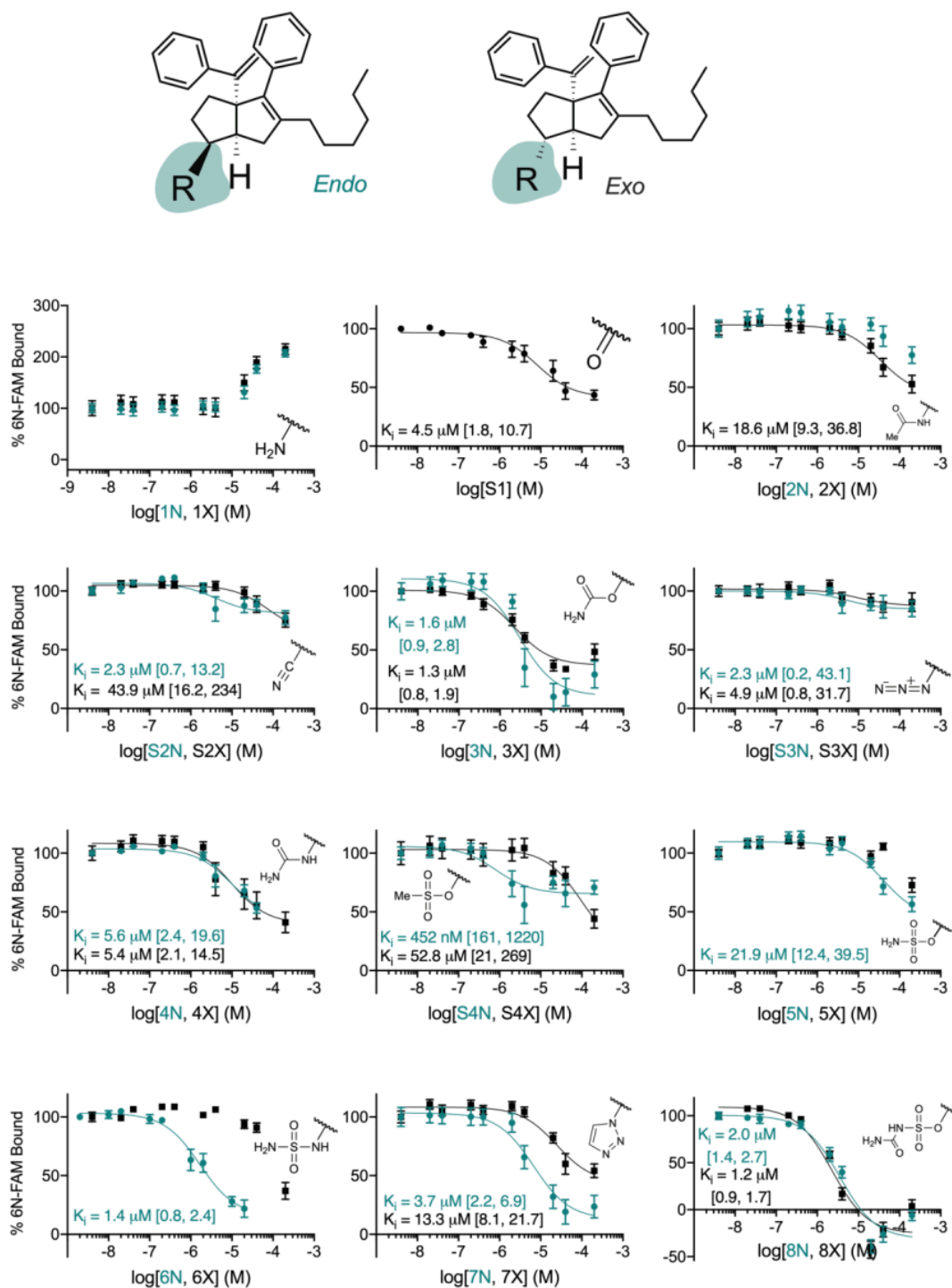


Figure S6.1. SF-1 binding to R¹ compounds. Curves for SF-1 binding to R¹ compounds are shown, with *endo* stereoisomers of the R¹ substituent in teal and *exo* stereoisomers in black. Experiments analyzed in Graphpad Prism, v7 using a one-site fit K_i curve (n=8). 95% confidence are reported for each K_i value; curves are not shown if confidence intervals or K_i values could not be calculated. Error bars are shown as SEM.

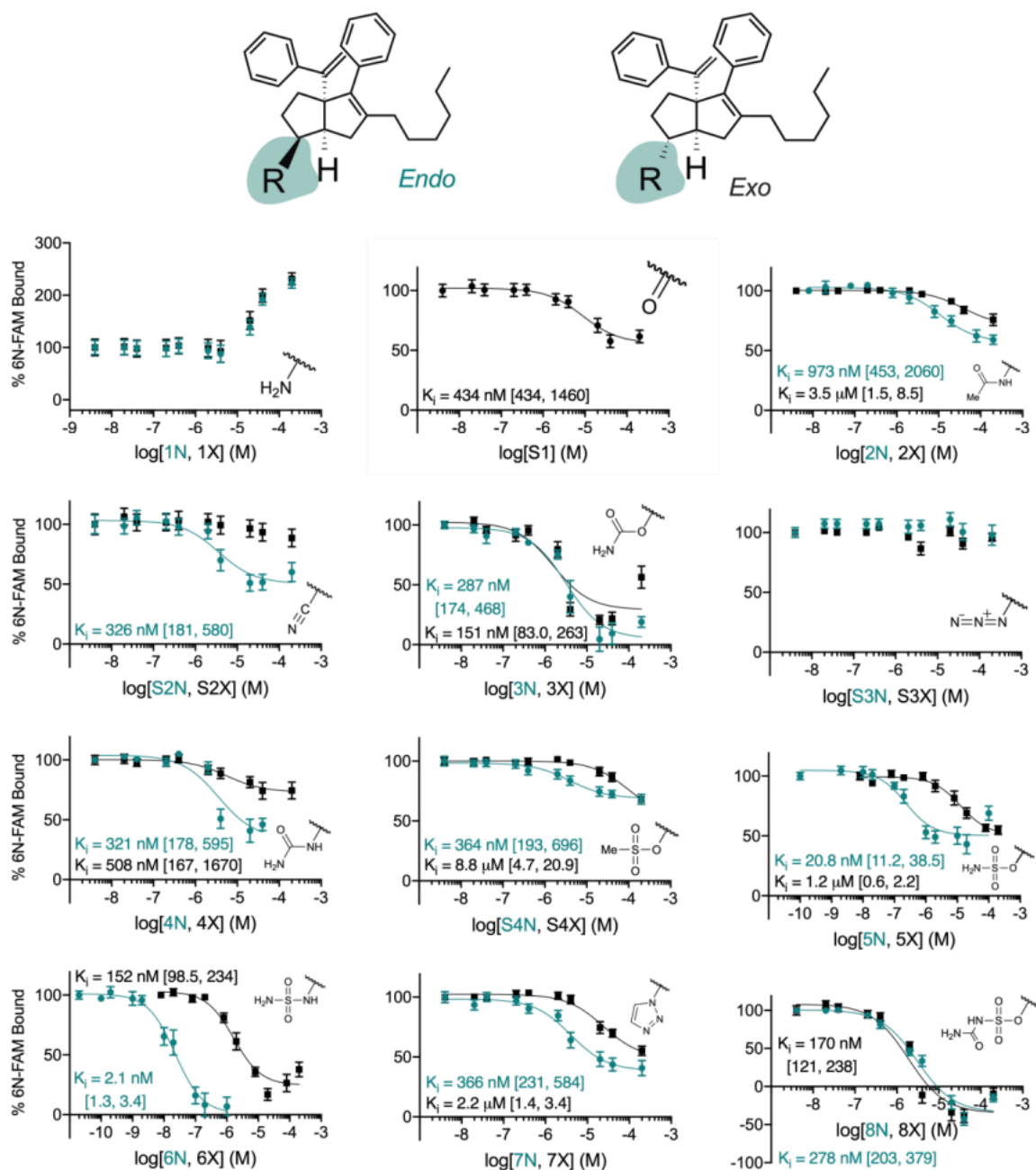


Figure S6.2. LRH-1 binding to R¹ compounds. Curves for LRH-1 binding to R¹ compounds are shown, with *endo* stereoisomers of the R¹ substituent in teal and *exo* stereoisomers in black. Experiments were analyzed in Graphpad Prism, v7 using a one-site fit K_i curve (n=8). 95% confidence are reported for each K_i value; curves are not shown if confidence intervals or K_i values could not be calculated. Error bars are shown as SEM.

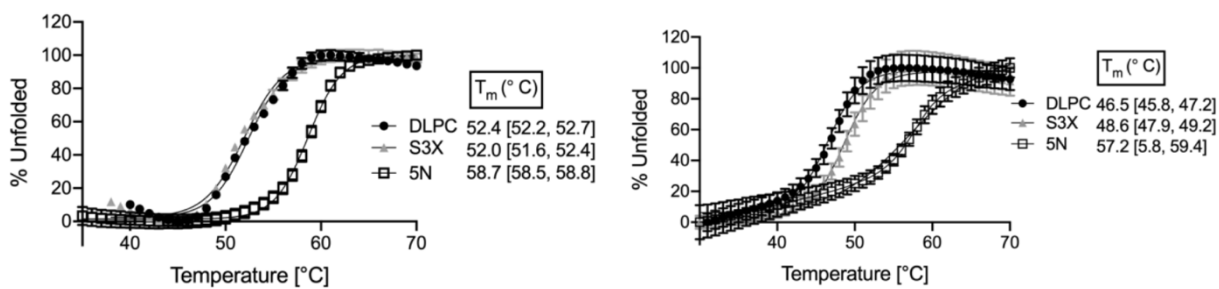


Figure S6.3. Representative thermal shift curves. Left, SF-1; right, LRH-1. Representative melting curves for DLPC and two synthetic agonists are shown. **S3X** stabilizes LRH-1, but not SF-1, whereas **5N** stabilizes both receptors. Experiments were analyzed in Graphpad Prism, v7 using the Boltzman equation ($n=9$). 95% confidence intervals are shown for each T_m value; error bars are shown as SEM.

LRH-1: Summary and Future Directions

To achieve precise control of inflammation in the gastrointestinal (GI) tract, we aimed to develop small molecule medicines that will define a new mode of action where activation of native anti-inflammatory machinery will restore intestinal health. Liver Receptor Homolog-1 (LRH-1) is a nuclear receptor that is expressed in the intestinal epithelium and has been recognized to maintain epithelial integrity and protect against inflammatory damage. Therefore, in the context of IBD, we hypothesized that upregulation of LRH-1's transcriptional activity will drive steroid production only at the site of inflammation. This will allow us to recapitulate the powerful protective anti-inflammatory effects of steroid treatment without the complications associated with systemic steroid delivery or global immunosuppression.

One of the major challenges associated with developing effective synthetic LRH-1 activators stems from the large and hydrophobic nature of the protein's ligand binding site. Using the previous best LRH-1 agonist, RJW100, we have studied the structure (via crystallography) and mechanism (via biochemical assays) of LRH-1 activation over the past few years.

Guided by early results from these efforts, we have undertaken an extensive structure-guided structure-activity relationship (SAR) study, based around a common hexahydropentalene scaffold. We have designed, synthesized, and evaluated compounds that make stabilizing contacts deep in the binding pocket of LRH-1, resulting in compound **6N** (which drives potency against LRH-1). In addition, we have developed a series of hybrid compounds that engage multiple regions of the LRH-1 ligand binding pocket in a completely new way: exemplified by compound **10CA**. These 'phospholipid mimics' display robust activation of LRH-1, achieving levels of LRH-1 transcriptional activity that were additive of DLPC and RJW100. The combination of both these

pharmacophores culminated in compound **6N-10CA**. This compound not only is the most potent agonist for LRH-1 to date, it induces high levels of LRH-1 transcriptional activity. All three compounds (**6N**, **10CA**, and **6N-10CA**) were interrogated using a combination of structural and biological studies. We found that our rational design approach positioned ligands in a consistent orientation in the binding pocket, as seen by the crystal structures of each of our compounds, which was extraordinarily enabling for the development of new LRH-1 agonists. We investigated **10CA** and **6N** in enteroids and found they drove transcription of anti-inflammatory genes. **10CA** was evaluated in a model of colitis induced by DSS, and was found to not only be tolerated, but reversed intestinal tissue damage in mice.

Building on the scaffold of **6N** and **10CA**, we also developed a sensitive fluorescent probe for polarization-based assays, which will greatly expedite future efforts to identify compounds that bind in the LBD of LRH-1 and its closest homologue, SF-1.

This work has been uniquely and powerfully enabling for the interrogation of LRH-1 biology and, crucially, the validity of LRH-1 as a drug target in a number of different contexts.

Part 2: Arene Dearomatization

A Call for Improved Dearomative Technologies.

Most drugs developed in the last 30 years contain or are comprised primarily of aromatic units.⁷⁴ This is largely due to the ease with which arene subunits can be synthesized, installed, and modified. Powerful technologies for the synthetic manipulation of aromatic petroleum resources (*i.e.* benzene, toluene, xylenes) have led to a deep pool of commercial aryl building blocks: arene nitration and subsequent reduction, diazotization, and Sandmeyer chemistry can deliver a wide range of aryl building blocks with excellent fidelity. The use of these building blocks to produce agrochemicals and pharmaceuticals has been particularly enabled by the extensive development of palladium catalyzed cross-coupling reactions (Suzuki-Miyaura, Buchwald-Hartwig, etc.), ionic aromatic substitution and C-H functionalization strategies.⁷⁵ The combination of easily accessible, cheap chemical precursors with reliable transformations has formed the landscape of drug discovery. However, the three-dimensional nature of enzymatic architecture often demands equally three-dimensional ligands, and in fact, it has recently been noted that compounds with many sp^3 carbons perform better in later stages of drug development and clinical trials.⁷⁶ However, highly three-dimensional scaffolds are more difficult and expensive to assemble from feedstocks,

⁷⁴ Mao, F.; Ni, W.; Xu, X.; Wang, H.; Wang, J.; Ji, M.; Li, J. Chemical Structure-Related Drug-like Criteria of Global Approved Drugs. *Molecules* **2016**, *21* (1), 1–18

⁷⁵ (a) Magano, J.; Dunetz, J. R. Large-Scale Applications of Transition Metal-Catalyzed Couplings for the Synthesis of Pharmaceuticals. *Chem. Rev.* **2011**, *111* (3), 2177–2250 (b) Watson, W. Transition Metal-Catalyzed Couplings in Process Chemistry: Case Studies from the Pharmaceutical Industry. *Org. Process Res. Dev.* **2014**, *18* (1), 277 (c) Devendar, P.; Qu, R.-Y.; Kang, W.-M.; He, B.; Yang, G.-F. Palladium-Catalyzed Cross-Coupling Reactions: A Powerful Tool for the Synthesis of Agrochemicals. *J. Agric. Food Chem.* **2018**, *66* (34), 8914–8934 (d) King, A. O.; Yasuda, N. Palladium-Catalyzed Cross-Coupling Reactions in the Synthesis of Pharmaceuticals BT - Organometallics in Process Chemistry; Springer Berlin Heidelberg: Berlin, Heidelberg, 2004; pp 205–245 (e) Ruiz-Castillo, P.; Buchwald, S. L. Applications of Palladium-Catalyzed C–N Cross-Coupling Reactions. *Chem. Rev.* **2016**, *116* (19), 12564–12649

⁷⁶ (a) Lovering, F.; Bikker, J.; Humblet, C. Escape from Flatland: Increasing Saturation as an Approach to Improving Clinical Success. *J. Med. Chem.* **2009**, *52* (21), 6752–6756 (b) Meyers, J.; Carter, M.; Mok, N. Y.; Brown, N. On the Origins of Three-Dimensionality in Drug-like Molecules. *Future Med. Chem.* **2016**, *8* (14), 1753–1767 (c) Kingwell, K. Exploring the Third Dimension. *Nat. Rev. Drug Discov.* **2009**, *8* (12), 931

so there is a demand for synthetic technologies that readily deliver sp^3 -rich scaffolds from abundant aromatic precursors.

In this vein, overcoming thermodynamic aromatic stabilization remains a key challenge. Aromatic units are reliable in cross-coupling and other (sometimes harsh) derivatization steps namely because of their remarkable stability.⁷⁷ Effective tools for dearomatization include high-pressure hydrogenation,⁷⁸ Birch reduction/alkylation,⁷⁹ and enzymatic oxidation.⁸⁰ In addition, an array of reactions that utilize phenols,⁸¹ photochemical arene cycloaddition,⁸² or other catalytic methods⁸³ have also been employed.

To facilitate rapid drug synthesis for compound containing sp^3 centers, we aimed to develop novel methods for the construction of complex three-dimensional architectures from aromatic systems.

⁷⁷ Wertjes, W. C.; Southgate, E. H.; Sarlah, D. Recent Advances in Chemical Dearomatization of Nonactivated Arenes. *Chem. Soc. Rev.* **2018**, *47* (21), 7996–8017

⁷⁸ Stanislaus, A.; Cooper, B. H. Aromatic Hydrogenation Catalysis: A Review. *Catal. Rev.* **1994**, *36* (1), 75–123

⁷⁹ (a) Birch, A. J. 117. Reduction by Dissolving Metals. Part I. *J. Chem. Soc.* **1944**, No. 430, 430 (b) Rabideau, P. W. The Birch Reduction of Aromatic Compounds. *Org. React.* **1992**, *42*, 1–334

⁸⁰ (a) Hudlicky, T.; Olivo, H. F.; McKibben, B. Microbial Oxidation of Aromatics in Enantiocontrolled Synthesis. 3. 1 Design of Amino Cyclitols (Exo-Nitrogenous) and Total Synthesis of (+)-Lycoricidine via Acylnitrosyl Cycloaddition to Polarized 1-Halo-1, 3-Cyclohexadienes. *J. Am. Chem. Soc.* **1994**, *116* (12), 5108–5115 (b) Boyd, D. R.; Bugg, T. D. H. Arene Cis-Dihydrodiol Formation: From Biology to Application. *Org. Biomol. Chem.* **2006**, *4* (2), 181–192

⁸¹ Pouységu, L.; Deffieux, D.; Quideau, S. Hypervalent Iodine-Mediated Phenol Dearomatization in Natural Product Synthesis. *Tetrahedron* **2010**, *66* (13), 2235–2261

⁸² (a) Cornelisse, J. The Meta Photocycloaddition of Arenes to Alkenes. *Chem. Rev.* **1993**, *93* (2), 615–669 (b) Okumura, M.; Nakamata Huynh, S. M.; Pospech, J.; Sarlah, D. Arenophile-Mediated Dearomative Reduction. *Angew. Chem. Int. Ed.* **2016**, *55* (51), 15910–15914

⁸³ (a) Zhuo, C. X.; Zhang, W.; You, S. L. Catalytic Asymmetric Dearomatization Reactions. *Angew. Chem. Int. Ed.* **2012**, *51* (51), 12662–12686 (b) Zheng, C.; You, S. L. Catalytic Asymmetric Dearomatization by Transition-Metal Catalysis: A Method for Transformations of Aromatic Compounds. *Chem* **2016**, *1* (6), 830–857

Principles of Photochemistry

Photochemical reactions harness photonic energy (from light) and transform it into electronic energy to drive a specific transformation. All organic molecules all have the ability to absorb specific wavelengths of light—that is, translate the energy from a photon (if it matches an energy gap between the HOMO and an unoccupied orbital) to promote an electron from a filled orbital into a higher energy empty antibonding orbital. This process can transform a previously stable molecule into a highly reactive one.

Direct photoexcitation of organic molecules in this fashion has been a powerful strategy for chemical synthesis since the 1800s,⁸⁴ however, direct photoexcitation is limited: by definition, the wavelength of light *must* match an absorption maxima in the compound to be excited,⁸⁵ limiting the scope and generalizability of a process and many conjugated organic compounds have similar absorption profiles,⁸⁶ leading to nonselective excitation.

The strategy to overcome these limitations lies in the development of *photoredox catalysts*. These molecules act as a mediator between light energy and electronic energy and are specifically designed to absorb wavelengths of light that most organic molecules do not (Fig. 7.1A). For example, the metal-centered tris(bipyridine)ruthenium(II) chloride absorbs blue light (450 nm) while most organic molecules do not absorb in this region.⁸⁷ The excited state of this photocatalyst

⁸⁴ (a) Trommsdorf, *Ann. Chem. Pharm.* **1834**, 11 (b) Roth, H. D. *Angew. Chem., Int. Ed. Engl.* **1989**, *28*, 1193 (c) Garcia-Garibay, M. A. *Acc. Chem. Res.* **2003**, *36*, 491.

⁸⁵ Baird, C. S. *Absorption of Electromagnetic Radiation*. McGraw-Hill Education February 27, 2019

⁸⁶ John D. Robert and Marjorie C. Caserio, **1977**, *Basic Principles of Organic Chemistry, Second Edition*. W. A. Benjamin, Inc.

⁸⁷ Select reviews on Ru(bpy)₃²⁺ as a photoredox catalyst: (a) Flamigni, L.; Barieri, A.; Sabatini, C.; Ventura, B.; Barigelletti, F. *Top. Curr. Chem.* **2007**, *281*, 143. (b) Campagna, S.; Puntoriero, F.; Nastasi, F.; Bergamini, G.; Balzani, V. *Top. Curr. Chem.* **2007**, *280*, 117 (c) Tucker, J. W.; Stephenson, C. R. J. *Shining Light on Photoredox Catalysis: Theory and Synthetic Applications. J. Org. Chem.* **2012**, *77* (4), 1617–1622

can then undergo a process called intersystem crossing, which gives a triplet excited state (Fig. 7.1B). This entire process allows the translation of photonic energy into electronic.

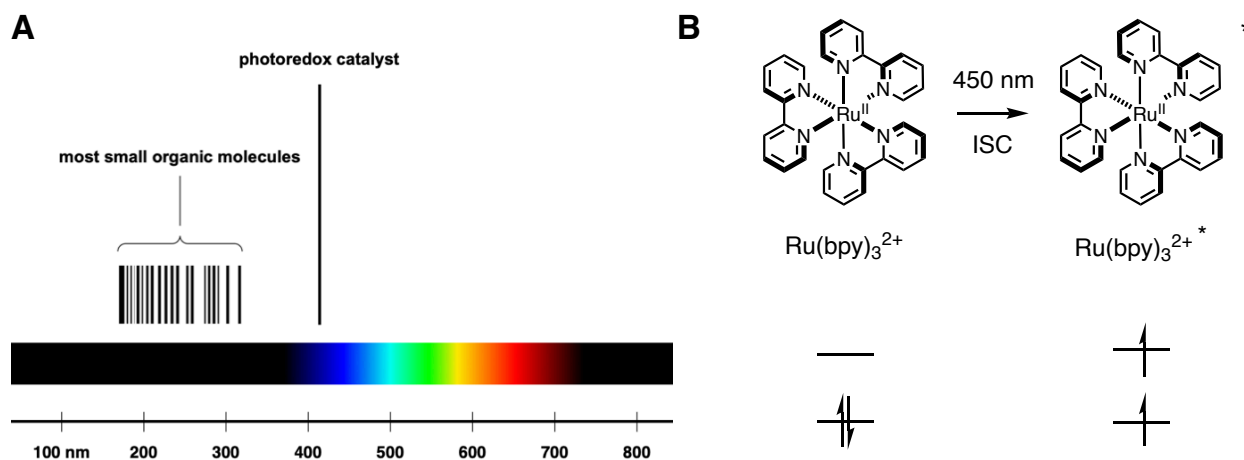


Figure 7.1 The principles of photoredox catalysis. (A) Photoredox catalysts absorb outside of the range of most small organic molecules. (B) An example of a photoredox catalyst: $\text{Ru}(\text{bpy})_3^{2+}$ absorbs blue light to reach its triplet excited state.

Photocatalytic triplet excited states are long-lived and can act both as reductants (by donating an electron) and oxidants (by accepting an electron). For example (Fig. 7.2), $\text{Ru}(\text{bpy})_3^{2+*}$ has a reduction potential of -0.81 V vs. SCE and an oxidation potential of 0.77 V vs. SCE. If the excited state $\text{Ru}(\text{bpy})_3^{2+*}$ loses an electron while reducing a species, (Fig. 7.2, termed oxidative quenching) it in turn becomes an even more potent oxidant ($E_{1/2}^{\text{II/III}} = 1.29$ V vs. SCE). If the opposite process occurs (reductive quenching) it becomes a highly potent reductant ($E_{1/2}^{\text{III/I}} = -1.33$ V vs. SCE). Chemists have taken advantage of these quenching processes to access the desired reactivity of photocatalysts by employing sacrificial oxidants or reductants—the ideal identify of

these are compounds that do not interfere with the desired reactivity and form easily removable byproducts.⁸⁸

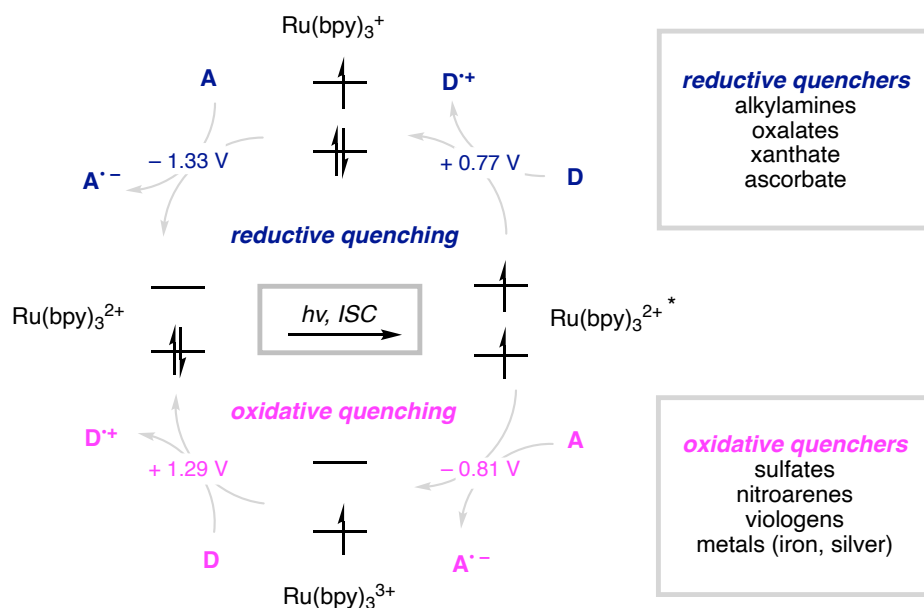


Figure 7.2. Photocatalytic quenching pathways, and common sacrificial oxidants and reductants.

Though rare earth metal-centered photoredox catalysts (ruthenium, iridium)⁸⁹ and other earth-abundant metal-centered catalysts (Cu^{I} , Zn^{II} , Ni^0 , V^{V} , Zr^{IV} , $\text{W}^{0, \text{IV}}$, Mo^0 , Cr^{III} , Co^{III} , Fe^{II})⁹⁰ have been commonplace and are well understood, recently there has been momentum in designing small organic molecules as photoredox catalysts. These catalysts operate similarly to metal-

⁸⁸ McAtee, R. C.; McClain, E. J.; Stephenson, C. R. J. Illuminating Photoredox Catalysis. *Trends Chem.* **2019**, *1* (1), 111–125

⁸⁹ Prier, C. K.; Rankic, D. A.; MacMillan, D. W. C. Visible Light Photoredox Catalysis with Transition Metal Complexes: Applications in Organic Synthesis. *Chem. Rev.* **2013**, *113* (7), 5322–5363

⁹⁰ Hockin, B. M.; Li, C.; Robertson, N.; Zysman-Colman, E. Photoredox Catalysts Based on Earth-Abundant Metal Complexes. *Catal. Sci. Technol.* **2019**, *9* (4), 889–915

centered photoredox catalysts, but are typically highly modular, tunable, cheaper, and more environmentally sustainable (some common classes are summarized in Fig. 7.3).⁹¹

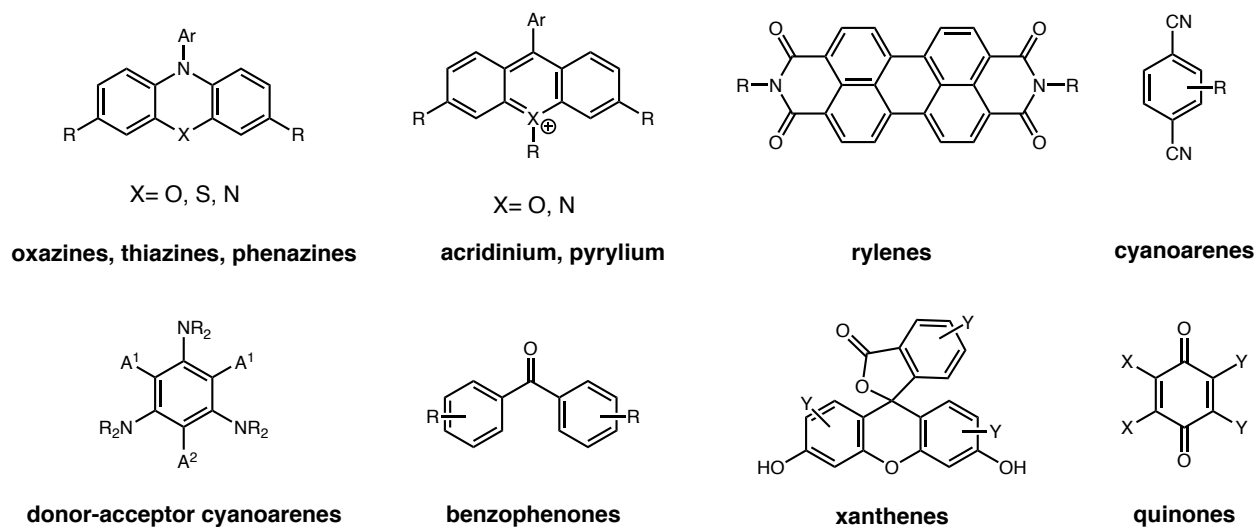


Figure 7.3. Structures of organic photoredox catalyst classes

Harnessing light energy for difficult organic transformations would be an impactful approach for organic transformations, and as such we aimed to develop sustainable and safe protocols for the reduction of aromatic units using visible light.

⁹¹ Romero, N. A.; Nicewicz, D. A. Organic Photoredox Catalysis. *Chem. Rev.* **2016**, *116* (17), 10075–10166

Chapter 7: Dearomatization via Radical Hydroarylation

Adapted and Reprinted in part from a preprint deposited at ChemRxiv
doi.org/10.26434.chemrxiv.9874454.v1

https://chemrxiv.org/articles/Arene_Dearomatization_via_Radical_Hydroarylation/9874454

7.1 Our Aromatic Functionalization Space

We have previously contributed to the growing number of aromatic functionalization reactions: our group has developed a series of photocatalytic hydroarylation systems that selectively engage a diverse series of olefinic substrates.⁹² A key element of this program arises from the understanding that catalytic single electron reduction can be generally employed to deliver highly reactive aryl radicals from the corresponding halides. Chemoselective olefin addition followed by a reduction event gives rise to the hydroarylation products with complete regiocontrol, a hallmark characteristic of Giese-type processes.⁹³ We questioned whether this mechanistic paradigm could be applied to aromatic substrates, where benzenoids would react to afford aryl cyclohexadiene derivatives. Because a vast array of olefin functionalization protocols have been developed,⁹⁴ this strategy would be attractive for the synthesis of highly-complex cyclohexane derivatives, particularly if it was safe (no hazardous or toxic reagents), economical (e.g. no precious metals), and sustainable (e.g. no stoichiometric metal waste, green solvent). Most important to us was developing a *predictable and selective* approach to dearomative hydroarylation. Ideally, this protocol would function on a range of arene substrates, such that the resulting diene olefins would be differentially reactive, allowing for selective elaboration of the carbon skeleton.

⁹² (a) Boyington, A. J.; Riu, M. L. Y.; Jui, N. T. Anti-Markovnikov Hydroarylation of Unactivated Olefins via Pyridyl Radical Intermediates. *J. Am. Chem. Soc.* **2017**, *139* (19), 6582–6585 (b) Seath, C. P.; Vogt, D. B.; Xu, Z.; Boyington, A. J.; Jui, N. T. Radical Hydroarylation of Functionalized Olefins and Mechanistic Investigation of Photocatalytic Pyridyl Radical Reactions. *J. Am. Chem. Soc.* **2018**, *140* (45), 15525–15534 (c) Boyington, A. J.; Seath, C. P.; Zearfoss, A. M.; Xu, Z.; Jui, N. T. Catalytic Strategy for Regioselective Arylethylamine Synthesis. *J. Am. Chem. Soc.* **2019**, *141* (9), 4147–4153 (d) Aycock, R. A.; Wang, H.; Jui, N. T. A Mild Catalytic System for Radical Conjugate Addition of Nitrogen Heterocycles. *Chem. Sci.* **2017**, *8* (4), 3121–3125 (e) Aycock, R. A.; Vogt, D. B.; Jui, N. T. A Practical and Scalable System for Heteroaryl Amino Acid Synthesis. *Chem. Sci.* **2017**, *8* (12), 7998–8003

⁹³ Giese, B. Formation of C-C Bonds by Addition of Free Radicals to Alkenes. *Angew. Chem. Int. Ed. English* **1983**, *22* (10), 753–764

⁹⁴ (a) Cristina Silva Costa, D. Additions to Non-Activated Alkenes: Recent Advances. *Arab. J. Chem.* **2017** (b) Dong, Z.; Ren, Z.; Thompson, S. J.; Xu, Y.; Dong, G. Transition-Metal-Catalyzed C-H Alkylation Using Alkenes. *Chem. Rev.* **2017**, *117* (13), 9333–9403

7.2 Dearomative Hydroarylation Design Strategy

Although aromatic systems experience significant thermodynamic stabilization, aromaticity is routinely broken (in a transient sense) in aromatic substitution pathways that operate through anionic,⁹⁵ cationic,⁹⁶ and radical intermediates.⁹⁷ Indeed, upon functionalization (bond-formation) within each of these mechanisms, aromaticity is rapidly restored. Within the radical pathway (i.e. Minisci radical arylation), this event typically involves an oxidation/deprotonation sequence.⁹⁸ To circumvent the thermodynamic well of rearomatization, we envisioned a radical-polar crossover mechanism that would involve reductive interception of a transient radical species to form corresponding anions, followed by quenching. Building on previous results from our lab and inspired by work from others,⁹⁹ we considered the dearomative cyclization of linear diaryl compounds. If successful, this approach would afford spirocyclic cyclohexadienes, a desirable general scaffold that is present in a range of molecules with diverse biological activities.¹⁰⁰ For

⁹⁵ Kwan, E. E.; Zeng, Y.; Besser, H. A.; Jacobsen, E. N. Concerted Nucleophilic Aromatic Substitutions. *Nat. Chem.* **2018**, *10* (9), 917–923

⁹⁶ Galabov, B.; Nalbantova, D.; Schleyer, P. V. R.; Schaefer, H. F. Electrophilic Aromatic Substitution: New Insights into an Old Class of Reactions. *Acc. Chem. Res.* **2016**, *49* (6), 1191–1199

⁹⁷ Scaiano, J. C.; Stewart, L. C. Phenyl Radical Kinetics. *J. Am. Chem. Soc.* **1983**, *105* (11), 3609–3614

⁹⁸ Minisci, F.; Bertini, F.; Galli, R.; Perchinijmmo, M. Nucleophilic Character of Alkyl Radicals–VI: A New Convenient Selective Alkylation of Heteroaromatic Bases. *Tetrahedron* **1971**, *27*, 3575–3579.

⁹⁹ (a) Jones, G. H.; Perkins, M. J. Internuclear Cyclisation. Part XXVI. Photolysis of 2-Iodo-N-Methyl-Benzanilide in Benzene. *J. Chem. Soc.* **1971**, No. 116, 116–122 (b) Collington, D. M.; Hey, D. H.; Rees, C. . Internuclear Cyclisation. Part XXIII. Formation and Rearrangement of 2-Methylisindoline-1 -Spirocyclohexa-2',5'-Diene-3,4'-Dione. Synthesis of the Octahydro-Derivative of an Unsaturated Dimer. *J. Chem. Soc.* **1968**, 1017–1020 (c) Escolano, C.; Jones, K. Aryl Radical Cyclisation onto Pyrroles: A Divergent Synthesis of Spiropyrrolidinyloxindoles and Pyrroloquinolines. *Tetrahedron Lett.* **2000**, *41* (46), 8951–8955 (d) Núñez, A.; Sánchez, A.; Burgos, C.; Alvarez-Builla, J. Pyridinium N-2'-Pyridylaminide: Radical Cyclization for the Synthesis of Benzonaphthyridine Derivatives. *Tetrahedron* **2007**, *63* (29), 6774–6783 (e) Crich, D.; Hao, X.; Lucas, M. A. Inhibition of Stannane-Mediated Radical Rearrangements by a Recoverable, Minimally Fluorous Selenol. *Org. Lett.* **1999**, *1* (2), 269–271 (f) Zhang, W.; Pugh, G. Free Radical Reactions for Heterocycle Synthesis. Part 5: Formation of Novel Bridged Spirolactones by Double Cyclizations. *Tetrahedron Lett.* **2001**, *42* (33), 5617–5620 (g) Bowman, W. R.; Storey, J. M. D. Synthesis Using Aromatic Homolytic Substitution - Recent Advances. *Chem. Soc. Rev.* **2007**, *36* (11), 1803–1822

¹⁰⁰ Sveiczzer, A.; North, A. J. P.; Mateu, N.; Kidd, S. L.; Sore, H. F.; Spring, D. R. Spirocycles as Rigidified Sp³-Rich Scaffolds for a Fragment Collection. *Org. Lett.* **2019**, *21* (12), 4600–4604

example, the spiro-fused dihydro-benzofuran, -indoline, and -oxindoles (Fig. 7.4) are effective modulators of cancer and obesity-associated targets.¹⁰¹

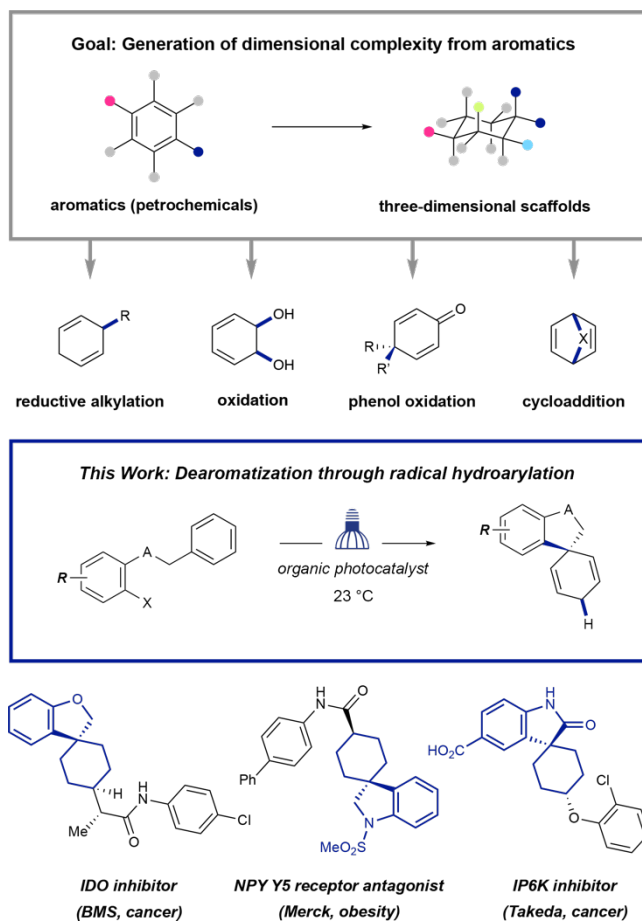


Figure 7.4. Dearomative radical hydroarylation strategy

¹⁰¹ (a) Terao, Y.; Takahashi, M.; Hara, R.; Hidaka, K.; Furukawa, H.; Yamasaki, T.; Kasai, S. Takeda Pharmaceutical Company Limited. IP6K Inhibitors. International Publication No. WO 2018/182051 A1. October, 4, **2018** (b) Sakamoto, T.; Moriya, M.; Haga, Y.; Takahashi, T.; Shibata, T.; Okamoto, O.; Nonoshita, K.; Kitazawa, H.; Hidaka, M.; Gomori, A.; Iwaasa, H.; Ishihara, A.; Kanatani, A.; Fukami, T.; Gao, Y. D.; MacNeil, D. J.; Yang, L. Identification of Novel and Orally Active Spiroindoline NPY Y5 Receptor Antagonists. *Bioorganic Med. Chem. Lett.* **2009**, *19* (6), 1564–1568. (c) Gao, Y.D.; Macneil, D.J.; Morin, N.R.; Fukami, T.; Kanatani, A.; Fukuroda, T. Ishii, Y.; Morin, M. Merck & Co., Inc. Spiro-indolines as Y5 Receptor Antagonists. International Publication No. WO 00/27845, May, 18, **2000**. (d) Seitz, S.P.; Cherney, E. C.; Zhu, X. Bristol-Myers Squibb Company. Inhibitors of Indoleamine 2,3- Dioxygenase and Methods of Their Use. International Publication No. WO 2019/074824 A1. April, 18, **2019**

We envisioned the catalytic blueprint shown in Figure 7.5A, where reduction of aryl iodide **1** would deliver aryl radical **2** via rapid mesolytic cleavage. Favored 5-*exo*-trig cyclization¹⁰² would generate cyclohexadienyl radical **3** which, after a second sequential reduction event ($E_{1/2}^{\circ} = -1.34$ V vs. SCE, see Supporting Information for details), would give rise to dienyl anion **4**. Finally, a protonation event would deliver the desired dearomatized spirocycle **5**.

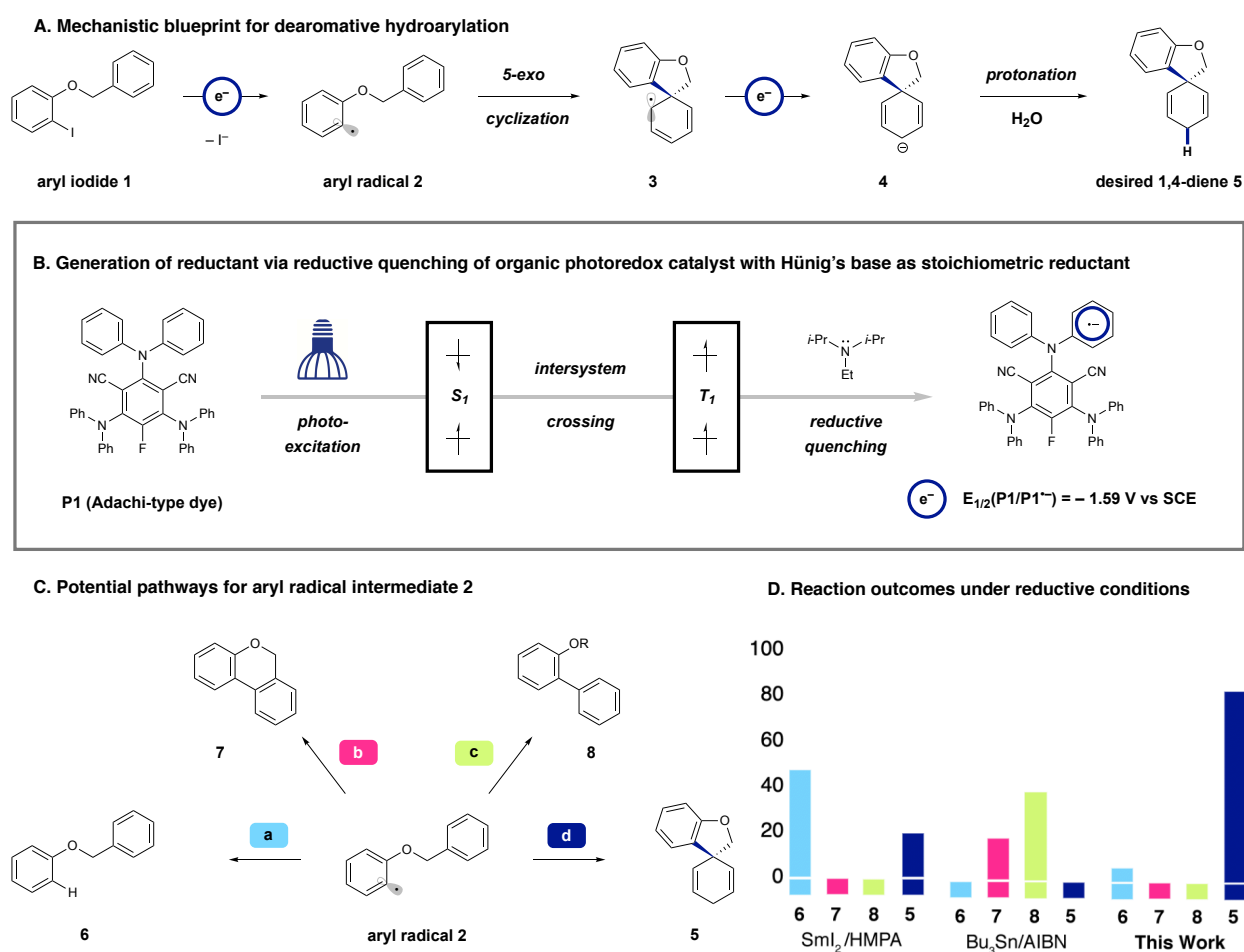


Figure 7.5. Design of dearomative spirocyclization reaction and support for each component. (A) Proposed arene hydroarylation mechanism to give spirocyclic 1,4-cyclohexadienes. (B) Generation of a catalytic reductant through reductive quenching with Hünig's base. (C) Demonstrated reaction pathways for aryl radical **2**. (D) Comparison of previously demonstrated reaction conditions with those described here.

¹⁰² Baldwin, B. J. E. Rules For Ring Closure. *J. Chem. Soc. Chem. Commun.* **1976**, 734–736

Crucial to this design would be identification of an effective system where constant generation of reductant would allow for this two-electron sequential reduction pathway. We found that in aqueous acetonitrile, several photocatalyst/stoichiometric reductant pairs are able to deliver the desired product (see Supporting Information for details). We found the most generally effective system to involve the Adachi-type¹⁰³ donor-acceptor cyanoarene 3DPAFIPN (**P1**, 5 mol%), *i*-Pr₂NEt (Hünig's base, 3 equiv), and commercial 15 W blue LEDs. As shown in Figure 7.5B, this proposal involves photoexcitation of **P1**, which undergoes intersystem crossing and facile reductive quenching with *i*-Pr₂NEt. Stern-Volmer quenching studies revealed that this quenching mechanism is fast under these conditions ($K_{SV} = \sim 1700$), giving rise to the ground state reductant ($P1^{\bullet-}$, $E_{1/2}^{\circ} = -1.59$ V vs. SCE).^{103b} This protocol for catalytic reductant generation is appealing, in part, because it utilizes inexpensive and readily accessible components to perform challenging substrate reduction under mild conditions.

7.3 Key Differences and Assets to Photochemical Dearomative Hydroarylation

While radical intermediate **2** has been accessed before, there are a number of competing reaction pathways that have been demonstrated. As indicated in Figure 7.5C, hydrodehalogenation of this radical species (pathway a) would give rise to arene **6**. Biaryl species **7** and **8** have also been produced through reductive formation of **2**, presumably through the desired 5-*exo* cyclization followed by neophyl rearrangement (pathway b) or fragmentation (pathway c), respectively. While treatment of **1** with SmI₂/HMPA was shown to deliver the desired product **5** as a mixture of

¹⁰³ (a) Uoyama, H.; Goushi, K.; Shizu, K.; Nomura, H.; Adachi, C. Highly Efficient Organic Light-Emitting Diodes from Delayed Fluorescence. *Nature* **2012**, *492* (7428), 234–238 (b) Speckmeier, E.; Fischer, T. G.; Zeitler, K. A Toolbox Approach To Construct Broadly Applicable Metal-Free Catalysts for Photoredox Chemistry: Deliberate Tuning of Redox Potentials and Importance of Halogens in Donor-Acceptor Cyanoarenes. *J. Am. Chem. Soc.* **2018**, *140* (45), 15353–15365

regioisomers, the major product under these conditions was the reduction product **6** (Fig. 7.5D) and attempts to generalize the reaction conditions across a panel of substrates gave inconsistent outcomes.¹⁰⁴ Atom-transfer conditions using Bu₃SnH/AIBN lead to arylation byproducts **7** and **8**.¹⁰⁵ In contrast, treating **1** with the photochemical conditions described here afford the desired dearomatized products with excellent selectivity (pathway d). The observed chemoselectivity under the photoreductive conditions described here is due to the constant generation of a catalytic amount of reductant, in contrast to abstracting conditions¹⁰⁵ or conditions that employ superstoichiometric amounts of reductant (samarium,^{104,104} electrochemical cell¹⁰⁶). This effectively suppresses undesired hydrodehalogenation through pathway a (when sequential reductions occur before dearomative spirocyclization) as well as eliminating undesired byproducts from inefficient trapping of radical intermediate **3** (pathways b, c, Bu₃SnH/AIBN conditions).

7.4 The Scope

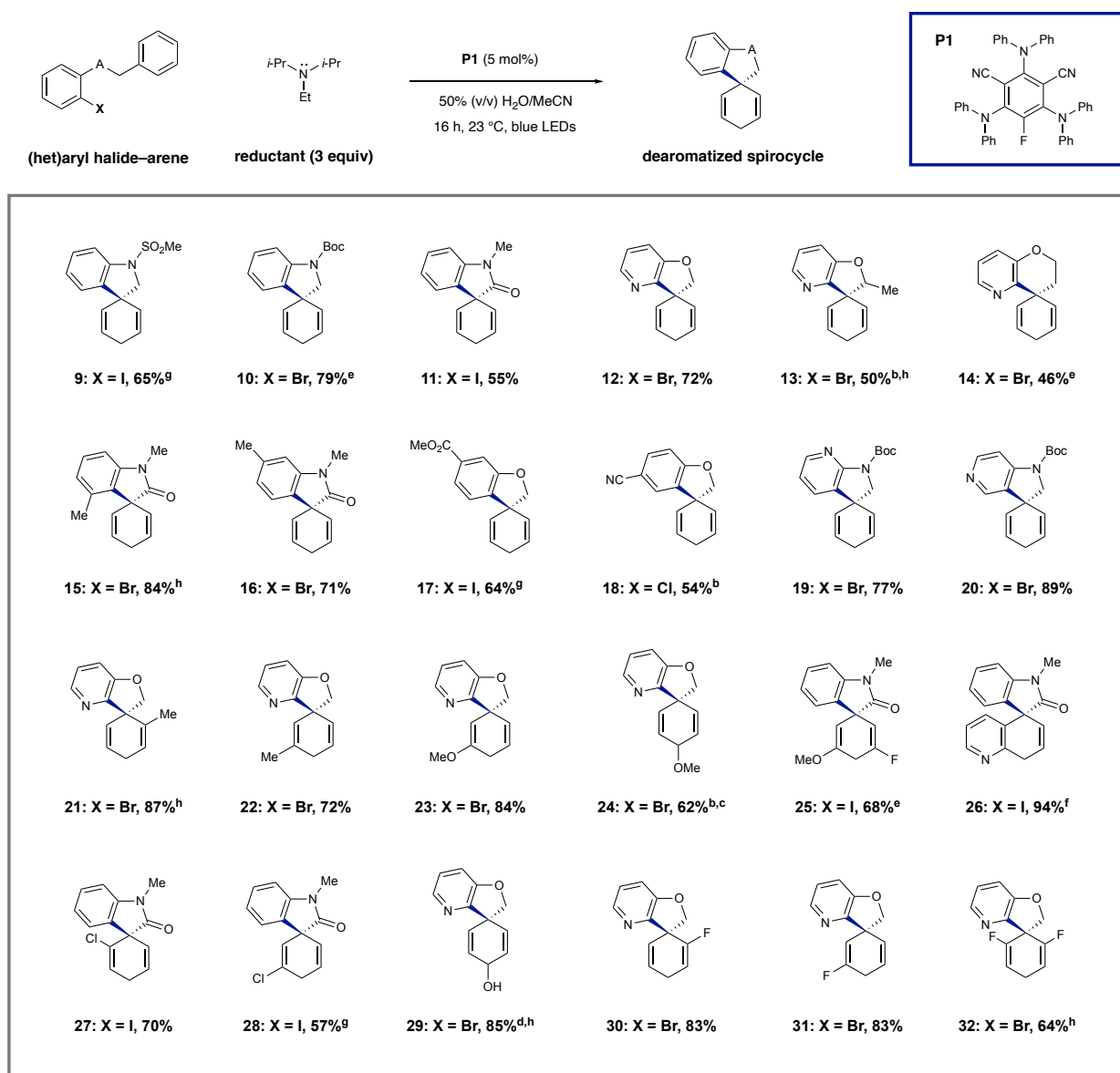
As illustrated in Table 7.1, this light-driven reaction effectively transforms a range of (hetero)aryl radical precursors with tethered aromatic radical acceptors to undergo dearomative spirocyclization. For example, the tether can be varied to give indoline derivatives **9** and **10** (65% and 79% yield, respectively). In addition, *N*-alkylated amide tethers (**11**, 55%) and ether linkers

¹⁰⁴ (a) Iwasaki, H.; Eguchi, T.; Tsutsui, N.; Ohno, H.; Tanaka, T. Samarium(II)-Mediated Spirocyclization by Intramolecular Aryl Radical Addition onto an Aromatic Ring. *J. Org. Chem.* **2008**, *73* (18), 7145–7152 (b) Wefelscheid, U. K.; Berndt, M.; Reißig, H. U. Samarium Diodide Mediated Ketyl-Aryl Coupling Reactions - Influence of Substituents and Trapping Experiments. *European J. Org. Chem.* **2008**, No. 21, 3635–3646 (c) Ohno, H.; Iwasaki, H.; Eguchi, T.; Tanaka, T. The First Samarium(II)-Mediated Aryl Radical Cyclisation onto an Aromatic Ring. *Chem. Commun.* **2004**, *10* (19), 2228–2229

¹⁰⁵ (a) Harrowven, D. C.; Nunn, M. I. T.; Newman, N. A.; Fenwick, D. R. A New Cascade Radical Reaction for the Synthesis of Biaryls and Triaryls from Benzyl Iodoaryl Ethers. *Tetrahedron Lett.* **2001**, *42* (5), 961–964 (b) Chen, Z. M.; Zhang, X. M.; Tu, Y. Q. Radical Aryl Migration Reactions and Synthetic Applications. *Chem. Soc. Rev.* **2015**, *44* (15), 5220–5245

¹⁰⁶ Peters, B. K.; Rodriguez, K. X.; Reisberg, S. H.; Beil, S. B.; Hickey, D. P.; Kawamata, Y.; Collins, M.; Starr, J.; Chen, L.; Udyavara, S.; Klunder, K.; Gorey, T. J.; Anderson, S. L.; Neurock, M.; Minter, S. D.; Baran, P. S. Scalable and Safe Synthetic Organic Electroreduction Inspired by Li-Ion Battery Chemistry. *Science*, **2019**, *363* (6429), 838–845

(**12**, 72%) are good substrates under these conditions. This allows further elaboration to give tethers that are either substituted (**13**, 50%), or extended to give 6-membered spirocycles (**14**, 46%). Altering the electronic properties of the aryl radical precursor was also tolerated; substrates containing either electron donating substituents (**15**, **16**) or withdrawing substituents (**17**, **18**) reacted to afford the corresponding products (54–84%). Radicals formed at the 3-position of pyridines also cyclize, giving hydroxyridylation products **19** and **20** in 77% and 89% yield, respectively.

Table 7.1. Photocatalytic Radical Hydroarylation of Aromatics: Scope of Spirocyclic Products^a

^aReaction conditions: (het)arylhalide-arene (0.5 mmol), **P1** (5 mol%), *i*-Pr₂NEt (1.5 mmol), MeCN:H₂O (1:1 v/v, 15 mL), blue LEDs, 23 °C, 16 h. Isolated yields shown. ^bReaction conducted with 10.0 equiv *i*-Pr₂NEt. ^c4:1 d.r., isolated yield of major diastereomer shown. ^d1.8:1 d.r., isolated yield of combined diastereomers shown. ^eReaction was conducted on a 0.2 mmol scale. ^fReaction was conducted on a 0.3 mmol scale, ^gReaction was conducted on a 0.4 mmol scale. ^hReaction was conducted on a 0.6 mmol scale.

The acceptor arene is also tolerant of substitution— donating substituents at the ortho, meta, or para positions dearomatize to give spirocycles **21–24** in 62–87% yield. A multi-substituted arene smoothly dearomatizes to give 1,4-cyclohexadiene **25**, which possesses two differentially reactive alkenes, in 68% isolated yield. Interestingly, quinolines can dearomatize to give a 5,8-dihydroquinoline in excellent yield (**26**, 94%). This is exciting due to the propensity for quinolines to dearomatize to 1,4-dihydroquinolines;¹⁰⁷ here we have disrupted the aromaticity of the canonically more stable aryl ring of the quinoline, complimentary to standard reductive processes. Halogenation is tolerated at the ortho (**27**, 70%; **30**, 83%) and meta positions (**28**, 57%; **31**, 83%) without any competitive dehalogenation observed. The resulting vinylic halogens are potential handles for further reactivity. When acceptor arenes with para-halogens are subjected to these conditions, they undergo the dearomative spirocyclization as expected; however, the product obtained is hydroxyl **29** (85%) which presumably arises from solvolysis of the halogenated products. This reactivity provides a direct alternative to phenol dearomatization and reduction to give allylic alcohols. A 3,5-difluorinated arene dearomatized under these conditions to spirocyclic product (**32**, 64%) without competitive observable defluorination.

7.5 Selectivity Rationale

Though we generally observed complete selectivity for the 1,4-spirocyclic diene products, a small number of amide-linked substrates also produced the corresponding phenanthridinones as minor side products (e.g. compound **33** in Fig. 7.6). These phenanthridinones presumably arise from neophyl rearrangement of the intermediate spirocyclic radical. To evaluate our hypothesis

¹⁰⁷ Von Ragué Schleyer, P.; Puhlhofer, F. Recommendations for the Evaluation of Aromatic Stabilization Energies. *Org. Lett.* **2002**, 4 (17), 2873–2876

that reductive interception of the radical intermediate mitigates competing pathways, we investigated the selectivity of the least selective amide-linked substrate in this study, which, under the conditions shown in Table 7.1, reacts to give rise to **11** and **33** in a roughly 2:1 ratio. We found that varying the equivalents of *i*-Pr₂NEt in the reaction, in turn influencing the effective concentration of reductant in the reaction, directly impacted the selectivity of the reaction. Specifically, fewer equivalents of amine results in a decrease in selectivity. Inversely, an increase in reductant concentration increases the rate of reduction of the radical intermediate, thereby limiting the ability of this intermediate to rearrange. These data are in accord with other observed aryl radical cyclization systems, where an increase in effective concentration of reductant is proportionally related to 5-*exo* cyclization versus neophyl rearrangement.¹⁰⁸

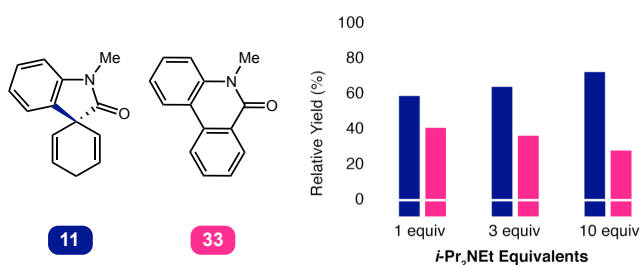


Figure 7.6. Modulation of lactam product ratios by reductant concentration.

¹⁰⁸ Chen, Z. M.; Zhang, X. M.; Tu, Y. Q. Radical Aryl Migration Reactions and Synthetic Applications. *Chem. Soc. Rev.* **2015**, *44* (15), 5220–5245

Given the net-reductive nature of this transformation, we questioned whether this reaction could be translated into an electrochemical system, and attempted to find conditions to give spirocyclic product **11** under this complementary two-electron manifold. Interestingly, preliminary results indicate this process is indeed possible. At constant current (50 mA), with Bu_4NBF_4 in acetonitrile, 8% yield of the desired product was obtained. However, hydrodehalogenation remained the major pathway under the most promising conditions (63%, see Supporting Information for details), with the remainder of the mass-balance being unreacted starting material.

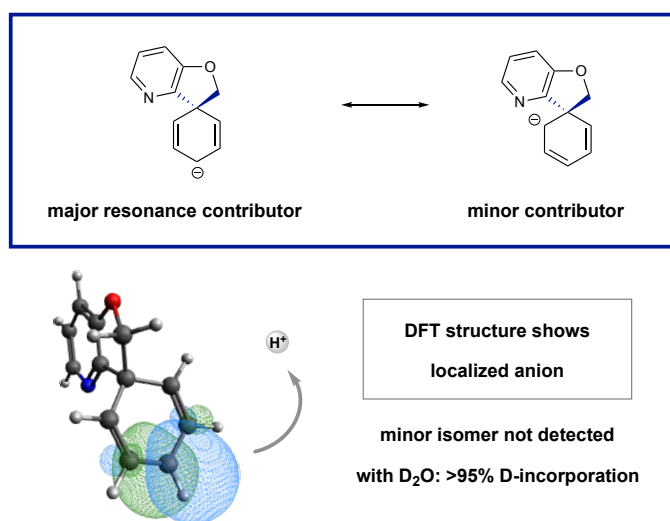


Figure 7.7. Computational structure of anion orbitals as a rationale for observed regioselectivity.

Selectivity for the 1,4-cyclohexadienyl product in our photochemical system is in accord with both previous studies on this type of anionic intermediate and DFT calculations.¹⁰⁹ The orbital that houses the lone pair is predicted to exist predominantly at the doubly allylic position (see DFT structure, Fig. 7.7). Protonation at this position gives the desired 1,4-cyclohexadienyl product, and

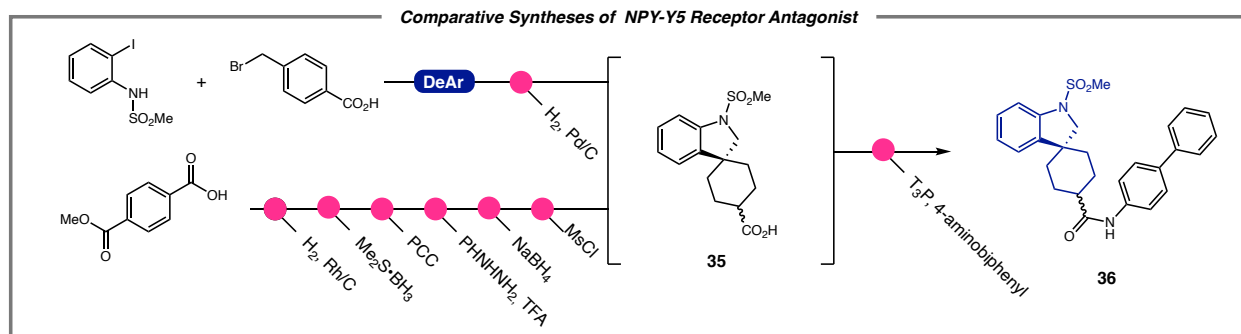
¹⁰⁹ Zimmerman, H. E. A Mechanistic Analysis of the Birch Reduction. *Acc. Chem. Res.* **2012**, *45* (2), 164–170

we have yet to detect undesired spirocyclic 1,3-cyclohexadienes. Replacement of water in our system with deuterium oxide resulted in complete (>95% by NMR) deuterium incorporation, supporting our proposed radical-polar crossover mechanism.

7.6 Comparative synthesis of a pharmaceutical candidate

To demonstrate the power of this dearomative method, we evaluated the comparative syntheses of a neuropeptide receptor Y5 antagonist, **36** (Fig. 7.8). The current route to **36** starts with exhaustive, high-pressure hydrogenation of a methylated terephthalic acid, followed by reduction of the carboxylic acid to corresponding alcohol. After re-oxidation of the resultant alcohol to an aldehyde, phenylhydrazine, trifluoroacetic acid, and sodium borohydride form the spirocyclic core. Mesylation followed by saponification gives common intermediate **35**.^{101b} Alternatively, following our photocatalytic dearomatization significantly streamlines this process (Fig. 7.8). Mesylation of iodoaniline followed by alkylation with methyl (4-bromomethyl) benzoate then saponification gives the linear arene precursor required for spirocyclization. Photocatalytic dearomatization of **34** is extremely efficient providing the corresponding spirocyclic product in near quantitative yield as detected by NMR (1:1 d.r.). Hydrogenation affords the common intermediate **35**. Amidation with propanephosphonic anhydride and 4-aminobiphenyl cleanly gives **36**. The photocatalytic dearomatization route described here is highly efficient, and the inherent high tolerance of the dearomative cyclization step lends to the modularity of potential structure-activity relationship studies for compounds of this or similar scaffolds

Figure 7.8. Photocatalytic dearomatization provides an efficient route to anti-obesity candidate **36**.



7.7 Conclusions

This spirocyclization operates under a distinctive reductive manifold where a photocatalyst (fueled by light and a stoichiometric amine reductant) delivers reducing electrons that deliver highly reactive aryl radicals. Following dearomative C–C bond formation, the resulting spirocyclic radical species is effectively intercepted via reductive radical-polar crossover, prohibiting undesired radical pathways. Finally, protonation occurs with high regioselectivity to afford the observed 1,4-diene systems. This mild and selective protocol for dearomative hydroarylation, delivers highly substituted, complex molecules from aromatic precursors in a single step.

7.8 Supporting Information

General Reagent Information

Solvents used in anhydrous reactions were purified by passing over activated alumina and storing under argon. Reagents were purchased from Sigma-Aldrich, Alfa Aesar, Acros Organics, Combi-Blocks, Oakwood Chemicals, Astatech, and TCI America and used as received, unless

stated otherwise. n-Butyllithium (n-BuLi) was used as a 1.6 M or 2.5 M solution in hexanes (Aldrich), and stored at 4 °C and titrated prior to use. Organic solutions were concentrated under reduced pressure on a rotary evaporator using a water bath. Chromatographic purification of products was accomplished using forced-flow chromatography on 230–400 mesh silica gel. Preparative HPLC was carried out using an Agilent Technologies 1260 Infinity HPLC with a 21.2 x 250 mm, 7µm pore size, ZORBAX Eclipse XDB-C18 Column. Eluents used were unmodified unless otherwise stated. Preparative thin-layer chromatography (PTLC) separations were carried out on 1000 µm SiliCycle silica gel F-254 plates. Thin-layer chromatography (TLC) was performed on 250 µm SiliCycle silica gel F-254 plates. Visualization of the developed chromatogram was performed by fluorescence quenching or staining using KMnO₄, p-anisaldehyde, or ninhydrin stains. All photoredox reactions were set up on the bench top and conducted under nitrogen atmosphere while subject to irradiation from blue LEDs, unless stated otherwise (LED wholesalers PAR38 Indoor Outdoor 16-Watt LED Flood Light Bulb, Blue; or Hydrofarm® PPB1002 PowerPAR LED Bulb-Blue 15W/E27 (available from Amazon)). Solvent was degassed by sonication under mild vacuum for 15 minutes. Photoredox catalysts 3DPAFIPN, 3DPA2FBN, 4CzIPN, 5CzBN, N-POX(Ph₂)₂ were all prepared according to literature procedures.¹¹⁰ All electrochemical procedures were carried out using an IKA ElectraSyn, available at <https://www.ika.com/en/Products-Lab-Eq/Electrochemistry-Kit-csp-516/ElectraSyn-20-Package-cpdt-20008980/>.

¹¹⁰ (a) Pearson, R. M.; Lim, C.-H.; McCarthy, B. G.; Musgrave, C. B.; Miyake, G. M. Organocatalyzed Atom Transfer Radical Polymerization Using N-Aryl Phenoxazines as Photoredox Catalysts. *J. Am. Chem. Soc.* **2016**, *138* (35), 11399–11407. (b) Speckmeier, E.; Fischer, T.; Zeitler, K. A Toolbox Approach to Construct Broadly Applicable Metal-Free Catalysts for Photoredox Chemistry: Deliberate Tuning of Redox Potentials and Importance of Halogens in Donor-Acceptor Cyanoarenes. *J. Am. Chem. Soc.* **2018**, *140* (45), 15354–15365.

General Analytical Information.

Unless otherwise noted, all yields refer to chromatographically and spectroscopically (^1H NMR) homogenous materials. New compounds were characterized by NMR, IR, HRMS, and melting point (when solid). ^1H and ^{13}C NMR spectra were obtained from the Emory University NMR facility and recorded on a Bruker Avance III HD 600 equipped with cryo-probe (600 MHz), INOVA 600 (600 MHz), INOVA 500 (500 MHz), INOVA 400 (400 MHz), VNMR 400 (400 MHz), or Mercury 300 (300 MHz), and are internally referenced to residual protio solvent signals. Data for ^1H NMR are reported as follows: chemical shift (ppm), multiplicity (s = singlet, d = doublet, t = triplet, q = quartet, m = multiplet, dd = doublet of doublets, dt = doublet of triplets, ddd = doublet of doublet of doublets, dtd = doublet of triplet of doublets, b = broad, etc.), coupling constant (Hz), integration, and assignment, when applicable. Data for decoupled ^{13}C NMR are reported in terms of chemical shift and multiplicity when applicable. IR spectra were recorded on a Thermo Fisher DiamondATR and reported in terms of frequency of absorption (cm^{-1}). High resolution mass spectra were obtained through the use of an Agilent 6230 electrospray ionization time-of-flight (ESI-TOF) mass spectrometer. Gas Chromatography Mass Spectrometry (GC-MS) was performed on an Agilent 5977A mass spectrometer with an Agilent 7890A gas chromatography inlet. Liquid Chromatography Mass Spectrometry (LC-MS) was performed on an Agilent 6120 mass spectrometer with an Agilent 1220 Infinity liquid chromatography inlet. Preparative High Pressure Liquid chromatography (Prep-HPLC) was performed on an Agilent 1200 Infinity Series chromatograph using an Agilent Prep-C18 30 x 250 mm 10 μm column, or an Agilent Prep-C18 21.2 x 100 mm, 5 μm column.

General Procedure A

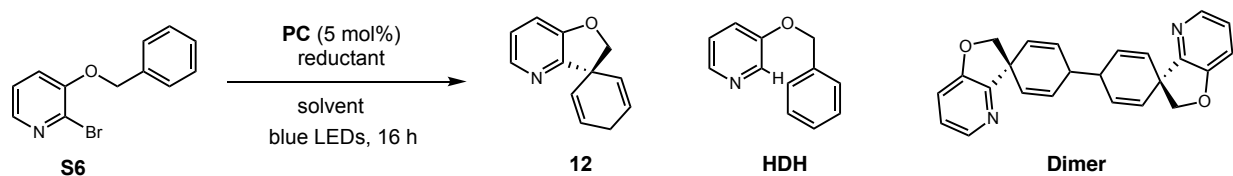
A 20 mL screw-top test tube was charged with photocatalyst (0.025 mmol, 5 mol%), and substrate (0.5 mmol, 1.0 equiv). The tube was equipped with a stir bar was sealed with a PTFE/silicon septa. The atmosphere was exchanged by applying vacuum and backfilling with nitrogen (this process was conducted a total of three times). Under nitrogen atmosphere, separate degassed solvent was added via syringe (7.5 mL of each MeCN and H₂O to give a 0.03 M solution), followed by DIPEA (3.0 equiv). The resulting mixture was stirred at 1400 RPM for 16 h under irradiation by blue LEDs, unless noted otherwise. The reaction was then extracted with ethyl acetate (3 x), dried with MgSO₄, and concentrated. The residue was purified on silica using the indicated solvent mixture as eluent to afford the title compound.

General Procedure B

A 20 mL screw-top test tube was charged with photocatalyst (0.025 mmol, 5 mol%), and substrate (0.5 mmol, 1.0 equiv). The tube was equipped with a stir bar was sealed with a PTFE/silicon septa. The atmosphere was exchanged by applying vacuum and backfilling with nitrogen (this process was conducted a total of three times). Under nitrogen atmosphere, separated degassed solvent was added via syringe (7.5 mL of each MeCN and H₂O to give a 0.03 M solution), followed by DIPEA (10.0 equiv). The resulting mixture was stirred at 1400 RPM for 16 h under irradiation by blue LEDs, unless noted otherwise. The reaction was then extracted with ethyl acetate (3 x), dried with MgSO₄, and concentrated. The residue was purified on silica using the indicated solvent mixture as eluent to afford the title compound.

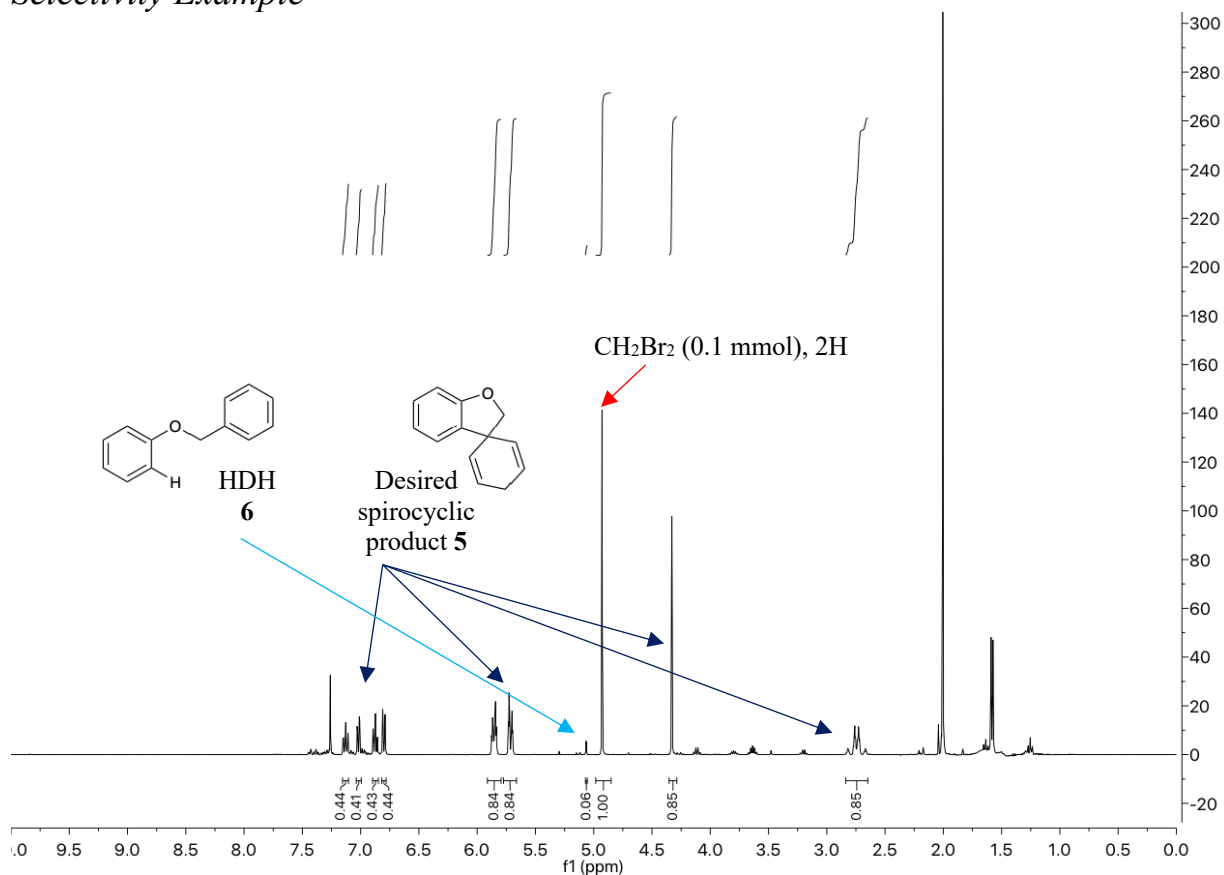
Optimization Procedure

An 8 mL screw-top test tube was charged with photocatalyst (0.005 mmol, 5 mol%) and 3-(benzyloxy)-2-bromopyridine (0.1 mmol, 1.0 equiv). The tube was equipped with a stir bar and sealed with a PTFE/silicon septa. The atmosphere was exchanged by applying vacuum and backfilling with nitrogen (this process was conducted a total of three times). Under nitrogen atmosphere, separately degassed solvent was added via syringe, followed by reductant. The resulting mixture was stirred at 800 RPM for 16 h under irradiation by blue LEDs, unless noted otherwise. The reaction was then extracted with ethyl acetate (3 x), washed with brine, dried with MgSO₄, and concentrated. Deutero-chloroform with an internal standard of dibromomethane (7 μ L, 0.1 mmol) was added. The sample was analyzed by ¹H NMR (d = 5 s), and the integral values were used to calculate the data given in Table S7.1.

Table S7.1: Optimization of arene dearomatization via hydroarylation reaction

entry	PC	reductant (equiv)	% water	cosolvent (rxn conc)	S6	12	HDH	dimer
1	3DPAFIPN	tributylamine (3)	10	DMF (0.1 M)	19	29	27	0
2	3DPAFIPN	tributylamine (3)	10	EtOH (0.1 M)	2	51	20	0
3	3DPAFIPN	tributylamine (3)	10	TFE (0.1 M)	0	57	7	15
4	3DPAFIPN	tributylamine (3)	10	DMSO (0.1 M)	11	43	7	0
5	3DPAFIPN	tributylamine (3)	10	MeCN (0.1 M)	0	60	19	0
6	3DPAFIPN	tributylamine (3)	50	MeCN (0.1 M)	0	71	14	0
7	3DPAFIPN	tributylamine (3)	80	MeCN (0.1M)	0	39	66	0
8	3DPAFIPN	DIPEA (3)	50	MeCN (0.1 M)	0	81	21	0
9	3DPAFIPN	DIPEA (0.5)	50	MeCN (0.1 M)	80	13	7	0
10	3DPAFIPN	DIPEA (2)	50	MeCN (0.1 M)	16	66	26	0
11	3DPAFIPN	DIPEA (10)	50	MeCN (0.1 M)	0	65	48	0
12	3DPAFIPN	DIPEA (3)	50	MeCN (0.03M)	5	86	6	0
13	4CzIPN	DIPEA (3)	50	MeCN (0.03 M)	46	49	5	0
14	5CzBN	DIPEA (3)	50	MeCN (0.03 M)	36	46	20	0
15	3DPA2FBN	DIPEA (3)	50	MeCN (0.03 M)	0	66	5	9
16	Ir(ppy) ₂ (dtbbpy) PF ₆	DIPEA (3)	50	MeCN (0.03 M)	14	66	15	0
17	Ir(ppy) ₃	DIPEA (3)	50	MeCN (0.03 M)	17	31	8	14
18	N-POX(Ph) ₂	HCOONa (3)	50	MeCN (0.03 M)	94	trace	trace	0
19	3DPAFIPN	DIPEA (3)	0	MeCN (0.03 M)	6	68	13	8
20 ^a	3DPAFIPN	DIPEA (3)	50	MeCN (0.03 M)	49	44	5	0
21	3DPAFIPN	triethylamine (3)	50	MeCN (0.03 M)	41	65	5	0
22	3DPAFIPN	none	50	MeCN (0.03 M)	100	0	0	0
23	none	DIPEA (3)	50	MeCN (0.03 M)	100	0	0	0
24 ^b	3DPAFIPN	DIPEA (3)	50	MeCN (0.03 M)	100	0	0	0

Selectivity Example



1-(benzyloxy)-2-iodobenzene (0.1 mmol) was subjected to General Conditions A. The reaction was then extracted with ethyl acetate (3 x), dried with MgSO_4 , and concentrated. Deuteriochloroform with an internal standard of dibromomethane (7 μL , 0.1 mmol) was added. The sample was analyzed by ^1H NMR ($d = 5$ s), and the integral values are shown in the crude NMR above. NMR was compared to (and was consistent with) reported literature values *J. Org. Chem.* **2008**, *73* (18), 7145–7152.

Fluorescence Quenching and Stern-Volmer Plots

All fluorescence measurements were recorded using a Horiba Scientific Dual-FL Fluorometer. Quenching studies were conducted in MeCN at 20 ± 0.5 °C (Peltier temperature controller) with a photocatalyst (3DPAFIPN) concentration of 9.01×10^{-6} M. Samples were prepared in Starna quartz cuvettes (3-Q-10-GL14-S) with septum seal caps. Dry N_2 was bubbled through the prepared sample for 4 minutes before analysis. Raw fluorescence intensity was measured at $\lambda = 542$ nm after excitation at $\lambda = 380$ nm in the quartz cuvettes with a path length of 1 cm and 0.1 second integration. Measurements of the quenchers shown were plotted using Igor Pro 8; data points were fit with a linear trend line.

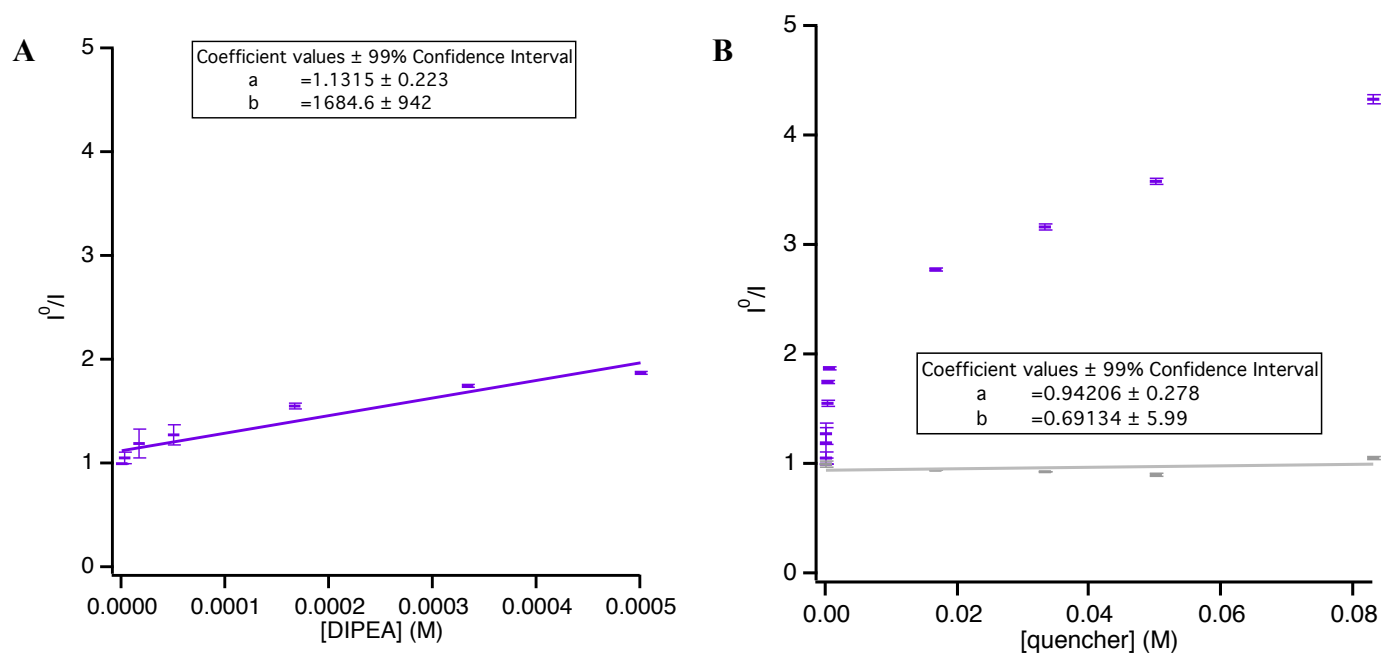


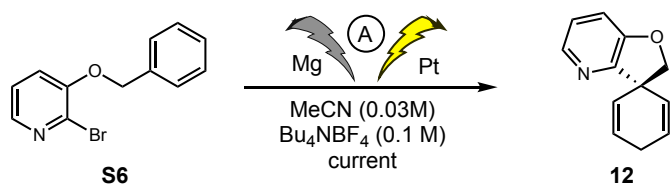
Figure S7.1: Stern-Volmer plots for (A) DIPEA at low concentrations and (B) DIPEA and 3-(benzyloxy)-2-bromopyridine up to $\sim 10,000$ equivalents with respect to photocatalyst 3DPAFIPN.

Table S7.2: Fluorescence Quenching Data

Compound (Quencher)	[Quencher] (M)	I ⁰ /I	Equiv vs PC	Coefficients
Diisopropylethylamine	0	1	0	y = a + bx
Diisopropylethylamine	3.3*10 ⁻⁶	1.06	0.4	a = 1.1 ± 0.2
Diisopropylethylamine	1.67*10 ⁻⁵	1.20	1.9	b = 1684 ± 942
Diisopropylethylamine	5.0*10 ⁻⁵	1.27	5.6	
Diisopropylethylamine	1.67*10 ⁻⁴	1.56	19	± 99% CI
Diisopropylethylamine	3.33*10 ⁻⁴	1.76	37	
Diisopropylethylamine	5.0*10 ⁻⁴	1.88	55	
Diisopropylethylamine	1.67*10 ⁻²	2.77	1854	
Diisopropylethylamine	3.33*10 ⁻²	3.16	3696	
Diisopropylethylamine	5.0*10 ⁻²	3.59	5549	
Diisopropylethylamine	8.3*10 ⁻²	4.33	9212	
3-(benzyloxy)-2-bromopyridine	0	1	0	y = a + bx
3-(benzyloxy)-2-bromopyridine	1.67*10 ⁻²	0.94	1854	a = 0.94 ± 0.28
3-(benzyloxy)-2-bromopyridine	3.33*10 ⁻²	0.94	3696	b = 0.69 ± 5.99
3-(benzyloxy)-2-bromopyridine	5.0*10 ⁻²	0.91	5549	
3-(benzyloxy)-2-bromopyridine	8.3*10 ⁻²	1.06	9212	± 99% CI

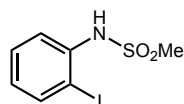
Electrochemical Reaction Optimization Procedure

To an ElectroSyn vial charged with stir bar was added 3-(benzyloxy)-2-bromopyridine (0.2 mmol, 1 equiv), electrolyte (to make the indicated concentration), and solvent (6 mL) An IKA Mg (anode) and Pt (cathode) plate electrodes were connected to an ElectroSyn vial cap. The ElectroSyn was setup as follows: New exp. > constant current > **X** (current from table) mA > no ref. electrode > total charge > 0.2 mmol, 3 F/mol > no alternating polarity > start. The reaction was allowed to run with stirring until the ElectroSyn had measured 3 F/mol input. The reaction was then concentrated. Deutro-chloroform with an internal standard of dibromomethane (7 μL, 0.1 mmol) was added. The sample was analyzed by ¹H NMR (d = 5 s), and the integral values were used to calculate the data given in Table S7.3.

Table S7.3: Preliminary results for electrochemical spirocyclization


entry	current	S6	12	HDH
1	2 mA	100	0	0
2	5 mA	71	0	30
3	10 mA	28	3	60
4	50 mA	29	8	63

Preparation of Starting Materials



***N*-(2-iodophenyl)methanesulfonamide (S1)**

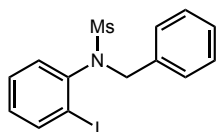
To a solution of 2-iodoaniline (572 mg, 2.6 mmol, 1 equiv) in dichloromethane was added methanesulfonyl chloride (250 μ L, 3.2 mmol, 1.2 equiv) dropwise via syringe, followed by pyridine (250 μ L, 2.8 mmol, 1.1 equiv). The resulting mixture was stirred at room temperature for 4 h and concentrated. The resulting residue was purified on silica gel (20–50% EtOAc/Hex eluent) to afford the title compound as a white solid (770 mg, >99%).

^1H NMR (399 MHz, CDCl_3) δ 7.80 (dd, $J = 8.0, 1.5$ Hz, 1H), 7.61 (dd, $J = 8.2, 1.5$ Hz, 1H), 7.35 (tdd, $J = 8.0, 1.5, 0.5$ Hz, 1H), 6.91 (ddd, $J = 8.0, 7.4, 1.5$ Hz, 1H), 6.67 (bs, 1H), 2.99 (s, 3H).

^{13}C NMR (100 MHz, CDCl_3) δ 139.4, 137.6, 129.9, 127.3, 122.6, 92.3, 40.2.

LRMS (APCI) m/z : $[M-H]^-$ calc'd. for $C_7H_7INO_2S$, 295.9; found 295.8

1H NMR spectrum is consistent with reported values.¹¹¹



***N*-benzyl-*N*-(2-iodophenyl)methanesulfonamide (S2)**

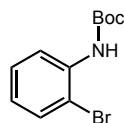
A 20 mL screw-top vial was charged with *N*-(2-iodophenyl)methanesulfonamide (**S1**), (459 mg, 1.6 mmol, 1.0 equiv) and K_2CO_3 (365 mg, 2.6 mmol, 1.6 equiv). DMF was added, followed by benzyl bromide (450 μ L, 3.7 mmol, 2.3 equiv). The reaction was stirred overnight (ca. 16 h) at room temperature, then heated to 60 °C until starting material was consumed (as determined by LCMS). The reaction was cooled to room temperature and then partitioned between EtOAc and water. The organic layer was washed with brine 3x, dried with $MgSO_4$ and purified on silica gel (10-50% EtOAc/Hex eluent) to afford the title compound as a colorless oil (394 mg, 66%).

1H NMR (399 MHz, $CDCl_3$) δ 7.89 (d, $J = 7.9$ Hz, 1H), 7.25 (s, 6H), 7.03 (d, $J = 7.9$ Hz, 1H), 6.99 (t, $J = 7.6$ Hz, 1H), 5.05 (d, $J = 14.6$ Hz, 1H), 4.54 (d, $J = 14.6$ Hz, 1H), 3.04 (s, 3H).

^{13}C NMR (100 MHz, $CDCl_3$) δ 140.7, 140.4, 135.4, 133.1, 130.2, 129.7, 129.0, 128.5, 128.2, 101.0, 54.9, 41.8.

LRMS (APCI) m/z : $[M+H]^+$ calc'd. for $C_{14}H_{15}INO_2S$, 387.9; found 387.7

¹¹¹ Fernández, A.; Varela, J.; Saá, C. Formation of Indoles, Dihydroisoquinolines, and Dihydroquinolines by Ruthenium-catalyzed Heterocyclizations. *Synthesis*, **2012**, 44, 3285–3295.

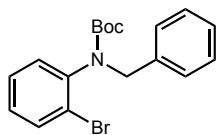


tert-butyl (2-bromophenyl)carbamate (S3): In a round bottom flask, 2-bromoaniline (15 g, 88 mmol, 1.0 equiv) was dissolved in DCM and cooled to 0 °C. Di-*tert*-butyl dicarbonate (43 g, 195 mmol, 2.2 equiv) was added slowly to the reaction over the course of 30 minutes. Dimethylaminopyridine (1.8 g, 15 mmol, 0.2 equiv) was then added slowly to the reaction mixture (caution: on this large scale significant exotherm and evolution of CO₂ is possible.). The resulting mixture was stirred until consumption of the starting material was detected by TLC. The reaction was then poured onto water, washed with concentrated aqueous NaHCO₃, and extracted with EtOAc (3 x). The combined organic layers were dried with MgSO₄. The crude oil was identified as the di-boc product by ¹H NMR. Mono-deprotection was achieved by stirring the crude oil in a dilute solution of TFA in DCM at 0 °C. This reaction was monitored carefully by TLC until the complete removal of one boc was detected. The reaction was then basified, poured onto water and extracted with EtOAc x3. The crude oil was purified on silica (10-30% EtOAc/Hex eluent) to afford the title product as a colorless oil (19 g, 80% over 2 steps).

¹H NMR (400 MHz, CDCl₃) δ 8.13 (d, *J* = 8.4 Hz, 1H), 7.48 (d, *J* = 8.0, 1.7 Hz, 1H), 7.32 – 7.16 (m, 1H), 6.97 (bs, 1H), 6.88 (t, *J* = 7.7 Hz, 1H), 1.52 (s, 9H).

¹H NMR spectrum is consistent with reported values¹¹²

¹¹² Zhang, Z.; Liu, Y-H.; Zhang, X.; Wang, X-C. KMnO₄-Mediated oxidative C-N bond cleavage of tertiary amines: synthesis of amides and sulfonamides. *Tetrahedron*, **2019**, 75, 2763–2770.

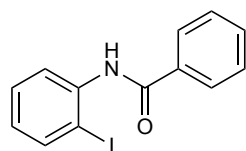


tert-butyl benzyl(2-bromophenyl)carbamate (S4): In a round bottom flask under nitrogen, sodium hydride as a 60% dispersion in mineral oil (180 mg, 4.5 mmol, 1.3 equiv) was suspended in DMF and cooled to 0 °C. **S3** as a solution in DMF (976 mg, 3.6 mmol, 1.0 equiv) was added dropwise to the sodium hydride suspension and stirred for 30 minutes before the addition of benzyl bromide (513 μ L, 4.3 mmol, 1.2 equiv). The reaction was removed from the ice bath, and after reacting for 4.5 h, was quenched with methanol then water at 0 °C. The resulting mixture was diluted with ethyl acetate and washed with brine 3x. The organic layer was dried with MgSO_4 , concentrated *in vacuo*, and purified on silica gel (0–5% EtOAc/Hex eluent) to afford the title compound as a colorless oil (238 mg, >99%).

$^1\text{H NMR}$ (500 MHz, CDCl_3 , 60 °C) δ 7.59 (bd, $J = 7.9$ Hz, 1H), 7.26 (bm, 5H), 7.10 (bm, 2H), 6.84 (bs, 1H), 5.21 (s, 1H), 4.23 (d, $J = 14.9$ Hz, 1H), 1.44 (bm, $J = 61.2$ Hz, 9H).

$^{13}\text{C NMR}$ (151 MHz, CDCl_3 , 60 °C) δ 154.4, 141.2, 137.9, 133.1, 130.9, 128.9, 128.4, 128.2, 127.6, 127.3, 123.8, 80.5, 52.7, 28.2.

LRMS (APCI) m/z : $[\text{M}-\text{C}_4\text{H}_9\text{H} + \text{H}]^+$ calc'd. for $\text{C}_{14}\text{H}_{12}\text{BrNO}_2$, 305.0; found 305.8.



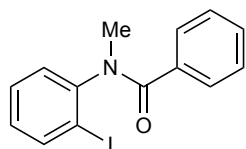
N-(2-iodophenyl)benzamide (S5): To a solution of 2-iodoaniline (641 mg, 2.9 mmol, 1.0 equiv) in dichloromethane was added benzoyl chloride (375 μ L, 3.2 mmol, 1.1 equiv) dropwise via syringe, followed by triethylamine (500 μ L, 3.6 mmol, 1.2 equiv). The resulting mixture was

stirred at room temperature for 4 h, quenched with methanol, and concentrated. The resulting solid was purified on silica gel (10–20% EtOAc/Hex eluent) to afford the title compound as a white solid. (945 mg, >99 %).

¹H NMR (399 MHz, CDCl₃) δ 8.42 (dd, *J* = 8.2, 1.6 Hz, 1H), 8.30 (bs, 1H), 8.01 – 7.88 (m, 2H), 7.79 (dd, *J* = 8.0, 1.5 Hz, 1H), 7.61 – 7.45 (m, 3H), 7.37 (ddd, *J* = 8.1, 7.4, 1.5 Hz, 1H), 6.86 (td, *J* = 7.7, 1.6 Hz, 1H).

¹³C NMR (100 MHz, CDCl₃) δ 165.3, 138.8, 138.3, 134.5, 132.2, 129.4, 128.9, 127.2, 126.1, 121.9, 90.4.

LRMS (APCI) *m/z*: [M+H]⁺ calc'd. for C₁₃H₁₁INO, 323.1; found 323.7



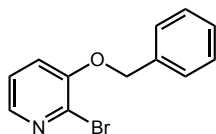
***N*-(2-iodophenyl)-*N*-methylbenzamide (S6):** In a vial under nitrogen, sodium hydride as a 60% dispersion in mineral oil (120 mg, 3.0 mmol, 2.0 equiv) was suspended in DMF and cooled to 0 °C. **S5** as a solution in DMF (476 mg, 1.5 mmol, 1.0 equiv) was added to the sodium hydride suspension and stirred for 30 minutes before the addition of methyl iodide (140 μL, 2.2 mmol, 1.5 equiv). The reaction was removed from the ice bath, and after reacting for 1.5 h, was quenched with methanol then water at 0 °C. The resulting mixture was diluted with ethyl acetate and washed with brine 3x. The organic layer was dried with MgSO₄, concentrated *in vacuo*, and purified on silica gel (10-25% EtOAc/Hex eluent) to afford the title compound as a white solid (312 mg, 62%).

¹H NMR (399 MHz, CDCl₃) δ 7.75 (dd, *J* = 8.0, 1.4 Hz, 1H), 7.43 – 7.27 (m, 2H), 7.20 – 7.01 (m, 5H), 6.85 (td, *J* = 7.6, 1.7 Hz, 1H), 3.35 (s, 3H).

^{13}C NMR (100 MHz, CDCl_3) δ 170.8, 146.9, 140.1, 135.6, 130.1, 129.8, 129.3, 129.1, 128.3, 127.6, 99.1, 37.5.

LRMS (APCI) m/z : $[\text{M}+\text{H}]^+$ calc'd. for $\text{C}_{14}\text{H}_{13}\text{INO}$, 337.9; found 337.7

^1H NMR spectrum is consistent with reported values¹¹³

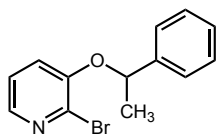


3-(benzyloxy)-2-bromopyridine (S7): A round bottom flask was charged with 2-bromo-3-hydroxypyridine (5.0 g, 29 mmol, 1.0 equiv) and K_2CO_3 (8.0 g, 58 mmol, 2.0 equiv). DMF was added, followed by benzyl bromide (3.7 mL, 31 mmol, 1.1 equiv). The reaction was heated to 80 °C and stirred for 16 h. The reaction was cooled to room temperature and then partitioned between EtOAc and water. The organic layer was washed with brine 3x, dried with MgSO_4 and purified on silica gel (20–50% EtOAc/Hex eluent) to afford the title compound as a white solid (7.5 g, 99%).

^1H NMR (400 MHz, CDCl_3) δ 7.96 (dd, $J = 3.8, 2.4$ Hz, 1H), 7.47 – 7.27 (m, 5H), 7.18 – 7.09 (m, 2H), 5.15 (s, 2H).

^{13}C NMR (126 MHz, CDCl_3) δ 152.0, 141.6, 135.5, 133.3, 128.7, 128.3, 127.0, 123.3, 120.5, 70.9.

LRMS (APCI) m/z : $[\text{M}+\text{H}]^+$ calc'd. for $\text{C}_{12}\text{H}_{11}\text{BrNO}$, 264.0; found 263.8



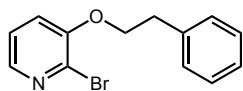
¹¹³ Colobert, F; Valdivia, V.; Choppin, S.; Leroux, F.; Fernández, I.; Álvarez, E.; Khair, N. Axial chirality control during Suzuki-Miyaura cross-coupling reactions: the tert-butylsulfinyl group as an efficient chiral auxiliary. *Org. Lett.* **2009**, 11 (25), 5130–5133.

(±) 2-bromo-3-(1-phenylethoxy)pyridine (S8): A round bottom flask was charged with 2-bromo-3-hydroxypyridine (522 mg, 3.0 mmol, 1.0 equiv) and K_2CO_3 (829 mg, 6.0 mmol, 2.0 equiv). MeCN (15 mL) was added, followed by (1-bromoethyl)benzene (0.41 mL, 3.0 mmol, 1.0 equiv). The reaction was heated to 60 °C and stirred for 18 h. The reaction was cooled to room temperature, diluted with water, and extracted with EtOAc 3x. The organic layer was washed with brine, dried with $MgSO_4$, and concentrated *in vacuo* to afford the title compound as a colorless oil (834 mg, >99%).

1H NMR (600 MHz, $CDCl_3$) δ 7.90 (dt, $J = 4.6, 1.3$ Hz, 1H), 7.41 – 7.37 (m, 2H), 7.35 (tt, $J = 6.5, 1.0$ Hz, 2H), 7.31 – 7.24 (m, 1H), 7.01 (ddt, $J = 8.2, 4.6, 1.2$ Hz, 1H), 6.99 – 6.95 (m, 1H), 5.35 (q, $J = 6.4$ Hz, 1H), 1.72 (dd, $J = 6.4, 1.1$ Hz, 3H).

^{13}C NMR (151 MHz, $CDCl_3$) δ 151.4, 141.5, 141.3, 133.8, 128.9, 128.0, 125.6, 123.2, 121.9, 77.8, 24.4.

LRMS (APCI) m/z : $[M+H]^+$ calc'd. for $C_{13}H_{13}BrNO$, 278.0; found 277.8.

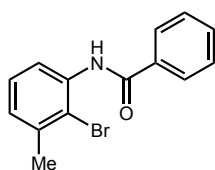


2-bromo-3-phenethoxy pyridine (S9): A 20mL screw-top vial was charged with 2-bromo-3-hydroxypyridine (452 mg, 2.6 mmol, 1.0 equiv) and K_2CO_3 (716 mg, 5.1 mmol, 2.0 equiv). DMF was added, followed by 2(bromoethyl)benzene (380 μ L, 2.9 mmol, 1.1 equiv). The reaction was heated to 80 °C and stirred for 16 h. The reaction was cooled to room temperature and then partitioned between EtOAc and water. The organic layer was washed with brine 3x, dried with

MgSO₄ and purified on silica gel (20–60% EtOAc/Hex eluent) to afford the title compound as a white solid (378 mg, 52%).

¹H NMR (399 MHz, CDCl₃) δ 7.93 (dd, *J* = 4.6, 1.6 Hz, 1H), 7.34 – 7.31 (m, 4H), 7.27 – 7.22 (m, 1H), 7.14 (dd, *J* = 8.1, 4.6 Hz, 1H), 7.04 (dd, *J* = 8.2, 1.5 Hz, 1H), 4.18 (t, *J* = 6.8 Hz, 2H), 3.15 (t, *J* = 6.8 Hz, 2H).

¹H NMR spectrum is consistent with reported values.¹¹⁴



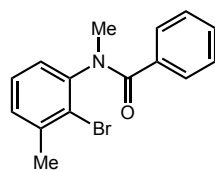
***N*-(2-bromo-3-methylphenyl)benzamide (S10):** To a solution of 2-bromo-3-methylaniline (0.41 mL, 3.3 mmol, 1.1 equiv) in dichloromethane was added benzoyl chloride (0.35 mL, 3.0 mmol, 1.0 equiv) dropwise via syringe, followed by triethylamine (0.46 mL, 3.3 mmol, 1.1 equiv). The resulting mixture was stirred at room temperature for 22 h, washed with 1 M HCl (aq), dried over MgSO₄, and concentrated *in vacuo* to afford the title compound as a white solid. (732 mg, 84%).

¹H NMR (400 MHz, CDCl₃) δ 8.60 (s, 1H), 8.43 – 8.37 (m, 1H), 7.99 – 7.91 (m, 2H), 7.64 – 7.56 (m, 1H), 7.56 – 7.49 (m, 2H), 7.29 (d, *J* = 7.8 Hz, 1H), 7.05 (ddd, *J* = 7.5, 1.7, 0.8 Hz, 1H), 2.46 (s, 3H) ppm.

¹³C NMR (151 MHz, CDCl₃) δ 165.5, 138.7, 136.1, 135.0, 132.3, 129.1, 127.9, 127.3, 126.4, 119.3, 116.7, 24.0 ppm.

LRMS (APCI) *m/z*: [M+H]⁺ calc'd. for C₁₄H₁₃BrNO, 290.0; found 289.7

¹¹⁴ Hu, Q.; Kunde, J.; Hanke, N.; Hartmann, R. Identification of 4-(4-nitro-2-phenethoxyphenyl)pyridine as a promising new lead for discovering inhibitors of both human and rat 11β-hydroxylase. *Eur. J. Med. Chem.* **2015**, 96, 139–150.

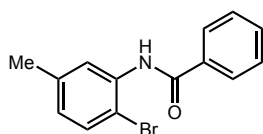


***N*-(2-bromo-3-methylphenyl)-*N*-methylbenzamide (S11):** In a vial under nitrogen, sodium hydride as a 60% dispersion in mineral oil (120 mg, 3.0 mmol, 1.5 equiv) was suspended in DMF and cooled to 0 °C. **S10** as a solution in DMF (580 mg, 2.0 mmol, 1.0 equiv) was added dropwise to the sodium hydride suspension and stirred for 30 minutes before the addition of methyl iodide (0.15 mL, 2.4 mmol, 1.2 equiv). The reaction was removed from the ice bath, and after reacting for 1.5 h, was quenched with water. The resulting mixture was diluted with ethyl acetate and washed with brine 3x. The organic layer was dried with MgSO₄ and concentrated *in vacuo* to afford the title compound as a light pink solid (573 mg, 94%).

¹H NMR (400 MHz, CDCl₃) δ 7.35 (dt, *J* = 7.0, 1.4 Hz, 2H), 7.26 – 7.17 (m, 1H), 7.14 (tt, *J* = 6.7, 1.7 Hz, 2H), 7.09 – 7.01 (m, 2H), 6.91 (dd, *J* = 7.5, 2.1 Hz, 1H), 3.38 (s, 3H), 2.39 (s, 3H) ppm.

¹³C NMR (151 MHz, CDCl₃) δ 171.2, 144.1, 140.4, 136.1, 129.9, 129.8, 128.2, 127.8, 127.7, 125.5, 37.3, 23.9 ppm.

LRMS (APCI) *m/z*: [M+H]⁺ calc'd. for C₁₅H₁₅BrNO, 304.0; found 303.7

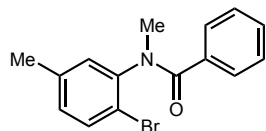


***N*-(2-bromo-5-methylphenyl)benzamide (S12):** To a solution of 2-bromo-5-methylaniline (614 mg, 3.3 mmol, 1.1 equiv) in dichloromethane was added benzoyl chloride (0.35 mL, 3.0 mmol, 1.0 equiv) dropwise via syringe, followed by triethylamine (0.46 mL, 3.3 mmol, 1.1 equiv). The resulting mixture was stirred at room temperature for 16 h, quenched with sat. aq. NH₄Cl, and extracted with DCM 3x. The combined organic layers were washed with 1 M HCl (aq) and brine,

dried over MgSO₄, and concentrated *in vacuo* to afford the title compound as an off-white solid (839 mg, 96%).

¹H NMR (400 MHz, CDCl₃) δ 8.46 – 8.37 (m, 2H), 7.92 (d, J = 7.0 Hz, 1H), 7.57 (t, J = 7.3 Hz, 1H), 7.51 (t, J = 7.3 Hz, 2H), 7.43 (d, J = 8.2 Hz, 1H), 6.83 (dd, J = 8.2, 2.1 Hz, 1H), 2.35 (s, 3H) ppm.

¹H NMR spectrum is consistent with reported values¹¹⁵



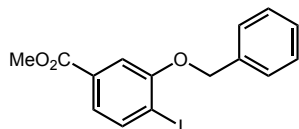
***N*-(2-bromo-5-methylphenyl)-*N*-methylbenzamide (S13):** In a vial under nitrogen, sodium hydride as a 60% dispersion in mineral oil (120 mg, 3.0 mmol, 1.5 equiv) was suspended in DMF and cooled to 0 °C. **S12** as a solution in DMF (580 mg, 2.0 mmol, 1.0 equiv) was added dropwise to the sodium hydride suspension and stirred for 30 minutes before the addition of methyl iodide (0.15 mL, 2.4 mmol, 1.2 equiv). The reaction was removed from the ice bath, and after reacting for 1 h was quenched with water and extracted with EtOAc 3x. The combined organic layers were washed with water and brine, dried with MgSO₄, and concentrated *in vacuo* to afford the title compound as a light yellow solid (577 mg, 95%).

¹H NMR (400 MHz, CDCl₃) δ 7.41 – 7.32 (m, 4H), 7.27 – 7.18 (m, 1H), 7.15 (t, J = 7.5 Hz, 2H), 6.92 – 6.83 (m, 2H), 3.37 (s, 3H), 2.17 (s, 3H) ppm.

¹³C NMR (126 MHz, CDCl₃) δ 171.0, 143.5, 138.8, 135.9, 133.4, 131.3, 130.0, 129.8, 128.2, 127.7, 119.3, 37.2, 20.8 ppm.

¹¹⁵ Zheng, N.; Anderson, K.; Huang, X.; Nguyen, H.; Buchwald, S. A palladium-catalyzed regiospecific synthesis of *N*-aryl benzimidazoles. *Angew. Chem. Int. Ed.* **2007**, 40, 7509–7512.

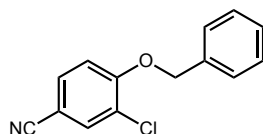
LRMS (APCI) m/z: $[M+H]^+$ calc'd. for $C_{15}H_{15}BrNO$, 304.0; found 303.7



Methyl 3-(benzyloxy)-4-iodobenzoate (S14): A round bottom flask was charged with methyl 3-hydroxy-4-iodobenzoate (417 mg, 1.5 mmol, 1.0 equiv) and K_2CO_3 (415 mg, 1.5 mmol, 1.0 equiv). MeCN (10 mL) was added, followed by benzyl bromide (0.18 mL, 3.0 mmol, 2.0 equiv). The reaction was heated to 60 °C and stirred for 18 h. The reaction was cooled to room temperature, diluted with water, and extracted with EtOAc 3x. The combined organic layers were washed with brine, dried over $MgSO_4$, and concentrated *in vacuo* to afford the title compound as a white solid (535 mg, 97%).

1H NMR (500 MHz, $CDCl_3$) δ 7.88 (d, $J = 8.1$ Hz, 1H), 7.56 – 7.50 (m, 3H), 7.44 – 7.37 (m, 3H), 7.34 (t, $J = 7.3$ Hz, 1H), 5.21 (s, 2H), 3.91 (s, 3H) ppm.

1H NMR spectra are consistent with reported values.¹¹⁶



4-(benzyloxy)-3-chlorobenzonitrile (S15): A round bottom flask was charged with 3-chloro-4-hydroxybenzonitrile (461 mg, 3.0 mmol, 1.0 equiv) and K_2CO_3 (829 mg, 6.0 mmol, 2.0 equiv). MeCN (15 mL) was added, followed by benzyl bromide (0.36 mL, 3.0 mmol, 1.0 equiv). The

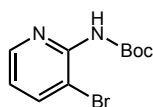
¹¹⁶ Palmerinin, C.; Tartacca, F.; Mazzoni, M.; Granieri, L.; Goracci, L.; Scrascia, A.; Lepri, S. Synthesis of new indole-based bisphosphonates and evaluation of their chelating ability in PE/CA-PJ15 cells. *Eur. J. Med. Chem.* **2015**, 102, 403–442.

reaction was heated to 60 °C and stirred for 16 h. The reaction was cooled to room temperature, diluted with water, and extracted with EtOAc 3x. The combined organic layers were washed with brine, dried over MgSO₄, and purified on silica gel (5–10% EtOAc/Hex eluent) to afford the title compound as a white solid (303 mg, 41%).

¹H NMR (400 MHz, CDCl₃) δ 7.68 (d, J = 2.0 Hz, 1H), 7.51 (ddd, J = 8.6, 2.1, 0.3 Hz, 1H), 7.47 – 7.31 (m, 5H), 7.01 (d, J = 8.6 Hz, 1H), 5.23 (s, 2H) ppm.

¹³C NMR (151 MHz, CDCl₃) δ 157.9, 135.3, 133.9, 132.5, 129.0, 128.7, 127.2, 124.4, 118.1, 113.9, 105.2, 71.2 ppm.

LRMS (EI) m/z: [M]⁺ calc'd. for C₁₄H₁₀ClNO, 243.1; found 243.1

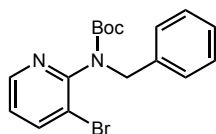


tert-butyl (3-bromopyridin-2-yl)carbamate (S16): To a solution of 2-amino-3-bromopyridine (692 mg, 4.0 mmol, 1.0 equiv) in THF was added triethylamine (1.3 mL, 9.6 mmol, 2.4 equiv), di-*tert*-butyl dicarbonate (1.92 g, 8.8 mmol, 2.2 equiv), and DMAP (49 mg, 0.4 mmol, 0.1 equiv). The resulting solution was stirred for 19 h, quenched with sat. aq. NH₄Cl, and extracted with EtOAc 3x. The combined organic layers were dried over MgSO₄ and concentrated *in vacuo*. The resulting solid was dissolved in DCM (40 mL) and cooled to 0 °C. Trifluoroacetic acid was added dropwise, and the resulting solution was stirred for 5.5 h, quenched with sat. aq. NaHCO₃, extracted with DCM 3x, dried over MgSO₄, and concentrated *in vacuo* to afford the title compound as a light yellow solid (997 mg, 91%).

¹H NMR (400 MHz, CDCl₃) δ 8.41 (dd, J = 4.8, 1.6 Hz, 2H), 7.82 (dd, J = 7.9, 1.7 Hz, 2H), 7.30 (s, 1H), 6.89 (dd, J = 7.9, 4.7 Hz, 2H), 1.55 (s, 17H) ppm.

^{13}C NMR (151 MHz, CDCl_3) δ 150.7, 148.8, 147.5, 141.0, 119.8, 109.4, 81.6, 28.3 ppm.

LRMS (APCI) m/z : $[\text{M}+\text{H}]^+$ calc'd. for $\text{C}_{10}\text{H}_{14}\text{BrN}_2\text{O}_2$, 273.0; found 272.7

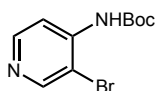


tert-butyl benzyl(3-bromopyridin-2-yl)carbamate (S17): In a round bottom flask under nitrogen, sodium hydride as a 60% dispersion in mineral oil (180 mg, 4.5 mmol, 1.5 equiv) was suspended in DMF and cooled to 0 °C. **S16** as a solution in DMF (819 mg, 3.0 mmol, 1.0 equiv) was added dropwise to the sodium hydride suspension and stirred for 30 minutes before the addition of benzyl bromide (0.43 mL, 3.6 mmol, 1.2 equiv). The reaction was removed from the ice bath, and after reacting for 1.5 h, was quenched with water and extracted with EtOAc 3x. The combined organic layers were washed with brine, dried over MgSO_4 , concentrated *in vacuo*, and purified on silica gel (10-20% EtOAc/Hex eluent) to afford the title compound as a white solid (830 mg, 76%).

^1H NMR (400 MHz, CDCl_3) δ 8.41 (d, J = 3.4 Hz, 1H), 7.85 (d, J = 7.9 Hz, 1H), 7.32 (s, 2H), 7.25 – 7.16 (m, 3H), 7.03 (dd, J = 7.9, 4.7 Hz, 1H), 5.00 (s, 1H), 4.89 (s, 1H), 1.41 (s, 9H) ppm.

^{13}C NMR (100 MHz, CDCl_3 , 50 °C) δ 153.7, 153.6, 147.5, 142.0, 137.9, 128.3, 127.3, 123.2, 120.8, 81.4, 52.4, 28.4 ppm.

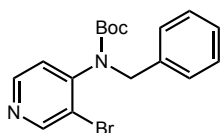
LRMS (APCI) m/z : $[\text{M}+\text{H}]^+$ calc'd. for $\text{C}_{17}\text{H}_{20}\text{BrN}_2\text{O}_2$, 363.0; found 362.8



tert-butyl (3-bromopyridin-4-yl)carbamate (S18): To a solution of 3-bromo-4-pyridinamine (692 mg, 4.0 mmol, 1.0 equiv) in THF (20 mL) was added triethylamine (1.3 mL, 9.6 mmol, 2.4 equiv), di-*tert*-butyl dicarbonate (1.92 g, 8.8 mmol, 2.2 equiv), and DMAP (49 mg, 0.4 mmol, 0.1 equiv). After stirring for 2.5 h, 1 M aq. HCl (20 mL) was added, and the resulting solution was stirred for 17 h. The reaction was neutralized with 1 M aq. NaOH (20 mL), extracted with EtOAc 3x, dried over MgSO₄, concentrated *in vacuo*, and purified on silica gel (30% EtOAc/Hex eluent) to afford the title compound as a white solid (807 mg, 74%).

¹H NMR (400 MHz, CDCl₃) δ 8.58 (d, J = 0.4 Hz, 1H), 8.37 (dd, J = 5.7, 0.6 Hz, 1H), 8.15 (d, J = 5.7 Hz, 1H), 7.17 (s, 1H), 1.54 (s, 9H) ppm.

¹H NMR spectrum is consistent with reported values.¹¹⁷



tert-butyl benzyl(3-bromopyridin-4-yl)carbamate (S19): In a round bottom flask under nitrogen, sodium hydride as a 60% dispersion in mineral oil (120 mg, 3.0 mmol, 1.5 equiv) was suspended in DMF and cooled to 0 °C. **S18** as a solution in DMF (546 mg, 2.0 mmol, 1.0 equiv) was added dropwise to the sodium hydride suspension and stirred for 30 minutes before the addition of benzyl bromide (0.29 mL, 2.4 mmol, 1.2 equiv). The reaction was removed from the ice bath, and after reacting for 4 h was quenched with water and extracted with EtOAc 3x. The

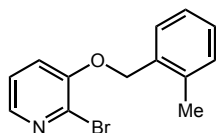
¹¹⁷ Fan, J.; Yao, Q.-J.; Liu, Y.-H.; Liao, G.; Zhang, S.; Shi, B.-F. Asymmetric total synthesis of TAN-1085 facilitated by Pd-catalyzed atroposelective C-H olefination. *Org. Lett.* **2019**, 21(9), 3352–3356.

combined organic layers were washed with water and brine, dried with MgSO_4 , concentrated *in vacuo*, and purified on silica gel (10-20% EtOAc/Hex eluent) to afford the title compound as a yellow oil (488 mg, 67%).

$^1\text{H NMR}$ (500 MHz, CDCl_3) δ 8.75 (s, 1H), 8.37 (d, $J = 5.1$ Hz, 1H), 7.30 – 7.26 (m, 3H), 7.21 (dd, $J = 7.5, 2.0$ Hz, 2H), 6.86 (s, 1H), 5.12 (s, 1H), 4.43 (s, 1H), 1.42 (s, 9H) ppm.

$^{13}\text{C NMR}$ (151 MHz, CDCl_3 , 50 °C) δ 153.5, 153.4, 149.3, 148.8, 137.2, 128.7, 127.9, 125.3, 122.0, 81.7, 65.4, 52.7, 28.3 ppm.

LRMS (APCI) m/z : $[\text{M}+\text{H}]^+$ calc'd. for $\text{C}_{17}\text{H}_{20}\text{BrN}_2\text{O}_2$, 363.0; found 362.8

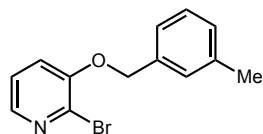


2-bromo-3-((2-methylbenzyl)oxy)pyridine (S20): A round bottom flask was charged with 2-bromo-3-hydroxypyridine (522 mg, 3.0 mmol, 1.0 equiv) and K_2CO_3 (829 mg, 6.0 mmol, 2.0 equiv). MeCN (15 mL) was added, followed by 2-methylbenzyl bromide (0.40 mL, 3.0 mmol, 1.0 equiv). The reaction was heated to 60 °C and stirred for 16 h. The reaction was cooled to room temperature, diluted with water, and extracted with EtOAc 3x. The combined organic layers were washed with brine, dried over MgSO_4 , and purified on silica gel (20% EtOAc/Hex eluent) to afford the title compound as a white solid (677 mg, 81%).

$^1\text{H NMR}$ (400 MHz, CDCl_3) δ 8.00 (t, $J = 3.1$ Hz, 1H), 7.47 – 7.41 (m, 1H), 7.32 – 7.22 (m, 4H), 7.20 (d, $J = 3.1$ Hz, 1H), 5.14 (s, 2H), 2.41 (s, 3H) ppm.

$^{13}\text{C NMR}$ (151 MHz, CDCl_3) δ 152.3, 141.7, 136.7, 133.6, 133.5, 130.7, 128.8, 128.5, 126.3, 123.5, 120.4, 69.8, 19.2 ppm.

LRMS (APCI) m/z : $[\text{M}+\text{H}]^+$ calc'd. for $\text{C}_{13}\text{H}_{13}\text{BrNO}$, 278.0; found 277.8

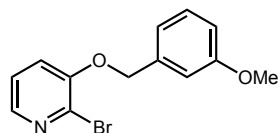


2-bromo-3-((3-methylbenzyl)oxy)pyridine (S21): A round bottom flask was charged with 2-bromo-3-hydroxypyridine (522 mg, 3.0 mmol, 1.0 equiv) and K_2CO_3 (829 mg, 6.0 mmol, 2.0 equiv). MeCN (15 mL) was added, followed by 1-(bromomethyl)-3-methylbenzene (0.41 mL, 3.0 mmol, 1.0 equiv). The reaction was heated to 60 °C and stirred for 15.5 h. The reaction was cooled to room temperature, diluted with water, and extracted with EtOAc 3x. The combined organic layers were washed with brine, dried over $MgSO_4$, and concentrated *in vacuo* to afford the title compound as a light brown solid (826 mg, 99%).

1H NMR (400 MHz, $CDCl_3$) δ 7.99 (dd, $J = 4.1, 2.1$ Hz, 1H), 7.32 – 7.22 (m, 3H), 7.19 – 7.11 (m, 3H), 5.15 (s, 2H), 2.38 (s, 3H) ppm.

^{13}C NMR (151 MHz, $CDCl_3$) δ 152.3, 141.7, 138.7, 135.6, 133.6, 129.3, 128.8, 127.9, 124.3, 123.5, 120.7, 71.2, 21.6 ppm.

LRMS (APCI) m/z : $[M+H]^+$ calc'd. for $C_{13}H_{13}BrNO$, 278.0; found 277.8



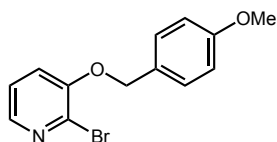
2-bromo-3-((3-methoxybenzyl)oxy)pyridine (S22): A round bottom flask was charged with 2-bromo-3-hydroxypyridine (522 mg, 3.0 mmol, 1.0 equiv) and K_2CO_3 (829 mg, 6.0 mmol, 2.0 equiv). MeCN (15 mL) was added, followed by 3-methoxybenzyl bromide (0.42 mL, 3.0 mmol, 1.0 equiv). The reaction was heated to 60 °C and stirred for 15 h. The reaction was cooled to room

temperature, diluted with water, and extracted with EtOAc 3x. The combined organic layers were washed with brine, dried over MgSO₄, and concentrated *in vacuo* to afford the title compound as a white solid (733 mg, 83%).

¹H NMR (600 MHz, CDCl₃) δ 7.99 (dd, *J* = 4.2, 2.0 Hz, 1H), 7.36 – 7.29 (m, 1H), 7.21 – 7.14 (m, 2H), 7.07 – 6.98 (m, 2H), 6.88 (ddd, *J* = 8.3, 2.6, 0.9 Hz, 1H), 5.17 (s, 2H), 3.83 (s, 3H).

¹³C NMR (151 MHz, CDCl₃) δ 156.0, 152.0, 141.6, 137.1, 133.3, 129.8, 123.4, 120.5, 119.1, 113.8, 112.4, 70.7, 55.3.

LRMS (APCI) *m/z*: [M+H]⁺ calc'd. for C₁₃H₁₃BrNO₂, 294.0; found 293.8.

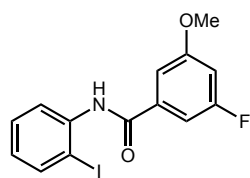


2-bromo-3-((4-methoxybenzyl)oxy)pyridine (S23): A round bottom flask was charged with 2-bromo-3-hydroxypyridine (522 mg, 3.0 mmol, 1.0 equiv) and K₂CO₃ (829 mg, 6.0 mmol, 2.0 equiv). MeCN (15 mL) was added, followed by 4-methoxybenzyl bromide (0.49 mL, 3.6 mmol, 1.2 equiv). The reaction was heated to 60 °C and stirred for 22 h. The reaction was cooled to room temperature, diluted with water, and extracted with EtOAc 3x. The combined organic layers were washed with brine, dried over MgSO₄, and purified on silica gel (10-40% EtOAc/Hex eluent) to afford the title compound as a white solid (699 mg, 79%).

¹H NMR (400 MHz, CDCl₃) δ 7.99 (dd, *J* = 3.7, 2.5 Hz, 1H), 7.38 (dt, *J* = 8.8, 0.6 Hz, 2H), 7.19 – 7.14 (m, 2H), 6.93 (d, *J* = 8.7 Hz, 2H), 5.11 (s, 2H), 3.82 (s, 3H) ppm.

¹³C NMR (151 MHz, CDCl₃) δ 159.9, 152.3, 141.7, 133.7, 129.0, 127.7, 123.5, 120.8, 114.3, 71.1, 55.5 ppm.

LRMS (APCI) *m/z*: [M+H]⁺ calc'd. for C₁₃H₁₃BrNO₂, 294.0; found 293.8



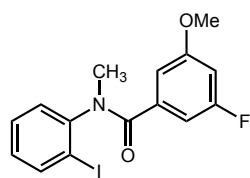
3-fluoro-*N*-(2-iodophenyl)-5-methoxybenzamide (S24): To a solution of 3-fluoro-5-methoxybenzoic acid (510 mg, 3.0 mmol, 1.0 equiv) was added HBTU (1.25 g, 3.3 mmol, 1.1 equiv), 2-iodoaniline (723 mg, 3.3 mmol, 1.1 equiv), and diisopropylethylamine (1.04 mL, 6.0 mmol, 2.0 equiv). After heating at 80 °C for 16.5 h, the reaction was quenched with sat. aq. NH₄Cl and extracted with EtOAc 3x. The combined organic layers were washed with water, 1M aq HCl, and brine, dried over MgSO₄, and purified on silica gel (5% EtOAc/Hex eluent) to afford the title compound as a light yellow solid (334 mg, 30%).

¹H NMR (400 MHz, CDCl₃) δ 8.42 (dd, *J* = 8.3, 1.6 Hz, 1H), 8.20 (s, 1H), 7.83 (dd, *J* = 8.0, 1.4 Hz, 1H), 7.46 – 7.37 (m, 1H), 7.30 (t, *J* = 1.9 Hz, 1H), 7.23 (dt, *J* = 8.6, 1.9 Hz, 1H), 6.91 (td, *J* = 7.7, 1.6 Hz, 1H), 6.83 (dt, *J* = 10.2, 2.3 Hz, 1H), 3.89 (s, 3H) ppm.

¹³C NMR (125 MHz, CDCl₃) δ 164.2 (d, ⁴*J*_{C-F} = 3.2 Hz), 163.7 (d, ¹*J*_{C-F} = 247.5 Hz), 161.5 (d, ³*J*_{C-F} = 11.1 Hz), 139.0, 138.1, 137.4 (d, ³*J*_{C-F} = 8.6 Hz), 129.6, 126.5, 122.0, 109.0 (d, ⁴*J*_{C-F} = 2.6 Hz), 106.6 (d, ²*J*_{C-F} = 23.5 Hz), 105.6 (d, ²*J*_{C-F} = 25.1 Hz), 90.5, 56.0 ppm.

¹⁹F NMR (376 MHz, CDCl₃) δ -109.6 (dd, *J* = 10.0, 8.5 Hz) ppm.

LRMS (APCI) *m/z*: [M+H]⁺ calc'd. for C₁₄H₁₂FINO₂, 372.0; found 371.6



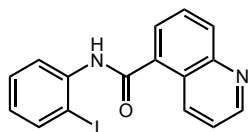
3-fluoro-*N*-(2-iodophenyl)-5-methoxy-*N*-methylbenzamide (S25): In a vial under nitrogen, sodium hydride as a 60% dispersion in mineral oil (48 mg, 1.2 mmol, 1.5 equiv) was suspended in DMF and cooled to 0 °C. **S24** as a solution in DMF (297 mg, 0.80 mmol, 1.0 equiv) was added dropwise to the sodium hydride suspension and stirred for 30 minutes before the addition of methyl iodide (60 μ L, 0.96 mmol, 1.5 equiv). The reaction was removed from the ice bath, and after reacting for 1 h, was quenched with water and extracted with EtOAc 3x. The combined organic layers were washed with water and brine, dried with MgSO₄, and concentrated *in vacuo* to afford the title compound as a yellow solid (287 mg, 93%).

¹H NMR (400 MHz, CDCl₃) δ 7.83 (dd, *J* = 7.9, 1.4 Hz, 1H), 7.25 – 7.21 (m, 1H), 7.09 (dd, *J* = 7.9, 1.6 Hz, 1H), 6.94 (td, *J* = 7.8, 1.6 Hz, 1H), 6.73 – 6.65 (m, 2H), 6.48 (dt, *J* = 10.4, 2.4 Hz, 1H), 3.66 (s, 3H), 3.36 (s, 3H) ppm.

¹³C NMR (126 MHz, CDCl₃) δ 169.2 (d, ⁴*J*_{C-F} = 3.3 Hz), 162.6 (d, ¹*J*_{C-F} = 246.0 Hz), 160.1 (d, ³*J*_{C-F} = 10.9 Hz), 146.6, 140.2, 138.0 (d, ³*J*_{C-F} = 8.3 Hz), 130.0, 129.5, 129.4, 109.2, 107.9 (d, ²*J*_{C-F} = 23.8 Hz), 103.8 (d, ⁴*J*_{C-F} = 24.5 Hz), 98.9, 55.6, 37.5 ppm.

¹⁹F NMR (376 MHz, CDCl₃) δ -111.5 (t, *J* = 9.6 Hz) ppm.

LRMS (APCI) *m/z*: [M+H]⁺ calc'd. for C₁₅H₁₄FINO₂, 386.0; found 385.6

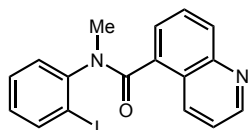


***N*-(2-iodophenyl)quinoline-5-carboxamide (S26):** To a solution of quinoline-5-carboxylic acid (520 mg, 3.0 mmol, 1.0 equiv) was added HBTU (1.25 g, 3.3 mmol, 1.1 equiv), 2-iodoaniline (723 mg, 3.3 mmol, 1.1 equiv), and diisopropylethylamine (1.04 mL, 6.0 mmol, 2.0 equiv). After heating at 80 °C for 20.5 h, the reaction was quenched with sat. aq. NH₄Cl and extracted with EtOAc 3x. The combined organic layers were washed with water, 1 M aq HCl, and brine, dried over MgSO₄, and purified on silica gel (30-50% EtOAc/Hex eluent) to afford the title compound as an off-white solid (385 mg, 34%).

¹H NMR (500 MHz, CDCl₃) δ 9.01 (dd, *J* = 4.3, 1.6 Hz, 1H), 8.95 (d, *J* = 8.7 Hz, 1H), 8.48 (d, *J* = 7.9 Hz, 1H), 8.33 (d, *J* = 8.5 Hz, 1H), 8.12 (s, 1H), 8.00 (d, *J* = 7.2 Hz, 1H), 7.86 (dd, *J* = 8.0, 1.4 Hz, 1H), 7.82 (t, *J* = 7.8 Hz, 1H), 7.55 (dd, *J* = 8.7, 4.2 Hz, 1H), 7.46 (dd, *J* = 8.5, 7.1 Hz, 1H), 6.97 – 6.92 (m, 1H) ppm.

¹³C NMR (151 MHz, CDCl₃) δ 166.3, 151.3, 148.5, 139.2, 138.4, 134.5, 134.0, 133.3, 129.7, 128.6, 126.8, 126.2, 125.9, 122.5, 122.4, 90.7 ppm.

LRMS (APCI) *m/z*: [M+H]⁺ calc'd. for C₁₆H₁₂IN₂O, 375.0; found 374.6



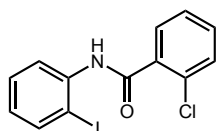
***N*-(2-iodophenyl)-*N*-methylquinoline-5-carboxamide (S27):** In a vial under nitrogen, sodium hydride as a 60% dispersion in mineral oil (48 mg, 1.2 mmol, 1.5 equiv) was suspended in DMF and cooled to 0 °C. **S26** as a solution in DMF (299 mg, 0.80 mmol, 1.0 equiv) was added dropwise

to the sodium hydride suspension and stirred for 30 minutes before the addition of methyl iodide (60 μL , 0.96 mmol, 1.5 equiv). The reaction was removed from the ice bath, and after reacting for 1 h, was quenched with water and extracted with EtOAc 3x. The combined organic layers were washed with water and brine, dried over MgSO_4 , and purified on silica gel (30-50% EtOAc/Hex eluent) to afford the title compound as a white solid (218 mg, 70%). Appeared as rotameric mixtures in ^1H NMR; no coalescence of peaks in CDCl_3 up to 60 $^\circ\text{C}$; major observed product reported.

^1H NMR (400 MHz, CDCl_3) δ 8.92 (dd, $J = 4.2, 1.7$ Hz, 1H), 8.66 – 8.60 (m, 1H), 7.95 (dt, $J = 8.2, 1.2$ Hz, 1H), 7.74 (dd, $J = 7.9, 1.4$ Hz, 1H), 7.53 – 7.37 (m, 3H), 7.04 – 6.92 (m, 2H), 6.80 (ddd, $J = 7.9, 7.2, 1.8$ Hz, 1H), 3.52 (s, 3H) ppm.

^{13}C NMR (126 MHz, CDCl_3) δ 169.3, 150.7, 148.1, 146.3, 140.4, 134.5, 133.8, 131.1, 129.5, 129.4, 129.4, 128.0, 126.0, 125.6, 121.7, 98.8, 37.2 ppm.

LRMS (APCI) m/z : $[\text{M}+\text{H}]^+$ calc'd. for $\text{C}_{17}\text{H}_{14}\text{IN}_2\text{O}$, 389.0; found 388.6

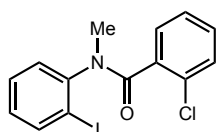


2-chloro-*N*-(2-iodophenyl)benzamide (S28): To a solution of 2-iodoaniline (604 mg, 2.8 mmol, 1.0 equiv) in dichloromethane was added 2-chlorobenzoyl chloride (390 μL , 3.0 mmol, 1.1 equiv) dropwise via syringe, followed by triethylamine (450 μL , 3.2 mmol, 1.1 equiv). The resulting mixture was stirred at room temperature for 4 h, quenched with methanol, and concentrated. The resulting solid was purified on silica gel (10–20% EtOAc/Hex eluent) to afford the title compound as a white solid. (695 mg, 71 %).

^1H NMR (399 MHz, CDCl_3) δ 8.39 (d, $J = 8.3$ Hz, 1H), 8.16 (s, 1H), 7.81 (dd, $J = 8.0, 1.5$ Hz, 1H), 7.76 (dd, $J = 7.5, 2.0$ Hz, 1H), 7.55 – 7.31 (m, 4H), 6.89 (td, $J = 7.7, 1.6$ Hz, 1H).

^{13}C NMR (100 MHz, CDCl_3) δ 164.6, 139.1, 138.2, 134.9, 131.9, 130.9, 130.6, 130.2, 129.3, 127.3, 126.5, 122.4, 90.1.

LRMS (APCI) m/z : $[\text{M}+\text{H}]^+$ calc'd. for $\text{C}_{13}\text{H}_{10}\text{ClINO}$, 357.9; found 357.6

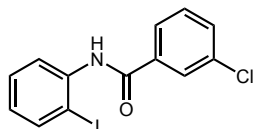


2-chloro-*N*-(2-iodophenyl)-*N*-methylbenzamide (S29): In a vial under nitrogen, sodium hydride as a 60% dispersion in mineral oil (90 mg, 2.2 mmol, 1.8 equiv) was suspended in DMF and cooled to 0 °C. **S28** as a solution in DMF (441 mg, 1.2 mmol, 1.0 equiv) was added to the sodium hydride suspension dropwise and stirred for 30 minutes before the addition of methyl iodide (120 μL , 1.8 mmol, 1.5 equiv). The reaction was removed from the ice bath, and after reacting for 1.5 h, was quenched with methanol then water at 0 °C. The resulting mixture was diluted with ethyl acetate and washed with brine 3x. The organic layer was dried with MgSO_4 , concentrated *in vacuo*, and purified on silica gel (10-25% EtOAc/Hex eluent) to afford the title compound as a white solid (384 mg, 84%). Appeared as rotameric mixtures in ^1H NMR; no coalescence of peaks in CDCl_3 up to 60 °C; major observed rotamer reported.

^1H NMR (400 MHz, CDCl_3) δ 7.75 (dd, $J = 7.9, 1.4$ Hz, 1H), 7.40 (dd, $J = 7.6, 1.8$ Hz, 1H), 7.35 (dd, $J = 7.8, 1.6$ Hz, 1H), 7.20 (dd, $J = 8.0, 1.3$ Hz, 1H), 7.14 (td, $J = 7.6, 1.4$ Hz, 1H), 7.07 (td, $J = 7.7, 1.8$ Hz, 1H), 7.00 (td, $J = 7.5, 1.3$ Hz, 1H), 6.83 (td, $J = 7.6, 1.6$ Hz, 1H), 3.39 (s, 3H).

^{13}C NMR (100 MHz, CDCl_3) δ 167.9, 145.4, 139.9, 136.0, 130.0, 129.6, 129.4, 129.3, 129.0, 127.9, 127.0, 126.20 98.8, 36.4.

LRMS (APCI) m/z: $[M+H]^+$ calc'd. for $C_{14}H_{12}ClINO$, 371.9; found 371.6

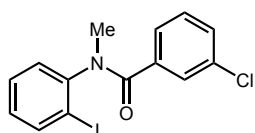


3-chloro-*N*-(2-iodophenyl)benzamide (S30): To a solution of 2-iodoaniline (608 mg, 2.8 mmol, 1.0 equiv) in dichloromethane was added 3-chlorobenzoyl chloride (380 μ L, 3.0 mmol, 1.1 equiv) dropwise via syringe, followed by triethylamine (450 μ L, 3.2 mmol, 1.1 equiv). The resulting mixture was stirred at room temperature for 4 h, quenched with methanol, and concentrated. The resulting solid was purified on silica gel (10–20% EtOAc/Hex eluent) to afford the title compound as a white solid. (767 mg, 77 %).

1H NMR (399 MHz, $CDCl_3$) δ 8.39 (dd, $J = 8.2, 1.6$ Hz, 1H), 8.20 (s, 1H), 8.01 – 7.90 (m, 1H), 7.86 – 7.75 (m, 2H), 7.55 (ddd, $J = 8.0, 2.1, 1.1$ Hz, 1H), 7.46 (t, $J = 7.9$ Hz, 1H), 7.40 (m, 1H), 6.89 (ddd, $J = 8.0, 7.3, 1.6$ Hz, 1H).

^{13}C NMR (100 MHz, $CDCl_3$) δ 163.9, 138.8, 137.9, 136.3, 135.2, 132.2, 130.2, 129.4, 127.7, 126.4, 125.0, 121.9, 90.4.

LRMS (APCI) m/z: $[M+H]^+$ calc'd. for $C_{13}H_{10}ClINO$, 357.9; found 357.6



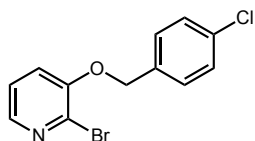
3-chloro-*N*-(2-iodophenyl)-*N*-methylbenzamide (S31): In a vial under nitrogen, sodium hydride as a 60% dispersion in mineral oil (66 mg, 1.7 mmol, 1.9 equiv) was suspended in DMF and cooled to 0 $^{\circ}C$. **S30** as a solution in DMF (321 mg, 0.9 mmol, 1.0 equiv) was added dropwise to the

sodium hydride suspension and stirred for 30 minutes before the addition of methyl iodide (90 μ L, 1.4 mmol, 1.6 equiv). The reaction was removed from the ice bath, and after reacting for 1.5 h, was quenched with methanol then water at 0 °C. The resulting mixture was diluted with ethyl acetate and washed with brine 3x. The organic layer was dried with MgSO₄, concentrated *in vacuo*, and purified on silica gel (10-25% EtOAc/Hex eluent) to afford the title compound as a white solid (215 mg, 64%).

¹H NMR (399 MHz, CDCl₃) δ 7.77 (dd, J = 7.9, 1.4 Hz, 1H), 7.39 (t, J = 1.9 Hz, 1H), 7.24 – 7.19 (m, 1H), 7.16 (dd, J = 7.9, 1.9 Hz, 2H), 7.09 (dd, J = 7.9, 1.6 Hz, 1H), 7.03 (dd, J = 8.4, 7.3 Hz, 1H), 6.90 (td, J = 7.7, 1.6 Hz, 1H), 3.34 (s, 3H).

¹³C NMR (100 MHz, CDCl₃) δ 169.2, 146.4, 140.2, 137.3, 133.7, 130.0, 129.9, 129.5, 129.4, 128.9, 128.6, 126.3, 98.9, 37.5.

LRMS (APCI) m/z : [M+H]⁺ calc'd. for C₁₄H₁₂ClINO, 371.9; found 371.6

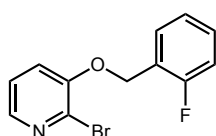


2-bromo-3-((4-chlorobenzyl)oxy)pyridine (S32): A round bottom flask was charged with 2-bromo-3-hydroxypyridine (522 mg, 3.0 mmol, 1.0 equiv) and K₂CO₃ (829 mg, 6.0 mmol, 2.0 equiv). MeCN (15 mL) was added, followed by 4-chlorobenzyl bromide (740 mg, 3.6 mmol, 1.2 equiv). The reaction was heated to 60 °C and stirred for 20 h. The reaction was cooled to room temperature, diluted with water, and extracted with EtOAc 3x. The combined organic layers were washed with brine, dried over MgSO₄, and purified on silica gel (20% EtOAc/Hex eluent) to afford the title compound as a white solid (771 mg, 86%).

¹H NMR (500 MHz, CDCl₃) δ 8.02 (dd, J = 4.6, 1.6 Hz, 1H), 7.44 – 7.34 (m, 4H), 7.19 (dd, J = 8.1, 4.6 Hz, 1H), 7.14 (dd, J = 8.1, 1.6 Hz, 1H), 5.15 (s, 2H) ppm.

¹³C NMR (151 MHz, CDCl₃) δ 151.9, 141.9, 134.3, 134.1, 133.5, 129.0, 128.5, 123.4, 120.5, 70.3 ppm.

LRMS (APCI) m/z: [M+H]⁺ calc'd. for C₁₂H₁₀BrClNO, 298.0; found 297.7



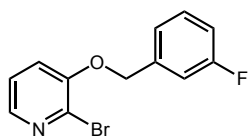
2-bromo-3-((2-fluorobenzyl)oxy)pyridine (S33): A round bottom flask was charged with 2-bromo-3-hydroxypyridine (522 mg, 3.0 mmol, 1.0 equiv) and K₂CO₃ (829 mg, 6.0 mmol, 2.0 equiv). MeCN (15 mL) was added, followed by 2-fluorobenzyl bromide (0.36 mL, 3.0 mmol, 1.0 equiv). The reaction was heated to 60 °C and stirred for 15 h. The reaction was cooled to room temperature, diluted with water, and extracted with EtOAc 3x. The combined organic layers were washed with brine, dried over MgSO₄, and purified on silica gel (10-30% EtOAc/Hex eluent) to afford the title compound as a white solid (753 mg, 89%).

¹H NMR (400 MHz, CDCl₃) δ 8.02 (dd, J = 3.8, 2.4 Hz, 1H), 7.60 (tdd, J = 7.5, 1.9, 0.8 Hz, 1H), 7.38 – 7.30 (m, 1H), 7.24 – 7.17 (m, 3H), 7.10 (ddd, J = 10.3, 8.2, 1.1 Hz, 1H), 5.25 (s, 3H) ppm.

¹³C NMR (151 MHz, CDCl₃) δ 160.3 (d, ¹J_{C-F} = 246.6 Hz), 152.0, 142.1, 133.6, 130.2 (d, ³J_{C-F} = 8.3 Hz), 129.5 (d, ³J_{C-F} = 3.8 Hz), 124.8 (d, ⁴J_{C-F} = 3.7 Hz), 123.6, 123.0 (d, ²J_{C-F} = 13.9 Hz), 120.5, 115.5 (d, ²J_{C-F} = 21.0 Hz), 64.8 (d, ³J_{C-F} = 4.6 Hz) ppm.

¹⁹F NMR (376 MHz, CDCl₃-d) δ -117.7 – -121.1 (m) ppm.

LRMS (APCI) m/z: [M+H]⁺ calc'd. for C₁₂H₁₀BrFNO, 282.0; found 281.8



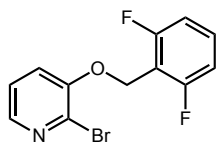
2-bromo-3-((3-fluorobenzyl)oxy)pyridine (S34): A round bottom flask was charged with 2-bromo-3-hydroxypyridine (522 mg, 3.0 mmol, 1.0 equiv) and K_2CO_3 (829 mg, 6.0 mmol, 2.0 equiv). MeCN (15 mL) was added, followed by 3-fluorobenzyl bromide (0.37 mL, 3.0 mmol, 1.0 equiv). The reaction was heated to 60 °C and stirred for 15 h. The reaction was cooled to room temperature, diluted with water, and extracted with EtOAc 3x. The combined organic layers were washed with brine, dried over $MgSO_4$, and purified on silica gel (10-30% EtOAc/Hex eluent) to afford the title compound as a white solid (765 mg, 90%).

1H NMR (400 MHz, $CDCl_3$) δ 8.02 (dd, $J = 4.6, 1.7$ Hz, 1H), 7.37 (td, $J = 7.9, 5.7$ Hz, 1H), 7.25 – 7.17 (m, 3H), 7.14 (dd, $J = 8.1, 1.7$ Hz, 1H), 7.04 (tdd, $J = 8.6, 2.7, 0.9$ Hz, 1H), 5.17 (s, 2H) ppm.

^{13}C NMR (151 MHz, $CDCl_3$) δ 163.2 (d, $^1J_{C-F} = 247.0$ Hz), 152.0, 142.1, 138.3 (d, $^3J_{C-F} = 7.4$ Hz), 133.6, 130.6 (d, $^3J_{C-F} = 8.3$ Hz), 123.5, 122.5 (d, $^4J_{C-F} = 3.0$ Hz), 120.5, 115.4 (d, $^2J_{C-F} = 21.2$ Hz), 114.1 (d, $^2J_{C-F} = 22.6$ Hz), 70.3 (d, $^4J_{C-F} = 2.1$ Hz) ppm.

^{19}F NMR (376 MHz, $CDCl_3$) δ -112.2 (td, $J = 9.1, 5.9$ Hz) ppm.

LRMS (APCI) m/z : $[M+H]^+$ calc'd. for $C_{12}H_{10}BrFNO$, 282.0; found 281.8



2-bromo-3-((2,6-difluorobenzyl)oxy)pyridine (S35): A round bottom flask was charged with 2-bromo-3-hydroxypyridine (522 mg, 3.0 mmol, 1.0 equiv) and K_2CO_3 (829 mg, 6.0 mmol, 2.0

equiv). MeCN (15 mL) was added, followed by 2,6-difluorobenzyl bromide (621 mg, 3.0 mmol, 1.0 equiv). The reaction was heated to 60 °C and stirred for 15 h. The reaction was cooled to room temperature, diluted with water, and extracted with EtOAc 3x. The combined organic layers were washed with brine, and dried over MgSO₄ to afford the title compound as an off-white solid (868 mg, 96%).

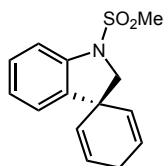
¹H NMR (400 MHz, CDCl₃) δ 8.04 – 8.00 (m, 1H), 7.41 – 7.31 (m, 2H), 7.25 – 7.21 (m, 1H), 6.96 (dd, J = 8.3, 7.4 Hz, 2H), 5.22 (s, 2H).

¹³C NMR (151 MHz, CDCl₃) δ 162.1 (dd, ¹J_{C-F} = 251.6, ³J_{C-F} = 7.3 Hz), 152.2, 142.4, 134.0, 131.5 (t, ³J_{C-F} = 10.5 Hz), 123.5, 121.4, 111.8 (dd, ²J_{C-F} = 21.0, ⁴J_{C-F} = 4.8 Hz), 111.7 (t, ²J_{C-F} = 18.8 Hz), 59.6 (t, ³J_{C-F} = 3.7 Hz) ppm.

¹⁹F NMR (376 MHz, CDCl₃) δ -114.1 (t, J = 6.8 Hz) ppm.

LRMS (APCI) m/z: [M+H]⁺ calc'd. for C₁₂H₉BrF₂NO, 300.0; found 299.8

Preparation of Products from the Substrate Table

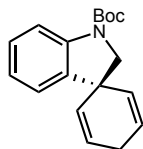


1'-(methylsulfonyl)spiro[cyclohexane-1,3'-indoline]-2,5-diene (9): Prepared according to General Procedure A using *N*-benzyl-*N*-(2 iodophenyl) methanesulfonamide (**S3**) (145 mg, 0.4 mmol, 1.0 equiv), DIPEA (210 μL, 1.2 mmol, 3 equiv) and 3DPAFIPN (12 mg, 5 mol%). After 16 h, the reaction was purified on silica (10 – 30% EtOAc/Hex) to provide the desired product as a colorless oil (63.3 mg, 65% yield).

¹H NMR (500 MHz, CDCl₃) δ 7.41 (d, *J* = 8.1, 0.7 Hz, 1H), 7.22 (ddd, *J* = 8.0, 5.2, 3.5 Hz, 1H), 7.08 – 7.03 (m, 3H), 5.91 (dtt, *J* = 10.3, 3.4, 1.1 Hz, 3H), 5.69 (app. dp, *J* = 10.4, 2.3 Hz, 2H), 3.81 (s, 2H), 2.92 (s, 3H), 2.85 – 2.70 (m, 3H).

¹³C NMR (126 MHz, CDCl₃) δ 140.3, 138.1, 128.6, 128.6, 125.5, 124.7, 124.1, 113.3, 63.4, 45.2, 34.5, 25.9.

HRMS (ESI) *m/z*: [M+H]⁺ calc'd. for C₁₄H₁₆NO₂S, 262.0824, found 262.0884.



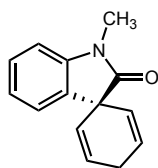
***tert*-butyl spiro[cyclohexane-1,3'-indoline]-2,5-diene-1'-carboxylate (10)**: Prepared according to General Procedure A using *tert*-butyl benzyl(2-bromophenyl)carbamate

(**S4**) (69 mg, 0.2 mmol, 1 equiv), DIPEA (105 μL, 0.6 mmol, 3 equiv) and 3DPAFIPN (6 mg, 5 mol%). After 16 h, the reaction was purified on silica (0–5% EtOAc/Hex) to provide the desired product as a light yellow oil (47 mg, 79% yield).

¹H NMR (600 MHz, CDCl₃) δ 7.68 (bs, 1H), 7.20 (ddd, *J* = 8.3, 7.4, 1.5 Hz, 1H), 7.02 (dd, *J* = 7.5, 1.3 Hz, 1H), 6.97 (td, *J* = 7.4, 1.1 Hz, 1H), 5.87 (dt, *J* = 10.2, 3.4 Hz, 2H), 5.71 (dt, *J* = 10.3, 2.0 Hz, 2H), 3.87 (s, 2H), 2.81 (dddd, *J* = 23.1, 5.4, 3.3, 2.1 Hz, 1H), 2.74 (dtt, *J* = 23.2, 3.5, 2.0 Hz, 1H), 1.60 (s, 9H).

¹³C NMR (151 MHz, CDCl₃) δ 152.4, 141.1, 138.1, 130.0, 128.0, 124.8, 123.4, 122.7, 114.7, 80.9, 61.7, 44.5, 28.5, 25.9.

HRMS (ESI) *m/z*: [M+H]⁺ calc'd. for C₁₈H₂₂NO, 284.1572; found 284.1657

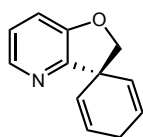


1'-methylspiro[cyclohexane-1,3'-indoline]-2,5-dien-2'-one (11): Prepared according to General Procedure A using *N*-(2-iodophenyl)-*N*-methylbenzamide (**S6**) (165 mg, 0.5 mmol, 1.0 equiv), DIPEA (260 μ L, 1.5 mmol, 3 equiv) and 3DPAFIPN (14 mg, 4 mol%). After 16 h, the reaction was purified on silica (10–20% EtOAc/Hex) to provide the desired product as a white solid (58 mg, 55% yield).

^1H NMR (500 MHz, CDCl_3) δ 7.29 (tt, $J = 7.7, 1.2$ Hz, 1H), 7.14 – 7.11 (m, 1H), 7.06 (tt, $J = 7.4, 1.0$ Hz, 1H), 6.85 (d, $J = 7.8, 0.8$ Hz, 1H), 6.14 (dtd, $J = 10.3, 3.4, 0.9$ Hz, 2H), 5.39 (dtd, $J = 10.5, 2.0, 0.9$ Hz, 2H), 3.23 (s, 3H), 3.02 – 2.94 (m, 1H), 2.90 – 2.81 (m, 1H).

^{13}C NMR (126 MHz, CDCl_3) δ 177.9, 143.0, 134.2, 128.4, 127.3, 124.7, 123.8, 122.9, 108.0, 51.8, 26.6, 25.7.

HRMS (ESI) m/z : $[\text{M}+\text{H}]^+$ calc'd. for $\text{C}_{14}\text{H}_{24}\text{NO}$, 212.0997; found 212.1118.

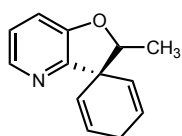


2'*H*-spiro[cyclohexane-1,3'-furo[3,2-*b*]pyridine]-2,5-diene (12): Prepared according to General Procedure A using 3-(benzyloxy)-2-bromopyridine (**S7**) (128 mg, 0.5 mmol, 1 equiv), DIPEA (270 μ L, 1.5 mmol, 3 equiv) and 3DPAFIPN (18 mg, 6 mol%). After 16 h, the reaction was purified on silica (20 – 40% Et_2O /Hex) to provide the desired product as a colorless oil (65 mg, 72% yield).

¹H NMR (600 MHz, CDCl₃) δ 8.14 (dd, *J* = 4.7, 1.4 Hz, 1H), 7.09 (dd, *J* = 8.1, 1.4 Hz, 1H), 7.05 (dd, *J* = 8.1, 4.7 Hz, 1H), 6.02 (dt, *J* = 10.2, 3.4 Hz, 2H), 5.75 (dt, *J* = 10.3, 2.0 Hz, 2H), 4.46 (s, 2H), 2.93 (dtt, *J* = 23.3, 3.3, 2.1 Hz, 1H), 2.74 (dtt, *J* = 23.4, 3.5, 2.1 Hz, 1H).

¹³C NMR (151 MHz, CDCl₃) δ 155.1, 152.6, 142.8, 127.0, 125.8, 122.8, 116.6, 83.0, 47.6, 26.0

HRMS (ESI) *m/z*: [M+H]⁺ calc'd. for C₁₃H₁₂NO, 186.0840; found 186.1081.

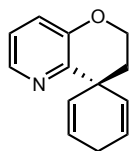


2'-methyl-2'*H*-spiro[cyclohexane-1,3'-furo[3,2-*b*]pyridine]-2,5-diene (13): Prepared according to General Procedure B using 2-bromo-3-(1-phenylethoxy)pyridine (**S8**) (152 mg, 0.6 mmol, 1 equiv), DIPEA (1.1 mL, 6.2 mmol, 10 equiv) and 3DPAFIPN (17 mg, 4 mol%). After 16 h, the reaction was purified on silica (15– 20% EtOAc/Hex) to provide the desired product as a yellow oil (54 mg, 50% yield).

¹H NMR (600 MHz, CDCl₃) δ 8.12 (dd, *J* = 4.5, 1.7 Hz, 1H), 7.07 (dd, *J* = 8.1, 1.7 Hz, 1H), 7.04 (dd, *J* = 8.1, 4.5 Hz, 1H), 6.15 (dtd, *J* = 10.0, 3.4, 1.6 Hz, 1H), 5.98 (dtd, *J* = 10.1, 3.4, 1.6 Hz, 1H), 5.67 (dq, *J* = 10.0, 2.1 Hz, 1H), 5.59 (dq, *J* = 10.1, 2.1 Hz, 1H), 4.57 (q, *J* = 6.6 Hz, 1H), 2.91 (dtt, *J* = 23.4, 3.7, 2.0 Hz, 1H), 2.76 (dtt, *J* = 23.3, 3.2, 2.2 Hz, 1H), 1.42 (d, *J* = 6.6 Hz, 3H).

¹³C NMR (151 MHz, CDCl₃) δ 156.3, 152.4, 142.7, 127.9, 126.4, 125.9, 124.5, 122.8, 116.4, 88.7, 50.7, 26.3, 15.2.

HRMS (ESI) *m/z*: [M+H]⁺ calc'd. for C₁₃H₁₄NO, 200.0997; found 200.1184

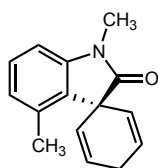


2',3'-dihydrospiro[cyclohexane-1,4'-pyrano[3,2-*b*]pyridine]-2,5-diene (14): Prepared according to General Procedure A using 2-bromo-3-phenethoxypyridine (**S9**) (59 mg, 0.2 mmol, 1 equiv) DIPEA (105 μ L, 0.6 mmol, 3 equiv) and 3DPAFIPN (6 mg, 5 mol%). After 16 h, the reaction was purified on silica (20 – 30% EtOAc/Hex) to provide the desired product as a colorless oil (18 mg, 46% yield).

$^1\text{H NMR}$ (500 MHz, CDCl_3) δ 8.24 (dd, $J = 4.5, 1.5$ Hz, 1H), 7.12 (dd, $J = 8.2, 1.5$ Hz, 1H), 7.05 (dd, $J = 8.2, 4.5$ Hz, 1H), 5.96 (dt, $J = 10.3, 3.4$ Hz, 2H), 5.77 (dt, $J = 10.4, 2.0$ Hz, 2H), 4.35 – 4.19 (m, 2H), 2.92 (dt, $J = 23.0, 3.6, 1.8$ Hz, 1H), 2.73 (dddd, $J = 23.0, 5.5, 3.1, 2.4$ Hz, 1H), 2.11 – 2.01 (m, 2H).

$^{13}\text{C NMR}$ (151 MHz, CDCl_3) δ 150.4, 148.4, 142.4, 131.0, 124.4, 124.4, 122.8, 77.2, 77.0, 76.8, 62.4, 39.3, 37.4, 26.2.

HRMS (ESI) m/z : $[\text{M}+\text{H}]^+$ calc'd. for $\text{C}_{13}\text{H}_{14}\text{NO}$, 200.0997, found 200.1247.

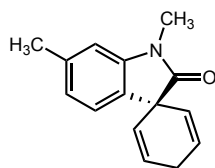


1',4'-dimethylspiro[cyclohexane-1,3'-indoline]-2,5-dien-2'-one (15): Prepared according to General Procedure A using *N*-(2-bromo-3-methylphenyl)-*N*-methylbenzamide (**S11**) (170 mg, 0.6 mmol, 1 equiv), DIPEA (300 μ L, 1.7 mmol, 3 equiv) and 3DPAFIPN (15 mg, 4 mol%). After 16 h, the reaction was purified on silica (20 % EtOAc/Hex) to provide the desired product as a yellow solid (106 mg, 84% yield).

$^1\text{H NMR}$ (600 MHz, CDCl_3) δ 7.22 (t, $J = 7.8$ Hz, 1H), 6.85 (dt, $J = 7.8, 0.8$ Hz, 1H), 6.72 (dt, $J = 7.7, 0.8$ Hz, 1H), 6.17 (dt, $J = 10.3, 3.4$ Hz, 2H), 5.36 (dt, $J = 10.3, 2.0$ Hz, 2H), 3.23 (s, 3H), 3.04 (dtt, $J = 23.3, 3.4, 2.1$ Hz, 1H), 2.82 (dtt, $J = 23.2, 3.4, 2.1$ Hz, 1H), 2.22 (s, 3H).

$^{13}\text{C NMR}$ (151 MHz, CDCl_3) δ 177.6, 143.1, 136.0, 130.1, 128.3, 127.7, 125.1, 122.7, 105.7, 51.8, 26.7, 25.8, 16.7.

HRMS (ESI) m/z : $[\text{M}+\text{H}]^+$ calc'd. for $\text{C}_{15}\text{H}_{16}\text{NO}$, 226.1154; found 226.1323.



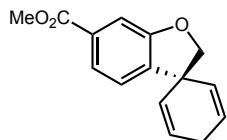
1',6'-dimethylspiro[cyclohexane-1,3'-indoline]-2,5-dien-2'-one (16)

Prepared according to General Procedure A using *N*-(2-bromo-5-methylphenyl)-*N*-methylbenzamide (**S13**) (152 mg, 0.5 mmol, 1 equiv), DIPEA (280 μL , 1.5 mmol, 3 equiv) and 3DPAFIPN (15 mg, 5 mol%). After 16 h, purification via preparative HPLC on an Agilent 1200 Infinity Series chromatograph using an Agilent PrepC18 30 x 250 mm 10 μm column, with a linear gradient using water and 0.1% formic acid (FA) (Solvent A) and MeCN and 0.1% FA (Solvent B); $t=0$ min, 50% B, $t = 25$ min, 99% B, with a flow rate 40 mL/min, to provide the desired product as a light yellow solid (80.0 mg, 71% yield).

$^1\text{H NMR}$ (400 MHz, CDCl_3) δ 7.00 (d, $J = 7.5$ Hz, 1H), 6.87 (ddd, $J = 7.4, 1.5, 0.8$ Hz, 1H), 6.67 (dd, $J = 1.6, 0.8$ Hz, 1H), 6.16 – 6.07 (m, 2H), 5.37 (dt, $J = 10.3, 2.0$ Hz, 2H), 3.21 (s, 3H), 2.97 (dtt, $J = 23.3, 3.3, 2.2$ Hz, 1H), 2.84 (dtt, $J = 23.2, 3.6, 2.0$ Hz, 1H), 2.39 (d, $J = 0.7$ Hz, 3H) ppm.

$^{13}\text{C NMR}$ (126 MHz, CDCl_3) δ 178.3, 143.2, 138.8, 131.5, 127.2, 124.6, 124.2, 123.5, 109.1, 51.7, 26.7, 25.9, 21.9 ppm.

HRMS (ESI) m/z: $[M+H]^+$ calc'd. for $C_{15}H_{16}NO$, 226.1154; found 226.1303.

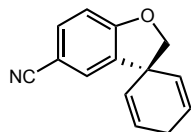


methyl 2*H*-spiro[benzofuran-3,1'-cyclohexane]-2',5'-diene-6-carboxylate (17): Prepared according to General Procedure A using methyl 3-(benzyloxy)-4-iodobenzoate (**S14**) (156 mg, 0.4 mmol, 1 equiv), DIPEA (260 μ L, 1.5 mmol, 3 equiv) and 3DPAFIPN (17 mg, 5 mol%). After 16 h, the reaction was purified on silica (10 – 30% EtOAc/Hex) to provide the desired product as a yellow oil (66 mg, 64% yield).

1H NMR (500 MHz, $CDCl_3$) δ 7.60 (dd, $J = 7.8, 1.5$ Hz, 1H), 7.44 (d, $J = 1.5$ Hz, 1H), 7.06 (d, $J = 7.7$ Hz, 1H), 5.90 (dt, $J = 10.1, 3.4$ Hz, 2H), 5.70 (dt, $J = 10.2, 2.0$ Hz, 2H), 4.39 (s, 2H), 3.89 (s, 3H), 2.81 (dddd, $J = 23.3, 5.4, 3.2, 2.1$ Hz, 1H), 2.72 (dtt, $J = 23.3, 3.5, 2.1$ Hz, 1H).

^{13}C NMR (151 MHz, $CDCl_3$) δ 166.9, 159.0, 139.7, 130.8, 128.3, 124.6, 124.6, 123.1, 110.7, 83.7, 77.2, 77.0, 76.8, 52.1, 47.4, 25.9.

HRMS (ESI) m/z: $[M+H]^+$ calc'd. for $C_{15}H_{15}O_3$, 243.0943; found 243.1062.

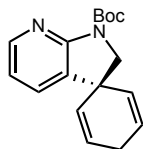


2*H*-spiro[benzofuran-3,1'-cyclohexane]-2',5'-diene-5-carbonitrile (18): Prepared according to General Procedure B using 4-(benzyloxy)-3-chlorobenzonitrile (**S15**) (119 mg, 0.5 mmol, 1 equiv), DIPEA (900 μ L, 5.2 mmol, 10 equiv) and 3DPAFIPN (18 mg, 6 mol%). After 16 h, the reaction was purified on silica (5% EtOAc/Hex) to provide the desired product as a yellow solid (55 mg, 54% yield).

¹H NMR (600 MHz, CDCl₃) δ 7.47 (dd, *J* = 8.3, 1.8 Hz, 1H), 7.31 (d, *J* = 1.8 Hz, 1H), 6.86 (d, *J* = 8.3 Hz, 1H), 5.94 (dt, *J* = 10.1, 3.4 Hz, 2H), 5.69 (dt, *J* = 10.2, 2.0 Hz, 2H), 4.44 (s, 2H), 2.83 (dddd, *J* = 23.4, 5.4, 3.4, 2.1 Hz, 1H), 2.75 (dtt, *J* = 23.4, 3.7, 2.0 Hz, 1H).

¹³C NMR (151 MHz, CDCl₃) δ 162.4, 136.1, 133.8, 129.3, 127.9, 125.1, 119.4, 110.7, 104.3, 84.3, 47.0, 25.8.

HRMS (ESI) *m/z*: [M+H]⁺ calc'd. for C₁₄H₁₂NO, 210.0841; found 210.0954.



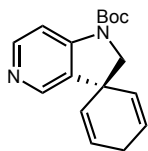
***tert*-butyl spiro[cyclohexane-1,3'-pyrrolo[2,3-*b*]pyridine]-2,5-diene-1'(2'*H*)-carboxylate (19):**

Prepared according to General Procedure A using *tert*-butyl benzyl(3-bromopyridin-2-yl)carbamate (**S17**) (182 mg, 0.5 mmol, 1 equiv), DIPEA (260 μL, 1.5 mmol, 3 equiv) and 3DPAFIPN (16 mg, 5 mol%). After 16 h, the reaction was purified on silica (10 – 30% EtOAc/Hex) to provide the desired product as a yellow oil (109 mg, 77% yield).

¹H NMR (600 MHz, CDCl₃) δ 8.25 (dd, *J* = 5.1, 1.7 Hz, 1H), 7.27 – 7.23 (m, 1H), 6.84 (dd, *J* = 7.4, 5.1 Hz, 1H), 5.88 (dt, *J* = 10.2, 3.4 Hz, 2H), 5.65 (dt, *J* = 10.3, 2.0 Hz, 2H), 3.85 (s, 2H), 2.78 (dtt, *J* = 23.3, 3.3, 2.1 Hz, 1H), 2.72 (dtt, *J* = 23.3, 3.4, 2.1 Hz, 1H), 1.55 (s, 9H) ppm.

¹³C NMR (151 MHz, CDCl₃) δ 155.4, 151.0, 148.1, 133.3, 131.7, 129.2, 124.4, 118.1, 81.6, 60.9, 42.5, 28.5, 26.0 ppm.

HRMS (ESI) *m/z*: [M+H]⁺ calc'd. for C₁₇H₂₁N₂O₂, 285.1525; found 285.1752.



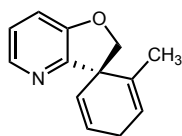
***tert*-butyl spiro[cyclohexane-1,3'-pyrrolo[3,2-*c*]pyridine]-2,5-diene-1'(2'*H*)-carboxylate (20):**

Prepared according to General Procedure A using *tert*-butyl benzyl(3-bromopyridin-4-yl)carbamate (**S19**) (182 mg, 0.5 mmol, 1 equiv), DIPEA (260 μ L, 1.5 mmol, 3 equiv) and 3DPAFIPN (16 mg, 5 mol%). After 16 h, the reaction was purified on silica (20-30% EtOAc/Hex) to provide the desired product as a yellow oil (127 mg, 89% yield).

¹H NMR (600 MHz, CDCl₃) δ 8.35 (d, *J* = 5.5 Hz, 1H), 8.12 (d, *J* = 0.8 Hz, 1H), 7.67 (s, 1H), 5.88 (dt, *J* = 10.1, 3.4 Hz, 2H), 5.67 (dt, *J* = 10.3, 2.0 Hz, 2H), 3.85 (s, 2H), 2.81 (dddd, *J* = 23.3, 5.4, 3.3, 2.1 Hz, 1H), 2.73 (dt, *J* = 23.4, 3.8, 2.1 Hz, 1H), 1.57 (s, 9H) ppm.

¹³C NMR (151 MHz, CDCl₃) δ 152.0, 149.8, 148.1, 146.7, 133.8, 129.2, 124.3, 109.5, 82.3, 62.2, 43.4, 28.5, 25.9 ppm.

HRMS (ESI) *m/z*: [M+H]⁺ calc'd. for C₁₇H₂₁N₂O₂, 285.1525; found 285.1696



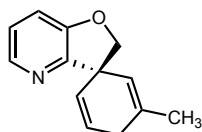
2-methyl-2'*H*-spiro[cyclohexane-1,3'-furo[3,2-*b*]pyridine]-2,5-diene (21): Prepared according to General Procedure A using 2-bromo-3-((2-methylbenzyl)oxy)pyridine

(**S20**) (156 mg, 0.6 mmol, 1 equiv) DIPEA (260 μ L, 1.5 mmol, 3 equiv) and 3DPAFIPN (16 mg, 4 mol%). After 16 h, the reaction was purified on silica (15 – 30% EtOAc/Hex) to provide the desired product as a yellow oil (97 mg, 87% yield).

¹H NMR (600 MHz, CDCl₃) δ 8.14 (dd, *J* = 4.7, 1.5 Hz, 1H), 7.07 (dd, *J* = 8.1, 1.6 Hz, 1H), 7.04 (dd, *J* = 8.1, 4.6 Hz, 1H), 6.00 (dtd, *J* = 9.9, 3.4, 1.5 Hz, 1H), 5.71 – 5.67 (m, 2H), 4.65 (d, *J* = 9.3 Hz, 1H), 4.37 (d, *J* = 9.3 Hz, 1H), 2.91 (dtt, *J* = 23.3, 3.7, 1.9 Hz, 1H), 2.73 (dtt, *J* = 23.3, 3.4, 1.9 Hz, 1H), 1.53 (q, *J* = 1.8 Hz, 3H).

¹³C NMR (151 MHz, CDCl₃) δ 154.5, 153.3, 142.8, 132.0, 127.7, 125.6, 122.7, 122.2, 116.6, 81.5, 50.6, 27.0, 19.0.

HRMS (ESI) *m/z*: [M+H]⁺ calc'd. for C₁₃H₁₃NO, 200.0997; found 200.1057.



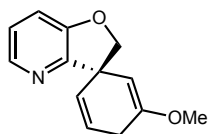
3-methyl-2'*H*-spiro[cyclohexane-1,3'-furo[3,2-*b*]pyridine]-2,5-diene (22): Prepared according to General Procedure A using 2-bromo-3-((3-methylbenzyl)oxy)pyridine

(**S21**) (131 mg, 0.5 mmol, 1 equiv), DIPEA (260 μL, 1.5 mmol, 3 equiv) and 3DPAFIPN (17 mg, 5 mol%). After 16 h, the reaction was purified on silica (20 – 30% EtOAc/Hex) to provide the desired product as a light yellow solid (94 mg, 72% yield).

¹H NMR (600 MHz, CDCl₃) δ 8.12 (dd, *J* = 4.8, 1.4 Hz, 1H), 7.07 (dd, *J* = 8.1, 1.4 Hz, 1H), 7.03 (dd, *J* = 8.1, 4.8 Hz, 1H), 5.99 (dt, *J* = 9.9, 3.4 Hz, 1H), 5.72 (dq, *J* = 9.9, 2.1 Hz, 1H), 5.46 (p, *J* = 1.7 Hz, 1H), 4.41 (d, *J* = 1.2 Hz, 2H), 2.82 (d, *J* = 23.2 Hz, 1H), 2.62 (d, *J* = 23.5 Hz, 1H), 1.79 (s, 3H).

¹³C NMR (151 MHz, CDCl₃) δ 155.4, 152.6, 142.7, 133.4, 126.9, 125.7, 122.7, 121.8, 116.5, 83.1, 48.8, 30.8, 23.2.

HRMS (ESI) *m/z*: [M+H]⁺ calc'd. for C₁₃H₁₄NO, 200.0997; found 200.1304

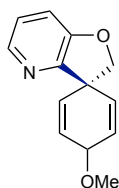


3-methoxy-2'*H*-spiro[cyclohexane-1,3'-furo[3,2-*b*]pyridine]-2,5-diene (23): Prepared according to General Procedure A using 2-bromo-3-((3-methoxybenzyl)oxy)pyridine (**S22**) (145 mg, 0.5 mmol, 1 equiv) DIPEA (260 μ L, 1.5 mmol, 3 equiv) and 3DPAFIPN (16 mg, 5 mol%). After 16 h, the reaction was purified on silica (20 – 30% EtOAc/Hex) to provide the desired product as an orange solid (89 mg, 84% yield).

$^1\text{H NMR}$ (600 MHz, CDCl_3) δ 8.14 (dd, $J = 4.8, 1.4$ Hz, 1H), 7.09 (dd, $J = 8.1, 1.4$ Hz, 1H), 7.05 (dd, $J = 8.1, 4.7$ Hz, 1H), 5.91 (dt, $J = 9.9, 3.5$ Hz, 1H), 5.71 (dq, $J = 9.8, 2.1$ Hz, 1H), 4.69 (q, $J = 1.3$ Hz, 1H), 4.47 (d, $J = 8.9$ Hz, 1H), 4.42 (d, $J = 9.0$ Hz, 1H), 3.57 (s, 3H), 2.97 (d, $J = 22.0$ Hz, 1H), 2.78 (d, $J = 22.0$ Hz, 1H).

$^{13}\text{C NMR}$ (151 MHz, CDCl_3) δ 155.6, 154.7, 152.5, 142.8, 127.4, 124.2, 122.7, 116.6, 95.5, 83.7, 54.0, 49.6, 28.6.

HRMS (ESI) m/z : $[\text{M}+\text{H}]^+$ calc'd. for $\text{C}_{13}\text{H}_{14}\text{NO}_2$, 216.0946; found 216.1049

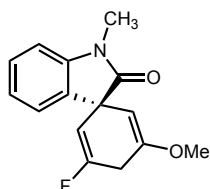


4-methoxy-2'*H*-spiro[cyclohexane-1,3'-furo[3,2-*b*]pyridine]-2,5-diene (24): Prepared according to General Procedure B using 2-bromo-3-((4-methoxybenzyl)oxy)pyridine (**S23**) (159 mg, 0.5 mmol, 1 equiv) DIPEA (900 μ L, 5.2 mmol, 10 equiv) and 3DPAFIPN (19 mg, 5 mol%). After 16 h, the reaction was purified on silica (20 – 50% EtOAc/Hex) to isolate a single diastereomer as a light yellow oil (72 mg, 62% yield).

¹H NMR (600 MHz, CDCl₃) δ 8.12 (dd, *J* = 4.8, 1.4 Hz, 1H), 7.13 (dd, *J* = 8.1, 1.4 Hz, 1H), 7.08 (dd, *J* = 8.1, 4.8 Hz, 1H), 6.13 (dd, *J* = 10.2, 3.2 Hz, 2H), 6.02 (dd, *J* = 10.1, 1.6 Hz, 2H), 4.61 (tt, *J* = 3.2, 1.6 Hz, 1H), 4.54 (s, 2H), 3.39 (s, 3H).

¹³C NMR (151 MHz, CDCl₃) δ 153.3, 153.1, 142.8, 130.7, 126.6, 123.2, 117.0, 80.7, 69.2, 54.4, 48.5.

HRMS (ESI) *m/z*: [M+H]⁺ calc'd. for C₁₃H₁₄NO₂, 216.0946; found 216.1081.



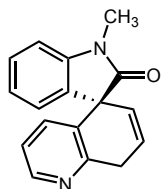
3-fluoro-5-methoxy-1'-methylspiro[cyclohexane-1,3'-indoline]-2,5-dien-2'-one (25): Prepared according to General Procedure A using 3-fluoro-*N*-(2-iodophenyl)-5-methoxy-*N*-methylbenzamide (**S25**) (77 mg, 0.2 mmol, 1 equiv), DIPEA (105 μL, 0.6 mmol, 3 equiv) and 3DPAFIPN (6 mg, 5 mol%). After 16 h, the reaction was purified on silica (10-30% EtOAc/Hex) to provide the desired product as a yellow oil (35 mg, 68% yield).

¹H NMR (400 MHz, CDCl₃) δ 7.30 (td, *J* = 7.6, 1.5 Hz, 1H), 7.13 (ddd, *J* = 7.4, 1.5, 0.6 Hz, 1H), 7.07 (td, *J* = 7.4, 1.0 Hz, 1H), 6.85 (dt, *J* = 7.8, 0.8 Hz, 1H), 4.98 (dq, *J* = 14.7, 1.5 Hz, 1H), 4.33 (t, *J* = 1.6 Hz, 1H), 3.54 (s, 3H), 3.24 (s, 3H), 3.24 (dt, *J* = 20.8, 1.5 Hz, 1H), 3.09 (dq, *J* = 21.0, 1.3 Hz, 1H) ppm.

¹³C NMR (126 MHz, CDCl₃) δ 178.2, 158.9 (d, ¹*J*_{C-F} = 257.2 Hz), 154.5 (d, ³*J*_{C-F} = 16.1 Hz), 142.8, 133.9, 128.7, 124.8, 123.2, 101.6 (d, ²*J*_{C-F} = 18.4 Hz), 92.9, 54.8, 52.1 (d, ³*J*_{C-F} = 9.2 Hz), 29.6 (d, ²*J*_{C-F} = 28.2 Hz), 26.76 ppm.

¹⁹F NMR (376 MHz, CDCl₃) δ -103.4 (d, *J* = 14.6 Hz) ppm.

HRMS (ESI) m/z: $[M+H]^+$ calc'd. for $C_{15}H_{15}FNO$, 260.1009; found 260.1191

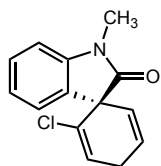


1-methyl-8'*H*-spiro[indoline-3,5'-quinolin]-2-one (26): Prepared according to General Procedure A using *N*-(2-iodophenyl)-*N*-methylquinoline-5-carboxamide (**S27**) (116 mg, 0.3 mmol, 1 equiv), DIPEA (160 μ L, 0.9 mmol, 3 equiv) and 3DPAFIPN (10 mg, 5 mol%). After 16 h, the reaction was purified on silica (30-100% EtOAc/Hex) to provide the desired product as a yellow solid (74 mg, 94% yield).

1H NMR (400 MHz, $CDCl_3$) δ 8.47 (dd, $J = 4.7, 1.7$ Hz, 1H), 7.35 (td, $J = 7.7, 1.4$ Hz, 1H), 7.07 (td, $J = 7.5, 1.0$ Hz, 1H), 7.03 – 6.97 (m, 2H), 6.95 (dt, $J = 7.8, 0.8$ Hz, 1H), 6.87 (dd, $J = 7.9, 1.7$ Hz, 1H), 6.37 (ddd, $J = 9.9, 4.1, 3.2$ Hz, 1H), 5.54 (ddd, $J = 9.9, 2.5, 1.8$ Hz, 1H), 3.92 (dt, $J = 22.7, 2.9$ Hz, 1H), 3.74 (ddd, $J = 22.6, 4.0, 1.8$ Hz, 1H), 3.28 (s, 3H) ppm.

^{13}C NMR (126 MHz, $CDCl_3$) δ 177.5, 154.6, 148.5, 143.5, 134.9, 134.7, 129.9, 128.9, 128.3, 124.7, 124.7, 123.5, 122.0, 108.4, 55.1, 33.0, 26.7 ppm.

HRMS (ESI) m/z: $[M+H]^+$ calc'd. for $C_{17}H_{15}N_2O$, 263.1106; found 263.1247.



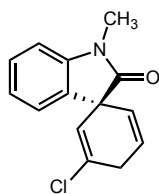
2-chloro-1'-methylspiro[cyclohexane-1,3'-indoline]-2,5-dien-2'-one (27): Prepared according to General Procedure A using 2-chloro-*N*-(2-iodophenyl)-*N*-methylbenzamide (**S29**) (186 mg, 0.5 mmol, 1 equiv), DIPEA (260 μ L, 1.5 mmol, 3 equiv), and 3DPAFIPN (16 mg, 5 mol%). After 16

h, the reaction was purified on silica (10–30% EtOAc/Hex) to provide the desired product as an off-white solid (86 mg, 70% yield).

¹H NMR (400 MHz, CDCl₃) δ 7.32 (t, *J* = 7.6 Hz, 1H), 7.14 (d, *J* = 8.1 Hz, 1H), 7.09 (d, *J* = 7.3 Hz, 1H), 6.85 (d, *J* = 7.8 Hz, 1H), 6.23 (t, *J* = 3.7 Hz, 1H), 6.04 (dt, *J* = 9.8, 3.4 Hz, 1H), 5.34 (dt, *J* = 9.8, 2.1 Hz, 1H), 3.25 (s, 3H), 3.16 – 3.05 (m, 1H), 3.05 – 2.95 (m, 1H).

¹³C NMR (126 MHz, CDCl₃) δ 175.4, 143.7, 131.6, 129.1, 128.0, 126.3, 125.5, 124.3, 124.2, 123.1, 108.2, 56.7, 28.3, 26.71.

HRMS (ESI) *m/z*: [M+H]⁺ calc'd. for C₁₄H₁₃ClNO, 246.0607; found 246.0675

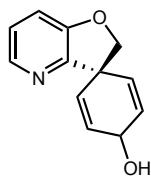


3-chloro-1'-methylspiro[cyclohexane-1,3'-indoline]-2,5-dien-2'-one (28): Prepared according to General Procedure A using 3-chloro-*N*-(2-iodophenyl)-*N*-methylbenzamide (**S31**) (159 mg, 0.4 mmol, 1 equiv), DIPEA (210 μL, 1.2 mmol, 3 equiv), and 3DPAFIPN (14.0 mg, 5 mol%). After 16 h, the reaction was purified on silica (10–20% EtOAc/Hex) to provide the desired product as light yellow solid (59.9 mg, 57% yield).

¹H NMR (500 MHz, CDCl₃) δ 7.31 (tt, *J* = 7.7, 1.3 Hz, 1H), 7.15 – 7.11 (m, 1H), 7.08 (tt, *J* = 7.4, 1.0 Hz, 1H), 6.88 – 6.82 (m, 1H), 6.06 (dtd, *J* = 9.8, 3.5, 1.0 Hz, 1H), 5.52 (q, *J* = 1.7 Hz, 1H), 5.40 – 5.35 (m, 1H), 3.31 – 3.06 (m, 5H).

¹³C NMR (126 MHz, CDCl₃) δ 176.4, 142.9, 133.4, 132.5, 128.9, 126.5, 124.9, 123.4, 123.1, 121.21, 121.20, 54.4, 33.2, 26.7.

HRMS (ESI) *m/z*: [M+H]⁺ calc'd. for C₁₄H₁₃ClNO, 246.0607; found 246.0770.



2'H-spiro[cyclohexane-1,3'-furo[3,2-*b*]pyridine]-2,5-dien-4-ol (29): Prepared according to General Procedure A using 2-bromo-3-((4-chlorobenzyl)oxy)pyridine (**S32**) (167 mg, 0.6 mmol, 1 equiv), DIPEA (315 μ L, 1.8 mmol, 3 equiv) and 3DPAFIPN (19 mg, 5 mol%). After 16 h, the reaction was purified on silica (100% EtOAc to 10% MeOH/EtOAc) to provide the desired product as a 1.8 : 1 mixture of diastereomers (combined yield 97 mg, 85% yield).

Major Diastereomer:

$^1\text{H NMR}$ (600 MHz, CDCl_3) δ 8.08 (dd, $J = 4.8, 1.3$ Hz, 1H), 7.11 (dd, $J = 8.1, 1.4$ Hz, 1H), 7.06 (dd, $J = 8.1, 4.8$ Hz, 1H), 6.20 (dd, $J = 9.8, 4.2$ Hz, 2H), 5.94 (d, $J = 9.1$ Hz, 2H), 4.54 (s, 2H), 4.50 (tt, $J = 4.1, 0.9$ Hz, 1H) ppm.

$^{13}\text{C NMR}$ (151 MHz, CDCl_3) δ 153.7, 152.1, 142.6, 131.5, 130.2, 123.3, 117.4, 81.7, 60.9, 49.0 ppm.

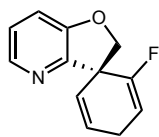
HRMS (ESI) m/z : $[\text{M}+\text{H}]$ calc'd for $\text{C}_{12}\text{H}_{13}\text{NO}_2$, 202.0790, found 202.0874

Minor Diastereomer:

$^1\text{H NMR}$ (600 MHz, CDCl_3) δ 8.06 (dd, $J = 4.8, 1.3$ Hz, 1H), 7.08 (dd, $J = 8.1, 1.3$ Hz, 1H), 7.03 (dd, $J = 8.1, 4.8$ Hz, 1H), 6.09 (dd, $J = 10.1, 3.2$ Hz, 2H), 5.88 (dd, $J = 10.0, 1.5$ Hz, 2H), 4.79 (s, 1H), 4.47 (s, 2H).

$^{13}\text{C NMR}$ (151 MHz, CDCl_3) δ 153.1, 153.1, 142.9, 129.3, 129.1, 123.2, 117.0, 80.7, 61.7, 48.3.

HRMS (ESI) m/z : $[\text{M}+\text{H}]$ calc'd for $\text{C}_{12}\text{H}_{13}\text{NO}_2$, 202.0790, found 202.0929



2-fluoro-2'*H*-spiro[cyclohexane-1,3'-furo[3,2-*b*]pyridine]-2,5-diene (30): Prepared according to General Procedure A using 2-bromo-3-((2-fluorobenzyl)oxy)pyridine

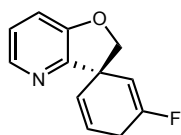
(**S33**) (144 mg, 0.5 mmol, 1 equiv), DIPEA (280 μ L, 1.6 mmol, 3 equiv) and 3DPAFIPN (17 mg, 5 mol%). After 16 h, the reaction was purified on silica (20 – 30% EtOAc/Hex) to provide the desired product as a yellow solid (86 mg, 83% yield).

^1H NMR (600 MHz, CDCl_3) δ 8.17 (dd, $J = 3.6, 2.5$ Hz, 1H), 7.11 (s, 1H), 7.10 (d, $J = 1.3$ Hz, 1H), 5.95 (dddd, $J = 10.7, 4.5, 3.4, 1.2$ Hz, 1H), 5.69 (tt, $J = 9.6, 2.0$ Hz, 1H), 5.54 (dtd, $J = 16.7, 3.6, 1.2$ Hz, 1H), 4.83 (d, $J = 9.3$ Hz, 1H), 4.45 (d, $J = 9.3$ Hz, 1H), 3.09 (ddtd, $J = 22.8, 5.4, 3.5, 2.0$ Hz, 1H), 2.91 (ddtd, $J = 22.8, 4.6, 3.5, 2.0$ Hz, 1H).

^{13}C NMR (151 MHz, CDCl_3) δ 156.2 (d, $^1J_{\text{C-F}} = 253.6$ Hz), 153.6, 151.3, 142.8, 127.1 (d, $^3J_{\text{C-F}} = 5.8$ Hz), 125.3 (d, $^4J_{\text{C-F}} = 2.4$ Hz), 123.5, 116.8, 102.5 (d, $^2J_{\text{C-F}} = 16.5$ Hz), 79.3, 49.8 (d, $^2J_{\text{C-F}} = 24.5$ Hz), 26.4 (d, $^3J_{\text{C-F}} = 6.7$ Hz).

^{19}F NMR (565 MHz, CDCl_3) δ -117.94 – -118.05 (1F, m).

HRMS (ESI) m/z : $[\text{M}+\text{H}]^+$ calc'd. for $\text{C}_{12}\text{H}_{11}\text{FNO}$, 204.0745; found 204.0956.



3-fluoro-2'*H*-spiro[cyclohexane-1,3'-furo[3,2-*b*]pyridine]-2,5-diene (31): Prepared according to General Procedure A using 2-bromo-3-((3-fluorobenzyl)oxy)pyridine

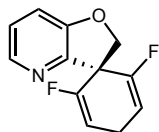
(**S34**) (152 mg, 0.5 mmol, 1 equiv), DIPEA (300 μ L, 1.7 mmol, 3 equiv) and 3DPAFIPN (17 mg, 5 mol%). After 16 h, the reaction was purified on silica (20 – 30% EtOAc/Hex) to provide the desired product as a colorless oil (91 mg, 83% yield).

$^1\text{H NMR}$ (600 MHz, CDCl_3) δ 8.14 (dd, $J = 4.6, 1.6$ Hz, 1H), 7.10 (dd, $J = 8.1, 1.6$ Hz, 1H), 7.07 (dd, $J = 8.1, 4.6$ Hz, 1H), 5.89 (ddt, $J = 9.8, 7.7, 3.5$ Hz, 2H), 5.73 – 5.69 (m, 2H), 5.32 (dq, $J = 16.3, 1.5$ Hz, 1H), 4.47 (dd, $J = 9.2, 1.4$ Hz, 1H), 4.44 (dd, $J = 9.2, 0.7$ Hz, 1H), 3.10 (ddt, $J = 22.3, 3.1, 1.5$ Hz, 2H), 2.92 (ddt, $J = 22.3, 3.4, 2.1$ Hz, 2H).

$^{13}\text{C NMR}$ (151 MHz, CDCl_3) δ 158.8 (d, $^1J_{\text{C-F}} = 258.2$ Hz), 153.9 (d, $^4J_{\text{C-F}} = 2.0$ Hz), 152.5, 142.9, 127.4 (d, $^3J_{\text{C-F}} = 2.8$ Hz), 123.2, 123.2, 123.1, 116.9, 104.0 (d, $^2J_{\text{C-F}} = 16.7$ Hz), 82.4 (d, $^4J_{\text{C-F}} = 2.8$ Hz), 50.0 (d, $^3J_{\text{C-F}} = 8.1$ Hz), 26.8 (d, $^2J_{\text{C-F}} = 26.1$ Hz).

$^{19}\text{F NMR}$ (565 MHz, CDCl_3) δ -103.27 (dd, $J = 16.9, 7.8$ Hz).

HRMS (ESI) m/z : $[\text{M}+\text{H}]^+$ calc'd. for $\text{C}_{12}\text{H}_{11}\text{FNO}$, 204.0746; found 204.1005.



2,6-difluoro-2'*H*-spiro[cyclohexane-1,3'-furo[3,2-*b*]pyridine]-2,5-diene (32**):** Prepared according to General Procedure A using 2-bromo-3-((2,6-difluorobenzyl)oxy)pyridine

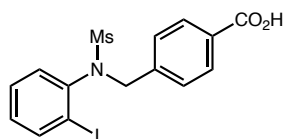
(**S35**) (175 mg, 0.6 mmol, 1 equiv), DIPEA (300 μ L, 1.5 mmol, 3 equiv) and 3DPAFIPN (16 mg, 4 mol%). After 16 h, the reaction was purified on silica (10 – 30% EtOAc/Hex) to provide the desired product as a light yellow solid (83 mg, 64% yield).

$^1\text{H NMR}$ (600 MHz, CDCl_3) δ 8.20 (dd, $J = 4.4, 1.7$ Hz, 1H), 7.16 (dd, $J = 8.2, 4.4$ Hz, 1H), 7.14 (dd, $J = 8.2, 1.7$ Hz, 1H), 5.58 (ddt, $J = 10.4, 5.3, 3.7$ Hz, 2H), 4.80 (s, 2H), 3.07 (dtt, $J = 22.2, 5.1, 3.7$ Hz, 1H), 2.89 (dtt, $J = 22.3, 4.9, 3.7$ Hz, 1H).

^{13}C NMR (151 MHz, CDCl_3) δ 154.4 (dd, $^1J_{\text{C-F}} = 254.8$, $^3J_{\text{C-F}} = 12.1$ Hz), 154.6, 147.7, 142.8, 124.2, 117.0, 102.3 (d, $^2J_{\text{C-F}} = 14.4$ Hz), 75.5, 52.1 (t, $^2J_{\text{C-F}} = 27.8$ Hz), 22.2 (t, $^3J_{\text{C-F}} = 8.0$ Hz).

^{19}F NMR (565 MHz, CDCl_3) δ -119.83 (dq, $J = 10.2$, 5.1 Hz).

HRMS (ESI) m/z : $[\text{M}+\text{H}]^+$ calc'd. for $\text{C}_{12}\text{H}_{10}\text{F}_2\text{NO}$, 222.0652; found 222.0972



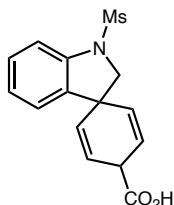
4-((*N*-(2-iodophenyl)methylsulfonamido)methyl)benzoic acid (S36)

A 100 mL round bottom flask was charged with *N*-(2-iodophenyl)methanesulfonamide (**S1**), (414 mg, 1.4 mmol, 1.0 equiv) and K_2CO_3 (480 mg, 3.5 mmol, 2.2 equiv). DMF was added (50 mL), followed by benzyl bromide (350 μL , 2.4 mmol, 2.3 equiv). The reaction was stirred overnight (ca. 16 h) at 50 $^\circ\text{C}$. The reaction was cooled to room temperature and then partitioned between EtOAc and water. The organic layer was washed with brine 3x, dried with MgSO_4 and concentrated. The crude oil was dissolved in THF/ H_2O (1:1 v/v) and lithium hydroxide (excess, ca 10 equiv) was added. The reaction was stirred at 50 $^\circ\text{C}$ until the reaction was complete as determined by TLC. The reaction was then cooled to room temperature and partitioned between EtOAc and water. The organic layer was washed 3x with 1 M NaOH. The organic layer was then discarded. EtOAc was added and the aqueous layer was re-acidified with conc. HCl. The aqueous layer was extracted with EtOAc (3 x). The combined organic layers were dried with Na_2SO_4 and concentrated. The desired product was purified by trituration with a minimal amount of EtOAc and was collected by filtration as a white solid (372 mg, 62% over 2 steps).

¹H NMR (400 MHz, CDCl₃) δ 8.04 (d, *J* = 8.3 Hz, 1H), 7.94 (dd, *J* = 7.9, 1.5 Hz, 1H), 7.40 (d, *J* = 8.3 Hz, 2H), 7.26 (dd, *J* = 7.4, 1.4 Hz, 1H), 7.09 (dd, *J* = 8.0, 1.6 Hz, 1H), 7.05 (td, *J* = 7.5, 1.6 Hz, 1H), 5.16 (d, *J* = 14.9 Hz, 1H), 4.66 (d, *J* = 14.9 Hz, 1H), 3.13 (s, 3H).

¹³C NMR (101 MHz, CDCl₃) δ 171.2, 141.6, 140.6, 140.2, 134.3, 130.4, 129.7, 129.2, 129.0, 126.6, 101.8, 55.2, 40.4.

LRMS (APCI) *m/z*: [M+H]⁺ calc'd. for C₁₅H₁₅INO₄S 432.0, found 431.6.



1'-(methylsulfonyl)spiro[cyclohexane-1,3'-indoline]-2,5-diene-4-carboxylic acid (S37)

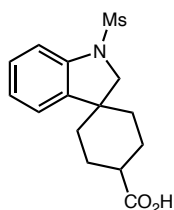
Prepared according to General Procedure A using 4-((*N*-(2-iodophenyl) methylsulfonamido) methyl) benzoic acid (624 mg, 1.4 mmol, 1.0 equiv), DIPEA (1.3 mL, 7.5 mmol, 5.4 equiv) and 3DPAFIPN (48 mg, 5 mol%). After 16 h, the reaction was purified on silica in 30–100% EtOAc/hex (1% acetic acid) to give the title compound as a 1:1 mixture of diastereomers. The crude mixture was carried on without further purification.

Diastereomer 1 signature peaks (elutes first):

¹H NMR (400 MHz, CDCl₃) δ 6.04 (dd, *J* = 10.1, 3.6 Hz, 1H), 5.91 (dd, *J* = 10.2, 2.1 Hz, 1H), 3.89 (m, 1H), 3.87 (s, 2H), 2.95 (s, 3H).

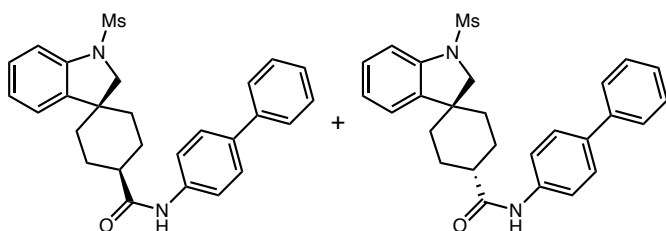
Diastereomer 2 signature peaks (elutes second):

¹H NMR (400 MHz, CDCl₃) δ 6.08 (dd, *J* = 10.1, 3.4 Hz, 1H), 5.92 (dd, *J* = 10.1, 2.2 Hz, 1H), 3.95 – 3.91 (m, 1H), 3.87 (s, 2H), 2.96 (s, 3H).



1'-(methylsulfonyl)spiro[cyclohexane-1,3'-indoline]-4-carboxylic acid (**35**)

A 4 mL vial was charged with 1'-(methylsulfonyl)spiro[cyclohexane-1,3'-indoline]-2,5-diene-4-carboxylic acid (**S37**) (15 mg, 0.05 mmol, 1 equiv), ~5 mg 5% Pd/C (wet basis), and a stir bar. To the vial was added 2 mL of 200-proof ethanol and the vial was placed in Parr high-pressure reactor. The reactor was sealed, evacuated, and backfilled with hydrogen at 1 PSI. This was repeated for a total of 5 times. The reactor was then pressurized to 40 PSI with hydrogen and stirred for 72 h. Upon reaction completion, the reactor was depressurized and dismantled. 0.5 mL of water was added to the reaction vial, then the reaction mixture was filtered through celite. The filtrate was concentrated then azeotroped with 10 mL of MeCN to remove the remaining water. Quantitative conversion to the hydrogenated product was detected by ^1H NMR and LRMS. The crude residue was used in the next step without further purification.



N-([1,1'-biphenyl]-4-yl)-1'-(methylsulfonyl)spiro[cyclohexane-1,3'-indoline]-4-carboxamide

(36-1, 36-2): In an 8 mL reaction tube equipped with a stir bar, 1'-(methylsulfonyl)spiro[cyclohexane-1,3'-indoline]-4-carboxylic acid (**35**) (15.4 mg, 0.05 mmol, 1.0 equiv) was dissolved in EtOAc to make a 0.1 M solution. 4-aminobiphenyl (10 mg, 0.06 mmol,

1.2 equiv) was added, followed by DIPEA (35 μ L, 0.2 mmol, 4.0 equiv). Propanephosphonic acid anhydride (as a 50% w/w solution in EtOAc) (55 μ L, 0.08 mmol, 1.6 equiv) was then added in one portion. The reaction mixture was allowed to stir for 3 h before being partitioned between water and EtOAc. The organic layer was washed with 1 M HCl (3x) then brine (3x). The organic layer was then dried with Na₂SO₄, filtered, and concentrated. The crude residue was purified by preparatory TLC (50% EtOAc/Hex eluent) to separate both diastereomers and afford the desired products as white solids. (Combined yield: 17.8 mg, 78% over 3 steps).

Diastereomer 1 (elutes first):

¹H NMR (600 MHz, CDCl₃) δ 7.61 (d, J = 8.5 Hz, 2H), 7.57 (d, J = 8.3 Hz, 4H), 7.46 – 7.39 (m, 3H), 7.37 – 7.31 (m, 1H), 7.27 – 7.21 (m, 2H), 7.15 (d, J = 7.6 Hz, 1H), 7.07 (t, J = 7.5 Hz, 1H), 3.87 (s, 2H), 2.92 (s, 3H), 2.43 – 2.32 (m, 1H), 2.08 (d, J = 11.4 Hz, 2H), 1.91 (d, J = 11.0 Hz, 2H), 1.83 – 1.71 (m, 4H).

¹³C NMR (151 MHz, CDCl₃) δ 173.0, 141.4, 140.5, 139.0, 137.8, 137.1, 129.3, 128.3, 127.7, 127.2, 126.9, 123.7, 122.9, 120.7, 115.5, 58.4, 45.8, 44.8, 43.9, 35.9, 34.7, 29.7, 26.2.

HRMS (ESI) m/z : [M+H]⁺ calc'd. for C₂₇H₂₉N₂O₃S, 461.1821, found 461.1875.

Diastereomer 2 (elutes second):

¹H NMR (600 MHz, CDCl₃) δ 7.63 (d, J = 8.6 Hz, 2H), 7.61 – 7.56 (m, 4H), 7.48 – 7.38 (m, 4H), 7.36 – 7.31 (m, 1H), 7.29 (s, 1H), 7.23 (dd, J = 8.1, 7.5 Hz, 1H), 7.06 (t, J = 7.5 Hz, 1H), 3.76 (s, 2H), 2.91 (s, 3H), 2.62 – 2.52 (m, 1H), 2.25 – 2.12 (m, 4H), 1.94 – 1.86 (m, 2H), 1.69 – 1.62 (m, 2H).

¹³C NMR (151 MHz, CDCl₃) δ 173.1, 141.1, 140.5, 139.1, 137.7, 137.1, 128.8, 128.5, 127.7, 127.2, 126.9, 124.9, 123.7, 120.1, 115.3, 61.7, 45.8, 43.3, 42.1, 34.3, 34.1, 30.2, 25.8.

HRMS (ESI) m/z : [M+H]⁺ calc'd. for C₂₇H₂₉N₂O₃S, 461.1821, found 461.1874.

Computational Details

All DFT calculations were carried out using the Gaussian 16 software package¹¹⁸ at the uM06¹¹⁹ level of theory with the 6-311+G(d,p)¹²⁰ basis set. The CPCM formalism for the Self Consistent Reaction Field (SCRF) model of solvation was employed in calculations to account for solvation in MeCN, and the default parameters as implemented in Gaussian were used. NBO charges were obtained using NBO Version 3.1 in Gaussian 16.¹²¹ Orbitals were visualized using Avagadro version 1.2.0.¹²²

Reduction potentials were calculated using a modified procedure as described by Nicewicz and coworkers.¹²³ Geometry optimizations were carried out for the reduced and neutral forms of each molecule, and frequency calculations were performed on the minimized structures to ensure no imaginary frequencies existed. Gibbs free energies (G_{298}) were obtained from the calculation and employed in the following equation equation:

$$E_{1/2}^{0,calc} = - \frac{(G_{298}[reduced] - G_{298}[oxidized])}{n_e F} - E_{1/2}^{0,SHE} + E_{1/2}^{0,SCE}$$

¹¹⁸ Frisch, M. J.; Trucks, G. W.; Schlegel, H. B.; Scuseria, G. E.; Robb, M. A.; Cheeseman, J. R.; Scalmani, G.; Barone, V.; Petersson, G. A.; Nakatsuji, H.; Li, X.; Caricato, M.; Marenich, A. V.; Bloino, J.; Janesko, B. G.; Gomperts, R.; Mennucci, B.; Hratchian, H. P.; Ortiz, J. V.; Izmaylov, A. F.; Sonnenberg, J. L.; Williams-Young, D.; Ding, F.; Lipparini, F.; Egidi, F.; Goings, J.; Peng, B.; Petrone, A.; Henderson, T.; Ranasinghe, D.; Zakrzewski, V. G.; Gao, J.; Rega, N.; Zheng, G.; Liang, W.; Hada, M.; Ehara, M.; Toyota, K.; Fukuda, R.; Hasegawa, J.; Ishida, M.; Nakajima, T.; Honda, Y.; Kitao, O.; Nakai, H.; Vreven, T.; Throssell, K.; Montgomery, J. A., Jr.; Peralta, J. E.; Ogliaro, F.; Bearpark, M. J.; Heyd, J. J.; Brothers, E. N.; Kudin, K. N.; Staroverov, V. N.; Keith, T. A.; Kobayashi, R.; Normand, J.; Raghavachari, K.; Rendell, A. P.; Burant, J. C.; Iyengar, S. S.; Tomasi, J.; Cossi, M.; Millam, J. M.; Klene, M.; Adamo, C.; Cammi, R.; Ochterski, J. W.; Martin, R. L.; Morokuma, K.; Farkas, O.; Foresman, J. B.; Fox, D. J. Gaussian Inc 16, Revision B.01. Gaussian Inc., Wallingford CT. **2016**

¹¹⁹ Zhao, Y.; Truhlar, D. G. The M06 Suite of Density Functionals for Main Group Thermochemistry, Thermochemical Kinetics, Noncovalent Interactions, Excited States, and Transition Elements: Two New Functionals and Systematic Testing of Four M06-Class Functionals and 12 Other Function. *Theor. Chem. Acc.* **2008**, 120 (1), 215–241

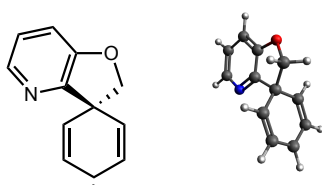
¹²⁰ McLean, A. D.; Chandler, G. S. Contracted Gaussian Basis Sets for Molecular Calculations. I. Second Row Atoms, Z=11–18. *J. Chem. Phys.* **1980**, 72 (10), 5639–5648

¹²¹ NBO Version 3.1, Glendening, E. D.; Reed, A. E.; Carpenter, J. E.; Weinhold, F.

¹²² Marcus D Hanwell, Donald E Curtis, David C Lonie, Tim Vandermeersch, Eva Zurek and Geoffrey R Hutchison; "Avogadro: An advanced semantic chemical editor, visualization, and analysis platform" *Journal of Cheminformatics* **2012**, 4:17

¹²³ Roth, H. G.; Romero, N. A.; Nicewicz, D. A. Experimental and Calculated Electrochemical Potentials of Common Organic Molecules for Applications to Single Electron Redox Chemistry. *Synlett* **2016**, 27 (05), 714–723

Where n_e is the number of electrons transferred ($n_e = 1$ for all calculations here), \mathcal{F} is the Faraday constant (value $23.061 \text{ kcal mol}^{-1} \text{ V}^{-1}$), $E_{1/2}^{0,SHE}$ is the absolute value for the standard hydrogen electrode (SHE, value = 4.281 V) and $E_{1/2}^{0,SCE}$ is the potential of the saturated calomel electrode (SCE) relative to the SHE in MeCN (value = -0.141V),¹²⁴ and $G_{298}[\text{oxidized}]$ and $G_{298}[\text{reduced}]$ are the Gibbs free energies in DMSO obtained from DFT calculations.

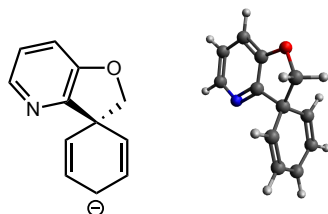


Charge: 0
 Multiplicity: 2
 Number of Imaginary Frequencies: 0
 Solvation: MeCN
 G_{298} : -592.774968 Hartree

C	2.1359520	-1.8896820	-0.0496070
C	3.1861070	-0.9987020	0.1321480
C	2.9431520	0.3713730	0.1841100
C	1.6254950	0.7551680	0.0419870
C	0.6391270	-0.2082310	-0.1308360
N	0.8577230	-1.5059140	-0.1734550
H	3.7393170	1.0946780	0.3238200
H	2.3295360	-2.9585960	-0.0925660
H	4.1976640	-1.3776000	0.2302670
O	1.1400950	2.0143860	0.0668640
C	-0.2220040	1.9418370	-0.4049320
H	-0.2233980	2.1681040	-1.4787000
H	-0.8062050	2.6922400	0.1295300
C	-0.7197230	0.4922050	-0.1623780
C	-1.5940820	-0.0037460	-1.2661860
C	-1.3538670	0.3427030	1.1893470
C	-2.7817220	-0.6228760	-1.0343270
H	-1.2186370	0.1187960	-2.2800550
C	-2.5460480	-0.2838250	1.3700900

¹²⁴ Isse, A. A.; Gennaro, A. Absolute Potential of the Standard Hydrogen Electrode and the Problem of Interconversion of Potentials in Different Solvents. *J. Phys. Chem. B*, **2010**, 114 (23), 7894–7899.

H	-0.7962480	0.7415160	2.0352210
C	-3.2796340	-0.7941480	0.2761670
H	-3.3647350	-0.9882490	-1.8752470
H	-2.9500320	-0.3834420	2.3738660
H	-4.2286040	-1.2935920	0.4396380



Charge: -1
 Multiplicity: 1
 Number of Imaginary Frequencies: 0
 Solvation: MeCN
 G₂₉₈: -592.888245 Hartree

C	2.076487	-1.923675	-0.112260
C	3.153155	-1.081021	0.121502
C	2.951311	0.296572	0.212533
C	1.650719	0.725897	0.059913
C	0.621043	-0.189039	-0.156695
N	0.812151	-1.493178	-0.247670
H	3.769359	0.989395	0.383874
H	2.235740	-2.997189	-0.193741
H	4.149697	-1.497808	0.224187
O	1.220503	2.653200	0.102935
C	-0.155812	1.989316	-0.358778
H	-0.152963	2.265084	-1.423647
H	-0.708878	2.739142	0.211695
C	-0.710632	0.558718	-0.164365
C	-1.671897	0.164641	-1.256064
C	-1.383810	0.481000	1.186441
C	-2.795092	-0.578860	-1.972200
H	-1.389390	0.419182	-2.278172
C	-2.512029	-0.354137	1.356645
H	-0.879557	0.854767	2.040930
C	-3.227819	-0.932789	0.286072
H	-3.399656	-0.881098	-1.867266
H	-2.895207	-0.471807	2.372384
H	-4.151973	-1.478266	0.448639

Chapter 8:
Photochemical Dearomatization of Benzenoids

8.1 Photochemical Activation of Monocyclic Aromatics

Visible-light mediated photocatalytic reduction of arenes is generally more difficult as reduction potential increases. In previous systems, however, we have shown that a large difference in reduction potential between the photocatalyst and arene can still lead to a productive reduction in the forward direction, if a photocatalyst with a long lifetime is employed and if the reduction is coupled to a sufficiently rapid process that acts as a thermodynamic driving force.¹²⁵

This is especially important because we aim to develop a method for the dearomatization of monocyclic aromatics. These substrates are challenging to access because of their particularly high reduction potentials (high-energy LUMO), but they are also the most widespread aromatic building blocks, making them attractive targets for dearomatization. Very recently, photochemical conditions that were able to perform dearomatization under photocatalytic conditions was reported, but this report was limited to polycyclic aromatics.¹²⁶ The authors identified that the first critical step in their system was energy transfer (EnT) between a sensitizer and polycyclic arene of interest. This was possible because of the close triplet energy levels of the sensitizer and polycyclic arene, coupled to a long-lived triplet excited state of the polyaromatic, which allows for electron transfer from an appropriate reductant to the newly formed LUMO of the polyaromatic. Notably, no examples of monocyclic aromatics were reported under these conditions, highlighting the difficulty in accessing this class of aromatics by sensitization techniques.

¹²⁵ Vogt, D. B.; Seath, C. P.; Wang, H.; Jui, N. T. Selective C–F Functionalization of Unactivated Trifluoromethylarenes. *J. Am. Chem. Soc.* **2019**, *141* (33), 13203–13211

¹²⁶ Chatterjee, A.; König, B. Birch-Type Photoreduction of Arenes and Heteroarenes by Sensitized Electron Transfer. *Angew. Chem. Int. Ed.* **2019**, 14289–14294

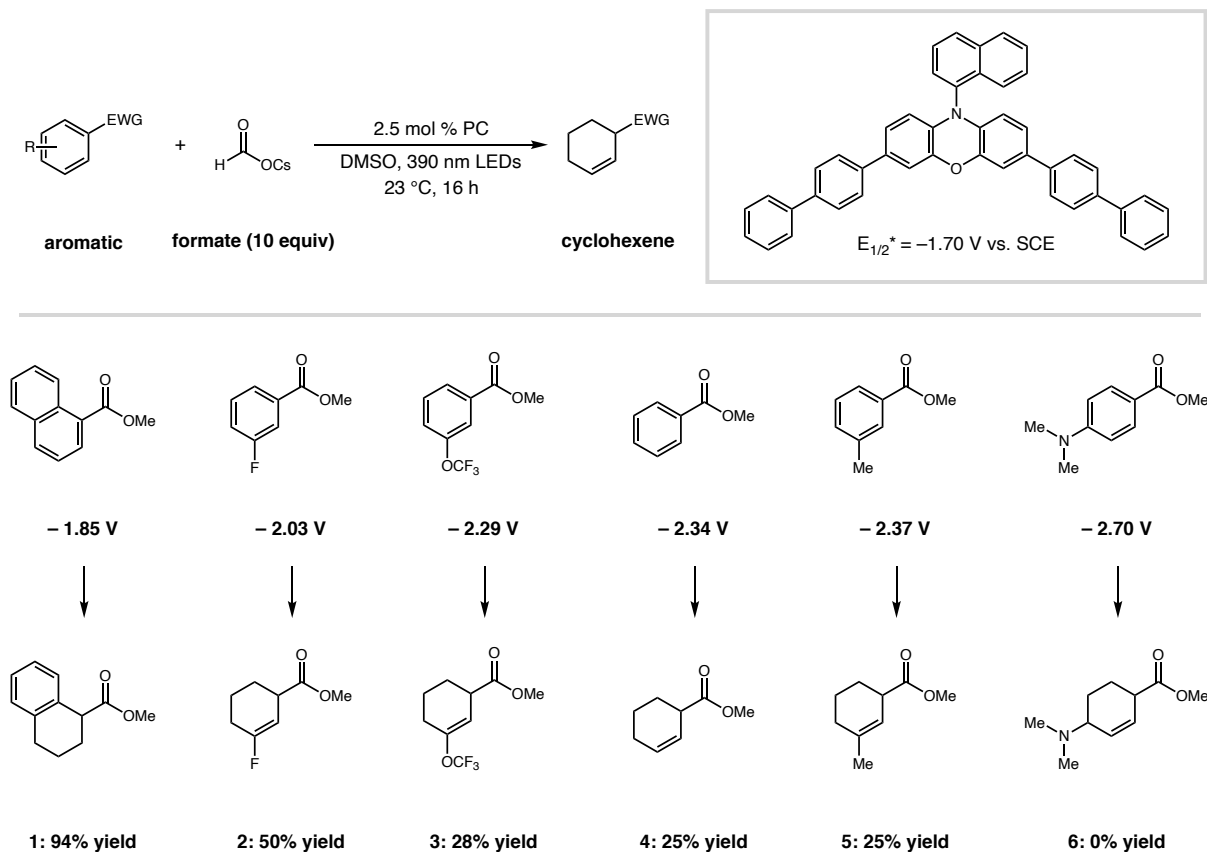
8.2 Proof-of-concept and preliminary scope

We have accomplished the dearomatization of monocyclic aromatics through endergonic electron transfer by utilizing a highly reducing organic dye with a particularly long triplet excited state (480 μ s).¹²⁷ With hydrated cesium formate as stoichiometric oxidant and DMSO as solvent, we were able to dearomatize methylnaphthoate to give tetrahydronaphthalene in 94% yield, imparting confidence that this system is indeed operational and could be elaborated to monocyclic aromatics.

When monocyclic benzenoids were subjected to these conditions, we excitingly observed dearomatized product in a number of substrates. The major (and often only detected) product under these conditions were 2-cyclohexenes, complementary to the traditional Diels-Alder retron, and completely different than Birch dearomatization. Under these preliminary conditions, meta-fluorinated methylbenzoate dearomatized to the 2-cyclohexene **2** in 50% yield, with vinyl fluoride retention. Similarly, 3-trifluoromethoxy methylbenzoate dearomatized to give the 2-cyclohexene **3** in 28% yield. Methylbenzoate dearomatizes to give **4** in 25% yield, as does meta-methyltoluate gives **5** in 25% yield. A trend in our preliminary data indicated reduction potential was tied to yield, with 0% conversion to **6** when the difference in catalyst and substrate potentials was ~ 1.0 V in the case of para-dimethylamino methylbenzoate.

¹²⁷ Du, Y.; Pearson, R. M.; Lim, C.-H.; Sartor, S. M.; Ryan, M. D.; Yang, H.; Damrauer, N. H.; Miyake, G. M. Strongly Reducing, Visible-Light Organic Photoredox Catalysts as Sustainable Alternatives to Precious Metals. *Chem. - Eur. J.* 2017, 23, 10962–10968

Scheme 8.1 Preliminary Results for Arene Dearomatization^a



^aReagents and Conditions: aromatic (0.2 mmol, 1.0 equiv), PC (2 mol%), cesium formate (2 mmol, 10 equiv), DMSO (0.1M), 390nm LEDs, 23°C, 16 h. Yields determined by ¹H NMR with dibromomethane as an internal standard.

8.3 Proposed Mechanism

We propose a mechanism similar to the one shown in Figure 8.1, where first, injection of an electron into a methylbenzoate gives a radical anion **7**, which protonates **3** or **5** to give dienyl radical **8**. This process likely proceeds through an initial endergonic SET to an aromatic unit. Stern-

Volmer quenching data suggests monocyclic aromatics here do not significantly quench the excited state of the catalyst, supporting evidence for endergonic SET.

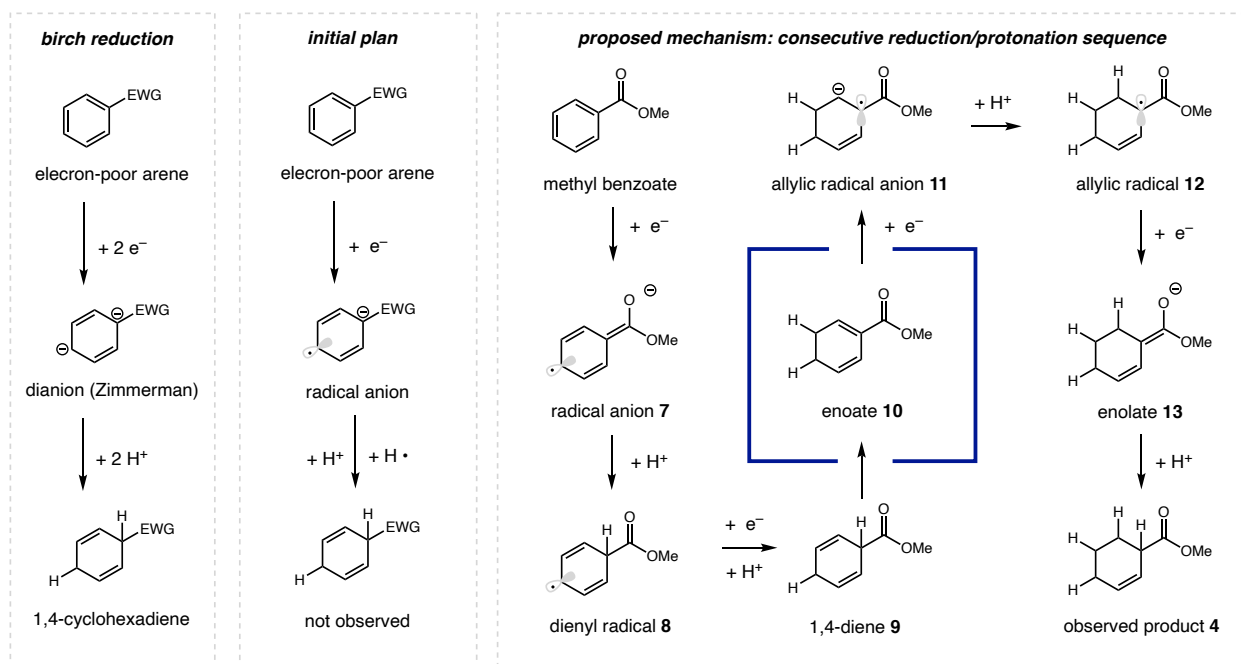


Figure 8.1. Mechanistic blueprint for photochemical arene dearomatization.

If significant quenching was observed (given the large difference in reduction potentials between the catalyst and substrate) it would indicate energy transfer (EnT) from the catalyst to the substrate. When photocatalyst is removed from the reaction, no conversion of the starting material is observed, which indicates a photocatalyst-driven process, and not direct excitation of the aromatic starting material. Subsequent reduction and protonation of dienyl radical **8** gives diene **9**, which would be the product of traditional Birch reduction. Here, our system diverts: at room temperature under these basic buffered conditions, the diene isomerizes to give enoate **10**, containing a reducible α,β -unsaturated ketone, which is a known participant in photoredox-

mediated processes. Upon reduction of enoate **10** to the corresponding radical anion **11**, protonation gives allylic radical **12**, which is reduced to enolate **13** and finally protonated to observed product **1**. This reductive sequence is reminiscent of the proposed mechanism in Chapter 7, where a radical-polar crossover event is key to preventing rearomatization.

8.4 Probing Mechanism with Experimentation

We questioned whether the initial reduction was EnT followed by electron transfer, or if this reduction was indeed a single electron transfer process. We conducted a luminescence quenching experiment that would investigate these pathways. Given the large differential in reduction potentials of the photocatalyst ($E_{1/2}^{0} \text{PC}^{*+/*} = -1.70 \text{ V vs. SCE}$) and substrate (here, methylbenzoate $E_{1/2}^{0} = -2.34 \text{ V vs. SCE}$), if efficient quenching of the excited state photocatalyst was observed ($K_{SV} \geq 30$) we reasoned that the operative quenching mechanism would be EnT. If little quenching was observed, ($K_{SV} < 30$) could be endergonic electron transfer.¹²⁸ In this experiment, we saw methylbenzoate was not an efficient quencher of the excited state photocatalyst, suggesting endergonic SET. Indeed, the K_{SV} we observed (0.06) is in line with other endergonic electron transfer processes (Fig. 8.2).¹²⁵

¹²⁸ Strieth-Kalthoff, F.; James, M. J.; Teders, M.; Pitzer, L.; Glorius, F. Energy Transfer Catalysis Mediated by Visible Light: Principles, Applications, Directions. *Chem. Soc. Rev.* **2018**, 47 (19), 7190–7202

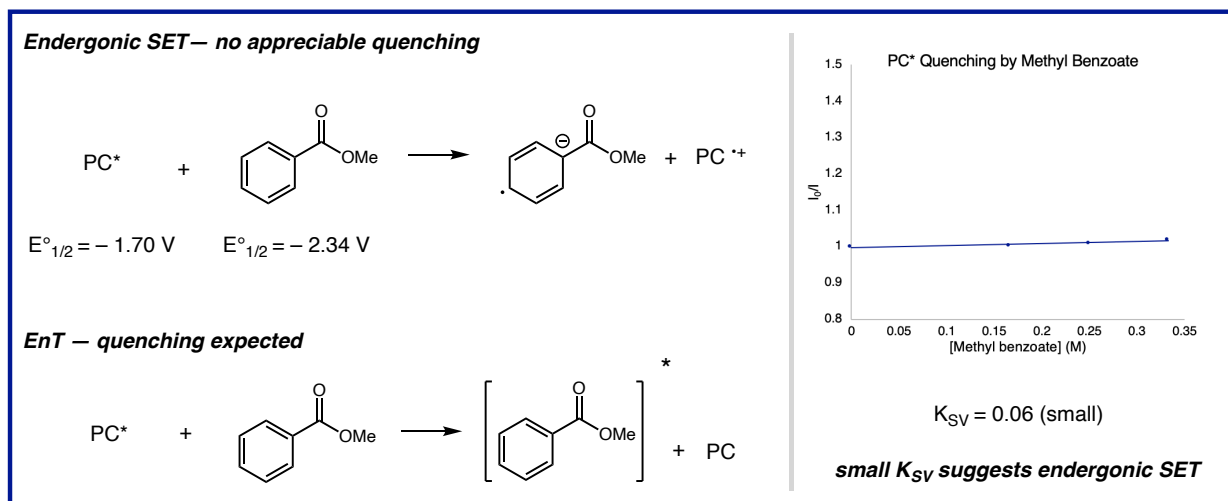


Figure 8.2. Luminescence quenching experiments suggest endergonic SET as operative reduction.

We next investigated if the electron transfer was facilitated by a proton-coupled electron transfer (PCET) mechanism. In PCET mechanisms, the protonation is only possible after increased basicity through the injection of an electron, and reduction is only possible once protonation occurs. The simultaneous barrier lowering events of both of these processes leads to a concerted protonation-reduction sequence—which may be a reasonable operative mechanism given the amount of acid and water in the reaction conditions.¹²⁹ We conducted a series of luminescence quenching experiments that aimed to investigate the PCET mechanism. These experiments are designed so that, in the case of a PCET-mediated process, catalyst quenching efficiency increases with increasing concentration of acid.¹³⁰ However, we did not see any increase in luminescence

¹²⁹ (a) Weinberg, D. R.; Gagliardi, C. J.; Hull, J. F.; Murphy, C. F.; Kent, C. A.; Westlake, B. C.; Paul, A.; Ess, D. H.; McCafferty, D. G.; Meyer, T. J. Proton-Coupled Electron Transfer. *Chem. Rev.* **2012**, *112* (7), 4016–4093 (b) Gentry, E. C.; Knowles, R. R. Synthetic Applications of Proton-Coupled Electron Transfer. *Acc. Chem. Res.* **2016**, *49* (8), 1546–1556

¹³⁰ Tarantino, K. T.; Liu, P.; Knowles, R. R. Catalytic Ketyl-Olefin Cyclizations Enabled by Proton-Coupled Electron Transfer. *J. Am. Chem. Soc.* **2013**, *135* (27), 10022–10025

quenching upon the addition of the acid used in the initial system (camphorsulfonic acid), nor did we see quenching in the presence of any acid with varying pK_a 's—which would be seen in a PCET mediated process (Fig. 8.3). Taken together with the lack of appreciable quenching on its own (precluding EnT), we concluded that the reduction of methylbenzoates is likely an endergonic electron transfer process. We hypothesize that the driving force for dearomatization, then, is the rapid protonation step after electron transfer facilitated by superstoichiometric number of protons from hydrated formate and wet DMSO available under these reaction conditions.

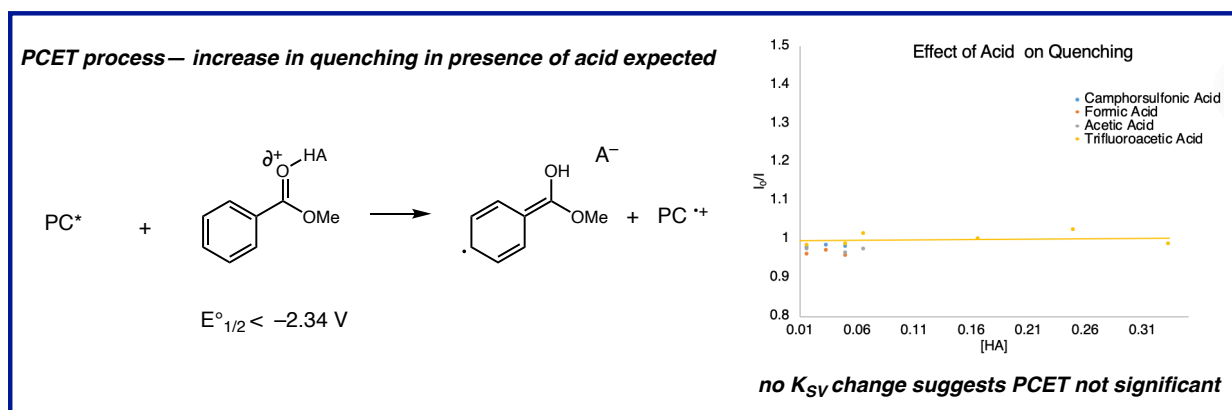


Figure 8.3. Varying concentrations and pK_a 's of acids does not change quenching efficiency.

To investigate the feasibility of the proposed protonation sequence we conducted a deuteration experiment to support either a radical-polar crossover mechanism (deuterium incorporation from solvent only), or a mechanism where protonation is followed by hydrogen atom transfer (HAT, deuterium incorporation from deuterio-formate), summarized in Figure 8.4.

We found that, with deuterio-formate, no deuterium incorporation was detected, precluding an H-atom transfer step from formate. With D_2O added to solvent, however, we indeed saw deuterium distribution and no appreciable amount of fully protonated product. However, in the

case of methylbenzoate the deuterium was incorporated as a distribution between 1–4 deuterium atoms present in the final product (with >90% D-incorporation at the α -position). In the case of methylnaphthoate, a substrate that fully converts to reduced product, we observed >90% D incorporation at the α , β , γ and δ , supporting four deuteration events (versus two deuteration and two HAT).

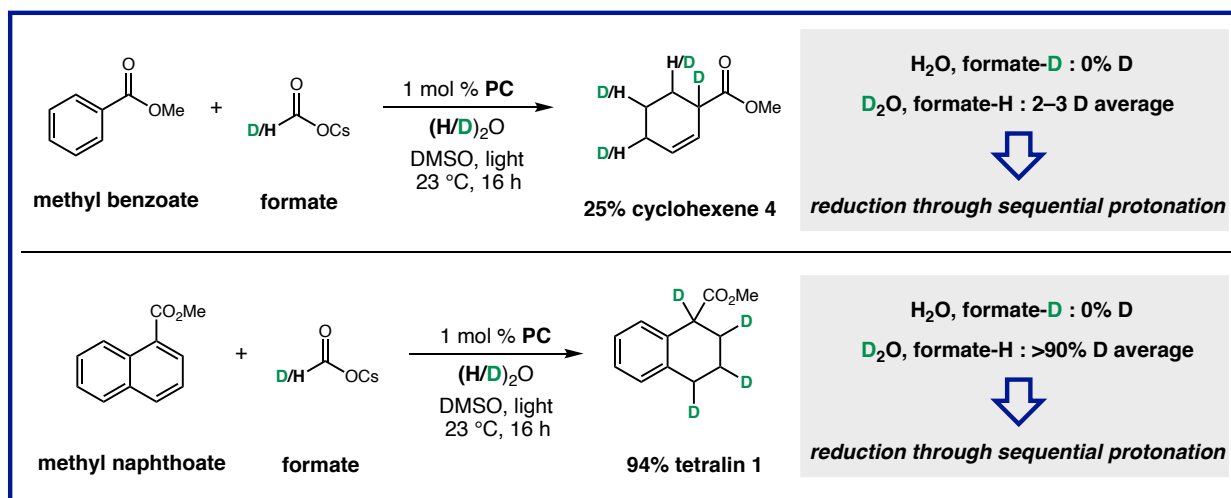


Figure 8.4. Deuterium experiments suggest consecutive reduction-protonation sequence.

With support for a consecutive reduction-protonation sequence, we began an attempt to further optimize our photocatalytic reduction system. We reasoned that a buffered system would facilitate both regeneration of our catalyst (through formate oxidation) and protonation of our substrate (through formic acid deprotonation). By choosing formic acid, we were able to keep the identity of the conjugate base the same as the stoichiometric oxidant. Indeed, with an increased amount of formic acid in the system, we were able to improve our reductive system to give 60% product.

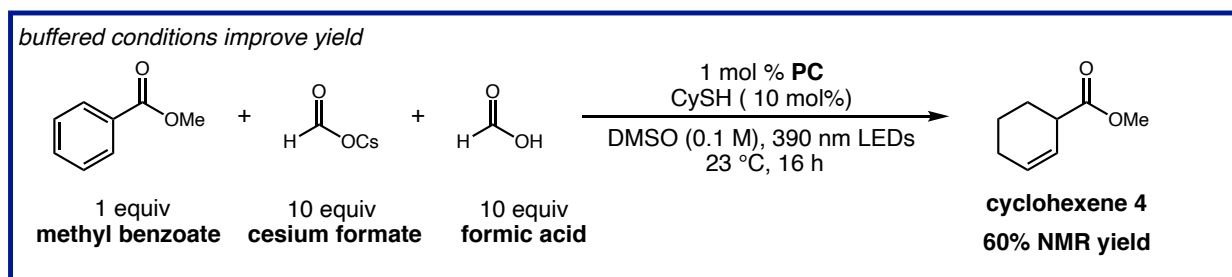


Figure 8.5. Current photochemical arene dearomatization conditions.

Under these buffered conditions, we are currently deeply investigating the mechanism of the reaction and evaluating the scope of our arene dearomatization.

8.5 Supporting Information

Optimization Procedure

An 8 mL screw-top test tube was charged with photocatalyst (0.001 mmol, 1 mol%) and reductant. The tube was equipped with a stir bar and sealed with a PTFE/silicon septa. The atmosphere was exchanged by applying vacuum and backfilling with nitrogen (this process was conducted a total of three times). Under nitrogen atmosphere, separately degassed solvent was added via syringe, followed by methyl benzoate (0.1 mmol, 1 equiv). The resulting mixture was stirred at 800 RPM for 16 h under irradiation by blue LEDs, unless noted otherwise. The reaction was then extracted with ethyl acetate (3 x), washed with brine, dried with MgSO₄, and concentrated. Deutero-chloroform with an internal standard of dibromomethane (7 μL, 0.1 mmol) was added. The sample was analyzed by ¹H NMR (d = 5 s), and the integral values were used to calculate the data given in Table S1.

Table S8.1: Optimization of Reduction Reaction



entry	PC	oxidant (equiv)	additive (equiv)	cosolvent (rxn conc)	SM	1	S2
1	N-POX(Ph ₂) ₂	NaCO ₂ H (3)	N/A	DMSO (0.1 M)	>99	tr	tr
2	N-POX(Ph ₂) ₂	CaCO ₂ H (3)	N/A	DMSO (0.1 M)	>99	0	0
3	N-POX(Ph ₂) ₂	KCO ₂ H (3)	N/A	DMSO (0.1 M)	>99	tr	tr
4	N-POX(Ph ₂) ₂	NH ₄ CO ₂ H (3)	N/A	DMSO (0.1 M)	>99	0	0
5	N-POX(Ph ₂) ₂	CsCO ₂ H (3)	N/A	DMSO (0.1 M)	80	17	3
6	N-POX(Ph ₂) ₂	NaCO ₂ H (3)	LiBF ₄ (1)	DMSO (0.1 M)	>99	tr	tr
7	N-POX(Ph ₂) ₂	NaCO ₂ H (3)	p-TsOH (1)	DMSO (0.1 M)	85	15	0
8	N-POX(Ph ₂) ₂	NaCO ₂ H (3)	La(OTf) ₃ (1)	DMSO (0.1 M)	>99	0	0
9	N-POX(Ph ₂) ₂	NaCO ₂ H (3)	urea (1)	DMSO (0.1 M)	>99	0	0
10	N-POX(Ph ₂) ₂	NaCO ₂ H (3)	MSA (1)	DMSO (0.1 M)	90	10	0
11	N-POX(Ph ₂) ₂	NaCO ₂ H (3)	TfOH (1)	DMSO (0.1 M)	95	5	0
12	N-POX(Ph ₂) ₂	NaCO ₂ H (3)	AcOH (1)	DMSO (0.1 M)	96	4	0
13	N-POX(Ph ₂) ₂	NaCO ₂ H (3)	CO ₂ H ₂ (1)	DMSO (0.1 M)	93	7	0
14	N-POX(Ph ₂) ₂	NaCO ₂ H (3)	TFA (1)	DMSO (0.1 M)	88	12	0
15	N-POX(Ph ₂) ₂	NaCO ₂ H (3)	NH ₄ Cl (1)	DMSO (0.1 M)	95	5	0
16 ^a	N-POX(Ph ₂) ₂	CsCO ₂ H (3)	MSA (1)	DMSO (0.1 M)	14	11	11
17 ^a	N-POX(Ph ₂) ₂	CsCO ₂ H (3)	AcOH (1)	DMSO (0.1 M)	16	14	13
18 ^a	N-POX(Ph ₂) ₂	CsCO ₂ H (3)	CO ₂ H ₂ (1)	DMSO (0.1 M)	31	25	0
19 ^a	N-POX(Ph ₂) ₂	CsCO ₂ H (3)	NH ₄ Cl (1)	DMSO (0.1 M)	23	25	5
20 ^a	N-POX(Ph ₂) ₂	CsCO ₂ H (3)	CO ₂ H ₂ (10)	DMSO (0.1 M)	64	15	0
21 ^{a,b}	N-POX(Ph ₂) ₂	CsCO ₂ H (3)	CO ₂ H ₂ (10)	DMSO (0.1 M)	7	44	5
22^{a,c}	N-POX(Ph₂)₂	CsCO₂H (3)	CO₂H₂ (10)	DMSO (0.1 M)	2	60	2

^a 390nm LEDs ^b 50 °C ^c 10 mol% CySH

Fluorescence Quenching and Stern-Volmer Plots

All fluorescence measurements were recorded using a Horiba Scientific Dual-FL Fluorometer. Quenching studies were conducted in MeCN at 20 ± 0.5 °C (Peltier temperature controller) with a N-POX(Ph₂)₂ concentration of 4.32×10^{-5} M. For measurements with constant methylbenzoate and varying concentrations of acid, the concentration of methyl benzoate was 0.005 M. Samples were prepared in Starna quartz cuvettes (3-Q-10-GL14-S) with septum seal caps. Dry N₂ was bubbled through the prepared sample for 3 minutes before analysis. Raw fluorescence intensity was measured at $\lambda = 500$ nm after excitation at $\lambda = 388$ nm in the quartz cuvettes with a path length of 1 cm and 0.1 second integration. Measurements of the quenchers shown were plotted using Microsoft Excel; data points were fit with a linear trend line.

Table S8.2: Fluorescence Quenching Data

Compound (Quencher)	[Quencher] (M)	I ⁰ /I	Coefficients
methylbenzoate	0	1	y = a + bx
methylbenzoate	0.167	1.004	a = 0.998
methylbenzoate	0.25	1.012	b = 0.06
methylbenzoate	0.33	1.019	R ² = 0.92
trifluoroacetic acid	0	1	y = a + bx
trifluoroacetic acid	0.0167	0.98	a = 0.996
trifluoroacetic acid	0.05	0.99	b = 0.02
trifluoroacetic acid	0.067	1.01	R ² = 0.02
trifluoroacetic acid	0.167	1.00	
trifluoroacetic acid	0.25	1.02	
trifluoroacetic acid	0.33	0.98	
formic acid	0	1	y = a + bx
formic acid	0.0167	0.96	a = 99
formic acid	0.033	0.98	b = - 0.7
formic acid	0.05	0.96	R ² = 0.6
acetic acid	0	1	y = a + bx
acetic acid	0.0167	0.97	a = 1.0
acetic acid	0.05	0.96	b = - 0.4
acetic acid	0.067	0.96	R ² = 0.53
camphorsulfonic acid	0	1	y = a + bx
camphorsulfonic acid	0.0167	0.97	a = 1.0
camphorsulfonic acid	0.033	0.98	b = - 0.3
camphorsulfonic acid	0.05	0.98	R ² = 0.37

Photochemical Dearomatization: Summary and Future Directions

Aromatic systems experience significant amounts of thermodynamic stabilization. Although disruption of these systems has not been trivial in a general sense, aromaticity is routinely broken in a transient sense.

Because radical addition to arenes is a well-studied process, we envisioned that we could build on this strong foundation to intercept transient dearomatized intermediates. Our strategy for this interception lies in radical-polar crossover, where we rapidly reduce a radical intermediate to an anion, which precludes common rearomatization pathways (oxidation and deprotonation, H-atom abstraction). This success has been largely successful in not only the dearomative processes shown here, but also a number of additional systems currently being investigated in our laboratory.

We hope this rapid radical-polar crossover (“reductive interception”) strategy will be generally used in the divergent synthesis of medicinally relevant scaffolds as well as the transformation of petrochemical and aromatic building blocks into complex, sp^3 -rich systems to aid drug discovery.